JPL D-18130/CL#04-2238
EOS MLS DRL 601 (part 5)
ATBD-MLS-05

Earth Observing System (EOS)

Microwave Limb Sounder (MLS) Forward Model Algorithm Theoretical Basis Document

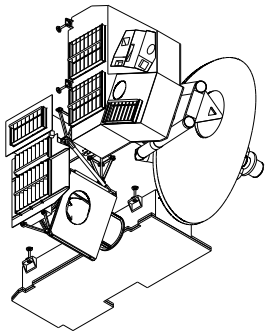

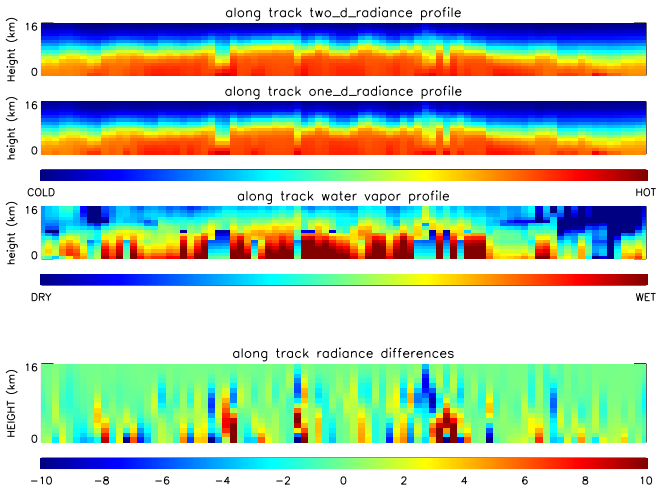

William G. Read, Zvi Shippony, and W. Van Snyder

Version 1.0
August 19, 2004

National Aeronautics and
Space Administration

JPL

Jet Propulsion Laboratory
California Institute of Technology
Pasadena, California, 91109-8099

In memory of my colleague and best friend
Zvi Shippony.
September 8, 1946 — July 24, 2002.
—Bill Read

Revision History

Version	Date	Comments
1.0	1 July 2004	Initial version

Contents

List of Figures

List of Tables

Chapter 1. Introduction

This document provides the physics contained in the signals measured by the Microwave Limb Sounder (MLS) experiment on the National Aeronautical and Space Administration (NASA) Earth Observing System (EOS) Aura (formerly CHEM) mission scheduled to launch in June 2004. The mathematical function solved herein is called the forward model and describes the relationship between measured signals and atmospheric composition. "Signal" for the purposes of this document is atmospheric spectral intensity in brightness (K). The conversion between brightness and the basic engineering measurements made by the instrument hardware itself is described in [5].

The EOS MLS is a follow-on and enhanced version of the microwave limb sounder flown on the Upper Atmosphere Research Satellite (UARS). The objective of these missions is to provide daily, global, vertically resolved atmospheric composition data of molecules important for understanding global environmental issues such as ozone depletion, climate change, and tropospheric pollution. Toward this end the EOS MLS measures temperature (T), water vapor (H_2O), ozone (O_3), carbon monoxide (CO), hydroxyl radical (OH), nitric acid (HNO_3), nitrous oxide (N_2O), hydrogen peroxy radical (HO_2), hydrochloric acid (HCl), chlorine monoxide (ClO), hypochlorous acid (HOCl), hydrogen cyanide (HCN), methyl cyanide (CH_3CN), and sulfur dioxide (SO_2), and ice water content (IWC) in clouds. The scientific significance of this measurement suite and basic measurement operations and requirements is given fully in [18].

The forward model is inverted, that is constituents as a function of signals, to extract the atmospheric compositions as described in [8]. The inversion algorithm requires a linear approximation to the forward model. This document provides the algorithms for computing the radiances and their first derivatives with respect to its state vector elements.

The forward model algorithm for EOS MLS takes advantage of lessons learned from UARS MLS and include some enhancements. The basic calculation is a non-scattering local thermodynamic equilibrium unpolarized radiative transfer calculation including instrument responses. Experience from UARS MLS demonstrated that for signals less than 120 K (single side band), the forward model is quite linear and pre-tabulated tables of radiances, state vectors, and derivatives from which to construct a Taylor series was an adequate representation. The data were stored in a Level 2 Processing Coefficients (L2PC) file. The details of those calculations are described in [14] and that document will form the basic infrastructure of the EOS MLS forward model. However there are some new added features. These include incorporating a different spherical representation of the Earth figure ellipse in the radiative transfer ray tracing. This change is implemented in order to have the vertical coordinate normal to the reference geoid used for geopotential and hydrostatic calculations which is heuristically a better definition than having the vertical coordinate pass through the Earth center of mass which is not normal to the surface. The EOS MLS forward model combines a two dimensional radiative transfer calculation which incorporates atmospheric gradients in height and along the line-of-sight (LOS) at a given height and a one dimensional scan and pointing model based on hydrostatic balance. The mounting of the MLS on the EOS Aura satellite allows measurements to be interleaved both horizontally and vertically in such a way that this information can be extracted without having to add any new state vector elements. This feature is discussed in [8] and is expected to significantly improve the accuracy of lower stratospheric constituent measurements of molecules having strongly inverted profiles (e.g. OH and O_3) and

for upper tropospheric humidity which has high horizontal variability. The EOS MLS experiment incorporate narrow banded digital auto-correlation spectrometers (DACS) and conventional UARS MLS type filters. The handling of the latter is expected to be nearly identical to UARS which has been described elsewhere but the former requires new techniques as described in [15]. The EOS MLS forward model will offer a choice of representation basis functions for the constituents. The choices are linear segments in mixing ratio (used for UARS) and linear segments in the logarithm of mixing ratio. The choice of functions allows added flexibility to characterize vertical profiles of constituents.

The major challenge with the EOS MLS forward model is execution time. The early versions of UARS L2 processing circumvented this by exclusively using L2PC files. But this led to some important compromises. Strong signal bands 5 and 6 for H_2O and O_3 had limited height coverage, which reduced precision and accuracy, and the center three channels of band 1 used for pointing are not processed. The UARS V5 retrieval rectified the former problem by iterating with a full forward model directly. Although time consuming, thanks to improvement in computers, the entire processing is kept within 25% of real time, but this only involves 30 channels being calculated in a 1 dimensional scheme. The 1 dimensional scheme (vertical gradients) can exploit horizontal symmetry which saves computational effort and time. The three center channels in band 1 are partially polarized and very non-linear in magnetic field. The magnetic calculation involving complex polarization tensors is inherently 8 times slower than an identical scalar calculation and this proved prohibitively time consuming—even for only three channels–for UARS MLS. Fortunately, for EOS MLS, the 118 GHz O_2 line splits into 3 (versus $\sim$ 50 for the 2 63 GHz lines measured by UARS MLS) and with faster computers, the polarized problem is more tractable. The evaluation of the partially polarized radiative transfer problem is discussed fully in [15].

The forward model accuracy is defined in terms of gridding convergence error. This is an estimate of the difference between a finitely gridded and an infinitely gridded calculation. Since the infinitely gridded calculation doesn't exist, it is represented by a calculation having a much finer grid than the test case. However, this deserves some caution because the convergence of difference can be very slow therefore the accuracy of the forward model is an estimate. The target values do not include the accuracy of the physics, e.g. lineshape functions, spectral parameters, the Fourier transform methodology for computing weighted averages, etc. The aim is to have the weak signal channels (maximum spectral signature difference less than 100 K, single side band across the band pass) and the O_2 which has no vertical mixing ratio gradient be about 0.2 K. The strong signal bands which are the remainder be 0.5 K. These were the same goals as for UARS and it is believed to have been achieved. The accuracy of the actual physics is tested through validation, laboratory experimentation and academic research.

This document will be a reasonably comprehensive description of the forward model, but is also a dynamic working document. Improved algorithms and new spectroscopic measurements will be included in future versions. Polarized and scattering radiative transfer models are described in [15] and [19] respectively.

Figure 1.1 Shows how the forward model calculation is organized in this document.

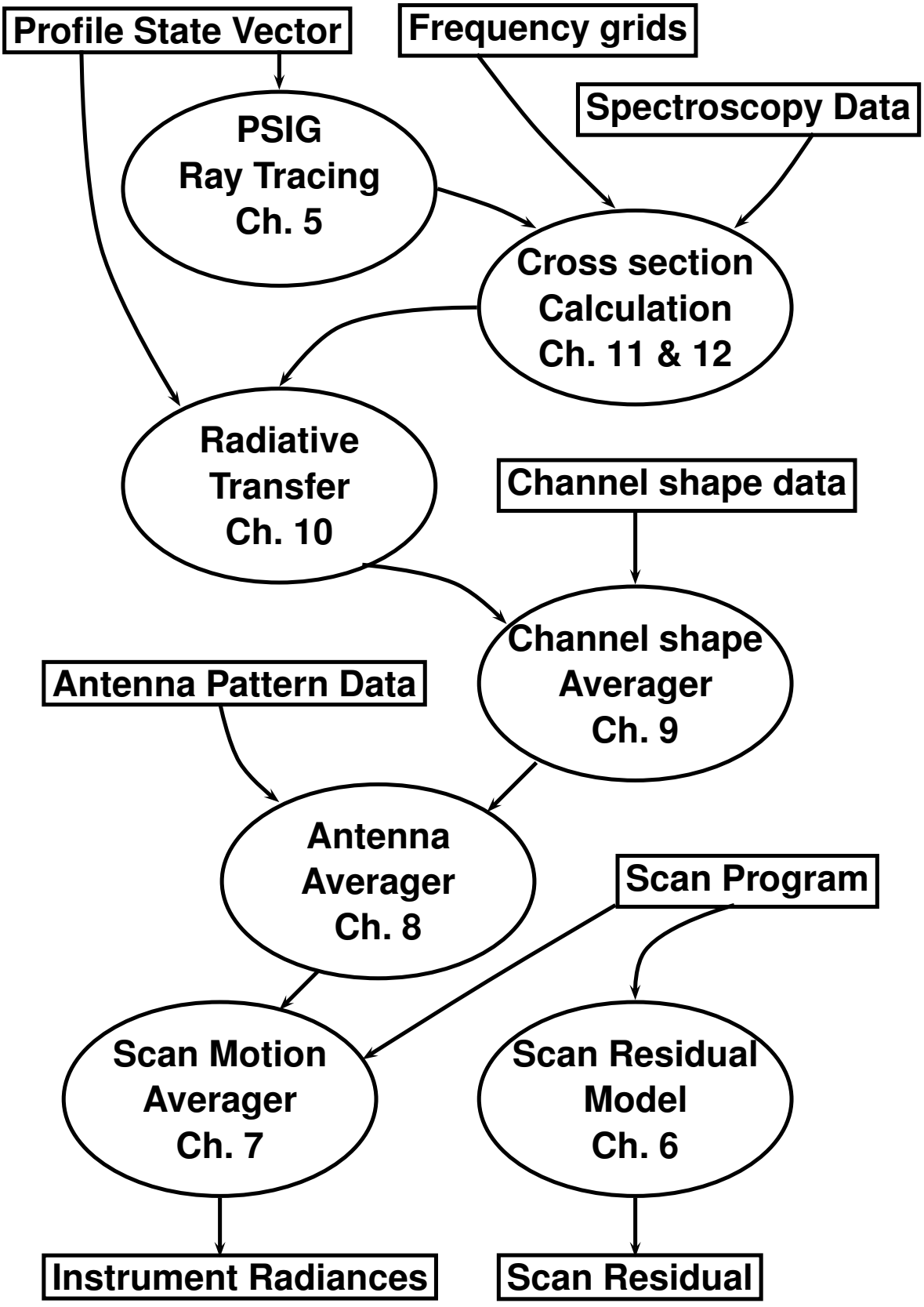

Figure 1.1: Forward model calculation organization.

Chapter 2. Measurement Description

The EOS MLS measures atmospheric thermal emission signals at specific frequencies between 118–2500 GHz (2500–120 μm). The instrument will fly on the EOS Aura satellite which is in a sun-synchronous polar orbit (98.14° inclination at 705 Km). The instrument views forward and the measurement coverage ranges from 82°S to 82°N. Vertical resolution is achieved by measuring the radiation through a high-gain antenna that scans the atmospheric limb. A complete vertical scan takes 24.7 seconds and there are 240 scans per orbit or $\approx$ 3500 scans per day. The limb tangent of the scans proceeds from near the surface to 90 km in a continuous movement and measurements are taken every 1/6 second. The upward scan movement keeps the limb tangent on a line that is nearly normal (or vertical) to the Earth surface. The forward viewing geometry couples the vertical limb tangent measurements with horizontal line-of-sight gradients, which will allow separation of both effects. In effect, the measurement and the sampled atmosphere are confined to the same two dimensions (height and orbit track) as shown in figure 2.1. This represents a significant improvement over the UARS viewing geometry where the atmosphere was viewed perpendicular to the spacecraft motion and therefore the measurement is affected by vertical, along measurement track, and line-of-sight variations, which is a three dimensional field. The UARS MLS measurement like EOS is two dimensional and does not allow for line-of-sight and along track variations to be separated.

The pre-launch version of the forward model uses a two-dimensional radiative transfer model combined with a vertical scan. Vertical and horizontal gradients in the atmospheric state are included in the radiance calculations. Also needed is the limb tangent horizontal and vertical positions, which we designate as ϕ_t and ζ_t respectively. Figure 2.2 shows the 2-D limb tangent loci of a typical EOS Aura scan in relation to the 1.5° horizontal basis function, the finest available horizontal resolution with Aura-MLS. As shown in figure 2.2, the scan varies slightly in ϕ_t. The current forward model implementation allows for ϕ_t to be independent of the profile horizontal basis (thereby allowing the scan to zig-zag). We assume, however, that the vertical coordinate for antenna smearing follows the vertical profile of ϕ_t. The true vertical profile smeared by the antenna is shown by the triangles which of course does not overlay the scan points (diamonds). The triangles, show the vertical and horizontal extent of the half-power beam width for the 118 GHz field-of-view (FOV), which has the largest amount of smearing. The proper calculation would require separate radiative transfer calculations along the smearing slant path for each tangent height, making this a very time consuming calculation; therefore, we are introducing some error in the interest of speed and simplicity. The error associated with this approximation is yet to be determined; however, it is not expected to be significant because the neglected horizontal smearing is less than 10% of the horizontal separations between radiance profile measurements. For interest, a refracted scan is shown (diamonds). Refraction actually helps minimize the antenna smearing errors due to the slant path. Separating the profile locations from the tangent ϕ_t is worthwhile because it allows arbitrary horizontal placement of the scan (i.e. accommodate its zig-zag behavior) yet allow a rigorous retrieval of a truly vertically-oriented state vector. For example, this would even allow for a downward scan where the horizontal loci of points are spread over a few 100 km; however, the antenna smearing algorithm would have to be modified to accurately account for the horizontal effects we are neglecting now because they would be considerably more substantial.

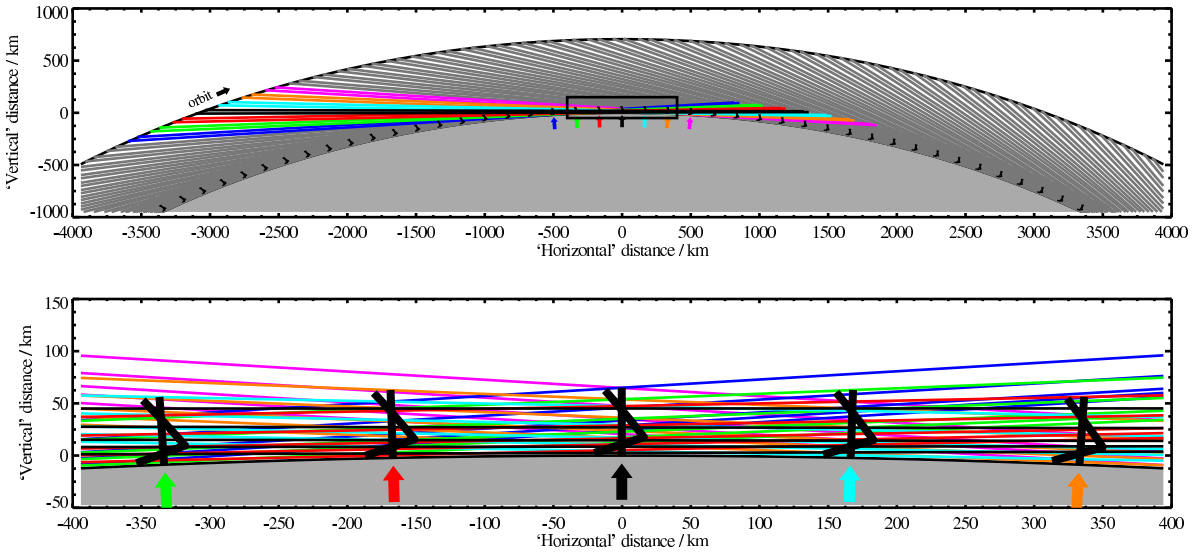

Figure 2.1: The EOS MLS limb viewing geometry in the orbit plane. The top panel shows a large section of the Earth which has been expanded in detail in the lower figure. The colored lines are measurements from a single scan whose tangent position is indicated by the colored arrow. The adjacent gray lines are the same but for adjacent scans. The tangent locus is the thick zig-zag line on top of the purely thick vertical line which would represent the measured profile positions. Notice that this geometry interleaves several profiles (above the colored arrows) in each scan position. The EOS MLS forward model is required to compute radiances and sensitivities for the two dimensional array of profiles shown. This figure is from [8].

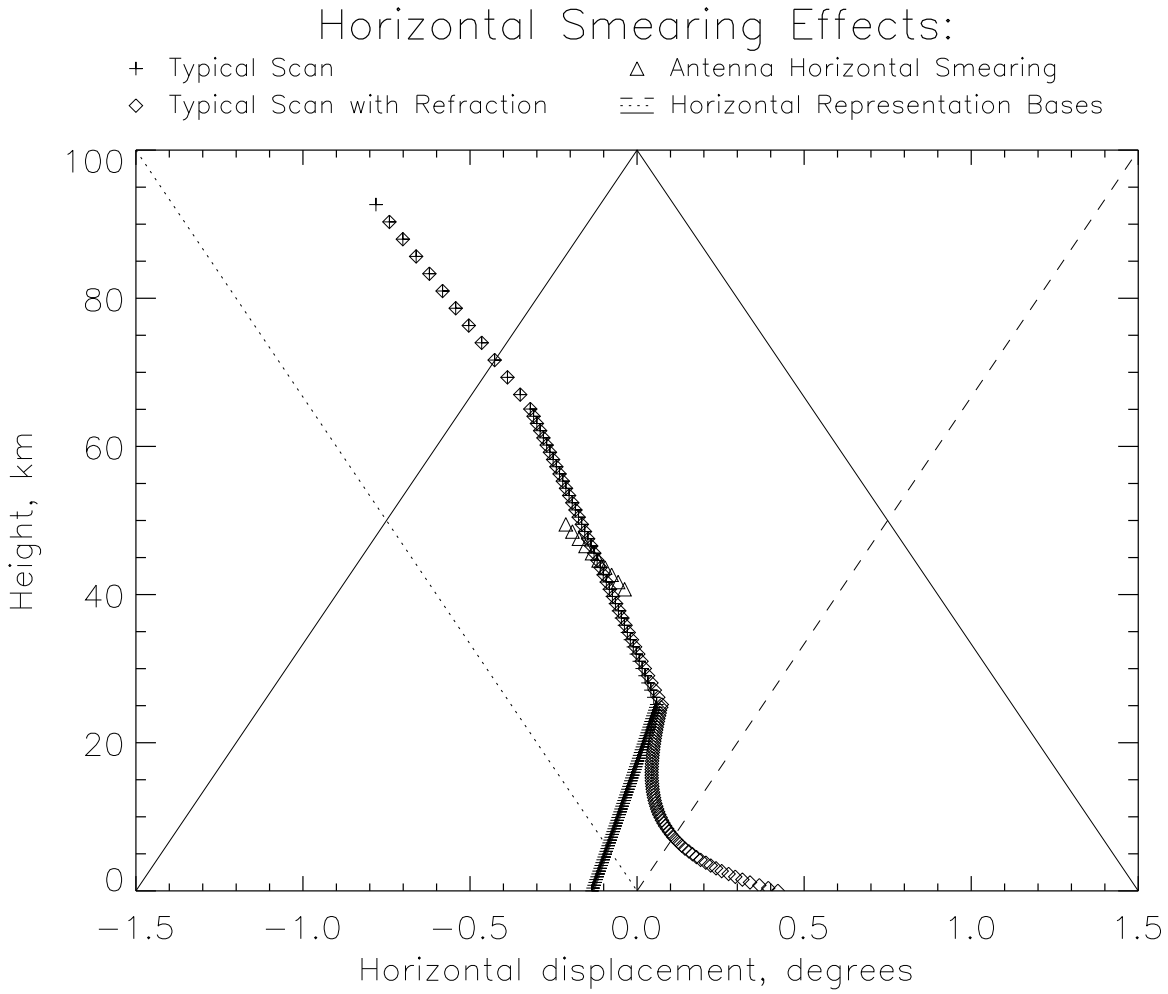

Figure 2.2: The horizontal variations expected due to scanning with and without refraction and antenna averaging. These are shown in comparison with a typical basis horizontal basis function.

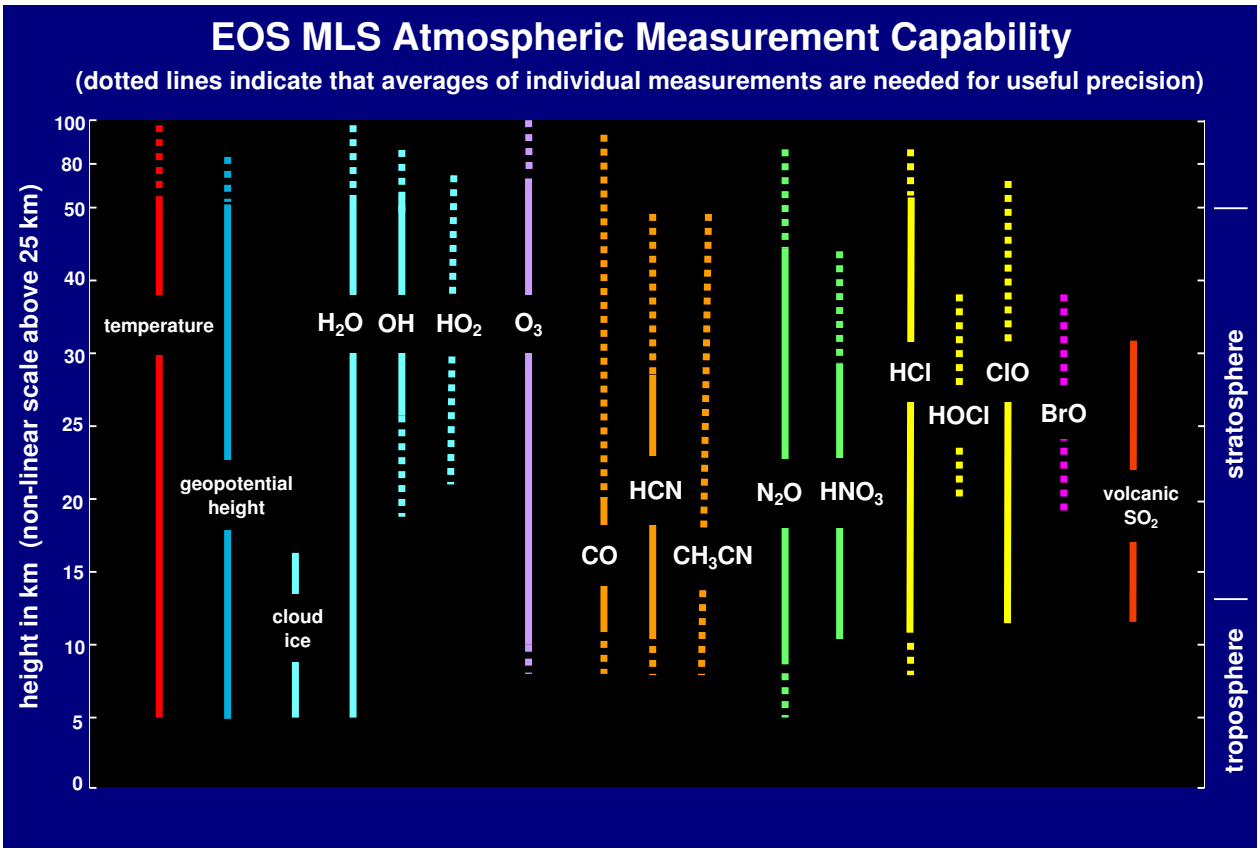

Figure 2.3: Geophysical measurements provided by EOS MLS (from [18]). Solid bars indicate vertical coverage of species with useful precision per radiance scan, dashed bars indicate vertical coverage available from a zonal or monthly mean. The signal from the spacecraft gyroscope is used with the pressure/temperature measurement to provide geopotential height.

The instrument has been tuned to measure emissions from molecules of scientific interest for understanding atmospheric chemistry, climate change and pollution. The EOS MLS has 5 radiometers. These are the spectral regions that the forward model needs to calculate. Due to the forward motion of the satellite, the molecular emissions will be Doppler shifted toward higher frequencies. The satellite flying at 7.5 km/sec shifts all the line frequencies by 1.000022 times their motionless position. Although this may seem very small, it is 20–30 times the Doppler width of a spectral line. A brief description of the radiometers is given in table 2.1. More details concerning scientific objectives and measurement operations are given in [18]. The anticipated vertical coverage of species measured by EOS MLS is given in figure 2.3, grouped by radiometer. Figure 2.4 shows EOS MLS spectral coverage and the deployment of bands, mid-bands, wide filters and digital autocorrelators. Bands are 1.2 GHz spectral regions processed through 25 variable width channels. A mid-band spectrometer is an 11 center channel subset of a band whose center is positioned on an additional target line that is within a 25 channel band. Band and mid band spectrometers are analogous to the 15 channel UARS MLS bands. A wide band filter is a 500 MHz wide channel that is positioned outside or between bands with the purpose of extending band width for tropospheric measurements. Digital autocorrelation spectrometer (DACS) is a 12 MHz, high resolution (0.1 MHz) spectrometer for resolving Doppler broadened lines in the mesosphere.

Table 2.1: MLS radiometers and primary measurement objective.

Radiometer	Measurement	Scientific Objective
R1A:118Ghz R1B:118GHz	O_2	Stratospheric Temperature, Pressure, and GPHeight. This is needed for accurate vertical registration of profiles. GPHeight is useful for atmospheric dynamics.
	cirrus	Climate studies.
R2:190GHz	H_2O	Atmospheric chemistry and climate variability/change.
	cirrus	Climate studies.
	HNO_3	Atmospheric chemistry studies.
	N_2O	Stratospheric tracer/dynamics.
	ClO	Chlorine catalyzed ozone depletion agent. —measurement common with UARS MLS.
	O_3	Ozone chemistry–measurement common with UARS MLS.
	HCN	Minor nitrogen source molecule.
	CH_3CN	Tropospheric pollution.
	SO_2	Large volcano detection.
R3:240GHz	O_3	Stratospheric and tropospheric chemistry.
	CO	Tropospheric tracer/dynamics.
	$O^{18}O$	Tropospheric pressure, temperature and GPHeight for vertical registration of profiles.
	HNO_3	Atmospheric chemistry studies.
	cirrus	Climate studies.
R4:640GHz	HCl	Chemistry and stratospheric chlorine loading.
	ClO	Chlorine catalyzed ozone depletion agent.
	N_2O	Stratospheric tracer/dynamics.
	HOCl	Chlorine chemistry studies.
	HO_2	Hydrogen chemistry studies.
	O_3	Ozone chemistry.
	BrO	Bromine catalyzed ozone depletion agent.
	CH_3CN	Tropospheric pollution.
	SO_2	Large volcano detection.
	cirrus	Climate studies.
R5H:2T5 R5V:2T5	O_2 OH	Pressure for vertical registration. Hydrogen catalyzed ozone depletion and Reactive hydrogen chemistry.

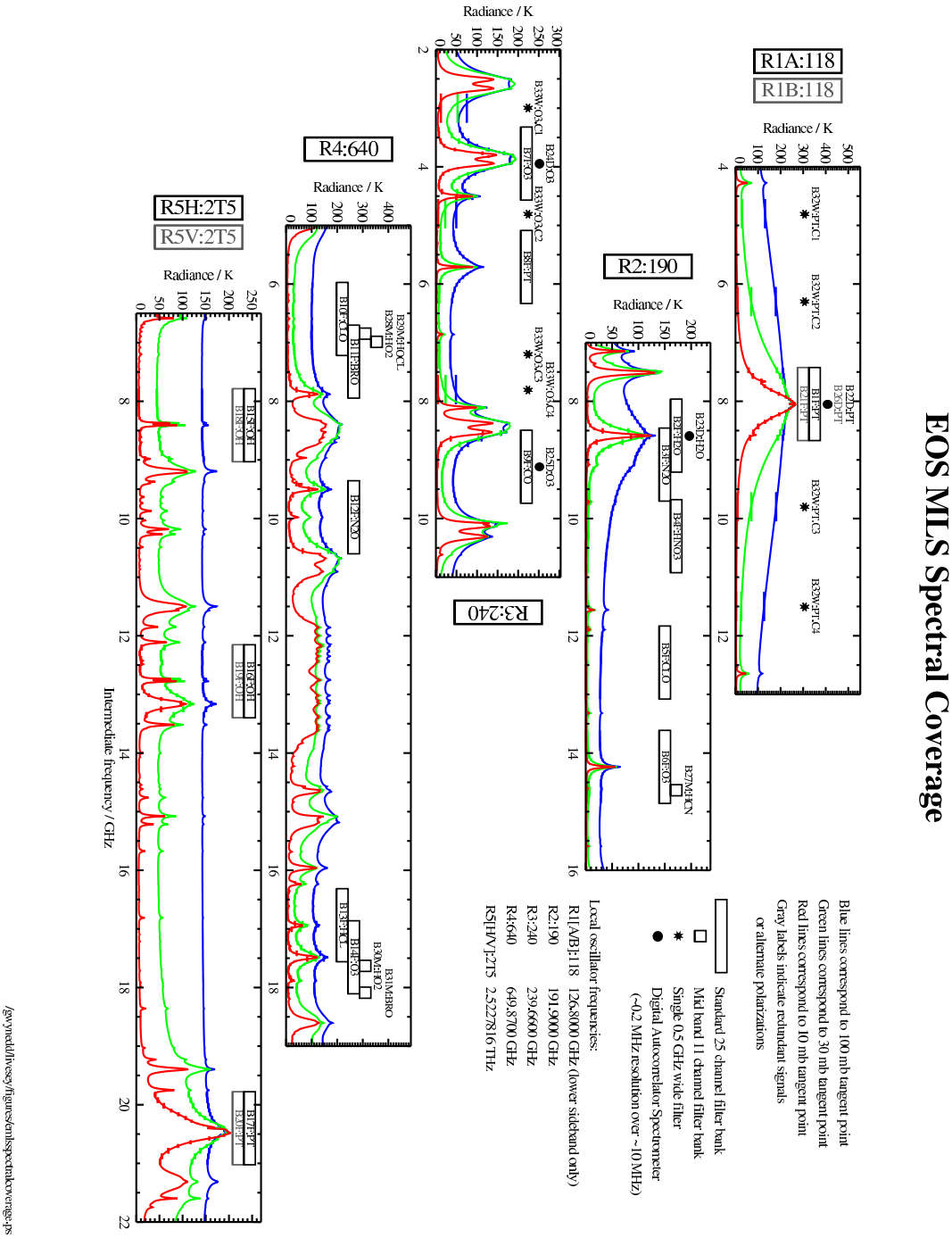

/gw/mls4/livesey/figures/emlsspectrakoverage.ps

Figure 2.4: Spectral regions measured by EOS MLS along with atmospheric signals in these regions. This figure was prepared by Dr. N.J.Livesey and Dr. M.J.Filipiak and taken from [8]. The frequency scale is relative to the local oscillator and includes signals above and below the LO frequency except R1 which is designed to receive frequencies below the LO.

2.1 R1:118 GHz Radiometer

There are actually two 118 GHz radiometers, each measuring orthogonal polarizations but only one will be used with the other a backup. The 118 GHz radiometer specifically targets the 118.7503 GHz O_2 line which will be slightly blue shifted as discussed previously due to spacecraft motion. This radiometer will employ a filter to block the upper sideband and therefore will be truly a single sideband radiometer. This line is used for establishing the pointing reference for the MLS FOV direction and measuring temperature. O_2 is a good molecule for this task because it has a constant and unvarying concentration of 0.2098 in the troposphere and stratosphere, which eliminates adjustable parameters in the radiance model. The signal is very strong, easily saturating, that is sensitive only to atmospheric temperature, in the stratosphere which is the main source of temperature information. Limb tangent pressure is measured from the optically thin radiances from the collision broadening. Combining the limb tangent pressure with the scan position knowledge, which gives limb tangent height is another method of measuring temperature. Using the hydrostatic balance condition, only two of the three variables, height, pressure, and temperature are independent. The scan provides height which is equivalent to temperature if pressure is known. But as will be discussed, in the limit where vertical resolution is dominated by the FOV width, the scan data and the optically thin radiances are not independent measurements.

An interesting issue is the resolution and information content of the pressure/temperature measurement. The vertical and horizontal resolution of the temperature measurement is limited by the FOV width–even despite having "independent" scan information. Independent is in quotes because it is not really independent as will be explained. The typical (and optimal) measurement situation is at altitudes where temperature information comes from saturated radiances and pressure from optically thin radiances. Saturated radiance is a condition where the atmosphere appears opaque at the given frequency and is a black body emitter. The atmospheric composition is indeterminate but its temperature can be measured. Optically thin is a condition where the atmosphere is highly transparent at the receiving frequency and the observed radiation is proportional to the density of the absorbers, hence is useful for measuring concentrations. Most of the temperature sensitivity of the optically thin radiances comes from the FOV width when it is broader than the LOS weighting function width. This occurs because the FOV width in pressure as a vertical coordinate changes with temperature in a fashion consistent with hydrostatic balance. In the UARS MLS case, virtually of all the temperature sensitivity in the optically thin radiances comes from the FOV width's sensitivity to pressure. Therefore, the saturated radiances and optically thin radiances provide two uncorrelated pieces of information to independently extract the pressure and temperature profiles, but the FOV width vertically smooths both. It is worth noting that in the case where the FOV width dominates the vertical smoothing, the functional relationship between pressure and temperature in the scan data is exactly the same as that obtained from optically thin radiances. The unfortunate consequence of this is that combining the scan with the optically thin radiances will not allow independent separation of temperature and pressure nor will increasing the scan resolution improve the resolution of the temperature profile. At best, the scan data decreases the uncertainty. As a cautionary note, small but unavoidable errors in the radiance and scan temperature derivative computations will break the perfectly correlated nature of these measurements, causing the paradoxical situation where a retrieval will struggle to get an accurate fit while pronouncing wonderful resolution and error statistics.

O_2 has a spin angular moment that interacts with the Earth magnetic field. This causes the

118 GHz line to split into three and the received radiation is partially polarized. The lines separate by a few MHz per Gauss and should be readily discernible above 40 km or so. The theory for handling this situation is given by [15]. The instrument is set up to simultaneously measure both polarizations and this will be a good validation of the polarized radiative transfer model. The instrument however will not normally operate in this mode but may occasionally operate this way.

2.2 R2:190 GHz Radiometer

This radiometer receives signals from H_2O, HNO_3, HCN, and CH_3CN in the lower side band and N_2O, O_3, SO_2 and ClO in the upper sideband. It provides very broad band coverage of the 183 GHz water line (6 GHz), which should allow good vertical coverage from the mesosphere well into the troposphere, especially including the tropopause region. The large bandwidth will use the spectral shape well down into the tropopause, which should improve accuracy. But to take advantage of this will require far wing lineshape studies. The continuum absorption that is different in the two sidebands is a new feature to be addressed. A laboratory measurement program led by F. De Lucia at The Ohio State University has been established for making absolute absorption measurements of dry-air and air-H_2O over the frequency range covered by EOS MLS. The dry air absorption and humidity itself determines the lowest altitude that humidity can be measured. Spectrometers have been centered on the H_2O, HNO_3, N_2O, ClO, O_3, and HCN emissions. These signals will be processed and measured very much in the same way as was done for UARS MLS, except the band width will be larger and better spectral resolution which should push the useful altitude coverage into the upper troposphere. A 12 MHz DACS, in addition to a standard 25 channel filter bank is used for measuring H_2O. Therefore H_2O profiles can be retrieved from the troposphere to the mesosphere. ClO is a free radical and has magnetic interactions leading to partially polarized radiation, a complication that is being ignored for now. The error caused by this needs to be quantified at in the future; however, it is expected that only the center channel would be most affected which will be most affected by the partial polarization. Since the magnetic splittings are small (0-2 MHz), ClO emissions at frequencies farther from line center will lose polarization and their strength determined by the channel weighted integrated lineshape which is not altered by the Zeeman effect. The R2 radiometer may detect SO_2 in the event of a stratovolcanic eruption.

R2 will also be sensitive to numerous contaminant species like vibrationally excited ozone, isotopic ozone, and $H_2^{18}O$, vibrationally excited N_2O, which are included in the current model. Optically thin channels in R2 will be used for the IWC measurement [19].

2.3 R3:240 GHz Radiometer

The R3 radiometer targets two very strong ozone lines, a pair in each sideband, which are folded onto each other in such a way so as to appear almost like one line in the band. A few wide-band filters have been dispersed throughout this band to establish the background absorption. The goal is to push the ozone measurement as low as possible into the troposphere. Despite using the strongest possible ozone lines, signals from water vapor and the dry continuum will dominate the ozone signal in the troposphere. The plan is to use a combination of 25 channel filter bank spectrometers and wide-band filters to discriminate the tropospheric ozone contribution from the stronger dry and wet continua contributions. Also critical is knowledge of the O_3 lineshape especially in the wings.

The linewidths of the important O_3 lines have been measured [3]. We also employ a DACS on one of the O_3 lines which extends its measurement into the mesosphere.

This radiometer has a 25 channel filter bank spectrometer and DACS centered on the 230 GHz CO line. CO can be measured from the mesosphere into the upper troposphere. Upper tropospheric CO is useful as a monitor of pollution and atmospheric circulations.

Throughout R3, there are some very strong HNO_3 lines which will extend its measurement into the upper troposphere.

The $O^{18}O$ molecule is also measured in this radiometer. This provides the tropospheric pointing reference. This is an interesting measurement because the isotopic oxygen is not quite strong enough to saturate the signal. The FOV width is also much narrower and does not dominate the vertical and horizontal resolution which will help establish better temperature and pressure separability when combined with the scan model. The strong ozone lines will also provide temperature data.

The optically thin channels in R3 are used in the IWC measurement [19].

2.4 R4:640 GHz Radiometer

The primary target lines in this radiometer are HCl and ClO, one in each sideband. The 649 GHz ClO line is 20 times stronger than the 204 GHz line measured by UARS MLS which more than compensates for the factor of 3 decrease in receiver sensitivity at the higher frequency. Other molecules measured in this radiometer are HOCl, HO_2, ^{81}BrO, N_2O, O_3 and CH_3CN. Modeling these molecules in the forward model is straightforward. The basic spectroscopic parameters have been measured in the JPL spectroscopy laboratory [2, 9]. The ClO and BrO molecules however have spin angular momentum, which interacts with the Earth magnetic field emitting partially polarized radiation. As with ClO in R2, it will mostly affect the interpretation of the center channel or mesospheric retrievals. We will need to quantify this effect in the future.

Optically thin channels in the 640 GHz radiometer are used in the IWC retrieval [19].

2.5 R5:2T5 or 2.5 THz Radiometer

This radiometer measures two polarizations at this frequency and is specifically designed to measure OH. The two polarizations are for improving the precision. Emission from the OH molecule is straightforward to model. It is a radical so one may expect magnetic field interactions and emit partially polarized radiation, a complication that is being ignored. The magnetic interactions will appear as an additional line broadening of 0-2 MHz on the $\sim$3.5 MHz Doppler linewidth. The terahertz radiometer receives both polarizations which can help validate a polarization calculation should one be necessary. Also there are gaps in its spectral data base and some of the key parameters like linewidth and temperature dependence may have to be determined in orbit if this data are not available from laboratory measurements.

R5 scans independently of R1–R4 and therefore needs an independent pointing measurement. Limb tangent pressure is obtained from a 2.5 THz O_2 line. This will be used to link in an absolute sense, the terahertz scan to the gigahertz scan.

R5 having the shortest wavelengths, is most sensitive to ice, however, the moist-air contin-

uum is very strong. Based on H_2O-air absorption measurements at 2.5 THz measured by H. M. Pickett [personal communication, 2003], the R5 signal only penetrates down to 100 hPa ($\sim$ 3% transmission). Therefore IWC retrievals from R5 is a research activity.

Chapter 3. Measurement Definitions

3.1 Radiances

Level 1 processing produces radiances from instrument engineering data (Level 0). The Level 1 radiance is assumed to mean,

$$\begin{aligned} \overset{\bullet}{I} - I_{\text{bsl}} &= \frac{1}{t_2 - t_1} \int_{t_1}^{t_2} r_{\text{u}} \left\{ \frac{\int_{\nu_{\text{lo}}}^{\infty} \int_{\Omega_A} I\left(\nu, \Omega, \mathbf{x}\right) \Phi\left(\nu\right) G\left(\Omega, \Omega_o\left(t\right), \nu\right) \text{d}\Omega \text{d}\nu}{\int_{\nu_{\text{lo}}}^{\infty} \int_{\Omega_A} \Phi\left(\nu\right) G\left(\Omega, \Omega_o\left(t\right), \nu\right) \text{d}\Omega \text{d}\nu} \right. \\ &+ \left. r_{\text{l}} \frac{\int_{-\infty}^{\nu_{\text{lo}}} \int_{\Omega_A} I\left(\nu, \Omega, \mathbf{x}\right) \Phi\left(\nu\right) G\left(\Omega, \Omega_o\left(t\right), \nu\right) \text{d}\Omega \text{d}\nu}{\int_{-\infty}^{\nu_{\text{lo}}} \int_{\Omega_A} \Phi\left(\nu\right) G\left(\Omega, \Omega_o\left(t\right), \nu\right) \text{d}\Omega \text{d}\nu} \right\} \text{d}t, \end{aligned} \tag{3.1}$$

where $\overset{\bullet}{I}$ is the Level 1 calibrated radiance at the switching mirror for one spectrometer channel, r_{u} is the higher frequency (relative to the local oscillator frequency ν_{lo}) side band fraction for the channel, r_{l} is the lower sideband fraction, $I\left(\nu, \Omega, \mathbf{x}\right)$ is the limb radiance, $\Phi\left(\nu\right)$ is the instrument spectral response, $G\left(\Omega, \Omega_o\left(t\right), \nu\right)$ is the antenna response or field-of-view (FOV), ν is frequency, $\mathbf{x}$ is the limb radiance state vector, Ω is solid angle, $\Omega_o\left(t\right)$ is the FOV direction and varies with time, t, during the measurement which is a consequence of the continuous scan, Ω_A is that portion of solid angle for which $G\left(\Omega, \Omega_o\left(t\right), \nu\right)$ is measured, and I_{bsl} is an additive radiance that may be a function of frequency and height. All the functions in eq. 3.1 are channel dependent and it is assumed that the antenna response is frequency independent across the highly weighted part of the filter response (< 500 MHz) but different for the two sidebands, and the spectral response is independent of Ω_o. The integrals in the denominator of eq. 3.1 are normalizations of instrument response functions and are there to emphasize that a relative response function is needed. In practice these are "constants" and are folded into $\Phi\left(\nu\right)$ and $G\left(\Omega, \Omega_o\left(t\right), \nu\right)$. The antenna normalizing gain integral is the integrated gain within Ω_A (~ 0.4 sterad) which is slightly less than 4π.

The instrument radiances are calibrated from signals received from the switching mirror that cycles among reference temperature (hot), background space (cold) and limb viewing geometries. The calibration procedure can account for losses in the optics system between the switching mirror and the receiver but not for the reflectors between the Earth and the switching mirror because the optical paths for the "hot" and "cold" calibration signals are different from that for the limb radiances. The EOS MLS reflector system introduces additional losses and emissions which should be corrected. Additional stray emission due to thermal emissivities of the reflectors and stray radiation spill-over and scattering (unintentional Earth and satellite emissions gathered by the optics outside of solid angle Ω_A) is I_{bsl} given by [5]

$$\begin{aligned} I_{\text{bsl}} &= \sum_{\text{sb}=1}^{2} r''_{\text{sb}} \left\{ \left(\prod_{k=1}^{3} \rho^k \right) \eta_{\text{sb}}^1 \left(1 - \eta_{\text{sb}}^{AA}\right) P_{\text{sb}}^{\text{SA}} \right. \\ &+ \left. \sum_{k=1}^{3} \left(\prod_{j=k+1}^{3} \rho^j \right) \left[\left(1 - \rho^k\right) \eta_{\text{sb}}^k P_{\text{sb}}^{\text{O}k} + \left(\eta_{\text{sb}}^{k+1} - \eta_{\text{sb}}^k \right) P_{\text{sb}}^{\text{S}k} \right] \right\}, \end{aligned} \tag{3.2}$$

where ρ^k are ohmic losses for reflector k, η_{sb}^{AA} is the transmission of the antenna system, η_{sb}^k is the transmission of reflector k, $P_{\text{sb}}^{\text{SA}}$ is the radiance power in the limb hemisphere outside the FOV

measurement angle, $P_{\rm sb}^{{\rm S}k}$ is the radiance power illuminating the spill-over solid angle for reflector k, and $P_{\rm sb}^{{\rm O}k}$ is the thermally emitted power from reflector k. The transmission efficiency of the antenna system, $\eta_{\rm sb}^{A} = \eta_{\rm sb}^{AA}\eta_{\rm sb}^{1}$. The definitions of these quantities are fully described in [5]. When the superscript of ρ^k or $\eta_{\rm sb}^k$ exceeds the number of reflectors then $\rho^4 = \eta_{\rm sb}^4 = 1$. Quantities $P_{\rm sb}^{\rm SA}$, $P_{\rm sb}^{{\rm S}k}$, and $P_{\rm sb}^{{\rm O}k}$ are radiance measurements which must be measured or estimated.

The sideband fractions, $r_{\rm u}$ and $r_{\rm l}$ include the loss of limb signal through the antenna system as a consequence of scattering, spill-over, absorption, and the efficiency of the receiver at each sideband frequency. The sideband fractions $r_{\rm u}$ and $r_{\rm l}$ are defined as

$$\begin{aligned}
r_{\rm u} &= \eta_{\rm u}^{A}\rho^{A}r'_{\rm u}, \\
r_{\rm l} &= \eta_{\rm l}^{A}\rho^{A}r'_{\rm l}, \\
r'_{\rm u} &= \frac{\eta_{\rm u}^{A}r''_{\rm u}}{\eta_{\rm u}^{A}r''_{\rm u} + \eta_{\rm l}^{A}r''_{\rm l}}, \\
r'_{\rm l} &= \frac{\eta_{\rm l}^{A}r''_{\rm l}}{\eta_{\rm u}^{A}r''_{\rm u} + \eta_{\rm l}^{A}r''_{\rm l}}, \\
r''_{\rm u} &= \frac{\int_{\nu_{\rm lo}}^{\infty}\Phi\left(\nu\right){\rm d}\nu}{\int_{-\infty}^{\infty}\Phi\left(\nu\right){\rm d}\nu}, \\
r''_{\rm l} &= \frac{\int_{-\infty}^{\nu_{\rm lo}}\Phi\left(\nu\right){\rm d}\nu}{\int_{-\infty}^{\infty}\Phi\left(\nu\right){\rm d}\nu},
\end{aligned} \tag{3.3}$$

where $\eta_{\rm u}^{A}$ is the antenna efficiency and ρ^A is the product of the ohmic losses of each reflector in the antenna system which is equal for both sidebands. The spectral function, Φ, has two peaked responses equidistant above and below the local oscillator frequency. The 118 GHz radiometer is an exception in that Φ has only one peaked response which is in the lower sideband. The radiometric sideband fractions $r''_{\rm u}$ and $r''_{\rm l}$ quantitatively describe the receiver's effectiveness at the sideband frequency. By definition, $r''_{\rm u} + r''_{\rm l} = 1$, but due to losses in the reflector system causes $r_{\rm u} + r_{\rm l} \leq 1$.

The terahertz module uses the switching mirror as its primary antenna. Consequently, the "hot," "cold," and "limb" radiances used in calibration share the same optics and in eq. 3.1 $r_{\rm u} = r''_{\rm u}$, $r_{\rm l} = r''_{\rm l}$, and $I_{\rm bsl} = 0$. Based on pre-launch calibration, $I_{\rm bsl} = 4.1$, 2.8, 4.7, and 10.1K for R1, R2, R3, and R4 respectively. It is expected that $I_{\rm bsl}$ is not scan dependent but it will vary with changing temperature of the antenna elements.

3.2 Level 1 Orbit Attitude data

Level 1 provides detailed information regarding the satellite location, velocity, and instrument limb tangent location. The instrument also provides encoder data which is the angular position of the FOV direction. This information when combined with the hydrostatic model can be used to measure temperature. The conversion of the instrument encoder into geometric heights is complicated (see a theoretical basis for this calculation in Appendix C). Therefore, the derived height from the encoder is used as a measurement. Chapter 4 describes the forward model we use for level 1 heights.

Chapter 4. Profile Representation

4.1 Independent Coordinates

The most fundamental issue is the choice of *independent* coordinates for gridding the state vector. The choice made here is based mostly on past heritage and data output requirements. The state vector components can vary vertically, horizontally (along track), and spectrally (which is synonymous with channel). For height, $\zeta = -\log(p)$ where p is pressure in hPa is the vertical coordinate. Throughout this document, $\log = \log_{10}$ and $\ln = \log_e$. Orbit plane geodetic angle, ϕ, is the horizontal coordinate. Frequency, ν, is the spectral coordinate. All except the ϕ coordinate are self-explanatory. ϕ is directly coupled to the Earth figure shape that will be incorporated into the EOS MLS forward model. This coordinate is convenient because it collapses the Earth figure ellipsoid into a plane and leads to simpler elliptical mathematical functions. There is an integral number (240) of equally spaced ϕ's per orbit. ϕ will be an accumulated quantity being reset at the beginning of each day. ϕ modulo 360° gives the angle relative to the suborbital ellipse with the following proposed convention: $0° \leq \phi < 90°$, northern hemisphere ascending node, $90° \leq \phi < 180°$, northern hemisphere descending node, $180° \leq \phi < 270°$, southern hemisphere descending node, and $270° \leq \phi < 360°$, southern hemisphere ascending node. The integer part of $\phi/360°$ gives the orbit number which is of no concern here.

4.2 Profile function

The EOS MLS forward model employs two kinds of representation basis functions, linear and logarithmic. Linear is good for weak and slowly varying constituents because it has a near linear relationship with radiance and allows for multiple profile averaging without introducing non-linear distortion in the final averaged result. The latter statement neglects *a priori* contributions. The linear representation basis is used for the majority of state vector components represented with vertical profiles. The logarithmic basis may be better than linear for vertically varying quantities that change several orders of magnitude. Examples are tropospheric water vapor, which due to thermodynamic constraints of the Clausius-Clapyron phase equilibrium equation naturally follows an exponential concentration gradient with temperature, and possibly extinction because it represents a molecular continuum proportional to P^2. The EOS MLS forward model can handle either[1]. All linear state vector quantities will be of the form:

$$\mathsf{f}^k(\zeta,\phi,\nu) = \sum_l^{\mathrm{NH}^k} \sum_m^{\mathrm{NP}^k} \sum_n^{\mathrm{NF}^k} f^k_{lmn} \eta^k_l(\zeta)\, \eta^k_m(\phi)\, \eta^k_n(\nu)\,, \tag{4.1}$$

or for the logarithmic form use

$$\ln \mathsf{f}^k(\zeta,\phi,\nu) = \sum_l^{\mathrm{NH}^k} \sum_m^{\mathrm{NP}^k} \sum_n^{\mathrm{NF}^k} \ln f^k_{lmn} \eta^k_l(\zeta)\, \eta^k_m(\phi)\, \eta^k_n(\nu)\,, \tag{4.2}$$

[1]Species can have either type of basis and the radiative transfer calculation can accommodate both types in a calculation; however, a species must have one type of function for its entire vertical range. It may be desirable to have separate functional forms for different height coverages. This can be accommodated by calling the same species by two different names and defining their representation basis such that they join at a common point.

where $\mathsf{f}^k(\zeta, \phi, \nu)$ is a *profile* that can have height, horizontal, and spectral variability. f^k is a state vector (or logarithm thereof) *component* identified by superscript k. f^k_{lmn} is an *element* (or logarithm thereof) of state vector component k. k covers everything to be differentiated by the forward model e.g., $k =$ "temperature", "ozone", or "radiometer sideband" are allowable choices. The η are basis functions in each of the three coordinates l, m, n for component k. NH, NP, and NF are the total number of basis functions in each of the three allowable dimensions. Any or all of these can be unity which allows components to have no dimensionality up to three dimensions. The representation basis functions use the standard UARS MLS "undelimited" form of the triangular representation basis given by

$$\eta^k_l(\zeta) = \begin{array}{cc} 0 & \zeta \geq \zeta^k_{l+1} \\ \frac{\zeta^k_{l+1} - \zeta}{\Delta\zeta^k_l} & \zeta^k_{l+1} > \zeta \geq \zeta^k_l \\ \frac{\zeta - \zeta^k_{l-1}}{\Delta\zeta^k_{l-1}} & \zeta^k_l > \zeta > \zeta^k_{l-1} \\ 0 & \zeta^k_{l-1} \geq \zeta \end{array}, \tag{4.3}$$

where $1 < l < \mathrm{NH}^k$, but when $l = 1$ use

$$\eta^k_1(\zeta) = \begin{array}{cc} 0 & \zeta \geq \zeta^k_2 \\ \frac{\zeta^k_2 - \zeta}{\Delta\zeta^k_1} & \zeta^k_2 > \zeta \geq \zeta^k_1 \\ 1 & \zeta^k_1 > \zeta \end{array}. \tag{4.4}$$

When $l = \mathrm{NH}^k$ use

$$\eta^k_{\mathrm{NH}}(\zeta) = \begin{array}{cc} 1 & \zeta \geq \zeta^k_{\mathrm{NH}} \\ \frac{\zeta - \zeta^k_{\mathrm{NH}-1}}{\Delta\zeta^k_{\mathrm{NH}-1}} & \zeta^k_{\mathrm{NH}} > \zeta > \zeta^k_{\mathrm{NH}-1} \\ 0 & \zeta^k_{\mathrm{NH}-1} \geq \zeta \end{array}. \tag{4.5}$$

This is slightly different from UARS MLS forward model, which used this definition for geophysical parameters like temperature, and a slightly modified form called "delimited" for the concentrations, where the basis functions for all elements are the same but have minimum and maximum values beyond which the function was zero. Although more realistic for some situations and somewhat simpler to implement in software because all the functions are the same, it has the annoying feature of needing two extra element points (NH + 2 ζ^k_l's) to characterize it. This feature is inconvenient and will be avoided for EOS MLS. The special case where NH^k = 1 uses

$$\eta^k_1(\zeta) = 1. \tag{4.6}$$

Identical forms are used for $\eta^k_m(\phi)$ and $\eta^k_n(\nu)$.

Chapter 5. Ray Tracing Model

5.1 Earth Figure Ellipse Function

The EOS MLS forward model models the Earth as an ellipsoid as given by,

$$1 = \frac{X^2 + Y^2}{a^2} + \frac{Z^2}{b^2}, \tag{5.1}$$

where X, Y, Z are coordinates in the Earth centered rotating (ECR) frame and a and b are the major and minor axes of the Earth (6378.137 km and 6356.7523141 Km—1980 Geodetic Reference System [17]). The ellipsoid defines the surface that profiles are normal to and the limb tangent height. It does not physically represent the surface of the Earth itself, which includes aberrations from mountains and sea. It also defines the Earth reflection boundary for radiative transfer calculations and in that respect, is not totally realistic. But in limb sounding for most cases, either the limb ray is above the surface or the atmosphere is opaque and the Earth intersecting ray doesn't see the surface. There will be some cases where this may not be true but inaccuracies caused by this simplification will be ignored as this is a research problem well beyond the scope of routine production processing. The ellipsoid defines the surface of constant geopotential ($U_o = 62.636860850 km^2/sec^2$). The distance from the ellipsoid center to its surface of constant geopotential only depends on limb tangent ϕ_t, as the other constants in the function are being adopted by definition. Therefore ϕ_t is the only new element added to the state vector by this function and the following discussions.

The measurement track defines a subellipse on the Earth reference ellipsoid. This is related to the orbit incline angle according to

$$1 = \frac{x^2}{a^2} + \frac{y^2}{c^2} \tag{5.2}$$

where x and y are Cartesian coordinates in the orbit plane and c is the orbit plane projected minor axis given by

$$c^2 = \frac{a^2 b^2}{a^2 \sin^2\beta + b^2 \cos^2\beta} \tag{5.3}$$

where β is an incline angle between the plane formed by the center of Earth, satellite, and limb tangent position and the Earth centered rotating frame z-axis incline angle. For EOS MLS it is well approximated by the orbital inclination angle (98.14 degrees nominal). This gives $c = 6357.17893191$ km for the projected ellipse. The line of sight (LOS) of the radiative transfer problem is contained in this plane.

Figure 5.1 shows the orbit plane slice of the Earth ellipsoid. This coordinate system is called the line-of-sight frame (LOSF). All ray tracing vectors in the LOSF are two dimensional. Figure 5.1 also shows the geocentric angle γ_t, which is the angle between $\vec{R^{\oplus}}$ at ϕ_t and the x-axis. It is not the geocentric angle of the tangent point because the vectors $\vec{R^{\oplus}}$ and $\vec{h_t}$ are not co-linear with $\vec{R_t}$. Any geodetic angle ϕ is related to γ according to

$$\sin^2\phi = \frac{a^4 \sin^2\gamma}{c^4 \cos^2\gamma + a^4 \sin^2\gamma},$$

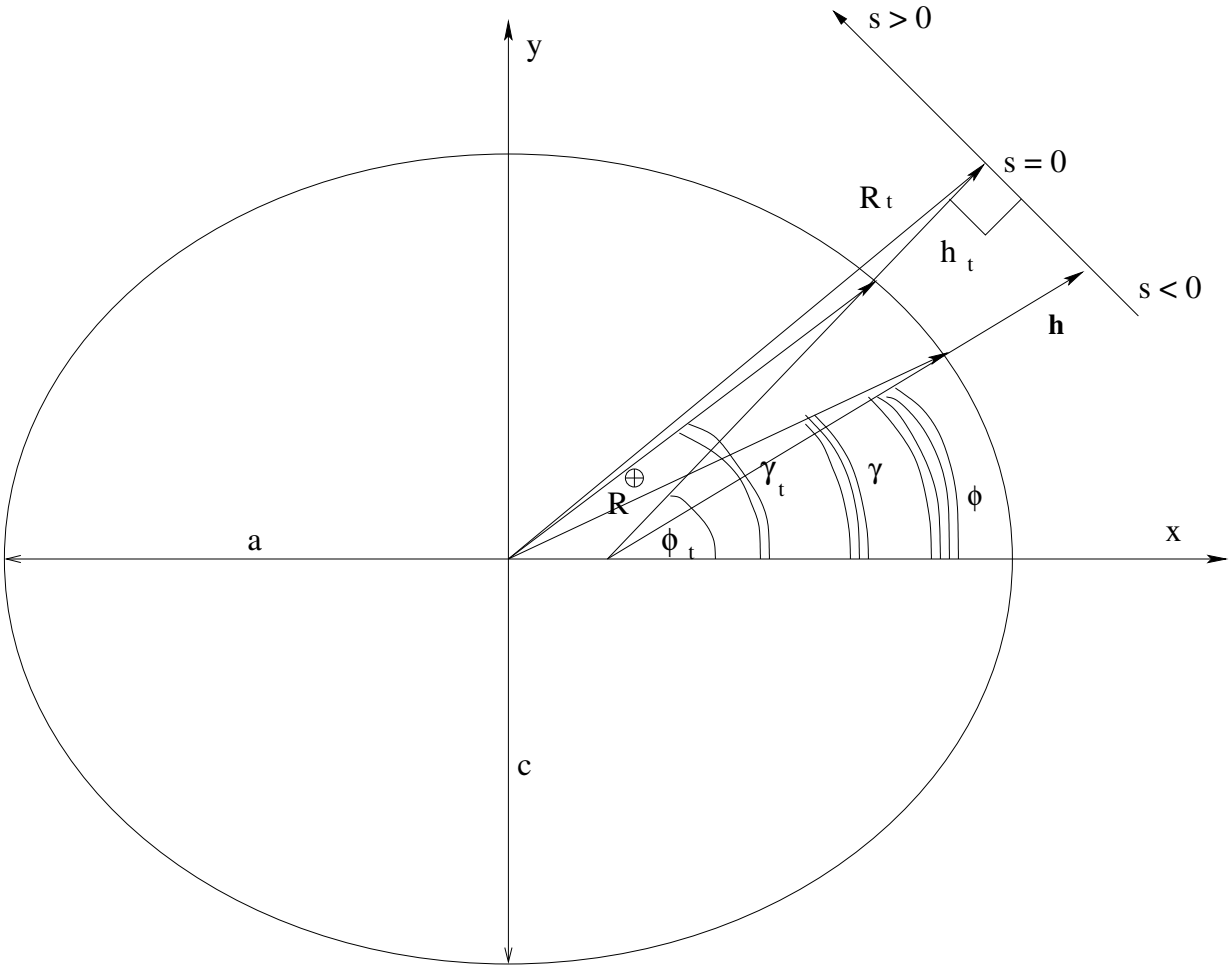

Figure 5.1: Variables illustrated in relation to the Earth figure ellipse projected onto the x-y plane of the Line of Sight Frame (LOSF). The z axis points out of the page.

$$\begin{aligned}
\sin^2\gamma &= \frac{c^4\sin^2\phi}{a^4\cos^2\phi + c^4\sin^2\phi}, \\
\cos^2\phi &= \frac{c^4\cos^2\gamma}{c^4\cos^2\gamma + a^4\sin^2\gamma}, \\
\cos^2\gamma &= \frac{a^4\cos^2\phi}{a^4\cos^2\phi + c^4\sin^2\phi}, \text{and} \\
\tan\phi &= \frac{a^2}{c^2}\tan\gamma. \qquad (5.4)
\end{aligned}$$

These equations can be used to convert between these angles. Another useful conversion is between geocentric latitude λ in the ECR frame and γ

$$\sin\lambda = \sin\gamma\sin\beta. \qquad (5.5)$$

Eq. 5.4 can be used to convert geocentric latitude into geodetic latitude by replacing c with b. Note that for the 98.14° orbit described here, when $\gamma = 90°$, $\lambda = 81.86°$.

5.2 Ray tracing

The two dimensional (2-D) LOS ray tracing algorithm is presented here. First we described the exact formulation for profiles that are normal to the 2-D Earth figure ellipse. Then an approximate "circular" form that is implemented in the EOS MLS forward model. Based on the orbit plane projected ellipse shown in fig 5.1 we relate the integration path coordinate to h, the normal vertical and ϕ, the geodetic angle. The LOS path vector, $\vec{R}$ is

$$\vec{R} = \vec{R}_t + \vec{n}_d s, \qquad (5.6)$$

where subscript t indicates tangent and $\vec{n}_d$ is a unit vector perpendicular to the limb tangent or tangent to the ellipse at ϕ_t, which is

$$\vec{n}_d = (-\sin\phi_t, \cos\phi_t, 0)\,. \qquad (5.7)$$

The tangent LOSF geodetic angle ϕ_t is a state vector quantity and must include the effects of refraction. A theoretical basis for its calculation is given in Appendices A and C. From the figure one can write

$$\vec{R}_t = \vec{R}^{\oplus} + \vec{h}_t. \qquad (5.8)$$

The Earth radius $\vec{R}^{\oplus}$ in the orbit plane projected ellipse is

$$\vec{R}^{\oplus} = \sqrt{\frac{a^4\cos^2\phi + c^4\sin^2\phi}{a^2\cos^2\phi + c^2\sin^2\phi}}\,(\cos\gamma, \sin\gamma, 0)\,. \qquad (5.9)$$

Substituting eq. 5.4 into eq. 5.9 and rearranging gives

$$\vec{R}^{\oplus} = N(\phi)\left(\cos\phi, \frac{c^2}{a^2}\sin\phi, 0\right), \qquad (5.10)$$

where $N(\phi) = a^2/\sqrt{a^2\cos^2\phi + c^2\sin^2\phi}$ is the radius of curvature in the prime vertical. Substituting eq. 5.4 and eq. 5.10 into eq. 5.8 and writing it out by components gives

$$\vec{R}_t = \left((N(\phi_t) + h_t)\cos\phi_t, \left(\frac{c^2}{a^2}N(\phi_t) + h_t\right)\sin\phi_t, 0 \right). \tag{5.11}$$

Substituting eqs. 5.7, 5.10, and 5.11 into eq. 5.6 and separating the x and y components of $\vec{h}$ gives two equations,

$$\begin{aligned} h\cos\phi &= (N(\phi_t) + h_t)\cos\phi_t - s\sin\phi_t - N(\phi)\cos\phi, \\ h\sin\phi &= \left(\frac{c^2}{a^2}N(\phi_t) + h_t\right)\sin\phi_t + s\cos\phi_t - \frac{c^2}{a^2}N(\phi)\sin\phi. \end{aligned} \tag{5.12}$$

These two equations have three unknowns h, ϕ, and s. This means that only one of the three is independent. Our choice would be to have h be the independent variable because it is convenient to use a vertical coordinate for fixing the integration boundaries but unfortunately so far this does not lend to simple expressions of ϕ or s as a function of h. The horizontal coordinate ϕ does. The two components in eq. 5.12 can be combined to create these expressions where ϕ is the independent variable.

$$\begin{aligned} h &= \frac{h_t + N(\phi_t)\left(\cos^2\phi_t + \frac{c^2}{a^2}\sin^2\phi_t\right) - N(\phi)\left(\cos\phi\cos\phi_t + \frac{c^2}{a^2}\sin\phi\sin\phi_t\right)}{\cos(\phi - \phi_t)}, \\ s &= h_t\tan(\phi - \phi_t) \\ &+ \frac{N(\phi_t)\left(\cos\phi_t\sin\phi - \frac{c^2}{a^2}\sin\phi_t\cos\phi\right) - N(\phi)\cos\phi\sin\phi\left(1 - \frac{c^2}{a^2}\right)}{\cos(\phi - \phi_t)}. \end{aligned} \tag{5.13}$$

Thus as one moves along ϕ, the values of h and s are known. Note that at ϕ_t, $s = 0$ and $h = h_t$. By convention $\phi = 0$ is the equator crossing on the *ascending* orbit, $\phi = 90.0$ is the northernmost polar crossing. $\phi = 180.0$ or -180.0 is the equator crossing on the *descending* orbit, and $\phi = -90.0$ or 270.0 is the southernmost polar crossing. $s > 0$ are path length distances from the tangent to a point in the atmosphere on the ray path segment that is heading away from the observer and $s < 0$ is the same but for the segment going toward the observer. Unfortunately the elliptic figure prevents the use of symmetry about the tangent normal while computing heights and path lengths.

Normally, the radiative transfer integral is evaluated at fixed pressure boundaries which has the nice feature of avoiding vertical interpolations in absorption coefficients and the boundaries coincide with representation breakpoint pressures, which increases the derivative calculation accuracy with fewer segments, and makes the calculation faster. Therefore it is really desirable to have h as the independent coordinate, which is equivalent to ζ through the hydrostatic function. So far, this will involve inverting eq. 5.13. This can be done by assuming the following circular equations,

$$\begin{aligned} h &= \frac{R_t^{\oplus} + h_t}{\cos(\phi - \phi_t)} - R_t^{\oplus}, \\ s &= \left(R_t^{\oplus} + h_t\right)\tan(\phi - \phi_t), \end{aligned} \tag{5.14}$$

for the initial guess, calculating derivatives and iterating with a Newton method until convergence is achieved. These equations make it rather easy to express s and ϕ as a function of h.

A special situation occurs when the limb ray intersects the Earth surface. A surface intersecting path occurs when $h_t < 0$. When this happens, the ray path is defined by

$$\vec{R} = \vec{R}_{\rm surf} + \vec{n}_d s, \tag{5.15}$$

where,

$$\vec{R}_{\rm surf} = \left(N\left(\phi_s\right)\cos\phi_{\rm surf}, \frac{c^2}{a^2} N\left(\phi_s\right)\sin\phi_{\rm surf}, 0 \right), \tag{5.16}$$

$\phi_{\rm surf}$ is the geodetic angle which intersects the earth. This is found by finding the value ϕ which gives $h = 0$, requiring,

$$\left(N\left(\phi_t\right) + h_t\right)\cos^2\phi_t + \left(\frac{c^2}{a^2} N\left(\phi_t\right) + h_t\right)\sin^2\phi_t = N\left(\phi_s\right)\left(\cos\phi_s\cos\phi_t + \frac{c^2}{a^2}\sin\phi_s\sin\phi_t\right). \tag{5.17}$$

$\phi_{\rm surf} < \phi_t$ because the Earth surface is closer to the observer than the actual tangent in an Earth intersecting ray. Once $\phi_{\rm surf}$ is found, then the heights and path lengths of the incoming path ($s < 0$) as a function of ϕ are

$$\begin{aligned} h &= \frac{N\left(\phi_{\rm surf}\right)\left(\cos\phi_{\rm surf}\cos\phi_t + \frac{c^2}{a^2}\sin\phi_{\rm surf}\sin\phi_t\right) - N\left(\phi\right)\left(\cos\phi\cos\phi_t + \frac{c^2}{a^2}\sin\phi\sin\phi_t\right)}{\cos\left(\phi - \phi_t\right)}, \\ s &= \frac{N\left(\phi_{\rm surf}\right)\left(\cos\phi_{\rm surf}\sin\phi - \frac{c^2}{a^2}\sin\phi_{\rm surf}\cos\phi\right) - N\left(\phi\right)\sin\phi\cos\phi\left(1 - \frac{c^2}{a^2}\right)}{\cos\left(\phi - \phi_t\right)}. \end{aligned} \tag{5.18}$$

The reflected path, which is going away from the observer having positive s is based on

$$\vec{R} = \vec{R}_{\rm surf} + \vec{n}_r s, \tag{5.19}$$

where $\vec{n}_r$ is the surface reflected unit vector, which is $\left(-\sin\left(2\phi_{\rm surf} - \phi_t\right), \cos\left(2\phi_{\rm surf} - \phi_t\right), 0\right)$. This gives

$$\begin{aligned} h &= \frac{N\left(\phi_{\rm surf}\right)\left(\cos\phi_{\rm surf}\cos\left(2\phi_{\rm surf} - \phi_t\right) + \frac{c^2}{a^2}\sin\phi_{\rm surf}\sin\left(2\phi_{\rm surf} - \phi_t\right)\right)}{\cos\left(\phi - 2\phi_{\rm surf} + \phi_t\right)} \\ &- \frac{N\left(\phi\right)\left(\cos\phi\cos\left(2\phi_{\rm surf} - \phi_t\right) + \frac{c^2}{a^2}\sin\phi\sin\left(2\phi_{\rm surf} - \phi_t\right)\right)}{\cos\left(\phi - 2\phi_{\rm surf} + \phi_t\right)}, \\ s &= \frac{N\left(\phi_{\rm surf}\right)\left(\cos\phi_{\rm surf}\sin\phi - \frac{c^2}{a^2}\sin\phi_{\rm surf}\cos\phi\right) - N\left(\phi\right)\sin\phi\cos\phi\left(1 - \frac{c^2}{a^2}\right)}{\cos\left(\phi - 2\phi_{\rm surf} + \phi_t\right)}. \end{aligned} \tag{5.20}$$

Note that in these cases $s = 0$ is the ray reflection point off the Earth.

As mentioned previously, these elliptic equations are awkward to work with. This motivated an investigation as to whether a circle whose origin lies along $\vec{h_t}$ with a closely matched radius of curvature could be used in lieu of the elliptical equations. The answer is YES(!) and the following circular Earth figure will be used for the radiative transfer ray tracings. The effective radius of curvature is obtained by finding the intersection of two normals to the orbit projected Earth figure ellipse (fig 5.1) which is slightly offset from ϕ_t. The resulting circular Earth is shown in Figure 5.2. This gives

$$R_{\rm eq}^{\oplus} \equiv H_t^{\oplus} = N\left(\phi_t\right)\sqrt{\sin^2\phi_t + \frac{c^4}{a^4}\cos^2\phi_t}. \tag{5.21}$$

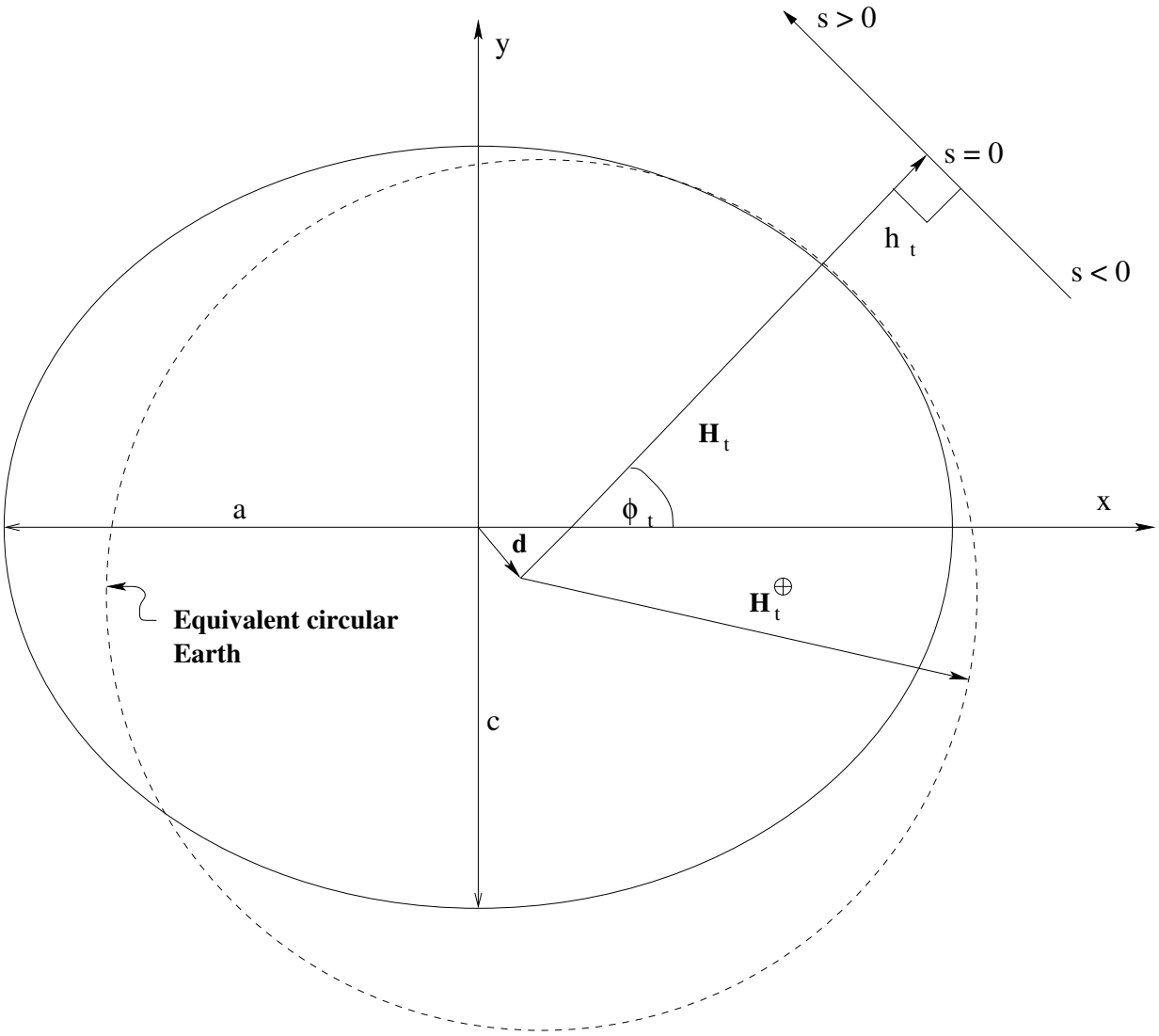

Figure 5.2: The equivalent circular Earth representation in the LOSF.

From now on we will refer to geocentric heights in the $R_{\rm eq}^{\oplus}$ coordinate system with H quantities and geocentric heights in the actual Earth ellipsoid coordinate system with R quantities. Heights in either system use h. Note that the origin of this circle is

$$\begin{aligned} x &= \left(N\left(\phi_t\right) - H_t^{\oplus}\right)\cos\phi_t, \\ y &= \left(\frac{c^2}{a^2}N\left(\phi_t\right) - H_t^{\oplus}\right)\sin\phi_t, \\ \vec{d} &= \left[x, y, 0\right]. \end{aligned} \tag{5.22}$$

This means that one will have to make an adjustment in the attitude offset angles if the above is used as an "instantaneous" representation of the Earth. This allows eqn. 5.13 to be replaced with

$$\begin{aligned} h &= \left(h_t + H_t^{\oplus}\right)/\cos\left(\phi - \phi_t\right) - H_t^{\oplus}, \\ s &= \left(h_t + H_t^{\oplus}\right)\tan\left(\phi - \phi_t\right). \end{aligned} \tag{5.23}$$

Figure 5.3 shows the differences of h and s computed with eq. 5.13 for the full ellipse and eq. 5.23 for the equivalent circle at $\phi_t = 45.0°$. The path length s, is accurate to 0.1% or better, and h better than 100 m. For the first three degrees of ϕ about ϕ_t, which covers 5 coefficients, h is accurate to 10 m and the s difference is negligible. At the orbital poles and equator, the errors are 10 times smaller. These errors show that the equivalent circle representation of the ellipse is acceptable. From the figure, it shows that the path length error at $s = \pm 500$ km about ϕ_t is 0.01%. Assuming a radiance weighting function 1000 km wide and optically thin situations, would lead to a radiance error of ∼0.01% or 0.01 K at 100 K. The error for optically thick situations should be smaller because the path length sensitivity is attenuated by transmission function. Therefore, the equivalent circle representation for ray-tracing is an excellent approximation.

The major benefit is that ϕ and s can now be written as a function of h and all the ray tracing features of the UARS forward model can now be used intact. The relevant functions are now

$$\begin{aligned} s &= \pm\sqrt{\left(h + H_t^{\oplus}\right)^2 - \left(h_t + H_t^{\oplus}\right)^2}, \\ \phi &= \phi_t \pm \arccos\left(\frac{\left(h_t + H_t^{\oplus}\right)}{\left(h + H_t^{\oplus}\right)}\right). \end{aligned} \tag{5.24}$$

The choice of the sign depends on which side of the tangent h is. These functions will also be used for the earth intersecting ray case too. The Earth intersecting ray is derived identically to the ellipse case except it uses the circular equations.

$$\begin{aligned} & & \text{Incoming} & & \text{Outgoing} \\ h &= H_t^{\oplus}\left(\tfrac{\cos(\phi_{\rm surf}-\phi_t)}{\cos(\phi-\phi_t)} - 1\right) & & H_t^{\oplus}\left(\tfrac{\cos(\phi_t-\phi_{\rm surf})}{\cos(\phi+\phi_t-2\phi_{\rm surf})} - 1\right) \\ s &= H_t^{\oplus}\tfrac{\sin(\phi-\phi_{\rm surf})}{\cos(\phi-\phi_t)} & & H_t^{\oplus}\tfrac{\sin(\phi-\phi_{\rm surf})}{\cos(\phi+\phi_t-2\phi_{\rm surf})}. \end{aligned} \tag{5.25}$$

$\phi_{\rm surf}$ has the same meaning as it does for the ellipse but is approximated by $\cos\left(\phi_t - \phi_{\rm surf}\right) = \left(H_t^{\oplus} + h_t\right)/H_t^{\oplus}$. Note that physically $\phi_{\rm surf} < \phi_t$. Since the independent variable ϕ appears in one place in eq 5.25 for h it is easy to write ϕ as a function of h.

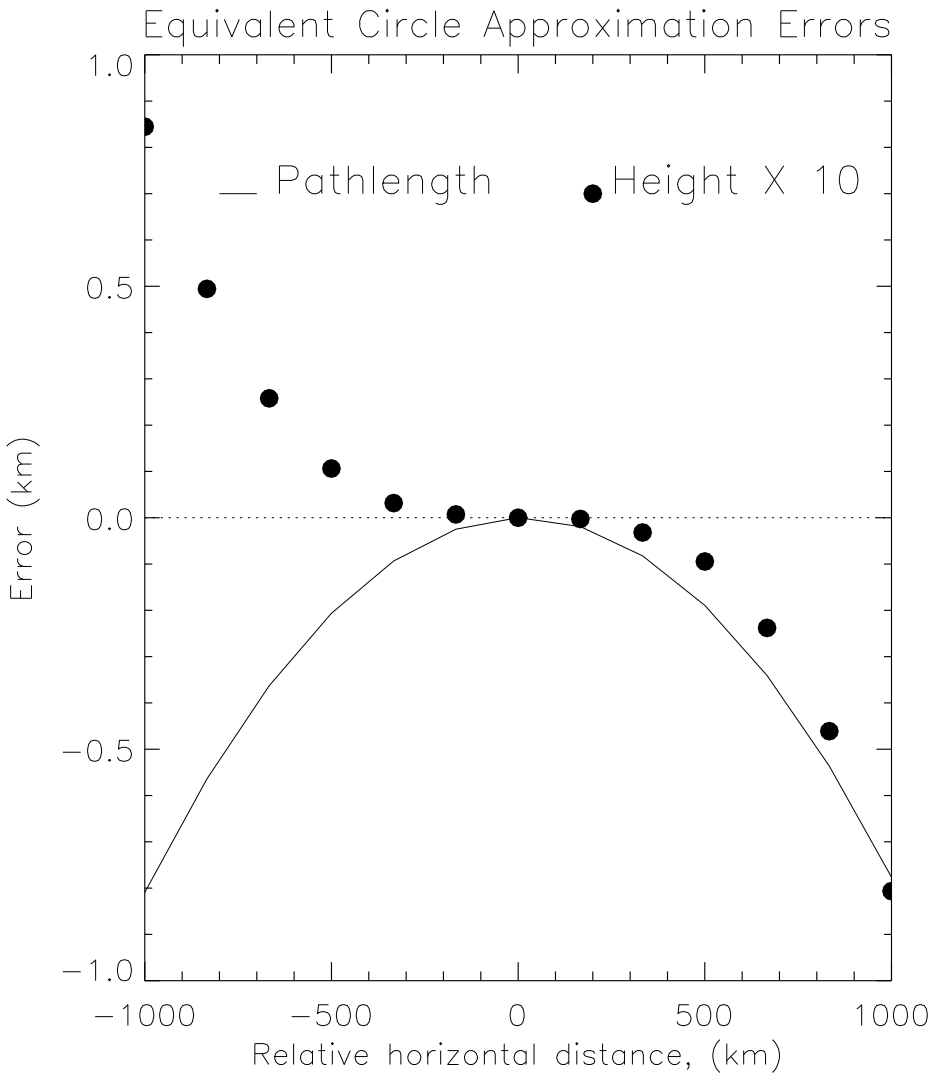

Figure 5.3: Difference of h and s computed for ellipse and equivalent circle representations of the Earth figure at $45.0°$.

5.3 Geopotential Function

The geopotential function defines the gravitational acceleration that is used in the hydrostatic and scan model. The function used here gives a constant geopotential for the locus of points described by the ellipsoid in eq. 5.1. The function is

$$U_r = \frac{GM}{R}\left(1 - \sum_{i=1}^{2} J_{2i} P_{2i}\left(\lambda\right)\left(\frac{a}{R}\right)^{2i}\right) + \frac{\omega^2 R^2 \cos^2\lambda}{2}, \tag{5.26}$$

where R is the distance from the center of the Earth, J_{2i} are form factors, P_{2i} are Legendre polynomials, GM is the Gravitational constant times the mass of the Earth, and ω is the angular velocity of the Earth. These constants are [17]:

$$\begin{aligned}
J_2 &= 0.0010826256, \\
J_4 &= -0.0000023709122, \\
GM &= 3986005 \times 10^8 \mathrm{m}^3\mathrm{s}^{-2}, \\
\omega &= 7292115 \times 10^{-11} \mathrm{rad\ s}^{-1}, \\
P_2 &= \tfrac{1}{2}\left(3\sin^2\lambda - 1\right), \\
P_4 &= \tfrac{1}{8}\left(35\sin^4\lambda - 30\sin^2\lambda + 3\right).
\end{aligned}$$

Expansion of eq. 5.26 to J_4 is adequate for our purposes. These values are somewhat different from that used from UARS MLS where the coefficients were taken from a very high order asymmetric geopotential model including longitudinal variations. This is rejected for now because the reference ellipsoid was not a constant geopotential surface. The differences between the UARS constants and those used here are tens of centimeters between 0–100 km and considered unimportant. The gradient of eq. 5.26 is the gravitational acceleration that is used in the hydrostatic model. For the purposes of state vector discussions, there are no added state vector elements because the only independent variables are R and λ which is uniquely defined by ϕ and ζ and the reference geopotential height. All the other constants and variables will be treated as errorless constants. This is acceptable because the geopotential function is adopted by definition and we are neglecting issues regarding surface aberrations.

5.4 Hydrostatic Model

The EOS MLS forward model assumes hydrostatic balance holds for the entire atmosphere. This is necessary because evaluating eq. 3.1 is a geometric and absorption problem that requires heights and pressures. The hydrostatic function interrelates heights with pressure and only one of these (the latter) is independent. The two dimensional hydrostatic function is based on eq. 30 in the forward model paper [14]

$$h\left(\zeta,\phi\right) = \frac{g_o \overset{\star}{R}_o^{\,2}}{g_o \overset{\star}{R}_o - \mathsf{k}\ln 10 \sum_l^{\mathrm{NH^T}} \sum_m^{\mathrm{NP}^T} \left(f_{lm}^T \eta_m^T\left(\phi\right) P_l\right)} - \overset{\star}{R}_o + R_o - R^{\oplus}, \tag{5.27}$$

where k, is the Boltzmann constant, P_l is the integral

$$P_l = \int_{\zeta_o}^{\zeta} \frac{\eta_l^T\left(\zeta\right)}{\mathcal{M}\left(\zeta\right)} \mathrm{d}\zeta, \tag{5.28}$$

ζ_o is a reference pressure where the absolute height with respect to the center of the Earth is known and is R_o, and $\mathcal{M}$ is the mean molecular mass of the atmosphere. The gravitational acceleration is given by

$$g_o = - \mid \vec{\nabla} U_r \left(R_o, \phi_o \right) \mid, \tag{5.29}$$

where $U_r \left(R_o, \phi_o \right)$ is the geopotential function evaluated at R_o and the equivalent latitude and longitude represented by ϕ_o. To simplistically yet accurately account for centrifugal effects, eq. 5.27 is derived assuming a $1/R^2$ gravitational fall-off satisfying the two boundary conditions that the gravitational acceleration and the vertical gravitational gradient are accurate. Eq. 5.29 defines the former and the latter is satisfied by defining a special "effective" height $\overset{\star}{R}_o$ according to

$$\overset{\star}{R}_o = \frac{2 g_o}{- \left(\partial g / \partial R \right)_{R=R_o}}. \tag{5.30}$$

The reference height R_o is the geometric height that is equivalent to the input reference geopotential height. We will use R_o to compute the surface pressure, then the reference height R_o will be reset to the surface of the Earth reference ellipsoid $R^{\oplus}$, which is convenient because it serves as a boundary condition of the radiative transfer for reflected rays. ζ_o in eq. 5.28 will be set to the computed surface pressure.

The radiance temperature derivatives need the hydrostatic temperature derivative of eq. 5.27 which is given by

$$\frac{\mathrm{d}h}{\mathrm{d}f_{lm}^T} = \frac{g_o \mathsf{k} \ln 10 \overset{\star}{R}_o^{\,2} \eta_m^T \left(\phi \right) P_l}{\left[g_o \overset{\star}{R}_o - \mathsf{k} \ln 10 \sum_l^{\mathrm{NT^T}} \sum_m^{\mathrm{NP^T}} \left(f_{lm}^T \eta_m^T \left(\phi \right) P_l \right) \right]^2}. \tag{5.31}$$

5.5 Radiative transfer Pre-Selected Integration Grid (PSIG)

The 2-D LOS radiative transfer equation is evaluated by taking a LOS path defined according to eq. 5.24 or 5.25 and chopping it into small segments that can be integrated accurately with quadrature. The division of the LOS path is based on the ζ coordinate so as to insure that the quadrature boundaries coincide with the profile vertical representation break-points. When the user calls the radiative transfer forward model, the forward model forms a mathematical union of all the inputted ζ_l^k basis breakpoints and mandates that each LOS path be chopped this way. The tangent heights of the calculation are also the same set of ζ's that are used for the LOS subdivision. This grid is called the Pre-Selected Integration grid (a matrix of path ζ's $\times$ tangent ζ's). The LOS path is then further divided into additional ζ's to accommodate the numerical quadrature to be used. For example, 3-point Gauss-Legendre is used for integrating the optical depth along the LOS. Therefore 3 additional ζ's are defined for each PSIG ζ. This grid is the coarsest that can be used that will provide accurate results; however, if there are sharp vertical gradients in the vertical mixing ratio profiles, a finer grid will be necessary. We have seen instances where this level of gridding has errors approaching 1 K. Therefore, a capability to oversample the PSIG grid formed from the union of representation basis ζ_l^k's is used. Oversampling not only adds more evaluation layers along the LOS but also adds more tangent heights to evaluate. The current forward model implementation uses $2\times$ oversampling in the troposphere and lower stratosphere.

Once the ζ PSIG is established, the corresponding LOS heights H's and geodetic angles ϕ's are needed. Eq. 5.27 is evaluated for at each unique ζ in the PSIG plus the extra quadrature ζ's at each ϕ_m in the temperature horizontal representation basis. This produces a reference 2-D heights matrix $h(\zeta, \phi_m)$. A reference geopotential height for a given pressure surface (nominally 100 hPa) is included in the hydrostatic calculation. The smallest ζ in the PSIG is defined as the designated surface pressure. The designated surface height of the designated surface pressure is computed at ϕ_t for the scan point nearest Earth surface using linear interpolation in ϕ_m. The value of the designated surface height is subtracted from $h(\zeta, \phi_m)$ and added to the equivalent circular Earth radius. This operation has no effect on the path lengths of the ray segments and therefore introduces no error in the radiative transfer equation. It does however define the pressure level at which intersecting rays reflect off the Earth and therefore there may be radiance differences for ray traces that reflect off a surface defined by the reference geopotential and those that reflect off a surface defined by the smallest PSIG ζ. The resulting error is obviously case dependent. The ray tracing program accommodates tangents that are geometrically below the designated surface pressure; however, the tangent pressure for these ray tracings is the designated surface pressure and an auxiliary vector of sub-surface heights (expressed as negative distance in km below the designated surface) must be supplied. Using an extrapolated tangent ζ coordinate for describing Earth reflected rays is not desirable because it causes errors in the reflected ray radiative transfer formulation for the temperature derivative.

Computing the 2-D ray tracings is done as follows. A vector of ray tracing ζ's is created from the ζ PSIG. For the lowermost tangent ray (which may reflect off the Earth surface), a reversed order ζ PSIG is concatenated to ζ PSIG producing a path ζ. Subsequent tangent height path ζ's are concatenated to the previous vector of path ζ's. For tangent heights having ζ_t that is less than the designated surface ζ, those ζ's in the PSIG that are greater than ζ_t are dropped from their path ζ. Paths with higher values of tangent ζ_t have fewer elements. The resulting long vector which may contain any number of individual path ζ's is called a compact vector formatted (CVF) ζ_{cvf}. From this a new reference height matrix $h_{\text{ref}}(\zeta_{\text{cvf}}, \phi_m)$ is established from $h(\zeta, \phi_m)$. Since the PSIG ζ's is a subset of ζ_{cvf}, $h_{\text{ref}}(\zeta_{\text{cvf}}, \phi_m)$ is merely a re-indexing of $h(\zeta, \phi_m)$. A guess for the path heights for all the ray-tracings is estimated by $h_{\text{cvf}} = h_{\text{ref}}(\zeta_{\text{cvf}}, \phi_{m=1})$. From h_{cvf} , ϕ_{cvf} is computed from eq. 5.24 or 5.25. The resulting ϕ_{cvf} is used to create a horizontal representation basis matrix $\eta^{\text{T}}(\phi_{\text{cvf}}, \phi_m)$ according to eqs. 4.3–4.6. A new heights estimate is created from $h\text{est}_{\text{cvf}} = \sum_m^{\text{NH}} h_{\text{ref}}(\zeta_{\text{cvf}})\, \eta^{\text{T}}(\phi_{\text{cvf}}, \phi_m)$. $h\text{est}_{\text{cvf}}$ is compared to h_{cvf} and where the differences are greater than some suitable threshold (10m), a new ϕ_{cvf}, $\eta^{\text{T}}(\phi_{\text{cvf}}, \phi_m)$ and $h\text{est}_{\text{cvf}}$ are computed until all elements in $h\text{est}_{\text{cvf}}$ differ less than the target threshold or a maximum number of iterations is exceeded. A limitation in the technique is its implied requirement that the minimum path ζ occurs where the path geodetic height is minimum. This is only true for the 1-D case or 2-D cases where the temperature gradient at the tangent is zero. In the general case, the minimum path ζ is slightly off the geodetic tangent. If the 2-D temperature gradient is large enough, it can cause convergence problems for the method outlined above. At present we do not have a capability for handling a variably adjusting ζ PSIG, therefore when non convergence occurs, linear interpolation is used to estimate the heights of pressures between ζ_t and its nearest converged ζ/h pair. A final set of ϕ_{cvf} is computed. the resulting ϕ_{cvf} are not corrected for refractive effects however, it is straightforward to do so (see Appendix A). Remember that ϕ_{cvf} computed this way is relative to the inputted ϕ_t which should include refraction.

The path 2-D fields for the constituents and temperature are computed from eq 4.1 or 4.2. The

derivatives of the ray traced heights with respect to temperature is evaluated with this procedure. The $\frac{\mathrm{d}h}{\mathrm{d}f_{lm}^T}$ (see eq. 5.31) is computed for each ζ in the PSIG and then resampled to the CVF path form as was done for height (except the resulting matrix has three dimensions, ζ_{CVF}, ϕ_m, and ζ_l). This matrix is multiplied by the CVF path $\eta^{\mathrm{T}}\left(\phi_{\mathrm{cvf}}, \phi_m\right)$ which is made 3-D by duplicating it NH times (forming a three dimensional $\eta^{\mathrm{T}}\left(\phi_{\mathrm{cvf}}, \phi_m, \mathrm{NH}\right)$).

Unlike the path ζs which are specified to fall on representation basis boundaries (or finer), the corresponding ϕ's will not coincide with the temperature basis ϕ_m. This algorithm assumes that h and $\frac{\mathrm{d}h}{\mathrm{d}f_{lm}^T}$ at $\phi \neq \phi_m$ is linear between adjacent ϕ_ms. This was tested against a more accurate method which requires running the hydrostatic function for each new ϕ and we find the linear interpolation method introduces no significant error. [1]

[1] This exercise was performed several years ago and regrettably I failed to document the actual error but had considered it negligible not to warrant further attention but it should be repeated.

Chapter 6. The Scan Model

The MLS FOV is scanned through the atmosphere and the FOV direction (ie angle) is measured and available for use. The scan measurement is encoder counts, which allows ϵ_t and α_t to be computed. Formally eq. D.11 is the model which relates this measurement to the state vector quantities previously described but it is a very messy calculation and was not done this way in UARS MLS. In UARS MLS which is adopted for EOS MLS, the orbit attitude service's estimate of height is fitted which is a derived quantity incorporating all the angles discussed above. This was extremely convenient because the calculated height folded together the effects of many angles, and the satellite motion into one measurement quantity and as long as one is not particularly interested in retrieving or properly accounting for errors in any of these quantities except for the raw measurement itself, then this approach is superior. The measurement to fit is

$$\vec{0} = \left[U_r\left(\vec{R}_t\right) - \Delta U_r\left(\vec{\zeta}_t\right) - U_r\left(R_{\rm ref}\right)\right]/g_o, \tag{6.1}$$

where $\vec{0}$ is the scan residual, $U_r\left(\vec{R}_t\right)$ is the geopotential (eq. 5.26) computed from heights given by orbit attitude measurements, $\Delta U_r\left(\vec{\zeta}_t\right)$ is the atmospheric geopotential offset relative to $Z_{\rm refgeopot}$, $U_r\left(R_{\rm ref}\right)$ is the geopotential of the reference geopotential height, $Z_{\rm refgeopot}$, $R_{\rm ref}$ is the reference geometric height, and $g_o = 9.80665\ {\rm ms}^{-2}$ (converts geopotential units to height units). The $\vec{\rm vector}$ designation means that this quantity is a profile on some arbitrary vertical measurement grid whose height points are given by state vector component "tangent pressure." These are sampling points during a single profile scan [18]. The scan residual $\vec{0}$ has geopotential height units (m) and uncertainty based on encoder uncertainty mapped into height units. The scan forward model is casted this way because all the terms on the right hand side depend on state vector quantities.

The orbit attitude derived heights do not include refraction; they are converted to a refracted height according to,

$$\vec{R}_t = \frac{\vec{R}_{\rm geom}}{\vec{\mathcal{N}}_t}, \tag{6.2}$$

where $\vec{R}_{\rm geom}$ are the orbit attitude estimated geocentric heights, and $\vec{\mathcal{N}}_t$ is the refractive index given by

$$\mathcal{N}_t = 1 + \frac{0.0000776}{\mathsf{f}_t^T\left(\zeta_t, \phi_t\right) 10^{\zeta_t}}\left(1 + 4810\frac{\mathsf{f}^{\rm H2O}\left(\zeta_t, \phi_t\right)}{\mathsf{f}_t^T\left(\zeta_t, \phi_t\right)}\right). \tag{6.3}$$

Tangent pressure for a subsurface height is not defined; however, to accommodate the level 2 retrieval which extrapolates tangent pressure downward, we freeze $\vec{\mathcal{N}}_t$ at the surface value for $\vec{R}$ pointing below the surface. As shown in figure 2.2, ϕ_t depends on refraction. The difference between the refracted and unrefracted ϕ_t (a level 1 quantity) is computed according to

$$\Delta\vec{\phi}_t = \int_{{\rm MAX}\left(\vec{\zeta}_t, \zeta_s\right)}^{2.5} \frac{\vec{\mathcal{N}}_t \vec{R}_t}{R}\frac{{\rm d}R}{{\rm d}\zeta}\left(\frac{1}{\sqrt{\mathcal{N}^2R^2 - \vec{\mathcal{N}}_t^2\vec{R}_t^2}} - \frac{1}{\sqrt{\vec{\mathcal{N}}_t^2R^2 - \vec{\mathcal{N}}_t^2\vec{R}_t^2}}\right){\rm d}\zeta, \tag{6.4}$$

where ζ_s is the negative logarithm of pressure at the Earth surface and $\vec{R}_t$ are the geocentric heights of the tangent ray, some may be less than the Earth radius. The upper integration limit of 2.5 is

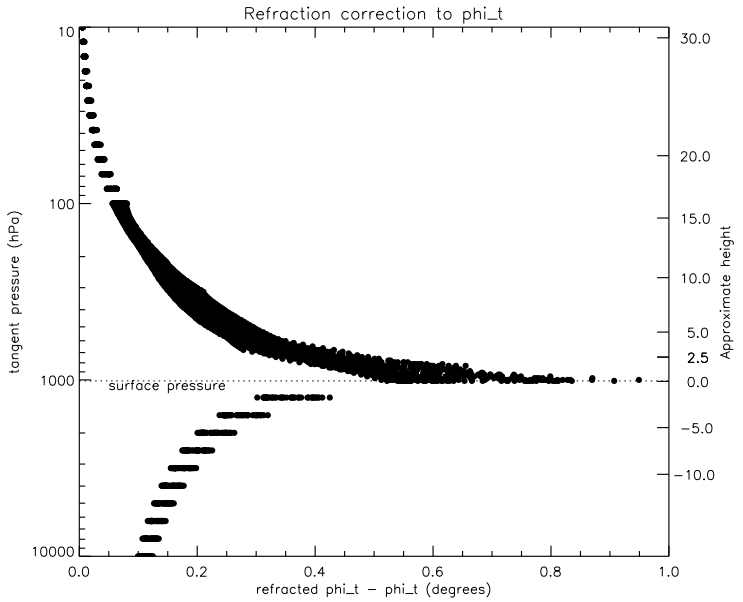

Figure 6.1: Computed difference between refracted ϕ_t and unrefracted ϕ_t for several February, 1996 profiles over 2 EOS orbits and several tangent pressure (and heights)

a ζ above which refractive effects are negligible. A full description and derivation of eq. 6.4 is given in Appendix A. The scan model may be a good place in the level 2 program to adjust ϕ_t for refraction. Figure 6.1 shows the correction for several profiles taken over two EOS orbits during a February day in 1996. Except in the boundary layer (lowermost 2 km in the Earth's atmosphere), the variability of the correction tends to be small relative to the 1.5° separations between horizontal basis components. We may simply apply a table of $\Delta\phi_t$ versus ζ_t as a method for correcting ϕ_t for refraction in the level 2 software.

$\Delta U\left(\vec{\zeta}_t\right)$ is the geopotential which is the second term in the denominator of eq. 5.27

$$\Delta U\left(\vec{\zeta}_t\right) = \mathsf{k}\ln 10 \sum_{l}^{\mathrm{NH^T}} \sum_{m}^{\mathrm{NP}^T} \left(f_{lm}^T \eta_m^T\left(\vec{\phi}_t\right) P_l\left(\vec{\zeta}_t\right)\right). \tag{6.5}$$

The reference geopotential is computed from the reference geometric height which is related to the reference geopotential height, $Z_{\mathbf{refgeopot}}$, according to

$$R_{\mathrm{ref}} = \frac{g_o^{\oplus}\left(\overset{\star}{R}_o^{\oplus}\right)^2}{g_o^{\oplus}\ \overset{\star}{R}_o^{\oplus} - g_o Z_{\mathrm{refgeopot}}} - \overset{\star}{R}_o^{\oplus} + R^{\oplus}, \tag{6.6}$$

where $g_o^{\oplus}$ and $\overset{\star}{R}_o^{\oplus}$ are the gravitational acceleration and effective Earth radius computed at the Earth surface with eq. 5.29 and eq. 5.30 respectively. Remember that $Z_{\mathbf{refgeopot}}$ is horizontally resolved (i.e. $Z_{\mathbf{refgeopot}} = \sum_m^{\mathrm{NH^T}} f_m^{\mathrm{refgeopot}} \eta_m^T\left(\vec{\phi}_t\right)$).

Formulas for the derivatives of the scan residual with respect to the limb tangent pressure,

temperature and reference geopotential are

$$\begin{aligned}
\frac{\mathrm{d}\vec{0}}{\mathrm{d}\vec{\zeta}_t} &= \mathsf{k}\ln 10 \sum_{l}^{\mathrm{NH^T}} \sum_{m}^{\mathrm{NP}^T} f_{lm}^T \eta_m^T\left(\vec{\phi}_t\right)\eta_l^T\left(\vec{\zeta}_t\right) / \left[g_o \mathcal{M}\left(\vec{\zeta}_t\right)\right] + \frac{\mathrm{d}U_r}{\mathrm{d}\vec{R}_t}\frac{\vec{R}_t}{g_o\vec{\mathcal{N}}_t} \\
&\times \left[\left(\vec{\mathcal{N}}_t - 1\right)\left(\ln 10 + \frac{\mathrm{d}\ln\vec{T}_t}{\mathrm{d}\vec{\zeta}_t}\right) + \frac{b'\vec{\mathsf{f}}_t^{H_2O}}{\vec{T}_t 10^{\vec{\zeta}_t}}\left(\frac{\mathrm{d}\ln\vec{\mathsf{f}}_t^{H_2O}}{\mathrm{d}\vec{\zeta}_t} - \frac{\mathrm{d}\ln\vec{T}_t}{\mathrm{d}\vec{\zeta}_t}\right)\right], \\
\frac{\mathrm{d}\vec{0}}{\mathrm{d}f_{lm}^T} &= \frac{\mathsf{k}\ln 10}{g_o}\eta_m^T\left(\vec{\phi}_t\right)\eta_l^T\left(\vec{\zeta}_t\right) + \frac{\mathrm{d}U_r}{\mathrm{d}\vec{R}_t}\frac{\vec{R}_t\left(\vec{\mathcal{N}}_t - 1 + \frac{b'\vec{\mathsf{f}}_t^{H_2O}}{\vec{T}_t^{\,2}10^{\vec{\zeta}_t}}\right)}{g_o\vec{T}_t\vec{\mathcal{N}}_t}\eta_l^T\left(\vec{\zeta}_t\right)\eta_m^T\left(\vec{\phi}_t\right), \\
\frac{\mathrm{d}\vec{0}}{\mathrm{d}f_m^{\mathrm{refgeopot}}} &= \frac{\mathrm{d}U_r}{\mathrm{d}R_{\mathrm{ref}}}\eta_m^T\left(\vec{\phi}_t\right)\frac{R_{\mathrm{ref}} - R^{\oplus} + \overset{\star}{R}^{\oplus}}{g_o^{\oplus}\overset{\star}{R}^{\oplus} - g_o\sum_m^{\mathrm{NH^T}} f_m^{\mathrm{refgeopot}}\eta_m^T\left(\vec{\phi}_t\right)}.
\end{aligned} \tag{6.7}$$

The $\frac{\mathrm{d}\vec{0}}{\mathrm{d}\vec{\zeta}_t}$ derivative is a sum of two terms. The first term is a hydrostatic contribution and the second term is an index of refraction contribution. When $R_t < R^{\oplus}$, the second term is zero, that is it is not added to the first term. Although water vapor is included in $\mathcal{N}_t$, we have not worked out the derivatives for it.

6.0.1 Improved scan model

The quantity $\vec{R}_{\mathrm{geom}}$, which is supplied by the orbit attitude services is a function that has R_s, ϵ_t, α_t, φ, ϑ, and ψ as independent variables. If these are considered important for error propagation purposes then $\vec{R}_{\mathrm{geom}}$ in eqn. 6.2 is substituted with the appropriate function involving instrument and spacecraft alignment and attitude angles. Beginning with the definition of a ray path

$$\vec{R}_t^{\oplus} + \vec{h}_t = \vec{R}_s + \vec{n}_d s_t, \tag{6.8}$$

where $\vec{n}_d$ is the unit vector in the pointing direction, $\vec{R}_t^{\oplus}$ is a geocentric vector to the Earth ellipsoid figure, $\vec{h}_t$ is geodetic height, $\vec{R}_s$ is the geocentric spacecraft location, and s_t is the path distance. Figure 5.1 shows some of these quantities but this equation applies to the full 3-D ellipsoid. The unit vector $\vec{n}_d$ depends on φ, ϑ, ψ, ϵ_t, α_t, and the spacecraft latitude, longitude, orbital incline angle, and ascend/descend node through a series of rotation matrices (eq. C.1). The limb tangent is defined as the minimum value of the geodetic height $\vec{h}$ given by,

$$\mid \vec{R}_{\mathrm{geom}} \mid = \mid \vec{R}_{\oplus} + \vec{h}_t \mid = \mid \vec{R}_s - \vec{n}_d\left[\vec{n}_d \cdot \left(\vec{R}_s - \vec{R}_{\oplus}\right)\right] \mid . \tag{6.9}$$

This is substituted into eq. 6.2 and provides a means to directly incorporate the encoder measurement into the scan model with capability for correct error propagation. *This material exists mostly for future reference.*

Chapter 7. Scan Averaging

The EOS MLS scan continuously moves while the radiometric measurement is being made, which means that there will be some height averaging. This is the time integral in eq. 3.1. The amount of movement is expected to be small relative to the FOV patterns and therefore less critical to modeling details *we hope*. The scan angle change with respect to time may follow a function like,

$$\chi_{\rm eq}^{\rm refr}(t) = \chi_{\rm eq}^{\rm refr}(t_1) + \frac{\Delta\chi^{\rm refr}}{\Delta t}(t-t_1) + \Delta\chi_A \sin\left(\omega t + \phi(t_1)\right), \tag{7.1}$$

where $\Delta\chi^{\rm refr} = \chi_{\rm eq}^{\rm refr}(t_2) - \chi_{\rm eq}^{\rm refr}(t_1)$ and $\Delta t = t_2 - t_1$. This equation assumes a linear (constant velocity) change in pointing angle with respect to time. Added to this is an oscillation (jitter) function having a peak-to-peak value of $2\Delta\chi_A$, frequency ω and initial phase $\phi(t_1)$. Let $\mathbf{I}_{\rm inst}$ be a vector of instantaneous radiances for the corresponding vector of $\vec{\zeta}_t$. There is a corresponding and known set of pointing angles $\chi_{\rm eq}^{\rm refr}$ in the equivalent circular Earth representation. These angles are a function of the existing state vector components and therefore are always available. Finally, a continuous and smooth $I_{\rm inst}$ can be made from a cubic spline, which also gives the first derivative $I'_{\rm inst}$ at any height. The time averaged radiance for an integration between t_1 and t_2 is

$$\begin{aligned}\overset{\bullet}{I} &= \frac{1}{\Delta t}\int_{t_1}^{t_2} I_{\rm inst}\left(\chi_{\rm eq}^{\rm refr}(t_1)\right)(1-x)^2(1+2x) + I_{\rm inst}\left(\chi_{\rm eq}^{\rm refr}(t_2)\right)x^2(3-2x) \\ &+ I'_{\rm inst}\left(\chi_{\rm eq}^{\rm refr}(t_1)\right)\Delta\chi_{\rm eq}^{\rm refr}x(1-x)^2 + I'_{\rm inst}\left(\chi_{\rm eq}^{\rm refr}(t_2)\right)\Delta\chi_{\rm eq}^{\rm refr}x^2(x-1)\,{\rm d}t,\end{aligned} \tag{7.2}$$

where $I_{\rm inst}$ and $I'_{\rm inst}$ are evaluated from a cubic spline of $\mathbf{I}_{\rm inst}$ evaluated at the boundary points t_1, and t_2, and x is $\left(\chi_{\rm eq}^{\rm refr}(t) - \chi_{\rm eq}^{\rm refr}(t_1)\right)/\Delta\chi_{\rm eq}^{\rm refr}$. Substituting eq. 7.1 into eq. 7.2 and integrating gives the result. If the jitter term in eq. 7.1 is ignored the scan motion integral is

$$\overset{\bullet}{I} = \frac{1}{2}\left(I_{\rm inst}\left(\chi_{\rm eq}^{\rm refr}(t_1)\right) + I_{\rm inst}\left(\chi_{\rm eq}^{\rm refr}(t_2)\right)\right) + \frac{\Delta\chi_{\rm eq}^{\rm refr}}{12}\left(I'_{\rm inst}\left(\chi_{\rm eq}^{\rm refr}(t_1)\right) - I'_{\rm inst}\left(\chi_{\rm eq}^{\rm refr}(t_2)\right)\right). \tag{7.3}$$

It is proposed that eq. 7.3 be used for the time averaging.

7.1 Derivative Form

The basic derivative form is

$$\frac{{\rm d}\overset{\bullet}{I}}{{\rm d}x} = \frac{1}{2}\left(\frac{{\rm d}I_{\rm inst1}}{{\rm d}x} + \frac{{\rm d}I_{\rm inst2}}{{\rm d}x}\right) + \frac{\Delta\chi_{\rm eq}^{\rm refr}}{12}\left(\frac{{\rm d}I'_{\rm inst1}}{{\rm d}x} - \frac{{\rm d}I'_{\rm inst2}}{{\rm d}x}\right), \tag{7.4}$$

where x is any statevector element. Note that both eq. 7.3 and eq. 7.4 require two pressure values (at t_1 and t_2) to be known for each scan measurement. Therefore the tangent pressure retrievable is pressure at the integration boundaries that is *two* tangent pressures per radiance. This is inconvenient and instead one may use eqs. 7.3 and 7.4 with a representative scan (i.e. $\chi_{\rm eq}^{\rm refr}(t)$) to smooth over the radiances and derivatives. $\overset{\bullet}{I}$ and $\frac{{\rm d}\overset{\bullet}{I}}{{\rm d}x}$ are functions of ζ_t.

The current Level 2 processing ignores scan averaging. The first term in eq. 7.3 is simply the average of the two instantaneous radiances at the boundaries. If the radiance growth between the breakpoints is linear and the antenna scans at constant velocity, the scan smoothed radiance field is the same as the instantaneous radiance at $t = 0.5\,(t_1 + t_2)$ which is consistent with the level 2 usage. However, non-linearities of the radiance growth field affect the scan averaging and within the limitations stated above, is given in the second term of eq. 7.3. Therefore the second term of eq. 7.3 can be used to estimate the errors caused by neglecting the scan motion. The typical maximum error is 0.15 K over that portion of the radiance profile where $\mid \frac{\mathrm{d}I_{\mathrm{inst}}}{\mathrm{d}\chi_{\mathrm{eq}}^{\mathrm{refr}}} \mid$ is largest; however, some notable exceptions are: R1 it is 0.3 K in the stratosphere and 0.6 K in the mesosphere and R5H or R5V it is 1.1 K in the troposphere, 0.05 K in the stratosphere and 0.2 K in the mesosphere. The higher values are consistent with the scan step size which is largest in the mesosphere. The R5 (terahertz) scan takes very large steps in the troposphere accounting for the its large error.

Chapter 8. Field of View Integration

The far-field beam width of the MLS receiving antenna contributes to the vertical shape of the radiance weighting function. This is the reason why in eq. 3.1 we include the weighted average of the antenna gain function G and the radiances I over the solid angle Ω.

8.1 Discussion of Issues and Approximations

Nominally it is expected that the UARS MLS approach for correcting radiances for antenna smoothing (FOV integration) will be satisfactory for EOS MLS; however, there will be some new aspects to consider. These include the two-dimensionality of the problem, and possibly the scan and frequency dependencies of the patterns themselves. The UARS MLS approach assumed horizontal homogeneity with no frequency or scan dependence within each radiometer. This is considered unsatisfactory for EOS MLS because the sideband separation is much larger; therefore, there will be multiple patterns for each radiometer. In addition the scan dependence of each pattern will be measured. The frequency dependence is easily dealt with by simply adding more pattern files. The frequency dependence of a pattern should be negligible over a channel width and the approximation where the frequency and spatial coordinates are separated is valid. More problematic is the possible scan dependence of the pattern. The UARS MLS approach, suggested for use here, requires that the pattern is scan independent because it uses the fast Fourier transform (FT) method for performing convolutions. In the worst case, the FT method is not valid except for the one height in the scan having the correct antenna function. Therefore the spatial integral in eq. 3.1 should be evaluated at each pointing position with a different pattern. This will be much slower and could be a problem when the retrieval program interactively needs computed radiances for non-linear inversions.

An idea for handling the scan dependence, if needed, is discussed here which allows continued use of the rapid convolution approach used in UARS MLS. As of August 19, 2004, the measured antenna patterns are sufficiently scan independent [5] such that this complication is unnecessary. An approach is to intelligently choose one specific pattern at a scan position that minimizes errors over the whole vertical range. This retains the single pattern concept for easy FT processing yet effectively includes the scan dependence. This would be implemented as follows. Antenna smearing effects are most important where the second derivative of the radiance versus height curve is maximal. This usually leads to two hopefully closely separated maxima. Since the height where this occurs is mostly determined by spectroscopy it can be known prior to launch and the appropriate pattern selected. Scan errors will be minimum beyond the rapid radiance change region because the pattern will behave more like a delta function and the shape details are unimportant. Across a band, the height where the radiances change rapidly will vary considerably and therefore different patterns selected by scan optimization could be used for each channel. This could allow the use of the UARS MLS approach while incorporating the scan dependence of the pattern in a way that will minimize errors without having to resort to the full multi-pattern and much slower integration approach.

Chapter 2 discussed neglecting horizontal smearing in the antenna smearing calculation. Based on that discussion it seems reasonable to neglect horizontal smearing in the pre-launch model. Not

neglecting it would mean among other things, that the efficient convolution approach described below is not beneficial because the radiance profile varies with each antenna pointing position. *An estimate of the error this approximation causes is not known and needs to be evaluated. This will require generation of a 2-D matrix of radiances as a function of ζ_t and ϕ_t. Then the antenna smoothing has to be done, one pointing at a time using the instantaneous radiance ζ_t and ϕ_t profile as received by the antenna. As a rough estimate, at a given ζ_t, the error should be proportional to the difference in the instantaneous difference between the antenna received ϕ_t and the scanned ϕ_t times the horizontal radiance gradient $\frac{\mathrm{d}I}{\mathrm{d}\phi_t}$.*

8.2 UARS MLS Approach

The antenna gain function is assumed to be frequency independent over a spectral channel bandwidth which is $< 0.5\%$ of the received frequency. The spatial averaging part of eq. 3.1 is expanded below

$$I\left(\epsilon_t, \alpha_t, \nu_{\mathrm{ch}}, \mathbf{x}\right) = \frac{1}{4\pi}\mathrm{Tr}\int_0^{2\pi}\int_{-\frac{\pi}{2}}^{\frac{\pi}{2}} \mathbf{I}\left(\epsilon, \alpha, \nu_{\mathrm{ch}}, \mathbf{x}\right)\mathbf{G}\left(\epsilon_t - \epsilon, \alpha_t - \alpha\right)\cos\epsilon \mathrm{d}\epsilon\mathrm{d}\alpha, \tag{8.1}$$

where $\mathbf{G}$ is the polarized far field antenna pattern, Tr is the trace of a matrix, $\mathbf{I}$ is the channel averaged radiance in polarized format, angles ϵ_t and α_t are elevation (vertical) and azimuth (cross-track) angles and the total integrated area under $\mathbf{G}$ is 4π. The angles ϵ_t and α_t are defined in the IFOVP frame. The solution of this equation is described in detail in [14, 15] and only the end result is given here. The general case, eq. 8.1 requires 4 pattern measurements and the polarization direction of the receiver (angle ξ in the level 1 ATBD [5], which is used in the polarized radiative transfer calculation). The polarized radiative transfer calculation and its application (mesospheric O_2 under the influence of Earth's magnetic field) is given in [15]. The unpolarized case, which is applicable to the other EOS molecules in the troposphere through the stratosphere is described here.

Eq. 8.1 is converted to a convolution integral where it can be evaluated by the Fast Fourier Transform (FFT). Since the cross-track smearing is small (< 20 km), the atmosphere is assumed to be homogeneous on this scale and the problem is collapsed into the elevation dimension only. We also smear the radiance field along the horizontal, $\vec{\phi}_t$, which differs from the actual horizontal smearing by $< \pm 20$ km (see figure 2.2). Making the appropriate coordinate conversion and assuming unpolarized radiation from the atmosphere gives the following

$$I\left(\chi_{\mathrm{eq}}^{\mathrm{refr}}, \nu_{\mathrm{ch}}, \mathbf{x}\right) = \int_{-\infty}^{\infty} I\left(\chi, \nu_{\mathrm{ch}}, \mathbf{x}\right)\overline{G}\left(\chi_{\mathrm{eq}}^{\mathrm{refr}} - \chi\right)\mathrm{d}\chi, \tag{8.2}$$

where $I\left(\chi_{\mathrm{eq}}^{\mathrm{refr}}, \nu_{\mathrm{ch}}, \mathbf{x}\right)$ is the channel averaged radiance (chapter 9), $\overline{G}\left(\chi_{\mathrm{eq}}^{\mathrm{refr}} - \chi\right)$ is the sum of the co and cross-polarized antenna gain functions in the angular pointing coordinate χ. $\overline{G}$ is normalized to unit area. See [14] for the development of eq. 8.2. The small angle approximation $\sin\left(\epsilon_t - \epsilon\right) \approx \chi_{\mathrm{eq}}^{\mathrm{refr}} - \chi$ is assumed. $\chi_{\mathrm{eq}}^{\mathrm{refr}}$ is related to geometric quantities according to

$$\sin\chi_{\mathrm{eq}}^{\mathrm{refr}} = \mathcal{N}_t\frac{H_t}{H_s}, \tag{8.3}$$

where $\chi_{\mathrm{eq}}^{\mathrm{refr}}$ is the refracted pointing angle in the x-y plane of the LOSF relative to the equivalent circular Earth representation. $\chi_{\mathrm{eq}}^{\mathrm{refr}}$ is related to the pointing angle χ^{refr} relative to the Earth figure

according to

$$\chi_{\rm eq}^{\rm refr} - \chi^{\rm refr} = \Delta\chi = \frac{R_s^2 + H_s^2 - d^2}{2R_s H_s}, \tag{8.4}$$

where H_s is the satellite orbit radius relative to the equivalent circular Earth figure in figure 5.2. Although H_s is straightforward to calculate, $\vec{H}_s = \vec{R}_s - \vec{d}$ ($\vec{d}$ is from eq. 5.22), to do so requires additional Level 1 data. $\vec{H}_s$ can be computed with adequate accuracy with the following empirical formula

$$H_s \approx R_s\,(\text{ECR or ECI}) + 38.9 \sin\left[2\left(\phi_t - 51.6\right)\right]. \tag{8.5}$$

For EOS MLS, the error in eq. 8.5 is less than 0.55 km. It can be shown that this will have negligible impact. The satellite radius only affects the accuracy of the forward model by distorting the antenna shape. A characteristic property of the antenna FOV is its half power beam width (HPBW) which is an angular property describing its resolving ability. More important is the projection of the antenna HPBW on the limb tangent. The following equation gives that projection

$$\Delta h_{\rm hpbw} = \Delta\chi_{\rm hpbw}\sqrt{H_s^2 - \left(H_t^{\oplus} + h\right)^2}, \tag{8.6}$$

where $\chi_{\rm hpbw}$ is the antenna HPBW in radians. Differentiating eq. 8.6 gives

$$\mathrm{d}\Delta h_{\rm hpbw} = \frac{\Delta\chi_{\rm hpbw}\left[H_s \mathrm{d}H_s - \left(H_t^{\oplus} + h\right)\left(\mathrm{d}H_t^{\oplus} + \frac{\mathrm{d}h}{\mathrm{d}T}\mathrm{d}T\right)\right]}{\sqrt{H_s^2 - \left(H_t^{\oplus} + h\right)^2}}. \tag{8.7}$$

According to eq. 8.7, an error of 0.6 km is equivalent to a HPBW error of 3 meters in tangent height for an antenna with a HPBW of 6 km. This is 0.05% of the HPBW which is entirely negligible compared to the uncertainty in knowledge of the antenna HPBW (a few percent). The integration variable χ is related to limb tangent heights according to eq. 8.3. The 1-dimensional antenna pattern is defined in a plane traced by ϵ_t or the y-z axes in the IFOVP frame. The $\chi_{\rm eq}^{\rm refr}$ is in the x-y axes in the LOSF. These planes are coincident only when $\alpha_t = 0$ (EOS MLS, 90 for UARS MLS), $\varphi = 0$ (EOS MLS), $\vartheta = 0$ (UARS MLS), $\psi = 0$, or 180. In general, $\alpha_t, \varphi, \vartheta$, and ψ are slightly deviant from ideal and the half-power beam width of $\overline{G}\left(\chi_{\rm eq}^{\rm refr} - \chi\right)$ is slightly wider in the plane defined by $\chi_{\rm eq}^{\rm refr}$. *The difference between integrating in the IFOVP and LOSF coordinates is a second order effect which is neglected for now but should be investigated when preparing error budgets for validation papers.*

One dimensional FFTs are applied to evaluate eq. 8.2. The Fourier transform theorem of convolutions is

$$\mathcal{F}t\left(I\left(\chi_{\rm eq}^{\rm refr}\right)\right) = \mathcal{F}t\left(I\left(\chi\right)\right) \times \mathcal{F}t\left(\overline{G}\left(\chi\right)\right). \tag{8.8}$$

The Fourier transform of the antenna gain pattern can be taken and stored as such. An advantage to doing this in addition to avoiding repetitive FFT calculations is that the resulting autocorrelation of the field pattern should be zero beyond twice the aperture distance and the first point in the pattern is the normalization factor. Truncating the aperture autocorrelation pattern provides some noise filtering. This was not done for UARS MLS because of uncertainty of the actual aperture size. For EOS MLS we are not truncating the aperture autocorrelation patterns for the GHz radiometers but are truncating them for the THz radiometer.

The derivative of the antenna smeared radiance with respect to a state vector element is given by

$$\begin{aligned}\frac{\mathrm{d}I}{\mathrm{d}x_j} &= \int_{-\infty}^{\infty}\left[\frac{\mathrm{d}I}{\mathrm{d}x_j} + I\frac{\mathrm{d}}{\mathrm{d}\chi}\left(\frac{\mathrm{d}\chi}{\mathrm{d}x_j}\right)\right]\overline{G}\left(\chi_{\mathrm{eq}}^{\mathrm{refr}}-\chi\right)\mathrm{d}\chi \\ &+ \frac{\mathrm{d}\chi_{\mathrm{eq}}^{\mathrm{refr}}}{\mathrm{d}x_j}\int_{-\infty}^{\infty} I\frac{\mathrm{d}\overline{G}\left(\chi_{\mathrm{eq}}^{\mathrm{refr}}-\chi\right)}{\mathrm{d}\left(\chi_{\mathrm{eq}}^{\mathrm{refr}}-\chi\right)}\mathrm{d}\chi - \int_{-\infty}^{\infty} I\frac{\mathrm{d}\chi}{\mathrm{d}x_j}\frac{\mathrm{d}\overline{G}\left(\chi_{\mathrm{eq}}^{\mathrm{refr}}-\chi\right)}{\mathrm{d}\left(\chi_{\mathrm{eq}}^{\mathrm{refr}}-\chi\right)}\mathrm{d}\chi, \end{aligned} \tag{8.9}$$

where x_j is a state vector element. In most cases, x_j is non geometrical (that is, has no effect on heights of pressure surfaces) and all the $\frac{\mathrm{d}\chi}{\mathrm{d}x_j} = 0$, simplifying eq. 8.9 considerably. Exceptions to this are temperature (affects heights through the hydrostatic model), Earth and satellite orbital radii. Although the antenna pattern is invariant in its angular properties, its beam width in *pressure* units does change whenever the observing geometry is altered.

The angular derivatives in eq. 8.9 are given by [14]

$$\begin{aligned}\frac{\mathrm{d}\chi}{\mathrm{d}f_{lm}^T} &= \frac{\tan\chi}{H_t}\frac{\mathrm{d}H_t}{\mathrm{d}f_{lm}^T}, \\ \frac{\mathrm{d}}{\mathrm{d}\chi}\left(\frac{\mathrm{d}\chi}{\mathrm{d}f_{lm}^T}\right) &= \frac{2+\tan^2\chi}{H_t}\frac{\mathrm{d}H_t}{\mathrm{d}f_{lm}^T} + \frac{\eta_l^T\eta_m^T}{T_t}, \\ &= \frac{\tan^2\chi}{H_t}\frac{\mathrm{d}H_t}{\mathrm{d}f_{lm}^T} + \frac{\mathrm{d}}{\mathrm{d}H_t}\left(\frac{\mathrm{d}H_t}{\mathrm{d}f_{lm}^T}\right), \\ \frac{\mathrm{d}\chi}{\mathrm{d}H_s} &= -\frac{\tan\chi}{H_s}, \\ \frac{\mathrm{d}}{\mathrm{d}\chi}\left(\frac{\mathrm{d}\chi}{\mathrm{d}H_s}\right) &= -\frac{1}{H_s\cos^2\chi}, \\ \frac{\mathrm{d}\chi}{\mathrm{d}H_t^{\oplus}} &= \frac{\tan\chi}{H_t}, \\ \frac{\mathrm{d}}{\mathrm{d}\chi}\left(\frac{\mathrm{d}\chi}{\mathrm{d}H_t^{\oplus}}\right), &= \frac{1}{H_t\cos^2\chi}, \end{aligned} \tag{8.10}$$

where T_t is temperature at the limb tangent. The derivations of the temperature forms are given in Appendix B. The H_t is evaluated for each tangent height for all the ray tracings. $\frac{\mathrm{d}\overline{G}\left(\chi_{\mathrm{eq}}^{\mathrm{refr}}-\chi\right)}{\mathrm{d}\left(\chi_{\mathrm{eq}}^{\mathrm{refr}}-\chi\right)}$ is evaluated using the FT derivative property

$$\mathcal{F}t\left(\frac{\mathrm{d}\overline{G}\left(\chi\right)}{\mathrm{d}\chi}\right) = iq\mathcal{F}t\left(\overline{G}\left(\chi\right)\right) \tag{8.11}$$

where q is the aperture independent coordinate (number of wavelengths), and $i = \sqrt{-1}$. This definition is convenient because the pattern is stored as $\mathcal{F}t\left(\overline{G}\left(\chi\right)\right)$ and ensures internal consistency between the pattern and its derivative.

Here we discuss some practical issues with evaluating eq. 8.9. First, since rays reflect off the Earth surface, temperature cannot influence H_t when it is less than $H_t^{\oplus}$ and state vector variable

ζ_t doesn't exist. If one ignores this fact by artificially extrapolating the pressure to larger values, an erroneous spike in the lowest coefficient of $\frac{\mathrm{d}I}{\mathrm{d}f_{lm}^T}$ occurs. To eliminate this and also do the calculation in the physically correct fashion, $\frac{\mathrm{d}\chi}{\mathrm{d}f_{lm}^T} = 0$ for all $\chi_{\mathrm{eq}}^{\mathrm{refr}}$ that point below $H_t^{\oplus}$. Therefore one has to be careful that the same Earth radius is used throughout the calculation. The second problem is numerical. The following must be true,

$$\int_{-\infty}^{\infty} \frac{\mathrm{d}}{\mathrm{d}\chi}\left(\frac{\mathrm{d}\chi}{\mathrm{d}x_j}\right)\overline{G}\left(\chi_{\mathrm{eq}}^{\mathrm{refr}}-\chi\right)\mathrm{d}\chi - \int_{-\infty}^{\infty}\frac{\mathrm{d}\chi}{\mathrm{d}x_j}\frac{\mathrm{d}\overline{G}\left(\chi_{\mathrm{eq}}^{\mathrm{refr}}-\chi\right)}{\mathrm{d}\left(\chi_{\mathrm{eq}}^{\mathrm{refr}}-\chi\right)}\mathrm{d}\chi = 0. \tag{8.12}$$

In other words there should be no sensitivity to the antenna beam shape if there is no gradient in the radiance profile. Calculations assuming constant I showed that this is not the case, a result of imperfect numerics. The error peaks at the maximum of $\frac{\mathrm{d}}{\mathrm{d}\chi}\left(\frac{\mathrm{d}\chi}{\mathrm{d}x_j}\right)$. Therefore to mitigate this error we subtract the anticipated error pattern from the calculation of eq. 8.9. This is easily done by setting $I = I - I_M$ in the first and third term (*I believe you can replace all the I's with* $I - I_M$) on the right-hand side of eq. 8.9, where I_M is I at the height where $\frac{\mathrm{d}}{\mathrm{d}\chi}\left(\frac{\mathrm{d}\chi}{\mathrm{d}x_j}\right)$ is maximum. This trick eliminated an annoying spike-like feature that affected all temperature coefficients affected by ϕ_t, and improved agreement with finite difference comparisons.

Chapter 9. Spectral Integration

The MLS instrument channels measure radiation over a finite bandwidth of frequencies. This causes the resulting signal to distort or spectrally smear the lineshape relative to a monochromatic measurement. The methodology for computing the spectral integral in eq. 3.1 is described here.

9.1 Evaluation

The radiative transfer equation (chapter 10) is evaluated at several frequencies and convolved with the spectral response as given in eq. 3.1. Since the radiative transfer calculations are time consuming there will be an effort to minimize the number of its computations. This is done by computing a radiative transfer spectrum at selected frequencies across the radiometer bandpass. The frequencies are selected such that brightness temperature for any frequency inside the radiometer bandpass can be accurately computed with interpolation. Each tangent pressure will have its own optimized spectral grid. This approach is more efficient than basing the gridding by channel, which was done in the UARS MLS forward model. The full band spectral computation was incorporated by Hugh Pumphrey [12] for the 183 GHz band in UARS MLS with very good results. The channel radiance for each height will be computed from

$$I\left(\mathbf{x}, \nu_{\mathrm{ch}}\right) = \frac{\int_{\nu_{\mathrm{lo}}}^{\infty} I\left(\mathbf{x}, \nu\right) \Phi\left(\nu_{\mathrm{ch}} - \nu\right) \mathrm{d}\nu}{\int_{\nu_{\mathrm{lo}}}^{\infty} \Phi\left(\nu_{\mathrm{ch}} - \nu\right) \mathrm{d}\nu} \tag{9.1}$$

There will be an analogous equation for the lower side-band (see eq. 3.1). The standard spectrometers which employ 25, 11 channel filter banks and wide-band channels having individually different responses will be integrated individually using a trapezoidal quadrature. The actual quadrature is not considered to be a critical issue since the frequency gridding of the radiative transfer calculation and the ability to interpolate in frequency is the accuracy-limiting aspect.

The digital autocorrelator spectrometers (DACS) consist of 129 channels having a $\Phi = \sin\left(\nu_{\mathrm{ch}} - \nu\right) / \left(\nu_{\mathrm{ch}} - \nu\right)$ shape preweighted by a bandpass filter. As a result of the large number of channels involved we evaluate the spectrally averaged result using the Fourier transform theorem of convolutions as is done with the antenna smearing evaluation. The DACS spectral integration is described in [15].

9.2 Derivatives

The forward model derivatives with respect to all the state vector elements need to be processed through the spectral averaging algorithms. The calculation is

$$\frac{\mathrm{d}I\left(\mathbf{x}, \nu_{\mathrm{ch}}\right)}{\mathrm{d}x_j} = \frac{\int_{\nu_{\mathrm{lo}}}^{\infty} \frac{\mathrm{d}I(\mathbf{x},\nu)}{\mathrm{d}x_j} \Phi\left(\nu_{\mathrm{ch}} - \nu\right) \mathrm{d}\nu}{\int_{\nu_{\mathrm{lo}}}^{\infty} \Phi\left(\nu_{\mathrm{ch}} - \nu\right) \mathrm{d}\nu} \tag{9.2}$$

None of the state vector quantities are expected to alter the channel filter shape so unlike the antenna averaging problem which required special differential forms, none are needed for spectral

averaging. The center frequency of the spectral channels may change during operations due to varying thermal environments. A first order correction for this effect can be done by shifting the molecular line position whose derivative forms are given in chapter 11.

Chapter 10. Radiance Calculation

The radiative transfer model described here is for the special case of local thermodynamic equilibrium without scattering and unpolarized radiation. The main emphasis is the rapid yet accurate calculation of derivatives that are needed by the inversion algorithm (Level 2). The basic mathematics has been described elsewhere [14], only a condensed discussion is given here.

10.1 Radiative Transfer Equation

The radiative transfer equation in local thermodynamic equilibrium through the atmosphere is a differential equation. It is converted to an integral equation and solved discretely with numerical quadratures. The notation used to designate levels and ray paths is shown in figure 10.1. The level indexing notation for the EOS MLS forward model is different and actually simpler than the UARS MLS case and takes advantage of the two dimensionality of the atmosphere. The atmosphere is partitioned into N concentric shells or levels. A ray path cuts through all the levels above the tangent level. The outermost level is 1 nearest the observer and each level is numbered consecutively to the tangent level t. The next level which initiates the ray on the atmospheric side opposite to the observer is $2N - t + 1$ and the levels are then numbered consecutively until the ray leaves the last level now on the far side of the observer, which is at $2N$. Note that level designations t and $2N - t + 1$ although indexically different point to the exact same spot in the atmosphere bounding a "zero-thickness" layer. The redundant designation actually makes the computer coding of the algorithm very simple and properly accounts for Earth surface emissions if the ray path reflects off the Earth. This is accomplished by choosing an appropriate value for the tangent level emission efficiency value Υ (= 1, for non Earth intersecting rays and is< 1, the Earth reflectivity coefficient otherwise). Since the state of the atmosphere on the right side is not the same as the left (except at t and $2N - t + 1$), as was assumed in UARS MLS, special indexing which took advantage of the symmetry is eliminated in this forward model and actually leads to simpler equations. However, the memory storage and some computations are twice as great. The boundaries in Figure 10.1 correspond to the PSIG ζ (without the extra quadrature points) described in chapter 5. Chapter 5 also provides the algorithm for computing ϕ, temperature and other profile quantities on the boundaries.

The radiative transfer equation (same as that used for UARS MLS but with different notation) is

$$I(\mathbf{x}) = \sum_{i=1}^{2N} \Delta B_i \mathcal{T}_i, \tag{10.1}$$

where ΔB_i is the source function in differential temperature format given by

$$\begin{aligned}
\Delta B_1 &= \frac{B_1 + B_2}{2}, \\
\Delta B_i &= \frac{B_{i+1} - B_{i-1}}{2}, \\
\Delta B_t &= \frac{B_{t+1} - B_{t-1}}{2}, \\
\Delta B_{2N-t+1} &= \frac{B_{2N-t+2} - B_{2N-t}}{2},
\end{aligned}$$

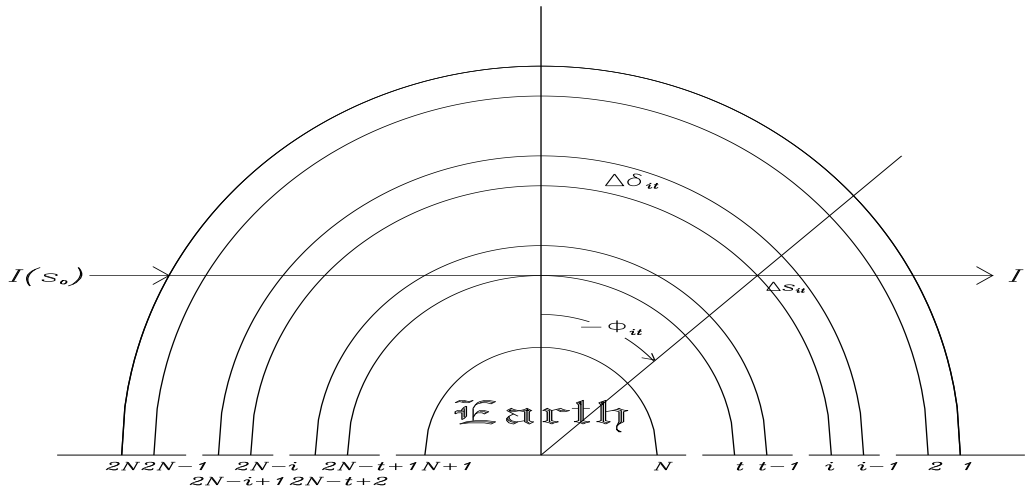

Figure 10.1: Level indexing notation for discrete radiative transfer calculations. Note that each line of sight path is associated with a tangent pressure, t, and a pressure/angle index, i. The atmospheric state including height can be different along an isobar curve (e.g. $i \rightarrow 2N - i$).

$$\begin{aligned} \Delta B_{2N-i+1} &= \frac{B_{2N-i+2} - B_{2N-i}}{2}, \\ \Delta B_{2N} &= I_o - \frac{B_{2N-1} + B_{2N}}{2}, \end{aligned} \tag{10.2}$$

where B is the thermal Planck radiation function

$$B_i = \frac{\mathsf{h}\nu}{\mathsf{k}\left(\exp\left\{\frac{\mathsf{h}\nu}{\mathsf{k}T_i}\right\} - 1\right)}. \tag{10.3}$$

where h is the Planck constant, k is the Boltzmann constant, ν is the radiation frequency and T_i is temperature at the ith level. $\mathcal{T}_i$ is the transmission function at the ith level. This is given by

$$\begin{aligned} \text{for } i &\leq t, \\ \mathcal{T}_1 &= 1, \\ \mathcal{T}_i &= \exp\left\{-\sum_{j=2}^{i} \Delta\delta_{j\rightarrow j-1}\right\}, \\ \text{for } t &< i < 2N - t + 1, \\ \mathcal{T}_i &= 0, \\ \text{for } i &= 2N - t + 1, \\ \mathcal{T}_{2N-t+1} &= \Upsilon\mathcal{T}_t, \\ \text{for } i &> 2N - t + 1, \\ \mathcal{T}_i &= \mathcal{T}_{2N-t+1} \exp\left\{-\sum_{j=2N-t+2}^{i} \Delta\delta_{j-1\rightarrow j}\right\}, \end{aligned} \tag{10.4}$$

where $\Delta\delta_{j\to j-1}$ is the incremental opacity integral between levels $j \to j-1$. The limits for the incremental opacity integral are reversed for $i > t$ to keep the lower limit closest to the tangent surface. Since in limb viewing it is very unlikely that the atmosphere is transmissive enough to see the surface, a sophisticated treatment of Earth reflection effects is not considered important.

There is sometimes confusion regarding how the differential temperature radiative transfer eq. 10.1 works in the vicinity of the tangent which we clarify now. Expanding eq. 10.1 and showing only the terms about $i = t$ gives

$$\begin{aligned} I(\mathbf{x}) &= \cdots + \Delta B_{t-1}\mathcal{T}_{t-1} + \Delta B_t\mathcal{T}_t + \Delta B_{t+1}\mathcal{T}_{t+1} + \Delta B_{t+2}\mathcal{T}_{t+2} + \cdots \\ &= \cdots + \frac{B_t - B_{t-2}}{2}\mathcal{T}_{t-1} + \frac{B_{t+1} - B_{t-1}}{2}\mathcal{T}_t + \frac{B_{t+2} - B_t}{2}\mathcal{T}_{t+1} + \frac{B_{t+3} - B_{t+1}}{2}\mathcal{T}_{t+2} + \cdots \end{aligned} \tag{10.5}$$

Recognize that index t and $t+1$ refer to the same point on the LOS path which requires $B_t = B_{t+1}$ and from eq 10.4, $\mathcal{T}_{t+1} = \Upsilon\mathcal{T}_t$. We will also set $\mathcal{T}_{t+2} = \Upsilon\mathcal{T}_t\Delta\mathcal{T}_{t+1\to t+2}$ where $\Delta\mathcal{T}_{t+1\to t+2} = \exp\{-\Delta\delta_{t+1\to t+2}\}$. Collecting all the terms that involve B_t and B_{t+1} gives

$$I(\mathbf{x}) = \cdots + \frac{B_t + B_{t-1}}{2}(\mathcal{T}_{t-1} - \mathcal{T}_t) + B_t(1-\Upsilon)\mathcal{T}_t + \frac{B_{t+1} + B_t}{2}\mathcal{T}_t\Upsilon(1 - \Delta\mathcal{T}_{t+1\to t+2}) + \cdots \tag{10.6}$$

The terms as arranged in this equation show that the linear average temperature in the layer is multiplied by the difference in the transmission function between the layer boundaries (first and third terms). The solution is exact if temperature is a linear in transmission. This result is consistent with the differential transmission form of the radiative transfer equation. The middle term contains the Earth reflectivity effect. If the LOS ray is above the Earth surface, then $\Upsilon = 1$ and the second term disappears. For Earth intersecting rays, $\Upsilon \neq 1$, the second term is the surface emission from the Earth attenuated by the atmospheric transmission, and the Earth intersecting part of the LOS is scaled by Earth reflectivity.

10.2 Radiative Transfer Derivative

The derivative form of eq. 10.1 is

$$\frac{\mathrm{d}I(\mathbf{x})}{\mathrm{d}x_k} = \sum_{i=1}^{2N} \mathcal{Q}_i\mathcal{T}_i, \tag{10.7}$$

where x_k is an element in state vector $(\mathbf{x})$. This is identical to eq. 10.1 except $\mathcal{Q}_i$ replaces ΔB_i and is given by

$$\mathcal{Q}_i = \frac{\partial\Delta B_i}{\partial x_k} - \Delta B_i\mathcal{W}_i, \tag{10.8}$$

where $\mathcal{W}_i$ is the transmittance derivative given by

$$\begin{aligned} \mathcal{W}_1 &= 0, \\ \text{for } i &\leq t, \\ \mathcal{W}_i &= \mathcal{W}_{i-1} + \frac{\partial\Delta\delta_{i\to i-1}}{\partial x_k}, \\ \text{for } t &< i < 2N - t + 1, \end{aligned}$$

$$\begin{aligned} \mathcal{W}_i &= 0, \\ \mathcal{W}_{2N-t+1} &= \mathcal{W}_t, \\ \text{for } i &> 2N-t+1, \\ \mathcal{W}_i &= \mathcal{W}_{i-1} + \frac{\partial \Delta\delta_{i-1\to i}}{\partial x_k}, \end{aligned} \tag{10.9}$$

where $\frac{\partial \Delta\delta_{i\to i-1}}{\partial x_k}$ is the layer opacity derivative with respect to state vector element x_k.

10.3 Opacity Integral

The opacity integral is given by

$$\Delta\delta_{i\to i-1} = \sum_{k=1}^{NS} \Delta\delta^k_{i\to i-1}, \tag{10.10}$$

which is a summation of each component opacity for each species. The representation basis functions are given by eq. 4.1 and eq. 4.2. The incremental opacity integral is

$$\begin{aligned} \Delta\delta^k_{i\to i-1} &= \frac{\Delta s^{\text{refr}}_{i\to i-1}}{\Delta s_{i\to i-1}} \int_{\zeta_i}^{\zeta_{i-1}} \mathsf{f}^k\left(\zeta, \phi\left(\zeta\right), \nu\right) \beta^k\left(P\left(\zeta\right), T\left(\zeta\right), \nu\right) \\ &\times \frac{\left(h\left(\zeta\right) + H^{\oplus}\left(\phi_t\right)\right)}{\sqrt{\left(h\left(\zeta\right) + H^{\oplus}\left(\phi_t\right)\right)^2 - \left(h\left(\zeta_t\right) + H^{\oplus}\left(\phi_t\right)\right)^2}} \\ &\times \frac{\left[h\left(\zeta\right) + \overset{\star}{R}_o\left(\phi\left(\zeta\right)\right) - R_o\left(\phi\left(\zeta\right)\right) + R^{\oplus}\left(\phi\left(\zeta\right)\right)\right]^2 T\left(\zeta\right) \mathsf{k} \ln 10}{g_o\left(\phi\left(\zeta\right)\right) \overset{\star}{R}^2_o\left(\phi\left(\zeta\right)\right) \mathcal{M}\left(\zeta\right)} \mathrm{d}\zeta, \end{aligned} \tag{10.11}$$

where f^k is either from eq. 4.1 or eq. 4.2 and $\beta\left(P\left(\zeta\right), T\left(\zeta\right), \nu\right)$ is the derivative of the species absorption coefficient with respect to volume mixing ratio or cross section for the kth species. ζ is the LOS path coordinate; it establishes h, and ϕ as described in chapter 4. The last two terms following the "$\times$" are $\frac{\mathrm{d}s}{\mathrm{d}h}\frac{\mathrm{d}h}{\mathrm{d}\zeta}$ respectively and are based on the geometric and hydrostatic models. The geometric model is based on the equivalent circular Earth and the hydrostatic model is based on a geocentric gravitational model and is the origin of the many different R's involved. Refraction causes a path lengthening effect relative to the straight-line path differences used here. This is compensated for by scaling the opacity integral by the ratio of the straight path length to the refracted one. Numerical experiments have shown this to be a completely satisfactory approximation. The path length ratio is given by

$$\frac{\Delta s^{\text{refr}}_{i\to i-1}}{\Delta s_{i\to i-1}} = \int_{\zeta_i}^{\zeta_{i-1}} \frac{\mathcal{N} H}{\sqrt{\mathcal{N}^2 H^2 - \mathcal{N}_t^2 H_t^2}} \frac{\mathrm{d}h}{\mathrm{d}\zeta} \mathrm{d}\zeta \Big/ \int_{\zeta_i}^{\zeta_{i-1}} \frac{\mathrm{d}s}{\mathrm{d}h}\frac{\mathrm{d}h}{\mathrm{d}\zeta} \mathrm{d}\zeta, \tag{10.12}$$

where $\mathcal{N}$ is the refractive index given in eq. 6.3. The derivation of eq. 10.12 is given in Appendix A. Another consideration is the effect of path lengthening on the ray traced ϕ. It is currently ignored but can be included by integrating eq. A.5. The statevector quantities such as temperature would be evaluated with the corrected ϕ. Note that ϕ_t is not affected and that the error (the horizontal component for evaluating state vector components) increases as the horizontal distance from the

tangent increases. *I do not know how large this error is. In future software upgrades, we will add the horizontal correction according to eq. A.5.*

These integrals are evaluated with a 3-point Gauss-Legendre quadrature based on pressure gridding. This is not as accurate as integrating in the path dimension s, partly because there is a singularity at the tangent point. A strategy that is quite effective is to replace the above integral with

$$\int_{\zeta_i}^{\zeta_{i-1}} G(\zeta) \frac{\mathrm{d}s}{\mathrm{d}h}\frac{\mathrm{d}h}{\mathrm{d}\zeta}\mathrm{d}\zeta = G(\zeta_i)\int_{\zeta_i}^{\zeta_{i-1}} \frac{\mathrm{d}s}{\mathrm{d}h}\frac{\mathrm{d}h}{\mathrm{d}\zeta}\mathrm{d}\zeta + \int_{\zeta_i}^{\zeta_{i-1}} [G(\zeta) - G(\zeta_i)] \frac{\mathrm{d}s}{\mathrm{d}h}\frac{\mathrm{d}h}{\mathrm{d}\zeta}\mathrm{d}\zeta, \qquad (10.13)$$

where $G(\zeta)$ contains a non-singular function. The first integral on the right of $=$ has a singularity but can be integrated analytically because it is the path length, $\Delta s_{i\rightarrow i-1}$. The second term right of $=$ still has a singularity but if the $G(\zeta) - G(\zeta_i)$ part is higher order than the path length derivative then a well behaved solution results. In this case G is proportional to β which is nearly exponential in ζ; the result is very well behaved and this trick provides a good solution. It is not quite as accurate as doing the integral in path length but there are some advantages to using a regular ζ grid, which include having the vertical breakpoints of representation basis functions coincide with the PSIG. A speed optimization strategy that is implemented is to compute the first integral right of the = in eq. 10.13 and evaluate the transmission function eq. 10.4. The path derivative of the $\mathcal{T}$ function is evaluated and based on a user supplied threshold, only that portion of the path where the derivative of $\mathcal{T}$ exceeds the threshold do we compute the second term right of the = in eq. 10.13. This saves 3 absorption coefficient evaluations for each PSIG point that is smaller than the threshold.

10.4 Opacity and Source Function Derivatives

The radiative transfer derivative in eq. 10.7 is a function of the opacity derivative and the differential temperature derivative (source function). For EOS MLS, this comes in three forms, mixing ratio, temperature, and β specific. These forms are given below

10.4.1 Mixing ratio

The derivative of the source function with respect to mixing ratio is zero so that term in eq. 10.8 vanishes. The opacity derivative with respect to mixing ratio using the linear basis is

$$\begin{aligned}\frac{\mathrm{d}\Delta\delta^k_{i\rightarrow i-1}}{\mathrm{d}f^k_{lmn}} &= \frac{\Delta s^{\mathrm{refr}}_{i\rightarrow i-1}}{\Delta s_{i\rightarrow i-1}}\int_{\zeta_i}^{\zeta_{i-1}} \eta^k_l(\zeta)\,\eta^k_m(\phi(\zeta))\,\eta^k_n(\nu) \\ &\times \beta^k(P(\zeta),T(\zeta),\nu)\frac{\mathrm{d}s}{\mathrm{d}h}\frac{\mathrm{d}h}{\mathrm{d}\zeta}\mathrm{d}\zeta. \qquad (10.14)\end{aligned}$$

It is worth noting that summing these integrals times the mixing ratio coeffient f^k_{lmn} over all four indices also gives the incremental opacity in eq. 10.10. The frequency dependence is retained because one of the species is likely to be *EXTINCTION* which will have $\beta^{\mathrm{ext}} \equiv 1$ but allows for spectral structure.

The opacity derivative with respect to mixing ratio using the logarithmic basis is

$$\frac{\mathrm{d}\Delta\delta^k_{i\rightarrow i-1}}{\mathrm{d}f^k_{lmn}} = \frac{\Delta s^{\mathrm{refr}}_{i\rightarrow i-1}}{\Delta s_{i\rightarrow i-1}}\int_{\zeta_i}^{\zeta_{i-1}} \frac{\eta^k_l(\zeta)\,\eta^k_m(\phi(\zeta))\,\eta^k_n(\nu)}{f^k_{lmn}}$$

$$\times \quad \mathsf{f}^k\left(\zeta,\phi\left(\zeta\right),\nu\right)\beta^k\left(P\left(\zeta\right),T\left(\zeta\right),\nu\right)\frac{\mathrm{d}s}{\mathrm{d}h}\frac{\mathrm{d}h}{\mathrm{d}\zeta}\mathrm{d}\zeta. \tag{10.15}$$

Note that $f^k_{lmn} > 0$ always; therefore this representation is not appropriate for weak and noisy products.

10.4.2 Temperature

The temperature derivative is quite complicated because the atmospheric absorption, hydrostatic model and the path length calculations depend on it. Some simplifying assumptions will be made to make this problem tractable. The sensitivity of these equations to the change in refraction due to temperature will be ignored and $\frac{\mathrm{d}h}{\mathrm{d}\zeta} = H^2\mathsf{k}T\ln 10/\left(g_oR_o^2\mathcal{M}\right)$ is assumed where H is in the equivalent circular Earth system. The path length derivative is $\frac{\mathrm{d}s}{\mathrm{d}h} = H/\sqrt{H^2-H_t^2}$. Since temperature is independent of frequency, the $\eta_n\left(\nu\right)$ representation basis will be dropped. The temperature derivative of the incremental opacity equation is

$$\begin{aligned}
&\frac{\mathrm{d}\Delta\delta^k_{i\to i-1}}{\mathrm{d}f^T_{lmn}} \approx \\
&\quad \frac{\Delta s^{\mathrm{refr}}_{i\to i-1}}{\Delta s_{i\to i-1}}\int_{\zeta_{i-1}}^{\zeta_i}\mathsf{f}^k\left(\zeta,\phi\left(\zeta\right),\nu\right)\frac{\mathrm{d}\beta^k\left(P\left(\zeta\right),T\left(\zeta\right),\nu\right)}{\mathrm{d}f^T_{lmn}}\frac{H^3}{\sqrt{H^2-H_t^2}}\frac{T\mathsf{k}\ln 10}{g_oR_o^2\mathcal{M}} \\
&+ \quad \mathsf{f}^k\left(\zeta,\phi\left(\zeta\right),\nu\right)\beta^k\left(P\left(\zeta\right),T\left(\zeta\right),\nu\right)\frac{T\mathsf{k}\ln 10}{g_oR_o^2\mathcal{M}}\frac{\mathrm{d}\left(H^3/\sqrt{H^2-H_t^2}\right)}{\mathrm{d}f^T_{lmn}} \\
&+ \quad \mathsf{f}^k\left(\zeta,\phi\left(\zeta\right),\nu\right)\beta^k\left(P\left(\zeta\right),T\left(\zeta\right),\nu\right)\frac{H^3}{\sqrt{H^2-H_t^2}}\frac{\mathrm{d}\left[T\mathsf{k}\ln 10/\left(g_oR_o^2\mathcal{M}\right)\right]}{\mathrm{d}f^T_{lmn}}\mathrm{d}\zeta.
\end{aligned} \tag{10.16}$$

A simplifying yet effective approximation is to assume $\beta^k = \overset{\star}{\beta}{}^k\left(T/\overset{\star}{T}\right)^{n^k}$, where $\overset{\star}{\beta}{}^k$ is the species k cross section evaluated at $\overset{\star}{T}$ and n^k is its temperature dependence. n^k is determined analytically by rationing the logarithm of βs computed at $\overset{\star}{T}\pm 10$. Substituting the empirical equation for β^k and expanding eq. 10.16 gives

$$\begin{aligned}
\frac{\mathrm{d}\Delta\delta^k_{i\to i-1}}{\mathrm{d}f^T_{lmn}} &= \frac{\Delta s^{\mathrm{refr}}_{i\to i-1}}{\Delta s_{i\to i-1}}\int_{\zeta_i}^{\zeta_{i-1}}\mathsf{f}^k\beta^k\frac{n^k\eta^T_l\left(\zeta\right)\eta^T_m\left(\phi\left(\zeta\right)\right)}{T}\frac{\mathrm{d}s}{\mathrm{d}h}\frac{\mathrm{d}h}{\mathrm{d}\zeta} \\
&+ \mathsf{f}^k\beta^k\frac{2H^2\frac{\mathrm{d}H}{\mathrm{d}f^T_{lm}}-3H_t^2\frac{\mathrm{d}H}{\mathrm{d}f^T_{lm}}+HH_t\frac{\mathrm{d}H_t}{\mathrm{d}f^T_{lm}}}{\left(H^2-H_t^2\right)^{\frac{3}{2}}}\frac{\mathrm{d}h}{\mathrm{d}\zeta} \\
&+ \mathsf{f}^k\beta^k\frac{\eta^T_l\left(\zeta\right)\eta^T_m\left(\phi\left(\zeta\right)\right)}{T}\frac{\mathrm{d}s}{\mathrm{d}h}\frac{\mathrm{d}h}{\mathrm{d}\zeta}\mathrm{d}\zeta.
\end{aligned} \tag{10.17}$$

The first term in eq. 10.17 is the temperature sensitivity due to the cross section and the second two terms are the temperature sensitivity to changes in the radiative transfer geometry that are brought about due to the hydrostatic relationship. Now it would seem quite natural to combine the first and third terms and integrate but there is a strategic reason for not doing this. These equations,

like eq. 10.11 have a singularity that can be taken out by performing the integration according to eq. 10.13. When that approach is used on the second two terms right of the $=$, the integral

$$\frac{\Delta s^{\text{refr}}_{i\to i-1}}{\Delta s_{i\to i-1}}\mathsf{f}^k_i\beta^k_i\int_{\zeta_{i-1}}^{\zeta_i}\frac{\mathrm{d}\frac{\mathrm{d}s}{\mathrm{d}h}\frac{\mathrm{d}h}{\mathrm{d}\zeta}}{\mathrm{d}T_{lm}}\mathrm{d}\zeta = \frac{\Delta s^{\text{refr}}_{i\to i-1}}{\Delta s_{i\to i-1}}\mathsf{f}^k_i\beta^k_i\left(\frac{H_i\frac{\mathrm{d}H_i}{\mathrm{d}T_{lm}}-H_t\frac{\mathrm{d}H_t}{\mathrm{d}T_{lm}}}{\sqrt{H_i^2-H_t^2}}-\frac{H_{i-1}\frac{\mathrm{d}H_{i-1}}{\mathrm{d}T_{lm}}-H_t\frac{\mathrm{d}H_t}{\mathrm{d}T_{lm}}}{\sqrt{H_{i-1}^2-H_t^2}}\right), \tag{10.18}$$

where H_i is the height (including the equivalent earth radius) at level i, is added and subtracted to both sides of eq. 10.17. When this is done, $\mathsf{f}^k_i\beta^k_i$ is subtracted from the integrand in the second two terms right of the $=$ in eq. 10.17 and integrated. *Do not use this and combine terms 1 and 3 or the wrong answer will be achieved.* The first term right of the $=$ is integrated like eq. 10.11.

The forward model currently computes $\frac{\mathrm{d}\beta^k}{\mathrm{d}T}$ analytically. Although more complicated, this enhancement is more accurate and faster to compute. Therefore we replace $\frac{\mathrm{d}\beta^k}{\mathrm{d}T}=n^k\beta^k/T$ which appears in the first term right of $=$ in eq. 10.17. The difference of temperature derivatives computed with the power law approximation as described following eq. 10.16 and the full analytical derivative $\frac{\mathrm{d}\beta^k}{\mathrm{d}T}$ is less than 1% showing that the power law is a good approximation. The error caused by the approximations mentioned here based on comparison with finite difference derivatives are better than 10%.

The source function derivative $\frac{\mathrm{d}\Delta B_i}{\mathrm{d}T_{lm}}$ for temperature is

$$\begin{aligned}\frac{\mathrm{d}\Delta B_i}{\mathrm{d}T_{lm}} &= \frac{\frac{\mathrm{d}B_{i+1}}{\mathrm{d}T_{lm}}-\frac{\mathrm{d}B_{i-1}}{\mathrm{d}T_{lm}}}{2}, \text{where,}\\ \frac{\mathrm{d}B_i}{\mathrm{d}T_{lm}} &= \frac{B_i^2\exp\left\{\frac{\mathsf{h}\nu}{\mathsf{k}T_i}\right\}}{T_i^2}\eta_l^T\left(\zeta_i\right)\eta_m^T\left(\phi\left(\zeta_i\right)\right).\end{aligned} \tag{10.19}$$

10.4.3 β derivatives

There is a class of derivatives that only affect β^k which are generally spectrosopically based and these are given by

$$\frac{\mathrm{d}\Delta\delta^k_{i\to i-1}}{\mathrm{d}x_j}=\frac{\Delta s^{\text{refr}}_{i\to i-1}}{\Delta s_{i\to i-1}}\int_{\zeta_i}^{\zeta_{i-1}}\mathsf{f}^k\frac{\mathrm{d}\beta^k}{\mathrm{d}x_j}\frac{\mathrm{d}s}{\mathrm{d}h}\frac{\mathrm{d}h}{\mathrm{d}\zeta}\mathrm{d}\zeta. \tag{10.20}$$

This is identical to the opacity integral (eq. 10.11) where β^k is replaced with $\frac{\mathrm{d}\beta^k}{\mathrm{d}x_j}$; it is evaluated accordingly. When the singularity separation is done, the differential term which now involves $\frac{\mathrm{d}\beta^k}{\mathrm{d}x_j}$ must go to zero faster than the singularity. Given that β behaves exponentially and satisfies the condition, the derivative will behave exponentially and should satisfy the condition also.

Chapter 11. Absorption Coefficient Calculations

This chapter describes the basic absorption cross-section calculation defined here as the derivative of the absorption coefficient with respect to concentration (in volume mixing ratio), or β^k used in the radiative transfer calculations. The algorithm for computing $\mathrm{d}\beta^k/\mathrm{d}X$ where X is temperature or a spectroscopic parameter such as line width is also presented.

11.1 Line Cross-section Theory

The cross-section β^k for the kth species is given by

$$\beta^k = \mathcal{R}^k \sqrt{\frac{\ln 2}{\pi}} \frac{10^{-13}}{\mathsf{k}} P \left[\sum_j 10^{\mathcal{S}_j^k} \mathrm{LineShape}\left(x_j^k(\nu), y_j^k(\nu), z_j^k(\nu) \right) \right] / \left(T w_d^k \right), \tag{11.1}$$

where

$$\begin{aligned} \mathcal{S}_j^k &= \mathcal{I}_j^k(300) + \frac{\mathsf{hc} E\ell_j^k}{\mathsf{k}} \left(\frac{1}{300} - \frac{1}{T} \right) \\ &+ \log \left[\frac{Q^k(300) \tanh\left\{ \mathsf{h}\nu / (2\mathsf{k}T) \right\} \left(1 + \exp\left\{ -\mathsf{h}\nu_j^k / (\mathsf{k}T) \right\} \right)}{Q^k(T) \left(1 - \exp\left\{ -\mathsf{h}\nu_{0j}^k / (\mathsf{k}300) \right\} \right)} \right], \end{aligned} \tag{11.2}$$

T is temperature in Kelvins, P is pressure in hPa, $\mathcal{R}^k$ is the isotopic fraction for the species, $\mathcal{I}_j^k(300)$ is the logarithm of the integrated intensity in nm^{2}MHz at 300 K, ν_j^k is the pressure shifted line center frequency in MHz, ν_{0j}^k is the non-pressure shifted line center frequency in MHz, $E\ell_j^k$ is the ground state energy in cm^{-1}, $Q^k(T)$ is the partition function, $w_d^k = \sqrt{2\ln 2\mathsf{k}}\,\nu\sqrt{\frac{T}{\mathcal{M}^k}}/\mathsf{c}$ is the Doppler width in MHz, $\mathcal{M}^k$ is the absorber molecular mass in amu, c is the speed-of-light, $\sqrt{\frac{\ln 2}{\pi}}\frac{10^{-13}}{\mathsf{k}}$ = 3.402136078 $\times 10^9$ K hPa^{-1}nm^{-2}km^{-1}, is proportional to the reciprocal Boltzmann constant, k in JK^{-1}, LineShape$\left(x_j^k(\nu), y_j^k(\nu), z_j^k(\nu) \right)$ is the lineshape function and j identifies the individual lines in the molecule. The constants, $\sqrt{2\ln 2\mathsf{k}}/\mathsf{c} = 3.58117369 \times 10^{-7}$ AMU$^{\frac{1}{2}}$T$^{-\frac{1}{2}}$, $\mathsf{k}/\mathsf{hc} = 1.600386$ cm^{-1}K^{-1}, $\mathsf{k}/\mathsf{h} = 20836.74$ MHz K^{-1}. The temperature dependence of the logarithm of the ratio of the partition function at 300K to T is approximated by

$$\log\left[\frac{Q^k(300)}{Q^k(T)} \right] = \log\left[\frac{Q^k(300)}{Q^k(T_0)} \right] + \frac{\log\left[\frac{Q^k(T_1)}{Q^k(T_0)} \right]}{\log\left[\frac{T_1}{T_0} \right]} \log\left[\frac{T_0}{T} \right]. \tag{11.3}$$

where $Q^k(T_1)$ and $Q^k(T_0)$ are tabulated partition functions at temperatures T_1 and T_0, which are, preferably, greater than and less than T (or vice-versa), respectively, and $Q^k(300)$ is the partition function evaluated at 300K. The partition function includes all the rotational, vibrational, and electronic states. The partition function for EOS MLS calculations is tabulated at 300, 225, and 150K.

The LineShape function is

$$\text{LineShape}\left(x_j^k(\nu), y_j^k(\nu), z_j^k(\nu)\right) = \left(\frac{\nu}{\nu_{0j}^k}\right)\left\{\frac{1}{\pi}\int_{-\infty}^{\infty}\frac{\left[y_j^k(\nu) - Y_j^k\left(x_j^k(\nu)-t\right)\right]\exp\{-t^2\}}{\left(y_j^k(\nu)\right)^2+\left(x_j^k(\nu)-t\right)^2}\mathrm{d}t + \frac{1}{\sqrt{\pi}}\frac{y_j^k(\nu) - Y_j^k z_j^k(\nu)}{\left(z_j^k(\nu)\right)^2+\left(y_j^k(\nu)\right)^2}\right\}, \tag{11.4}$$

where $x_j^k(\nu) = \frac{\sqrt{\ln 2}\left(\nu-\nu_j'^k\right)}{w_d^k}$, $y_j^k(\nu) = \frac{\sqrt{\ln 2}w_{cj}^k P}{w_d^k}\left(\frac{300}{T}\right)^{n_{cj}^k}$, $z_j^k(\nu) = \frac{\sqrt{\ln 2}\left(\nu+\nu_j'^k\right)}{w_d^k}$, w_{cj}^k is the collision width in MHz hPa^{-1} at 300 Kelvins, n_{cj}^k is its temperature dependence, Y_j^k is an intramolecular line interference coefficient, ν_j^k is the line position frequency in MHz, and ν is the radiation frequency in MHz. The $\left(\frac{\nu}{\nu_{0j}^k}\right)$ term, which is virtually constant over a Doppler width, has been pulled outside the integral. The integral is related to the Fadeeva function (eq. 7.1.4 in [1]). The numerator of the integrand with $y_j^k(\nu)$ is a Voigt function (real part of the Fadeeva function). The numerator of the integrand with $y_j^k(\nu)$ is the imaginary part of the Fadeeva function. The Fadeeva function is evaluated according to [16]. The line center frequency is pressure shifted and Doppler shifted according to

$$\begin{aligned}
\nu_j^k &= \left[\nu_{0j}^k + \Delta\nu_{0j}^k P\left(\frac{300}{T}\right)^{n_{\Delta\nu_{0j}^k}}\right], \\
\nu_j'^k &= \nu_j^k v_c, \\
v_c &= 1 + \left[\vec{v}\,(\mathbf{ACF})^t\right]_z/\mathsf{c},
\end{aligned} \tag{11.5}$$

where ν_{0j}^k is the unshifted rest line center frequency in MHz, v_c is the Doppler shift of the line position due to the z-axis component of the spacecraft and Earth velocities, $\vec{v}$, in the IFOVP frame (see text following eq. C.3). $\Delta\nu_{0j}^k$ is the pressure shift parameter in MHz hPa^{-1}, and $n_{\Delta\nu_{0j}^k}$ is its temperature dependence. The temperature dependence of the shift is often not known for the few cases where the shift is measured. In those cases we use $n_{\Delta\nu_{0j}^k} = \left(1+6n_{cj}^k\right)/4$ based on a theory developed by [11]. The interference coefficient is parameterized according to

$$Y_j^k = P\left[\delta_j^k\left(\frac{300}{T}\right)^{n_{\delta j}^k} + \gamma_j^k\left(\frac{300}{T}\right)^{n_{\gamma j}^k}\right]; \tag{11.6}$$

at this it time applies only to O_2 [7] and is zero otherwise.

The isotopic fraction $\mathcal{R}^k$ allows the user to input a volume mixing ratio for the total molecule yet have the computed radiances adjusted accordingly. The software implements a feature that allows the user to combine a number of molecules and treat the combination as one. The feature allows one to combine the most abundant isotope with its excited vibrational states, and lesser abundant isotopic components of the same molecule. The combined β^k is simply a sum over the individual β^k's of the combined species, times their isotopic fractions $\mathcal{R}^k$. The software can also be run where the isotopic fraction is ignored, that is, $\mathcal{R}^k = 1$. The two options are necessary because for some molecules (e.g. H_2O), the isotopic fractions in the upper atmosphere differ significantly from that found at the Earth's surface.

11.2 Storage and Calculation

The parameters needed to evaluate eq. 11.1 are given in chapter 12. Initially it was thought that evaluating eq. 11.1 over several pressures, temperatures and frequencies and using a look-up table would be the most efficient and fastest computational technique, however it has been found that for molecules having fewer than 4 lines per radiometer sideband, it is faster to apply eq. 11.1 directly. Therefore an elaborate method of storing and accessing data described in earlier versions of this document are no longer being implemented. To facilitate the speed, we have used a special modified Voigt evaluation method based on [16].

11.3 Temperature Derivative

The temperature derivative of eq. 11.1 is expanded as follows. First we write eq. 11.1 as

$$\begin{aligned}\beta^k &= \sum_j \beta_j^k \\ \beta_j^k &= \mathcal{S}_j'^k \tanh\left\{\frac{\mathsf{h}\nu}{2\mathsf{k}T}\right\} \text{LineShape}\left(x_j^k(\nu), y_j^k(\nu), z_j^k(\nu)\right) \end{aligned} \tag{11.7}$$

where,

$$\mathcal{S}_j'^k = \sqrt{\frac{\ln 2}{\pi}} \frac{\mathcal{R}^k 10^{-13} P}{\mathsf{k}T w_d^k} \frac{\left(1+\exp\left\{-\mathsf{h}\nu_j^k/(\mathsf{k}T)\right\}\right)}{\left(1-\exp\left\{-\mathsf{h}\nu_{0j}^k/(\mathsf{k}300)\right\}\right)} 10^{\mathcal{I}_j^k(300)+\frac{\mathsf{h}E\ell_j^k}{\mathsf{k}}\left(\frac{1}{300}-\frac{1}{T}\right)+\log\left\{Q^k(300)/Q^k(T)\right\}}.$$

The temperature derivative is

$$\begin{aligned}\frac{\mathrm{d}\beta_j^k}{\mathrm{d}T} &= \frac{\mathrm{d}\mathcal{S}_j^{k\prime}}{\mathrm{d}T}\tanh\left\{\frac{\mathsf{h}\nu}{2\mathsf{k}T}\right\}\text{LineShape}\left(x_j^k(\nu), y_j^k(\nu), z_j^k(\nu)\right) \\ &+ \mathcal{S}_j^{k\prime}\frac{\mathrm{d}\tanh\left\{\frac{\mathsf{h}\nu}{2\mathsf{k}T}\right\}}{\mathrm{d}T}\text{LineShape}\left(x_j^k(\nu), y_j^k(\nu), z_j^k(\nu)\right) \\ &+ \mathcal{S}_j^{k\prime}\tanh\left\{\frac{\mathsf{h}\nu}{2\mathsf{k}T}\right\}\frac{\mathrm{d}\text{LineShape}\left(x_j^k(\nu), y_j^k(\nu), z_j^k(\nu)\right)}{\mathrm{d}T}. \end{aligned} \tag{11.8}$$

where

$$\begin{aligned}\frac{\mathrm{d}\mathcal{S}_j^{k\prime}}{\mathrm{d}T} &= -\mathcal{S}_j^{k\prime}\left\{\frac{3}{2T}\right. \\ &+ \frac{\mathsf{h}\exp\left\{-\mathsf{h}\nu_j^k/(\mathsf{k}T)\right\}\left[\nu_{0j}^k v_c n_{\Delta\nu_{0j}}^k - \nu_j^k\left(n_{\Delta\nu_{0j}^k}+1\right)\right]}{\mathsf{k}T^2\left(1+\exp\left\{-\mathsf{h}\nu_j^k/(\mathsf{k}T)\right\}\right)} \\ &- \left.\frac{\ln 10\,\mathsf{h}E\ell_j^k}{\mathsf{k}T^2} + \frac{\log\left[\frac{Q^k(T_1)}{Q^k(T_0)}\right]}{T\log\left[\frac{T_1}{T_0}\right]}\right\}, \\ \frac{\mathrm{d}\tanh\left\{\frac{\mathsf{h}\nu}{2\mathsf{k}T}\right\}}{\mathrm{d}T} &= \frac{\mathsf{h}\nu}{2\mathsf{k}T^2}\left(\tanh^2\left\{\frac{\mathsf{h}\nu}{2\mathsf{k}T}\right\}-1\right), \text{and} \end{aligned}$$

$$\begin{aligned}
\frac{\mathrm{dLineShape}\left(x_j^k(\nu), y_j^k(\nu), z_j^k(\nu)\right)}{\mathrm{d}T} &= \frac{\mathrm{d}\mathcal{U}\left(x_j^k(\nu), y_j^k(\nu)\right)}{\mathrm{d}x_j^k(\nu)}\frac{\mathrm{d}x_j^k(\nu)}{\mathrm{d}T} \\
&+ \frac{\mathrm{d}\mathcal{U}\left(x_j^k(\nu), y_j^k(\nu)\right)}{\mathrm{d}y_j}\frac{\mathrm{d}y_j^k(\nu)}{\mathrm{d}T} - \mathcal{V}\left(x_j^k(\nu), y_j^k(\nu)\right)\frac{\mathrm{d}Y_j^k}{\mathrm{d}T} \\
&- Y_j^k\frac{\mathrm{d}\mathcal{V}\left(x_j^k(\nu), y_j^k(\nu)\right)}{\mathrm{d}x_j^k(\nu)}\frac{\mathrm{d}x_j^k(\nu)}{\mathrm{d}T} - Y_j^k\frac{\mathrm{d}\mathcal{V}\left(x_j^k(\nu), y_j^k(\nu)\right)}{\mathrm{d}y_j^k(\nu)}\frac{\mathrm{d}y_j^k(\nu)}{\mathrm{d}T} \\
&+ \frac{\left[\left(z_j^k(\nu)\right)^2 + \left(y_j^k(\nu)\right)^2\right]\left(\frac{\mathrm{d}y_j^k(\nu)}{\mathrm{d}T} - \frac{\mathrm{d}Y_j^k}{\mathrm{d}T}z_j^k(\nu) - Y_j^k\frac{\mathrm{d}z_j}{\mathrm{d}T}\right)}{\sqrt{\pi}\left[\left(z_j^k(\nu)\right)^2 + \left(y_j^k(\nu)\right)^2\right]^2} \\
&- \frac{2\left(z_j^k(\nu)\frac{\mathrm{d}z_j^k(\nu)}{\mathrm{d}T} + y_j^k(\nu)\frac{\mathrm{d}y_j^k(\nu)}{\mathrm{d}T}\right)\left(y_j^k(\nu) - Y_j^k z_j^k(\nu)\right)}{\sqrt{\pi}\left[\left(z_j^k(\nu)\right)^2 + \left(y_j^k(\nu)\right)^2\right]^2},
\end{aligned}$$

$\mathcal{U}\left(x_j^k(\nu), y_j^k(\nu)\right)$ and $\mathcal{V}\left(x_j^k(\nu), y_j^k(\nu)\right)$ are the real and imaginary parts of the Fadeeva function. The derivatives of the Fadeeva function are: $\frac{\partial\mathcal{U}\left(x_j^k(\nu), y_j^k(\nu)\right)}{\partial x_j^k(\nu)} = \frac{\partial\mathcal{V}\left(x_j^k(\nu), y_j^k(\nu)\right)}{\partial y_j^k(\nu)} = 2\mathcal{V}\left(x_j^k(\nu), y_j^k(\nu)\right)y_j^k(\nu) - 2\mathcal{U}\left(x_j^k(\nu), y_j^k(\nu)\right)x_j^k(\nu)$, and $\frac{\partial\mathcal{U}\left(x_j^k(\nu), y_j^k(\nu)\right)}{\partial y_j^k(\nu)} = -\frac{\partial\mathcal{V}\left(x_j^k(\nu), y_j^k(\nu)\right)}{\partial x_j^k(\nu)} = 2\mathcal{V}\left(x_j^k(\nu), y_j^k(\nu)\right)x_j^k(\nu) + 2\mathcal{U}\left(x_j^k(\nu), y_j^k(\nu)\right)y_j^k(\nu) - 2/\sqrt{\pi}$ [1]. The temperature derivatives of $x_j^k(\nu)$, $y_j^k(\nu)$, $y_j^k(\nu)$, and ν_j^k are:

$$\begin{aligned}
\frac{\mathrm{d}\nu_j^k}{\mathrm{d}T} &= \frac{\left(\nu_{0j}^k v_c - \nu_j^k\right)n_{\Delta\nu_{0j}}^k}{T} \\
\frac{\mathrm{d}x_j^k(\nu)}{\mathrm{d}T} &= -\frac{x_j^k(\nu)}{2T} - \frac{\sqrt{\ln 2}\left(\nu_{0j}^k v_c - \nu_j\right)n_{\Delta\nu_{0j}}^k}{Tw_d^k} \\
\frac{\mathrm{d}y_j^k(\nu)}{\mathrm{d}T} &= -\frac{y_j^k(\nu)\left(n_{cj}^k + \frac{1}{2}\right)}{T} \\
\frac{\mathrm{d}Y_j^k}{\mathrm{d}T} &= -P\left(\frac{n_{\delta j}^k\delta_j^k}{T}\left(\frac{300}{T}\right)^{n_{\delta j}^k} + \frac{n_{\gamma j}^k\gamma_j^k}{T}\left(\frac{300}{T}\right)^{n_{\gamma j}^k}\right)
\end{aligned} \tag{11.9}$$

Despite its complexity, computing the temperature derivative of β directly will be faster than using the empirical temperature power function, $\beta^k = \overset{\star}{\beta}^k\left(T/\overset{\star}{T}\right)^{n^k}$ in eq. 10.17, because most of the time consuming exponential and Voigt function evaluations have been done while computing β^k whereas computing the n^k requires two additional β^k evaluations.

11.4 Spectral Derivatives

The EOS forward model will supply radiance sensitivities to w_c^k, n_c^k, and ν_j^k. The ν_j^k derivative can be used to study or correct for pressure shifts, filter shifts, and even atmospheric winds. The

derivative computations will take advantage of the following assumptions in order to simplify the calculations:

1. Ignore contributions from the image frequency $z_j^k(\nu)$ term.
2. Ignore anything involving the Van-Vleck Weiskopf Lorentz lineshape correction $\left(\frac{\nu}{\nu_{0j}^k}\right)$. This is exact because the ν_{0j}^k dependence is canceled by one in $10^{\mathcal{I}_j^k}$.
3. Ignore anything involving the interference term Y_j^k.
4. Ignore anything involving the $\mathcal{S}_j^k$ term. *The goodness of this needs to be checked!*

Accordingly for purposes of derivative calculations, β^k is approximately

$$\beta^k \approx 3.4 \times 10^9 \mathcal{R}^k P \sum_j 10^{\mathcal{S}_j^k} \mathcal{U}\left(x_j^k(\nu), y_j^k(\nu)\right). \tag{11.10}$$

Taking the derivative of eq. 11.10 with respect to X and incorporating the assumptions above gives

$$\frac{\mathrm{d}\beta^k}{\mathrm{d}X} \approx 3.4 \times 10^9 \mathcal{R}^k P \sum_j 10^{\mathcal{S}_j^k} \left(\frac{\partial \mathcal{U}\left(x_j^k(\nu), y_j^k(\nu)\right)}{\partial x_j^k(\nu)} \frac{\mathrm{d}x_j^k(\nu)}{\mathrm{d}X} + \frac{\partial \mathcal{U}\left(x_j^k(\nu), y_j^k(\nu)\right)}{\partial y_j^k(\nu)} \frac{\mathrm{d}y_j^k(\nu)}{\mathrm{d}X} \right) \tag{11.11}$$

The remaining terms are easy to evaluate depending on whether X = w_{cj}^k, n_{cj}^k, and ν_j^k.

$$\begin{array}{ccccc} X & = & w_{cj}^k & n_{cj}^k & \nu_j^k \\ \frac{\partial x_j^k(\nu)}{\partial X} & = & 0 & 0 & -\frac{\sqrt{\ln 2}}{w_d^k} \\ \frac{\partial y_j^k(\nu)}{\partial X} & = & \frac{y_j^k(\nu)}{w_c^k} & y_j^k(\nu) \ln\left(\frac{300}{T}\right) & 0 \end{array} \tag{11.12}$$

All j lines for a given parameter X are computed together. This is done so that only one file per molecule per EOS band is created; however, one will not be able to fit individual line parameters for a given molecule within an EOS band.

Chapter 12. Spectroscopy

The molecules and their line-by-line spectroscopic parameters are presented. Table 12.1 gives parameters that are specific for each molecule, such as the partition function. Table 12.2 has the line-by-line data base for each molecule. Table 12.3 lists the lines of molecules to be included by band. In addition to the line spectrum, each band includes continuum emissions from EXTINCTION, N_2, H_2O and O_2. The continuum parameters are given in Table 12.1. Except for EXTINCTION, N_2, and O_2, the continuum parametrization is given by

$$\beta^k_{\rm cont} = {\rm cont\_1}^k \nu^2 P^2 \left(300/T\right)^{{\rm cont\_2}^k}, \tag{12.1}$$

where subscript $\rm cont$ implies that species k may have a line-by-line contribution that must be added to the cross section above to yield the total cross section. Eq. 12.1 is the continuum due to collisions in dry air, therefore in the case of H_2O, the self-absorption (which has different parameters and scales by $\left(\mathbf{f}^{H_2O}\right)^2$ is ignored). The continuum function for EXTINCTION is

$$\beta^{\rm EXTINCTION} = {\rm cont\_1}^{\rm EXTINCTION}, \tag{12.2}$$

Where ${\rm cont\_1}^{\rm EXTINCTION}$ is in $\rm km^{-1}$ and $\beta^{\rm EXTINCTION}$ is the total cross section. The N_2 cross section is parameterized according to [19]

$$\begin{aligned} \beta^{N_2} &= P^2\nu^2 \left(300/T\right)^{{\rm cont\_2}^{N_2}} \left[{\rm cont\_1}^{N_2} \exp\left\{-{\rm cont\_3}^{\rm N_2}\nu^2\left(\frac{300}{T}\right)\right\}\right. \\ &+ \left. {\rm cont\_4}^{\rm N_2} \exp\left\{-{\rm cont\_5}^{\rm N_2}\nu^2\left(\frac{300}{T}\right)\right\}\left(\left\{{\rm cont\_6}^{N_2}\right\}^2 + \nu^2\right)\right]. \end{aligned} \tag{12.3}$$

Eq 12.3 is an empirical function which fits the N_2 Collision Induced Absorption (CIA) spectrum from 0–3 THz. The N_2 absorption coefficient is $\left(\mathbf{f}^{N_2}\right)^2 \beta^{N_2}$ where $\mathbf{f}^{N_2} = 0.79$. Pardo [10] has found that in the atmosphere, dry absorption due to N_2–N_2, N_2–O_2, O_2–N_2, and O_2–O_2 pairs can be adequately fitted by multiplying eq. 12.3 by 0.81 = (1.29×0.79^2). The continuum parameterization for O_2 is the Debye spectrum according to [6]

$$\beta^{\rm O_2}_{\rm cont} = \frac{{\rm cont\_1}^{\rm O_2}\nu^2 P^2 \left(300/T\right)^{{\rm cont\_2}^{\rm O_2}}}{\nu^2 + \left({\rm cont\_3}^{\rm O_2} P \left(300/T\right)^{{\rm cont\_4}^{\rm O_2}}\right)^2}. \tag{12.4}$$

The Debye continuum absorption coefficient is $\mathbf{f}^{O_2} \times \beta^{\rm O_2}_{\rm cont}$. Eq. 12.4 must be added to the line by line contribution for O_2 to yield the total cross section for O_2.

The water vapor continuum consists of two parts. The first part which is under the H_2O heading in Table 12.1 is excess water vapor absorption (divided by $\mathbf{f}^{H_2O}$, self absorption effects are neglected) after performing a full line by line calculation up to 4 THz. The total absorption is based on laboratory measurements from DeLucia and Meshkov [personal communication, 2003]. For rapid computation of the cross section, for any individual radiometer we only include a small subset of H_2O lines in the line by line computation and approximate the contribution of the neglected lines with a secondary continuum contribution which is radiometer dependent. This continuum cross-section which is to be added to the total H_2O cross-section calculation is listed under the molecule name H_2O-rX (X = 1a, 1b, 2, 3, 4, 5h, 5v).

12.1 Temperature Derivative

The temperature derivative of the species cross section will need to have the temperature derivative of the continuum added to them. We give the temperature derivatives of the various continuum functions considered here.

$$\frac{\mathrm{d}\beta^k_{\mathrm{cont}}}{\mathrm{d}T} = -\beta^k_{\mathrm{cont}}\frac{\mathrm{cont\_2}^k}{T} \tag{12.5}$$

$$\frac{\mathrm{d}\beta^{\mathrm{EXTINCTION}}}{\mathrm{d}T} = 0 \tag{12.6}$$

$$\begin{aligned}\frac{\mathrm{d}\beta^{N_2}}{\mathrm{d}T} = \frac{1}{T}\Big[&-\beta^{N_2}\mathrm{cont\_2}^{N_2} \\ &+ P^2\nu^4\left(300/T\right)^{\mathrm{cont\_2}^{N_2}+1}\Big(\mathrm{cont\_1}^{N_2}\ \mathrm{cont\_3}^{N_2}\exp\left\{-\mathrm{cont\_3}^{N_2}\nu^2\left(300/T\right)\right\} \\ &+ \mathrm{cont\_4}^{N_2}\ \mathrm{cont\_5}^{N_2}\left(\left\{\mathrm{cont\_6}^{N_2}\right\}^2+\nu^2\right)\exp\left\{-\mathrm{cont\_5}^{N_2}\nu^2\left(300/T\right)\right\}\Big)\Big]\end{aligned} \tag{12.7}$$

$$\frac{\mathrm{d}\beta^{\mathrm{O_2}}_{\mathrm{cont}}}{\mathrm{d}T} = \frac{\beta^{\mathrm{O_2}}_{\mathrm{cont}}}{T}\left(\frac{2\ \mathrm{cont\_4}^{\mathrm{O_2}}\left(\mathrm{cont\_3}^{\mathrm{O_2}}P\left(300/T\right)^{\mathrm{cont\_4}^{\mathrm{O_2}}}\right)^2}{\nu^2+\left(\mathrm{cont\_3}^{\mathrm{O_2}}P\left(300/T\right)^{\mathrm{cont\_4}^{\mathrm{O_2}}}\right)^2}-\mathrm{cont\_2}^{\mathrm{O_2}}\right) \tag{12.8}$$

12.2 Line Selection

The line selection is performed by automatic data base maintenance programs which search the JPL and HITRAN catalogues for lines based on strength thresholds and frequency windows. The programs that do this job are described in appendix F. The target strength sensitivity thresholds for the pre-launch version of EOS MLS bands are using the "Initial" values in table F.1. As of now, CPU processing time for Level 2 prevents us from being more ambitious at this time.

12.3 Spectroscopy Tables for UARS and EOS MLS

These tables are generated from the actual database tables that are under CVS software management control. The reader should always compare the CVS version tag given at the foot of each table to that which is currently in the MLSPGS database for the heritage of data herein. The units in Table 12.1 are for eq. 12.1 and eq. 12.3. The units for $\mathrm{cont\_1}^{\mathrm{O_2}}$ in eq. 12.4 is $\mathrm{hPa}^{-2}\mathrm{km}^{-1}$ and $\mathrm{cont\_3}^{\mathrm{O_2}}$ is hPa^{-1}.

Table 12.1: Spectroscopy data base for MLS signals.

molecule, k	isotopic abundance $\mathcal{R}^k$	mass $\mathcal{M}^k$ AMU	Partition Function Q^K at 300 K	225 K	150 K	cont_1^k ($\mathrm{km^{-1}hPa^{-2}MHz^{-2}}$)	cont_2^k	cont_3^k ($\mathrm{MHz^{-2}}$)	cont_4^k ($\mathrm{km^{-1}hPa^{-1}MHz^{-4}}$)	cont_5^k ($\mathrm{MHz^{-2}}$)	cont_6^k MHz
^{79}BrO	0.5042	94.913	4063.505	2961.240	1951.762	0.000	0.0	0.000	0.000	0.000	0.000
^{79}BrO(ν_1)	0.5042	94.913	4063.505	2961.240	1951.762	0.000	0.0	0.000	0.000	0.000	0.000
^{81}BrO	0.4934	96.911	4081.5688	2973.5390	1959.8684	0.000	0.0	0.000	0.000	0.000	0.000
^{81}BrO(ν_1)	0.4934	96.911	4081.5688	2973.5390	1959.8684	0.000	0.0	0.000	0.000	0.000	0.000
CH_3COCH_3	0.96386	58.04189	1361190.4081	884098.8930	480996.8409	0.000	0.0	0.000	0.000	0.000	0.000
CH_3CN	0.97395	41.027	41079.2740	23622.3423	11400.2610	0.000	0.0	0.000	0.000	0.000	0.000
$CH_3^{35}Cl$	0.74894	49.99234	29627.476	18552.970	9981.683	0.000	0.0	0.000	0.000	0.000	0.000
$CH_3^{37}Cl$	0.23949	51.98939	30096.981	18846.881	10139.724	0.000	0.0	0.000	0.000	0.000	0.000
CH_3OH	0.98592	32.02623	6413.5724	4165.8152	2267.7752	0.000	0.0	0.000	0.000	0.000	0.000
CO	0.98654	27.995	108.8679	81.7147	54.5758	0.000	0.0	0.000	0.000	0.000	0.000
^{13}CO	0.011080	28.998	113.868	85.467	57.082	0.000	0.0	0.000	0.000	0.000	0.000
C^{17}O	0.000368	28.999	111.686	83.830	55.989	0.000	0.0	0.000	0.000	0.000	0.000
C^{18}O	0.001978	29.999	114.288	85.783	57.293	0.000	0.0	0.000	0.000	0.000	0.000
^{35}ClO	0.75348	50.964	3349.653	2307.8097	1424.6232	0.000	0.0	0.000	0.000	0.000	0.000
^{35}ClO(ν_1)	0.75348	50.964	3349.653	2307.8097	1424.6232	0.000	0.0	0.000	0.000	0.000	0.000
^{37}ClO	0.24172	52.961	3409.573	2347.4697	1449.1055	0.000	0.0	0.000	0.000	0.000	0.000
^{37}ClO(ν_1)	0.24172	52.961	3409.573	2347.4697	1449.1055	0.000	0.0	0.000	0.000	0.000	0.000
COF_2	0.98654	65.992	71946.972	42222.127	21914.815	0.000	0.0	0.000	0.000	0.000	0.000
^{35}ClOO^{35}Cl	0.57134	101.928	426874.29	277268.16	151112.36	0.000	0.0	0.000	0.000	0.000	0.000
^{35}ClOO^{37}Cl	0.36541	103.925	439238.10	285233.15	155417.53	0.000	0.0	0.000	0.000	0.000	0.000
$^{35}ClONO_2$	0.74957	96.957	614327.56	372305.97	181426.20	0.000	0.0	0.000	0.000	0.000	0.000
$^{37}ClONO_2$	0.23970	98.953	629941.18	381768.42	186080.13	0.000	0.0	0.000	0.000	0.000	0.000
EXTINCTION	1.00000	0.000	0.000	0.000	0.000	1.000	0.0	0.000	0.000	0.000	0.000
H^{79}Br	0.50678	79.926	103.4189	78.3610	53.3458	0.000	0.0	0.000	0.000	0.000	0.000
H^{81}Br	0.49306	81.824	103.4427	78.3971	53.3580	0.000	0.0	0.000	0.000	0.000	0.000
H^{35}Cl	0.75759	35.977	83.387	63.358	43.341	0.000	0.0	0.000	0.000	0.000	0.000
H^{37}Cl	0.24226	37.974	83.522	63.445	43.401	0.000	0.0	0.000	0.000	0.000	0.000
D^{35}Cl	0.000112	36.982	156.3148	117.5168	78.7590	0.000	0.0	0.000	0.000	0.000	0.000
D^{37}Cl	0.0000359	38.980	156.7834	117.8691	78.9951	0.000	0.0	0.000	0.000	0.000	0.000
HCN	0.98509	27.011	438.244	321.850	212.849	0.000	0.0	0.000	0.000	0.000	0.000
HCN(ν_2)	0.98509	27.011	438.244	321.850	212.849	0.000	0.0	0.000	0.000	0.000	0.000
H^{13}CN	0.01107	28.014	449.693	330.410	218.510	0.000	0.0	0.000	0.000	0.000	0.000
HC^{15}N	0.00362	28.007	150.458	110.498	73.0755	0.000	0.0	0.000	0.000	0.000	0.000
HCOOH	0.98390	46.005	10035.1878	6025.4318	3167.86358	0.000	0.0	0.000	0.000	0.000	0.000
HF	0.99984	20.006	10.5027	7.9598	5.4238	0.000	0.0	0.000	0.000	0.000	0.000
DF	0.00015	21.013	19.5749	14.7605	9.9495	0.000	0.0	0.000	0.000	0.000	0.000
H_2CO	0.98624	30.011	2906.284	1875.7246	1020.4879	0.000	0.0	0.000	0.000	0.000	0.000

Continued on next page

molecule, k	isotopic abundance $\mathcal{R}^k$	mass $\mathcal{M}^k$ AMU	Partition Function Q^K at 300 K	225 K	150 K	cont_1^k ($\mathrm{km^{-1}hPa^{-2}MHz^{-2}}$)	cont_2^k	cont_3^k ($\mathrm{MHz^{-2}}$)	cont_4^k ($\mathrm{km^{-1}hPa^{-1}MHz^{-4}}$)	cont_5^k ($\mathrm{MHz^{-2}}$)	cont_6^k MHz
$H_2^{13}CO$	0.01108	31.014	2979.9127	1925.3070	1047.6109	0.000	0.0	0.000	0.000	0.000	0.000
$H_2C^{18}O$	0.00198	32.0151	3017.1715	1959.7470	1066.8417	0.000	0.0	0.000	0.000	0.000	0.000
H_2O	0.99729	18.011	178.115	116.011	63.680	5.376×10^{-16}	4.80	0.000	0.000	0.000	0.000
H_2O-r1a	0.99729	18.011	0.0000	0.0000	0.0000	2.531×10^{-16}	3.445	0.000	0.000	0.000	0.000
H_2O-r1b	0.99729	18.011	0.0000	0.0000	0.0000	2.531×10^{-16}	3.445	0.000	0.000	0.000	0.000
H_2O-r2	0.99729	18.011	0.0000	0.0000	0.0000	2.446×10^{-16}	3.495	0.000	0.000	0.000	0.000
H_2O-r3	0.99729	18.011	0.0000	0.0000	0.0000	3.401×10^{-16}	3.499	0.000	0.000	0.000	0.000
H_2O-r4	0.99729	18.011	0.0000	0.0000	0.0000	2.123×10^{-16}	3.126	0.000	0.000	0.000	0.000
H_2O-r5h	0.99729	18.011	0.0000	0.0000	0.0000	1.584×10^{-15}	1.344	0.000	0.000	0.000	0.000
H_2O-r5v	0.99729	18.011	0.0000	0.0000	0.0000	1.584×10^{-15}	1.344	0.000	0.000	0.000	0.000
$H_2O(\nu_2)$	0.99729	18.011	178.115	116.011	63.680	0.000	0.0	0.000	0.000	0.000	0.000
$H_2^{17}O$	0.000372	19.015	178.8134	116.5199	63.9588	0.000	0.0	0.000	0.000	0.000	0.000
$H_2^{17}O(\nu_2)$	0.000372	19.015	178.8134	116.5199	63.9588	0.000	0.0	0.000	0.000	0.000	0.000
$H_2^{18}O$	0.00204	20.015	179.639	117.004	64.210	0.000	0.0	0.000	0.000	0.000	0.000
$H_2^{18}O(\nu_2)$	0.00204	20.015	179.639	117.004	64.210	0.000	0.0	0.000	0.000	0.000	0.000
D_2O	0.00000002	20.023	1044.7202	679.5164	371.1932	0.000	0.0	0.000	0.000	0.000	0.000
HDO	0.00031	19.0167	146.8589	95.5652	52.2998	0.000	0.0	0.000	0.000	0.000	0.000
$HDO(\nu_2)$	0.00031	19.0167	0.0000	0.0000	0.0000	0.000	0.0	0.000	0.000	0.000	0.000
$HD^{17}O$	0.000000116	20.021	0.0000	0.0000	0.0000	0.000	0.0	0.000	0.000	0.000	0.000
$HD^{18}O$	0.000000623	21.021	148.7305	96.7832	52.9541	0.000	0.0	0.000	0.000	0.000	0.000
H_2O_2	0.99489	34.005	10095.9933	5800.2031	2814.265	0.000	0.0	0.000	0.000	0.000	0.000
$H_2^{32}S$	0.94988	33.988	514.3989	334.5030	182.7679	0.000	0.0	0.000	0.000	0.000	0.000
$H_2^{32}SO_4$	0.94079	97.967	155955.25	101274.47	55118.83	0.000	0.0	0.000	0.000	0.000	0.000
HNO_3	0.98897	62.996	36797.943	20244.661	10080.001	0.000	0.0	0.000	0.000	0.000	0.000
$HNO_3(\nu_5)$	0.98897	62.996	36797.943	20244.661	10080.001	0.000	0.0	0.000	0.000	0.000	0.000
$HNO_3(\nu_6)$	0.98897	62.996	36797.943	20244.661	10080.001	0.000	0.0	0.000	0.000	0.000	0.000
$HNO_3(\nu_7)$	0.98897	62.996	36797.943	20244.661	10080.001	0.000	0.0	0.000	0.000	0.000	0.000
$HNO_3(\nu_8)$	0.98897	62.996	36797.943	20244.661	10080.001	0.000	0.0	0.000	0.000	0.000	0.000
$HNO_3(\nu_9)$	0.98897	62.996	36797.943	20244.661	10080.001	0.000	0.0	0.000	0.000	0.000	0.000
$H^{15}NO_3$	0.00363	63.993	0.0000	0.0000	0.0000	0.000	0.0	0.000	0.000	0.000	0.000
$HO^{79}Br$	0.50560	95.921	13551.8951	8796.2993	4786.3009	0.000	0.0	0.000	0.000	0.000	0.000
$HO^{81}Br$	0.49190	97.919	13611.3123	8834.8667	4806.1796	0.000	0.0	0.000	0.000	0.000	0.000
$HO^{35}Cl$	0.75576	51.972	9521.381	6181.587	3363.566	0.000	0.0	0.000	0.000	0.000	0.000
$HO^{37}Cl$	0.24168	53.969	9689.470	6290.716	3422.946	0.000	0.0	0.000	0.000	0.000	0.000
HO_2	0.99504	32.998	4389.8069	2841.7306	1547.2823	0.000	0.0	0.000	0.000	0.000	0.000
$HOONO_2$	0.98677	62.996	120032.817	86596.432	49796.6354	0.000	0.0	0.000	0.000	0.000	0.000
NO	0.99397	29.998	1160.7503	816.9585	492.2662	0.000	0.0	0.000	0.000	0.000	0.000
NO_2	0.99162	45.993	13875.1958	8816.0960	4764.3099	0.000	0.0	0.000	0.000	0.000	0.000
N_2	0.99269	28.006	0.000	0.000	0.000	5.727×10^{-20}	3.964	1.669×10^{-12}	9.997×10^{-33}	1.113×10^{-13}	1.798×10^{6}

Continued on next page

molecule, k	isotopic abundance $\mathcal{R}^k$	mass $\mathcal{M}^k$ AMU	Partition Function Q^K at 300 K	225 K	150 K	cont_1^k ($\mathrm{km^{-1}hPa^{-2}MHz^{-2}}$)	cont_2^k	cont_3^k ($\mathrm{MHz^{-2}}$)	cont_4^k ($\mathrm{km^{-1}hPa^{-1}MHz^{-4}}$)	cont_5^k ($\mathrm{MHz^{-2}}$)	cont_6^k MHz
N_2O	0.99030	44.001	566.0444	392.6434	251.3676	0.000	0.0	0.000	0.000	0.000	0.000
$N_2O(\nu_1)$	0.99030	44.001	566.0444	392.6434	251.3676	0.000	0.0	0.000	0.000	0.000	0.000
$N_2O(\nu_2)$	0.99030	44.001	566.0444	392.6434	251.3676	0.000	0.0	0.000	0.000	0.000	0.000
$N_2O(2\nu_2)$	0.99030	44.001	566.0444	392.6434	251.3676	0.000	0.0	0.000	0.000	0.000	0.000
^{15}NNO	0.00364	44.998	587.1479	406.7990	260.2050	0.000	0.0	0.000	0.000	0.000	0.000
$N^{15}NO$	0.00364	44.998	570.8418	394.3303	251.6273	0.000	0.0	0.000	0.000	0.000	0.000
$N_2^{17}O$	0.000369	45.005	0.0000	0.0000	0.0000	0.000	0.0	0.000	0.000	0.000	0.000
$N_2^{18}O$	0.00199	46.005	601.5296	416.5139	266.3258	0.000	0.0	0.000	0.000	0.000	0.000
O	0.99763	15.995	6.7406	6.3241	5.7703	0.000	0.0	0.000	0.000	0.000	0.000
^{17}O	0.000374	16.99914	0.0000	0.0000	0.0000	0.000	0.0	0.000	0.000	0.000	0.000
^{18}O	0.002039	17.99946	0.0000	0.0000	0.0000	0.000	0.0	0.000	0.000	0.000	0.000
$OC^{18}O$	0.0039471	45.994	620.0804	438.8584	284.9883	0.000	0.0	0.000	0.000	0.000	0.000
$O^{35}ClO$	0.75410	66.959	52517.011	35416.040	19301.897	0.000	0.0	0.000	0.000	0.000	0.000
$O^{37}ClO$	0.24120	68.956	52420.360	34905.993	19173.438	0.000	0.0	0.000	0.000	0.000	0.000
$OC^{32}S$	0.93739	59.967	1246.5206	835.6316	522.4917	0.000	0.0	0.000	0.000	0.000	0.000
$OC^{34}S$	0.04158	61.963	1277.7595	856.5686	535.5788	0.000	0.0	0.000	0.000	0.000	0.000
$O^{13}C^{32}S$	0.01053	60.970	1267.5148	844.3118	525.1707	0.000	0.0	0.000	0.000	0.000	0.000
OH	0.99744	17.003	81.5086	60.3097	40.1570	0.000	0.0	0.000	0.000	0.000	0.000
^{18}OH	0.00200	19.007	82.0367	60.6851	40.3827	0.000	0.0	0.000	0.000	0.000	0.000
OD	0.00016	18.009	212.422	153.391	97.4765	0.000	0.0	0.000	0.000	0.000	0.000
O_2	0.99519	31.990	218.6754	164.1345	109.5973	6.87×10^{-9}	2.8	0.56	0.8	0.000	0.000
$O_2(\nu_1)$	0.99519	31.990	218.6754	164.1345	109.5973	0.000	0.0	0.000	0.000	0.000	0.000
$^1\Delta_g O_2$	0.99519	31.990	149.5547	112.7457	75.9277	0.000	0.0	0.000	0.000	0.000	0.000
$O^{17}O$	0.000742	32.994	2692.775	2018.8311	1345.8604	0.000	0.0	0.000	0.000	0.000	0.000
$O^{18}O$	0.00407	33.994	461.087	345.728	230.431	0.000	0.0	0.000	0.000	0.000	0.000
$O^{18}O(\nu_1)$	0.00407	33.994	0.0000	0.0000	0.0000	0.000	0.0	0.000	0.000	0.000	0.000
$^1\Delta_g^{18}OO$	0.00407	33.994	0.0000	0.0000	0.0000	0.000	0.0	0.000	0.000	0.000	0.000
O_3	0.99279	47.984	3563.3512	2235.0190	1200.4721	0.000	0.0	0.000	0.000	0.000	0.000
$O_3(\nu_{1,3})$	0.99279	47.984	3563.3512	2235.0190	1200.4721	0.000	0.0	0.000	0.000	0.000	0.000
$O_3(\nu_2)$	0.99279	47.984	3563.3512	2235.0190	1200.4721	0.000	0.0	0.000	0.000	0.000	0.000
$O_3(2\nu_2)$	0.99279	47.984	3563.3512	2235.0190	1200.4721	0.000	0.0	0.000	0.000	0.000	0.000
$O_3(\nu_{1,3}+\nu_2)$	0.99279	47.984	3563.3512	2235.0190	1200.4721	0.000	0.0	0.000	0.000	0.000	0.000
$O_2^{17}O$	0.00074	48.989	44324.2078	27768.8958	14905.4993	0.000	0.0	0.000	0.000	0.000	0.000
$O^{17}OO$	0.00037	48.989	21895.8859	13718.0208	7364.7181	0.000	0.0	0.000	0.000	0.000	0.000
$O_2^{18}O$	0.00406	49.989	7637.3743	4779.4115	2563.8530	0.000	0.0	0.000	0.000	0.000	0.000
$O_2^{18}O(\nu_2)$	0.00406	49.989	7637.3743	4779.4115	2563.8530	0.000	0.0	0.000	0.000	0.000	0.000
$O^{18}OO$	0.00203	49.989	3730.9603	2334.9508	1252.9579	0.000	0.0	0.000	0.000	0.000	0.000
$O^{18}OO(\nu_2)$	0.00203	49.989	3730.9603	2334.9508	1252.9579	0.000	0.0	0.000	0.000	0.000	0.000
$^{32}SO_2$	0.94548	63.962	6491.5387	3989.7541	2104.6337	0.000	0.0	0.000	0.000	0.000	0.000

Continued on next page

molecule, k	isotopic abundance $\mathcal{R}^k$	mass $\mathcal{M}^k$ AMU	Partition Function Q^K at 300 K	225 K	150 K	cont_1^k ($\mathrm{km^{-1}hPa^{-2}MHz^{-2}}$)	cont_2^k	cont_3^k ($\mathrm{MHz^{-2}}$)	cont_4^k ($\mathrm{km^{-1}hPa^{-1}MHz^{-4}}$)	cont_5^k ($\mathrm{MHz^{-2}}$)	cont_6^k MHz
$^{32}SO_2(\nu_2)$	0.94548	63.962	6491.5387	3989.7541	2104.6337	0.000	0.0	0.000	0.000	0.000	0.000
$^{33}SO_2$	0.00754	64.961	23883.6116	15502.4379	8433.3476	0.000	0.0	0.000	0.000	0.000	0.000
$^{34}SO_2$	0.04195	65.958	6520.96385	4007.8991	2126.1799	0.000	0.0	0.000	0.000	0.000	0.000

Id: mol_data_table.tex,v 1.13 2004/02/12 00:10:05 bill Exp

Table 12.2: Species line data for MLS signals.

molecule	ν_{0j}^k (MHz)	$\mathcal{I}_j^k$ (nm^2MHz)	$E\ell_j^k$ (cm^{-1})	w_{cj}^k (MHz hPa^{-1})	n_{cj}^k	$\Delta\nu_{0j}^k$ (MHz hPa^{-1})	$n_{\Delta\nu_{0j}}^k$	δ_j^k (hPa^{-1})	$n_{\delta_j}^k$	γ_j^k (hPa^{-1})	$n_{\gamma_j}^k$
^{79}BrO	652880.5319	−1.8010	265.4432	2.251	0.817	0.000	0.000	0.00e+00	0.00	0.00e+00	0.00
	652881.8917	−1.8181	265.4474	2.251	0.817	0.000	0.000	0.00e+00	0.00	0.00e+00	0.00
	652882.5651	−1.8010	265.4437	2.251	0.817	0.000	0.000	0.00e+00	0.00	0.00e+00	0.00
	652883.2781	−1.8352	265.4460	2.251	0.817	0.000	0.000	0.00e+00	0.00	0.00e+00	0.00
	652883.7212	−1.8181	265.4479	2.251	0.817	0.000	0.000	0.00e+00	0.00	0.00e+00	0.00
	652883.9628	−1.8522	265.4395	2.251	0.817	0.000	0.000	0.00e+00	0.00	0.00e+00	0.00
	652885.0993	−1.8352	265.4464	2.251	0.817	0.000	0.000	0.00e+00	0.00	0.00e+00	0.00
	652885.9708	−1.8522	265.4401	2.251	0.817	0.000	0.000	0.00e+00	0.00	0.00e+00	0.00
^{81}BrO	624764.8570	−1.8110	243.5061	2.263	0.788	0.000	0.000	0.00e+00	0.00	0.00e+00	0.00
	624766.3907	−1.8288	243.5093	2.263	0.788	0.000	0.000	0.00e+00	0.00	0.00e+00	0.00
	624766.7040	−1.8110	243.5066	2.263	0.788	0.000	0.000	0.00e+00	0.00	0.00e+00	0.00
	624767.9257	−1.8466	243.5078	2.263	0.788	0.000	0.000	0.00e+00	0.00	0.00e+00	0.00
	624768.0666	−1.8288	243.5097	2.263	0.788	0.000	0.000	0.00e+00	0.00	0.00e+00	0.00
	624768.8034	−1.8644	243.5020	2.263	0.788	0.000	0.000	0.00e+00	0.00	0.00e+00	0.00
	624769.5930	−1.8466	243.5082	2.263	0.788	0.000	0.000	0.00e+00	0.00	0.00e+00	0.00
	624770.6246	−1.8644	243.5026	2.263	0.788	0.000	0.000	0.00e+00	0.00	0.00e+00	0.00
	650175.8041	−1.8041	264.3460	2.251	0.817	0.000	0.000	0.00e+00	0.00	0.00e+00	0.00
	650177.2087	−1.8212	264.3493	2.251	0.817	0.000	0.000	0.00e+00	0.00	0.00e+00	0.00
	650177.7979	−1.8041	264.3465	2.251	0.817	0.000	0.000	0.00e+00	0.00	0.00e+00	0.00
	650178.6151	−1.8383	264.3478	2.251	0.817	0.000	0.000	0.00e+00	0.00	0.00e+00	0.00
	650179.0310	−1.8212	264.3497	2.251	0.817	0.000	0.000	0.00e+00	0.00	0.00e+00	0.00
	650179.4142	−1.8554	264.3421	2.251	0.817	0.000	0.000	0.00e+00	0.00	0.00e+00	0.00
	650180.4285	−1.8383	264.3482	2.251	0.817	0.000	0.000	0.00e+00	0.00	0.00e+00	0.00
	650181.3811	−1.8554	264.3427	2.251	0.817	0.000	0.000	0.00e+00	0.00	0.00e+00	0.00
CH_3COCH_3	176754.0405	−3.8253	44.4658	3.000	0.750	0.000	0.000	0.00e+00	0.00	0.00e+00	0.00
	176756.3792	−3.8253	44.4657	3.000	0.750	0.000	0.000	0.00e+00	0.00	0.00e+00	0.00
	177786.1645	−3.4309	47.3498	3.000	0.750	0.000	0.000	0.00e+00	0.00	0.00e+00	0.00
	177837.1126	−3.9346	47.2975	3.000	0.750	0.000	0.000	0.00e+00	0.00	0.00e+00	0.00
	178874.8160	−3.3510	49.6727	3.000	0.750	0.000	0.000	0.00e+00	0.00	0.00e+00	0.00
	178912.0856	−3.8558	49.6161	3.000	0.750	0.000	0.000	0.00e+00	0.00	0.00e+00	0.00
	179982.9373	−3.2825	51.4414	3.000	0.750	0.000	0.000	0.00e+00	0.00	0.00e+00	0.00

Continued on next page

molecule	ν_{0j}^k (MHz)	$\mathcal{I}_j^k$ ($\mathrm{nm^2MHz}$)	$E\ell_j^k$ ($\mathrm{cm^{-1}}$)	w_{cj}^k ($\mathrm{MHz\,hPa^{-1}}$)	n_{cj}^k	$\Delta\nu_{0j}^k$ ($\mathrm{MHz\,hPa^{-1}}$)	$n_{\Delta\nu_{0j}}^k$	δ_j^k ($\mathrm{hPa^{-1}}$)	$n_{\delta_j}^k$	γ_j^k ($\mathrm{hPa^{-1}}$)	$n_{\gamma_j}^k$
	179987.0518	−3.8010	23.6871	3.000	0.750	0.000	0.000	0.00e+00	0.00	0.00e+00	0.00
	180005.8142	−3.7874	51.3786	3.000	0.750	0.000	0.000	0.00e+00	0.00	0.00e+00	0.00
	180149.9393	−3.8001	23.7563	3.000	0.750	0.000	0.000	0.00e+00	0.00	0.00e+00	0.00
	181098.1317	−3.2214	52.6589	3.000	0.750	0.000	0.000	0.00e+00	0.00	0.00e+00	0.00
	181105.1070	−3.7263	52.5878	3.000	0.750	0.000	0.000	0.00e+00	0.00	0.00e+00	0.00
	182561.9008	−3.8255	275.7505	3.000	0.750	0.000	0.000	0.00e+00	0.00	0.00e+00	0.00
	182614.1018	−4.3225	275.7719	3.000	0.750	0.000	0.000	0.00e+00	0.00	0.00e+00	0.00
	183191.6768	−3.8138	255.4971	3.000	0.750	0.000	0.000	0.00e+00	0.00	0.00e+00	0.00
	183262.8573	−4.3124	255.5147	3.000	0.750	0.000	0.000	0.00e+00	0.00	0.00e+00	0.00
	183671.7576	−4.5301	235.8304	3.000	0.750	0.000	0.000	0.00e+00	0.00	0.00e+00	0.00
	183682.1932	−4.4469	42.8499	3.000	0.750	0.000	0.000	0.00e+00	0.00	0.00e+00	0.00
	183702.0583	−4.6218	42.8494	3.000	0.750	0.000	0.000	0.00e+00	0.00	0.00e+00	0.00
	183754.6747	−4.0205	42.8031	3.000	0.750	0.000	0.000	0.00e+00	0.00	0.00e+00	0.00
	183763.7798	−3.8082	235.8431	3.000	0.750	0.000	0.000	0.00e+00	0.00	0.00e+00	0.00
	183817.4001	−4.2252	42.7565	3.000	0.750	0.000	0.000	0.00e+00	0.00	0.00e+00	0.00
	183855.8615	−4.1030	235.8559	3.000	0.750	0.000	0.000	0.00e+00	0.00	0.00e+00	0.00
	184168.0210	−4.5306	216.7829	3.000	0.750	0.000	0.000	0.00e+00	0.00	0.00e+00	0.00
	184282.8181	−3.8075	216.7899	3.000	0.750	0.000	0.000	0.00e+00	0.00	0.00e+00	0.00
	184397.6856	−4.1032	216.7969	3.000	0.750	0.000	0.000	0.00e+00	0.00	0.00e+00	0.00
	184613.7154	−4.5376	198.3383	3.000	0.750	0.000	0.000	0.00e+00	0.00	0.00e+00	0.00
	184753.0708	−3.8142	198.3387	3.000	0.750	0.000	0.000	0.00e+00	0.00	0.00e+00	0.00
	184892.4682	−4.1098	198.3392	3.000	0.750	0.000	0.000	0.00e+00	0.00	0.00e+00	0.00
	185012.8380	−4.5524	180.4979	3.000	0.750	0.000	0.000	0.00e+00	0.00	0.00e+00	0.00
	185178.3735	−3.8279	180.4908	3.000	0.750	0.000	0.000	0.00e+00	0.00	0.00e+00	0.00
	185308.9356	−4.4439	44.3269	3.000	0.750	0.000	0.000	0.00e+00	0.00	0.00e+00	0.00
	185343.9727	−4.1244	180.4838	3.000	0.750	0.000	0.000	0.00e+00	0.00	0.00e+00	0.00
	185388.9197	−4.2375	44.3693	3.000	0.750	0.000	0.000	0.00e+00	0.00	0.00e+00	0.00
	185527.7604	−4.4534	46.9179	3.000	0.750	0.000	0.000	0.00e+00	0.00	0.00e+00	0.00
	185562.3433	−3.8528	163.2475	3.000	0.750	0.000	0.000	0.00e+00	0.00	0.00e+00	0.00
	185581.0777	−4.0555	46.9164	3.000	0.750	0.000	0.000	0.00e+00	0.00	0.00e+00	0.00
	185605.3445	−3.8514	46.8714	3.000	0.750	0.000	0.000	0.00e+00	0.00	0.00e+00	0.00
	185660.6378	−3.8510	46.8698	3.000	0.750	0.000	0.000	0.00e+00	0.00	0.00e+00	0.00
	185683.1733	−4.2772	46.8249	3.000	0.750	0.000	0.000	0.00e+00	0.00	0.00e+00	0.00

Continued on next page

molecule	ν_{0j}^k (MHz)	$\mathcal{I}_j^k$ ($\mathrm{nm^2MHz}$)	$E\ell_j^k$ ($\mathrm{cm^{-1}}$)	u_{cj}^k ($\mathrm{MHz\,hPa^{-1}}$)	n_{cj}^k	$\Delta\nu_{0j}^k$ ($\mathrm{MHz\,hPa^{-1}}$)	$n_{\Delta\nu_{0j}}^k$	δ_j^k ($\mathrm{hPa^{-1}}$)	$n_{\delta_j}^k$	γ_j^k ($\mathrm{hPa^{-1}}$)	$n_{\gamma_j}^k$
	185740.2509	−4.0551	46.8233	3.000	0.750	0.000	0.000	0.00e+00	0.00	0.00e+00	0.00
	185755.6357	−4.1489	163.2320	3.000	0.750	0.000	0.000	0.00e+00	0.00	0.00e+00	0.00
	185800.2002	−4.2847	26.7937	3.000	0.750	0.000	0.000	0.00e+00	0.00	0.00e+00	0.00
	185908.2369	−3.8895	146.6098	3.000	0.750	0.000	0.000	0.00e+00	0.00	0.00e+00	0.00
	186130.6072	−4.3907	146.5850	3.000	0.750	0.000	0.000	0.00e+00	0.00	0.00e+00	0.00
	186219.1622	−3.9463	130.5789	3.000	0.750	0.000	0.000	0.00e+00	0.00	0.00e+00	0.00
	186325.7509	−4.3912	26.8381	3.000	0.750	0.000	0.000	0.00e+00	0.00	0.00e+00	0.00
	186471.7851	−4.4471	130.5440	3.000	0.750	0.000	0.000	0.00e+00	0.00	0.00e+00	0.00
	186480.3668	−4.1704	50.4094	3.000	0.750	0.000	0.000	0.00e+00	0.00	0.00e+00	0.00
	186480.5197	−4.3463	50.4094	3.000	0.750	0.000	0.000	0.00e+00	0.00	0.00e+00	0.00
	186480.8924	−4.3463	50.4094	3.000	0.750	0.000	0.000	0.00e+00	0.00	0.00e+00	0.00
	186497.9323	−4.0299	115.1558	3.000	0.750	0.000	0.000	0.00e+00	0.00	0.00e+00	0.00
	186544.1505	−3.4431	50.3617	3.000	0.750	0.000	0.000	0.00e+00	0.00	0.00e+00	0.00
	186607.6564	−3.7439	50.3140	3.000	0.750	0.000	0.000	0.00e+00	0.00	0.00e+00	0.00
	186747.2480	−4.1676	100.3415	3.000	0.750	0.000	0.000	0.00e+00	0.00	0.00e+00	0.00
	186765.8630	−4.5999	42.7691	3.000	0.750	0.000	0.000	0.00e+00	0.00	0.00e+00	0.00
	186781.8432	−4.5324	115.1099	3.000	0.750	0.000	0.000	0.00e+00	0.00	0.00e+00	0.00
	186782.1196	−4.1642	26.7332	3.000	0.750	0.000	0.000	0.00e+00	0.00	0.00e+00	0.00
	186917.3539	−3.9979	42.7202	3.000	0.750	0.000	0.000	0.00e+00	0.00	0.00e+00	0.00
	199590.9109	−3.8925	63.8372	3.000	0.750	0.000	0.000	0.00e+00	0.00	0.00e+00	0.00
	199613.4146	−3.1654	63.7759	3.000	0.750	0.000	0.000	0.00e+00	0.00	0.00e+00	0.00
	199635.8342	−3.4662	63.7147	3.000	0.750	0.000	0.000	0.00e+00	0.00	0.00e+00	0.00
	200026.5430	−4.2737	29.6903	3.000	0.750	0.000	0.000	0.00e+00	0.00	0.00e+00	0.00
	200153.9218	−4.0971	29.7652	3.000	0.750	0.000	0.000	0.00e+00	0.00	0.00e+00	0.00
	200158.9722	−4.5742	29.7651	3.000	0.750	0.000	0.000	0.00e+00	0.00	0.00e+00	0.00
	200162.2289	−3.8107	305.0115	3.000	0.750	0.000	0.000	0.00e+00	0.00	0.00e+00	0.00
	200208.8474	−4.3015	305.0355	3.000	0.750	0.000	0.000	0.00e+00	0.00	0.00e+00	0.00
	200287.0720	−4.2726	29.8399	3.000	0.750	0.000	0.000	0.00e+00	0.00	0.00e+00	0.00
	200328.3162	−3.6702	29.6908	3.000	0.750	0.000	0.000	0.00e+00	0.00	0.00e+00	0.00
	200458.8932	−3.6696	29.7655	3.000	0.750	0.000	0.000	0.00e+00	0.00	0.00e+00	0.00
	200627.6726	−3.8728	29.6911	3.000	0.750	0.000	0.000	0.00e+00	0.00	0.00e+00	0.00
	200632.4703	−4.0946	29.6910	3.000	0.750	0.000	0.000	0.00e+00	0.00	0.00e+00	0.00
	200673.3797	−4.5118	283.5019	3.000	0.750	0.000	0.000	0.00e+00	0.00	0.00e+00	0.00

Continued on next page

molecule	ν_{0j}^k (MHz)	$\mathcal{I}_j^k$ ($\mathrm{nm^2MHz}$)	$E\ell_j^k$ ($\mathrm{cm^{-1}}$)	w_{cj}^k ($\mathrm{MHz\,hPa^{-1}}$)	n_{cj}^k	$\Delta\nu_{0j}^k$ ($\mathrm{MHz\,hPa^{-1}}$)	$n_{\Delta\nu_{0j}}^k$	δ_j^k ($\mathrm{hPa^{-1}}$)	$n_{\delta_j}^k$	γ_j^k ($\mathrm{hPa^{-1}}$)	$n_{\gamma_j}^k$
	200724.1429	−3.8383	65.1385	3.000	0.750	0.000	0.000	0.00e+00	0.00	0.00e+00	0.00
	200724.1429	−3.7134	65.1385	3.000	0.750	0.000	0.000	0.00e+00	0.00	0.00e+00	0.00
	200724.1429	−3.7134	65.1384	3.000	0.750	0.000	0.000	0.00e+00	0.00	0.00e+00	0.00
	200730.8313	−3.1112	65.0679	3.000	0.750	0.000	0.000	0.00e+00	0.00	0.00e+00	0.00
	200737.5084	−3.4120	64.9973	3.000	0.750	0.000	0.000	0.00e+00	0.00	0.00e+00	0.00
	200740.1407	−3.7947	283.5224	3.000	0.750	0.000	0.000	0.00e+00	0.00	0.00e+00	0.00
	200806.7995	−4.0851	283.5430	3.000	0.750	0.000	0.000	0.00e+00	0.00	0.00e+00	0.00
	200813.1771	−4.4892	37.7154	3.000	0.750	0.000	0.000	0.00e+00	0.00	0.00e+00	0.00
	200826.8877	−4.6031	50.7812	3.000	0.750	0.000	0.000	0.00e+00	0.00	0.00e+00	0.00
	200835.8153	−4.0024	50.7406	3.000	0.750	0.000	0.000	0.00e+00	0.00	0.00e+00	0.00
	200868.0670	−4.4296	50.6994	3.000	0.750	0.000	0.000	0.00e+00	0.00	0.00e+00	0.00
	201049.7229	−4.0610	37.6630	3.000	0.750	0.000	0.000	0.00e+00	0.00	0.00e+00	0.00
	201179.9793	−4.5046	262.6173	3.000	0.750	0.000	0.000	0.00e+00	0.00	0.00e+00	0.00
	201269.2721	−3.7852	262.6334	3.000	0.750	0.000	0.000	0.00e+00	0.00	0.00e+00	0.00
	201358.4285	−4.0776	262.6495	3.000	0.750	0.000	0.000	0.00e+00	0.00	0.00e+00	0.00
	201376.1853	−4.2609	37.6097	3.000	0.750	0.000	0.000	0.00e+00	0.00	0.00e+00	0.00
	201639.3599	−4.5028	242.3349	3.000	0.750	0.000	0.000	0.00e+00	0.00	0.00e+00	0.00
	201753.2897	−3.7814	242.3455	3.000	0.750	0.000	0.000	0.00e+00	0.00	0.00e+00	0.00
	201867.0030	−4.0756	242.3562	3.000	0.750	0.000	0.000	0.00e+00	0.00	0.00e+00	0.00
	202054.7773	−4.5076	222.6559	3.000	0.750	0.000	0.000	0.00e+00	0.00	0.00e+00	0.00
	202195.3860	−3.7853	222.6601	3.000	0.750	0.000	0.000	0.00e+00	0.00	0.00e+00	0.00
	202335.9752	−4.0800	222.6643	3.000	0.750	0.000	0.000	0.00e+00	0.00	0.00e+00	0.00
	202429.3424	−4.5203	203.5815	3.000	0.750	0.000	0.000	0.00e+00	0.00	0.00e+00	0.00
	202599.0701	−3.7964	203.5782	3.000	0.750	0.000	0.000	0.00e+00	0.00	0.00e+00	0.00
	202765.6692	−4.5429	185.1128	3.000	0.750	0.000	0.000	0.00e+00	0.00	0.00e+00	0.00
	202768.5492	−4.0924	203.5749	3.000	0.750	0.000	0.000	0.00e+00	0.00	0.00e+00	0.00
	203603.5815	−3.9076	149.9646	3.000	0.750	0.000	0.000	0.00e+00	0.00	0.00e+00	0.00
	203872.0102	−4.4086	149.9326	3.000	0.750	0.000	0.000	0.00e+00	0.00	0.00e+00	0.00
	203879.0805	−3.9891	133.3075	3.000	0.750	0.000	0.000	0.00e+00	0.00	0.00e+00	0.00
	203911.7643	−4.6370	43.9795	3.000	0.750	0.000	0.000	0.00e+00	0.00	0.00e+00	0.00
	204127.8920	−4.1247	117.2591	3.000	0.750	0.000	0.000	0.00e+00	0.00	0.00e+00	0.00
	204182.9997	−4.4918	133.2639	3.000	0.750	0.000	0.000	0.00e+00	0.00	0.00e+00	0.00
	204183.6408	−4.2252	55.4844	3.000	0.750	0.000	0.000	0.00e+00	0.00	0.00e+00	0.00

Continued on next page

molecule	ν_{0j}^k (MHz)	$\mathcal{I}_j^k$ ($\mathrm{nm^2MHz}$)	$E\ell_j^k$ ($\mathrm{cm^{-1}}$)	u_{cj}^k ($\mathrm{MHz\,hPa^{-1}}$)	n_{cj}^k	$\Delta\nu_{0j}^k$ ($\mathrm{MHz\,hPa^{-1}}$)	$n_{\Delta\nu_{0j}}^k$	δ_j^k ($\mathrm{hPa^{-1}}$)	$n_{\delta_j}^k$	γ_j^k ($\mathrm{hPa^{-1}}$)	$n_{\gamma_j}^k$
	204184.7932	−4.4007	55.4843	3.000	0.750	0.000	0.000	0.00e+00	0.00	0.00e+00	0.00
	204220.5632	−4.0333	43.9285	3.000	0.750	0.000	0.000	0.00e+00	0.00	0.00e+00	0.00
	204271.4822	−3.7988	55.4434	3.000	0.750	0.000	0.000	0.00e+00	0.00	0.00e+00	0.00
	204358.7716	−4.0029	55.4025	3.000	0.750	0.000	0.000	0.00e+00	0.00	0.00e+00	0.00
	204370.2129	−4.3998	55.4792	3.000	0.750	0.000	0.000	0.00e+00	0.00	0.00e+00	0.00
	204464.1283	−3.7977	55.4381	3.000	0.750	0.000	0.000	0.00e+00	0.00	0.00e+00	0.00
	204486.8164	−4.4582	43.8785	3.000	0.750	0.000	0.000	0.00e+00	0.00	0.00e+00	0.00
	204557.2508	−4.2237	55.3970	3.000	0.750	0.000	0.000	0.00e+00	0.00	0.00e+00	0.00
	205062.8358	−4.1149	59.6210	3.000	0.750	0.000	0.000	0.00e+00	0.00	0.00e+00	0.00
	205064.5777	−3.8931	59.6210	3.000	0.750	0.000	0.000	0.00e+00	0.00	0.00e+00	0.00
	205136.7427	−3.6887	59.5797	3.000	0.750	0.000	0.000	0.00e+00	0.00	0.00e+00	0.00
	205138.5639	−3.6887	59.5796	3.000	0.750	0.000	0.000	0.00e+00	0.00	0.00e+00	0.00
	205210.6487	−4.1145	59.5383	3.000	0.750	0.000	0.000	0.00e+00	0.00	0.00e+00	0.00
	205212.5450	−3.8927	59.5383	3.000	0.750	0.000	0.000	0.00e+00	0.00	0.00e+00	0.00
	205318.5636	−4.4174	439.6484	3.000	0.750	0.000	0.000	0.00e+00	0.00	0.00e+00	0.00
	205337.8535	−4.4455	60.9935	3.000	0.750	0.000	0.000	0.00e+00	0.00	0.00e+00	0.00
	206077.8980	−3.6040	63.1768	3.000	0.750	0.000	0.000	0.00e+00	0.00	0.00e+00	0.00
	206138.9278	−3.3028	63.1333	3.000	0.750	0.000	0.000	0.00e+00	0.00	0.00e+00	0.00
	206168.4024	−4.3865	414.5613	3.000	0.750	0.000	0.000	0.00e+00	0.00	0.00e+00	0.00
	206199.7596	−3.8076	63.0899	3.000	0.750	0.000	0.000	0.00e+00	0.00	0.00e+00	0.00
	206199.7596	−3.6035	63.0899	3.000	0.750	0.000	0.000	0.00e+00	0.00	0.00e+00	0.00
	206603.9920	−4.6349	33.0626	3.000	0.750	0.000	0.000	0.00e+00	0.00	0.00e+00	0.00
	207212.9118	−3.2315	66.1223	3.000	0.750	0.000	0.000	0.00e+00	0.00	0.00e+00	0.00
	207261.5274	−3.7364	66.0750	3.000	0.750	0.000	0.000	0.00e+00	0.00	0.00e+00	0.00
	624458.8035	−3.5171	587.4466	3.000	0.750	0.000	0.000	0.00e+00	0.00	0.00e+00	0.00
	624484.1342	−3.0120	587.4209	3.000	0.750	0.000	0.000	0.00e+00	0.00	0.00e+00	0.00
	624666.9312	−3.7966	179.2289	3.000	0.750	0.000	0.000	0.00e+00	0.00	0.00e+00	0.00
	624670.4364	−3.7966	179.2289	3.000	0.750	0.000	0.000	0.00e+00	0.00	0.00e+00	0.00
	624787.3645	−2.9301	643.0445	3.000	0.750	0.000	0.000	0.00e+00	0.00	0.00e+00	0.00
	624804.9332	−3.4350	643.0728	3.000	0.750	0.000	0.000	0.00e+00	0.00	0.00e+00	0.00
	624838.5155	−3.1592	325.1884	3.000	0.750	0.000	0.000	0.00e+00	0.00	0.00e+00	0.00
	624839.9336	−3.6665	321.6274	3.000	0.750	0.000	0.000	0.00e+00	0.00	0.00e+00	0.00
	624850.8608	−3.3418	325.2111	3.000	0.750	0.000	0.000	0.00e+00	0.00	0.00e+00	0.00

Continued on next page

molecule	ν_{0j}^k (MHz)	$\mathcal{I}_j^k$ (nm^{2}MHz)	$E\ell_j^k$ (cm^{-1})	w_{cj}^k (MHz hPa^{-1})	n_{cj}^k	$\Delta\nu_{0j}^k$ (MHz hPa^{-1})	$n_{\Delta\nu_{0j}}^k$	δ_j^k (hPa^{-1})	$n_{\delta_j}^k$	γ_j^k (hPa^{-1})	$n_{\gamma_j}^k$
	624862.7086	−3.2408	321.6044	3.000	0.750	0.000	0.000	0.00e+00	0.00	0.00e+00	0.00
	624867.9658	−3.5641	325.1645	3.000	0.750	0.000	0.000	0.00e+00	0.00	0.00e+00	0.00
	624981.5533	−3.5728	316.8889	3.000	0.750	0.000	0.000	0.00e+00	0.00	0.00e+00	0.00
	625051.4489	−2.9704	316.9154	3.000	0.750	0.000	0.000	0.00e+00	0.00	0.00e+00	0.00
	625118.5039	−3.3960	316.9414	3.000	0.750	0.000	0.000	0.00e+00	0.00	0.00e+00	0.00
	625121.9134	−3.1742	316.9414	3.000	0.750	0.000	0.000	0.00e+00	0.00	0.00e+00	0.00
	625149.4917	−3.3969	316.8765	3.000	0.750	0.000	0.000	0.00e+00	0.00	0.00e+00	0.00
	625214.9148	−2.9702	316.9030	3.000	0.750	0.000	0.000	0.00e+00	0.00	0.00e+00	0.00
	625312.5684	−3.5722	316.8643	3.000	0.750	0.000	0.000	0.00e+00	0.00	0.00e+00	0.00
	625498.4002	−3.5097	598.1629	3.000	0.750	0.000	0.000	0.00e+00	0.00	0.00e+00	0.00
	625520.8596	−3.0046	598.1361	3.000	0.750	0.000	0.000	0.00e+00	0.00	0.00e+00	0.00
	625778.3140	−3.3650	312.1095	3.000	0.750	0.000	0.000	0.00e+00	0.00	0.00e+00	0.00
	625799.7547	−2.7630	312.1922	3.000	0.750	0.000	0.000	0.00e+00	0.00	0.00e+00	0.00
	625821.4055	−2.7631	312.2748	3.000	0.750	0.000	0.000	0.00e+00	0.00	0.00e+00	0.00
	625965.5985	−2.9218	648.7555	3.000	0.750	0.000	0.000	0.00e+00	0.00	0.00e+00	0.00
	625988.1987	−3.4269	648.7796	3.000	0.750	0.000	0.000	0.00e+00	0.00	0.00e+00	0.00
	626042.8376	−3.0637	312.1409	3.000	0.750	0.000	0.000	0.00e+00	0.00	0.00e+00	0.00
	626065.0045	−2.7627	312.2235	3.000	0.750	0.000	0.000	0.00e+00	0.00	0.00e+00	0.00
	626307.7811	−3.3643	312.1720	3.000	0.750	0.000	0.000	0.00e+00	0.00	0.00e+00	0.00
	626569.6534	−3.5029	608.3179	3.000	0.750	0.000	0.000	0.00e+00	0.00	0.00e+00	0.00
	626588.7876	−2.9978	608.2900	3.000	0.750	0.000	0.000	0.00e+00	0.00	0.00e+00	0.00
	626912.4796	−3.5614	325.1646	3.000	0.750	0.000	0.000	0.00e+00	0.00	0.00e+00	0.00
	626956.9594	−3.1570	325.1409	3.000	0.750	0.000	0.000	0.00e+00	0.00	0.00e+00	0.00
	632212.0287	−3.5496	585.0747	3.000	0.750	0.000	0.000	0.00e+00	0.00	0.00e+00	0.00
	632212.0378	−2.9658	650.7465	3.000	0.750	0.000	0.000	0.00e+00	0.00	0.00e+00	0.00
	632216.8170	−3.4708	650.7784	3.000	0.750	0.000	0.000	0.00e+00	0.00	0.00e+00	0.00
	632243.7575	−3.0444	585.0517	3.000	0.750	0.000	0.000	0.00e+00	0.00	0.00e+00	0.00
	632637.0342	−3.2682	329.0454	3.000	0.750	0.000	0.000	0.00e+00	0.00	0.00e+00	0.00
	632664.6671	−3.6869	329.0033	3.000	0.750	0.000	0.000	0.00e+00	0.00	0.00e+00	0.00
	632678.7391	−3.4907	328.9950	3.000	0.750	0.000	0.000	0.00e+00	0.00	0.00e+00	0.00
	632700.6596	−3.1423	329.0237	3.000	0.750	0.000	0.000	0.00e+00	0.00	0.00e+00	0.00
	632826.7957	−3.6637	221.0643	3.000	0.750	0.000	0.000	0.00e+00	0.00	0.00e+00	0.00
	632847.4916	−3.1423	329.0120	3.000	0.750	0.000	0.000	0.00e+00	0.00	0.00e+00	0.00

Continued on next page

molecule	ν_{0j}^k (MHz)	$\mathcal{I}_j^k$ (nm^2MHz)	$E\ell_j^k$ (cm^{-1})	w_{cj}^k (MHz hPa^{-1})	n_{cj}^k	$\Delta\nu_{0j}^k$ (MHz hPa^{-1})	$n_{\Delta\nu_{0j}}^k$	δ_j^k (hPa^{-1})	$n_{\delta_j}^k$	γ_j^k (hPa^{-1})	$n_{\gamma_j}^k$
	632866.7451	−3.4897	329.0401	3.000	0.750	0.000	0.000	0.00e+00	0.00	0.00e+00	0.00
	632927.1414	−3.6868	328.9815	3.000	0.750	0.000	0.000	0.00e+00	0.00	0.00e+00	0.00
	633168.1041	−3.5413	596.9608	3.000	0.750	0.000	0.000	0.00e+00	0.00	0.00e+00	0.00
	633197.7241	−3.0361	596.9369	3.000	0.750	0.000	0.000	0.00e+00	0.00	0.00e+00	0.00
	633374.8170	−2.9601	657.5891	3.000	0.750	0.000	0.000	0.00e+00	0.00	0.00e+00	0.00
	633385.4845	−3.4639	657.6202	3.000	0.750	0.000	0.000	0.00e+00	0.00	0.00e+00	0.00
	634437.0853	−2.8098	321.4641	3.000	0.750	0.000	0.000	0.00e+00	0.00	0.00e+00	0.00
	634492.7001	−2.8098	321.5313	3.000	0.750	0.000	0.000	0.00e+00	0.00	0.00e+00	0.00
	634547.1516	−2.9519	663.8851	3.000	0.750	0.000	0.000	0.00e+00	0.00	0.00e+00	0.00
	634563.6259	−3.4567	663.9141	3.000	0.750	0.000	0.000	0.00e+00	0.00	0.00e+00	0.00
	634628.0619	−3.1107	321.4138	3.000	0.750	0.000	0.000	0.00e+00	0.00	0.00e+00	0.00
	634683.3872	−2.8094	321.4809	3.000	0.750	0.000	0.000	0.00e+00	0.00	0.00e+00	0.00
	634873.3676	−3.4112	321.4305	3.000	0.750	0.000	0.000	0.00e+00	0.00	0.00e+00	0.00
	635224.7746	−3.5276	619.0272	3.000	0.750	0.000	0.000	0.00e+00	0.00	0.00e+00	0.00
	635249.0050	−3.0225	619.0012	3.000	0.750	0.000	0.000	0.00e+00	0.00	0.00e+00	0.00
	635352.9646	−3.5514	174.5692	3.000	0.750	0.000	0.000	0.00e+00	0.00	0.00e+00	0.00
	635387.6431	−3.6361	342.4698	3.000	0.750	0.000	0.000	0.00e+00	0.00	0.00e+00	0.00
	635407.4553	−3.2103	342.4476	3.000	0.750	0.000	0.000	0.00e+00	0.00	0.00e+00	0.00
	635728.3277	−2.9439	669.6355	3.000	0.750	0.000	0.000	0.00e+00	0.00	0.00e+00	0.00
	635750.0632	−3.4490	669.6603	3.000	0.750	0.000	0.000	0.00e+00	0.00	0.00e+00	0.00
	636302.1082	−3.5216	629.2180	3.000	0.750	0.000	0.000	0.00e+00	0.00	0.00e+00	0.00
	636322.9889	−3.0165	629.1907	3.000	0.750	0.000	0.000	0.00e+00	0.00	0.00e+00	0.00
	637011.5617	−3.4964	326.3828	3.000	0.750	0.000	0.000	0.00e+00	0.00	0.00e+00	0.00
	637085.4436	−2.8941	326.4245	3.000	0.750	0.000	0.000	0.00e+00	0.00	0.00e+00	0.00
	637160.5773	−2.8938	326.4658	3.000	0.750	0.000	0.000	0.00e+00	0.00	0.00e+00	0.00
	637216.4495	−3.3203	326.3807	3.000	0.750	0.000	0.000	0.00e+00	0.00	0.00e+00	0.00
	637289.5615	−2.8937	326.4221	3.000	0.750	0.000	0.000	0.00e+00	0.00	0.00e+00	0.00
	637402.7158	−3.5159	638.8521	3.000	0.750	0.000	0.000	0.00e+00	0.00	0.00e+00	0.00
	648392.1602	−3.5518	338.8568	3.000	0.750	0.000	0.000	0.00e+00	0.00	0.00e+00	0.00
	648415.1283	−3.3475	338.8334	3.000	0.750	0.000	0.000	0.00e+00	0.00	0.00e+00	0.00
	648422.7222	−3.6452	558.9616	3.000	0.750	0.000	0.000	0.00e+00	0.00	0.00e+00	0.00
	648460.4078	−3.7737	338.8101	3.000	0.750	0.000	0.000	0.00e+00	0.00	0.00e+00	0.00
	648611.4259	−3.6251	573.9231	3.000	0.750	0.000	0.000	0.00e+00	0.00	0.00e+00	0.00

Continued on next page

molecule	ν_{0j}^k (MHz)	I_j^k ($\mathrm{nm^2MHz}$)	$E\ell_j^k$ ($\mathrm{cm^{-1}}$)	w_{cj}^k ($\mathrm{MHz\,hPa^{-1}}$)	n_{cj}^k	$\Delta\nu_{0j}^k$ ($\mathrm{MHz\,hPa^{-1}}$)	$n_{\Delta\nu_{0j}}^k$	δ_j^k ($\mathrm{hPa^{-1}}$)	$n_{\delta_j}^k$	γ_j^k ($\mathrm{hPa^{-1}}$)	$n_{\gamma_j}^k$
	648615.8408	−3.6490	238.6814	3.000	0.750	0.000	0.000	0.00e+00	0.00	0.00e+00	0.00
	648777.1645	−3.4382	336.9214	3.000	0.750	0.000	0.000	0.00e+00	0.00	0.00e+00	0.00
	648797.2636	−3.6746	543.3072	3.000	0.750	0.000	0.000	0.00e+00	0.00	0.00e+00	0.00
	648828.6017	−2.8361	336.9815	3.000	0.750	0.000	0.000	0.00e+00	0.00	0.00e+00	0.00
	648881.4045	−2.8360	337.0415	3.000	0.750	0.000	0.000	0.00e+00	0.00	0.00e+00	0.00
	649006.4714	−3.1371	336.9361	3.000	0.750	0.000	0.000	0.00e+00	0.00	0.00e+00	0.00
	649058.5459	−2.8357	336.9961	3.000	0.750	0.000	0.000	0.00e+00	0.00	0.00e+00	0.00
	649126.1157	−3.6104	588.2405	3.000	0.750	0.000	0.000	0.00e+00	0.00	0.00e+00	0.00
	649235.1963	−3.4375	336.9506	3.000	0.750	0.000	0.000	0.00e+00	0.00	0.00e+00	0.00
	649400.6346	−3.5264	677.7969	3.000	0.750	0.000	0.000	0.00e+00	0.00	0.00e+00	0.00
	649837.4307	−3.5991	601.9434	3.000	0.750	0.000	0.000	0.00e+00	0.00	0.00e+00	0.00
	650552.8406	−3.5211	685.8131	3.000	0.750	0.000	0.000	0.00e+00	0.00	0.00e+00	0.00
	650675.5449	−3.5903	615.0505	3.000	0.750	0.000	0.000	0.00e+00	0.00	0.00e+00	0.00
	651301.5484	−3.5283	342.5482	3.000	0.750	0.000	0.000	0.00e+00	0.00	0.00e+00	0.00
	651716.9611	−3.5156	693.2806	3.000	0.750	0.000	0.000	0.00e+00	0.00	0.00e+00	0.00
	652362.6384	−3.7994	191.1281	3.000	0.750	0.000	0.000	0.00e+00	0.00	0.00e+00	0.00
	652363.3640	−3.7994	191.1281	3.000	0.750	0.000	0.000	0.00e+00	0.00	0.00e+00	0.00
	652584.0251	−3.5771	639.5250	3.000	0.750	0.000	0.000	0.00e+00	0.00	0.00e+00	0.00
	652891.7722	−3.5097	700.2005	3.000	0.750	0.000	0.000	0.00e+00	0.00	0.00e+00	0.00
	653056.9170	−3.6730	350.1067	3.000	0.750	0.000	0.000	0.00e+00	0.00	0.00e+00	0.00
	653058.5797	−3.4781	350.1503	3.000	0.750	0.000	0.000	0.00e+00	0.00	0.00e+00	0.00
	653082.3445	−3.1210	350.1283	3.000	0.750	0.000	0.000	0.00e+00	0.00	0.00e+00	0.00
	653159.1605	−3.2562	350.1479	3.000	0.750	0.000	0.000	0.00e+00	0.00	0.00e+00	0.00
	653210.7728	−3.1209	350.1216	3.000	0.750	0.000	0.000	0.00e+00	0.00	0.00e+00	0.00
	653235.2940	−3.4787	350.0989	3.000	0.750	0.000	0.000	0.00e+00	0.00	0.00e+00	0.00
	653311.8791	−3.6728	350.0937	3.000	0.750	0.000	0.000	0.00e+00	0.00	0.00e+00	0.00
	653612.7817	−3.5719	650.9082	3.000	0.750	0.000	0.000	0.00e+00	0.00	0.00e+00	0.00
	658736.4294	−3.6248	609.8930	3.000	0.750	0.000	0.000	0.00e+00	0.00	0.00e+00	0.00
	659141.9589	−3.5493	699.4586	3.000	0.750	0.000	0.000	0.00e+00	0.00	0.00e+00	0.00
	659394.5600	−3.6168	354.5299	3.000	0.750	0.000	0.000	0.00e+00	0.00	0.00e+00	0.00
	659429.8682	−3.0495	354.5550	3.000	0.750	0.000	0.000	0.00e+00	0.00	0.00e+00	0.00
	659458.8662	−3.4279	354.5796	3.000	0.750	0.000	0.000	0.00e+00	0.00	0.00e+00	0.00
	659466.9782	−3.2061	354.5794	3.000	0.750	0.000	0.000	0.00e+00	0.00	0.00e+00	0.00

Continued on next page

molecule	ν_{0j}^k (MHz)	$\mathcal{I}_j^k$ (nm^2MHz)	$E\ell_j^k$ (cm^{-1})	w_{cj}^k (MHz hPa^{-1})	n_{cj}^k	$\Delta\nu_{0j}^k$ (MHz hPa^{-1})	$n_{\Delta\nu_{0j}}^k$	δ_j^k (hPa^{-1})	$n_{\delta_j}^k$	γ_j^k (hPa^{-1})	$n_{\gamma_j}^k$
	659489.6115	−3.6154	623.6196	3.000	0.750	0.000	0.000	0.00e+00	0.00	0.00e+00	0.00
	659545.9211	−3.4288	354.5249	3.000	0.750	0.000	0.000	0.00e+00	0.00	0.00e+00	0.00
	659573.0392	−3.0493	354.5501	3.000	0.750	0.000	0.000	0.00e+00	0.00	0.00e+00	0.00
	659687.5133	−3.6163	354.5204	3.000	0.750	0.000	0.000	0.00e+00	0.00	0.00e+00	0.00
	660297.3018	−3.5446	707.5132	3.000	0.750	0.000	0.000	0.00e+00	0.00	0.00e+00	0.00
	660354.3088	−3.6080	636.7547	3.000	0.750	0.000	0.000	0.00e+00	0.00	0.00e+00	0.00
	660416.3709	−2.7902	348.5832	3.000	0.750	0.000	0.000	0.00e+00	0.00	0.00e+00	0.00
	660421.6529	−2.7901	348.5063	3.000	0.750	0.000	0.000	0.00e+00	0.00	0.00e+00	0.00
	660427.2895	−3.3920	348.4295	3.000	0.750	0.000	0.000	0.00e+00	0.00	0.00e+00	0.00
	660584.0327	−3.6633	234.8316	3.000	0.750	0.000	0.000	0.00e+00	0.00	0.00e+00	0.00
	660658.4791	−2.7898	348.5428	3.000	0.750	0.000	0.000	0.00e+00	0.00	0.00e+00	0.00
	660663.2810	−3.0908	348.4660	3.000	0.750	0.000	0.000	0.00e+00	0.00	0.00e+00	0.00
	660899.6418	−3.3915	348.5022	3.000	0.750	0.000	0.000	0.00e+00	0.00	0.00e+00	0.00
	661295.8745	−3.6020	649.3097	3.000	0.750	0.000	0.000	0.00e+00	0.00	0.00e+00	0.00
	661398.7990	−3.6627	234.8306	3.000	0.750	0.000	0.000	0.00e+00	0.00	0.00e+00	0.00
	661464.4956	−3.5395	715.0196	3.000	0.750	0.000	0.000	0.00e+00	0.00	0.00e+00	0.00
	661538.4666	−3.6034	363.6640	3.000	0.750	0.000	0.000	0.00e+00	0.00	0.00e+00	0.00
CH_3CN	183835.0975	−3.1065	206.2774	4.684	0.890	0.000	0.000	0.00e+00	0.00	0.00e+00	0.00
	183835.4437	−2.8034	206.2773	4.684	0.890	0.000	0.000	0.00e+00	0.00	0.00e+00	0.00
	183874.2327	−2.7463	151.7119	4.684	0.890	0.000	0.000	0.00e+00	0.00	0.00e+00	0.00
	183906.0868	−2.6039	107.0505	4.684	0.890	0.000	0.000	0.00e+00	0.00	0.00e+00	0.00
	183930.8684	−2.1956	72.3033	4.684	0.890	0.000	0.000	0.00e+00	0.00	0.00e+00	0.00
	183948.4900	−2.4216	47.4782	4.684	0.890	0.000	0.000	0.00e+00	0.00	0.00e+00	0.00
	183959.0800	−2.3772	32.5809	4.684	0.890	0.000	0.000	0.00e+00	0.00	0.00e+00	0.00
	183962.6200	−2.8849	27.6148	4.684	0.890	0.000	0.000	0.00e+00	0.00	0.00e+00	0.00
	183962.6200	−2.8410	27.6147	4.684	0.890	0.000	0.000	0.00e+00	0.00	0.00e+00	0.00
	183962.6200	−2.7971	27.6148	4.684	0.890	0.000	0.000	0.00e+00	0.00	0.00e+00	0.00
	202215.3769	−2.4763	212.4094	4.401	0.660	0.000	0.000	0.00e+00	0.00	0.00e+00	0.00
	202258.1607	−2.6106	157.8453	4.401	0.660	0.000	0.000	0.00e+00	0.00	0.00e+00	0.00
	202293.1896	−2.4785	113.1849	4.401	0.660	0.000	0.000	0.00e+00	0.00	0.00e+00	0.00
	202320.4492	−2.0770	78.4386	4.401	0.660	0.000	0.000	0.00e+00	0.00	0.00e+00	0.00
	202340.1000	−2.7457	53.6141	4.401	0.660	0.000	0.000	0.00e+00	0.00	0.00e+00	0.00
	202340.1000	−2.3073	53.6141	4.401	0.660	0.000	0.000	0.00e+00	0.00	0.00e+00	0.00

Continued on next page

molecule	ν_{0j}^k (MHz)	$\mathcal{I}_j^k$ ($\mathrm{nm^2MHz}$)	$E\ell_j^k$ ($\mathrm{cm^{-1}}$)	w_{cj}^k ($\mathrm{MHz\,hPa^{-1}}$)	n_{cj}^k	$\Delta\nu_{0j}^k$ ($\mathrm{MHz\,hPa^{-1}}$)	$n_{\Delta\nu_{0j}}^k$	δ_j^k ($\mathrm{hPa^{-1}}$)	$n_{\delta_j}^k$	γ_j^k ($\mathrm{hPa^{-1}}$)	$n_{\gamma_j}^k$
	202351.4500	−2.7435	38.7171	4.401	0.660	0.000	0.000	0.00e+00	0.00	0.00e+00	0.00
	202351.4500	−2.7037	38.7172	4.401	0.660	0.000	0.000	0.00e+00	0.00	0.00e+00	0.00
	202351.4500	−2.7833	38.7172	4.401	0.660	0.000	0.000	0.00e+00	0.00	0.00e+00	0.00
	202355.6100	−2.2512	33.7511	4.401	0.660	0.000	0.000	0.00e+00	0.00	0.00e+00	0.00
	624344.0986	−2.4431	586.9401	3.324	0.650	0.000	0.000	0.00e+00	0.00	0.00e+00	0.00
	624344.1105	−2.1419	586.9402	3.324	0.650	0.000	0.000	0.00e+00	0.00	0.00e+00	0.00
	624498.4440	−1.5255	522.5616	3.337	0.620	0.000	0.000	0.00e+00	0.00	0.00e+00	0.00
	624629.1049	−1.8911	468.0627	3.349	0.590	0.000	0.000	0.00e+00	0.00	0.00e+00	0.00
	624629.1122	−2.1730	468.0628	3.349	0.590	0.000	0.000	0.00e+00	0.00	0.00e+00	0.00
	624736.0997	−2.0893	423.4558	3.324	0.650	0.000	0.000	0.00e+00	0.00	0.00e+00	0.00
	624736.1036	−1.7881	423.4559	3.324	0.650	0.000	0.000	0.00e+00	0.00	0.00e+00	0.00
	624819.3430	−1.7260	388.7511	3.337	0.620	0.000	0.000	0.00e+00	0.00	0.00e+00	0.00
	624819.3430	−1.7132	388.7510	3.337	0.620	0.000	0.000	0.00e+00	0.00	0.00e+00	0.00
	624819.3430	−1.7004	388.7511	3.337	0.620	0.000	0.000	0.00e+00	0.00	0.00e+00	0.00
	624878.8642	−1.4834	363.9563	3.337	0.620	0.000	0.000	0.00e+00	0.00	0.00e+00	0.00
	624914.5729	−1.4512	349.0772	3.337	0.620	0.000	0.000	0.00e+00	0.00	0.00e+00	0.00
	624926.4775	−1.4405	344.1171	3.337	0.620	0.000	0.000	0.00e+00	0.00	0.00e+00	0.00
	660994.4320	−2.1488	629.2032	3.381	0.540	0.000	0.000	0.00e+00	0.00	0.00e+00	0.00
	661157.5676	−1.5389	564.8351	3.381	0.540	0.000	0.000	0.00e+00	0.00	0.00e+00	0.00
	661295.7173	−1.7225	510.3451	3.381	0.540	0.000	0.000	0.00e+00	0.00	0.00e+00	0.00
	661408.8233	−2.1036	465.7454	3.381	0.540	0.000	0.000	0.00e+00	0.00	0.00e+00	0.00
	661408.8266	−1.8024	465.7455	3.381	0.540	0.000	0.000	0.00e+00	0.00	0.00e+00	0.00
	661496.8230	−1.2506	431.0463	3.381	0.540	0.000	0.000	0.00e+00	0.00	0.00e+00	0.00
	661559.7415	−1.9875	406.2556	3.381	0.540	0.000	0.000	0.00e+00	0.00	0.00e+00	0.00
	661559.7435	−1.9754	406.2555	3.381	0.540	0.000	0.000	0.00e+00	0.00	0.00e+00	0.00
	661559.7472	−1.9633	406.2556	3.381	0.540	0.000	0.000	0.00e+00	0.00	0.00e+00	0.00
$CH_3^{35}Cl$	185968.0370	−4.1016	206.0033	2.500	0.500	0.000	0.000	0.00e+00	0.00	0.00e+00	0.00
	185980.0370	−4.0379	206.0023	2.500	0.500	0.000	0.000	0.00e+00	0.00	0.00e+00	0.00
	186000.8870	−4.0170	148.7477	2.500	0.500	0.000	0.000	0.00e+00	0.00	0.00e+00	0.00
	186003.0590	−4.0818	148.7476	2.500	0.500	0.000	0.000	0.00e+00	0.00	0.00e+00	0.00
	186009.2240	−3.9532	148.7472	2.500	0.500	0.000	0.000	0.00e+00	0.00	0.00e+00	0.00
	186011.4060	−4.1464	148.7471	2.500	0.500	0.000	0.000	0.00e+00	0.00	0.00e+00	0.00
	186027.7810	−3.7810	101.9023	2.500	0.500	0.000	0.000	0.00e+00	0.00	0.00e+00	0.00

Continued on next page

molecule	ν_{0j}^k (MHz)	I_j^k ($\mathrm{nm^2MHz}$)	$E\ell_j^k$ ($\mathrm{cm^{-1}}$)	w_{cj}^k ($\mathrm{MHz\,hPa^{-1}}$)	n_{cj}^k	$\Delta\nu_{0j}^k$ ($\mathrm{MHz\,hPa^{-1}}$)	$n_{\Delta\nu_{0j}}^k$	δ_j^k ($\mathrm{hPa^{-1}}$)	$n_{\delta_j}^k$	γ_j^k ($\mathrm{hPa^{-1}}$)	$n_{\gamma_j}^k$
	186028.9560	−3.8458	101.9022	2.500	0.500	0.000	0.000	0.00e+00	0.00	0.00e+00	0.00
	186033.1230	−3.7173	101.9022	2.500	0.500	0.000	0.000	0.00e+00	0.00	0.00e+00	0.00
	186034.2980	−3.9104	101.9022	2.500	0.500	0.000	0.000	0.00e+00	0.00	0.00e+00	0.00
	186048.7630	−3.3204	65.4669	2.500	0.500	0.000	0.000	0.00e+00	0.00	0.00e+00	0.00
	186049.1430	−3.3852	65.4670	2.500	0.500	0.000	0.000	0.00e+00	0.00	0.00e+00	0.00
	186051.7820	−3.2567	65.4671	2.500	0.500	0.000	0.000	0.00e+00	0.00	0.00e+00	0.00
	186052.1450	−3.4498	65.4672	2.500	0.500	0.000	0.000	0.00e+00	0.00	0.00e+00	0.00
	186063.5228	−3.5808	39.4418	2.500	0.500	0.000	0.000	0.00e+00	0.00	0.00e+00	0.00
	186063.6898	−3.5161	39.4417	2.500	0.500	0.000	0.000	0.00e+00	0.00	0.00e+00	0.00
	186064.8555	−3.6454	39.4422	2.500	0.500	0.000	0.000	0.00e+00	0.00	0.00e+00	0.00
	186065.0270	−3.4523	39.4421	2.500	0.500	0.000	0.000	0.00e+00	0.00	0.00e+00	0.00
	186072.1696	−3.5202	23.8267	2.500	0.500	0.000	0.000	0.00e+00	0.00	0.00e+00	0.00
	186072.5014	−3.5848	23.8272	2.500	0.500	0.000	0.000	0.00e+00	0.00	0.00e+00	0.00
	186072.6720	−3.4555	23.8265	2.500	0.500	0.000	0.000	0.00e+00	0.00	0.00e+00	0.00
	186073.0078	−3.3917	23.8271	2.500	0.500	0.000	0.000	0.00e+00	0.00	0.00e+00	0.00
	186075.1170	−3.5650	18.6222	2.500	0.500	0.000	0.000	0.00e+00	0.00	0.00e+00	0.00
	186075.1170	−3.5004	18.6216	2.500	0.500	0.000	0.000	0.00e+00	0.00	0.00e+00	0.00
	186075.6160	−3.4356	18.6215	2.500	0.500	0.000	0.000	0.00e+00	0.00	0.00e+00	0.00
	186075.6160	−3.3719	18.6221	2.500	0.500	0.000	0.000	0.00e+00	0.00	0.00e+00	0.00
	636288.1819	−2.6768	665.9084	2.500	0.500	0.000	0.000	0.00e+00	0.00	0.00e+00	0.00
	636288.8365	−2.9507	665.9087	2.500	0.500	0.000	0.000	0.00e+00	0.00	0.00e+00	0.00
	636288.8439	−3.0051	665.9088	2.500	0.500	0.000	0.000	0.00e+00	0.00	0.00e+00	0.00
	636449.0467	−2.7788	577.4800	2.500	0.500	0.000	0.000	0.00e+00	0.00	0.00e+00	0.00
	636449.5669	−2.7780	577.4804	2.500	0.500	0.000	0.000	0.00e+00	0.00	0.00e+00	0.00
	636591.1990	−2.6035	499.4550	2.500	0.500	0.000	0.000	0.00e+00	0.00	0.00e+00	0.00
	636591.5976	−2.6028	499.4555	2.500	0.500	0.000	0.000	0.00e+00	0.00	0.00e+00	0.00
	636714.5472	−2.4611	431.8335	2.500	0.500	0.000	0.000	0.00e+00	0.00	0.00e+00	0.00
	636714.5705	−2.4429	431.8334	2.500	0.500	0.000	0.000	0.00e+00	0.00	0.00e+00	0.00
	636714.8377	−2.4793	431.8340	2.500	0.500	0.000	0.000	0.00e+00	0.00	0.00e+00	0.00
	636714.8650	−2.4248	431.8339	2.500	0.500	0.000	0.000	0.00e+00	0.00	0.00e+00	0.00
	636819.0577	−2.3239	374.6152	2.500	0.500	0.000	0.000	0.00e+00	0.00	0.00e+00	0.00
	636819.2426	−2.6522	374.6158	2.500	0.500	0.000	0.000	0.00e+00	0.00	0.00e+00	0.00
	636819.2783	−2.5978	374.6157	2.500	0.500	0.000	0.000	0.00e+00	0.00	0.00e+00	0.00

Continued on next page

molecule	ν_{0j}^k (MHz)	$\mathcal{I}_j^k$ ($\mathrm{nm^2MHz}$)	$E\ell_j^k$ ($\mathrm{cm^{-1}}$)	w_{cj}^k ($\mathrm{MHz\,hPa^{-1}}$)	n_{cj}^k	$\Delta\nu_{0j}^k$ ($\mathrm{MHz\,hPa^{-1}}$)	$n_{\Delta\nu_j}^k$	δ_j^k ($\mathrm{hPa^{-1}}$)	$n_{\delta_j}^k$	γ_j^k ($\mathrm{hPa^{-1}}$)	$n_{\gamma_j}^k$
	636904.6166	−2.5294	327.8004	2.500	0.500	0.000	0.000	0.00e+00	0.00	0.00e+00	0.00
	636904.6553	−2.5112	327.8003	2.500	0.500	0.000	0.000	0.00e+00	0.00	0.00e+00	0.00
	636904.7673	−2.2184	327.8009	2.500	0.500	0.000	0.000	0.00e+00	0.00	0.00e+00	0.00
	636971.2472	−1.8368	291.3888	2.500	0.500	0.000	0.000	0.00e+00	0.00	0.00e+00	0.00
	636971.3213	−1.8361	291.3894	2.500	0.500	0.000	0.000	0.00e+00	0.00	0.00e+00	0.00
	637018.8285	−2.3900	265.3806	2.500	0.500	0.000	0.000	0.00e+00	0.00	0.00e+00	0.00
	637018.8590	−2.4082	265.3812	2.500	0.500	0.000	0.000	0.00e+00	0.00	0.00e+00	0.00
	637018.8763	−2.3719	265.3805	2.500	0.500	0.000	0.000	0.00e+00	0.00	0.00e+00	0.00
	637018.9108	−2.3537	265.3811	2.500	0.500	0.000	0.000	0.00e+00	0.00	0.00e+00	0.00
	637047.4014	−2.3552	249.7756	2.500	0.500	0.000	0.000	0.00e+00	0.00	0.00e+00	0.00
	637047.4075	−2.3734	249.7762	2.500	0.500	0.000	0.000	0.00e+00	0.00	0.00e+00	0.00
	637047.4516	−2.3371	249.7756	2.500	0.500	0.000	0.000	0.00e+00	0.00	0.00e+00	0.00
	637047.4617	−2.3189	249.7762	2.500	0.500	0.000	0.000	0.00e+00	0.00	0.00e+00	0.00
	637056.9255	−2.3617	244.5746	2.500	0.500	0.000	0.000	0.00e+00	0.00	0.00e+00	0.00
	637056.9275	−2.3436	244.5740	2.500	0.500	0.000	0.000	0.00e+00	0.00	0.00e+00	0.00
	637056.9784	−2.3254	244.5739	2.500	0.500	0.000	0.000	0.00e+00	0.00	0.00e+00	0.00
	637056.9804	−2.3073	244.5746	2.500	0.500	0.000	0.000	0.00e+00	0.00	0.00e+00	0.00
$CH_3^{37}Cl$	183184.7324	−3.0720	65.1803	2.500	0.500	0.000	0.000	0.00e+00	0.00	0.00e+00	0.00
	183186.9584	−3.2781	65.1804	2.500	0.500	0.000	0.000	0.00e+00	0.00	0.00e+00	0.00
	183187.2631	−3.4712	65.1805	2.500	0.500	0.000	0.000	0.00e+00	0.00	0.00e+00	0.00
	183198.8300	−3.6022	39.1551	2.500	0.500	0.000	0.000	0.00e+00	0.00	0.00e+00	0.00
	183198.9617	−3.5375	39.1550	2.500	0.500	0.000	0.000	0.00e+00	0.00	0.00e+00	0.00
	183199.9626	−3.2586	39.1554	2.500	0.500	0.000	0.000	0.00e+00	0.00	0.00e+00	0.00
	183207.1922	−3.5416	23.5400	2.500	0.500	0.000	0.000	0.00e+00	0.00	0.00e+00	0.00
	183207.4536	−3.6062	23.5404	2.500	0.500	0.000	0.000	0.00e+00	0.00	0.00e+00	0.00
	183207.5882	−3.4769	23.5398	2.500	0.500	0.000	0.000	0.00e+00	0.00	0.00e+00	0.00
	183207.8529	−3.4131	23.5403	2.500	0.500	0.000	0.000	0.00e+00	0.00	0.00e+00	0.00
	183209.9786	−3.5864	18.3354	2.500	0.500	0.000	0.000	0.00e+00	0.00	0.00e+00	0.00
	183209.9802	−3.5218	18.3349	2.500	0.500	0.000	0.000	0.00e+00	0.00	0.00e+00	0.00
	183210.4642	−3.4570	18.3348	2.500	0.500	0.000	0.000	0.00e+00	0.00	0.00e+00	0.00
	183210.4659	−3.3933	18.3353	2.500	0.500	0.000	0.000	0.00e+00	0.00	0.00e+00	0.00
	626926.9793	−2.4750	428.0732	2.500	0.500	0.000	0.000	0.00e+00	0.00	0.00e+00	0.00
	626926.9977	−2.4568	428.0731	2.500	0.500	0.000	0.000	0.00e+00	0.00	0.00e+00	0.00

Continued on next page

molecule	ν_{0j}^k (MHz)	$\mathcal{I}_j^k$ ($\mathrm{nm^2MHz}$)	$E\ell_j^k$ ($\mathrm{cm^{-1}}$)	w_{cj}^k ($\mathrm{MHz\,hPa^{-1}}$)	n_{cj}^k	$\Delta\nu_{0j}^k$ ($\mathrm{MHz\,hPa^{-1}}$)	$n_{\Delta\nu_{0j}}^k$	δ_j^k ($\mathrm{hPa^{-1}}$)	$n_{\delta_j}^k$	γ_j^k ($\mathrm{hPa^{-1}}$)	$n_{\gamma_j}^k$
	626927.2082	−2.4932	428.0736	2.500	0.500	0.000	0.000	0.00e+00	0.00	0.00e+00	0.00
	626927.2299	−2.4387	428.0735	2.500	0.500	0.000	0.000	0.00e+00	0.00	0.00e+00	0.00
	627028.7082	−2.3378	370.8539	2.500	0.500	0.000	0.000	0.00e+00	0.00	0.00e+00	0.00
	627028.8690	−2.3370	370.8543	2.500	0.500	0.000	0.000	0.00e+00	0.00	0.00e+00	0.00
	652962.8523	−2.1538	448.9852	2.500	0.500	0.000	0.000	0.00e+00	0.00	0.00e+00	0.00
	652963.0568	−2.1532	448.9856	2.500	0.500	0.000	0.000	0.00e+00	0.00	0.00e+00	0.00
	653068.7870	−2.3275	391.7693	2.500	0.500	0.000	0.000	0.00e+00	0.00	0.00e+00	0.00
	653068.9292	−2.3268	391.7697	2.500	0.500	0.000	0.000	0.00e+00	0.00	0.00e+00	0.00
	653155.5452	−2.2234	344.9563	2.500	0.500	0.000	0.000	0.00e+00	0.00	0.00e+00	0.00
	653155.6365	−2.2228	344.9568	2.500	0.500	0.000	0.000	0.00e+00	0.00	0.00e+00	0.00
	653223.0762	−1.8415	308.5463	2.500	0.500	0.000	0.000	0.00e+00	0.00	0.00e+00	0.00
	653223.1280	−1.8408	308.5467	2.500	0.500	0.000	0.000	0.00e+00	0.00	0.00e+00	0.00
	653271.3230	−2.3946	282.5391	2.500	0.500	0.000	0.000	0.00e+00	0.00	0.00e+00	0.00
	653271.3440	−2.4120	282.5396	2.500	0.500	0.000	0.000	0.00e+00	0.00	0.00e+00	0.00
	653271.3581	−2.3772	282.5391	2.500	0.500	0.000	0.000	0.00e+00	0.00	0.00e+00	0.00
	653271.3824	−2.3598	282.5396	2.500	0.500	0.000	0.000	0.00e+00	0.00	0.00e+00	0.00
	653300.2922	−2.3600	266.9348	2.500	0.500	0.000	0.000	0.00e+00	0.00	0.00e+00	0.00
	653300.2962	−2.3774	266.9353	2.500	0.500	0.000	0.000	0.00e+00	0.00	0.00e+00	0.00
	653300.3289	−2.3426	266.9348	2.500	0.500	0.000	0.000	0.00e+00	0.00	0.00e+00	0.00
	653300.3362	−2.3251	266.9353	2.500	0.500	0.000	0.000	0.00e+00	0.00	0.00e+00	0.00
	653309.9488	−2.3658	261.7339	2.500	0.500	0.000	0.000	0.00e+00	0.00	0.00e+00	0.00
	653309.9505	−2.3484	261.7334	2.500	0.500	0.000	0.000	0.00e+00	0.00	0.00e+00	0.00
	653309.9877	−2.3310	261.7333	2.500	0.500	0.000	0.000	0.00e+00	0.00	0.00e+00	0.00
	653309.9893	−2.3136	261.7338	2.500	0.500	0.000	0.000	0.00e+00	0.00	0.00e+00	0.00
CH_3OH	181296.0300	−3.9714	42.9881	3.000	0.500	0.000	0.000	0.00e+00	0.00	0.00e+00	0.00
	181771.0500	−4.4518	28.0738	3.000	0.500	0.000	0.000	0.00e+00	0.00	0.00e+00	0.00
	183124.9773	−4.3189	92.6906	3.000	0.500	0.000	0.000	0.00e+00	0.00	0.00e+00	0.00
	183853.0000	−4.3733	44.2782	3.000	0.500	0.000	0.000	0.00e+00	0.00	0.00e+00	0.00
	183879.9600	−4.3154	92.6903	3.000	0.500	0.000	0.000	0.00e+00	0.00	0.00e+00	0.00
	186300.9500	−4.7410	88.7681	3.000	0.500	0.000	0.000	0.00e+00	0.00	0.00e+00	0.00
	201072.0504	−4.3865	107.2083	3.000	0.500	0.000	0.000	0.00e+00	0.00	0.00e+00	0.00
	201089.2756	−4.3864	107.2078	3.000	0.500	0.000	0.000	0.00e+00	0.00	0.00e+00	0.00
	201445.4885	−4.2933	43.6940	3.000	0.500	0.000	0.000	0.00e+00	0.00	0.00e+00	0.00

Continued on next page

molecule	ν_{0j}^k (MHz)	$\mathcal{I}_j^k$ ($\mathrm{nm^2MHz}$)	$E\ell_j^k$ ($\mathrm{cm^{-1}}$)	u_{cj}^k ($\mathrm{MHz\,hPa^{-1}}$)	n_{cj}^k	$\Delta\nu_{0j}^k$ ($\mathrm{MHz\,hPa^{-1}}$)	$n_{\Delta\nu_{0j}}^k$	δ_j^k ($\mathrm{hPa^{-1}}$)	$n_{\delta_j}^k$	γ_j^k ($\mathrm{hPa^{-1}}$)	$n_{\gamma_j}^k$
	205791.2813	−4.3790	4.8405	3.000	0.500	0.000	0.000	0.00e+00	0.00	0.00e+00	0.00
	626626.1888	−2.9614	14.9878	3.000	0.500	0.000	0.000	0.00e+00	0.00	0.00e+00	0.00
	636238.2680	−2.6714	160.4325	3.000	0.500	0.000	0.000	0.00e+00	0.00	0.00e+00	0.00
	636259.8546	−2.6739	141.0791	3.000	0.500	0.000	0.000	0.00e+00	0.00	0.00e+00	0.00
	636263.3859	−2.6739	141.0804	3.000	0.500	0.000	0.000	0.00e+00	0.00	0.00e+00	0.00
	636264.0656	−2.6853	123.3384	3.000	0.500	0.000	0.000	0.00e+00	0.00	0.00e+00	0.00
	636274.0770	−2.6853	123.3375	3.000	0.500	0.000	0.000	0.00e+00	0.00	0.00e+00	0.00
	636279.9980	−2.7071	107.2083	3.000	0.500	0.000	0.000	0.00e+00	0.00	0.00e+00	0.00
	636287.1936	−2.6714	160.4342	3.000	0.500	0.000	0.000	0.00e+00	0.00	0.00e+00	0.00
	636290.7110	−2.7071	107.2078	3.000	0.500	0.000	0.000	0.00e+00	0.00	0.00e+00	0.00
	636304.3550	−2.7422	92.6906	3.000	0.500	0.000	0.000	0.00e+00	0.00	0.00e+00	0.00
	636311.6900	−2.7422	92.6903	3.000	0.500	0.000	0.000	0.00e+00	0.00	0.00e+00	0.00
	636333.4700	−2.7952	79.7853	3.000	0.500	0.000	0.000	0.00e+00	0.00	0.00e+00	0.00
	636337.4190	−2.7951	79.7852	3.000	0.500	0.000	0.000	0.00e+00	0.00	0.00e+00	0.00
	636363.8430	−2.8751	68.4927	3.000	0.500	0.000	0.000	0.00e+00	0.00	0.00e+00	0.00
	636366.2480	−2.8751	68.4927	3.000	0.500	0.000	0.000	0.00e+00	0.00	0.00e+00	0.00
	636393.5680	−2.7022	58.8130	3.000	0.500	0.000	0.000	0.00e+00	0.00	0.00e+00	0.00
	636420.2310	−2.9486	50.7463	3.000	0.500	0.000	0.000	0.00e+00	0.00	0.00e+00	0.00
CO	230538.0000	−4.1197	3.8450	2.197	0.760	0.000	0.000	0.00e+00	0.00	0.00e+00	0.00
^{13}CO	661067.2801	−2.8687	55.1341	1.833	0.690	0.000	0.000	0.00e+00	0.00	0.00e+00	0.00
^{35}ClO	204293.8478	−4.4911	13.0222	2.499	0.500	0.000	0.000	0.00e+00	0.00	0.00e+00	0.00
	204295.0210	−4.4911	13.0222	2.499	0.500	0.000	0.000	0.00e+00	0.00	0.00e+00	0.00
	204327.6084	−4.0695	13.0203	2.529	0.620	0.000	0.000	0.00e+00	0.00	0.00e+00	0.00
	204346.0000	−2.7855	13.0222	2.529	0.620	0.000	0.000	0.00e+00	0.00	0.00e+00	0.00
	204350.9229	−4.1913	13.0193	2.499	0.500	0.000	0.000	0.00e+00	0.00	0.00e+00	0.00
	204351.6300	−3.1688	13.0203	2.529	0.620	0.000	0.000	0.00e+00	0.00	0.00e+00	0.00
	204352.2200	−3.1688	13.0203	2.529	0.620	0.000	0.000	0.00e+00	0.00	0.00e+00	0.00
	204356.8600	−3.2535	13.0193	2.529	0.620	0.000	0.000	0.00e+00	0.00	0.00e+00	0.00
	204357.4800	−3.2535	13.0193	2.529	0.620	0.000	0.000	0.00e+00	0.00	0.00e+00	0.00
	204362.5570	−3.0373	13.0189	2.529	0.620	0.000	0.000	0.00e+00	0.00	0.00e+00	0.00
	204491.5050	−3.7256	334.5504	2.499	0.500	0.000	0.000	0.00e+00	0.00	0.00e+00	0.00
	204491.9374	−3.8079	334.5525	2.499	0.500	0.000	0.000	0.00e+00	0.00	0.00e+00	0.00
	204493.3344	−3.8926	334.5551	2.499	0.500	0.000	0.000	0.00e+00	0.00	0.00e+00	0.00

Continued on next page

molecule	ν_{0j}^k (MHz)	I_j^k (nm^2MHz)	$E\ell_j^k$ (cm^{-1})	w_{cj}^k (MHz hPa^{-1})	n_{cj}^k	$\Delta\nu_{0j}^k$ (MHz hPa^{-1})	$n_{\Delta\nu_{0j}}^k$	δ_j^k (hPa^{-1})	$n_{\delta_j}^k$	γ_j^k (hPa^{-1})	$n_{\gamma_j}^k$
	204497.9715	−3.9774	334.5578	2.499	0.500	0.000	0.000	0.00e+00	0.00	0.00e+00	0.00
	205168.7432	−3.7230	334.6707	2.499	0.500	0.000	0.000	0.00e+00	0.00	0.00e+00	0.00
	205175.4649	−3.8054	334.6658	2.499	0.500	0.000	0.000	0.00e+00	0.00	0.00e+00	0.00
	205176.8563	−3.9748	334.6606	2.499	0.500	0.000	0.000	0.00e+00	0.00	0.00e+00	0.00
	205177.4267	−3.8900	334.6626	2.499	0.500	0.000	0.000	0.00e+00	0.00	0.00e+00	0.00
	649445.0400	−1.9671	176.5276	2.144	0.769	0.000	0.000	0.00e+00	0.00	0.00e+00	0.00
	649445.0400	−1.9920	176.5265	2.144	0.769	0.000	0.000	0.00e+00	0.00	0.00e+00	0.00
	649445.0400	−2.0170	176.5262	2.144	0.769	0.000	0.000	0.00e+00	0.00	0.00e+00	0.00
	649445.0400	−2.0420	176.5265	2.144	0.769	0.000	0.000	0.00e+00	0.00	0.00e+00	0.00
	649451.1700	−1.9671	176.5287	2.144	0.769	0.000	0.000	0.00e+00	0.00	0.00e+00	0.00
	649451.1700	−1.9920	176.5276	2.144	0.769	0.000	0.000	0.00e+00	0.00	0.00e+00	0.00
	649451.1700	−2.0170	176.5272	2.144	0.769	0.000	0.000	0.00e+00	0.00	0.00e+00	0.00
	649451.1700	−2.0420	176.5275	2.144	0.769	0.000	0.000	0.00e+00	0.00	0.00e+00	0.00
	650628.9967	−2.6329	498.3054	2.499	0.500	0.000	0.000	0.00e+00	0.00	0.00e+00	0.00
	650629.1177	−2.6579	498.3077	2.499	0.500	0.000	0.000	0.00e+00	0.00	0.00e+00	0.00
	650629.3322	−2.6829	498.3105	2.499	0.500	0.000	0.000	0.00e+00	0.00	0.00e+00	0.00
	650629.8570	−2.7078	498.3138	2.499	0.500	0.000	0.000	0.00e+00	0.00	0.00e+00	0.00
	651298.1297	−2.6329	498.6952	2.499	0.500	0.000	0.000	0.00e+00	0.00	0.00e+00	0.00
	651298.7393	−2.6578	498.6912	2.499	0.500	0.000	0.000	0.00e+00	0.00	0.00e+00	0.00
	651298.9924	−2.6828	498.6883	2.499	0.500	0.000	0.000	0.00e+00	0.00	0.00e+00	0.00
	651299.1048	−2.7077	498.6862	2.499	0.500	0.000	0.000	0.00e+00	0.00	0.00e+00	0.00
^{37}ClO	200882.1646	−4.0901	12.7996	2.529	0.620	0.000	0.000	0.00e+00	0.00	0.00e+00	0.00
	200897.3378	−3.1071	12.8011	2.529	0.620	0.000	0.000	0.00e+00	0.00	0.00e+00	0.00
	200897.8638	−3.1071	12.8012	2.529	0.620	0.000	0.000	0.00e+00	0.00	0.00e+00	0.00
	200902.3004	−3.1894	12.7996	2.529	0.620	0.000	0.000	0.00e+00	0.00	0.00e+00	0.00
	200902.9097	−3.1894	12.7996	2.529	0.620	0.000	0.000	0.00e+00	0.00	0.00e+00	0.00
	200906.6905	−3.2741	12.7987	2.529	0.620	0.000	0.000	0.00e+00	0.00	0.00e+00	0.00
	200907.2946	−3.2741	12.7988	2.529	0.620	0.000	0.000	0.00e+00	0.00	0.00e+00	0.00
	200911.1624	−3.3589	12.7984	2.529	0.620	0.000	0.000	0.00e+00	0.00	0.00e+00	0.00
	200911.6721	−3.3589	12.7984	2.529	0.620	0.000	0.000	0.00e+00	0.00	0.00e+00	0.00
	201027.2255	−3.7463	334.3268	2.499	0.500	0.000	0.000	0.00e+00	0.00	0.00e+00	0.00
	201027.5892	−3.8286	334.3286	2.499	0.500	0.000	0.000	0.00e+00	0.00	0.00e+00	0.00
	201028.8033	−3.9133	334.3308	2.499	0.500	0.000	0.000	0.00e+00	0.00	0.00e+00	0.00

Continued on next page

molecule	ν_{0j}^k (MHz)	$\mathcal{I}_j^k$ (nm^{2}MHz)	$E\ell_j^k$ (cm^{-1})	w_{cj}^k (MHz hPa^{-1})	n_{cj}^k	$\Delta\nu_{0j}^k$ (MHz hPa^{-1})	$n_{\Delta\nu_{0j}}^k$	δ_j^k (hPa^{-1})	$n_{\delta_j}^k$	γ_j^k (hPa^{-1})	$n_{\gamma_j}^k$
	201032.6599	−3.9981	334.3329	2.499	0.500	0.000	0.000	0.00e+00	0.00	0.00e+00	0.00
	201692.5232	−3.7437	334.4439	2.499	0.500	0.000	0.000	0.00e+00	0.00	0.00e+00	0.00
	201698.1377	−3.8260	334.4399	2.499	0.500	0.000	0.000	0.00e+00	0.00	0.00e+00	0.00
	201699.3266	−3.9955	334.4355	2.499	0.500	0.000	0.000	0.00e+00	0.00	0.00e+00	0.00
	201699.8196	−3.9107	334.4372	2.499	0.500	0.000	0.000	0.00e+00	0.00	0.00e+00	0.00
^{35}ClOO^{35}Cl	184670.4272	−4.6335	129.4034	2.750	0.750	0.000	0.000	0.00e+00	0.00	0.00e+00	0.00
	185356.6423	−4.5386	131.1088	2.750	0.750	0.000	0.000	0.00e+00	0.00	0.00e+00	0.00
	201586.7461	−4.5590	154.8783	2.750	0.750	0.000	0.000	0.00e+00	0.00	0.00e+00	0.00
	202362.0204	−4.4744	156.6914	2.750	0.750	0.000	0.000	0.00e+00	0.00	0.00e+00	0.00
	205747.6470	−4.5434	161.6025	2.750	0.750	0.000	0.000	0.00e+00	0.00	0.00e+00	0.00
	205991.6776	−4.6487	159.1894	2.750	0.750	0.000	0.000	0.00e+00	0.00	0.00e+00	0.00
	206611.2336	−4.4607	163.4415	2.750	0.750	0.000	0.000	0.00e+00	0.00	0.00e+00	0.00
H^{35}Cl	625901.6030	−1.3118	0.0000	2.541	0.723	0.109	0.417	0.00e+00	0.00	0.00e+00	0.00
	625918.7560	−1.1357	0.0000	2.541	0.723	0.109	0.417	0.00e+00	0.00	0.00e+00	0.00
	625932.0070	−1.6128	0.0000	2.541	0.723	0.109	0.417	0.00e+00	0.00	0.00e+00	0.00
H^{37}Cl	624964.3740	−1.3137	0.0000	2.541	0.723	0.109	0.417	0.00e+00	0.00	0.00e+00	0.00
	624977.8210	−1.1376	0.0000	2.541	0.723	0.109	0.417	0.00e+00	0.00	0.00e+00	0.00
	624988.3340	−1.6147	0.0000	2.541	0.723	0.109	0.417	0.00e+00	0.00	0.00e+00	0.00
HCN	177259.8176	−2.3132	2.9564	4.577	0.500	0.000	0.000	0.00e+00	0.00	0.00e+00	0.00
	177261.1836	−1.7466	2.9564	4.577	0.500	0.000	0.000	0.00e+00	0.00	0.00e+00	0.00
	177263.4450	−2.6811	2.9564	4.577	0.500	0.000	0.000	0.00e+00	0.00	0.00e+00	0.00
H_2CO	653970.1550	−1.6143	120.1291	3.145	0.500	0.000	0.000	0.00e+00	0.00	0.00e+00	0.00
H_2O	22235.0800	−5.8875	446.5107	2.658	0.640	0.000	0.000	0.00e+00	0.00	0.00e+00	0.00
	183310.1170	−3.6465	136.1639	2.950	0.800	−0.060	1.375	0.00e+00	0.00	0.00e+00	0.00
	321225.6400	−5.1005	1282.9191	2.148	0.640	0.000	0.000	0.00e+00	0.00	0.00e+00	0.00
	325152.9190	−3.5737	315.7795	2.725	0.640	0.000	0.000	0.00e+00	0.00	0.00e+00	0.00
	380197.3720	−2.6163	212.1564	2.863	0.720	0.000	0.000	0.00e+00	0.00	0.00e+00	0.00
	390134.5080	−6.0426	1525.1360	1.907	0.640	0.000	0.000	0.00e+00	0.00	0.00e+00	0.00
	437346.6670	−4.8155	1045.0583	1.370	0.640	0.000	0.000	0.00e+00	0.00	0.00e+00	0.00
	439150.8120	−3.6583	742.0763	1.643	0.640	0.000	0.000	0.00e+00	0.00	0.00e+00	0.00
	443018.2950	−4.3272	1045.0579	1.411	0.640	0.000	0.000	0.00e+00	0.00	0.00e+00	0.00
	448001.0750	−2.5931	285.4186	2.385	0.640	0.000	0.000	0.00e+00	0.00	0.00e+00	0.00
	470888.9470	−4.0745	742.0730	1.793	0.640	0.000	0.000	0.00e+00	0.00	0.00e+00	0.00

Continued on next page

molecule	ν_{0j}^k (MHz)	$\mathcal{I}_j^k$ (nm^{2}MHz)	$E\ell_j^k$ (cm^{-1})	w_{cj}^k (MHz hPa^{-1})	n_{cj}^k	$\Delta\nu_{0j}^k$ (MHz hPa^{-1})	$n_{\Delta\nu_{0j}}^k$	δ_j^k (hPa^{-1})	$n_{\delta_j}^k$	γ_j^k (hPa^{-1})	$n_{\gamma_j}^k$
	474689.1270	−3.4842	488.1342	1.983	0.640	0.000	0.000	0.00e+00	0.00	0.00e+00	0.00
	488491.1330	−4.1823	586.4792	2.497	0.640	0.000	0.000	0.00e+00	0.00	0.00e+00	0.00
	503568.5320	−4.9795	1394.8142	1.156	0.640	0.000	0.000	0.00e+00	0.00	0.00e+00	0.00
	504482.6920	−5.4550	1394.8141	1.162	0.640	0.000	0.000	0.00e+00	0.00	0.00e+00	0.00
	556936.0020	−0.8180	23.7944	3.069	0.640	0.000	0.000	0.00e+00	0.00	0.00e+00	0.00
	620700.8070	−2.7675	488.1077	2.212	0.640	0.000	0.000	0.00e+00	0.00	0.00e+00	0.00
	645766.0100	−6.0872	1789.0428	1.001	0.640	0.000	0.000	0.00e+00	0.00	0.00e+00	0.00
	645905.6200	−5.6099	1789.0428	1.003	0.640	0.000	0.000	0.00e+00	0.00	0.00e+00	0.00
	752033.2270	−0.9975	70.0908	2.908	0.640	0.000	0.000	0.00e+00	0.00	0.00e+00	0.00
	766793.5803	−6.2648	1960.2074	1.144	0.640	0.000	0.000	0.00e+00	0.00	0.00e+00	0.00
	841051.1620	−5.2267	1690.6644	1.414	0.640	0.000	0.000	0.00e+00	0.00	0.00e+00	0.00
	854050.4341	−6.2615	2246.8848	0.951	0.640	0.000	0.000	0.00e+00	0.00	0.00e+00	0.00
	863838.9300	−6.2833	2225.4692	0.895	0.640	0.000	0.000	0.00e+00	0.00	0.00e+00	0.00
	906206.1180	−4.0529	1050.1577	2.347	0.640	0.000	0.000	0.00e+00	0.00	0.00e+00	0.00
	916171.5820	−2.3745	285.2193	2.503	0.640	0.000	0.000	0.00e+00	0.00	0.00e+00	0.00
	970315.0220	−2.3214	383.8425	2.403	0.640	0.000	0.000	0.00e+00	0.00	0.00e+00	0.00
	987926.7640	−1.1368	37.1371	2.896	0.640	0.000	0.000	0.00e+00	0.00	0.00e+00	0.00
	1097364.7910	−0.3212	136.7617	2.852	0.640	0.000	0.000	0.00e+00	0.00	0.00e+00	0.00
	1109597.5937	−5.0968	1437.9686	1.558	0.640	0.000	0.000	0.00e+00	0.00	0.00e+00	0.00
	1113342.9640	−0.8389	0.0000	2.787	0.640	0.000	0.000	0.00e+00	0.00	0.00e+00	0.00
	1146621.1610	−3.4704	744.1627	2.253	0.640	0.000	0.000	0.00e+00	0.00	0.00e+00	0.00
	1153126.8220	−1.1310	134.9016	2.743	0.640	0.000	0.000	0.00e+00	0.00	0.00e+00	0.00
	1153370.9104	−5.2607	1774.7511	1.687	0.640	0.000	0.000	0.00e+00	0.00	0.00e+00	0.00
	1158323.7430	−2.1310	610.3412	2.022	0.640	0.000	0.000	0.00e+00	0.00	0.00e+00	0.00
	1162911.5930	−0.2819	173.3658	2.679	0.640	0.000	0.000	0.00e+00	0.00	0.00e+00	0.00
	1168358.5260	−3.4472	1216.1945	1.405	0.640	0.000	0.000	0.00e+00	0.00	0.00e+00	0.00
	1172525.8350	−3.2063	888.6326	1.702	0.640	0.000	0.000	0.00e+00	0.00	0.00e+00	0.00
	1190828.8780	−3.9077	1216.1898	1.514	0.640	0.000	0.000	0.00e+00	0.00	0.00e+00	0.00
	1207638.7140	−0.7849	275.4970	2.708	0.640	0.000	0.000	0.00e+00	0.00	0.00e+00	0.00
	1215801.6760	−4.6959	1590.6907	1.215	0.640	0.000	0.000	0.00e+00	0.00	0.00e+00	0.00
	1219943.7360	−4.2158	1590.6899	1.241	0.640	0.000	0.000	0.00e+00	0.00	0.00e+00	0.00
	1228788.7720	−0.8537	95.1759	2.770	0.640	0.000	0.000	0.00e+00	0.00	0.00e+00	0.00
	1271472.9734	−6.0621	2205.6526	1.851	0.640	0.000	0.000	0.00e+00	0.00	0.00e+00	0.00

Continued on next page

molecule	ν_{0j}^k (MHz)	I_j^k ($\mathrm{nm^2MHz}$)	$E\ell_j^k$ ($\mathrm{cm^{-1}}$)	w_{cj}^k ($\mathrm{MHz\,hPa^{-1}}$)	n_{cj}^k	$\Delta\nu_{0j}^k$ ($\mathrm{MHz\,hPa^{-1}}$)	$n_{\Delta\nu_{0j}}^k$	δ_j^k ($\mathrm{hPa^{-1}}$)	$n_{\delta_j}^k$	γ_j^k ($\mathrm{hPa^{-1}}$)	$n_{\gamma_j}^k$
	1278265.9460	−2.6523	888.5987	1.969	0.640	0.000	0.000	0.00e+00	0.00	0.00e+00	0.00
	1296411.0330	−2.6752	842.3566	2.424	0.640	0.000	0.000	0.00e+00	0.00	0.00e+00	0.00
	1307963.1240	−3.7929	1079.0796	1.719	0.640	0.000	0.000	0.00e+00	0.00	0.00e+00	0.00
	1322064.8030	−1.7682	508.8121	2.432	0.640	0.000	0.000	0.00e+00	0.00	0.00e+00	0.00
	1335279.3261	−5.0287	2009.8051	1.083	0.640	0.000	0.000	0.00e+00	0.00	0.00e+00	0.00
	1335984.7344	−5.5054	2009.8051	1.086	0.640	0.000	0.000	0.00e+00	0.00	0.00e+00	0.00
	1344676.4880	−3.9359	882.8903	1.775	0.640	0.000	0.000	0.00e+00	0.00	0.00e+00	0.00
	1410618.0740	−0.3754	399.4575	2.740	0.640	0.000	0.000	0.00e+00	0.00	0.00e+00	0.00
	1435008.3752	−4.6059	1293.0181	1.385	0.640	0.000	0.000	0.00e+00	0.00	0.00e+00	0.00
	1440781.5440	−2.5489	661.5489	2.421	0.640	0.000	0.000	0.00e+00	0.00	0.00e+00	0.00
	1529245.7164	−5.8830	2471.2549	0.986	0.640	0.000	0.000	0.00e+00	0.00	0.00e+00	0.00
	1541966.7850	−2.3337	610.1144	2.377	0.640	0.000	0.000	0.00e+00	0.00	0.00e+00	0.00
	1574232.0730	−3.1643	704.2140	1.948	0.640	0.000	0.000	0.00e+00	0.00	0.00e+00	0.00
	1596252.4612	−4.0848	1201.9215	1.872	0.640	0.000	0.000	0.00e+00	0.00	0.00e+00	0.00
	1602219.1820	−0.6933	222.0528	2.817	0.640	0.000	0.000	0.00e+00	0.00	0.00e+00	0.00
	1661007.6370	−0.2764	79.4964	2.749	0.640	0.000	0.000	0.00e+00	0.00	0.00e+00	0.00
	1669904.7750	0.0980	23.7944	2.961	0.640	0.000	0.000	0.00e+00	0.00	0.00e+00	0.00
	1693469.7422	−4.4777	1524.8479	1.174	0.640	0.000	0.000	0.00e+00	0.00	0.00e+00	0.00
	1713882.9730	−2.6366	325.3479	2.236	0.640	0.000	0.000	0.00e+00	0.00	0.00e+00	0.00
	1716769.6330	0.0700	79.4964	2.873	0.640	0.000	0.000	0.00e+00	0.00	0.00e+00	0.00
	1716956.6161	−3.1971	446.6966	2.107	0.640	0.000	0.000	0.00e+00	0.00	0.00e+00	0.00
	1762042.7910	−1.0368	602.7735	2.667	0.640	0.000	0.000	0.00e+00	0.00	0.00e+00	0.00
	1766198.7480	−2.3765	757.7802	2.054	0.640	0.000	0.000	0.00e+00	0.00	0.00e+00	0.00
	1794788.9530	−0.9542	542.9058	2.664	0.640	0.000	0.000	0.00e+00	0.00	0.00e+00	0.00
	1797158.7620	−0.8300	782.4098	2.670	0.640	0.000	0.000	0.00e+00	0.00	0.00e+00	0.00
	1851205.5969	−5.2441	1813.2234	1.869	0.640	0.000	0.000	0.00e+00	0.00	0.00e+00	0.00
	1867748.5940	−0.3319	446.5107	2.641	0.640	0.000	0.000	0.00e+00	0.00	0.00e+00	0.00
	1879750.1209	−4.0201	920.2100	1.998	0.640	0.000	0.000	0.00e+00	0.00	0.00e+00	0.00
	1880752.3612	−2.8849	586.2435	2.007	0.640	0.000	0.000	0.00e+00	0.00	0.00e+00	0.00
	1884887.8220	−2.4647	1059.8354	1.743	0.640	0.000	0.000	0.00e+00	0.00	0.00e+00	0.00
	1893686.5446	−3.2447	222.0528	2.532	0.640	0.000	0.000	0.00e+00	0.00	0.00e+00	0.00
	1898852.2438	−3.6864	1411.6418	1.476	0.640	0.000	0.000	0.00e+00	0.00	0.00e+00	0.00
	1903497.2554	−5.9467	2042.3741	1.397	0.640	0.000	0.000	0.00e+00	0.00	0.00e+00	0.00

Continued on next page

molecule	ν_{0j}^k (MHz)	$\mathcal{I}_j^k$ ($\mathrm{nm^2MHz}$)	$E\ell_j^k$ ($\mathrm{cm^{-1}}$)	w_{cj}^k ($\mathrm{MHz\,hPa^{-1}}$)	n_{cj}^k	$\Delta\nu_{0j}^k$ ($\mathrm{MHz\,hPa^{-1}}$)	$n_{\Delta\nu_{0j}}^k$	δ_j^k ($\mathrm{hPa^{-1}}$)	$n_{\delta_j}^k$	γ_j^k ($\mathrm{hPa^{-1}}$)	$n_{\gamma_j}^k$
	1903643.6988	−4.4834	1899.0082	2.060	0.640	0.000	0.000	0.00e+00	0.00	0.00e+00	0.00
	1918485.3240	−1.0615	382.5169	2.597	0.640	0.000	0.000	0.00e+00	0.00	0.00e+00	0.00
	1919359.5310	−0.5767	142.2785	2.691	0.640	0.000	0.000	0.00e+00	0.00	0.00e+00	0.00
	1930215.9655	−4.0436	1810.5879	1.268	0.640	0.000	0.000	0.00e+00	0.00	0.00e+00	0.00
	1945009.9169	−4.5142	1810.5833	1.314	0.640	0.000	0.000	0.00e+00	0.00	0.00e+00	0.00
	1969214.4157	−3.1773	1411.6115	1.634	0.640	0.000	0.000	0.00e+00	0.00	0.00e+00	0.00
	2014864.5323	−3.4932	542.9058	2.306	0.640	0.000	0.000	0.00e+00	0.00	0.00e+00	0.00
	2015982.8280	−1.5992	982.9117	2.567	0.640	0.000	0.000	0.00e+00	0.00	0.00e+00	0.00
	2024457.3939	−5.4154	2254.2844	1.141	0.640	0.000	0.000	0.00e+00	0.00	0.00e+00	0.00
	2027255.5289	−4.9371	2254.2837	1.150	0.640	0.000	0.000	0.00e+00	0.00	0.00e+00	0.00
	2040476.8100	−0.6634	315.7795	2.567	0.640	0.000	0.000	0.00e+00	0.00	0.00e+00	0.00
	2050980.0553	−5.3387	1774.6163	0.974	0.640	0.000	0.000	0.00e+00	0.00	0.00e+00	0.00
	2074432.3050	−0.8348	206.3014	2.746	0.640	0.000	0.000	0.00e+00	0.00	0.00e+00	0.00
	2162370.4976	−2.8144	1059.6466	2.113	0.640	0.000	0.000	0.00e+00	0.00	0.00e+00	0.00
	2164131.9800	−0.1090	70.0908	2.917	0.640	0.000	0.000	0.00e+00	0.00	0.00e+00	0.00
	2177409.7043	−3.5765	744.0637	1.819	0.640	0.000	0.000	0.00e+00	0.00	0.00e+00	0.00
	2191225.4895	−5.8877	2740.4209	1.045	0.640	0.000	0.000	0.00e+00	0.00	0.00e+00	0.00
	2196345.7560	−0.2064	212.1564	2.476	0.640	0.000	0.000	0.00e+00	0.00	0.00e+00	0.00
	2221750.5000	−0.1982	325.3479	2.641	0.640	0.000	0.000	0.00e+00	0.00	0.00e+00	0.00
	2244810.9240	−1.9819	931.2371	2.089	0.640	0.000	0.000	0.00e+00	0.00	0.00e+00	0.00
	2264149.6500	−0.0590	224.8384	2.541	0.640	0.000	0.000	0.00e+00	0.00	0.00e+00	0.00
	2300455.7163	−4.2058	982.9117	2.198	0.640	0.000	0.000	0.00e+00	0.00	0.00e+00	0.00
	2317882.1600	−1.5916	1282.9191	2.503	0.640	0.000	0.000	0.00e+00	0.00	0.00e+00	0.00
	2344250.3350	−0.6255	704.2140	2.429	0.640	0.000	0.000	0.00e+00	0.00	0.00e+00	0.00
	2347482.1720	−2.5304	1538.1495	2.429	0.640	0.000	0.000	0.00e+00	0.00	0.00e+00	0.00
	2356835.9575	−4.0562	1616.4530	2.162	0.640	0.000	0.000	0.00e+00	0.00	0.00e+00	0.00
	2365899.6590	−0.6359	206.3014	2.406	0.640	0.000	0.000	0.00e+00	0.00	0.00e+00	0.00
	2391572.6280	−0.0617	142.2785	2.752	0.640	0.000	0.000	0.00e+00	0.00	0.00e+00	0.00
	2428247.2090	−1.4374	1201.9215	2.339	0.640	0.000	0.000	0.00e+00	0.00	0.00e+00	0.00
	2446843.2450	−1.6380	1050.1577	2.561	0.640	0.000	0.000	0.00e+00	0.00	0.00e+00	0.00
	2462933.0320	−0.0738	300.3623	2.377	0.640	0.000	0.000	0.00e+00	0.00	0.00e+00	0.00
	2477509.1475	−5.2935	2042.3105	0.824	0.640	0.000	0.000	0.00e+00	0.00	0.00e+00	0.00
	2531917.8110	−2.7836	1131.7756	2.118	0.640	0.000	0.000	0.00e+00	0.00	0.00e+00	0.00

Continued on next page

molecule	ν_{0j}^k (MHz)	I_j^k ($\mathrm{nm^2MHz}$)	$E\ell_j^k$ ($\mathrm{cm^{-1}}$)	w_{cj}^k ($\mathrm{MHz\,hPa^{-1}}$)	n_{cj}^k	$\Delta\nu_{0j}^k$ ($\mathrm{MHz\,hPa^{-1}}$)	$n_{\Delta\nu_{0j}}^k$	δ_j^k ($\mathrm{hPa^{-1}}$)	$n_{\delta_j}^k$	γ_j^k ($\mathrm{hPa^{-1}}$)	$n_{\gamma_j}^k$
	2547436.4782	−2.9621	1255.9115	1.693	0.640	0.000	0.000	0.00e+00	0.00	0.00e+00	0.00
	2567177.1320	−1.4962	756.7248	2.479	0.640	0.000	0.000	0.00e+00	0.00	0.00e+00	0.00
	2571762.6300	−2.5339	1813.2234	2.250	0.640	0.000	0.000	0.00e+00	0.00	0.00e+00	0.00
	2575004.6340	−2.8471	1360.2354	2.162	0.640	0.000	0.000	0.00e+00	0.00	0.00e+00	0.00
	2576644.1382	−3.3607	920.1683	1.473	0.640	0.000	0.000	0.00e+00	0.00	0.00e+00	0.00
	2602481.8493	−5.8579	2327.9141	1.053	0.640	0.000	0.000	0.00e+00	0.00	0.00e+00	0.00
	2618261.5475	−3.2416	1631.3831	1.458	0.640	0.000	0.000	0.00e+00	0.00	0.00e+00	0.00
	2619333.9790	−3.7589	1114.5499	1.696	0.640	0.000	0.000	0.00e+00	0.00	0.00e+00	0.00
	2630959.5200	−0.6133	416.2087	2.283	0.640	0.000	0.000	0.00e+00	0.00	0.00e+00	0.00
	2640473.8360	0.5303	136.7617	2.823	0.640	0.000	0.000	0.00e+00	0.00	0.00e+00	0.00
	2645039.6296	−4.5991	2054.3687	1.270	0.640	0.000	0.000	0.00e+00	0.00	0.00e+00	0.00
	2657665.3396	−3.1955	399.4575	2.380	0.640	0.000	0.000	0.00e+00	0.00	0.00e+00	0.00
	2664570.7040	−0.7824	842.3566	2.561	0.640	0.000	0.000	0.00e+00	0.00	0.00e+00	0.00
	2685638.9690	−0.5767	326.6255	2.283	0.640	0.000	0.000	0.00e+00	0.00	0.00e+00	0.00
	2689170.0317	−4.1076	2054.3452	1.332	0.640	0.000	0.000	0.00e+00	0.00	0.00e+00	0.00
	2714161.5927	−5.0796	2522.2651	1.136	0.640	0.000	0.000	0.00e+00	0.00	0.00e+00	0.00
	2723413.6662	−5.5539	2522.2612	1.153	0.640	0.000	0.000	0.00e+00	0.00	0.00e+00	0.00
	2773976.5880	0.4655	42.3717	2.870	0.640	0.000	0.000	0.00e+00	0.00	0.00e+00	0.00
	2790947.7072	−5.2130	1538.1495	1.981	0.640	0.000	0.000	0.00e+00	0.00	0.00e+00	0.00
	2801857.6359	−3.6576	1631.2455	1.705	0.640	0.000	0.000	0.00e+00	0.00	0.00e+00	0.00
	2848996.2600	−3.7146	2205.6526	2.154	0.640	0.000	0.000	0.00e+00	0.00	0.00e+00	0.00
	2864256.1638	−3.8711	2533.7932	2.083	0.640	0.000	0.000	0.00e+00	0.00	0.00e+00	0.00
	2880025.3690	−0.2776	552.9114	2.130	0.640	0.000	0.000	0.00e+00	0.00	0.00e+00	0.00
	2884278.9400	−0.7376	446.6966	2.294	0.640	0.000	0.000	0.00e+00	0.00	0.00e+00	0.00
	2884941.0520	−0.9578	661.5489	2.468	0.640	0.000	0.000	0.00e+00	0.00	0.00e+00	0.00
	2962111.0940	−1.1545	503.9681	2.594	0.640	0.000	0.000	0.00e+00	0.00	0.00e+00	0.00
	2968748.6540	−0.0295	37.1371	2.755	0.640	0.000	0.000	0.00e+00	0.00	0.00e+00	0.00
	2970800.2440	0.0204	300.3623	2.661	0.640	0.000	0.000	0.00e+00	0.00	0.00e+00	0.00
	2991473.5590	−3.5123	2105.8679	1.978	0.640	0.000	0.000	0.00e+00	0.00	0.00e+00	0.00
	2997539.1600	−2.6324	1899.0082	2.250	0.640	0.000	0.000	0.00e+00	0.00	0.00e+00	0.00
	2998565.7220	−1.3068	882.8903	2.130	0.640	0.000	0.000	0.00e+00	0.00	0.00e+00	0.00
	3003347.5660	−2.2648	1437.9686	2.051	0.640	0.000	0.000	0.00e+00	0.00	0.00e+00	0.00
	3013199.5660	0.5635	224.8384	2.456	0.640	0.000	0.000	0.00e+00	0.00	0.00e+00	0.00

Continued on next page

molecule	ν_{0j}^k (MHz)	$\mathcal{I}_j^k$ ($\mathrm{nm^2MHz}$)	$E\ell_j^k$ ($\mathrm{cm^{-1}}$)	w_{cj}^k ($\mathrm{MHz\,hPa^{-1}}$)	n_{cj}^k	$\Delta\nu_{0j}^k$ ($\mathrm{MHz\,hPa^{-1}}$)	$n_{\Delta\nu_{0j}}^k$	δ_j^k ($\mathrm{hPa^{-1}}$)	$n_{\delta_j}^k$	γ_j^k ($\mathrm{hPa^{-1}}$)	$n_{\gamma_j}^k$
	3043766.1490	−0.2896	508.8121	2.300	0.640	0.000	0.000	0.00e+00	0.00	0.00e+00	0.00
	3048859.6233	−4.1476	1114.5322	1.273	0.640	0.000	0.000	0.00e+00	0.00	0.00e+00	0.00
	3074733.5164	−5.0011	2880.8342	1.910	0.640	0.000	0.000	0.00e+00	0.00	0.00e+00	0.00
	3118998.5120	−2.7010	1477.2974	1.655	0.640	0.000	0.000	0.00e+00	0.00	0.00e+00	0.00
	3126585.0700	−0.7612	383.8425	2.089	0.640	0.000	0.000	0.00e+00	0.00	0.00e+00	0.00
	3135010.9510	0.1294	222.0528	2.573	0.640	0.000	0.000	0.00e+00	0.00	0.00e+00	0.00
	3149876.8980	−2.2722	1255.1667	2.218	0.640	0.000	0.000	0.00e+00	0.00	0.00e+00	0.00
	3165532.7340	−0.2741	382.5169	1.963	0.640	0.000	0.000	0.00e+00	0.00	0.00e+00	0.00
	3167578.2370	−0.2065	447.2524	1.972	0.640	0.000	0.000	0.00e+00	0.00	0.00e+00	0.00
	3182186.8480	−0.7319	503.9681	2.033	0.640	0.000	0.000	0.00e+00	0.00	0.00e+00	0.00
	3183463.5937	−3.6205	782.4098	2.274	0.640	0.000	0.000	0.00e+00	0.00	0.00e+00	0.00
	3210358.1960	−0.9561	709.6082	1.919	0.640	0.000	0.000	0.00e+00	0.00	0.00e+00	0.00
	3230146.5250	−0.3962	648.9787	2.022	0.640	0.000	0.000	0.00e+00	0.00	0.00e+00	0.00
	3245323.5730	−2.5486	1616.4530	2.312	0.640	0.000	0.000	0.00e+00	0.00	0.00e+00	0.00
	3307402.5320	−3.9241	1875.4618	1.376	0.640	0.000	0.000	0.00e+00	0.00	0.00e+00	0.00
	3323228.5998	−4.5475	1327.1176	1.320	0.640	0.000	0.000	0.00e+00	0.00	0.00e+00	0.00
	3329185.2390	−1.1018	816.6942	1.954	0.640	0.000	0.000	0.00e+00	0.00	0.00e+00	0.00
	3331458.3760	0.0650	95.1759	2.814	0.640	0.000	0.000	0.00e+00	0.00	0.00e+00	0.00
	3354519.7223	−4.3608	2321.9058	1.212	0.640	0.000	0.000	0.00e+00	0.00	0.00e+00	0.00
	3468263.9729	−4.8085	2321.8130	1.317	0.640	0.000	0.000	0.00e+00	0.00	0.00e+00	0.00
	3495358.1100	−0.9165	1006.1159	1.816	0.640	0.000	0.000	0.00e+00	0.00	0.00e+00	0.00
	3498248.8293	−5.1971	2629.3345	1.846	0.640	0.000	0.000	0.00e+00	0.00	0.00e+00	0.00
	3509431.2780	−1.5716	1360.2354	2.268	0.640	0.000	0.000	0.00e+00	0.00	0.00e+00	0.00
	3536666.8070	−0.3993	586.2435	1.834	0.640	0.000	0.000	0.00e+00	0.00	0.00e+00	0.00
	3538892.9168	−5.1431	2983.3962	1.872	0.640	0.000	0.000	0.00e+00	0.00	0.00e+00	0.00
	3547271.5146	−3.5637	1724.7054	1.652	0.640	0.000	0.000	0.00e+00	0.00	0.00e+00	0.00
	3568076.8522	−4.0294	1327.1100	1.109	0.640	0.000	0.000	0.00e+00	0.00	0.00e+00	0.00
	3569620.1055	−3.5663	2414.7234	1.714	0.640	0.000	0.000	0.00e+00	0.00	0.00e+00	0.00
	3599641.7080	0.1122	326.6255	2.057	0.640	0.000	0.000	0.00e+00	0.00	0.00e+00	0.00
	3612970.6230	−0.7338	885.6002	1.670	0.640	0.000	0.000	0.00e+00	0.00	0.00e+00	0.00
	3654603.2820	0.6052	325.3479	2.145	0.640	0.000	0.000	0.00e+00	0.00	0.00e+00	0.00
	3669872.2510	−1.8461	927.7439	2.471	0.640	0.000	0.000	0.00e+00	0.00	0.00e+00	0.00
	3674226.9950	−2.1828	1690.6644	1.766	0.640	0.000	0.000	0.00e+00	0.00	0.00e+00	0.00

Continued on next page

molecule	ν_{0j}^k (MHz)	$\mathcal{I}_j^k$ (nm^2MHz)	$E\ell_j^k$ (cm^{-1})	w_{cj}^k (MHz hPa^{-1})	n_{cj}^k	$\Delta\nu_{0j}^k$ (MHz hPa^{-1})	$n_{\Delta\nu_{0j}}^k$	δ_j^k (hPa^{-1})	$n_{\delta_j}^k$	γ_j^k (hPa^{-1})	$n_{\gamma_j}^k$
	3682708.1050	−1.0949	1079.0796	1.766	0.640	0.000	0.000	0.00e+00	0.00	0.00e+00	0.00
	3691315.3090	−0.8505	586.4792	1.628	0.640	0.000	0.000	0.00e+00	0.00	0.00e+00	0.00
	3718095.9400	−3.3365	1874.9730	1.810	0.640	0.000	0.000	0.00e+00	0.00	0.00e+00	0.00
	3721502.7960	−1.6267	1131.7756	2.165	0.640	0.000	0.000	0.00e+00	0.00	0.00e+00	0.00
	3737021.5320	−1.7381	1216.2312	1.608	0.640	0.000	0.000	0.00e+00	0.00	0.00e+00	0.00
	3762739.9680	−4.8220	2300.6851	1.831	0.640	0.000	0.000	0.00e+00	0.00	0.00e+00	0.00
	3776068.4569	−3.6362	1998.9952	1.743	0.640	0.000	0.000	0.00e+00	0.00	0.00e+00	0.00
	3798281.6380	−0.2997	416.2087	2.424	0.640	0.000	0.000	0.00e+00	0.00	0.00e+00	0.00
	3807258.4120	0.5531	173.3658	2.773	0.640	0.000	0.000	0.00e+00	0.00	0.00e+00	0.00
	3809788.3097	−3.9425	2629.3345	1.948	0.640	0.000	0.000	0.00e+00	0.00	0.00e+00	0.00
	3855281.5950	−0.8207	931.2371	2.019	0.640	0.000	0.000	0.00e+00	0.00	0.00e+00	0.00
	3858098.9708	−4.4385	1282.9191	2.227	0.640	0.000	0.000	0.00e+00	0.00	0.00e+00	0.00
	3922858.1360	−1.0817	757.7802	1.843	0.640	0.000	0.000	0.00e+00	0.00	0.00e+00	0.00
	3937072.7604	−3.7900	2144.0464	1.253	0.640	0.000	0.000	0.00e+00	0.00	0.00e+00	0.00
	3949321.6415	−0.5669	610.3412	1.649	0.640	0.000	0.000	0.00e+00	0.00	0.00e+00	0.00
	3953481.2619	−0.5978	756.7248	1.693	0.640	0.000	0.000	0.00e+00	0.00	0.00e+00	0.00
	3954343.4650	−1.2759	927.7439	1.737	0.640	0.000	0.000	0.00e+00	0.00	0.00e+00	0.00
	3956018.7052	−1.0425	610.1144	1.593	0.640	0.000	0.000	0.00e+00	0.00	0.00e+00	0.00
	3970997.4050	−1.0946	1122.7085	1.722	0.640	0.000	0.000	0.00e+00	0.00	0.00e+00	0.00
	3977046.4810	0.4516	79.4964	2.799	0.640	0.000	0.000	0.00e+00	0.00	0.00e+00	0.00
	3981742.6229	−4.4546	1557.8478	0.954	0.640	0.000	0.000	0.00e+00	0.00	0.00e+00	0.00
$H_2^{18}O$	203407.5200	−3.5657	134.7832	2.245	0.900	0.000	0.000	0.00e+00	0.00	0.00e+00	0.00
	322465.1700	−3.6110	314.4594	2.465	0.640	0.000	0.000	0.00e+00	0.00	0.00e+00	0.00
	390607.7600	−2.6125	210.7993	2.535	0.640	0.000	0.000	0.00e+00	0.00	0.00e+00	0.00
	489054.2600	−2.5218	282.3071	2.341	0.640	0.000	0.000	0.00e+00	0.00	0.00e+00	0.00
	517181.9600	−4.1772	583.9863	2.315	0.640	0.000	0.000	0.00e+00	0.00	0.00e+00	0.00
	520137.3200	−3.5221	733.6831	1.708	0.640	0.000	0.000	0.00e+00	0.00	0.00e+00	0.00
	537337.5700	−3.3827	482.6726	2.048	0.640	0.000	0.000	0.00e+00	0.00	0.00e+00	0.00
	539895.9582	−4.1734	1033.1943	1.429	0.640	0.000	0.000	0.00e+00	0.00	0.00e+00	0.00
	547676.4400	−0.8324	23.7549	2.925	0.640	0.000	0.000	0.00e+00	0.00	0.00e+00	0.00
	554859.8700	−3.9425	733.6794	1.804	0.640	0.000	0.000	0.00e+00	0.00	0.00e+00	0.00
	692079.1400	−2.6779	482.6435	2.186	0.640	0.000	0.000	0.00e+00	0.00	0.00e+00	0.00
	745320.2000	−1.0069	69.9275	2.787	0.640	0.000	0.000	0.00e+00	0.00	0.00e+00	0.00

Continued on next page

molecule	ν_{0j}^k (MHz)	I_j^k ($\mathrm{nm^2MHz}$)	$E\ell_j^k$ ($\mathrm{cm^{-1}}$)	w_{cj}^k ($\mathrm{MHz\,hPa^{-1}}$)	n_{cj}^k	$\Delta\nu_{0j}^k$ ($\mathrm{MHz\,hPa^{-1}}$)	$n_{\Delta\nu_{0j}}^k$	δ_j^k ($\mathrm{hPa^{-1}}$)	$n_{\delta_j}^k$	γ_j^k ($\mathrm{hPa^{-1}}$)	$n_{\gamma_j}^k$
	856844.6259	−4.1545	1047.3287	2.162	0.640	0.000	0.000	0.00e+00	0.00	0.00e+00	0.00
	970272.0405	−2.3235	282.0946	2.462	0.640	0.000	0.000	0.00e+00	0.00	0.00e+00	0.00
	994675.1291	−1.1267	36.7487	2.784	0.640	0.000	0.000	0.00e+00	0.00	0.00e+00	0.00
	1003277.5999	−2.3026	380.7025	2.271	0.640	0.000	0.000	0.00e+00	0.00	0.00e+00	0.00
	1095627.3929	−0.3260	136.3367	2.702	0.640	0.000	0.000	0.00e+00	0.00	0.00e+00	0.00
	1101698.2565	−0.8479	0.0000	2.256	0.640	0.000	0.000	0.00e+00	0.00	0.00e+00	0.00
	1136703.5794	−0.2968	172.8829	2.579	0.640	0.000	0.000	0.00e+00	0.00	0.00e+00	0.00
	1181394.0281	−1.1042	133.4759	2.579	0.640	0.000	0.000	0.00e+00	0.00	0.00e+00	0.00
	1182806.2449	−3.4929	740.9986	2.039	0.640	0.000	0.000	0.00e+00	0.00	0.00e+00	0.00
	1188863.1256	−0.7953	274.8032	2.579	0.640	0.000	0.000	0.00e+00	0.00	0.00e+00	0.00
	1199005.6352	−0.8704	94.7887	2.664	0.640	0.000	0.000	0.00e+00	0.00	0.00e+00	0.00
	1210585.2182	−3.5266	1725.0170	2.702	0.640	0.000	0.000	0.00e+00	0.00	0.00e+00	0.00
	1216850.4219	−2.0964	604.7929	2.033	0.640	0.000	0.000	0.00e+00	0.00	0.00e+00	0.00
	1252571.4543	−3.1609	880.1147	1.743	0.640	0.000	0.000	0.00e+00	0.00	0.00e+00	0.00
	1255321.4709	−3.8672	1074.7634	1.699	0.640	0.000	0.000	0.00e+00	0.00	0.00e+00	0.00
	1264940.6114	−3.3975	1204.1749	1.435	0.640	0.000	0.000	0.00e+00	0.00	0.00e+00	0.00
	1270077.6044	−2.7363	839.5494	2.359	0.640	0.000	0.000	0.00e+00	0.00	0.00e+00	0.00
	1271139.8842	−4.0108	879.4953	1.760	0.640	0.000	0.000	0.00e+00	0.00	0.00e+00	0.00
	1290218.3431	−3.8573	1204.1694	1.587	0.640	0.000	0.000	0.00e+00	0.00	0.00e+00	0.00
	1340739.2220	−1.7754	505.7288	2.324	0.640	0.000	0.000	0.00e+00	0.00	0.00e+00	0.00
	1367763.9605	−2.6047	880.0763	1.969	0.640	0.000	0.000	0.00e+00	0.00	0.00e+00	0.00
	1375824.2733	−3.4723	1765.3977	2.579	0.640	0.000	0.000	0.00e+00	0.00	0.00e+00	0.00
	1402966.0331	−0.3792	398.3605	2.603	0.640	0.000	0.000	0.00e+00	0.00	0.00e+00	0.00
	1438648.6106	−2.5817	658.6100	2.409	0.640	0.000	0.000	0.00e+00	0.00	0.00e+00	0.00
	1479129.7195	−3.2313	701.6946	1.887	0.640	0.000	0.000	0.00e+00	0.00	0.00e+00	0.00
	1578273.6476	−3.5909	1993.2765	2.603	0.640	0.000	0.000	0.00e+00	0.00	0.00e+00	0.00
	1605962.4600	−0.6944	221.2341	2.597	0.640	0.000	0.000	0.00e+00	0.00	0.00e+00	0.00
	1620851.5585	−2.2943	604.5442	2.409	0.640	0.000	0.000	0.00e+00	0.00	0.00e+00	0.00
	1633483.5998	−0.2901	78.9887	2.650	0.640	0.000	0.000	0.00e+00	0.00	0.00e+00	0.00
	1648236.8203	−3.2906	1670.0377	2.749	0.640	0.000	0.000	0.00e+00	0.00	0.00e+00	0.00
	1655867.6270	0.0913	23.7549	2.878	0.640	0.000	0.000	0.00e+00	0.00	0.00e+00	0.00
	1656202.0540	−2.6794	324.0467	2.177	0.640	0.000	0.000	0.00e+00	0.00	0.00e+00	0.00
	1671349.9472	−3.2442	444.8461	2.069	0.640	0.000	0.000	0.00e+00	0.00	0.00e+00	0.00

Continued on next page

molecule	ν_{0j}^k (MHz)	$\mathcal{I}_j^k$ (nm^{2}MHz)	$E\ell_j^k$ (cm^{-1})	w_{cj}^k (MHz hPa^{-1})	n_{cj}^k	$\Delta\nu_{0j}^k$ (MHz hPa^{-1})	$n_{\Delta\nu_{0j}}^k$	δ_j^k (hPa^{-1})	$n_{\delta_j}^k$	γ_j^k (hPa^{-1})	$n_{\gamma_j}^k$
	1719250.2351	0.0760	78.9887	2.749	0.640	0.000	0.000	0.00e+00	0.00	0.00e+00	0.00
	1719981.2923	−1.0481	601.2376	2.564	0.640	0.000	0.000	0.00e+00	0.00	0.00e+00	0.00
	1738483.5248	−3.1774	1612.0481	2.878	0.640	0.000	0.000	0.00e+00	0.00	0.00e+00	0.00
	1771674.5587	−0.8345	780.4527	2.559	0.640	0.000	0.000	0.00e+00	0.00	0.00e+00	0.00
	1800474.6081	−0.9516	541.1803	2.497	0.640	0.000	0.000	0.00e+00	0.00	0.00e+00	0.00
	1815853.4107	−0.3469	445.1585	2.541	0.640	0.000	0.000	0.00e+00	0.00	0.00e+00	0.00
	1815973.2499	−2.3648	752.1876	1.995	0.640	0.000	0.000	0.00e+00	0.00	0.00e+00	0.00
	1824553.5451	−3.2787	221.2341	2.462	0.640	0.000	0.000	0.00e+00	0.00	0.00e+00	0.00
	1846872.2757	−2.9343	583.7777	1.978	0.640	0.000	0.000	0.00e+00	0.00	0.00e+00	0.00
	1894323.8233	−0.5871	141.5681	2.620	0.640	0.000	0.000	0.00e+00	0.00	0.00e+00	0.00
	1899604.3420	−3.5445	541.1803	2.236	0.640	0.000	0.000	0.00e+00	0.00	0.00e+00	0.00
	1916534.3133	−4.0584	916.2937	1.875	0.640	0.000	0.000	0.00e+00	0.00	0.00e+00	0.00
	1924106.0100	−3.4714	1670.0377	2.650	0.640	0.000	0.000	0.00e+00	0.00	0.00e+00	0.00
	1961635.6544	−2.4439	1051.2032	1.740	0.640	0.000	0.000	0.00e+00	0.00	0.00e+00	0.00
	1974635.8699	−1.0323	379.2917	2.482	0.640	0.000	0.000	0.00e+00	0.00	0.00e+00	0.00
	1985919.1496	−0.6801	314.4594	2.479	0.640	0.000	0.000	0.00e+00	0.00	0.00e+00	0.00
	1995278.2565	−3.6644	1399.4634	1.488	0.640	0.000	0.000	0.00e+00	0.00	0.00e+00	0.00
	2011797.1616	−1.5951	980.2224	2.491	0.640	0.000	0.000	0.00e+00	0.00	0.00e+00	0.00
	2074107.4911	−3.1527	1399.4280	1.678	0.640	0.000	0.000	0.00e+00	0.00	0.00e+00	0.00
	2099963.2169	−0.8162	204.7560	2.556	0.640	0.000	0.000	0.00e+00	0.00	0.00e+00	0.00
	2143751.5400	−0.2237	210.7993	2.450	0.640	0.000	0.000	0.00e+00	0.00	0.00e+00	0.00
	2147732.5366	−0.1136	69.9275	2.773	0.640	0.000	0.000	0.00e+00	0.00	0.00e+00	0.00
	2153999.7814	−3.6289	740.9122	1.781	0.640	0.000	0.000	0.00e+00	0.00	0.00e+00	0.00
	2197901.5928	−3.7751	1732.2623	2.620	0.640	0.000	0.000	0.00e+00	0.00	0.00e+00	0.00
	2216284.3762	−3.4006	1658.3350	2.773	0.640	0.000	0.000	0.00e+00	0.00	0.00e+00	0.00
	2227871.8907	−0.1958	324.0467	2.476	0.640	0.000	0.000	0.00e+00	0.00	0.00e+00	0.00
	2234437.9986	−3.5403	2045.9221	2.541	0.640	0.000	0.000	0.00e+00	0.00	0.00e+00	0.00
	2242197.9273	−0.0656	223.8286	2.473	0.640	0.000	0.000	0.00e+00	0.00	0.00e+00	0.00
	2260499.9239	−1.5969	1279.7979	2.418	0.640	0.000	0.000	0.00e+00	0.00	0.00e+00	0.00
	2261914.3636	−2.7865	1050.9904	2.080	0.640	0.000	0.000	0.00e+00	0.00	0.00e+00	0.00
	2278608.6960	−1.9890	925.7000	2.089	0.640	0.000	0.000	0.00e+00	0.00	0.00e+00	0.00
	2316972.0670	−2.5269	1534.3687	2.353	0.640	0.000	0.000	0.00e+00	0.00	0.00e+00	0.00
	2318554.3020	−0.6509	204.7560	2.415	0.640	0.000	0.000	0.00e+00	0.00	0.00e+00	0.00

Continued on next page

molecule	ν_{0j}^k (MHz)	I_j^k ($\mathrm{nm^2MHz}$)	$E\ell_j^k$ ($\mathrm{cm^{-1}}$)	w_{cj}^k ($\mathrm{MHz\,hPa^{-1}}$)	n_{cj}^k	$\Delta\nu_{0j}^k$ ($\mathrm{MHz\,hPa^{-1}}$)	$n_{\Delta\nu_{0j}}^k$	δ_j^k ($\mathrm{hPa^{-1}}$)	$n_{\delta_j}^k$	γ_j^k ($\mathrm{hPa^{-1}}$)	$n_{\gamma_j}^k$
	2336117.3839	−3.4028	1732.2623	2.652	0.640	0.000	0.000	0.00e+00	0.00	0.00e+00	0.00
	2361110.6108	−0.6173	701.6946	2.339	0.640	0.000	0.000	0.00e+00	0.00	0.00e+00	0.00
	2371686.7133	−1.6490	1047.3287	2.506	0.640	0.000	0.000	0.00e+00	0.00	0.00e+00	0.00
	2388324.5802	−0.0582	141.5681	2.652	0.640	0.000	0.000	0.00e+00	0.00	0.00e+00	0.00
	2405970.2080	−3.4105	1913.0220	2.476	0.640	0.000	0.000	0.00e+00	0.00	0.00e+00	0.00
	2418469.3088	−0.0860	298.6202	2.350	0.640	0.000	0.000	0.00e+00	0.00	0.00e+00	0.00
	2446247.6254	−1.4250	1198.2000	2.277	0.640	0.000	0.000	0.00e+00	0.00	0.00e+00	0.00
	2526740.8769	−3.2299	398.3605	2.321	0.640	0.000	0.000	0.00e+00	0.00	0.00e+00	0.00
	2540639.4392	−2.8122	1126.4397	2.077	0.640	0.000	0.000	0.00e+00	0.00	0.00e+00	0.00
	2550886.7864	−2.9010	1355.2001	2.189	0.640	0.000	0.000	0.00e+00	0.00	0.00e+00	0.00
	2561676.9731	−3.4180	916.2579	1.432	0.640	0.000	0.000	0.00e+00	0.00	0.00e+00	0.00
	2563889.5168	−3.2598	1814.0861	2.473	0.640	0.000	0.000	0.00e+00	0.00	0.00e+00	0.00
	2573240.0980	−2.5198	1808.3622	2.212	0.640	0.000	0.000	0.00e+00	0.00	0.00e+00	0.00
	2582730.2138	−0.7964	839.5494	2.506	0.640	0.000	0.000	0.00e+00	0.00	0.00e+00	0.00
	2588332.7234	−3.4213	1811.2903	2.450	0.640	0.000	0.000	0.00e+00	0.00	0.00e+00	0.00
	2591047.2572	−0.6218	414.1683	2.230	0.640	0.000	0.000	0.00e+00	0.00	0.00e+00	0.00
	2616384.3462	−2.9562	1247.2064	1.658	0.640	0.000	0.000	0.00e+00	0.00	0.00e+00	0.00
	2622938.7881	0.5280	136.3367	2.676	0.640	0.000	0.000	0.00e+00	0.00	0.00e+00	0.00
	2650084.3209	−3.8112	1109.8026	1.602	0.640	0.000	0.000	0.00e+00	0.00	0.00e+00	0.00
	2653655.4500	−1.4686	751.0330	2.479	0.640	0.000	0.000	0.00e+00	0.00	0.00e+00	0.00
	2666731.6426	−0.5792	325.2157	2.218	0.640	0.000	0.000	0.00e+00	0.00	0.00e+00	0.00
	2670222.4181	−2.7736	1725.0170	2.676	0.640	0.000	0.000	0.00e+00	0.00	0.00e+00	0.00
	2712657.0147	−3.2339	1619.0560	1.420	0.640	0.000	0.000	0.00e+00	0.00	0.00e+00	0.00
	2741674.7720	0.4557	42.0234	2.746	0.640	0.000	0.000	0.00e+00	0.00	0.00e+00	0.00
	2805384.3905	−0.9731	658.6100	2.427	0.640	0.000	0.000	0.00e+00	0.00	0.00e+00	0.00
	2808108.3007	−3.3895	1899.6082	2.535	0.640	0.000	0.000	0.00e+00	0.00	0.00e+00	0.00
	2845979.6153	−0.2816	550.4510	2.080	0.640	0.000	0.000	0.00e+00	0.00	0.00e+00	0.00
	2850890.0446	−3.2965	1899.6082	2.350	0.640	0.000	0.000	0.00e+00	0.00	0.00e+00	0.00
	2888025.8578	−0.7319	444.8461	2.268	0.640	0.000	0.000	0.00e+00	0.00	0.00e+00	0.00
	2897777.4846	−2.6368	1894.1962	2.221	0.640	0.000	0.000	0.00e+00	0.00	0.00e+00	0.00
	2917091.7659	−3.6440	1618.8966	1.722	0.640	0.000	0.000	0.00e+00	0.00	0.00e+00	0.00
	2939000.1481	−0.0404	36.7487	2.655	0.640	0.000	0.000	0.00e+00	0.00	0.00e+00	0.00
	2966027.6095	−2.7657	1814.0861	2.388	0.640	0.000	0.000	0.00e+00	0.00	0.00e+00	0.00

Continued on next page

molecule	ν_{0j}^k (MHz)	I_j^k (nm^2MHz)	$E\ell_j^k$ (cm^{-1})	w_{cj}^k (MHz hPa^{-1})	n_{cj}^k	$\Delta\nu_{0j}^k$ (MHz hPa^{-1})	$n_{\Delta\nu_{0j}}^k$	δ_j^k (hPa^{-1})	$n_{\delta_j}^k$	γ_j^k (hPa^{-1})	$n_{\gamma_j}^k$
	2969868.4153	−0.3054	505.7288	2.294	0.640	0.000	0.000	0.00e+00	0.00	0.00e+00	0.00
	2986640.8120	−3.6762	780.4527	2.201	0.640	0.000	0.000	0.00e+00	0.00	0.00e+00	0.00
	2990139.1456	0.0354	298.6202	2.535	0.640	0.000	0.000	0.00e+00	0.00	0.00e+00	0.00
H_2O_2	184679.2200	−2.9133	399.5130	2.940	0.500	0.000	0.000	0.00e+00	0.00	0.00e+00	0.00
	204574.7000	−2.9336	475.3351	2.940	0.500	0.000	0.000	0.00e+00	0.00	0.00e+00	0.00
	625044.1800	−2.4432	362.0153	2.940	0.500	0.000	0.000	0.00e+00	0.00	0.00e+00	0.00
	626608.9004	−3.1681	109.8849	2.940	0.500	0.000	0.000	0.00e+00	0.00	0.00e+00	0.00
	661379.1913	−2.7196	386.6541	2.900	0.800	0.000	0.000	0.00e+00	0.00	0.00e+00	0.00
$H_2^{32}S$	626474.6250	−2.2695	505.7564	2.344	0.750	0.000	0.000	0.00e+00	0.00	0.00e+00	0.00
	650374.1860	−1.9795	173.9673	2.344	0.750	0.000	0.000	0.00e+00	0.00	0.00e+00	0.00
$H_2^{32}SO_4$	182630.8124	−3.4602	51.3867	2.750	0.750	0.000	0.000	0.00e+00	0.00	0.00e+00	0.00
	182705.1880	−3.3621	50.7218	2.750	0.750	0.000	0.000	0.00e+00	0.00	0.00e+00	0.00
	183178.8227	−3.4511	51.4993	2.750	0.750	0.000	0.000	0.00e+00	0.00	0.00e+00	0.00
	183582.6085	−3.4376	51.6374	2.750	0.750	0.000	0.000	0.00e+00	0.00	0.00e+00	0.00
	183984.2424	−3.4226	51.7916	2.750	0.750	0.000	0.000	0.00e+00	0.00	0.00e+00	0.00
	184377.3103	−3.4063	51.9614	2.750	0.750	0.000	0.000	0.00e+00	0.00	0.00e+00	0.00
	184766.4116	−3.3893	52.1460	2.750	0.750	0.000	0.000	0.00e+00	0.00	0.00e+00	0.00
	185153.1233	−3.3717	52.3449	2.750	0.750	0.000	0.000	0.00e+00	0.00	0.00e+00	0.00
	185538.2793	−3.3538	52.5578	2.750	0.750	0.000	0.000	0.00e+00	0.00	0.00e+00	0.00
	202208.6055	−3.3424	63.7057	2.750	0.750	0.000	0.000	0.00e+00	0.00	0.00e+00	0.00
	202409.1997	−3.3898	63.5319	2.750	0.750	0.000	0.000	0.00e+00	0.00	0.00e+00	0.00
	202698.1878	−3.3924	63.5383	2.750	0.750	0.000	0.000	0.00e+00	0.00	0.00e+00	0.00
	202873.4206	−3.4714	63.2472	2.750	0.750	0.000	0.000	0.00e+00	0.00	0.00e+00	0.00
	202878.8675	−3.4714	63.2472	2.750	0.750	0.000	0.000	0.00e+00	0.00	0.00e+00	0.00
	203816.8132	−3.3320	64.0638	2.750	0.750	0.000	0.000	0.00e+00	0.00	0.00e+00	0.00
	204220.0048	−3.3190	64.2289	2.750	0.750	0.000	0.000	0.00e+00	0.00	0.00e+00	0.00
	204615.6177	−3.3050	64.4098	2.750	0.750	0.000	0.000	0.00e+00	0.00	0.00e+00	0.00
	205006.0779	−3.2901	64.6058	2.750	0.750	0.000	0.000	0.00e+00	0.00	0.00e+00	0.00
	205393.4428	−3.2747	64.8164	2.750	0.750	0.000	0.000	0.00e+00	0.00	0.00e+00	0.00
	205778.7456	−3.2589	65.0410	2.750	0.750	0.000	0.000	0.00e+00	0.00	0.00e+00	0.00
	206162.5525	−3.1180	65.2795	2.750	0.750	0.000	0.000	0.00e+00	0.00	0.00e+00	0.00
HNO_3	176828.3550	−4.2611	478.6182	3.223	0.750	0.000	0.000	0.00e+00	0.00	0.00e+00	0.00
	177398.2186	−4.2118	449.5038	3.223	0.750	0.000	0.000	0.00e+00	0.00	0.00e+00	0.00

Continued on next page

molecule	ν_{0j}^k (MHz)	$\mathcal{I}_j^k$ ($\mathrm{nm^2MHz}$)	$E\ell_j^k$ ($\mathrm{cm^{-1}}$)	u_{cj}^k ($\mathrm{MHz\,hPa^{-1}}$)	n_{cj}^k	$\Delta\nu_{0j}^k$ ($\mathrm{MHz\,hPa^{-1}}$)	$n_{\Delta\nu_{0j}}^k$	δ_j^k ($\mathrm{hPa^{-1}}$)	$n_{\delta_j}^k$	γ_j^k ($\mathrm{hPa^{-1}}$)	$n_{\gamma_j}^k$
	177834.1207	−4.9584	10.6509	3.223	0.750	0.000	0.000	0.00e+00	0.00	0.00e+00	0.00
	177918.0674	−4.1654	421.2101	3.223	0.750	0.000	0.000	0.00e+00	0.00	0.00e+00	0.00
	178391.8006	−4.0199	393.7383	3.223	0.750	0.000	0.000	0.00e+00	0.00	0.00e+00	0.00
	178646.4767	−4.6517	17.7804	3.223	0.750	0.000	0.000	0.00e+00	0.00	0.00e+00	0.00
	178822.9762	−3.9810	367.0891	3.223	0.750	0.000	0.000	0.00e+00	0.00	0.00e+00	0.00
	179214.8564	−3.9453	341.2637	3.223	0.750	0.000	0.000	0.00e+00	0.00	0.00e+00	0.00
	179570.4437	−3.9131	316.2629	3.223	0.750	0.000	0.000	0.00e+00	0.00	0.00e+00	0.00
	179892.5122	−3.8845	292.0875	3.223	0.750	0.000	0.000	0.00e+00	0.00	0.00e+00	0.00
	180035.1820	−5.0235	11.7338	3.223	0.750	0.000	0.000	0.00e+00	0.00	0.00e+00	0.00
	180101.5200	−4.0220	22.9315	3.223	0.750	0.000	0.000	0.00e+00	0.00	0.00e+00	0.00
	180183.6335	−3.8598	268.7384	3.223	0.750	0.000	0.000	0.00e+00	0.00	0.00e+00	0.00
	180446.1425	−3.8393	246.2165	3.223	0.750	0.000	0.000	0.00e+00	0.00	0.00e+00	0.00
	180625.2698	−4.6486	17.7391	3.223	0.750	0.000	0.000	0.00e+00	0.00	0.00e+00	0.00
	180682.4323	−3.8233	224.5223	3.223	0.750	0.000	0.000	0.00e+00	0.00	0.00e+00	0.00
	180725.3575	−4.8636	28.2003	3.223	0.750	0.000	0.000	0.00e+00	0.00	0.00e+00	0.00
	180894.4179	−3.8125	203.6568	3.223	0.750	0.000	0.000	0.00e+00	0.00	0.00e+00	0.00
	181084.1006	−3.8075	183.6205	3.223	0.750	0.000	0.000	0.00e+00	0.00	0.00e+00	0.00
	181179.1123	−4.0033	28.2003	3.223	0.750	0.000	0.000	0.00e+00	0.00	0.00e+00	0.00
	181253.3038	−3.8093	164.4142	3.223	0.750	0.000	0.000	0.00e+00	0.00	0.00e+00	0.00
	181403.7376	−3.8193	146.0384	3.223	0.750	0.000	0.000	0.00e+00	0.00	0.00e+00	0.00
	181537.0375	−3.8395	128.4939	3.223	0.750	0.000	0.000	0.00e+00	0.00	0.00e+00	0.00
	181559.8656	−3.2092	40.7280	3.223	0.750	0.000	0.000	0.00e+00	0.00	0.00e+00	0.00
	181594.4162	−3.2736	39.9040	3.223	0.750	0.000	0.000	0.00e+00	0.00	0.00e+00	0.00
	181630.5718	−3.3458	38.2393	3.223	0.750	0.000	0.000	0.00e+00	0.00	0.00e+00	0.00
	181654.6355	−3.8731	111.7811	3.223	0.750	0.000	0.000	0.00e+00	0.00	0.00e+00	0.00
	181677.9981	−3.4285	35.7326	3.223	0.750	0.000	0.000	0.00e+00	0.00	0.00e+00	0.00
	181758.0067	−3.9255	95.9006	3.223	0.750	0.000	0.000	0.00e+00	0.00	0.00e+00	0.00
	181770.4400	−4.6628	32.3799	3.223	0.750	0.000	0.000	0.00e+00	0.00	0.00e+00	0.00
	181772.0400	−3.8940	32.3799	3.223	0.750	0.000	0.000	0.00e+00	0.00	0.00e+00	0.00
	181789.2000	−3.8939	32.3793	3.223	0.750	0.000	0.000	0.00e+00	0.00	0.00e+00	0.00
	181790.8200	−4.6626	32.3793	3.223	0.750	0.000	0.000	0.00e+00	0.00	0.00e+00	0.00
	181848.4498	−4.0069	80.8529	3.223	0.750	0.000	0.000	0.00e+00	0.00	0.00e+00	0.00
	181927.2235	−4.1404	66.6385	3.223	0.750	0.000	0.000	0.00e+00	0.00	0.00e+00	0.00

Continued on next page

molecule	ν_{0j}^k (MHz)	$\mathcal{I}_j^k$ (nm^{2}MHz)	$E\ell_j^k$ (cm^{-1})	u_{cj}^k (MHz hPa^{-1})	n_{cj}^k	$\Delta\nu_{0j}^k$ (MHz hPa^{-1})	$n_{\Delta\nu_{0j}}^k$	δ_j^k (hPa^{-1})	$n_{\delta_j}^k$	γ_j^k (hPa^{-1})	$n_{\gamma_j}^k$
	181995.4626	−4.4891	53.2579	3.223	0.750	0.000	0.000	0.00e+00	0.00	0.00e+00	0.00
	182549.7633	−5.1197	808.5518	3.400	0.800	0.000	0.000	0.00e+00	0.00	0.00e+00	0.00
	183005.8585	−5.4216	257.5064	3.400	0.800	0.000	0.000	0.00e+00	0.00	0.00e+00	0.00
	183371.1814	−5.0002	10.6571	3.223	0.750	0.000	0.000	0.00e+00	0.00	0.00e+00	0.00
	183413.8725	−3.9814	28.1106	3.223	0.750	0.000	0.000	0.00e+00	0.00	0.00e+00	0.00
	183555.2076	−5.6816	10.6509	3.400	0.800	0.000	0.000	0.00e+00	0.00	0.00e+00	0.00
	183616.1012	−5.0444	771.2618	3.400	0.800	0.000	0.000	0.00e+00	0.00	0.00e+00	0.00
	183634.5213	−5.0443	771.2617	3.400	0.800	0.000	0.000	0.00e+00	0.00	0.00e+00	0.00
	183867.6273	−4.8317	28.1106	3.223	0.750	0.000	0.000	0.00e+00	0.00	0.00e+00	0.00
	184408.8272	−5.5113	45.5346	3.400	0.800	0.000	0.000	0.00e+00	0.00	0.00e+00	0.00
	184472.3222	−5.2947	327.6540	3.400	0.800	0.000	0.000	0.00e+00	0.00	0.00e+00	0.00
	184482.4318	−5.4122	307.4957	3.400	0.800	0.000	0.000	0.00e+00	0.00	0.00e+00	0.00
	184561.8609	−5.1660	29.4000	3.400	0.800	0.000	0.000	0.00e+00	0.00	0.00e+00	0.00
	184606.3294	−5.0017	16.7737	3.223	0.750	0.000	0.000	0.00e+00	0.00	0.00e+00	0.00
	184624.9639	−4.9717	734.7820	3.400	0.800	0.000	0.000	0.00e+00	0.00	0.00e+00	0.00
	184625.5890	−5.4944	734.7819	3.400	0.800	0.000	0.000	0.00e+00	0.00	0.00e+00	0.00
	184633.6557	−5.4944	734.7820	3.400	0.800	0.000	0.000	0.00e+00	0.00	0.00e+00	0.00
	184634.2809	−4.9716	734.7819	3.400	0.800	0.000	0.000	0.00e+00	0.00	0.00e+00	0.00
	185212.0242	−5.2724	348.7306	3.400	0.800	0.000	0.000	0.00e+00	0.00	0.00e+00	0.00
	185550.5506	−4.7895	699.1139	3.400	0.800	0.000	0.000	0.00e+00	0.00	0.00e+00	0.00
	185555.0316	−4.7895	699.1139	3.400	0.800	0.000	0.000	0.00e+00	0.00	0.00e+00	0.00
	185770.5934	−5.7696	53.6980	3.400	0.800	0.000	0.000	0.00e+00	0.00	0.00e+00	0.00
	186400.6680	−4.7239	664.2589	3.400	0.800	0.000	0.000	0.00e+00	0.00	0.00e+00	0.00
	186402.8437	−4.7239	664.2589	3.400	0.800	0.000	0.000	0.00e+00	0.00	0.00e+00	0.00
	186741.0155	−5.5184	628.9120	3.400	0.800	0.000	0.000	0.00e+00	0.00	0.00e+00	0.00
	186942.6933	−5.5067	236.7484	3.400	0.800	0.000	0.000	0.00e+00	0.00	0.00e+00	0.00
	199548.2214	−4.5231	692.4577	3.400	0.800	0.000	0.000	0.00e+00	0.00	0.00e+00	0.00
	200243.8295	−4.4582	657.5795	3.400	0.800	0.000	0.000	0.00e+00	0.00	0.00e+00	0.00
	200243.8295	−4.3508	657.5795	3.400	0.800	0.000	0.000	0.00e+00	0.00	0.00e+00	0.00
	200289.2525	−5.5462	287.6875	3.400	0.800	0.000	0.000	0.00e+00	0.00	0.00e+00	0.00
	200291.9577	−5.3588	15.6699	3.400	0.800	0.000	0.000	0.00e+00	0.00	0.00e+00	0.00
	200517.9997	−5.7595	247.8096	3.400	0.800	0.000	0.000	0.00e+00	0.00	0.00e+00	0.00
	200831.2765	−4.6727	15.6519	3.223	0.750	0.000	0.000	0.00e+00	0.00	0.00e+00	0.00

Continued on next page

molecule	ν_{0j}^k (MHz)	$\mathcal{I}_j^k$ ($\mathrm{nm^2MHz}$)	$E\ell_j^k$ ($\mathrm{cm^{-1}}$)	w_{cj}^k ($\mathrm{MHz\,hPa^{-1}}$)	n_{cj}^k	$\Delta\nu_{0j}^k$ ($\mathrm{MHz\,hPa^{-1}}$)	$n_{\Delta\nu_{0j}}^k$	δ_j^k ($\mathrm{hPa^{-1}}$)	$n_{\delta_j}^k$	γ_j^k ($\mathrm{hPa^{-1}}$)	$n_{\gamma_j}^k$
	200886.9849	−4.3959	623.5174	3.170	0.800	0.000	0.000	0.00e+00	0.00	0.00e+00	0.00
	200886.9849	−4.2897	623.5174	3.170	0.800	0.000	0.000	0.00e+00	0.00	0.00e+00	0.00
	200892.0425	−5.7581	247.7971	3.400	0.800	0.000	0.000	0.00e+00	0.00	0.00e+00	0.00
	201481.4027	−4.3363	590.2726	3.170	0.800	0.000	0.000	0.00e+00	0.00	0.00e+00	0.00
	201481.4027	−4.2313	590.2726	3.170	0.800	0.000	0.000	0.00e+00	0.00	0.00e+00	0.00
	201510.0713	−5.3373	396.0224	3.400	0.800	0.000	0.000	0.00e+00	0.00	0.00e+00	0.00
	201813.5724	−5.5407	287.6369	3.400	0.800	0.000	0.000	0.00e+00	0.00	0.00e+00	0.00
	201900.7160	−5.4127	330.5959	3.400	0.800	0.000	0.000	0.00e+00	0.00	0.00e+00	0.00
	202013.2952	−5.3416	376.6626	3.400	0.800	0.000	0.000	0.00e+00	0.00	0.00e+00	0.00
	202030.4782	−4.2794	557.8461	3.170	0.800	0.000	0.000	0.00e+00	0.00	0.00e+00	0.00
	202030.4782	−4.1755	557.8461	3.170	0.800	0.000	0.000	0.00e+00	0.00	0.00e+00	0.00
	202300.3556	−5.3210	422.5238	3.400	0.800	0.000	0.000	0.00e+00	0.00	0.00e+00	0.00
	202333.8827	−5.3989	402.7440	3.400	0.800	0.000	0.000	0.00e+00	0.00	0.00e+00	0.00
	202485.9261	−3.9186	29.5996	3.680	0.640	0.000	0.000	0.00e+00	0.00	0.00e+00	0.00
	202537.3282	−4.1224	526.2390	3.170	0.800	0.000	0.000	0.00e+00	0.00	0.00e+00	0.00
	202537.3283	−4.2253	526.2390	3.170	0.800	0.000	0.000	0.00e+00	0.00	0.00e+00	0.00
	202750.9847	−5.3716	370.3379	3.400	0.800	0.000	0.000	0.00e+00	0.00	0.00e+00	0.00
	203004.8250	−4.1740	495.4521	3.170	0.800	0.000	0.000	0.00e+00	0.00	0.00e+00	0.00
	203320.6304	−4.7998	28.9390	3.680	0.640	0.000	0.000	0.00e+00	0.00	0.00e+00	0.00
	203435.6245	−4.1256	465.4866	3.170	0.800	0.000	0.000	0.00e+00	0.00	0.00e+00	0.00
	203658.1385	−5.5642	661.6716	3.400	0.800	0.000	0.000	0.00e+00	0.00	0.00e+00	0.00
	203733.5256	−5.3152	425.8074	3.400	0.800	0.000	0.000	0.00e+00	0.00	0.00e+00	0.00
	203832.1916	−3.9802	436.3433	3.170	0.800	0.000	0.000	0.00e+00	0.00	0.00e+00	0.00
	204196.8195	−3.9388	408.0232	3.170	0.800	0.000	0.000	0.00e+00	0.00	0.00e+00	0.00
	204337.4451	−5.1907	36.9928	3.400	0.800	0.000	0.000	0.00e+00	0.00	0.00e+00	0.00
	204450.6288	−5.4120	54.8105	3.400	0.800	0.000	0.000	0.00e+00	0.00	0.00e+00	0.00
	204531.6485	−3.9006	380.5270	3.170	0.800	0.000	0.000	0.00e+00	0.00	0.00e+00	0.00
	204718.8340	−4.7891	35.7211	3.680	0.640	0.000	0.000	0.00e+00	0.00	0.00e+00	0.00
	204838.6805	−3.8657	353.8556	3.170	0.800	0.000	0.000	0.00e+00	0.00	0.00e+00	0.00
	205014.9591	−5.3207	449.8442	3.400	0.800	0.000	0.000	0.00e+00	0.00	0.00e+00	0.00
	205062.5770	−4.4718	23.7641	3.680	0.640	0.000	0.000	0.00e+00	0.00	0.00e+00	0.00
	205119.7921	−3.8345	328.0099	3.150	0.800	0.000	0.000	0.00e+00	0.00	0.00e+00	0.00
	205265.1608	−5.4186	481.8919	3.400	0.800	0.000	0.000	0.00e+00	0.00	0.00e+00	0.00

Continued on next page

molecule	ν_{0j}^k (MHz)	$\mathcal{I}_j^k$ (nm^{2}MHz)	$E\ell_j^k$ (cm^{-1})	w_{cj}^k (MHz hPa^{-1})	n_{cj}^k	$\Delta\nu_{0j}^k$ (MHz hPa^{-1})	$n_{\Delta\nu_{0j}}^k$	δ_j^k (hPa^{-1})	$n_{\delta_j}^k$	γ_j^k (hPa^{-1})	$n_{\gamma_j}^k$
	205363.6832	−5.8226	179.3890	3.400	0.800	0.000	0.000	0.00e+00	0.00	0.00e+00	0.00
	205376.7458	−3.8070	302.9905	3.170	0.800	0.000	0.000	0.00e+00	0.00	0.00e+00	0.00
	205611.2000	−3.7837	278.7983	3.170	0.800	0.000	0.000	0.00e+00	0.00	0.00e+00	0.00
	205630.3245	−5.4768	568.2051	3.400	0.800	0.000	0.000	0.00e+00	0.00	0.00e+00	0.00
	205736.9662	−3.8803	35.7211	3.680	0.640	0.000	0.000	0.00e+00	0.00	0.00e+00	0.00
	205824.7169	−3.7651	255.4339	3.170	0.800	0.000	0.000	0.00e+00	0.00	0.00e+00	0.00
	205991.6018	−5.4238	345.4691	3.400	0.800	0.000	0.000	0.00e+00	0.00	0.00e+00	0.00
	206018.7703	−3.7514	232.8980	3.165	0.850	0.000	0.000	0.00e+00	0.00	0.00e+00	0.00
	206194.7518	−3.7437	211.1912	3.255	0.730	0.000	0.000	0.00e+00	0.00	0.00e+00	0.00
	206230.4862	−4.4695	23.7394	3.680	0.640	0.000	0.000	0.00e+00	0.00	0.00e+00	0.00
	206353.9761	−3.7428	190.3143	3.158	0.880	0.000	0.000	0.00e+00	0.00	0.00e+00	0.00
	206497.6860	−3.7501	170.2678	3.170	0.800	0.000	0.000	0.00e+00	0.00	0.00e+00	0.00
	206569.9483	−5.3524	993.8232	3.400	0.800	0.000	0.000	0.00e+00	0.00	0.00e+00	0.00
	206577.0565	−5.3524	993.8232	3.400	0.800	0.000	0.000	0.00e+00	0.00	0.00e+00	0.00
	206594.6855	−3.0642	53.2579	3.323	0.700	0.000	0.000	0.00e+00	0.00	0.00e+00	0.00
	206627.0566	−3.7676	151.0523	3.170	0.800	0.000	0.000	0.00e+00	0.00	0.00e+00	0.00
	206628.6816	−3.1196	52.4362	3.430	0.640	0.000	0.000	0.00e+00	0.00	0.00e+00	0.00
	206663.1951	−3.1804	50.7739	3.642	0.610	0.000	0.000	0.00e+00	0.00	0.00e+00	0.00
	206703.2186	−3.2481	48.2702	3.615	0.670	0.000	0.000	0.00e+00	0.00	0.00e+00	0.00
	206743.1987	−3.7987	132.6683	3.170	0.800	0.000	0.000	0.00e+00	0.00	0.00e+00	0.00
	206757.5006	−5.6470	7.3117	3.400	0.800	0.000	0.000	0.00e+00	0.00	0.00e+00	0.00
	206765.0232	−3.3250	44.9231	3.470	0.640	0.000	0.000	0.00e+00	0.00	0.00e+00	0.00
	206774.2822	−5.6470	7.3117	3.400	0.800	0.000	0.000	0.00e+00	0.00	0.00e+00	0.00
	206847.1622	−3.8486	115.1164	3.170	0.800	0.000	0.000	0.00e+00	0.00	0.00e+00	0.00
	206895.9348	−4.5658	40.7262	3.700	0.640	0.000	0.000	0.00e+00	0.00	0.00e+00	0.00
	206901.4468	−3.7796	40.7262	3.700	0.640	0.000	0.000	0.00e+00	0.00	0.00e+00	0.00
	206939.9384	−3.9277	98.3970	3.170	0.800	0.000	0.000	0.00e+00	0.00	0.00e+00	0.00
	206951.2528	−3.7793	40.7244	3.700	0.640	0.000	0.000	0.00e+00	0.00	0.00e+00	0.00
	206956.7648	−4.5654	40.7244	3.700	0.640	0.000	0.000	0.00e+00	0.00	0.00e+00	0.00
	207022.4627	−4.0589	82.5107	3.170	0.800	0.000	0.000	0.00e+00	0.00	0.00e+00	0.00
	207095.6166	−4.4056	67.4579	3.223	0.750	0.000	0.000	0.00e+00	0.00	0.00e+00	0.00
	230012.5652	−3.7753	44.0823	3.223	0.750	0.000	0.000	0.00e+00	0.00	0.00e+00	0.00
	231627.3370	−3.0205	67.4579	3.263	0.650	0.000	0.000	0.00e+00	0.00	0.00e+00	0.00

Continued on next page

molecule	ν_{0j}^k (MHz)	$\mathcal{I}_j^k$ ($\mathrm{nm^2MHz}$)	$E\ell_j^k$ ($\mathrm{cm^{-1}}$)	w_{cj}^k ($\mathrm{MHz\,hPa^{-1}}$)	n_{cj}^k	$\Delta\nu_{0j}^k$ ($\mathrm{MHz\,hPa^{-1}}$)	$n_{\Delta\nu_{0j}}^k$	δ_j^k ($\mathrm{hPa^{-1}}$)	$n_{\delta_j}^k$	γ_j^k ($\mathrm{hPa^{-1}}$)	$n_{\gamma_j}^k$
	231661.0304	−3.0684	66.6385	3.223	0.750	0.000	0.000	0.00e+00	0.00	0.00e+00	0.00
	231694.3543	−3.1198	64.9784	3.223	0.750	0.000	0.000	0.00e+00	0.00	0.00e+00	0.00
	231730.5651	−3.1756	62.4774	3.223	0.750	0.000	0.000	0.00e+00	0.00	0.00e+00	0.00
	231777.6757	−3.2369	59.1341	3.223	0.750	0.000	0.000	0.00e+00	0.00	0.00e+00	0.00
	231862.6453	−3.3047	54.9454	3.223	0.750	0.000	0.000	0.00e+00	0.00	0.00e+00	0.00
	232050.6553	−3.6790	49.9019	3.223	0.750	0.000	0.000	0.00e+00	0.00	0.00e+00	0.00
	232178.5970	−3.6784	49.8971	3.223	0.750	0.000	0.000	0.00e+00	0.00	0.00e+00	0.00
	235167.5730	−3.8626	45.4428	3.223	0.750	0.000	0.000	0.00e+00	0.00	0.00e+00	0.00
	236148.0695	−3.7114	43.8088	3.223	0.750	0.000	0.000	0.00e+00	0.00	0.00e+00	0.00
	244142.8772	−2.9672	75.1842	3.223	0.750	0.000	0.000	0.00e+00	0.00	0.00e+00	0.00
	244176.3496	−3.0123	74.3659	3.223	0.750	0.000	0.000	0.00e+00	0.00	0.00e+00	0.00
	244209.1879	−3.0604	72.7069	3.223	0.750	0.000	0.000	0.00e+00	0.00	0.00e+00	0.00
	244244.0750	−3.1121	70.2071	3.223	0.750	0.000	0.000	0.00e+00	0.00	0.00e+00	0.00
	244287.0548	−3.1684	66.8654	3.223	0.750	0.000	0.000	0.00e+00	0.00	0.00e+00	0.00
	244356.1585	−3.2302	62.6795	3.223	0.750	0.000	0.000	0.00e+00	0.00	0.00e+00	0.00
	244369.9016	−3.6706	51.7547	3.223	0.750	0.000	0.000	0.00e+00	0.00	0.00e+00	0.00
	244513.3716	−3.5984	57.6423	3.223	0.750	0.000	0.000	0.00e+00	0.00	0.00e+00	0.00
	244528.0770	−3.5983	57.6418	3.223	0.750	0.000	0.000	0.00e+00	0.00	0.00e+00	0.00
	244731.9485	−3.7898	45.5346	3.223	0.750	0.000	0.000	0.00e+00	0.00	0.00e+00	0.00
	246093.7146	−3.6597	51.6858	3.223	0.750	0.000	0.000	0.00e+00	0.00	0.00e+00	0.00
	247810.6065	−3.6352	44.6036	3.223	0.750	0.000	0.000	0.00e+00	0.00	0.00e+00	0.00
	624484.4450	−3.3030	337.3292	3.223	0.750	0.000	0.000	0.00e+00	0.00	0.00e+00	0.00
	624775.5300	−3.3026	337.3306	3.223	0.750	0.000	0.000	0.00e+00	0.00	0.00e+00	0.00
	625344.9466	−3.5135	182.3848	3.223	0.750	0.000	0.000	0.00e+00	0.00	0.00e+00	0.00
	626621.9820	−4.2786	182.3422	3.223	0.750	0.000	0.000	0.00e+00	0.00	0.00e+00	0.00
	626825.2410	−3.5774	187.3097	3.223	0.750	0.000	0.000	0.00e+00	0.00	0.00e+00	0.00
	631750.8291	−2.6473	509.2607	3.400	0.800	0.000	0.000	0.00e+00	0.00	0.00e+00	0.00
	631759.4840	−2.6578	504.2625	3.400	0.800	0.000	0.000	0.00e+00	0.00	0.00e+00	0.00
	631766.8126	−2.6674	498.4238	3.400	0.800	0.000	0.000	0.00e+00	0.00	0.00e+00	0.00
	631770.0138	−3.6167	247.8096	3.223	0.750	0.000	0.000	0.00e+00	0.00	0.00e+00	0.00
	631774.1257	−2.6761	491.7449	3.400	0.800	0.000	0.000	0.00e+00	0.00	0.00e+00	0.00
	631782.6466	−2.6842	484.2261	3.400	0.800	0.000	0.000	0.00e+00	0.00	0.00e+00	0.00
	631794.4115	−2.6915	475.8673	3.400	0.800	0.000	0.000	0.00e+00	0.00	0.00e+00	0.00

Continued on next page

molecule	ν_{0j}^k (MHz)	$\mathcal{I}_j^k$ (nm^{2}MHz)	$E\ell_j^k$ (cm^{-1})	w_{cj}^k (MHz hPa^{-1})	n_{cj}^k	$\Delta\nu_{0j}^k$ (MHz hPa^{-1})	$n_{\Delta\nu_{0j}}^k$	δ_j^k (hPa^{-1})	$n_{\delta_j}^k$	γ_j^k (hPa^{-1})	$n_{\gamma_j}^k$
	631811.6338	−2.6982	466.6682	3.400	0.800	0.000	0.000	0.00e+00	0.00	0.00e+00	0.00
	631837.6664	−2.7043	456.6282	3.400	0.800	0.000	0.000	0.00e+00	0.00	0.00e+00	0.00
	631858.1117	−3.0788	327.6540	3.223	0.750	0.000	0.000	0.00e+00	0.00	0.00e+00	0.00
	631877.4590	−2.7100	445.7462	3.400	0.800	0.000	0.000	0.00e+00	0.00	0.00e+00	0.00
	631896.3016	−4.1681	742.8669	3.400	0.800	0.000	0.000	0.00e+00	0.00	0.00e+00	0.00
	631938.8027	−2.7153	434.0204	3.223	0.750	0.000	0.000	0.00e+00	0.00	0.00e+00	0.00
	632034.8446	−2.7201	421.4477	3.223	0.750	0.000	0.000	0.00e+00	0.00	0.00e+00	0.00
	632148.8480	−3.6870	107.6041	3.223	0.750	0.000	0.000	0.00e+00	0.00	0.00e+00	0.00
	632189.1235	−2.7246	408.0232	3.223	0.750	0.000	0.000	0.00e+00	0.00	0.00e+00	0.00
	632219.7624	−4.1648	696.9618	3.400	0.800	0.000	0.000	0.00e+00	0.00	0.00e+00	0.00
	632360.1195	−3.6160	247.7971	3.223	0.750	0.000	0.000	0.00e+00	0.00	0.00e+00	0.00
	632448.0967	−2.7286	393.7383	3.223	0.750	0.000	0.000	0.00e+00	0.00	0.00e+00	0.00
	632535.8512	−4.1911	651.8781	3.400	0.800	0.000	0.000	0.00e+00	0.00	0.00e+00	0.00
	632597.8138	−3.1948	333.8074	3.223	0.750	0.000	0.000	0.00e+00	0.00	0.00e+00	0.00
	632844.6590	−4.2702	607.6165	3.400	0.800	0.000	0.000	0.00e+00	0.00	0.00e+00	0.00
	632876.3616	−4.1524	80.8529	3.223	0.750	0.000	0.000	0.00e+00	0.00	0.00e+00	0.00
	632880.9913	−3.4505	200.5850	3.223	0.750	0.000	0.000	0.00e+00	0.00	0.00e+00	0.00
	632912.7602	−2.7314	378.5771	3.223	0.750	0.000	0.000	0.00e+00	0.00	0.00e+00	0.00
	633027.6914	−3.6483	374.9006	3.400	0.800	0.000	0.000	0.00e+00	0.00	0.00e+00	0.00
	633146.2743	−4.4759	564.1777	3.400	0.800	0.000	0.000	0.00e+00	0.00	0.00e+00	0.00
	633578.8659	−4.8322	484.9734	3.223	0.750	0.000	0.000	0.00e+00	0.00	0.00e+00	0.00
	633770.9327	−3.1211	330.5959	3.223	0.750	0.000	0.000	0.00e+00	0.00	0.00e+00	0.00
	633825.8146	−3.9555	362.5070	3.223	0.750	0.000	0.000	0.00e+00	0.00	0.00e+00	0.00
	633829.8071	−3.0886	362.5070	3.223	0.750	0.000	0.000	0.00e+00	0.00	0.00e+00	0.00
	633848.8746	−3.8796	263.6108	3.223	0.750	0.000	0.000	0.00e+00	0.00	0.00e+00	0.00
	633854.1264	−3.0886	362.5060	3.223	0.750	0.000	0.000	0.00e+00	0.00	0.00e+00	0.00
	633858.1189	−3.9554	362.5060	3.223	0.750	0.000	0.000	0.00e+00	0.00	0.00e+00	0.00
	635089.2789	−4.0196	345.4691	3.223	0.750	0.000	0.000	0.00e+00	0.00	0.00e+00	0.00
	635432.1434	−3.0777	345.4691	3.223	0.750	0.000	0.000	0.00e+00	0.00	0.00e+00	0.00
	635439.0872	−4.2619	179.3890	3.223	0.750	0.000	0.000	0.00e+00	0.00	0.00e+00	0.00
	635546.7294	−3.5533	179.3854	3.223	0.750	0.000	0.000	0.00e+00	0.00	0.00e+00	0.00
	636414.7874	−2.9733	305.4334	3.223	0.750	0.000	0.000	0.00e+00	0.00	0.00e+00	0.00
	636423.7620	−3.3403	370.2694	3.223	0.750	0.000	0.000	0.00e+00	0.00	0.00e+00	0.00

Continued on next page

molecule	ν_{0j}^k (MHz)	I_j^k ($\mathrm{nm^2MHz}$)	$E\ell_j^k$ ($\mathrm{cm^{-1}}$)	w_{cj}^k ($\mathrm{MHz\,hPa^{-1}}$)	n_{cj}^k	$\Delta\nu_{0j}^k$ ($\mathrm{MHz\,hPa^{-1}}$)	$n_{\Delta\nu_{0j}}^k$	δ_j^k ($\mathrm{hPa^{-1}}$)	$n_{\delta_j}^k$	γ_j^k ($\mathrm{hPa^{-1}}$)	$n_{\gamma_j}^k$
	636850.0072	−3.0749	345.4104	3.223	0.750	0.000	0.000	0.00e+00	0.00	0.00e+00	0.00
	637192.8717	−4.0150	345.4104	3.223	0.750	0.000	0.000	0.00e+00	0.00	0.00e+00	0.00
	637234.7106	−3.5339	250.9911	3.223	0.750	0.000	0.000	0.00e+00	0.00	0.00e+00	0.00
	637259.9950	−4.1855	177.4516	3.223	0.750	0.000	0.000	0.00e+00	0.00	0.00e+00	0.00
	637267.8610	−3.5338	250.9904	3.223	0.750	0.000	0.000	0.00e+00	0.00	0.00e+00	0.00
	637269.3732	−4.1855	177.4512	3.223	0.750	0.000	0.000	0.00e+00	0.00	0.00e+00	0.00
	648337.4208	−3.4968	203.2441	3.223	0.750	0.000	0.000	0.00e+00	0.00	0.00e+00	0.00
	648916.5334	−4.1854	219.7609	3.223	0.750	0.000	0.000	0.00e+00	0.00	0.00e+00	0.00
	649032.1913	−3.5724	205.9474	3.223	0.750	0.000	0.000	0.00e+00	0.00	0.00e+00	0.00
	650287.6161	−3.0033	326.6619	3.223	0.750	0.000	0.000	0.00e+00	0.00	0.00e+00	0.00
	650483.0066	−3.4846	200.6619	3.223	0.750	0.000	0.000	0.00e+00	0.00	0.00e+00	0.00
	650582.7236	−3.7045	265.9358	3.223	0.750	0.000	0.000	0.00e+00	0.00	0.00e+00	0.00
	650713.1148	−3.2210	358.1598	3.223	0.750	0.000	0.000	0.00e+00	0.00	0.00e+00	0.00
	651934.0981	−4.2830	175.9352	3.223	0.750	0.000	0.000	0.00e+00	0.00	0.00e+00	0.00
	651940.4017	−3.5986	175.9350	3.223	0.750	0.000	0.000	0.00e+00	0.00	0.00e+00	0.00
	652156.4541	−3.5985	175.9352	3.223	0.750	0.000	0.000	0.00e+00	0.00	0.00e+00	0.00
	652162.7577	−4.2829	175.9350	3.223	0.750	0.000	0.000	0.00e+00	0.00	0.00e+00	0.00
	652428.6213	−3.2183	358.1708	3.223	0.750	0.000	0.000	0.00e+00	0.00	0.00e+00	0.00
	652790.5934	−4.2798	200.5850	3.223	0.750	0.000	0.000	0.00e+00	0.00	0.00e+00	0.00
	652899.0599	−3.4033	219.6281	3.223	0.750	0.000	0.000	0.00e+00	0.00	0.00e+00	0.00
	653893.2885	−3.6746	400.8148	3.400	0.800	0.000	0.000	0.00e+00	0.00	0.00e+00	0.00
	658918.9445	−4.9109	186.2392	3.223	0.750	0.000	0.000	0.00e+00	0.00	0.00e+00	0.00
	659083.5267	−4.0694	348.3532	3.223	0.750	0.000	0.000	0.00e+00	0.00	0.00e+00	0.00
	659149.3708	−3.9776	388.2566	3.223	0.750	0.000	0.000	0.00e+00	0.00	0.00e+00	0.00
	659157.9297	−3.0984	388.2566	3.223	0.750	0.000	0.000	0.00e+00	0.00	0.00e+00	0.00
	659197.9058	−2.9835	328.4549	3.223	0.750	0.000	0.000	0.00e+00	0.00	0.00e+00	0.00
	659206.8279	−3.0983	388.2547	3.223	0.750	0.000	0.000	0.00e+00	0.00	0.00e+00	0.00
	659215.3868	−3.9775	388.2547	3.223	0.750	0.000	0.000	0.00e+00	0.00	0.00e+00	0.00
	659610.9966	−3.8739	263.1104	3.223	0.750	0.000	0.000	0.00e+00	0.00	0.00e+00	0.00
	660198.7192	−4.0472	370.3379	3.223	0.750	0.000	0.000	0.00e+00	0.00	0.00e+00	0.00
	660833.4591	−3.0836	370.3379	3.223	0.750	0.000	0.000	0.00e+00	0.00	0.00e+00	0.00
	661197.9981	−3.4836	391.4982	3.223	0.750	0.000	0.000	0.00e+00	0.00	0.00e+00	0.00
	661204.0841	−3.4836	391.4982	3.223	0.750	0.000	0.000	0.00e+00	0.00	0.00e+00	0.00

Continued on next page

molecule	ν_{0j}^k (MHz)	$\mathcal{I}_j^k$ (nm^2MHz)	$E\ell_j^k$ (cm^{-1})	w_{cj}^k (MHz hPa^{-1})	n_{cj}^k	$\Delta\nu_{0j}^k$ (MHz hPa^{-1})	$n_{\Delta\nu_{0j}}^k$	δ_j^k (hPa^{-1})	$n_{\delta_j}^k$	γ_j^k (hPa^{-1})	$n_{\gamma_j}^k$
	661516.2296	−4.9418	148.2836	3.400	0.800	0.000	0.000	0.00e+00	0.00	0.00e+00	0.00
$HNO_3(\nu_5)$	205984.9148	−4.9741	931.7017	3.323	0.700	0.000	0.000	0.00e+00	0.00	0.00e+00	0.00
	206028.1620	−5.0285	930.8858	3.430	0.640	0.000	0.000	0.00e+00	0.00	0.00e+00	0.00
	206070.1894	−5.0879	929.2305	3.642	0.610	0.000	0.000	0.00e+00	0.00	0.00e+00	0.00
$HNO_3(\nu_6)$	183461.8066	−5.3247	674.8520	3.400	0.800	0.000	0.000	0.00e+00	0.00	0.00e+00	0.00
	201486.2753	−5.2747	676.3423	3.680	0.640	0.000	0.000	0.00e+00	0.00	0.00e+00	0.00
	204769.5845	−5.1915	837.0552	3.158	0.880	0.000	0.000	0.00e+00	0.00	0.00e+00	0.00
	204923.8235	−5.1981	817.0504	3.170	0.800	0.000	0.000	0.00e+00	0.00	0.00e+00	0.00
	205062.4532	−5.2151	797.8746	3.170	0.800	0.000	0.000	0.00e+00	0.00	0.00e+00	0.00
	205409.3277	−5.2271	682.4597	3.680	0.640	0.000	0.000	0.00e+00	0.00	0.00e+00	0.00
	206866.2019	−4.7419	691.6870	3.470	0.640	0.000	0.000	0.00e+00	0.00	0.00e+00	0.00
	206872.8020	−5.1251	687.4692	3.700	0.640	0.000	0.000	0.00e+00	0.00	0.00e+00	0.00
	207130.3913	−4.5417	699.3232	3.430	0.640	0.000	0.000	0.00e+00	0.00	0.00e+00	0.00
	207228.9863	−4.4868	700.2066	3.323	0.700	0.000	0.000	0.00e+00	0.00	0.00e+00	0.00
	626353.6227	−4.5546	980.0617	3.400	0.800	0.000	0.000	0.00e+00	0.00	0.00e+00	0.00
	632085.0641	−4.1336	1067.7795	3.400	0.800	0.000	0.000	0.00e+00	0.00	0.00e+00	0.00
	632110.1209	−4.1305	1080.4219	3.400	0.800	0.000	0.000	0.00e+00	0.00	0.00e+00	0.00
	632122.1764	−4.1359	1054.2941	3.400	0.800	0.000	0.000	0.00e+00	0.00	0.00e+00	0.00
	632171.1923	−4.1267	1092.2264	3.400	0.800	0.000	0.000	0.00e+00	0.00	0.00e+00	0.00
	632253.7847	−4.1222	1103.1967	3.400	0.800	0.000	0.000	0.00e+00	0.00	0.00e+00	0.00
	632272.8340	−4.1369	1039.9563	3.400	0.800	0.000	0.000	0.00e+00	0.00	0.00e+00	0.00
	632349.2741	−4.1171	1113.3341	3.400	0.800	0.000	0.000	0.00e+00	0.00	0.00e+00	0.00
	632452.1889	−4.1113	1122.6403	3.400	0.800	0.000	0.000	0.00e+00	0.00	0.00e+00	0.00
	632558.8404	−4.1048	1131.1154	3.400	0.800	0.000	0.000	0.00e+00	0.00	0.00e+00	0.00
	632649.6401	−4.1358	1024.7487	3.400	0.800	0.000	0.000	0.00e+00	0.00	0.00e+00	0.00
	632666.5927	−4.0976	1138.7596	3.400	0.800	0.000	0.000	0.00e+00	0.00	0.00e+00	0.00
	632773.4467	−4.0895	1145.5732	3.400	0.800	0.000	0.000	0.00e+00	0.00	0.00e+00	0.00
	632877.8473	−4.0805	1151.5557	3.400	0.800	0.000	0.000	0.00e+00	0.00	0.00e+00	0.00
	632978.4548	−4.0707	1156.7065	3.400	0.800	0.000	0.000	0.00e+00	0.00	0.00e+00	0.00
	633074.1444	−4.0598	1161.0250	3.400	0.800	0.000	0.000	0.00e+00	0.00	0.00e+00	0.00
	633163.9080	−4.0480	1164.5104	3.400	0.800	0.000	0.000	0.00e+00	0.00	0.00e+00	0.00
	633246.8274	−4.0350	1167.1617	3.400	0.800	0.000	0.000	0.00e+00	0.00	0.00e+00	0.00
	633322.0509	−4.0210	1168.9781	3.400	0.800	0.000	0.000	0.00e+00	0.00	0.00e+00	0.00

Continued on next page

molecule	ν_{0j}^k (MHz)	$\mathcal{I}_j^k$ (nm^2MHz)	$E\ell_j^k$ (cm^{-1})	w_{cj}^k (MHz hPa^{-1})	n_{cj}^k	$\Delta\nu_{0j}^k$ (MHz hPa^{-1})	$n_{\Delta\nu_{0j}}^k$	δ_j^k (hPa^{-1})	$n_{\delta_j}^k$	γ_j^k (hPa^{-1})	$n_{\gamma_j}^k$
	633388.7783	−4.0058	1169.9584	3.400	0.800	0.000	0.000	0.00e+00	0.00	0.00e+00	0.00
	633525.1451	−4.4318	1008.6349	3.400	0.800	0.000	0.000	0.00e+00	0.00	0.00e+00	0.00
	633565.4857	−4.4317	1008.6334	3.400	0.800	0.000	0.000	0.00e+00	0.00	0.00e+00	0.00
	633909.2417	−4.3227	951.4430	3.400	0.800	0.000	0.000	0.00e+00	0.00	0.00e+00	0.00
	635000.3006	−4.4202	991.5566	3.400	0.800	0.000	0.000	0.00e+00	0.00	0.00e+00	0.00
	637042.0547	−4.4160	991.4706	3.400	0.800	0.000	0.000	0.00e+00	0.00	0.00e+00	0.00
	648400.5846	−4.7395	865.9379	3.400	0.800	0.000	0.000	0.00e+00	0.00	0.00e+00	0.00
	650614.5741	−4.3364	972.5879	3.400	0.800	0.000	0.000	0.00e+00	0.00	0.00e+00	0.00
	651971.6874	−4.4928	1000.9546	3.400	0.800	0.000	0.000	0.00e+00	0.00	0.00e+00	0.00
	652935.1501	−4.4378	997.8153	3.400	0.800	0.000	0.000	0.00e+00	0.00	0.00e+00	0.00
	658840.5959	−4.4412	1034.3188	3.400	0.800	0.000	0.000	0.00e+00	0.00	0.00e+00	0.00
	658921.3152	−4.4411	1034.3157	3.400	0.800	0.000	0.000	0.00e+00	0.00	0.00e+00	0.00
	659693.2415	−4.4775	1001.0318	3.400	0.800	0.000	0.000	0.00e+00	0.00	0.00e+00	0.00
	660301.0002	−4.4259	1016.3605	3.400	0.800	0.000	0.000	0.00e+00	0.00	0.00e+00	0.00
$HNO_3(\nu_7)$	179981.9689	−4.4998	619.3993	3.400	0.800	0.000	0.000	0.00e+00	0.00	0.00e+00	0.00
	180264.9863	−4.5622	618.6752	3.400	0.800	0.000	0.000	0.00e+00	0.00	0.00e+00	0.00
	182557.2066	−5.1159	803.1835	3.400	0.800	0.000	0.000	0.00e+00	0.00	0.00e+00	0.00
	182777.1455	−5.1042	782.3067	3.400	0.800	0.000	0.000	0.00e+00	0.00	0.00e+00	0.00
	182974.0090	−5.0984	762.2594	3.400	0.800	0.000	0.000	0.00e+00	0.00	0.00e+00	0.00
	183142.4991	−5.1879	607.1052	3.400	0.800	0.000	0.000	0.00e+00	0.00	0.00e+00	0.00
	183149.6830	−5.0995	743.0423	3.400	0.800	0.000	0.000	0.00e+00	0.00	0.00e+00	0.00
	183305.9356	−5.1087	724.6561	3.400	0.800	0.000	0.000	0.00e+00	0.00	0.00e+00	0.00
	183444.4257	−5.1282	707.1014	3.400	0.800	0.000	0.000	0.00e+00	0.00	0.00e+00	0.00
	183566.7097	−5.1612	690.3788	3.400	0.800	0.000	0.000	0.00e+00	0.00	0.00e+00	0.00
	183674.2479	−5.2130	674.4888	3.400	0.800	0.000	0.000	0.00e+00	0.00	0.00e+00	0.00
	202225.9859	−5.1266	608.6125	3.680	0.640	0.000	0.000	0.00e+00	0.00	0.00e+00	0.00
	204784.7830	−4.3546	631.8201	3.323	0.700	0.000	0.000	0.00e+00	0.00	0.00e+00	0.00
	204784.7830	−4.2768	631.8201	3.323	0.700	0.000	0.000	0.00e+00	0.00	0.00e+00	0.00
	205066.3443	−4.3314	631.1148	3.430	0.640	0.000	0.000	0.00e+00	0.00	0.00e+00	0.00
	205066.3461	−4.4084	631.1148	3.430	0.640	0.000	0.000	0.00e+00	0.00	0.00e+00	0.00
	205349.3406	−4.3913	629.5517	3.642	0.610	0.000	0.000	0.00e+00	0.00	0.00e+00	0.00
	205349.3440	−4.4671	629.5517	3.642	0.610	0.000	0.000	0.00e+00	0.00	0.00e+00	0.00
	205379.5040	−5.0874	614.7238	3.680	0.640	0.000	0.000	0.00e+00	0.00	0.00e+00	0.00

Continued on next page

molecule	ν_{0j}^k (MHz)	I_j^k ($\mathrm{nm^2MHz}$)	$E\ell_j^k$ ($\mathrm{cm^{-1}}$)	w_{cj}^k ($\mathrm{MHz\,hPa^{-1}}$)	n_{cj}^k	$\Delta\nu_{0j}^k$ ($\mathrm{MHz\,hPa^{-1}}$)	$n_{\Delta\nu_{0j}}^k$	δ_j^k ($\mathrm{hPa^{-1}}$)	$n_{\delta_j}^k$	γ_j^k ($\mathrm{hPa^{-1}}$)	$n_{\gamma_j}^k$
	205638.8086	−4.4582	627.1300	3.615	0.670	0.000	0.000	0.00e+00	0.00	0.00e+00	0.00
	205638.8099	−4.5322	627.1300	3.615	0.670	0.000	0.000	0.00e+00	0.00	0.00e+00	0.00
	205951.4550	−4.6052	623.8475	3.470	0.640	0.000	0.000	0.00e+00	0.00	0.00e+00	0.00
	206341.0968	−4.9875	619.6977	3.700	0.640	0.000	0.000	0.00e+00	0.00	0.00e+00	0.00
	206393.9350	−4.9872	619.6957	3.700	0.640	0.000	0.000	0.00e+00	0.00	0.00e+00	0.00
	626166.3604	−3.8616	1096.0524	3.400	0.800	0.000	0.000	0.00e+00	0.00	0.00e+00	0.00
	626412.1046	−3.8776	1095.6483	3.400	0.800	0.000	0.000	0.00e+00	0.00	0.00e+00	0.00
	626414.9281	−4.7185	761.3763	3.400	0.800	0.000	0.000	0.00e+00	0.00	0.00e+00	0.00
	626653.1461	−3.8924	1094.3844	3.400	0.800	0.000	0.000	0.00e+00	0.00	0.00e+00	0.00
	626890.4827	−3.9060	1092.2614	3.400	0.800	0.000	0.000	0.00e+00	0.00	0.00e+00	0.00
	627060.8108	−4.2683	886.5711	3.400	0.800	0.000	0.000	0.00e+00	0.00	0.00e+00	0.00
	632721.5576	−4.3292	909.6971	3.400	0.800	0.000	0.000	0.00e+00	0.00	0.00e+00	0.00
	632799.0808	−4.2952	941.4383	3.400	0.800	0.000	0.000	0.00e+00	0.00	0.00e+00	0.00
	632826.1549	−4.2951	941.4372	3.400	0.800	0.000	0.000	0.00e+00	0.00	0.00e+00	0.00
	633190.7436	−4.6535	779.5782	3.400	0.800	0.000	0.000	0.00e+00	0.00	0.00e+00	0.00
	634677.0351	−4.2839	924.4640	3.400	0.800	0.000	0.000	0.00e+00	0.00	0.00e+00	0.00
	635859.0265	−4.1798	884.4556	3.400	0.800	0.000	0.000	0.00e+00	0.00	0.00e+00	0.00
	636220.2437	−4.2808	924.4000	3.400	0.800	0.000	0.000	0.00e+00	0.00	0.00e+00	0.00
	636481.7563	−4.7577	758.3475	3.400	0.800	0.000	0.000	0.00e+00	0.00	0.00e+00	0.00
	649411.2209	−4.4300	937.3387	3.400	0.800	0.000	0.000	0.00e+00	0.00	0.00e+00	0.00
	649774.3276	−4.7037	782.2712	3.400	0.800	0.000	0.000	0.00e+00	0.00	0.00e+00	0.00
	650184.0758	−4.2069	905.6656	3.400	0.800	0.000	0.000	0.00e+00	0.00	0.00e+00	0.00
	650927.7925	−3.8995	1138.2386	3.400	0.800	0.000	0.000	0.00e+00	0.00	0.00e+00	0.00
	651027.2113	−4.4275	937.3490	3.400	0.800	0.000	0.000	0.00e+00	0.00	0.00e+00	0.00
	651079.3631	−4.7812	785.0006	3.400	0.800	0.000	0.000	0.00e+00	0.00	0.00e+00	0.00
	651171.0657	−3.9148	1137.8510	3.400	0.800	0.000	0.000	0.00e+00	0.00	0.00e+00	0.00
	651874.4817	−3.9536	1131.5305	3.400	0.800	0.000	0.000	0.00e+00	0.00	0.00e+00	0.00
	652103.5264	−3.9642	1127.7075	3.400	0.800	0.000	0.000	0.00e+00	0.00	0.00e+00	0.00
	652331.5856	−3.9737	1123.0276	3.400	0.800	0.000	0.000	0.00e+00	0.00	0.00e+00	0.00
	652559.7686	−3.9821	1117.4915	3.400	0.800	0.000	0.000	0.00e+00	0.00	0.00e+00	0.00
	652789.2855	−3.9896	1111.0991	3.400	0.800	0.000	0.000	0.00e+00	0.00	0.00e+00	0.00
	653021.5114	−3.9961	1103.8511	3.400	0.800	0.000	0.000	0.00e+00	0.00	0.00e+00	0.00
	653154.5640	−4.6057	798.6252	3.400	0.800	0.000	0.000	0.00e+00	0.00	0.00e+00	0.00

Continued on next page

molecule	ν_{0j}^k (MHz)	I_j^k (nm^2MHz)	$E\ell_j^k$ (cm^{-1})	a_{cj}^k (MHz hPa^{-1})	n_{cj}^k	$\Delta\nu_{0j}^k$ (MHz hPa^{-1})	$n_{\Delta\nu_{0j}}^k$	δ_j^k (hPa^{-1})	$n_{\delta_j}^k$	γ_j^k (hPa^{-1})	$n_{\gamma_j}^k$
	653184.1016	−4.8029	754.8631	3.400	0.800	0.000	0.000	0.00e+00	0.00	0.00e+00	0.00
	653258.0855	−4.0017	1095.7472	3.400	0.800	0.000	0.000	0.00e+00	0.00	0.00e+00	0.00
	653419.0929	−4.8027	754.8633	3.400	0.800	0.000	0.000	0.00e+00	0.00	0.00e+00	0.00
	653501.0720	−4.0065	1086.7874	3.400	0.800	0.000	0.000	0.00e+00	0.00	0.00e+00	0.00
	653753.2260	−4.0104	1076.9708	3.400	0.800	0.000	0.000	0.00e+00	0.00	0.00e+00	0.00
	658726.7466	−4.7831	784.7255	3.400	0.800	0.000	0.000	0.00e+00	0.00	0.00e+00	0.00
	658771.9978	−4.7218	776.6510	3.400	0.800	0.000	0.000	0.00e+00	0.00	0.00e+00	0.00
	659723.0210	−4.6932	970.8425	3.400	0.800	0.000	0.000	0.00e+00	0.00	0.00e+00	0.00
	659728.5791	−4.6932	970.8425	3.400	0.800	0.000	0.000	0.00e+00	0.00	0.00e+00	0.00
	660087.1556	−4.2897	949.3408	3.400	0.800	0.000	0.000	0.00e+00	0.00	0.00e+00	0.00
$HNO_3(\nu_8)$	204673.8526	−5.4709	798.7676	3.680	0.640	0.000	0.000	0.00e+00	0.00	0.00e+00	0.00
	206261.5593	−4.9857	807.9616	3.470	0.640	0.000	0.000	0.00e+00	0.00	0.00e+00	0.00
	206297.1097	−5.3681	803.7568	3.700	0.640	0.000	0.000	0.00e+00	0.00	0.00e+00	0.00
	206307.9283	−4.9121	811.3260	3.615	0.670	0.000	0.000	0.00e+00	0.00	0.00e+00	0.00
	206374.6253	−5.3677	803.7539	3.700	0.640	0.000	0.000	0.00e+00	0.00	0.00e+00	0.00
	206380.8054	−4.8461	813.8576	3.642	0.610	0.000	0.000	0.00e+00	0.00	0.00e+00	0.00
	206460.7534	−4.7864	815.5587	3.430	0.640	0.000	0.000	0.00e+00	0.00	0.00e+00	0.00
	206542.2256	−4.7317	816.4305	3.323	0.700	0.000	0.000	0.00e+00	0.00	0.00e+00	0.00
	636311.7392	−4.6531	1106.8336	3.400	0.800	0.000	0.000	0.00e+00	0.00	0.00e+00	0.00
	649634.7465	−4.5684	1087.8773	3.400	0.800	0.000	0.000	0.00e+00	0.00	0.00e+00	0.00
	650859.1985	−4.5930	1089.8046	3.400	0.800	0.000	0.000	0.00e+00	0.00	0.00e+00	0.00
$HNO_3(\nu_9)$	181240.9944	−4.1554	493.8461	3.400	0.800	0.000	0.000	0.00e+00	0.00	0.00e+00	0.00
	181262.6503	−4.8484	490.4886	3.400	0.800	0.000	0.000	0.00e+00	0.00	0.00e+00	0.00
	181262.6520	−4.8484	490.4885	3.400	0.800	0.000	0.000	0.00e+00	0.00	0.00e+00	0.00
	181271.8094	−4.0754	496.3652	3.400	0.800	0.000	0.000	0.00e+00	0.00	0.00e+00	0.00
	181288.1016	−4.8482	490.4877	3.400	0.800	0.000	0.000	0.00e+00	0.00	0.00e+00	0.00
	181288.1033	−4.8482	490.4876	3.400	0.800	0.000	0.000	0.00e+00	0.00	0.00e+00	0.00
	181315.8486	−4.3057	498.0506	3.400	0.800	0.000	0.000	0.00e+00	0.00	0.00e+00	0.00
	181315.8547	−4.3057	498.0507	3.400	0.800	0.000	0.000	0.00e+00	0.00	0.00e+00	0.00
	181362.3790	−3.9412	498.9038	3.400	0.800	0.000	0.000	0.00e+00	0.00	0.00e+00	0.00
	183134.4554	−4.6296	486.2069	3.400	0.800	0.000	0.000	0.00e+00	0.00	0.00e+00	0.00
	200439.4517	−4.8901	487.7084	3.400	0.800	0.000	0.000	0.00e+00	0.00	0.00e+00	0.00
	200439.4684	−4.8901	487.7083	3.400	0.800	0.000	0.000	0.00e+00	0.00	0.00e+00	0.00

Continued on next page

molecule	ν_{0j}^k (MHz)	$\mathcal{I}_j^k$ ($\mathrm{nm^2MHz}$)	$E\ell_j^k$ ($\mathrm{cm^{-1}}$)	w_{cj}^k ($\mathrm{MHz\,hPa^{-1}}$)	n_{cj}^k	$\Delta\nu_{0j}^k$ ($\mathrm{MHz\,hPa^{-1}}$)	$n_{\Delta\nu_{0j}}^k$	δ_j^k ($\mathrm{hPa^{-1}}$)	$n_{\delta_j}^k$	γ_j^k ($\mathrm{hPa^{-1}}$)	$n_{\gamma_j}^k$
	201885.4512	−5.0452	892.9137	3.400	0.800	0.000	0.000	0.00e+00	0.00	0.00e+00	0.00
	201885.4866	−5.0452	892.9136	3.400	0.800	0.000	0.000	0.00e+00	0.00	0.00e+00	0.00
	202304.0944	−4.7016	864.7192	3.400	0.800	0.000	0.000	0.00e+00	0.00	0.00e+00	0.00
	202687.5744	−4.6623	837.3443	3.400	0.800	0.000	0.000	0.00e+00	0.00	0.00e+00	0.00
	203650.8464	−4.5658	760.1458	3.400	0.800	0.000	0.000	0.00e+00	0.00	0.00e+00	0.00
	203916.6841	−4.5417	736.0578	3.400	0.800	0.000	0.000	0.00e+00	0.00	0.00e+00	0.00
	204158.1136	−4.8232	712.7936	3.400	0.800	0.000	0.000	0.00e+00	0.00	0.00e+00	0.00
	204158.1470	−4.8232	712.7935	3.400	0.800	0.000	0.000	0.00e+00	0.00	0.00e+00	0.00
	204376.9507	−4.5078	690.3538	3.400	0.800	0.000	0.000	0.00e+00	0.00	0.00e+00	0.00
	204574.7905	−4.8004	668.7393	3.400	0.800	0.000	0.000	0.00e+00	0.00	0.00e+00	0.00
	204574.8236	−4.8004	668.7392	3.400	0.800	0.000	0.000	0.00e+00	0.00	0.00e+00	0.00
	204748.2657	−4.8358	493.8098	3.400	0.800	0.000	0.000	0.00e+00	0.00	0.00e+00	0.00
	204748.2734	−4.8358	493.8097	3.400	0.800	0.000	0.000	0.00e+00	0.00	0.00e+00	0.00
	204753.2489	−4.7987	647.9506	3.400	0.800	0.000	0.000	0.00e+00	0.00	0.00e+00	0.00
	204753.2818	−4.7987	647.9505	3.400	0.800	0.000	0.000	0.00e+00	0.00	0.00e+00	0.00
	204876.7704	−5.4226	481.9445	3.400	0.800	0.000	0.000	0.00e+00	0.00	0.00e+00	0.00
	204880.1851	−5.4226	481.9444	3.400	0.800	0.000	0.000	0.00e+00	0.00	0.00e+00	0.00
	204913.7859	−4.8054	627.9884	3.400	0.800	0.000	0.000	0.00e+00	0.00	0.00e+00	0.00
	204913.8186	−4.8054	627.9883	3.400	0.800	0.000	0.000	0.00e+00	0.00	0.00e+00	0.00
	205057.7946	−4.8224	608.8534	3.400	0.800	0.000	0.000	0.00e+00	0.00	0.00e+00	0.00
	205057.8272	−4.8224	608.8533	3.400	0.800	0.000	0.000	0.00e+00	0.00	0.00e+00	0.00
	205186.5896	−4.8528	590.5461	3.400	0.800	0.000	0.000	0.00e+00	0.00	0.00e+00	0.00
	205186.6222	−4.8528	590.5460	3.400	0.800	0.000	0.000	0.00e+00	0.00	0.00e+00	0.00
	205301.4116	−4.9023	573.0671	3.400	0.800	0.000	0.000	0.00e+00	0.00	0.00e+00	0.00
	205301.4441	−4.9023	573.0670	3.400	0.800	0.000	0.000	0.00e+00	0.00	0.00e+00	0.00
	205403.4304	−4.9809	556.4170	3.400	0.800	0.000	0.000	0.00e+00	0.00	0.00e+00	0.00
	205403.4628	−4.9809	556.4169	3.400	0.800	0.000	0.000	0.00e+00	0.00	0.00e+00	0.00
	205493.7486	−5.1117	540.5962	3.400	0.800	0.000	0.000	0.00e+00	0.00	0.00e+00	0.00
	205493.7809	−5.1117	540.5961	3.400	0.800	0.000	0.000	0.00e+00	0.00	0.00e+00	0.00
	205838.5144	−5.4206	481.9239	3.400	0.800	0.000	0.000	0.00e+00	0.00	0.00e+00	0.00
	205841.9295	−5.4206	481.9238	3.400	0.800	0.000	0.000	0.00e+00	0.00	0.00e+00	0.00
	206227.6347	−5.4049	502.9975	3.400	0.800	0.000	0.000	0.00e+00	0.00	0.00e+00	0.00
	206227.8770	−5.4049	502.9974	3.400	0.800	0.000	0.000	0.00e+00	0.00	0.00e+00	0.00

Continued on next page

molecule	ν_{0j}^k (MHz)	$\mathcal{I}_j^k$ ($\mathrm{nm^2MHz}$)	$E\ell_j^k$ ($\mathrm{cm^{-1}}$)	w_{cj}^k ($\mathrm{MHz\,hPa^{-1}}$)	n_{cj}^k	$\Delta\nu_{0j}^k$ ($\mathrm{MHz\,hPa^{-1}}$)	$n_{\Delta\nu_{0j}}^k$	δ_j^k ($\mathrm{hPa^{-1}}$)	$n_{\delta_j}^k$	γ_j^k ($\mathrm{hPa^{-1}}$)	$n_{\gamma_j}^k$
	206229.3526	−4.6520	502.9975	3.400	0.800	0.000	0.000	0.00e+00	0.00	0.00e+00	0.00
	206229.4915	−4.1749	502.9974	3.400	0.800	0.000	0.000	0.00e+00	0.00	0.00e+00	0.00
	206231.1576	−5.1039	502.9974	3.400	0.800	0.000	0.000	0.00e+00	0.00	0.00e+00	0.00
	206241.3195	−5.0101	506.3542	3.400	0.800	0.000	0.000	0.00e+00	0.00	0.00e+00	0.00
	206243.0382	−3.9764	506.3542	3.400	0.800	0.000	0.000	0.00e+00	0.00	0.00e+00	0.00
	206244.7569	−5.0101	506.3542	3.400	0.800	0.000	0.000	0.00e+00	0.00	0.00e+00	0.00
	206280.6022	−4.9322	508.8755	3.400	0.800	0.000	0.000	0.00e+00	0.00	0.00e+00	0.00
	206282.3452	−3.9104	508.8755	3.400	0.800	0.000	0.000	0.00e+00	0.00	0.00e+00	0.00
	206284.0881	−4.9322	508.8755	3.400	0.800	0.000	0.000	0.00e+00	0.00	0.00e+00	0.00
	206286.3290	−5.5269	498.7979	3.400	0.800	0.000	0.000	0.00e+00	0.00	0.00e+00	0.00
	206289.7076	−5.5269	498.7979	3.400	0.800	0.000	0.000	0.00e+00	0.00	0.00e+00	0.00
	206297.0141	−4.4324	498.7979	3.400	0.800	0.000	0.000	0.00e+00	0.00	0.00e+00	0.00
	206326.6025	−4.8647	510.5639	3.400	0.800	0.000	0.000	0.00e+00	0.00	0.00e+00	0.00
	206328.3762	−3.8508	510.5639	3.400	0.800	0.000	0.000	0.00e+00	0.00	0.00e+00	0.00
	206330.1498	−4.8646	510.5639	3.400	0.800	0.000	0.000	0.00e+00	0.00	0.00e+00	0.00
	206370.8296	−4.4320	498.7951	3.400	0.800	0.000	0.000	0.00e+00	0.00	0.00e+00	0.00
	206373.6322	−4.8044	511.4202	3.400	0.800	0.000	0.000	0.00e+00	0.00	0.00e+00	0.00
	206375.4431	−3.7961	511.4202	3.400	0.800	0.000	0.000	0.00e+00	0.00	0.00e+00	0.00
	206377.2539	−4.8044	511.4202	3.400	0.800	0.000	0.000	0.00e+00	0.00	0.00e+00	0.00
	206378.1362	−5.5263	498.7951	3.400	0.800	0.000	0.000	0.00e+00	0.00	0.00e+00	0.00
	206381.5146	−5.5263	498.7951	3.400	0.800	0.000	0.000	0.00e+00	0.00	0.00e+00	0.00
	624314.3397	−3.8649	790.8922	3.400	0.800	0.000	0.000	0.00e+00	0.00	0.00e+00	0.00
	624352.8456	−4.6013	616.0375	3.400	0.800	0.000	0.000	0.00e+00	0.00	0.00e+00	0.00
	624352.8940	−4.6013	616.0374	3.400	0.800	0.000	0.000	0.00e+00	0.00	0.00e+00	0.00
	625085.6322	−4.3890	657.8790	3.400	0.800	0.000	0.000	0.00e+00	0.00	0.00e+00	0.00
	625085.7032	−4.3890	657.8789	3.400	0.800	0.000	0.000	0.00e+00	0.00	0.00e+00	0.00
	626452.5348	−4.4208	661.4528	3.400	0.800	0.000	0.000	0.00e+00	0.00	0.00e+00	0.00
	626452.5486	−4.4208	661.4529	3.400	0.800	0.000	0.000	0.00e+00	0.00	0.00e+00	0.00
	632080.5403	−3.7363	819.1949	3.400	0.800	0.000	0.000	0.00e+00	0.00	0.00e+00	0.00
	632137.3061	−4.0372	819.1927	3.400	0.800	0.000	0.000	0.00e+00	0.00	0.00e+00	0.00
	632137.3200	−4.0372	819.1926	3.400	0.800	0.000	0.000	0.00e+00	0.00	0.00e+00	0.00
	633436.2757	−4.1262	823.3417	3.400	0.800	0.000	0.000	0.00e+00	0.00	0.00e+00	0.00
	633441.3435	−4.1262	823.3417	3.400	0.800	0.000	0.000	0.00e+00	0.00	0.00e+00	0.00

Continued on next page

molecule	ν_{0j}^k (MHz)	I_j^k ($\mathrm{nm^2MHz}$)	$E\ell_j^k$ ($\mathrm{cm^{-1}}$)	w_{cj}^k ($\mathrm{MHz\,hPa^{-1}}$)	n_{cj}^k	$\Delta\nu_{0j}^k$ ($\mathrm{MHz\,hPa^{-1}}$)	$n_{\Delta\nu_{0j}}^k$	δ_j^k ($\mathrm{hPa^{-1}}$)	$n_{\delta_j}^k$	γ_j^k ($\mathrm{hPa^{-1}}$)	$n_{\gamma_j}^k$
	633600.8042	−4.0251	802.1466	3.400	0.800	0.000	0.000	0.00e+00	0.00	0.00e+00	0.00
	633600.8219	−4.0251	802.1465	3.400	0.800	0.000	0.000	0.00e+00	0.00	0.00e+00	0.00
	633826.2903	−4.2085	636.8636	3.400	0.800	0.000	0.000	0.00e+00	0.00	0.00e+00	0.00
	636191.9062	−4.4818	708.5949	3.400	0.800	0.000	0.000	0.00e+00	0.00	0.00e+00	0.00
	636194.7659	−4.4818	708.5949	3.400	0.800	0.000	0.000	0.00e+00	0.00	0.00e+00	0.00
	636209.1040	−4.4818	708.5946	3.400	0.800	0.000	0.000	0.00e+00	0.00	0.00e+00	0.00
	636211.9636	−4.4818	708.5945	3.400	0.800	0.000	0.000	0.00e+00	0.00	0.00e+00	0.00
	636219.6352	−4.0197	802.0349	3.400	0.800	0.000	0.000	0.00e+00	0.00	0.00e+00	0.00
	636219.6427	−4.0197	802.0348	3.400	0.800	0.000	0.000	0.00e+00	0.00	0.00e+00	0.00
	636572.6435	−4.0666	787.6118	3.400	0.800	0.000	0.000	0.00e+00	0.00	0.00e+00	0.00
	636572.7197	−4.0666	787.6117	3.400	0.800	0.000	0.000	0.00e+00	0.00	0.00e+00	0.00
	648486.9195	−3.8046	811.6563	3.400	0.800	0.000	0.000	0.00e+00	0.00	0.00e+00	0.00
	648694.6807	−4.4723	660.5840	3.400	0.800	0.000	0.000	0.00e+00	0.00	0.00e+00	0.00
	648694.6974	−4.4723	660.5839	3.400	0.800	0.000	0.000	0.00e+00	0.00	0.00e+00	0.00
	649728.3300	−3.6348	783.1054	3.400	0.800	0.000	0.000	0.00e+00	0.00	0.00e+00	0.00
	650018.9228	−4.6359	723.1495	3.400	0.800	0.000	0.000	0.00e+00	0.00	0.00e+00	0.00
	650021.6410	−4.6358	723.1494	3.400	0.800	0.000	0.000	0.00e+00	0.00	0.00e+00	0.00
	650199.9431	−3.7464	808.4427	3.400	0.800	0.000	0.000	0.00e+00	0.00	0.00e+00	0.00
	650303.8379	−4.0341	853.5926	3.400	0.800	0.000	0.000	0.00e+00	0.00	0.00e+00	0.00
	651715.2943	−4.4732	655.0602	3.400	0.800	0.000	0.000	0.00e+00	0.00	0.00e+00	0.00
	651715.3606	−4.4732	655.0601	3.400	0.800	0.000	0.000	0.00e+00	0.00	0.00e+00	0.00
	651859.4050	−3.6541	785.0129	3.400	0.800	0.000	0.000	0.00e+00	0.00	0.00e+00	0.00
	651869.7697	−4.7109	607.8479	3.400	0.800	0.000	0.000	0.00e+00	0.00	0.00e+00	0.00
	651869.8196	−4.7109	607.8478	3.400	0.800	0.000	0.000	0.00e+00	0.00	0.00e+00	0.00
	651870.3762	−4.7109	607.8479	3.400	0.800	0.000	0.000	0.00e+00	0.00	0.00e+00	0.00
	651870.4260	−4.7109	607.8478	3.400	0.800	0.000	0.000	0.00e+00	0.00	0.00e+00	0.00
	652349.5192	−4.6336	723.1008	3.400	0.800	0.000	0.000	0.00e+00	0.00	0.00e+00	0.00
	652352.2394	−4.6336	723.1008	3.400	0.800	0.000	0.000	0.00e+00	0.00	0.00e+00	0.00
	653867.7700	−4.2580	663.2667	3.400	0.800	0.000	0.000	0.00e+00	0.00	0.00e+00	0.00
	658805.1738	−3.7298	826.8891	3.400	0.800	0.000	0.000	0.00e+00	0.00	0.00e+00	0.00
	659380.2908	−4.2575	663.0704	3.400	0.800	0.000	0.000	0.00e+00	0.00	0.00e+00	0.00
	660084.0947	−4.4420	680.2930	3.400	0.800	0.000	0.000	0.00e+00	0.00	0.00e+00	0.00
	660084.1128	−4.4420	680.2931	3.400	0.800	0.000	0.000	0.00e+00	0.00	0.00e+00	0.00

Continued on next page

molecule	ν_{0j}^k (MHz)	$\mathcal{I}_j^k$ (nm^{2}MHz)	$E\ell_j^k$ (cm^{-1})	w_{cj}^k (MHz hPa^{-1})	n_{cj}^k	$\Delta\nu_{0j}^k$ (MHz hPa^{-1})	$n_{\Delta\nu_{0j}}^k$	δ_j^k (hPa^{-1})	$n_{\delta_j}^k$	γ_j^k (hPa^{-1})	$n_{\gamma_j}^k$
$HO^{35}Cl$	625074.8710	−1.7217	135.2941	2.886	0.650	−0.056	0.400	0.00e+00	0.00	0.00e+00	0.00
	632057.8077	−1.7376	170.0846	2.886	0.650	−0.056	0.400	0.00e+00	0.00	0.00e+00	0.00
	635870.0222	−1.7504	188.9661	2.886	0.650	−0.056	0.400	0.00e+00	0.00	0.00e+00	0.00
	648618.0026	−1.8064	251.5493	2.886	0.650	−0.056	0.400	0.00e+00	0.00	0.00e+00	0.00
	653312.9426	−1.8307	274.3879	2.886	0.650	−0.056	0.400	0.00e+00	0.00	0.00e+00	0.00
	2502016.9641	−1.3530	345.1560	1.764	0.500	0.000	0.000	0.00e+00	0.00	0.00e+00	0.00
$HO^{37}Cl$	624378.8940	−1.7250	132.9422	2.886	0.650	−0.056	0.400	0.00e+00	0.00	0.00e+00	0.00
	634788.5280	−1.7521	185.6824	2.886	0.650	−0.056	0.400	0.00e+00	0.00	0.00e+00	0.00
	661305.9426	−1.8850	317.4194	1.764	0.500	0.000	0.000	0.00e+00	0.00	0.00e+00	0.00
HO_2	184194.5500	−3.9371	85.1861	3.138	0.670	0.000	0.000	0.00e+00	0.00	0.00e+00	0.00
	184196.7600	−4.1289	85.1856	3.138	0.670	0.000	0.000	0.00e+00	0.00	0.00e+00	0.00
	184212.6400	−3.9370	85.1862	3.138	0.670	0.000	0.000	0.00e+00	0.00	0.00e+00	0.00
	184214.8700	−4.1289	85.1857	3.138	0.670	0.000	0.000	0.00e+00	0.00	0.00e+00	0.00
	184373.8100	−3.4818	137.2257	3.138	0.670	0.000	0.000	0.00e+00	0.00	0.00e+00	0.00
	184378.3000	−3.5234	137.2252	3.138	0.670	0.000	0.000	0.00e+00	0.00	0.00e+00	0.00
	200615.7200	−3.5785	25.5092	3.138	0.670	0.000	0.000	0.00e+00	0.00	0.00e+00	0.00
	200617.4700	−3.4482	25.5087	3.138	0.670	0.000	0.000	0.00e+00	0.00	0.00e+00	0.00
	202869.9800	−3.9067	82.2612	3.138	0.670	0.000	0.000	0.00e+00	0.00	0.00e+00	0.00
	202872.1900	−3.7763	82.2606	3.138	0.670	0.000	0.000	0.00e+00	0.00	0.00e+00	0.00
	202885.9400	−3.9066	82.2614	3.138	0.670	0.000	0.000	0.00e+00	0.00	0.00e+00	0.00
	202888.1800	−3.7763	82.2607	3.138	0.670	0.000	0.000	0.00e+00	0.00	0.00e+00	0.00
	625660.3542	−2.1256	119.4374	2.223	0.750	0.000	0.000	0.00e+00	0.00	0.00e+00	0.00
	625663.7997	−2.0859	119.4370	2.223	0.750	0.000	0.000	0.00e+00	0.00	0.00e+00	0.00
	626579.9359	−3.0550	0.0009	3.138	0.670	0.000	0.000	0.00e+00	0.00	0.00e+00	0.00
	626587.0677	−2.6569	0.0000	3.138	0.670	0.000	0.000	0.00e+00	0.00	0.00e+00	0.00
	626607.4541	−3.3555	0.0000	3.138	0.670	0.000	0.000	0.00e+00	0.00	0.00e+00	0.00
	633329.0046	−2.1141	119.5077	3.138	0.670	0.000	0.000	0.00e+00	0.00	0.00e+00	0.00
	633333.7137	−2.1578	119.5074	3.138	0.670	0.000	0.000	0.00e+00	0.00	0.00e+00	0.00
	636598.8986	−2.1240	143.2996	3.138	0.670	0.000	0.000	0.00e+00	0.00	0.00e+00	0.00
	636602.4359	−2.0876	143.2991	3.138	0.670	0.000	0.000	0.00e+00	0.00	0.00e+00	0.00
	648613.8526	−2.1297	169.3204	3.138	0.670	0.000	0.000	0.00e+00	0.00	0.00e+00	0.00
	648617.4877	−2.0961	169.3200	3.138	0.670	0.000	0.000	0.00e+00	0.00	0.00e+00	0.00
	649701.4773	−2.3462	175.3035	2.061	−0.200	0.000	0.000	0.00e+00	0.00	0.00e+00	0.00

Continued on next page

molecule	ν_{0j}^k (MHz)	$\mathcal{I}_j^k$ (nm^2MHz)	$E\ell_j^k$ (cm^{-1})	w_{cj}^k (MHz hPa^{-1})	n_{cj}^k	$\Delta\nu_{0j}^k$ (MHz hPa^{-1})	$n_{\Delta\nu_{0j}}^k$	δ_j^k (hPa^{-1})	$n_{\delta_j}^k$	γ_j^k (hPa^{-1})	$n_{\gamma_j}^k$
	649701.5134	−2.3001	175.3039	2.061	−0.200	0.000	0.000	0.00e+00	0.00	0.00e+00	0.00
	650426.8147	−2.2993	175.3525	2.061	−0.200	0.000	0.000	0.00e+00	0.00	0.00e+00	0.00
	650426.8484	−2.3453	175.3522	2.061	−0.200	0.000	0.000	0.00e+00	0.00	0.00e+00	0.00
	650575.0063	−2.1209	97.7365	3.138	0.670	0.000	0.000	0.00e+00	0.00	0.00e+00	0.00
	650575.0245	−2.0792	97.7361	3.138	0.670	0.000	0.000	0.00e+00	0.00	0.00e+00	0.00
	650595.2013	−2.9516	283.6823	3.138	0.670	0.000	0.000	0.00e+00	0.00	0.00e+00	0.00
	650599.5548	−2.9215	283.6825	3.138	0.670	0.000	0.000	0.00e+00	0.00	0.00e+00	0.00
	650795.8109	−2.1250	97.7995	3.138	0.670	0.000	0.000	0.00e+00	0.00	0.00e+00	0.00
	650796.1034	−2.1711	97.7991	3.138	0.670	0.000	0.000	0.00e+00	0.00	0.00e+00	0.00
	652077.6973	−2.2973	174.3048	3.138	0.670	0.000	0.000	0.00e+00	0.00	0.00e+00	0.00
	652077.8316	−2.2557	174.3044	3.138	0.670	0.000	0.000	0.00e+00	0.00	0.00e+00	0.00
	652782.0864	−2.2964	174.3514	3.138	0.670	0.000	0.000	0.00e+00	0.00	0.00e+00	0.00
	652782.2730	−2.2549	174.3510	3.138	0.670	0.000	0.000	0.00e+00	0.00	0.00e+00	0.00
	653223.8481	−2.5192	269.8187	3.138	0.670	0.000	0.000	0.00e+00	0.00	0.00e+00	0.00
	653224.0584	−2.4776	269.8182	3.138	0.670	0.000	0.000	0.00e+00	0.00	0.00e+00	0.00
	653228.7041	−2.5192	269.8189	3.138	0.670	0.000	0.000	0.00e+00	0.00	0.00e+00	0.00
	653228.9149	−2.4776	269.8184	3.138	0.670	0.000	0.000	0.00e+00	0.00	0.00e+00	0.00
	660115.6907	−2.2023	118.6140	2.090	0.630	0.000	0.000	0.00e+00	0.00	0.00e+00	0.00
	660115.8615	−2.1563	118.6142	2.090	0.630	0.000	0.000	0.00e+00	0.00	0.00e+00	0.00
	660485.6655	−2.1541	118.2757	2.090	0.630	0.000	0.000	0.00e+00	0.00	0.00e+00	0.00
	660485.7114	−2.1125	118.2754	2.090	0.630	0.000	0.000	0.00e+00	0.00	0.00e+00	0.00
	2509318.5449	−1.5048	137.2257	3.138	0.670	0.000	0.000	0.00e+00	0.00	0.00e+00	0.00
	2509318.5449	−1.5464	137.2252	3.138	0.670	0.000	0.000	0.00e+00	0.00	0.00e+00	0.00
	2511090.2884	−1.5506	191.2681	3.138	0.670	0.000	0.000	0.00e+00	0.00	0.00e+00	0.00
	2511090.2884	−1.5158	191.2684	3.138	0.670	0.000	0.000	0.00e+00	0.00	0.00e+00	0.00
$HOONO_2$	186372.3129	−4.3783	78.4660	2.750	0.750	0.000	0.000	0.00e+00	0.00	0.00e+00	0.00
	186377.4349	−4.3782	78.4095	2.750	0.750	0.000	0.000	0.00e+00	0.00	0.00e+00	0.00
	186385.4620	−4.3588	80.3912	2.750	0.750	0.000	0.000	0.00e+00	0.00	0.00e+00	0.00
	186389.7521	−4.3587	80.3343	2.750	0.750	0.000	0.000	0.00e+00	0.00	0.00e+00	0.00
	186391.9506	−4.3588	80.3908	2.750	0.750	0.000	0.000	0.00e+00	0.00	0.00e+00	0.00
	186396.2405	−4.3587	80.3338	2.750	0.750	0.000	0.000	0.00e+00	0.00	0.00e+00	0.00
	186500.5868	−4.0369	81.6966	2.750	0.750	0.000	0.000	0.00e+00	0.00	0.00e+00	0.00
	186503.9421	−4.3378	81.6391	2.750	0.750	0.000	0.000	0.00e+00	0.00	0.00e+00	0.00

Continued on next page

molecule	ν_{0j}^k (MHz)	I_j^k ($\mathrm{nm^2MHz}$)	$E\ell_j^k$ ($\mathrm{cm^{-1}}$)	w_{cj}^k ($\mathrm{MHz\,hPa^{-1}}$)	n_{cj}^k	$\Delta\nu_{0j}^k$ ($\mathrm{MHz\,hPa^{-1}}$)	$n_{\Delta\nu_{0j}}^k$	δ_j^k ($\mathrm{hPa^{-1}}$)	$n_{\delta_j}^k$	γ_j^k ($\mathrm{hPa^{-1}}$)	$n_{\gamma_j}^k$
	186504.0461	−4.3378	81.6390	2.750	0.750	0.000	0.000	0.00e+00	0.00	0.00e+00	0.00
	186567.9967	−4.3774	78.4509	2.750	0.750	0.000	0.000	0.00e+00	0.00	0.00e+00	0.00
	186573.1205	−4.3772	78.3944	2.750	0.750	0.000	0.000	0.00e+00	0.00	0.00e+00	0.00
	186673.0329	−4.0151	82.4228	2.750	0.750	0.000	0.000	0.00e+00	0.00	0.00e+00	0.00
	186675.4767	−4.0150	82.3645	2.750	0.750	0.000	0.000	0.00e+00	0.00	0.00e+00	0.00
	199853.8184	−4.3251	88.5468	2.750	0.750	0.000	0.000	0.00e+00	0.00	0.00e+00	0.00
	199859.9087	−4.3249	88.4910	2.750	0.750	0.000	0.000	0.00e+00	0.00	0.00e+00	0.00
	199927.4314	−4.3081	91.1256	2.750	0.750	0.000	0.000	0.00e+00	0.00	0.00e+00	0.00
	199932.7338	−4.3080	91.0695	2.750	0.750	0.000	0.000	0.00e+00	0.00	0.00e+00	0.00
	199943.0919	−4.2902	93.0516	2.750	0.750	0.000	0.000	0.00e+00	0.00	0.00e+00	0.00
	199944.8897	−4.2902	93.0515	2.750	0.750	0.000	0.000	0.00e+00	0.00	0.00e+00	0.00
	199947.5663	−4.2901	92.9950	2.750	0.750	0.000	0.000	0.00e+00	0.00	0.00e+00	0.00
	199949.3641	−4.2901	92.9949	2.750	0.750	0.000	0.000	0.00e+00	0.00	0.00e+00	0.00
	199966.5372	−4.3453	79.9453	2.750	0.750	0.000	0.000	0.00e+00	0.00	0.00e+00	0.00
	199974.4260	−4.3452	79.8896	2.750	0.750	0.000	0.000	0.00e+00	0.00	0.00e+00	0.00
	199989.8852	−4.3569	88.7767	2.750	0.750	0.000	0.000	0.00e+00	0.00	0.00e+00	0.00
	199991.5437	−4.3078	91.1209	2.750	0.750	0.000	0.000	0.00e+00	0.00	0.00e+00	0.00
	199996.0350	−4.3567	88.7215	2.750	0.750	0.000	0.000	0.00e+00	0.00	0.00e+00	0.00
	199996.8457	−4.3077	91.0647	2.750	0.750	0.000	0.000	0.00e+00	0.00	0.00e+00	0.00
	200070.9454	−3.9700	94.3649	2.750	0.750	0.000	0.000	0.00e+00	0.00	0.00e+00	0.00
	200074.5308	−3.9698	94.3076	2.750	0.750	0.000	0.000	0.00e+00	0.00	0.00e+00	0.00
	200246.2620	−3.9498	95.1026	2.750	0.750	0.000	0.000	0.00e+00	0.00	0.00e+00	0.00
	200248.8682	−3.9497	95.0446	2.750	0.750	0.000	0.000	0.00e+00	0.00	0.00e+00	0.00
	200988.8911	−4.3196	88.4497	2.750	0.750	0.000	0.000	0.00e+00	0.00	0.00e+00	0.00
	200995.0234	−4.3195	88.3938	2.750	0.750	0.000	0.000	0.00e+00	0.00	0.00e+00	0.00
	201923.0645	−4.2882	25.1586	2.750	0.750	0.000	0.000	0.00e+00	0.00	0.00e+00	0.00
	202036.2458	−4.6293	31.4479	2.750	0.750	0.000	0.000	0.00e+00	0.00	0.00e+00	0.00
	202101.0320	−4.6024	27.4488	2.750	0.750	0.000	0.000	0.00e+00	0.00	0.00e+00	0.00
	202111.9593	−4.6033	27.4484	2.750	0.750	0.000	0.000	0.00e+00	0.00	0.00e+00	0.00
	202624.7285	−4.8157	226.6660	2.750	0.750	0.000	0.000	0.00e+00	0.00	0.00e+00	0.00
	202665.9615	−4.8078	226.6648	2.750	0.750	0.000	0.000	0.00e+00	0.00	0.00e+00	0.00
	202767.0133	−4.8281	88.4497	2.750	0.750	0.000	0.000	0.00e+00	0.00	0.00e+00	0.00
	202773.1862	−4.8211	88.3938	2.750	0.750	0.000	0.000	0.00e+00	0.00	0.00e+00	0.00

Continued on next page

molecule	ν_{0j}^k (MHz)	I_j^k ($\mathrm{nm^2MHz}$)	$E\ell_j^k$ ($\mathrm{cm^{-1}}$)	u_{cj}^k ($\mathrm{MHz\,hPa^{-1}}$)	n_{cj}^k	$\Delta\nu_{0j}^k$ ($\mathrm{MHz\,hPa^{-1}}$)	$n_{\Delta\nu_{0j}}^k$	δ_j^k ($\mathrm{hPa^{-1}}$)	$n_{\delta_j}^k$	γ_j^k ($\mathrm{hPa^{-1}}$)	$n_{\gamma_j}^k$
	202773.2855	−4.8165	31.9321	2.750	0.750	0.000	0.000	0.00e+00	0.00	0.00e+00	0.00
	202821.2235	−4.4736	47.4384	2.750	0.750	0.000	0.000	0.00e+00	0.00	0.00e+00	0.00
	203578.1536	−4.3378	149.0662	2.750	0.750	0.000	0.000	0.00e+00	0.00	0.00e+00	0.00
	203585.1372	−4.3376	149.0108	2.750	0.750	0.000	0.000	0.00e+00	0.00	0.00e+00	0.00
	203676.5561	−4.7851	192.4695	2.750	0.750	0.000	0.000	0.00e+00	0.00	0.00e+00	0.00
	203777.9465	−4.5928	37.0558	2.750	0.750	0.000	0.000	0.00e+00	0.00	0.00e+00	0.00
	203788.8516	−4.7982	216.7165	2.750	0.750	0.000	0.000	0.00e+00	0.00	0.00e+00	0.00
	203805.5570	−4.2848	140.8996	2.750	0.750	0.000	0.000	0.00e+00	0.00	0.00e+00	0.00
	203808.9680	−4.7944	216.7159	2.750	0.750	0.000	0.000	0.00e+00	0.00	0.00e+00	0.00
	203812.6607	−4.2846	140.8439	2.750	0.750	0.000	0.000	0.00e+00	0.00	0.00e+00	0.00
	204080.2237	−4.2373	133.2715	2.750	0.750	0.000	0.000	0.00e+00	0.00	0.00e+00	0.00
	204087.4605	−4.2372	133.2155	2.750	0.750	0.000	0.000	0.00e+00	0.00	0.00e+00	0.00
	204191.2403	−4.8111	31.9376	2.750	0.750	0.000	0.000	0.00e+00	0.00	0.00e+00	0.00
	204264.1793	−4.6254	35.4581	2.750	0.750	0.000	0.000	0.00e+00	0.00	0.00e+00	0.00
	204367.5431	−4.6603	34.5776	2.750	0.750	0.000	0.000	0.00e+00	0.00	0.00e+00	0.00
	204422.5807	−4.1946	126.1851	2.750	0.750	0.000	0.000	0.00e+00	0.00	0.00e+00	0.00
	204429.9700	−4.1945	126.1290	2.750	0.750	0.000	0.000	0.00e+00	0.00	0.00e+00	0.00
	204430.9506	−4.8087	236.8570	2.750	0.750	0.000	0.000	0.00e+00	0.00	0.00e+00	0.00
	204484.7927	−4.8012	270.9026	2.750	0.750	0.000	0.000	0.00e+00	0.00	0.00e+00	0.00
	204484.7927	−4.8012	270.9185	2.750	0.750	0.000	0.000	0.00e+00	0.00	0.00e+00	0.00
	204484.7945	−4.8012	270.9026	2.750	0.750	0.000	0.000	0.00e+00	0.00	0.00e+00	0.00
	204484.7945	−4.8012	270.9185	2.750	0.750	0.000	0.000	0.00e+00	0.00	0.00e+00	0.00
	204516.5866	−4.6206	229.6098	2.750	0.750	0.000	0.000	0.00e+00	0.00	0.00e+00	0.00
	204516.5866	−4.6206	229.6256	2.750	0.750	0.000	0.000	0.00e+00	0.00	0.00e+00	0.00
	204552.8773	−4.3139	84.6101	2.750	0.750	0.000	0.000	0.00e+00	0.00	0.00e+00	0.00
	204560.1893	−4.3138	84.5544	2.750	0.750	0.000	0.000	0.00e+00	0.00	0.00e+00	0.00
	204626.3922	−4.7810	192.4537	2.750	0.750	0.000	0.000	0.00e+00	0.00	0.00e+00	0.00
	204827.4501	−4.7840	207.0584	2.750	0.750	0.000	0.000	0.00e+00	0.00	0.00e+00	0.00
	204836.9957	−4.7822	207.0581	2.750	0.750	0.000	0.000	0.00e+00	0.00	0.00e+00	0.00
	204857.2626	−4.1560	119.6450	2.750	0.750	0.000	0.000	0.00e+00	0.00	0.00e+00	0.00
	204864.8367	−4.1558	119.5888	2.750	0.750	0.000	0.000	0.00e+00	0.00	0.00e+00	0.00
	204918.1540	−4.7627	264.4158	2.750	0.750	0.000	0.000	0.00e+00	0.00	0.00e+00	0.00
	204918.1540	−4.7627	264.4316	2.750	0.750	0.000	0.000	0.00e+00	0.00	0.00e+00	0.00

Continued on next page

molecule	ν_{0j}^k (MHz)	$\mathcal{I}_j^k$ (nm^2MHz)	$E\ell_j^k$ (cm^{-1})	w_{cj}^k (MHz hPa^{-1})	n_{cj}^k	$\Delta\nu_{0j}^k$ (MHz hPa^{-1})	$n_{\Delta\nu_j}^k$	δ_j^k (hPa^{-1})	$n_{\delta_j}^k$	γ_j^k (hPa^{-1})	$n_{\gamma_j}^k$
	204918.2034	−4.7627	264.4158	2.750	0.750	0.000	0.000	0.00e+00	0.00	0.00e+00	0.00
	204918.2034	−4.7627	264.4316	2.750	0.750	0.000	0.000	0.00e+00	0.00	0.00e+00	0.00
	205075.2242	−4.3343	89.0635	2.750	0.750	0.000	0.000	0.00e+00	0.00	0.00e+00	0.00
	205082.1969	−4.3342	89.0085	2.750	0.750	0.000	0.000	0.00e+00	0.00	0.00e+00	0.00
	205118.1854	−4.6404	234.0283	2.750	0.750	0.000	0.000	0.00e+00	0.00	0.00e+00	0.00
	205118.1854	−4.6405	234.0442	2.750	0.750	0.000	0.000	0.00e+00	0.00	0.00e+00	0.00
	205436.7073	−4.3131	92.0438	2.750	0.750	0.000	0.000	0.00e+00	0.00	0.00e+00	0.00
	205443.5429	−4.3129	91.9884	2.750	0.750	0.000	0.000	0.00e+00	0.00	0.00e+00	0.00
	206696.2538	−4.2763	97.7945	2.750	0.750	0.000	0.000	0.00e+00	0.00	0.00e+00	0.00
	206701.6496	−4.2762	97.7385	2.750	0.750	0.000	0.000	0.00e+00	0.00	0.00e+00	0.00
	206718.3103	−4.2921	95.2132	2.750	0.750	0.000	0.000	0.00e+00	0.00	0.00e+00	0.00
	206722.2779	−4.2591	99.7210	2.750	0.750	0.000	0.000	0.00e+00	0.00	0.00e+00	0.00
	206723.2132	−4.2591	99.7210	2.750	0.750	0.000	0.000	0.00e+00	0.00	0.00e+00	0.00
	206724.4931	−4.2919	95.1576	2.750	0.750	0.000	0.000	0.00e+00	0.00	0.00e+00	0.00
	206726.8470	−4.2590	99.6645	2.750	0.750	0.000	0.000	0.00e+00	0.00	0.00e+00	0.00
	206727.7823	−4.2590	99.6645	2.750	0.750	0.000	0.000	0.00e+00	0.00	0.00e+00	0.00
	206732.1598	−4.2762	97.7919	2.750	0.750	0.000	0.000	0.00e+00	0.00	0.00e+00	0.00
	206737.5552	−4.2760	97.7359	2.750	0.750	0.000	0.000	0.00e+00	0.00	0.00e+00	0.00
	206855.6541	−3.9396	101.0385	2.750	0.750	0.000	0.000	0.00e+00	0.00	0.00e+00	0.00
	206859.3304	−3.9395	100.9814	2.750	0.750	0.000	0.000	0.00e+00	0.00	0.00e+00	0.00
NO	651771.4200	−3.4882	58.5617	1.764	0.500	0.000	0.000	0.00e+00	0.00	0.00e+00	0.00
	651772.9276	−3.6253	58.5572	1.764	0.500	0.000	0.000	0.00e+00	0.00	0.00e+00	0.00
	651773.1484	−3.5566	58.5593	1.764	0.500	0.000	0.000	0.00e+00	0.00	0.00e+00	0.00
NO_2	653126.2317	−5.0381	190.6094	1.970	0.500	0.000	0.000	0.00e+00	0.00	0.00e+00	0.00
	653251.6802	−4.6010	190.6080	1.970	0.500	0.000	0.000	0.00e+00	0.00	0.00e+00	0.00
	653288.4701	−4.6059	190.6014	1.970	0.500	0.000	0.000	0.00e+00	0.00	0.00e+00	0.00
	653327.8563	−4.7619	190.6027	1.970	0.500	0.000	0.000	0.00e+00	0.00	0.00e+00	0.00
N_2O	200975.2600	−4.0623	23.4641	2.466	0.970	0.000	0.000	0.00e+00	0.00	0.00e+00	0.00
	652833.7897	−3.0608	272.2826	2.143	0.570	0.000	0.000	0.00e+00	0.00	0.00e+00	0.00
$N_2O(\nu_2)$	201055.2631	−5.2962	612.2415	2.400	0.800	0.000	0.000	0.00e+00	0.00	0.00e+00	0.00
	201435.1295	−5.2947	612.2859	2.400	0.800	0.000	0.000	0.00e+00	0.00	0.00e+00	0.00
	653089.2474	−4.2888	861.1584	2.400	0.800	0.000	0.000	0.00e+00	0.00	0.00e+00	0.00
$N_2O(2\nu_2)$	201407.0037	−6.4947	1191.6471	2.400	0.800	0.000	0.000	0.00e+00	0.00	0.00e+00	0.00

Continued on next page

molecule	ν_{0j}^k (MHz)	$\mathcal{I}_j^k$ (nm^2MHz)	$E\ell_j^k$ (cm^{-1})	u_{cj}^k (MHz hPa^{-1})	n_{cj}^k	$\Delta\nu_{0j}^k$ (MHz hPa^{-1})	$n_{\Delta\nu_{0j}}^k$	δ_j^k (hPa^{-1})	$n_{\delta_j}^k$	γ_j^k (hPa^{-1})	$n_{\gamma_j}^k$
	201509.9336	−6.5423	1201.2708	2.400	0.800	0.000	0.000	0.00e+00	0.00	0.00e+00	0.00
	201513.5634	−6.5423	1201.2710	2.400	0.800	0.000	0.000	0.00e+00	0.00	0.00e+00	0.00
$N^{15}NO$	200960.9139	−4.0671	23.4624	2.466	0.970	0.000	0.000	0.00e+00	0.00	0.00e+00	0.00
	652787.0903	−3.0656	272.2633	2.143	0.570	0.000	0.000	0.00e+00	0.00	0.00e+00	0.00
$OC^{32}S$	182427.1956	−2.9604	42.5980	2.058	0.500	0.000	0.000	0.00e+00	0.00	0.00e+00	0.00
	206745.1610	−2.8244	55.1738	2.058	0.500	0.000	0.000	0.00e+00	0.00	0.00e+00	0.00
OH	2509935.4400	−0.8049	0.0018	2.651	0.940	0.000	0.000	0.00e+00	0.00	0.00e+00	0.00
	2509949.0100	0.3412	0.0018	2.651	0.940	0.000	0.000	0.00e+00	0.00	0.00e+00	0.00
	2509988.1500	0.1493	0.0000	2.651	0.940	0.000	0.000	0.00e+00	0.00	0.00e+00	0.00
	2514298.7300	−0.8037	0.0574	2.651	0.940	0.000	0.000	0.00e+00	0.00	0.00e+00	0.00
	2514316.7050	0.3424	0.0574	2.651	0.940	0.000	0.000	0.00e+00	0.00	0.00e+00	0.00
	2514353.4900	0.1505	0.0556	2.651	0.940	0.000	0.000	0.00e+00	0.00	0.00e+00	0.00
O_2	49962.4752	−10.3309	2230.4143	0.938	0.710	0.000	0.000	0.00e+00	0.00	0.00e+00	0.00
	50474.2042	−9.8881	2011.2062	0.890	0.800	0.000	0.000	2.40e-04	0.80	7.90e-04	1.80
	50987.7278	−9.4699	1803.1726	0.910	0.800	0.000	0.000	2.20e-04	0.80	7.80e-04	1.80
	51503.3389	−9.0764	1606.3473	0.940	0.800	0.000	0.000	1.97e-04	0.80	7.74e-04	1.80
	52021.4047	−8.7079	1420.7625	0.970	0.800	0.000	0.000	1.66e-04	0.80	7.64e-04	1.80
	52542.3925	−8.3648	1246.4482	0.990	0.800	0.000	0.000	1.36e-04	0.80	7.51e-04	1.80
	53066.9079	−8.0472	1083.4329	1.020	0.800	0.000	0.000	1.31e-04	0.80	7.14e-04	1.80
	53595.7507	−7.7555	931.7430	1.050	0.800	0.000	0.000	2.30e-04	0.80	5.84e-04	1.80
	54130.0016	−7.4901	791.4030	1.070	0.800	0.000	0.000	3.35e-04	0.80	4.31e-04	1.80
	54671.1450	−7.2516	662.4358	1.100	0.800	0.000	0.000	3.74e-04	0.80	3.05e-04	1.80
	55221.3720	−7.0406	544.8622	1.130	0.800	0.000	0.000	2.58e-04	0.80	3.39e-04	1.80
	55783.8190	−6.8578	438.7010	1.170	0.800	0.000	0.000	-1.16e-04	0.80	7.05e-04	1.80
	56264.7660	−7.0947	2.0843	1.730	0.800	0.000	0.000	3.90e-04	0.80	-1.13e-04	1.80
	56363.3930	−6.7045	343.9694	1.200	0.800	0.000	0.000	-2.97e-04	0.80	7.53e-04	1.80
	56968.1800	−6.5822	260.6825	1.240	0.800	0.000	0.000	-4.16e-04	0.80	7.42e-04	1.80
	57612.4802	−6.4931	188.8531	1.280	0.800	0.000	0.000	-6.13e-04	0.80	6.97e-04	1.80
	58323.8850	−6.4408	128.4920	1.330	0.800	0.000	0.000	-2.05e-04	0.80	5.10e-05	1.80
	58446.5800	−6.6543	16.3876	1.520	0.800	0.000	0.000	7.48e-04	0.80	-1.46e-04	1.80
	59164.2150	−6.4313	79.6070	1.390	0.800	0.000	0.000	-7.22e-04	0.80	2.66e-04	1.80
	59590.9780	−6.4845	42.2240	1.430	0.800	0.000	0.000	7.65e-04	0.80	-9.00e-05	1.80
	60306.0440	−6.4767	42.2001	1.450	0.800	0.000	0.000	-7.05e-04	0.80	8.10e-05	1.80

Continued on next page

molecule	ν_{0j}^k (MHz)	$\mathcal{I}_j^k$ (nm^2MHz)	$E\ell_j^k$ (cm^{-1})	u_{cj}^k (MHz hPa^{-1})	n_{cj}^k	$\Delta\nu_{0j}^k$ (MHz hPa^{-1})	$n_{\Delta\nu_{0j}}^k$	δ_j^k (hPa^{-1})	$n_{\delta j}^k$	γ_j^k (hPa^{-1})	$n_{\gamma j}^k$
	60434.7760	−6.4119	79.5646	1.360	0.800	0.000	0.000	6.97e-04	0.80	-3.24e-04	1.80
	61150.5700	−6.3991	128.3978	1.310	0.800	0.000	0.000	1.04e-04	0.80	-6.70e-05	1.80
	61800.1550	−6.4318	188.7134	1.270	0.800	0.000	0.000	5.70e-04	0.80	-7.61e-04	1.80
	62411.2230	−6.5026	260.5009	1.230	0.800	0.000	0.000	3.60e-04	0.80	-7.77e-04	1.80
	62486.2550	−6.6072	16.2529	1.540	0.800	0.000	0.000	-4.98e-04	0.80	9.70e-05	1.80
	62997.9772	−6.6076	343.7481	1.200	0.800	0.000	0.000	2.39e-04	0.80	-7.68e-04	1.80
	63568.5200	−6.7440	438.4414	1.170	0.800	0.000	0.000	1.08e-04	0.80	-7.06e-04	1.80
	64127.7770	−6.9103	544.5651	1.130	0.800	0.000	0.000	-3.11e-04	0.80	-3.32e-04	1.80
	64678.8985	−7.1052	662.1020	1.100	0.800	0.000	0.000	-4.21e-04	0.80	-2.98e-04	1.80
	65224.0647	−7.3278	791.0330	1.070	0.800	0.000	0.000	-3.75e-04	0.80	-4.23e-04	1.80
	65764.7440	−7.5773	931.3370	1.050	0.800	0.000	0.000	-2.67e-04	0.80	-5.75e-04	1.80
	66302.0821	−7.8533	1082.9915	1.020	0.800	0.000	0.000	-1.68e-04	0.80	-7.00e-04	1.80
	66836.8204	−8.1552	1245.9714	0.990	0.800	0.000	0.000	-1.69e-04	0.80	-7.35e-04	1.80
	67369.5887	−8.4828	1420.2505	0.970	0.800	0.000	0.000	-2.00e-04	0.80	-7.44e-04	1.80
	67900.8670	−8.8357	1605.8004	0.940	0.800	0.000	0.000	-2.28e-04	0.80	-7.53e-04	1.80
	68431.0050	−9.2137	1802.5907	0.920	0.800	0.000	0.000	-2.40e-04	0.80	-7.60e-04	1.80
	68960.3120	−9.6164	2010.5895	0.900	0.800	0.000	0.000	-2.50e-04	0.80	-7.65e-04	1.80
	69489.0300	−10.0437	2229.7629	0.938	0.710	0.000	0.000	0.00e+00	0.00	0.00e+00	0.00
	70017.3699	−10.4954	2460.0750	0.938	0.710	0.000	0.000	0.00e+00	0.00	0.00e+00	0.00
	118750.3430	−6.5312	0.0000	1.528	0.979	−0.140	1.360	-3.60e-05	0.80	9.00e-06	1.80
	368498.3443	−7.1917	3.9611	1.920	0.200	0.000	0.000	0.00e+00	0.00	0.00e+00	0.00
	424763.1200	−6.1477	2.0843	1.596	0.712	0.000	0.000	0.00e+00	0.00	0.00e+00	0.00
	487249.3755	−6.5101	2.0843	1.597	0.750	0.000	0.000	0.00e+00	0.00	0.00e+00	0.00
	715393.0720	−6.7458	18.3372	1.810	0.200	0.000	0.000	0.00e+00	0.00	0.00e+00	0.00
	773839.6910	−5.9341	16.3876	1.604	0.750	0.000	0.000	0.00e+00	0.00	0.00e+00	0.00
	834145.7191	−6.3844	16.3876	1.470	0.750	0.000	0.000	0.00e+00	0.00	0.00e+00	0.00
	1061124.0518	−6.5891	44.2117	1.260	0.710	0.000	0.000	0.00e+00	0.00	0.00e+00	0.00
	1120715.0358	−5.8400	42.2240	1.482	0.750	0.000	0.000	0.00e+00	0.00	0.00e+00	0.00
	1179879.2388	−6.3252	42.2240	1.231	0.710	0.000	0.000	0.00e+00	0.00	0.00e+00	0.00
	1406372.3689	−6.5348	81.5805	1.246	0.710	0.000	0.000	0.00e+00	0.00	0.00e+00	0.00
	1466807.1330	−5.8128	79.5646	1.202	0.710	0.000	0.000	0.00e+00	0.00	0.00e+00	0.00
	1525131.0204	−6.3153	79.5646	1.202	0.710	0.000	0.000	0.00e+00	0.00	0.00e+00	0.00
	1751254.8766	−6.5425	130.4375	1.217	0.710	0.000	0.000	0.00e+00	0.00	0.00e+00	0.00

Continued on next page

molecule	ν_{0j}^k (MHz)	$\mathcal{I}_j^k$ ($\mathrm{nm^2MHz}$)	$E\ell_j^k$ ($\mathrm{cm^{-1}}$)	w_{cj}^k ($\mathrm{MHz\,hPa^{-1}}$)	n_{cj}^k	$\Delta\nu_{0j}^k$ ($\mathrm{MHz\,hPa^{-1}}$)	$n_{\Delta\nu_{0j}}^k$	δ_j^k ($\mathrm{hPa^{-1}}$)	$n_{\delta_j}^k$	γ_j^k ($\mathrm{hPa^{-1}}$)	$n_{\gamma_j}^k$
	1812405.5390	−5.8342	128.3978	1.173	0.710	0.000	0.000	0.00e+00	0.00	0.00e+00	0.00
	1870017.9181	−6.3459	128.3978	1.173	0.710	0.000	0.000	0.00e+00	0.00	0.00e+00	0.00
	2095777.6612	−6.5966	190.7748	1.173	0.710	0.000	0.000	0.00e+00	0.00	0.00e+00	0.00
	2157577.7730	−5.8954	188.7134	1.143	0.710	0.000	0.000	0.00e+00	0.00	0.00e+00	0.00
	2214546.0193	−6.4119	188.7134	1.143	0.710	0.000	0.000	0.00e+00	0.00	0.00e+00	0.00
	2439912.6415	−6.6894	262.5827	1.129	0.710	0.000	0.000	0.00e+00	0.00	0.00e+00	0.00
	2502323.9230	−5.9917	260.5009	1.280	0.750	0.000	0.000	0.00e+00	0.00	0.00e+00	0.00
	2558687.2443	−6.5104	260.5009	1.114	0.710	0.000	0.000	0.00e+00	0.00	0.00e+00	0.00
	2783618.3155	−6.8166	345.8495	1.055	0.710	0.000	0.000	0.00e+00	0.00	0.00e+00	0.00
	2846616.2927	−6.1200	343.7481	0.997	0.710	0.000	0.000	0.00e+00	0.00	0.00e+00	0.00
	2902400.0929	−6.6393	343.7481	0.997	0.710	0.000	0.000	0.00e+00	0.00	0.00e+00	0.00
$O_2(\nu_1)$	62525.5416	−9.8479	1572.4576	1.540	0.800	0.000	0.000	-4.98e-04	0.80	9.70e-05	1.80
	62583.5000	−9.7355	1814.0099	1.230	0.800	0.000	0.000	3.60e-04	0.80	-7.77e-04	1.80
	63169.1700	−9.8386	1896.3390	1.200	0.800	0.000	0.000	2.39e-04	0.80	-7.68e-04	1.80
	63739.5411	−9.9729	1989.9875	1.170	0.800	0.000	0.000	1.08e-04	0.80	-7.06e-04	1.80
	119039.3139	−9.7704	1556.3547	1.528	0.979	−0.140	1.360	-3.60e-05	0.80	9.00e-06	1.80
$O^{17}O$	62240.0039	−7.6367	16.4685	1.636	0.710	0.000	0.000	0.00e+00	0.00	0.00e+00	0.00
	62266.4942	−7.6060	253.5234	1.389	0.710	0.000	0.000	0.00e+00	0.00	0.00e+00	0.00
	62305.3120	−7.4643	217.2839	1.407	0.710	0.000	0.000	0.00e+00	0.00	0.00e+00	0.00
	62368.0444	−7.7113	292.5392	1.375	0.710	0.000	0.000	0.00e+00	0.00	0.00e+00	0.00
	62369.5256	−7.5728	253.5201	1.389	0.710	0.000	0.000	0.00e+00	0.00	0.00e+00	0.00
	62381.8528	−7.8348	16.4633	1.636	0.710	0.000	0.000	0.00e+00	0.00	0.00e+00	0.00
	62457.7596	−7.6806	292.5362	1.375	0.710	0.000	0.000	0.00e+00	0.00	0.00e+00	0.00
	62479.6170	−7.5397	253.5165	1.389	0.710	0.000	0.000	0.00e+00	0.00	0.00e+00	0.00
	62554.0748	−7.6497	292.5331	1.375	0.710	0.000	0.000	0.00e+00	0.00	0.00e+00	0.00
	62596.7649	−7.5067	253.5128	1.389	0.710	0.000	0.000	0.00e+00	0.00	0.00e+00	0.00
	62656.9858	−7.6187	292.5297	1.375	0.710	0.000	0.000	0.00e+00	0.00	0.00e+00	0.00
	62766.4891	−7.5878	292.5262	1.375	0.710	0.000	0.000	0.00e+00	0.00	0.00e+00	0.00
	62836.8614	−7.7017	334.3221	1.357	0.710	0.000	0.000	0.00e+00	0.00	0.00e+00	0.00
	62882.5809	−7.5570	292.5225	1.375	0.710	0.000	0.000	0.00e+00	0.00	0.00e+00	0.00
	62939.6688	−7.6727	334.3187	1.357	0.710	0.000	0.000	0.00e+00	0.00	0.00e+00	0.00
	63048.6585	−7.6436	334.3152	1.357	0.710	0.000	0.000	0.00e+00	0.00	0.00e+00	0.00
	63163.8268	−7.6147	334.3115	1.357	0.710	0.000	0.000	0.00e+00	0.00	0.00e+00	0.00

Continued on next page

molecule	ν_{0j}^k (MHz)	$\mathcal{I}_j^k$ (nm^2MHz)	$E\ell_j^k$ (cm^{-1})	u_{cj}^k (MHz hPa^{-1})	n_{cj}^k	$\Delta\nu_{0j}^k$ (MHz hPa^{-1})	$n_{\Delta\nu_{0j}}^k$	δ_j^k (hPa^{-1})	$n_{\delta_j}^k$	γ_j^k (hPa^{-1})	$n_{\gamma_j}^k$
	63441.3106	−7.6797	378.8782	1.334	0.710	0.000	0.000	0.00e+00	0.00	0.00e+00	0.00
	118687.6979	−7.4972	0.6304	1.762	0.710	0.000	0.000	0.00e+00	0.00	0.00e+00	0.00
	118737.7202	−7.3217	0.6304	1.762	0.710	0.000	0.000	0.00e+00	0.00	0.00e+00	0.00
	118804.0320	−7.1975	0.6304	1.762	0.710	0.000	0.000	0.00e+00	0.00	0.00e+00	0.00
$O^{18}O$	62293.8371	−6.7992	246.7181	1.230	0.800	0.000	0.000	3.60e-04	0.80	-7.77e-04	1.80
	62570.0516	−6.8432	284.6816	1.055	0.710	0.000	0.000	0.00e+00	0.00	0.00e+00	0.00
	62842.0333	−6.8950	325.3501	1.200	0.800	0.000	0.000	2.39e-04	0.80	-7.68e-04	1.80
	63110.5315	−6.9544	368.7220	1.026	0.710	0.000	0.000	0.00e+00	0.00	0.00e+00	0.00
	63376.1335	−7.0211	414.7957	1.170	0.800	0.000	0.000	1.08e-04	0.80	-7.06e-04	1.80
	63639.3063	−7.0948	463.5694	1.026	0.710	0.000	0.000	0.00e+00	0.00	0.00e+00	0.00
	63900.4262	−7.1756	515.0412	1.130	0.800	0.000	0.000	-3.11e-04	0.80	-3.32e-04	1.80
	64159.7995	−7.2631	569.2091	1.026	0.710	0.000	0.000	0.00e+00	0.00	0.00e+00	0.00
	118759.8102	−6.8560	0.5633	1.528	0.979	−0.140	1.360	-3.60e-05	0.80	9.00e-06	1.80
	233946.1790	−6.6822	0.0000	1.685	0.760	0.000	0.000	0.00e+00	0.00	0.00e+00	0.00
O_3	63078.7400	−6.0667	550.3134	2.121	0.760	0.000	0.000	0.00e+00	0.00	0.00e+00	0.00
	114979.2000	−5.2493	21.2944	2.308	0.760	0.000	0.000	0.00e+00	0.00	0.00e+00	0.00
	118364.5000	−5.1315	0.0000	2.396	0.760	0.000	0.000	0.00e+00	0.00	0.00e+00	0.00
	119277.6200	−5.2811	392.1784	2.115	0.760	0.000	0.000	0.00e+00	0.00	0.00e+00	0.00
	176829.2761	−6.9643	1493.3408	1.898	0.760	0.000	0.000	0.00e+00	0.00	0.00e+00	0.00
	178577.0671	−5.7769	744.3066	1.971	0.760	0.000	0.000	0.00e+00	0.00	0.00e+00	0.00
	180001.2900	−5.5831	676.7956	1.986	0.760	0.000	0.000	0.00e+00	0.00	0.00e+00	0.00
	182682.8258	−7.7229	1891.6455	1.892	0.760	0.000	0.000	0.00e+00	0.00	0.00e+00	0.00
	183967.0403	−6.0043	1022.2396	1.933	0.760	0.000	0.000	0.00e+00	0.00	0.00e+00	0.00
	184377.8200	−4.0805	39.7506	2.367	0.700	0.000	0.000	0.00e+00	0.00	0.00e+00	0.00
	184748.7200	−4.5663	222.5716	2.138	0.750	0.000	0.000	0.00e+00	0.00	0.00e+00	0.00
	185128.6740	−7.3803	1736.8529	1.892	0.760	0.000	0.000	0.00e+00	0.00	0.00e+00	0.00
	185556.8300	−5.1658	550.3134	2.109	0.760	0.000	0.000	0.00e+00	0.00	0.00e+00	0.00
	199384.3602	−4.8227	416.3526	2.162	0.760	0.000	0.000	0.00e+00	0.00	0.00e+00	0.00
	203352.3120	−6.7564	1447.1622	1.901	0.760	0.000	0.000	0.00e+00	0.00	0.00e+00	0.00
	203453.1720	−5.2535	670.0092	1.995	0.760	0.000	0.000	0.00e+00	0.00	0.00e+00	0.00
	206132.0490	−4.7285	323.6207	2.170	0.760	0.000	0.000	0.00e+00	0.00	0.00e+00	0.00
	229575.0227	−4.6148	302.6370	2.100	0.760	0.000	0.000	0.00e+00	0.00	0.00e+00	0.00
	231281.4919	−3.8341	112.5424	2.222	0.703	0.000	0.000	0.00e+00	0.00	0.00e+00	0.00

Continued on next page

molecule	ν_{0j}^k (MHz)	$\mathcal{I}_j^k$ (nm^{2}MHz)	$E\ell_j^k$ (cm^{-1})	w_{cj}^k (MHz hPa^{-1})	n_{cj}^k	$\Delta\nu_{0j}^k$ (MHz hPa^{-1})	$n_{\Delta\nu_{0j}}^k$	δ_j^k (hPa^{-1})	$n_{\delta_j}^k$	γ_j^k (hPa^{-1})	$n_{\gamma_j}^k$
	232986.7731	−5.9577	1102.3590	1.922	0.760	0.000	0.000	0.00e+00	0.00	0.00e+00	0.00
	235709.8400	−3.6754	120.2571	2.263	0.655	0.000	0.000	0.00e+00	0.00	0.00e+00	0.00
	237146.1921	−3.6913	93.6687	2.257	0.693	0.000	0.000	0.00e+00	0.00	0.00e+00	0.00
	242318.7357	−3.7179	70.4557	2.307	0.663	0.000	0.000	0.00e+00	0.00	0.00e+00	0.00
	243453.7000	−3.7622	56.8050	2.276	0.685	0.000	0.000	0.00e+00	0.00	0.00e+00	0.00
	244145.6952	−5.2621	735.7845	1.986	0.760	0.000	0.000	0.00e+00	0.00	0.00e+00	0.00
	244158.0400	−4.5516	50.3021	2.362	0.749	0.000	0.000	0.00e+00	0.00	0.00e+00	0.00
	247761.7700	−4.4169	142.7128	2.240	0.685	0.000	0.000	0.00e+00	0.00	0.00e+00	0.00
	248183.3800	−3.6595	183.4307	2.192	0.680	0.000	0.000	0.00e+00	0.00	0.00e+00	0.00
	249788.6000	−3.8968	17.5973	2.405	0.674	0.000	0.000	0.00e+00	0.00	0.00e+00	0.00
	624480.5315	−6.7649	1387.9606	1.895	0.760	0.000	0.000	0.00e+00	0.00	0.00e+00	0.00
	625371.4686	−3.8747	192.5235	2.220	0.745	0.000	0.000	0.00e+00	0.00	0.00e+00	0.00
	625894.7151	−5.2346	1121.6884	1.939	0.760	0.000	0.000	0.00e+00	0.00	0.00e+00	0.00
	626397.2442	−5.6131	1714.3823	1.892	0.760	0.000	0.000	0.00e+00	0.00	0.00e+00	0.00
	632177.0500	−3.2267	327.5579	2.109	0.760	0.000	0.000	0.00e+00	0.00	0.00e+00	0.00
	633352.9979	−3.9520	344.5328	2.071	0.760	0.000	0.000	0.00e+00	0.00	0.00e+00	0.00
	634028.0793	−6.6507	1860.8002	1.892	0.760	0.000	0.000	0.00e+00	0.00	0.00e+00	0.00
	634461.7341	−3.1172	241.8317	2.141	0.760	0.000	0.000	0.00e+00	0.00	0.00e+00	0.00
	634519.7678	−4.2213	707.1504	1.980	0.760	0.000	0.000	0.00e+00	0.00	0.00e+00	0.00
	650732.9663	−3.8711	179.0698	2.071	0.760	0.000	0.000	0.00e+00	0.00	0.00e+00	0.00
	651723.7773	−6.4353	1143.7693	1.907	0.760	0.000	0.000	0.00e+00	0.00	0.00e+00	0.00
	653762.5698	−3.0571	116.5520	2.109	0.760	0.000	0.000	0.00e+00	0.00	0.00e+00	0.00
	658815.2932	−3.9122	325.1934	2.071	0.760	0.000	0.000	0.00e+00	0.00	0.00e+00	0.00
	659594.8149	−6.5237	1811.4114	1.892	0.760	0.000	0.000	0.00e+00	0.00	0.00e+00	0.00
	660360.2258	−5.7949	1822.0275	1.892	0.760	0.000	0.000	0.00e+00	0.00	0.00e+00	0.00
	661458.3584	−3.2086	346.2320	2.121	0.760	0.000	0.000	0.00e+00	0.00	0.00e+00	0.00
	2501411.4461	−2.4537	464.3759	2.056	0.760	0.000	0.000	0.00e+00	0.00	0.00e+00	0.00
	2501727.5474	−6.2598	874.9194	1.951	0.760	0.000	0.000	0.00e+00	0.00	0.00e+00	0.00
	2502751.7710	−5.8245	1508.3408	1.892	0.760	0.000	0.000	0.00e+00	0.00	0.00e+00	0.00
	2509560.4399	−3.0037	759.2807	2.004	0.760	0.000	0.000	0.00e+00	0.00	0.00e+00	0.00
	2509611.2736	−5.3814	205.3285	2.118	0.760	0.000	0.000	0.00e+00	0.00	0.00e+00	0.00
	2510614.2022	−4.4576	360.4138	2.159	0.760	0.000	0.000	0.00e+00	0.00	0.00e+00	0.00
	2510875.7362	−4.8191	308.4246	2.121	0.760	0.000	0.000	0.00e+00	0.00	0.00e+00	0.00

Continued on next page

molecule	ν_{0j}^k (MHz)	$\mathcal{I}_j^k$ ($\mathrm{nm^2MHz}$)	$E\ell_j^k$ ($\mathrm{cm^{-1}}$)	w_{cj}^k ($\mathrm{MHz\,hPa^{-1}}$)	n_{cj}^k	$\Delta\nu_{0j}^k$ ($\mathrm{MHz\,hPa^{-1}}$)	$n_{\Delta\nu_j}^k$	δ_j^k ($\mathrm{hPa^{-1}}$)	$n_{\delta_j}^k$	γ_j^k ($\mathrm{hPa^{-1}}$)	$n_{\gamma_j}^k$
	2510933.7261	−6.2351	839.3328	1.957	0.760	0.000	0.000	0.00e+00	0.00	0.00e+00	0.00
	2536301.7542	−5.5723	762.2312	1.951	0.760	0.000	0.000	0.00e+00	0.00	0.00e+00	0.00
	2542119.3911	−3.5194	1023.0811	1.939	0.760	0.000	0.000	0.00e+00	0.00	0.00e+00	0.00
	2543208.4034	−2.7659	643.1247	2.056	0.760	0.000	0.000	0.00e+00	0.00	0.00e+00	0.00
$O_3(\nu_{1,3})$	177420.9586	−6.9897	1290.9767	2.118	0.760	0.000	0.000	0.00e+00	0.00	0.00e+00	0.00
	177915.5696	−6.8832	1109.5260	2.133	0.760	0.000	0.000	0.00e+00	0.00	0.00e+00	0.00
	180424.1450	−7.2010	1518.8818	2.162	0.760	0.000	0.000	0.00e+00	0.00	0.00e+00	0.00
	180631.7528	−7.1549	1448.3398	2.109	0.760	0.000	0.000	0.00e+00	0.00	0.00e+00	0.00
	182377.0023	−6.3958	1142.9371	2.326	0.760	0.000	0.000	0.00e+00	0.00	0.00e+00	0.00
	183854.7692	−6.5307	1047.0529	2.270	0.760	0.000	0.000	0.00e+00	0.00	0.00e+00	0.00
	183892.9893	−6.5026	1141.2266	2.112	0.760	0.000	0.000	0.00e+00	0.00	0.00e+00	0.00
	184950.7733	−7.4273	1672.5137	2.004	0.760	0.000	0.000	0.00e+00	0.00	0.00e+00	0.00
	185320.4566	−6.1331	1116.5826	2.115	0.760	0.000	0.000	0.00e+00	0.00	0.00e+00	0.00
	186340.1091	−7.3800	1053.1855	2.235	0.760	0.000	0.000	0.00e+00	0.00	0.00e+00	0.00
	186460.3917	−6.2472	1190.3132	2.311	0.760	0.000	0.000	0.00e+00	0.00	0.00e+00	0.00
	203881.8298	−7.1897	1557.6290	2.021	0.760	0.000	0.000	0.00e+00	0.00	0.00e+00	0.00
	206438.9550	−7.5947	1800.5298	1.980	0.760	0.000	0.000	0.00e+00	0.00	0.00e+00	0.00
	231990.9848	−5.8596	1147.3606	2.100	0.760	0.000	0.000	0.00e+00	0.00	0.00e+00	0.00
	234355.3078	−5.8832	1122.7642	2.115	0.760	0.000	0.000	0.00e+00	0.00	0.00e+00	0.00
	234557.5814	−5.8429	1175.2635	2.086	0.760	0.000	0.000	0.00e+00	0.00	0.00e+00	0.00
	236067.7980	−5.9778	1223.0594	2.270	0.760	0.000	0.000	0.00e+00	0.00	0.00e+00	0.00
	237314.4297	−6.0353	1252.9349	2.259	0.760	0.000	0.000	0.00e+00	0.00	0.00e+00	0.00
	243063.5194	−5.8295	1206.4340	2.068	0.760	0.000	0.000	0.00e+00	0.00	0.00e+00	0.00
	244217.2315	−5.9693	1286.1281	2.247	0.760	0.000	0.000	0.00e+00	0.00	0.00e+00	0.00
	244404.1242	−6.0173	1173.3816	2.285	0.760	0.000	0.000	0.00e+00	0.00	0.00e+00	0.00
	248720.8421	−5.9738	1083.6143	2.147	0.760	0.000	0.000	0.00e+00	0.00	0.00e+00	0.00
	625011.4391	−6.6789	2112.0935	1.922	0.760	0.000	0.000	0.00e+00	0.00	0.00e+00	0.00
	625051.2336	−5.2762	1262.3696	2.048	0.760	0.000	0.000	0.00e+00	0.00	0.00e+00	0.00
	625797.9205	−6.3711	1578.3297	2.021	0.760	0.000	0.000	0.00e+00	0.00	0.00e+00	0.00
	626784.5400	−6.3141	1923.1816	1.939	0.760	0.000	0.000	0.00e+00	0.00	0.00e+00	0.00
	632833.8294	−5.9291	1506.8578	2.051	0.760	0.000	0.000	0.00e+00	0.00	0.00e+00	0.00
	632949.7372	−5.2457	1228.0027	2.068	0.760	0.000	0.000	0.00e+00	0.00	0.00e+00	0.00
	633243.8371	−6.2020	1793.3206	1.971	0.760	0.000	0.000	0.00e+00	0.00	0.00e+00	0.00

Continued on next page

molecule	ν_{0j}^k (MHz)	$\mathcal{I}_j^k$ ($\mathrm{nm^2MHz}$)	$E\ell_j^k$ ($\mathrm{cm^{-1}}$)	a_{cj}^k ($\mathrm{MHz\,hPa^{-1}}$)	n_{cj}^k	$\Delta\nu_{0j}^k$ ($\mathrm{MHz\,hPa^{-1}}$)	$n_{\Delta\nu_{0j}}^k$	δ_j^k ($\mathrm{hPa^{-1}}$)	$n_{\delta_j}^k$	γ_j^k ($\mathrm{hPa^{-1}}$)	$n_{\gamma_j}^k$
	633377.2058	−6.9575	1924.9194	1.986	0.760	0.000	0.000	0.00e+00	0.00	0.00e+00	0.00
	633855.9280	−5.6359	1486.7418	2.021	0.760	0.000	0.000	0.00e+00	0.00	0.00e+00	0.00
	634020.9595	−5.2919	1206.4340	2.068	0.760	0.000	0.000	0.00e+00	0.00	0.00e+00	0.00
	635316.5654	−5.0922	1324.0380	2.036	0.760	0.000	0.000	0.00e+00	0.00	0.00e+00	0.00
	636672.3675	−5.4269	1071.8220	2.188	0.760	0.000	0.000	0.00e+00	0.00	0.00e+00	0.00
	648890.8087	−5.9965	1602.2275	2.112	0.760	0.000	0.000	0.00e+00	0.00	0.00e+00	0.00
	650510.8450	−5.3529	1275.1962	2.124	0.760	0.000	0.000	0.00e+00	0.00	0.00e+00	0.00
	650978.7020	−5.7402	1413.9343	2.021	0.760	0.000	0.000	0.00e+00	0.00	0.00e+00	0.00
	650983.0165	−5.3513	1361.2935	2.036	0.760	0.000	0.000	0.00e+00	0.00	0.00e+00	0.00
	651225.6634	−6.3095	1553.4397	2.018	0.760	0.000	0.000	0.00e+00	0.00	0.00e+00	0.00
	652066.8398	−5.8931	1638.1635	1.969	0.760	0.000	0.000	0.00e+00	0.00	0.00e+00	0.00
	652842.8928	−6.1634	1282.1796	2.071	0.760	0.000	0.000	0.00e+00	0.00	0.00e+00	0.00
	653417.9746	−5.3460	1245.6863	2.115	0.760	0.000	0.000	0.00e+00	0.00	0.00e+00	0.00
	658757.9619	−6.8757	1893.0692	1.995	0.760	0.000	0.000	0.00e+00	0.00	0.00e+00	0.00
	659212.6286	−5.3827	1077.7053	2.168	0.760	0.000	0.000	0.00e+00	0.00	0.00e+00	0.00
	659465.1985	−5.2601	1240.8279	2.048	0.760	0.000	0.000	0.00e+00	0.00	0.00e+00	0.00
	660962.4607	−5.5063	1448.8875	2.121	0.760	0.000	0.000	0.00e+00	0.00	0.00e+00	0.00
	2509599.8979	−5.0050	1697.0256	2.059	0.760	0.000	0.000	0.00e+00	0.00	0.00e+00	0.00
	2513510.4489	−4.8444	1553.6113	2.068	0.760	0.000	0.000	0.00e+00	0.00	0.00e+00	0.00
	2514240.3740	−5.8047	1625.4521	2.051	0.760	0.000	0.000	0.00e+00	0.00	0.00e+00	0.00
	2534560.2526	−5.0405	1721.3582	2.059	0.760	0.000	0.000	0.00e+00	0.00	0.00e+00	0.00
	2535126.4983	−5.8145	1641.4181	2.051	0.760	0.000	0.000	0.00e+00	0.00	0.00e+00	0.00
	2542175.6118	−5.9924	1490.1013	2.080	0.760	0.000	0.000	0.00e+00	0.00	0.00e+00	0.00
	2542657.8486	−5.3620	1893.0692	1.995	0.760	0.000	0.000	0.00e+00	0.00	0.00e+00	0.00
$O_3(\nu_2)$	177028.2271	−6.6969	1279.2695	2.103	0.760	0.000	0.000	0.00e+00	0.00	0.00e+00	0.00
	178714.3385	−6.6700	712.7403	2.314	0.760	0.000	0.000	0.00e+00	0.00	0.00e+00	0.00
	182180.0402	−5.5519	740.5513	2.367	0.700	0.000	0.000	0.00e+00	0.00	0.00e+00	0.00
	204958.6184	−7.0516	1538.4984	1.957	0.760	0.000	0.000	0.00e+00	0.00	0.00e+00	0.00
	205214.0363	−6.0589	768.8169	2.174	0.760	0.000	0.000	0.00e+00	0.00	0.00e+00	0.00
	206496.0360	−6.0194	873.1248	2.121	0.760	0.000	0.000	0.00e+00	0.00	0.00e+00	0.00
	206504.4510	−6.5209	1250.6364	2.109	0.760	0.000	0.000	0.00e+00	0.00	0.00e+00	0.00
	235867.6556	−5.2777	812.9482	2.222	0.703	0.000	0.000	0.00e+00	0.00	0.00e+00	0.00
	243382.3207	−5.1099	850.6339	2.215	0.692	0.000	0.000	0.00e+00	0.00	0.00e+00	0.00

Continued on next page

molecule	ν_{0j}^k (MHz)	$\mathcal{I}_j^k$ (nm^{2}MHz)	$E\ell_j^k$ (cm^{-1})	w_{cj}^k (MHz hPa^{-1})	n_{cj}^k	$\Delta\nu_{0j}^k$ (MHz hPa^{-1})	$n_{\Delta\nu_{0j}}^k$	δ_j^k (hPa^{-1})	$n_{\delta_j}^k$	γ_j^k (hPa^{-1})	$n_{\gamma_j}^k$
	246512.6283	−5.1638	771.2002	2.307	0.663	0.000	0.000	0.00e+00	0.00	0.00e+00	0.00
	246551.3991	−6.0073	1003.3897	2.100	0.760	0.000	0.000	0.00e+00	0.00	0.00e+00	0.00
	625280.8257	−5.6817	1406.2328	1.980	0.760	0.000	0.000	0.00e+00	0.00	0.00e+00	0.00
	625324.2654	−5.9626	1832.3977	1.913	0.760	0.000	0.000	0.00e+00	0.00	0.00e+00	0.00
	625611.7040	−6.1803	1556.6555	1.980	0.760	0.000	0.000	0.00e+00	0.00	0.00e+00	0.00
	625793.5621	−7.1379	1296.5992	1.986	0.760	0.000	0.000	0.00e+00	0.00	0.00e+00	0.00
	626654.6988	−5.0093	1053.2765	2.065	0.760	0.000	0.000	0.00e+00	0.00	0.00e+00	0.00
	626723.5181	−6.3439	1726.7479	1.928	0.760	0.000	0.000	0.00e+00	0.00	0.00e+00	0.00
	631906.3437	−5.5937	789.5505	2.089	0.760	0.000	0.000	0.00e+00	0.00	0.00e+00	0.00
	648489.8807	−5.7914	1747.6532	1.922	0.760	0.000	0.000	0.00e+00	0.00	0.00e+00	0.00
	651192.8448	−6.0954	1524.0315	1.986	0.760	0.000	0.000	0.00e+00	0.00	0.00e+00	0.00
	651250.7562	−7.1107	1480.8032	1.957	0.760	0.000	0.000	0.00e+00	0.00	0.00e+00	0.00
	651819.8765	−4.3696	986.0609	2.056	0.760	0.000	0.000	0.00e+00	0.00	0.00e+00	0.00
	652188.1959	−4.9530	1177.4709	2.074	0.760	0.000	0.000	0.00e+00	0.00	0.00e+00	0.00
	652270.6460	−4.6953	731.2869	2.185	0.760	0.000	0.000	0.00e+00	0.00	0.00e+00	0.00
	653460.2649	−4.5245	906.0238	2.133	0.760	0.000	0.000	0.00e+00	0.00	0.00e+00	0.00
	659091.0854	−4.5020	873.1248	2.124	0.760	0.000	0.000	0.00e+00	0.00	0.00e+00	0.00
	659753.5588	−6.6220	1823.2760	1.939	0.760	0.000	0.000	0.00e+00	0.00	0.00e+00	0.00
	2502324.3793	−5.8121	1748.9291	1.919	0.760	0.000	0.000	0.00e+00	0.00	0.00e+00	0.00
	2502973.9957	−3.9807	1193.2393	2.068	0.760	0.000	0.000	0.00e+00	0.00	0.00e+00	0.00
	2509207.0106	−3.9125	1159.6021	2.048	0.760	0.000	0.000	0.00e+00	0.00	0.00e+00	0.00
	2509247.0031	−5.5275	1970.9839	1.907	0.760	0.000	0.000	0.00e+00	0.00	0.00e+00	0.00
	2514385.5333	−5.8121	2216.1091	1.922	0.760	0.000	0.000	0.00e+00	0.00	0.00e+00	0.00
	2514593.0117	−5.7397	2176.0647	1.928	0.760	0.000	0.000	0.00e+00	0.00	0.00e+00	0.00
	2514784.7726	−5.6693	2136.8491	1.933	0.760	0.000	0.000	0.00e+00	0.00	0.00e+00	0.00
	2514961.5137	−5.6009	2098.4626	1.939	0.760	0.000	0.000	0.00e+00	0.00	0.00e+00	0.00
	2515123.9199	−5.5346	2060.9058	1.945	0.760	0.000	0.000	0.00e+00	0.00	0.00e+00	0.00
	2515272.6626	−5.4704	2024.1785	1.951	0.760	0.000	0.000	0.00e+00	0.00	0.00e+00	0.00
	2515408.4005	−5.4083	1988.2815	1.957	0.760	0.000	0.000	0.00e+00	0.00	0.00e+00	0.00
	2543331.2660	−5.8056	1296.5992	1.986	0.760	0.000	0.000	0.00e+00	0.00	0.00e+00	0.00
	2544322.6785	−4.2010	1321.6418	2.059	0.760	0.000	0.000	0.00e+00	0.00	0.00e+00	0.00
$O_3(2\nu_2)$	179922.8155	−7.0167	1438.7604	2.367	0.700	0.000	0.000	0.00e+00	0.00	0.00e+00	0.00
	202771.3420	−7.4927	1586.9775	2.118	0.760	0.000	0.000	0.00e+00	0.00	0.00e+00	0.00

Continued on next page

molecule	ν_{0j}^k (MHz)	$\mathcal{I}_j^k$ (nm^{2}MHz)	$E\ell_j^k$ (cm^{-1})	w_{cj}^k (MHz hPa^{-1})	n_{cj}^k	$\Delta\nu_{0j}^k$ (MHz hPa^{-1})	$n_{\Delta\nu_{0j}}^k$	δ_j^k (hPa^{-1})	$n_{\delta_j}^k$	γ_j^k (hPa^{-1})	$n_{\gamma_j}^k$
	203207.6007	−6.8054	1485.6147	2.311	0.760	0.000	0.000	0.00e+00	0.00	0.00e+00	0.00
	205320.8744	−7.1399	1511.9310	2.250	0.760	0.000	0.000	0.00e+00	0.00	0.00e+00	0.00
	624182.6861	−6.1448	1724.4404	2.109	0.760	0.000	0.000	0.00e+00	0.00	0.00e+00	0.00
	633538.2627	−6.3296	1820.9072	2.086	0.760	0.000	0.000	0.00e+00	0.00	0.00e+00	0.00
	636155.1303	−6.1886	1424.7426	2.185	0.760	0.000	0.000	0.00e+00	0.00	0.00e+00	0.00
	659760.7611	−6.5673	1896.0497	2.112	0.760	0.000	0.000	0.00e+00	0.00	0.00e+00	0.00
	660004.8028	−6.1402	1429.7810	2.185	0.760	0.000	0.000	0.00e+00	0.00	0.00e+00	0.00
	2543146.7986	−5.3695	1864.2002	2.048	0.760	0.000	0.000	0.00e+00	0.00	0.00e+00	0.00
$O_3(\nu_{1,3}+\nu_2)$	625303.2213	−6.7289	1984.1699	2.033	0.760	0.000	0.000	0.00e+00	0.00	0.00e+00	0.00
	631929.2002	−6.5177	2007.1578	2.036	0.760	0.000	0.000	0.00e+00	0.00	0.00e+00	0.00
	634988.3326	−6.7137	1890.3179	2.068	0.760	0.000	0.000	0.00e+00	0.00	0.00e+00	0.00
	636266.8508	−6.6842	1946.4941	2.048	0.760	0.000	0.000	0.00e+00	0.00	0.00e+00	0.00
	649584.2351	−6.6391	1881.4623	2.086	0.760	0.000	0.000	0.00e+00	0.00	0.00e+00	0.00
	650111.6106	−6.8367	2037.1606	2.141	0.760	0.000	0.000	0.00e+00	0.00	0.00e+00	0.00
	652737.5290	−6.9733	1826.5981	2.185	0.760	0.000	0.000	0.00e+00	0.00	0.00e+00	0.00
	653091.9105	−6.6400	1854.0483	2.100	0.760	0.000	0.000	0.00e+00	0.00	0.00e+00	0.00
	653606.3783	−6.6505	2081.6233	2.056	0.760	0.000	0.000	0.00e+00	0.00	0.00e+00	0.00
	658828.3385	−6.7133	2002.8525	2.036	0.760	0.000	0.000	0.00e+00	0.00	0.00e+00	0.00
	659847.7538	−6.6825	1924.5775	2.048	0.760	0.000	0.000	0.00e+00	0.00	0.00e+00	0.00
$O_2^{17}O$	183915.8815	−5.2611	4.8924	2.270	0.760	0.000	0.000	0.00e+00	0.00	0.00e+00	0.00
	183916.9099	−5.6581	4.8924	2.270	0.760	0.000	0.000	0.00e+00	0.00	0.00e+00	0.00
	183917.5302	−5.1402	4.8924	2.270	0.760	0.000	0.000	0.00e+00	0.00	0.00e+00	0.00
	199987.3720	−5.6241	66.2231	2.174	0.760	0.000	0.000	0.00e+00	0.00	0.00e+00	0.00
	201390.9495	−4.8522	110.1172	2.250	0.760	0.000	0.000	0.00e+00	0.00	0.00e+00	0.00
	201391.4698	−5.3851	110.1173	2.250	0.760	0.000	0.000	0.00e+00	0.00	0.00e+00	0.00
	201392.3028	−5.0373	110.1173	2.250	0.760	0.000	0.000	0.00e+00	0.00	0.00e+00	0.00
	202832.8581	−5.5305	234.7488	2.048	0.760	0.000	0.000	0.00e+00	0.00	0.00e+00	0.00
	204860.8300	−5.6542	8.1503	2.387	0.760	0.000	0.000	0.00e+00	0.00	0.00e+00	0.00
	204861.6800	−4.9819	8.1502	2.387	0.760	0.000	0.000	0.00e+00	0.00	0.00e+00	0.00
	204862.6300	−5.0222	8.1502	2.387	0.760	0.000	0.000	0.00e+00	0.00	0.00e+00	0.00
	204863.3910	−5.3117	8.1502	2.387	0.760	0.000	0.000	0.00e+00	0.00	0.00e+00	0.00
	205498.7940	−4.5078	96.6599	2.100	0.760	0.000	0.000	0.00e+00	0.00	0.00e+00	0.00
	205499.9100	−5.0421	96.6600	2.100	0.760	0.000	0.000	0.00e+00	0.00	0.00e+00	0.00

Continued on next page

molecule	ν_{0j}^k (MHz)	I_j^k ($\mathrm{nm^2MHz}$)	$E\ell_j^k$ ($\mathrm{cm^{-1}}$)	w_{cj}^k ($\mathrm{MHz\,hPa^{-1}}$)	n_{cj}^k	$\Delta\nu_{0j}^k$ ($\mathrm{MHz\,hPa^{-1}}$)	$n_{\Delta\nu_{0j}}^k$	δ_j^k ($\mathrm{hPa^{-1}}$)	$n_{\delta_j}^k$	γ_j^k ($\mathrm{hPa^{-1}}$)	$n_{\gamma_j}^k$
	205500.8730	−4.9237	96.6599	2.100	0.760	0.000	0.000	0.00e+00	0.00	0.00e+00	0.00
	205501.6230	−5.0666	96.6600	2.100	0.760	0.000	0.000	0.00e+00	0.00	0.00e+00	0.00
	205601.8144	−4.4506	46.5942	2.144	0.760	0.000	0.000	0.00e+00	0.00	0.00e+00	0.00
	205602.7260	−4.7425	46.5942	2.144	0.760	0.000	0.000	0.00e+00	0.00	0.00e+00	0.00
	625009.5694	−4.5892	465.2112	2.074	0.760	0.000	0.000	0.00e+00	0.00	0.00e+00	0.00
	625009.7126	−4.6022	465.2112	2.074	0.760	0.000	0.000	0.00e+00	0.00	0.00e+00	0.00
	625009.7872	−4.5758	465.2112	2.074	0.760	0.000	0.000	0.00e+00	0.00	0.00e+00	0.00
	625010.1853	−4.6149	465.2112	2.074	0.760	0.000	0.000	0.00e+00	0.00	0.00e+00	0.00
	625010.3980	−4.5620	465.2112	2.074	0.760	0.000	0.000	0.00e+00	0.00	0.00e+00	0.00
	625010.9574	−4.6271	465.2112	2.074	0.760	0.000	0.000	0.00e+00	0.00	0.00e+00	0.00
	627011.8296	−3.2481	278.8344	2.036	0.760	0.000	0.000	0.00e+00	0.00	0.00e+00	0.00
	631902.3885	−3.9025	235.4045	2.141	0.760	0.000	0.000	0.00e+00	0.00	0.00e+00	0.00
	631902.6927	−4.1786	235.4044	2.141	0.760	0.000	0.000	0.00e+00	0.00	0.00e+00	0.00
	631902.8045	−4.2373	235.4045	2.141	0.760	0.000	0.000	0.00e+00	0.00	0.00e+00	0.00
	631902.9204	−3.9077	235.4044	2.141	0.760	0.000	0.000	0.00e+00	0.00	0.00e+00	0.00
	635763.2268	−3.8837	217.2691	2.048	0.760	0.000	0.000	0.00e+00	0.00	0.00e+00	0.00
	635763.4934	−4.1588	217.2690	2.048	0.760	0.000	0.000	0.00e+00	0.00	0.00e+00	0.00
	635763.6269	−4.2204	217.2691	2.048	0.760	0.000	0.000	0.00e+00	0.00	0.00e+00	0.00
	635763.7172	−3.8894	217.2690	2.048	0.760	0.000	0.000	0.00e+00	0.00	0.00e+00	0.00
	636396.0542	−4.2219	29.6078	2.185	0.760	0.000	0.000	0.00e+00	0.00	0.00e+00	0.00
	636396.6046	−4.2863	29.6078	2.185	0.760	0.000	0.000	0.00e+00	0.00	0.00e+00	0.00
	636396.7385	−4.2215	29.6079	2.185	0.760	0.000	0.000	0.00e+00	0.00	0.00e+00	0.00
	636396.8567	−4.0846	29.6078	2.185	0.760	0.000	0.000	0.00e+00	0.00	0.00e+00	0.00
	636997.5285	−4.5295	55.2749	2.270	0.760	0.000	0.000	0.00e+00	0.00	0.00e+00	0.00
	636997.9465	−4.5668	55.2749	2.270	0.760	0.000	0.000	0.00e+00	0.00	0.00e+00	0.00
	636998.0732	−4.4923	55.2749	2.270	0.760	0.000	0.000	0.00e+00	0.00	0.00e+00	0.00
	636999.1116	−4.6042	55.2749	2.270	0.760	0.000	0.000	0.00e+00	0.00	0.00e+00	0.00
	636999.8142	−4.4556	55.2749	2.270	0.760	0.000	0.000	0.00e+00	0.00	0.00e+00	0.00
	637000.8255	−4.6413	55.2749	2.270	0.760	0.000	0.000	0.00e+00	0.00	0.00e+00	0.00
	648373.6161	−3.7976	126.0812	2.100	0.760	0.000	0.000	0.00e+00	0.00	0.00e+00	0.00
	648373.9670	−4.2259	126.0813	2.100	0.760	0.000	0.000	0.00e+00	0.00	0.00e+00	0.00
	648373.9787	−4.1453	126.0812	2.100	0.760	0.000	0.000	0.00e+00	0.00	0.00e+00	0.00
	648374.0518	−4.2014	126.0813	2.100	0.760	0.000	0.000	0.00e+00	0.00	0.00e+00	0.00

Continued on next page

molecule	ν_{0j}^k (MHz)	$\mathcal{I}_j^k$ ($\mathrm{nm^2MHz}$)	$E\ell_j^k$ ($\mathrm{cm^{-1}}$)	w_{cj}^k ($\mathrm{MHz\,hPa^{-1}}$)	n_{cj}^k	$\Delta\nu_{0j}^k$ ($\mathrm{MHz\,hPa^{-1}}$)	$n_{\Delta\nu_{0j}}^k$	δ_j^k ($\mathrm{hPa^{-1}}$)	$n_{\delta_j}^k$	γ_j^k ($\mathrm{hPa^{-1}}$)	$n_{\gamma_j}^k$
	648374.0615	−4.1744	126.0812	2.100	0.760	0.000	0.000	0.00e+00	0.00	0.00e+00	0.00
	649275.2349	−4.0869	113.7952	2.109	0.760	0.000	0.000	0.00e+00	0.00	0.00e+00	0.00
	649275.6618	−3.8362	113.7951	2.109	0.760	0.000	0.000	0.00e+00	0.00	0.00e+00	0.00
	649275.8339	−3.7354	113.7952	2.109	0.760	0.000	0.000	0.00e+00	0.00	0.00e+00	0.00
	649970.1201	−4.0950	102.3350	2.115	0.760	0.000	0.000	0.00e+00	0.00	0.00e+00	0.00
	649970.4631	−4.1321	102.3350	2.115	0.760	0.000	0.000	0.00e+00	0.00	0.00e+00	0.00
	649970.6726	−4.1677	102.3350	2.115	0.760	0.000	0.000	0.00e+00	0.00	0.00e+00	0.00
	649970.7157	−4.2600	102.3351	2.115	0.760	0.000	0.000	0.00e+00	0.00	0.00e+00	0.00
	649970.7749	−3.9157	102.3350	2.115	0.760	0.000	0.000	0.00e+00	0.00	0.00e+00	0.00
	649981.3999	−3.4431	183.2408	2.118	0.760	0.000	0.000	0.00e+00	0.00	0.00e+00	0.00
	649981.6061	−4.2086	183.2409	2.118	0.760	0.000	0.000	0.00e+00	0.00	0.00e+00	0.00
	650010.5882	−3.5385	199.5937	2.062	0.760	0.000	0.000	0.00e+00	0.00	0.00e+00	0.00
	650010.8169	−3.9035	199.5938	2.062	0.760	0.000	0.000	0.00e+00	0.00	0.00e+00	0.00
	650042.5398	−3.4373	167.7052	2.080	0.760	0.000	0.000	0.00e+00	0.00	0.00e+00	0.00
	650042.7459	−4.2065	167.7053	2.080	0.760	0.000	0.000	0.00e+00	0.00	0.00e+00	0.00
	650159.5639	−4.1208	216.7634	2.124	0.760	0.000	0.000	0.00e+00	0.00	0.00e+00	0.00
	650159.7719	−3.6866	216.7633	2.124	0.760	0.000	0.000	0.00e+00	0.00	0.00e+00	0.00
	650159.9428	−3.9126	216.7634	2.124	0.760	0.000	0.000	0.00e+00	0.00	0.00e+00	0.00
	650167.9240	−3.3671	152.9876	2.115	0.760	0.000	0.000	0.00e+00	0.00	0.00e+00	0.00
	650334.5414	−4.0796	139.0883	2.097	0.760	0.000	0.000	0.00e+00	0.00	0.00e+00	0.00
	650334.7582	−4.1092	139.0883	2.097	0.760	0.000	0.000	0.00e+00	0.00	0.00e+00	0.00
	650334.9084	−4.1378	139.0883	2.097	0.760	0.000	0.000	0.00e+00	0.00	0.00e+00	0.00
	650335.0010	−4.1649	139.0883	2.097	0.760	0.000	0.000	0.00e+00	0.00	0.00e+00	0.00
	650335.0448	−4.1903	139.0883	2.097	0.760	0.000	0.000	0.00e+00	0.00	0.00e+00	0.00
	650335.0478	−4.2135	139.0884	2.097	0.760	0.000	0.000	0.00e+00	0.00	0.00e+00	0.00
	650461.4706	−3.4779	234.7488	2.048	0.760	0.000	0.000	0.00e+00	0.00	0.00e+00	0.00
	650461.6905	−4.2345	234.7489	2.048	0.760	0.000	0.000	0.00e+00	0.00	0.00e+00	0.00
	650496.9314	−4.1078	91.6991	2.106	0.760	0.000	0.000	0.00e+00	0.00	0.00e+00	0.00
	650497.4014	−3.8663	91.6990	2.106	0.760	0.000	0.000	0.00e+00	0.00	0.00e+00	0.00
	650497.6139	−3.7782	91.6991	2.106	0.760	0.000	0.000	0.00e+00	0.00	0.00e+00	0.00
	650523.9865	−4.0806	126.0077	2.112	0.760	0.000	0.000	0.00e+00	0.00	0.00e+00	0.00
	650524.2255	−4.1123	126.0077	2.112	0.760	0.000	0.000	0.00e+00	0.00	0.00e+00	0.00
	650524.3879	−4.1429	126.0077	2.112	0.760	0.000	0.000	0.00e+00	0.00	0.00e+00	0.00

Continued on next page

molecule	ν_{0j}^k (MHz)	$\mathcal{I}_j^k$ ($\mathrm{nm^2MHz}$)	$E\ell_j^k$ ($\mathrm{cm^{-1}}$)	w_{cj}^k ($\mathrm{MHz\,hPa^{-1}}$)	n_{cj}^k	$\Delta\nu_{0j}^k$ ($\mathrm{MHz\,hPa^{-1}}$)	$n_{\Delta\nu_{0j}}^k$	δ_j^k ($\mathrm{hPa^{-1}}$)	$n_{\delta_j}^k$	γ_j^k ($\mathrm{hPa^{-1}}$)	$n_{\gamma_j}^k$
	650524.4849	−4.1720	126.0077	2.112	0.760	0.000	0.000	0.00e+00	0.00	0.00e+00	0.00
	650524.5238	−4.2235	126.0077	2.112	0.760	0.000	0.000	0.00e+00	0.00	0.00e+00	0.00
	650524.5270	−4.1990	126.0077	2.112	0.760	0.000	0.000	0.00e+00	0.00	0.00e+00	0.00
	650720.4274	−4.0853	113.7459	2.112	0.760	0.000	0.000	0.00e+00	0.00	0.00e+00	0.00
	650720.6912	−4.1195	113.7459	2.112	0.760	0.000	0.000	0.00e+00	0.00	0.00e+00	0.00
	650720.8672	−4.1524	113.7459	2.112	0.760	0.000	0.000	0.00e+00	0.00	0.00e+00	0.00
	650720.9691	−4.1836	113.7459	2.112	0.760	0.000	0.000	0.00e+00	0.00	0.00e+00	0.00
	650721.0000	−4.2384	113.7460	2.112	0.760	0.000	0.000	0.00e+00	0.00	0.00e+00	0.00
	650721.0095	−4.2125	113.7459	2.112	0.760	0.000	0.000	0.00e+00	0.00	0.00e+00	0.00
	650857.0769	−3.7032	299.9138	2.045	0.760	0.000	0.000	0.00e+00	0.00	0.00e+00	0.00
	650857.0860	−4.0277	299.9139	2.045	0.760	0.000	0.000	0.00e+00	0.00	0.00e+00	0.00
	650857.1135	−3.5493	299.9138	2.045	0.760	0.000	0.000	0.00e+00	0.00	0.00e+00	0.00
	650889.0320	−4.1260	81.8858	2.133	0.760	0.000	0.000	0.00e+00	0.00	0.00e+00	0.00
	650889.4268	−4.1706	81.8858	2.133	0.760	0.000	0.000	0.00e+00	0.00	0.00e+00	0.00
	650889.6667	−4.2135	81.8858	2.133	0.760	0.000	0.000	0.00e+00	0.00	0.00e+00	0.00
	650889.7352	−4.3217	81.8859	2.133	0.760	0.000	0.000	0.00e+00	0.00	0.00e+00	0.00
	650889.7877	−3.9707	81.8858	2.133	0.760	0.000	0.000	0.00e+00	0.00	0.00e+00	0.00
	650911.7313	−4.0939	102.3030	2.106	0.760	0.000	0.000	0.00e+00	0.00	0.00e+00	0.00
	650912.0235	−4.1310	102.3030	2.106	0.760	0.000	0.000	0.00e+00	0.00	0.00e+00	0.00
	650912.2151	−4.1667	102.3030	2.106	0.760	0.000	0.000	0.00e+00	0.00	0.00e+00	0.00
	650912.3224	−4.2004	102.3030	2.106	0.760	0.000	0.000	0.00e+00	0.00	0.00e+00	0.00
	650912.3442	−4.2590	102.3031	2.106	0.760	0.000	0.000	0.00e+00	0.00	0.00e+00	0.00
	650912.3608	−4.2315	102.3030	2.106	0.760	0.000	0.000	0.00e+00	0.00	0.00e+00	0.00
	650951.1646	−4.1557	253.5491	2.124	0.760	0.000	0.000	0.00e+00	0.00	0.00e+00	0.00
	650951.2825	−3.8845	253.5490	2.124	0.760	0.000	0.000	0.00e+00	0.00	0.00e+00	0.00
	650951.4690	−3.7543	253.5491	2.124	0.760	0.000	0.000	0.00e+00	0.00	0.00e+00	0.00
	651088.9544	−4.1072	91.6790	2.127	0.760	0.000	0.000	0.00e+00	0.00	0.00e+00	0.00
	651089.2805	−4.1476	91.6790	2.127	0.760	0.000	0.000	0.00e+00	0.00	0.00e+00	0.00
	651089.4900	−4.1866	91.6790	2.127	0.760	0.000	0.000	0.00e+00	0.00	0.00e+00	0.00
	651089.6032	−4.2233	91.6790	2.127	0.760	0.000	0.000	0.00e+00	0.00	0.00e+00	0.00
	651089.6136	−4.2862	91.6791	2.127	0.760	0.000	0.000	0.00e+00	0.00	0.00e+00	0.00
	651089.6387	−4.2569	91.6790	2.127	0.760	0.000	0.000	0.00e+00	0.00	0.00e+00	0.00
	651174.7048	−4.1506	72.8939	2.106	0.760	0.000	0.000	0.00e+00	0.00	0.00e+00	0.00

Continued on next page

molecule	ν_{0j}^k (MHz)	$\mathcal{I}_j^k$ (nm^2MHz)	$E\ell_j^k$ (cm^{-1})	w_{cj}^k (MHz hPa^{-1})	n_{cj}^k	$\Delta\nu_{0j}^k$ (MHz hPa^{-1})	$n_{\Delta\nu_{0j}}^k$	δ_j^k (hPa^{-1})	$n_{\delta_j}^k$	γ_j^k (hPa^{-1})	$n_{\gamma_j}^k$
	651175.1442	−4.2001	72.8939	2.106	0.760	0.000	0.000	0.00e+00	0.00	0.00e+00	0.00
	651175.4069	−4.2478	72.8939	2.106	0.760	0.000	0.000	0.00e+00	0.00	0.00e+00	0.00
	651175.4728	−4.3664	72.8940	2.106	0.760	0.000	0.000	0.00e+00	0.00	0.00e+00	0.00
	651175.5281	−4.2925	72.8939	2.106	0.760	0.000	0.000	0.00e+00	0.00	0.00e+00	0.00
	651175.5403	−4.3328	72.8940	2.106	0.760	0.000	0.000	0.00e+00	0.00	0.00e+00	0.00
	651246.0665	−4.1256	81.8737	2.106	0.760	0.000	0.000	0.00e+00	0.00	0.00e+00	0.00
	651246.4343	−4.1702	81.8737	2.106	0.760	0.000	0.000	0.00e+00	0.00	0.00e+00	0.00
	651246.6651	−4.2131	81.8737	2.106	0.760	0.000	0.000	0.00e+00	0.00	0.00e+00	0.00
	651246.7791	−4.3213	81.8738	2.106	0.760	0.000	0.000	0.00e+00	0.00	0.00e+00	0.00
	651246.7843	−4.2534	81.8737	2.106	0.760	0.000	0.000	0.00e+00	0.00	0.00e+00	0.00
	651246.8152	−4.2900	81.8738	2.106	0.760	0.000	0.000	0.00e+00	0.00	0.00e+00	0.00
	651706.3065	−4.5968	40.2225	2.118	0.760	0.000	0.000	0.00e+00	0.00	0.00e+00	0.00
	651706.6745	−4.9030	40.2226	2.118	0.760	0.000	0.000	0.00e+00	0.00	0.00e+00	0.00
	651706.8353	−4.7075	40.2225	2.118	0.760	0.000	0.000	0.00e+00	0.00	0.00e+00	0.00
	651706.8930	−4.8132	40.2226	2.118	0.760	0.000	0.000	0.00e+00	0.00	0.00e+00	0.00
	651719.2363	−4.7229	36.1413	2.106	0.760	0.000	0.000	0.00e+00	0.00	0.00e+00	0.00
	651720.0848	−4.7229	36.1413	2.235	0.760	0.000	0.000	0.00e+00	0.00	0.00e+00	0.00
	651721.0174	−4.8673	36.1414	2.106	0.760	0.000	0.000	0.00e+00	0.00	0.00e+00	0.00
	651721.8654	−4.8673	36.1413	2.235	0.760	0.000	0.000	0.00e+00	0.00	0.00e+00	0.00
	652649.3584	−3.5357	293.5895	2.124	0.760	0.000	0.000	0.00e+00	0.00	0.00e+00	0.00
	652649.6139	−4.2855	293.5896	2.124	0.760	0.000	0.000	0.00e+00	0.00	0.00e+00	0.00
	653939.0769	−3.5596	314.8270	2.036	0.760	0.000	0.000	0.00e+00	0.00	0.00e+00	0.00
	653939.3493	−4.3074	314.8271	2.036	0.760	0.000	0.000	0.00e+00	0.00	0.00e+00	0.00
	659880.6775	−3.2287	299.7493	2.027	0.760	0.000	0.000	0.00e+00	0.00	0.00e+00	0.00
	659974.6147	−4.2388	416.8095	2.021	0.760	0.000	0.000	0.00e+00	0.00	0.00e+00	0.00
	659975.7197	−4.6881	416.8095	2.021	0.760	0.000	0.000	0.00e+00	0.00	0.00e+00	0.00
	660080.3628	−4.0348	383.3902	2.118	0.760	0.000	0.000	0.00e+00	0.00	0.00e+00	0.00
	660080.5427	−3.7545	383.3903	2.118	0.760	0.000	0.000	0.00e+00	0.00	0.00e+00	0.00
	660238.0752	−4.1893	35.3451	2.168	0.760	0.000	0.000	0.00e+00	0.00	0.00e+00	0.00
	660238.6076	−4.2452	35.3451	2.168	0.760	0.000	0.000	0.00e+00	0.00	0.00e+00	0.00
	660238.7111	−4.1465	35.3452	2.168	0.760	0.000	0.000	0.00e+00	0.00	0.00e+00	0.00
	660238.8557	−4.0297	35.3451	2.168	0.760	0.000	0.000	0.00e+00	0.00	0.00e+00	0.00
$O^{17}OO$	203838.2437	−4.5873	8.3730	2.387	0.760	0.000	0.000	0.00e+00	0.00	0.00e+00	0.00

Continued on next page

molecule	ν_{0j}^k (MHz)	$\mathcal{I}_j^k$ (nm^{2}MHz)	$E\ell_j^k$ (cm^{-1})	w_{cj}^k (MHz hPa^{-1})	n_{cj}^k	$\Delta\nu_{0j}^k$ (MHz hPa^{-1})	$n_{\Delta\nu_{0j}}^k$	δ_j^k (hPa^{-1})	$n_{\delta_j}^k$	γ_j^k (hPa^{-1})	$n_{\gamma_j}^k$
	203838.9878	−4.5258	8.3729	2.387	0.760	0.000	0.000	0.00e+00	0.00	0.00e+00	0.00
	624294.2586	−3.1133	115.1509	2.109	0.760	0.000	0.000	0.00e+00	0.00	0.00e+00	0.00
	625771.8878	−3.8260	186.5115	2.118	0.760	0.000	0.000	0.00e+00	0.00	0.00e+00	0.00
	625772.0998	−3.3965	186.5114	2.118	0.760	0.000	0.000	0.00e+00	0.00	0.00e+00	0.00
	625772.1813	−3.6275	186.5115	2.118	0.760	0.000	0.000	0.00e+00	0.00	0.00e+00	0.00
	625782.9166	−3.8108	155.4173	2.115	0.760	0.000	0.000	0.00e+00	0.00	0.00e+00	0.00
	625783.1392	−3.5506	155.4172	2.115	0.760	0.000	0.000	0.00e+00	0.00	0.00e+00	0.00
	625783.2331	−3.9368	155.4173	2.115	0.760	0.000	0.000	0.00e+00	0.00	0.00e+00	0.00
	625783.2556	−3.6016	155.4172	2.115	0.760	0.000	0.000	0.00e+00	0.00	0.00e+00	0.00
	625869.5705	−3.5529	92.4293	2.106	0.760	0.000	0.000	0.00e+00	0.00	0.00e+00	0.00
	625869.8353	−4.0132	92.4294	2.106	0.760	0.000	0.000	0.00e+00	0.00	0.00e+00	0.00
	625869.9452	−3.4712	92.4293	2.106	0.760	0.000	0.000	0.00e+00	0.00	0.00e+00	0.00
	626087.3102	−3.3617	127.6861	2.112	0.760	0.000	0.000	0.00e+00	0.00	0.00e+00	0.00
	626087.4871	−3.9511	127.6862	2.112	0.760	0.000	0.000	0.00e+00	0.00	0.00e+00	0.00
	626087.5337	−3.6118	127.6861	2.112	0.760	0.000	0.000	0.00e+00	0.00	0.00e+00	0.00
	626316.5749	−3.1949	220.9630	2.124	0.760	0.000	0.000	0.00e+00	0.00	0.00e+00	0.00
	626316.6915	−3.9542	220.9631	2.124	0.760	0.000	0.000	0.00e+00	0.00	0.00e+00	0.00
	626490.4223	−3.8205	103.3213	2.106	0.760	0.000	0.000	0.00e+00	0.00	0.00e+00	0.00
	626490.6886	−3.8576	103.3212	2.106	0.760	0.000	0.000	0.00e+00	0.00	0.00e+00	0.00
	626490.8207	−3.9855	103.3213	2.106	0.760	0.000	0.000	0.00e+00	0.00	0.00e+00	0.00
	626490.8434	−3.8933	103.3212	2.106	0.760	0.000	0.000	0.00e+00	0.00	0.00e+00	0.00
	626490.8992	−3.6412	103.3213	2.106	0.760	0.000	0.000	0.00e+00	0.00	0.00e+00	0.00
	626739.7505	−3.8760	73.0967	2.106	0.760	0.000	0.000	0.00e+00	0.00	0.00e+00	0.00
	626740.1668	−3.9255	73.0966	2.106	0.760	0.000	0.000	0.00e+00	0.00	0.00e+00	0.00
	626740.3135	−3.7736	73.0967	2.106	0.760	0.000	0.000	0.00e+00	0.00	0.00e+00	0.00
	626740.3841	−3.9732	73.0966	2.106	0.760	0.000	0.000	0.00e+00	0.00	0.00e+00	0.00
	626740.4437	−4.0179	73.0967	2.106	0.760	0.000	0.000	0.00e+00	0.00	0.00e+00	0.00
	626867.1427	−3.8513	82.3236	2.106	0.760	0.000	0.000	0.00e+00	0.00	0.00e+00	0.00
	626867.4905	−3.8959	82.3235	2.106	0.760	0.000	0.000	0.00e+00	0.00	0.00e+00	0.00
	626867.5992	−4.0470	82.3236	2.106	0.760	0.000	0.000	0.00e+00	0.00	0.00e+00	0.00
	626867.6809	−3.9387	82.3235	2.106	0.760	0.000	0.000	0.00e+00	0.00	0.00e+00	0.00
	626867.7085	−4.0156	82.3236	2.106	0.760	0.000	0.000	0.00e+00	0.00	0.00e+00	0.00
	626867.7442	−3.9790	82.3235	2.106	0.760	0.000	0.000	0.00e+00	0.00	0.00e+00	0.00

Continued on next page

molecule	ν_{0j}^k (MHz)	$\mathcal{I}_j^k$ (nm^{2}MHz)	$E\ell_j^k$ (cm^{-1})	w_{cj}^k (MHz hPa^{-1})	n_{cj}^k	$\Delta\nu_{0j}^k$ (MHz hPa^{-1})	$n_{\Delta\nu_{0j}}^k$	δ_j^k (hPa^{-1})	$n_{\delta_j}^k$	γ_j^k (hPa^{-1})	$n_{\gamma_j}^k$
	633130.4022	−3.8346	476.4069	2.074	0.760	0.000	0.000	0.00e+00	0.00	0.00e+00	0.00
	633130.7602	−3.8461	476.4070	2.074	0.760	0.000	0.000	0.00e+00	0.00	0.00e+00	0.00
	634713.6891	−3.9871	344.3630	2.121	0.760	0.000	0.000	0.00e+00	0.00	0.00e+00	0.00
	634713.7493	−3.5431	344.3629	2.121	0.760	0.000	0.000	0.00e+00	0.00	0.00e+00	0.00
	634713.8846	−3.7581	344.3630	2.121	0.760	0.000	0.000	0.00e+00	0.00	0.00e+00	0.00
	648791.8277	−3.9477	182.9455	2.200	0.760	0.000	0.000	0.00e+00	0.00	0.00e+00	0.00
	648791.8712	−3.8435	182.9454	2.200	0.760	0.000	0.000	0.00e+00	0.00	0.00e+00	0.00
	648792.1789	−3.9269	182.9454	2.200	0.760	0.000	0.000	0.00e+00	0.00	0.00e+00	0.00
	648792.2674	−3.8642	182.9454	2.200	0.760	0.000	0.000	0.00e+00	0.00	0.00e+00	0.00
	648792.3892	−3.9060	182.9454	2.200	0.760	0.000	0.000	0.00e+00	0.00	0.00e+00	0.00
	648792.4291	−3.8851	182.9454	2.200	0.760	0.000	0.000	0.00e+00	0.00	0.00e+00	0.00
	649794.7104	−3.4459	443.1934	2.112	0.760	0.000	0.000	0.00e+00	0.00	0.00e+00	0.00
	649794.9197	−4.1861	443.1935	2.112	0.760	0.000	0.000	0.00e+00	0.00	0.00e+00	0.00
	650605.6360	−3.4242	35.4385	2.179	0.760	0.000	0.000	0.00e+00	0.00	0.00e+00	0.00
	650605.8348	−4.0122	35.4384	2.179	0.760	0.000	0.000	0.00e+00	0.00	0.00e+00	0.00
	650605.8560	−4.0705	35.4385	2.179	0.760	0.000	0.000	0.00e+00	0.00	0.00e+00	0.00
	651273.7164	−3.6559	285.3497	2.056	0.760	0.000	0.000	0.00e+00	0.00	0.00e+00	0.00
	651273.7186	−3.7367	285.3498	2.056	0.760	0.000	0.000	0.00e+00	0.00	0.00e+00	0.00
	651273.7536	−3.0938	285.3497	2.056	0.760	0.000	0.000	0.00e+00	0.00	0.00e+00	0.00
	661271.3080	−3.5195	497.5259	2.103	0.760	0.000	0.000	0.00e+00	0.00	0.00e+00	0.00
	661271.5427	−4.2572	497.5260	2.103	0.760	0.000	0.000	0.00e+00	0.00	0.00e+00	0.00
$O_2^{18}O$	181023.4500	−4.7050	4.7615	2.270	0.760	0.000	0.000	0.00e+00	0.00	0.00e+00	0.00
	181090.1200	−5.1752	350.1151	2.109	0.760	0.000	0.000	0.00e+00	0.00	0.00e+00	0.00
	181430.4698	−4.9932	74.2096	2.127	0.760	0.000	0.000	0.00e+00	0.00	0.00e+00	0.00
	183815.9900	−4.2833	82.4771	2.311	0.760	0.000	0.000	0.00e+00	0.00	0.00e+00	0.00
	184087.0920	−4.8881	229.0204	2.048	0.760	0.000	0.000	0.00e+00	0.00	0.00e+00	0.00
	185124.4600	−4.9655	179.1488	2.068	0.760	0.000	0.000	0.00e+00	0.00	0.00e+00	0.00
	185790.9811	−5.1981	419.4258	2.021	0.760	0.000	0.000	0.00e+00	0.00	0.00e+00	0.00
	201466.8808	−4.5355	7.9323	2.387	0.760	0.000	0.000	0.00e+00	0.00	0.00e+00	0.00
	202229.5092	−5.0558	328.7227	2.109	0.760	0.000	0.000	0.00e+00	0.00	0.00e+00	0.00
	202385.5621	−5.7844	7.9927	2.000	0.800	0.000	0.000	0.00e+00	0.00	0.00e+00	0.00
	203997.9605	−4.9270	64.7069	2.174	0.760	0.000	0.000	0.00e+00	0.00	0.00e+00	0.00
	205502.6039	−5.8834	830.5477	2.000	0.800	0.000	0.000	0.00e+00	0.00	0.00e+00	0.00

Continued on next page

molecule	ν_{0j}^k (MHz)	I_j^k ($\mathrm{nm^2MHz}$)	$E\ell_j^k$ ($\mathrm{cm^{-1}}$)	a_{cj}^k ($\mathrm{MHz\,hPa^{-1}}$)	n_{cj}^k	$\Delta\nu_{0j}^k$ ($\mathrm{MHz\,hPa^{-1}}$)	$n_{\Delta\nu_{0j}}^k$	δ_j^k ($\mathrm{hPa^{-1}}$)	$n_{\delta_j}^k$	γ_j^k ($\mathrm{hPa^{-1}}$)	$n_{\gamma_j}^k$
	205730.4003	−5.0413	328.6091	2.036	0.760	0.000	0.000	0.00e+00	0.00	0.00e+00	0.00
	232525.0900	−4.0110	113.7392	2.263	0.655	0.000	0.000	0.00e+00	0.00	0.00e+00	0.00
	232723.6689	−4.0054	127.4955	2.086	0.760	0.000	0.000	0.00e+00	0.00	0.00e+00	0.00
	233351.1600	−4.0183	100.7757	2.100	0.760	0.000	0.000	0.00e+00	0.00	0.00e+00	0.00
	234056.0600	−4.0012	142.0410	2.215	0.692	0.000	0.000	0.00e+00	0.00	0.00e+00	0.00
	234183.6000	−4.1541	119.6839	2.086	0.760	0.000	0.000	0.00e+00	0.00	0.00e+00	0.00
	235082.0900	−4.0279	88.6085	2.257	0.693	0.000	0.000	0.00e+00	0.00	0.00e+00	0.00
	236620.9400	−3.9980	157.3717	2.068	0.760	0.000	0.000	0.00e+00	0.00	0.00e+00	0.00
	244355.1638	−4.0760	56.9131	2.133	0.760	0.000	0.000	0.00e+00	0.00	0.00e+00	0.00
	245795.8877	−3.9934	190.3719	2.048	0.760	0.000	0.000	0.00e+00	0.00	0.00e+00	0.00
	248321.2300	−4.1007	47.9582	2.347	0.675	0.000	0.000	0.00e+00	0.00	0.00e+00	0.00
	625090.4623	−4.2634	349.3619	2.071	0.760	0.000	0.000	0.00e+00	0.00	0.00e+00	0.00
	625091.8080	−4.2634	349.3618	2.036	0.760	0.000	0.000	0.00e+00	0.00	0.00e+00	0.00
	625563.6585	−3.4532	248.0632	2.033	0.760	0.000	0.000	0.00e+00	0.00	0.00e+00	0.00
	625939.4177	−3.8498	479.6934	2.001	0.760	0.000	0.000	0.00e+00	0.00	0.00e+00	0.00
	631775.2923	−3.4628	157.3717	2.068	0.760	0.000	0.000	0.00e+00	0.00	0.00e+00	0.00
	633178.4482	−3.4147	211.9664	2.048	0.760	0.000	0.000	0.00e+00	0.00	0.00e+00	0.00
	633597.3311	−3.2644	292.2070	2.045	0.760	0.000	0.000	0.00e+00	0.00	0.00e+00	0.00
	633760.9558	−4.1752	185.1975	2.220	0.745	0.000	0.000	0.00e+00	0.00	0.00e+00	0.00
	633762.0906	−4.1752	185.1974	2.097	0.760	0.000	0.000	0.00e+00	0.00	0.00e+00	0.00
	636124.0614	−3.4004	195.1492	2.133	0.760	0.000	0.000	0.00e+00	0.00	0.00e+00	0.00
	649137.1089	−3.4919	306.9562	2.036	0.760	0.000	0.000	0.00e+00	0.00	0.00e+00	0.00
	649138.5046	−4.2063	685.5488	1.963	0.760	0.000	0.000	0.00e+00	0.00	0.00e+00	0.00
	649152.1201	−4.2237	330.2889	2.033	0.760	0.000	0.000	0.00e+00	0.00	0.00e+00	0.00
	649152.9292	−4.2237	330.2888	2.071	0.760	0.000	0.000	0.00e+00	0.00	0.00e+00	0.00
	650552.6825	−3.5168	328.4150	2.121	0.760	0.000	0.000	0.00e+00	0.00	0.00e+00	0.00
	652162.9684	−3.5482	34.6496	2.168	0.760	0.000	0.000	0.00e+00	0.00	0.00e+00	0.00
	652321.8443	−3.5438	350.6610	2.030	0.760	0.000	0.000	0.00e+00	0.00	0.00e+00	0.00
	653052.3818	−4.5832	785.4567	1.986	0.760	0.000	0.000	0.00e+00	0.00	0.00e+00	0.00
	653769.0994	−4.0359	456.8287	2.030	0.760	0.000	0.000	0.00e+00	0.00	0.00e+00	0.00
	660150.1537	−3.6361	422.1055	2.112	0.760	0.000	0.000	0.00e+00	0.00	0.00e+00	0.00
	661263.8286	−3.7614	63.1082	2.127	0.760	0.000	0.000	0.00e+00	0.00	0.00e+00	0.00
	2513742.9096	−2.6315	545.3744	2.036	0.760	0.000	0.000	0.00e+00	0.00	0.00e+00	0.00

Continued on next page

molecule	ν_{0j}^k (MHz)	$\mathcal{I}_j^k$ (nm^{2}MHz)	$E\ell_j^k$ (cm^{-1})	w_{cj}^k (MHz hPa^{-1})	n_{cj}^k	$\Delta\nu_{0j}^k$ (MHz hPa^{-1})	$n_{\Delta\nu_{0j}}^k$	δ_j^k (hPa^{-1})	$n_{\delta_j}^k$	γ_j^k (hPa^{-1})	$n_{\gamma_j}^k$
$O_2^{18}O(\nu_2)$	202329.9852	−5.9751	700.8997	2.000	0.800	0.000	0.000	0.00e+00	0.00	0.00e+00	0.00
	202854.3799	−5.6639	786.7170	2.000	0.800	0.000	0.000	0.00e+00	0.00	0.00e+00	0.00
	625288.0490	−4.9332	979.9084	2.027	0.760	0.000	0.000	0.00e+00	0.00	0.00e+00	0.00
	632137.4749	−4.9044	849.8707	2.068	0.760	0.000	0.000	0.00e+00	0.00	0.00e+00	0.00
	635776.4506	−4.8819	940.6570	2.033	0.760	0.000	0.000	0.00e+00	0.00	0.00e+00	0.00
	635928.1758	−5.0281	722.2060	2.185	0.760	0.000	0.000	0.00e+00	0.00	0.00e+00	0.00
	637047.7805	−5.0272	722.1694	2.188	0.760	0.000	0.000	0.00e+00	0.00	0.00e+00	0.00
	649088.2012	−4.8188	872.0065	2.068	0.760	0.000	0.000	0.00e+00	0.00	0.00e+00	0.00
	651149.6155	−4.8115	856.8796	2.124	0.760	0.000	0.000	0.00e+00	0.00	0.00e+00	0.00
	652824.9209	−4.8079	842.5614	2.086	0.760	0.000	0.000	0.00e+00	0.00	0.00e+00	0.00
	653326.2707	−4.7043	1004.9926	2.030	0.760	0.000	0.000	0.00e+00	0.00	0.00e+00	0.00
	658787.5784	−4.8972	978.7047	2.124	0.760	0.000	0.000	0.00e+00	0.00	0.00e+00	0.00
	659055.3845	−4.9830	727.7660	2.168	0.760	0.000	0.000	0.00e+00	0.00	0.00e+00	0.00
	659918.0986	−4.9199	999.2913	2.036	0.760	0.000	0.000	0.00e+00	0.00	0.00e+00	0.00
	661075.4086	−4.9814	727.7003	2.179	0.760	0.000	0.000	0.00e+00	0.00	0.00e+00	0.00
	661369.6259	−4.9447	1020.6632	2.121	0.760	0.000	0.000	0.00e+00	0.00	0.00e+00	0.00
$O^{18}OO$	177776.8700	−5.0823	461.6517	2.100	0.760	0.000	0.000	0.00e+00	0.00	0.00e+00	0.00
	199549.0969	−4.2310	8.3557	2.387	0.760	0.000	0.000	0.00e+00	0.00	0.00e+00	0.00
	205850.8977	−4.9231	436.3999	2.095	0.760	0.000	0.000	0.00e+00	0.00	0.00e+00	0.00
	206272.3015	−4.7160	49.1007	2.362	0.749	0.000	0.000	0.00e+00	0.00	0.00e+00	0.00
	234339.9800	−3.9213	33.9264	2.300	0.760	0.000	0.000	0.00e+00	0.00	0.00e+00	0.00
	236876.3866	−3.8722	111.7433	2.222	0.703	0.000	0.000	0.00e+00	0.00	0.00e+00	0.00
	242998.1087	−4.0241	20.9983	2.308	0.760	0.000	0.000	0.00e+00	0.00	0.00e+00	0.00
	631959.6261	−3.2692	34.9013	2.179	0.760	0.000	0.000	0.00e+00	0.00	0.00e+00	0.00
	633860.4277	−3.1310	182.4760	2.200	0.760	0.000	0.000	0.00e+00	0.00	0.00e+00	0.00
	634438.7221	−3.5196	56.1857	2.270	0.760	0.000	0.000	0.00e+00	0.00	0.00e+00	0.00
	635241.1461	−4.8127	884.2387	2.000	0.800	0.000	0.000	0.00e+00	0.00	0.00e+00	0.00
	635573.4715	−3.9449	262.2469	2.071	0.760	0.000	0.000	0.00e+00	0.00	0.00e+00	0.00
	652818.5971	−3.2296	41.7431	2.182	0.760	0.000	0.000	0.00e+00	0.00	0.00e+00	0.00
	653357.8186	−4.0626	412.4078	2.071	0.760	0.000	0.000	0.00e+00	0.00	0.00e+00	0.00
	659110.3746	−3.5565	552.8475	2.001	0.760	0.000	0.000	0.00e+00	0.00	0.00e+00	0.00
	660762.6847	−4.7294	851.6061	1.986	0.760	0.000	0.000	0.00e+00	0.00	0.00e+00	0.00
	660877.3393	−3.9272	246.3322	2.074	0.760	0.000	0.000	0.00e+00	0.00	0.00e+00	0.00

Continued on next page

molecule	ν_{0j}^k (MHz)	$\mathcal{I}_j^k$ (nm^2MHz)	$E\ell_j^k$ (cm^{-1})	u_{cj}^k (MHz hPa^{-1})	n_{cj}^k	$\Delta\nu_{0j}^k$ (MHz hPa^{-1})	$n_{\Delta\nu_{0j}}^k$	δ_j^k (hPa^{-1})	$n_{\delta_j}^k$	γ_j^k (hPa^{-1})	$n_{\gamma_j}^k$
	661047.7728	−3.1003	218.7333	2.177	0.760	0.000	0.000	0.00e+00	0.00	0.00e+00	0.00
	2510299.3261	−2.7649	625.1990	2.051	0.760	0.000	0.000	0.00e+00	0.00	0.00e+00	0.00
	2513320.8019	−2.5407	510.3609	2.033	0.760	0.000	0.000	0.00e+00	0.00	0.00e+00	0.00
	2535208.0603	−2.8015	649.4622	2.051	0.760	0.000	0.000	0.00e+00	0.00	0.00e+00	0.00
	2542168.8045	−3.0705	788.8491	2.004	0.760	0.000	0.000	0.00e+00	0.00	0.00e+00	0.00
	2543721.7419	−3.4438	975.0917	1.951	0.760	0.000	0.000	0.00e+00	0.00	0.00e+00	0.00
$O^{18}OO(\nu_2)$	200319.5404	−5.6398	686.3190	2.000	0.800	0.000	0.000	0.00e+00	0.00	0.00e+00	0.00
	201803.3743	−5.3618	764.1583	2.000	0.800	0.000	0.000	0.00e+00	0.00	0.00e+00	0.00
	633034.3066	−4.5423	859.8457	2.200	0.760	0.000	0.000	0.00e+00	0.00	0.00e+00	0.00
	659555.3155	−4.5120	895.9494	2.177	0.760	0.000	0.000	0.00e+00	0.00	0.00e+00	0.00
	659643.0706	−4.6332	719.8269	2.182	0.760	0.000	0.000	0.00e+00	0.00	0.00e+00	0.00
$^{32}SO_2$	179006.1051	−4.9879	13.2258	3.234	0.500	0.000	0.000	0.00e+00	0.00	0.00e+00	0.00
	179560.9541	−4.0944	269.2654	3.234	0.500	0.000	0.000	0.00e+00	0.00	0.00e+00	0.00
	180045.2785	−3.8586	204.1386	3.234	0.500	0.000	0.000	0.00e+00	0.00	0.00e+00	0.00
	182705.8900	−3.5192	64.6273	3.234	0.500	0.000	0.000	0.00e+00	0.00	0.00e+00	0.00
	183582.7100	−4.2184	380.9500	3.234	0.500	0.000	0.000	0.00e+00	0.00	0.00e+00	0.00
	184969.8000	−3.1903	138.2275	3.234	0.500	0.000	0.000	0.00e+00	0.00	0.00e+00	0.00
	185278.6000	−4.2025	44.1151	3.234	0.500	0.000	0.000	0.00e+00	0.00	0.00e+00	0.00
	199415.8756	−3.9997	253.2431	3.234	0.500	0.000	0.000	0.00e+00	0.00	0.00e+00	0.00
	200287.5300	−3.1026	203.4634	2.935	0.710	0.000	0.000	0.00e+00	0.00	0.00e+00	0.00
	200809.1800	−3.3496	84.1184	3.234	0.500	0.000	0.000	0.00e+00	0.00	0.00e+00	0.00
	203391.5500	−3.1150	41.9534	3.234	0.500	0.000	0.000	0.00e+00	0.00	0.00e+00	0.00
	203570.1500	−4.1127	361.7197	3.234	0.500	0.000	0.000	0.00e+00	0.00	0.00e+00	0.00
	204246.7598	−3.0842	118.6848	2.842	0.806	0.000	0.000	0.00e+00	0.00	0.00e+00	0.00
	204384.3000	−4.2293	38.3677	3.234	0.500	0.000	0.000	0.00e+00	0.00	0.00e+00	0.00
	205300.5700	−3.3743	41.9534	3.234	0.500	0.000	0.000	0.00e+00	0.00	0.00e+00	0.00
	234187.0526	−3.0840	272.3113	3.234	0.500	0.000	0.000	0.00e+00	0.00	0.00e+00	0.00
	235151.7201	−3.6054	5.3820	3.337	0.699	0.000	0.000	0.00e+00	0.00	0.00e+00	0.00
	236216.6848	−3.2153	82.9373	3.234	0.500	0.000	0.000	0.00e+00	0.00	0.00e+00	0.00
	237068.8700	−3.1022	57.3978	3.234	0.500	0.000	0.000	0.00e+00	0.00	0.00e+00	0.00
	244254.2177	−2.8932	57.1170	3.234	0.500	0.000	0.000	0.00e+00	0.00	0.00e+00	0.00
	245339.2295	−3.5959	235.6194	3.234	0.500	0.000	0.000	0.00e+00	0.00	0.00e+00	0.00
	245563.4226	−3.1436	42.3467	3.234	0.500	0.000	0.000	0.00e+00	0.00	0.00e+00	0.00

Continued on next page

molecule	ν_{0j}^k (MHz)	I_j^k ($\mathrm{nm^2MHz}$)	$E\ell_j^k$ ($\mathrm{cm^{-1}}$)	w_{cj}^k ($\mathrm{MHz\,hPa^{-1}}$)	n_{cj}^k	$\Delta\nu_{0j}^k$ ($\mathrm{MHz\,hPa^{-1}}$)	$n_{\Delta\nu_{0j}}^k$	δ_j^k ($\mathrm{hPa^{-1}}$)	$n_{\delta_j}^k$	γ_j^k ($\mathrm{hPa^{-1}}$)	$n_{\gamma_j}^k$
	248057.4013	−3.2160	74.6630	3.234	0.500	0.000	0.000	0.00e+00	0.00	0.00e+00	0.00
	624344.4890	−2.2371	358.8905	3.234	0.500	0.000	0.000	0.00e+00	0.00	0.00e+00	0.00
	624887.4758	−3.2265	595.6228	3.234	0.500	0.000	0.000	0.00e+00	0.00	0.00e+00	0.00
	626087.3249	−2.4460	73.5514	3.234	0.500	0.000	0.000	0.00e+00	0.00	0.00e+00	0.00
	626168.2253	−2.8578	588.0673	3.234	0.500	0.000	0.000	0.00e+00	0.00	0.00e+00	0.00
	626491.4639	−4.1158	1002.6498	3.234	0.500	0.000	0.000	0.00e+00	0.00	0.00e+00	0.00
	626809.5350	−3.5699	464.9364	3.234	0.500	0.000	0.000	0.00e+00	0.00	0.00e+00	0.00
	632193.3697	−2.3924	50.2953	3.234	0.500	0.000	0.000	0.00e+00	0.00	0.00e+00	0.00
	633349.4620	−4.2574	936.5057	3.234	0.500	0.000	0.000	0.00e+00	0.00	0.00e+00	0.00
	633791.4652	−3.1760	786.0961	3.234	0.500	0.000	0.000	0.00e+00	0.00	0.00e+00	0.00
	633849.2943	−3.5191	959.9871	3.234	0.500	0.000	0.000	0.00e+00	0.00	0.00e+00	0.00
	634782.4646	−3.9061	158.7910	3.234	0.500	0.000	0.000	0.00e+00	0.00	0.00e+00	0.00
	634898.4145	−2.4719	310.2576	3.234	0.500	0.000	0.000	0.00e+00	0.00	0.00e+00	0.00
	635127.0040	−3.2835	848.5906	3.234	0.500	0.000	0.000	0.00e+00	0.00	0.00e+00	0.00
	635324.7873	−2.7679	536.9456	3.234	0.500	0.000	0.000	0.00e+00	0.00	0.00e+00	0.00
	636086.5257	−3.6421	786.0961	3.234	0.500	0.000	0.000	0.00e+00	0.00	0.00e+00	0.00
	636090.0579	−2.9755	668.7700	3.234	0.500	0.000	0.000	0.00e+00	0.00	0.00e+00	0.00
	648381.4661	−2.6469	465.1802	3.234	0.500	0.000	0.000	0.00e+00	0.00	0.00e+00	0.00
	648694.4365	−3.6975	581.7480	3.234	0.500	0.000	0.000	0.00e+00	0.00	0.00e+00	0.00
	649052.1202	−2.8260	477.8320	3.234	0.500	0.000	0.000	0.00e+00	0.00	0.00e+00	0.00
	649236.3027	−3.1219	591.1776	3.234	0.500	0.000	0.000	0.00e+00	0.00	0.00e+00	0.00
	650796.7454	−3.2220	725.4476	3.234	0.500	0.000	0.000	0.00e+00	0.00	0.00e+00	0.00
	650861.9971	−3.9172	735.7471	3.234	0.500	0.000	0.000	0.00e+00	0.00	0.00e+00	0.00
	651299.9130	−2.3651	56.0457	3.234	0.500	0.000	0.000	0.00e+00	0.00	0.00e+00	0.00
	651306.2637	−2.5822	420.7944	3.234	0.500	0.000	0.000	0.00e+00	0.00	0.00e+00	0.00
	652529.7204	−4.1952	909.0086	3.234	0.500	0.000	0.000	0.00e+00	0.00	0.00e+00	0.00
	653109.7211	−2.6577	103.7124	3.234	0.500	0.000	0.000	0.00e+00	0.00	0.00e+00	0.00
	653882.8936	−2.5251	379.0139	3.234	0.500	0.000	0.000	0.00e+00	0.00	0.00e+00	0.00
	653928.0468	−4.1281	151.1269	3.234	0.500	0.000	0.000	0.00e+00	0.00	0.00e+00	0.00
	659079.8201	−3.6249	1029.1396	3.234	0.500	0.000	0.000	0.00e+00	0.00	0.00e+00	0.00
	659338.2952	−2.4032	269.2654	3.234	0.500	0.000	0.000	0.00e+00	0.00	0.00e+00	0.00
	659421.0105	−2.2523	401.1254	3.234	0.500	0.000	0.000	0.00e+00	0.00	0.00e+00	0.00
	659885.9532	−3.2044	492.6171	3.234	0.500	0.000	0.000	0.00e+00	0.00	0.00e+00	0.00

Continued on next page

molecule	ν_{0j}^k (MHz)	$\mathcal{I}_j^k$ (nm^{2}MHz)	$E\ell_j^k$ (cm^{-1})	w_{cj}^k (MHz hPa^{-1})	n_{cj}^k	$\Delta\nu_{0j}^k$ (MHz hPa^{-1})	$n_{\Delta\nu_{0j}}^k$	δ_j^k (hPa^{-1})	$n_{\delta_j}^k$	γ_j^k (hPa^{-1})	$n_{\gamma_j}^k$
	659898.5409	−2.3908	253.2431	3.234	0.500	0.000	0.000	0.00e+00	0.00	0.00e+00	0.00
	660472.6960	−2.3807	237.8639	2.791	0.689	0.000	0.000	0.00e+00	0.00	0.00e+00	0.00
	660918.3140	−2.3732	223.1323	2.778	0.719	0.000	0.000	0.00e+00	0.00	0.00e+00	0.00
	661332.4780	−2.3684	209.0446	3.234	0.500	0.000	0.000	0.00e+00	0.00	0.00e+00	0.00
	661510.7760	−2.5195	415.7610	3.234	0.500	0.000	0.000	0.00e+00	0.00	0.00e+00	0.00
	2509357.0265	−2.4727	925.6946	3.234	0.500	0.000	0.000	0.00e+00	0.00	0.00e+00	0.00
	2510469.9025	−3.2065	1281.1863	3.234	0.500	0.000	0.000	0.00e+00	0.00	0.00e+00	0.00
	2513384.4424	−2.7591	1065.1204	3.234	0.500	0.000	0.000	0.00e+00	0.00	0.00e+00	0.00
	2544199.8515	−2.4495	923.6210	3.234	0.500	0.000	0.000	0.00e+00	0.00	0.00e+00	0.00
$^{32}SO_2(\nu_2)$	179076.3654	−4.6649	536.5928	2.900	0.800	0.000	0.000	0.00e+00	0.00	0.00e+00	0.00
	179941.2004	−4.6168	582.4937	2.900	0.800	0.000	0.000	0.00e+00	0.00	0.00e+00	0.00
	199756.9742	−4.1645	690.5203	2.900	0.800	0.000	0.000	0.00e+00	0.00	0.00e+00	0.00
	200888.3407	−5.0387	612.7675	2.900	0.800	0.000	0.000	0.00e+00	0.00	0.00e+00	0.00
	201308.4885	−5.2245	900.4099	2.900	0.800	0.000	0.000	0.00e+00	0.00	0.00e+00	0.00
	201972.1800	−4.1561	662.2452	2.900	0.800	0.000	0.000	0.00e+00	0.00	0.00e+00	0.00
	202562.4700	−4.2016	559.6926	2.900	0.800	0.000	0.000	0.00e+00	0.00	0.00e+00	0.00
	203652.7000	−4.4163	601.7935	2.900	0.800	0.000	0.000	0.00e+00	0.00	0.00e+00	0.00
	204331.6700	−4.1674	721.3052	2.935	0.710	0.000	0.000	0.00e+00	0.00	0.00e+00	0.00
	625311.3135	−4.2735	1214.0306	2.900	0.800	0.000	0.000	0.00e+00	0.00	0.00e+00	0.00
	625933.5079	−4.2156	1185.6608	2.900	0.800	0.000	0.000	0.00e+00	0.00	0.00e+00	0.00
	632195.9831	−4.2939	592.3602	2.900	0.800	0.000	0.000	0.00e+00	0.00	0.00e+00	0.00
	634692.0861	−4.2184	962.8582	2.900	0.800	0.000	0.000	0.00e+00	0.00	0.00e+00	0.00
	637056.6346	−3.5544	828.0967	2.900	0.800	0.000	0.000	0.00e+00	0.00	0.00e+00	0.00
	648946.2944	−4.1384	1244.8781	2.900	0.800	0.000	0.000	0.00e+00	0.00	0.00e+00	0.00
	650669.2850	−3.8327	1055.7740	2.900	0.800	0.000	0.000	0.00e+00	0.00	0.00e+00	0.00
	650916.7971	−4.0407	1187.5302	2.900	0.800	0.000	0.000	0.00e+00	0.00	0.00e+00	0.00
	653385.2828	−4.2419	985.9882	2.900	0.800	0.000	0.000	0.00e+00	0.00	0.00e+00	0.00
	653711.4804	−3.9489	1132.7657	2.900	0.800	0.000	0.000	0.00e+00	0.00	0.00e+00	0.00
	658749.3593	−3.7283	621.5503	2.900	0.800	0.000	0.000	0.00e+00	0.00	0.00e+00	0.00
	659897.0724	−4.1870	1108.5524	2.900	0.800	0.000	0.000	0.00e+00	0.00	0.00e+00	0.00
	660076.5090	−3.6061	933.6227	2.900	0.800	0.000	0.000	0.00e+00	0.00	0.00e+00	0.00
	660266.8785	−3.7843	1031.0280	2.900	0.800	0.000	0.000	0.00e+00	0.00	0.00e+00	0.00
	660849.8281	−4.6033	756.3643	2.900	0.800	0.000	0.000	0.00e+00	0.00	0.00e+00	0.00

Continued on next page

molecule	ν_{0j}^k (MHz)	I_j^k (nm^2MHz)	$E\ell_j^k$ (cm^{-1})	w_{cj}^k (MHz hPa^{-1})	n_{cj}^k	$\Delta\nu_{0j}^k$ (MHz hPa^{-1})	$n_{\Delta\nu_{0j}}^k$	δ_j^k (hPa^{-1})	$n_{\delta_j}^k$	γ_j^k (hPa^{-1})	$n_{\gamma_j}^k$
	661138.2660	−4.2881	1243.0918	2.900	0.800	0.000	0.000	0.00e+00	0.00	0.00e+00	0.00
$^{34}SO_2$	184287.7358	−3.5023	29.0331	2.900	0.800	0.000	0.000	0.00e+00	0.00	0.00e+00	0.00
	201376.4835	−3.3978	41.7544	2.900	0.800	0.000	0.000	0.00e+00	0.00	0.00e+00	0.00
	203504.2123	−3.3561	83.7811	3.234	0.500	0.000	0.000	0.00e+00	0.00	0.00e+00	0.00
	204136.2298	−3.1076	41.7544	2.900	0.800	0.000	0.000	0.00e+00	0.00	0.00e+00	0.00
	204525.1791	−3.1131	95.2943	2.900	0.800	0.000	0.000	0.00e+00	0.00	0.00e+00	0.00
	624243.5693	−2.4696	309.2806	2.900	0.800	0.000	0.000	0.00e+00	0.00	0.00e+00	0.00
	624254.4853	−2.6724	462.4498	2.900	0.800	0.000	0.000	0.00e+00	0.00	0.00e+00	0.00
	626043.4993	−2.4537	82.0736	2.900	0.800	0.000	0.000	0.00e+00	0.00	0.00e+00	0.00
	632474.6378	−2.5014	337.2599	2.900	0.800	0.000	0.000	0.00e+00	0.00	0.00e+00	0.00
	633147.7364	−2.4805	318.6828	2.900	0.800	0.000	0.000	0.00e+00	0.00	0.00e+00	0.00
	634454.2164	−2.4607	300.7287	2.900	0.800	0.000	0.000	0.00e+00	0.00	0.00e+00	0.00
	635051.0139	−2.3871	55.0488	2.900	0.800	0.000	0.000	0.00e+00	0.00	0.00e+00	0.00
	635144.2269	−2.4438	283.4406	2.900	0.800	0.000	0.000	0.00e+00	0.00	0.00e+00	0.00
	636052.9909	−2.4287	266.7889	2.900	0.800	0.000	0.000	0.00e+00	0.00	0.00e+00	0.00
	636659.6978	−2.4163	250.7912	2.900	0.800	0.000	0.000	0.00e+00	0.00	0.00e+00	0.00
	637307.2949	−2.4062	235.4350	2.791	0.689	0.000	0.000	0.00e+00	0.00	0.00e+00	0.00
	648737.5970	−2.6895	103.2244	2.900	0.800	0.000	0.000	0.00e+00	0.00	0.00e+00	0.00
	650055.9800	−3.1305	588.6748	3.234	0.500	0.000	0.000	0.00e+00	0.00	0.00e+00	0.00
	652652.8650	−2.4324	91.4486	2.900	0.800	0.000	0.000	0.00e+00	0.00	0.00e+00	0.00
	652745.7910	−3.1557	593.2377	2.900	0.800	0.000	0.000	0.00e+00	0.00	0.00e+00	0.00
	653367.5968	−3.2273	722.4864	2.900	0.800	0.000	0.000	0.00e+00	0.00	0.00e+00	0.00
	658797.5170	−3.2162	490.4862	3.234	0.500	0.000	0.000	0.00e+00	0.00	0.00e+00	0.00

Id: line_data_table.tex,v 1.19 2004/02/12 00:09:46 bill Exp

Table 12.3: Molecules and lines considered for each radiometer.

R1A:118.B1LF:PT.C1-25	
O_2	118750.3430
$O_2(\nu_1)$	119039.3139
$O^{17}O$	118687.6979
	118737.7202
	118804.0320
$O^{18}O$	118759.8102
O_3	114979.2000
	118364.5000
	119277.6200
R2:190.B2LF:H2O.C1-25	
CH_3COCH_3	176754.0405
	176756.3792
	177786.1645
	177837.1126
	178874.8160
	178912.0856
	179982.9373
	179987.0518
	180005.8142
	180149.9393
	181098.1317
	181105.1070
CH_3CN	183930.8684
CH_3OH	181296.0300
	181771.0500
	183124.9773
	183853.0000
	183879.9600
HCN	177259.8176
	177261.1836
	177263.4450
H_2O	183310.1170
HNO_3	176828.3550
	177398.2186
	177834.1207
	177918.0674
	178391.8006
	178646.4767
	178822.9762
	179214.8564
	179570.4437
	179892.5122
	180035.1820
	180101.5200
	180183.6335
	180446.1425
	180625.2698
	180682.4323
	180725.3575
	180894.4179
	181084.1006
	181179.1123
	181253.3038
	181403.7376
	181537.0375
	181559.8656
	181594.4162
	181630.5718
	181654.6355
	181677.9981
	181758.0067
	181770.4400
	181772.0400
	181789.2000
	181790.8200
	181848.4498
	181927.2235
	181995.4626
	183371.1814
	183413.8725
	183867.6273
$HNO_3(\nu_7)$	179981.9689
	180264.9863
$HNO_3(\nu_9)$	181240.9944
	181262.6503
	181262.6520
	181271.8094
	181288.1016
	181288.1033
	181315.8486
	181315.8547
	181362.3790
$OC^{32}S$	182427.1956
O_3	176829.2761
	178577.0671
	180001.2900
	183967.0403
	184377.8200
$O_3(\nu_{1,3})$	177420.9586
	177915.5696
	180424.1450
	180631.7528
	182377.0023
	183854.7692
	183892.9893
$O_3(\nu_2)$	177028.2271
	178714.3385
	182180.0402
$O_3(2\nu_2)$	179922.8155
$O_2^{18}O$	181023.4500
	181090.1200
	181430.4698
	183815.9900
	184087.0920
$O^{18}OO$	177776.8700
$^{32}SO_2$	179006.1051
	179560.9541
	180045.2785
	182705.8900
	183582.7100
$^{32}SO_2(\nu_2)$	179076.3654
	179941.2004
$^{34}SO_2$	184287.7358
R2:190.B2UF:H2O.C1-25	
CH_3COCH_3	199590.9109
	199613.4146
	199635.8342
	200328.3162
	200458.8932

Continues next page

Table 12.4: Table 12.3 continued

	200627.6726		200906.6905		206743.1987
	200724.1429		200907.2946		206765.0232
	200730.8313		200911.1624		206847.1622
	200737.5084		200911.6721		206895.9348
	204271.4822	H_2O	183310.1170		206901.4468
	204464.1283	$H_2^{18}O$	203407.5200		206939.9384
	205136.7427	H_2O_2	204574.7000		206951.2528
	205138.5639	HNO_3	199548.2214		206956.7648
	205212.5450		200243.8295		207022.4627
	206138.9278		200831.2765		207095.6166
	206199.7596		200886.9849	$HNO_3(\nu_6)$	207130.3913
	207212.9118		201481.4027		207228.9863
	207261.5274		202030.4782	$HNO_3(\nu_7)$	204784.7830
CH_3CN	202320.4492		202485.9261		205066.3461
	202340.1000		202537.3283		205349.3440
	202351.4500		203004.8250		205638.8099
	202351.4500		203320.6304		205951.4550
	202355.6100		203435.6245	$HNO_3(\nu_9)$	200439.4517
CH_3OH	201072.0504		203832.1916		200439.4684
	201089.2756		204196.8195		204748.2657
	201445.4885		204337.4451		204748.2734
	205791.2813		204531.6485		206229.3526
^{35}ClO	204346.0000		204718.8340		206229.4915
	204351.6300		204838.6805		206243.0382
	204352.2200		205062.5770		206282.3452
	204356.8600		205119.7921		206297.0141
	204357.4800		205376.7458		206328.3762
	204362.5570		205611.2000		206370.8296
	204491.5050		205736.9662		206375.4431
	204491.9374		205824.7169	HO_2	200617.4700
	204493.3344		206018.7703	N_2O	200975.2600
	204497.9715		206194.7518	$N_2O(\nu_2)$	201055.2631
	205168.7432		206230.4862		201435.1295
	205175.4649		206353.9761	$OC^{32}S$	206745.1610
	205176.8563		206497.6860	O_3	199384.3602
	205177.4267		206594.6855		203352.3120
^{37}ClO	200897.3378		206627.0566		203453.1720
	200897.8638		206628.6816		206132.0490
	200902.3004		206663.1951	$O_3(\nu_{1,3})$	203881.8298
	200902.9097		206703.2186	$O_3(\nu_2)$	204958.6184

Continues next page

Table 12.5: Table 12.3 continued

	205214.0363		181098.1317		181758.0067
	206496.0360		181105.1070		181770.4400
	206504.4510	CH_3CN	183930.8684		181772.0400
$O_3(2\nu_2)$	203207.6007	CH_3OH	181296.0300		181789.2000
	205320.8744		181771.0500		181790.8200
$O_2^{18}O$	201466.8808		183124.9773		181848.4498
	202229.5092		183853.0000		181927.2235
	203997.9605		183879.9600		181995.4626
	205730.4003	HCN	177259.8176		183371.1814
$O^{18}OO$	199549.0969		177261.1836		183413.8725
	205850.8977		177263.4450		183867.6273
	206272.3015	H_2O	183310.1170	$HNO_3(\nu_7)$	179981.9689
$^{32}SO_2$	199415.8756	HNO_3	176828.3550		180264.9863
	200287.5300		177398.2186	$HNO_3(\nu_9)$	181240.9944
	200809.1800		177834.1207		181262.6503
	203391.5500		177918.0674		181262.6520
	203570.1500		178391.8006		181271.8094
	204246.7598		178646.4767		181288.1016
	204384.3000		178822.9762		181288.1033
	205300.5700		179214.8564		181315.8486
$^{32}SO_2(\nu_2)$	199756.9742		179570.4437		181315.8547
	201972.1800		179892.5122		181362.3790
	202562.4700		180035.1820	$OC^{32}S$	182427.1956
	203652.7000		180101.5200	O_3	176829.2761
	204331.6700		180183.6335		178577.0671
$^{34}SO_2$	201376.4835		180446.1425		180001.2900
	203504.2123		180625.2698		183967.0403
	204136.2298		180682.4323		184377.8200
	204525.1791		180725.3575	$O_3(\nu_{1,3})$	177420.9586
R2:190.B3LF:N2O.C1-25			180894.4179		177915.5696
CH_3COCH_3	176754.0405		181084.1006		180424.1450
	176756.3792		181179.1123		180631.7528
	177786.1645		181253.3038		182377.0023
	177837.1126		181403.7376		183854.7692
	178874.8160		181537.0375		183892.9893
	178912.0856		181559.8656	$O_3(\nu_2)$	177028.2271
	179982.9373		181594.4162		178714.3385
	179987.0518		181630.5718		182180.0402
	180005.8142		181654.6355	$O_3(2\nu_2)$	179922.8155
	180149.9393		181677.9981	$O_2^{18}O$	181023.4500

Continues next page

Table 12.6: Table 12.3 continued

	181090.1200		205791.2813		204531.6485
	181430.4698	^{35}ClO	204346.0000		204718.8340
	183815.9900		204351.6300		204838.6805
	184087.0920		204352.2200		205062.5770
$O^{18}OO$	177776.8700		204356.8600		205119.7921
$^{32}SO_2$	179006.1051		204357.4800		205376.7458
	179560.9541		204362.5570		205611.2000
	180045.2785		204491.5050		205736.9662
	182705.8900		204491.9374		205824.7169
	183582.7100		204493.3344		206018.7703
$^{32}SO_2(\nu_2)$	179076.3654		204497.9715		206194.7518
	179941.2004		205168.7432		206230.4862
$^{34}SO_2$	184287.7358		205175.4649		206353.9761
R2:190.B3UF:N2O.C1-25			205176.8563		206497.6860
CH_3COCH_3	199590.9109		205177.4267		206594.6855
	199613.4146	^{37}ClO	200897.3378		206627.0566
	199635.8342		200897.8638		206628.6816
	200328.3162		200902.3004		206663.1951
	200458.8932		200902.9097		206703.2186
	200627.6726		200906.6905		206743.1987
	200724.1429		200907.2946		206765.0232
	200730.8313		200911.1624		206847.1622
	200737.5084		200911.6721		206895.9348
	204271.4822	H_2O	183310.1170		206901.4468
	204464.1283	$H_2^{18}O$	203407.5200		206939.9384
	205136.7427	H_2O_2	204574.7000		206951.2528
	205138.5639	HNO_3	199548.2214		206956.7648
	205212.5450		200243.8295		207022.4627
	206138.9278		200831.2765		207095.6166
	206199.7596		200886.9849	$HNO_3(\nu_6)$	207130.3913
	207212.9118		201481.4027		207228.9863
	207261.5274		202030.4782	$HNO_3(\nu_7)$	204784.7830
CH_3CN	202320.4492		202485.9261		205066.3461
	202340.1000		202537.3283		205349.3440
	202351.4500		203004.8250		205638.8099
	202351.4500		203320.6304		205951.4550
	202355.6100		203435.6245	$HNO_3(\nu_9)$	200439.4517
CH_3OH	201072.0504		203832.1916		200439.4684
	201089.2756		204196.8195		204748.2657
	201445.4885		204337.4451		204748.2734

Continues next page

Table 12.7: Table 12.3 continued

	206229.3526		201972.1800		179892.5122
	206229.4915		202562.4700		180035.1820
	206243.0382		203652.7000		180101.5200
	206282.3452		204331.6700		180183.6335
	206297.0141	$^{34}SO_2$	201376.4835		180446.1425
	206328.3762		203504.2123		180625.2698
	206370.8296		204136.2298		180682.4323
	206375.4431		204525.1791		180725.3575
HO_2	200617.4700	R2:190.B4LF:HNO3.C1-25			180894.4179
N_2O	200975.2600	CH_3COCH_3	176754.0405		181084.1006
$N_2O(\nu_2)$	201055.2631		176756.3792		181179.1123
	201435.1295		177786.1645		181253.3038
$OC^{32}S$	206745.1610		177837.1126		181403.7376
O_3	199384.3602		178874.8160		181537.0375
	203352.3120		178912.0856		181559.8656
	203453.1720		179982.9373		181594.4162
	206132.0490		179987.0518		181630.5718
$O_3(\nu_{1,3})$	203881.8298		180005.8142		181654.6355
$O_3(\nu_2)$	204958.6184		180149.9393		181677.9981
	205214.0363		181098.1317		181758.0067
	206496.0360		181105.1070		181770.4400
	206504.4510	CH_3CN	183930.8684		181772.0400
$O_3(2\nu_2)$	203207.6007	CH_3OH	181296.0300		181789.2000
	205320.8744		181771.0500		181790.8200
$O_2^{18}O$	201466.8808		183124.9773		181848.4498
	202229.5092		183853.0000		181927.2235
	203997.9605		183879.9600		181995.4626
	205730.4003	HCN	177259.8176		183371.1814
$O^{18}OO$	199549.0969		177261.1836		183413.8725
	205850.8977		177263.4450		183867.6273
	206272.3015	H_2O	183310.1170	$HNO_3(\nu_7)$	179981.9689
$^{32}SO_2$	199415.8756	HNO_3	176828.3550		180264.9863
	200287.5300		177398.2186	$HNO_3(\nu_9)$	181240.9944
	200809.1800		177834.1207		181262.6503
	203391.5500		177918.0674		181262.6520
	203570.1500		178391.8006		181271.8094
	204246.7598		178646.4767		181288.1016
	204384.3000		178822.9762		181288.1033
	205300.5700		179214.8564		181315.8486
$^{32}SO_2(\nu_2)$	199756.9742		179570.4437		181315.8547

Continues next page

Table 12.8: Table 12.3 continued

	181362.3790		200730.8313		200911.1624
$OC^{32}S$	182427.1956		200737.5084		200911.6721
O_3	176829.2761		204271.4822	H_2O	183310.1170
	178577.0671		204464.1283	$H_2^{18}O$	203407.5200
	180001.2900		205136.7427	H_2O_2	204574.7000
	183967.0403		205138.5639	HNO_3	199548.2214
	184377.8200		205212.5450		200243.8295
$O_3(\nu_{1,3})$	177420.9586		206138.9278		200831.2765
	177915.5696		206199.7596		200886.9849
	180424.1450		207212.9118		201481.4027
	180631.7528		207261.5274		202030.4782
	182377.0023	CH_3CN	202320.4492		202485.9261
	183854.7692		202340.1000		202537.3283
	183892.9893		202351.4500		203004.8250
$O_3(\nu_2)$	177028.2271		202351.4500		203320.6304
	178714.3385		202355.6100		203435.6245
	182180.0402	CH_3OH	201072.0504		203832.1916
$O_3(2\nu_2)$	179922.8155		201089.2756		204196.8195
$O_2^{18}O$	181023.4500		201445.4885		204337.4451
	181090.1200		205791.2813		204531.6485
	181430.4698	^{35}ClO	204346.0000		204718.8340
	183815.9900		204351.6300		204838.6805
	184087.0920		204352.2200		205062.5770
$O^{18}OO$	177776.8700		204356.8600		205119.7921
$^{32}SO_2$	179006.1051		204357.4800		205376.7458
	179560.9541		204362.5570		205611.2000
	180045.2785		204491.5050		205736.9662
	182705.8900		204491.9374		205824.7169
	183582.7100		204493.3344		206018.7703
$^{32}SO_2(\nu_2)$	179076.3654		204497.9715		206194.7518
	179941.2004		205168.7432		206230.4862
$^{34}SO_2$	184287.7358		205175.4649		206353.9761
R2:190.B4UF:HNO3.C1-25			205176.8563		206497.6860
CH_3COCH_3	199590.9109		205177.4267		206594.6855
	199613.4146	^{37}ClO	200897.3378		206627.0566
	199635.8342		200897.8638		206628.6816
	200328.3162		200902.3004		206663.1951
	200458.8932		200902.9097		206703.2186
	200627.6726		200906.6905		206743.1987
	200724.1429		200907.2946		206765.0232

Continues next page

Table 12.9: Table 12.3 continued

	206847.1622		206504.4510	CH_3CN	183930.8684
	206895.9348	$O_3(2\nu_2)$	203207.6007	CH_3OH	181296.0300
	206901.4468		205320.8744		181771.0500
	206939.9384	$O_2^{18}O$	201466.8808		183124.9773
	206951.2528		202229.5092		183853.0000
	206956.7648		203997.9605		183879.9600
	207022.4627		205730.4003	HCN	177259.8176
	207095.6166	$O^{18}OO$	199549.0969		177261.1836
$HNO_3(\nu_6)$	207130.3913		205850.8977		177263.4450
	207228.9863		206272.3015	H_2O	183310.1170
$HNO_3(\nu_7)$	204784.7830	$^{32}SO_2$	199415.8756	HNO_3	176828.3550
	205066.3461		200287.5300		177398.2186
	205349.3440		200809.1800		177834.1207
	205638.8099		203391.5500		177918.0674
	205951.4550		203570.1500		178391.8006
$HNO_3(\nu_9)$	200439.4517		204246.7598		178646.4767
	200439.4684		204384.3000		178822.9762
	204748.2657		205300.5700		179214.8564
	204748.2734	$^{32}SO_2(\nu_2)$	199756.9742		179570.4437
	206229.3526		201972.1800		179892.5122
	206229.4915		202562.4700		180035.1820
	206243.0382		203652.7000		180101.5200
	206282.3452		204331.6700		180183.6335
	206297.0141	$^{34}SO_2$	201376.4835		180446.1425
	206328.3762		203504.2123		180625.2698
	206370.8296		204136.2298		180682.4323
	206375.4431		204525.1791		180725.3575
HO_2	200617.4700	R2:190.B5LF:CLO.C1-25			180894.4179
N_2O	200975.2600	CH_3COCH_3	176754.0405		181084.1006
$N_2O(\nu_2)$	201055.2631		176756.3792		181179.1123
	201435.1295		177786.1645		181253.3038
$OC^{32}S$	206745.1610		177837.1126		181403.7376
O_3	199384.3602		178874.8160		181537.0375
	203352.3120		178912.0856		181559.8656
	203453.1720		179982.9373		181594.4162
	206132.0490		179987.0518		181630.5718
$O_3(\nu_{1,3})$	203881.8298		180005.8142		181654.6355
$O_3(\nu_2)$	204958.6184		180149.9393		181677.9981
	205214.0363		181098.1317		181758.0067
	206496.0360		181105.1070		181770.4400

Continues next page

Table 12.10: Table 12.3 continued

	181772.0400		183815.9900		204351.6300
	181789.2000		184087.0920		204352.2200
	181790.8200	$O^{18}OO$	177776.8700		204356.8600
	181848.4498	$^{32}SO_2$	179006.1051		204357.4800
	181927.2235		179560.9541		204362.5570
	181995.4626		180045.2785		204491.5050
	183371.1814		182705.8900		204491.9374
	183413.8725		183582.7100		204493.3344
	183867.6273	$^{32}SO_2(\nu_2)$	179076.3654		204497.9715
$HNO_3(\nu_7)$	179981.9689		179941.2004		205168.7432
	180264.9863	$^{34}SO_2$	184287.7358		205175.4649
$HNO_3(\nu_9)$	181240.9944	R2:190.B5UF:CLO.C1-25			205176.8563
	181262.6503	CH_3COCH_3	199590.9109		205177.4267
	181262.6520		199613.4146	^{37}ClO	200897.3378
	181271.8094		199635.8342		200897.8638
	181288.1016		200328.3162		200902.3004
	181288.1033		200458.8932		200902.9097
	181315.8486		200627.6726		200906.6905
	181315.8547		200724.1429		200907.2946
	181362.3790		200730.8313		200911.1624
$OC^{32}S$	182427.1956		200737.5084		200911.6721
O_3	176829.2761		204271.4822	H_2O	183310.1170
	178577.0671		204464.1283	$H_2^{18}O$	203407.5200
	180001.2900		205136.7427	H_2O_2	204574.7000
	183967.0403		205138.5639	HNO_3	199548.2214
	184377.8200		205212.5450		200243.8295
$O_3(\nu_{1,3})$	177420.9586		206138.9278		200831.2765
	177915.5696		206199.7596		200886.9849
	180424.1450		207212.9118		201481.4027
	180631.7528		207261.5274		202030.4782
	182377.0023	CH_3CN	202320.4492		202485.9261
	183854.7692		202340.1000		202537.3283
	183892.9893		202351.4500		203004.8250
$O_3(\nu_2)$	177028.2271		202351.4500		203320.6304
	178714.3385		202355.6100		203435.6245
	182180.0402	CH_3OH	201072.0504		203832.1916
$O_3(2\nu_2)$	179922.8155		201089.2756		204196.8195
$O_2^{18}O$	181023.4500		201445.4885		204337.4451
	181090.1200		205791.2813		204531.6485
	181430.4698	^{35}ClO	204346.0000		204718.8340

Continues next page

Table 12.11: Table 12.3 continued

	204838.6805		206243.0382		203652.7000
	205062.5770		206282.3452		204331.6700
	205119.7921		206297.0141	$^{34}SO_2$	201376.4835
	205376.7458		206328.3762		203504.2123
	205611.2000		206370.8296		204136.2298
	205736.9662		206375.4431		204525.1791
	205824.7169	HO_2	200617.4700	R2:190.B6LF:O3.C1-25	
	206018.7703	N_2O	200975.2600	CH_3COCH_3	176754.0405
	206194.7518	$N_2O(\nu_2)$	201055.2631		176756.3792
	206230.4862		201435.1295		177786.1645
	206353.9761	$OC^{32}S$	206745.1610		177837.1126
	206497.6860	O_3	199384.3602		178874.8160
	206594.6855		203352.3120		178912.0856
	206627.0566		203453.1720		179982.9373
	206628.6816		206132.0490		179987.0518
	206663.1951	$O_3(\nu_{1,3})$	203881.8298		180005.8142
	206703.2186	$O_3(\nu_2)$	204958.6184		180149.9393
	206743.1987		205214.0363		181098.1317
	206765.0232		206496.0360		181105.1070
	206847.1622		206504.4510	CH_3CN	183930.8684
	206895.9348	$O_3(2\nu_2)$	203207.6007	CH_3OH	181296.0300
	206901.4468		205320.8744		181771.0500
	206939.9384	$O_2^{18}O$	201466.8808		183124.9773
	206951.2528		202229.5092		183853.0000
	206956.7648		203997.9605		183879.9600
	207022.4627		205730.4003	HCN	177259.8176
	207095.6166	$O^{18}OO$	199549.0969		177261.1836
$HNO_3(\nu_6)$	207130.3913		205850.8977		177263.4450
	207228.9863		206272.3015	H_2O	183310.1170
$HNO_3(\nu_7)$	204784.7830	$^{32}SO_2$	199415.8756	HNO_3	176828.3550
	205066.3461		200287.5300		177398.2186
	205349.3440		200809.1800		177834.1207
	205638.8099		203391.5500		177918.0674
	205951.4550		203570.1500		178391.8006
$HNO_3(\nu_9)$	200439.4517		204246.7598		178646.4767
	200439.4684		204384.3000		178822.9762
	204748.2657		205300.5700		179214.8564
	204748.2734	$^{32}SO_2(\nu_2)$	199756.9742		179570.4437
	206229.3526		201972.1800		179892.5122
	206229.4915		202562.4700		180035.1820

Continues next page

Table 12.12: Table 12.3 continued

	180101.5200	O_3	176829.2761		204271.4822
	180183.6335		178577.0671		204464.1283
	180446.1425		180001.2900		205136.7427
	180625.2698		183967.0403		205138.5639
	180682.4323		184377.8200		205212.5450
	180725.3575	$O_3(\nu_{1,3})$	177420.9586		206138.9278
	180894.4179		177915.5696		206199.7596
	181084.1006		180424.1450		207212.9118
	181179.1123		180631.7528		207261.5274
	181253.3038		182377.0023	CH_3CN	202320.4492
	181403.7376		183854.7692		202340.1000
	181537.0375		183892.9893		202351.4500
	181559.8656	$O_3(\nu_2)$	177028.2271		202351.4500
	181594.4162		178714.3385		202355.6100
	181630.5718		182180.0402	CH_3OH	201072.0504
	181654.6355	$O_3(2\nu_2)$	179922.8155		201089.2756
	181677.9981	$O_2^{18}O$	181023.4500		201445.4885
	181758.0067		181090.1200		205791.2813
	181770.4400		181430.4698	^{35}ClO	204346.0000
	181772.0400		183815.9900		204351.6300
	181789.2000		184087.0920		204352.2200
	181790.8200	$O^{18}OO$	177776.8700		204356.8600
	181848.4498	$^{32}SO_2$	179006.1051		204357.4800
	181927.2235		179560.9541		204362.5570
	181995.4626		180045.2785		204491.5050
	183371.1814		182705.8900		204491.9374
	183413.8725		183582.7100		204493.3344
	183867.6273	$^{32}SO_2(\nu_2)$	179076.3654		204497.9715
$HNO_3(\nu_7)$	179981.9689		179941.2004		205168.7432
	180264.9863	$^{34}SO_2$	184287.7358		205175.4649
$HNO_3(\nu_9)$	181240.9944	R2:190.B6UF:O3.C1-25			205176.8563
	181262.6503	CH_3COCH_3	199590.9109		205177.4267
	181262.6520		199613.4146	^{37}ClO	200897.3378
	181271.8094		199635.8342		200897.8638
	181288.1016		200328.3162		200902.3004
	181288.1033		200458.8932		200902.9097
	181315.8486		200627.6726		200906.6905
	181315.8547		200724.1429		200907.2946
	181362.3790		200730.8313		200911.1624
$OC^{32}S$	182427.1956		200737.5084		200911.6721

Continues next page

Table 12.13: Table 12.3 continued

H_2O	183310.1170		206901.4468		205320.8744
$H_2^{18}O$	203407.5200		206939.9384	$O_2^{18}O$	201466.8808
H_2O_2	204574.7000		206951.2528		202229.5092
HNO_3	199548.2214		206956.7648		203997.9605
	200243.8295		207022.4627		205730.4003
	200831.2765		207095.6166	$O^{18}OO$	199549.0969
	200886.9849	$HNO_3(\nu_6)$	207130.3913		205850.8977
	201481.4027		207228.9863		206272.3015
	202030.4782	$HNO_3(\nu_7)$	204784.7830	$^{32}SO_2$	199415.8756
	202485.9261		205066.3461		200287.5300
	202537.3283		205349.3440		200809.1800
	203004.8250		205638.8099		203391.5500
	203320.6304		205951.4550		203570.1500
	203435.6245	$HNO_3(\nu_9)$	200439.4517		204246.7598
	203832.1916		200439.4684		204384.3000
	204196.8195		204748.2657		205300.5700
	204337.4451		204748.2734	$^{32}SO_2(\nu_2)$	199756.9742
	204531.6485		206229.3526		201972.1800
	204718.8340		206229.4915		202562.4700
	204838.6805		206243.0382		203652.7000
	205062.5770		206282.3452		204331.6700
	205119.7921		206297.0141	$^{34}SO_2$	201376.4835
	205376.7458		206328.3762		203504.2123
	205611.2000		206370.8296		204136.2298
	205736.9662		206375.4431		204525.1791
	205824.7169	HO_2	200617.4700	R3:240.B7LF:O3.C1-25	
	206018.7703	N_2O	200975.2600	CO	230538.0000
	206194.7518	$N_2O(\nu_2)$	201055.2631	HNO_3	230012.5652
	206230.4862		201435.1295		231627.3370
	206353.9761	$OC^{32}S$	206745.1610		231661.0304
	206497.6860	O_3	199384.3602		231694.3543
	206594.6855		203352.3120		231730.5651
	206627.0566		203453.1720		231777.6757
	206628.6816		206132.0490		231862.6453
	206663.1951	$O_3(\nu_{1,3})$	203881.8298		232050.6553
	206703.2186	$O_3(\nu_2)$	204958.6184		232178.5970
	206743.1987		205214.0363		235167.5730
	206765.0232		206496.0360		236148.0695
	206847.1622		206504.4510	$O^{18}O$	233946.1790
	206895.9348	$O_3(2\nu_2)$	203207.6007	O_3	229575.0227

Continues next page

Table 12.14: Table 12.3 continued

	231281.4919
	232986.7731
	235709.8400
	237146.1921
$O_3(\nu_{1,3})$	231990.9848
	234355.3078
	234557.5814
	236067.7980
	237314.4297
$O_3(\nu_2)$	235867.6556
$O_2^{18}O$	232525.0900
	232723.6689
	233351.1600
	234056.0600
	234183.6000
	235082.0900
	236620.9400
$O^{18}OO$	234339.9800
	236876.3866
$^{32}SO_2$	234187.0526
	235151.7201
	236216.6848
	237068.8700
R3:240.B7UF:O3.C1-25	
HNO_3	244142.8772
	244176.3496
	244209.1879
	244244.0750
	244287.0548
	244356.1585
	244369.9016
	244513.3716
	244528.0770
	244731.9485
	246093.7146
	247810.6065
O_3	242318.7357
	243453.7000
	244145.6952
	244158.0400
	247761.7700
	248183.3800
	249788.6000
$O_3(\nu_{1,3})$	243063.5194
	244217.2315
	244404.1242
	248720.8421
$O_3(\nu_2)$	243382.3207
	246512.6283
	246551.3991
$O_2^{18}O$	244355.1638
	245795.8877
	248321.2300
$O^{18}OO$	242998.1087
$^{32}SO_2$	244254.2177
	245339.2295
	245563.4226
	248057.4013
R3:240.B8LF:PT.C1-25	
CO	230538.0000
HNO_3	230012.5652
	231627.3370
	231661.0304
	231694.3543
	231730.5651
	231777.6757
	231862.6453
	232050.6553
	232178.5970
	235167.5730
	236148.0695
$O^{18}O$	233946.1790
O_3	229575.0227
	231281.4919
	232986.7731
	235709.8400
	237146.1921
$O_3(\nu_{1,3})$	231990.9848
	234355.3078
	234557.5814
	236067.7980
	237314.4297
$O_3(\nu_2)$	235867.6556
$O_2^{18}O$	232525.0900
	232723.6689
	233351.1600
	234056.0600
	234183.6000
	235082.0900
	236620.9400
$O^{18}OO$	234339.9800
	236876.3866
$^{32}SO_2$	234187.0526
	235151.7201
	236216.6848
	237068.8700
R3:240.B8UF:PT.C1-25	
HNO_3	244142.8772
	244176.3496
	244209.1879
	244244.0750
	244287.0548
	244356.1585
	244369.9016
	244513.3716
	244528.0770
	244731.9485
	246093.7146
	247810.6065
O_3	242318.7357
	243453.7000
	244145.6952
	244158.0400
	247761.7700
	248183.3800
	249788.6000
$O_3(\nu_{1,3})$	243063.5194
	244217.2315
	244404.1242
	248720.8421

Continues next page

Table 12.15: Table 12.3 continued

$O_3(\nu_2)$	243382.3207
	246512.6283
	246551.3991
$O_2^{18}O$	244355.1638
	245795.8877
	248321.2300
$O^{18}OO$	242998.1087
$^{32}SO_2$	244254.2177
	245339.2295
	245563.4226
	248057.4013
R3:240.B9LF:CO.C1-25	
CO	230538.0000
HNO_3	230012.5652
	231627.3370
	231661.0304
	231694.3543
	231730.5651
	231777.6757
	231862.6453
	232050.6553
	232178.5970
	235167.5730
	236148.0695
$O^{18}O$	233946.1790
O_3	229575.0227
	231281.4919
	232986.7731
	235709.8400
	237146.1921
$O_3(\nu_{1,3})$	231990.9848
	234355.3078
	234557.5814
	236067.7980
	237314.4297
$O_3(\nu_2)$	235867.6556
$O_2^{18}O$	232525.0900
	232723.6689
	233351.1600
	234056.0600
	234183.6000
	235082.0900
	236620.9400
$O^{18}OO$	234339.9800
	236876.3866
$^{32}SO_2$	234187.0526
	235151.7201
	236216.6848
	237068.8700
R3:240.B9UF:CO.C1-25	
HNO_3	244142.8772
	244176.3496
	244209.1879
	244244.0750
	244287.0548
	244356.1585
	244369.9016
	244513.3716
	244528.0770
	244731.9485
	246093.7146
	247810.6065
O_3	242318.7357
	243453.7000
	244145.6952
	244158.0400
	247761.7700
	248183.3800
	249788.6000
$O_3(\nu_{1,3})$	243063.5194
	244217.2315
	244404.1242
	248720.8421
$O_3(\nu_2)$	243382.3207
	246512.6283
	246551.3991
$O_2^{18}O$	244355.1638
	245795.8877
	248321.2300
$O^{18}OO$	242998.1087
$^{32}SO_2$	244254.2177
	245339.2295
	245563.4226
	248057.4013
R4:640.B10LF:CLO.C1-25	
CH_3COCH_3	634437.0853
	634492.7001
	634547.1516
	634563.6259
	634628.0619
	634683.3872
	634873.3676
	635224.7746
	635249.0050
	635352.9646
	635387.6431
	635407.4553
	635728.3277
	635750.0632
	636302.1082
	636322.9889
	637011.5617
	637085.4436
	637160.5773
	637216.4495
	637289.5615
	637402.7158
$CH_3^{35}Cl$	636288.1819
	636288.8365
	636288.8439
	636449.0467
	636449.5669
	636591.1990
	636591.5976
	636714.5472
	636714.5705
	636714.8377
	636714.8650
	636819.0577
	636819.2426

Continues next page

Table 12.16: Table 12.3 continued

	636819.2783		635432.1434		635763.7172
	636904.6166		635439.0872		636396.0542
	636904.6553		635546.7294		636396.6046
	636904.7673		636414.7874		636396.7385
	636971.2472		636423.7620		636396.8567
	636971.3213		636850.0072		636997.5285
	637018.8285		637192.8717		636997.9465
	637018.8590		637234.7106		636998.0732
	637018.8763		637259.9950		636999.1116
	637018.9108		637267.8610		636999.8142
	637047.4014		637269.3732		637000.8255
	637047.4075	$HNO_3(\nu_6)$	635000.3006	$O^{17}OO$	634713.6891
	637047.4516		637042.0547		634713.7493
	637047.4617	$HNO_3(\nu_7)$	634677.0351		634713.8846
	637056.9255		635859.0265	$O_2^{18}O$	636124.0614
	637056.9275		636220.2437	$O_2^{18}O(\nu_2)$	635776.4506
	637056.9784		636481.7563		635928.1758
	637056.9804	$HNO_3(\nu_8)$	636311.7392		637047.7805
CH_3OH	636238.2680	$HNO_3(\nu_9)$	636191.9062	$O^{18}OO$	634438.7221
	636259.8546		636194.7659		635241.1461
	636263.3859		636209.1040		635573.4715
	636264.0656		636211.9636	$^{32}SO_2$	634782.4646
	636274.0770		636219.6352		634898.4145
	636279.9980		636219.6427		635127.0040
	636287.1936		636572.6435		635324.7873
	636290.7110		636572.7197		636086.5257
	636304.3550	$HO^{35}Cl$	635870.0222		636090.0579
	636311.6900	$HO^{37}Cl$	634788.5280	$^{32}SO_2(\nu_2)$	634692.0861
	636333.4700	HO_2	636598.8986		637056.6346
	636337.4190		636602.4359	$^{34}SO_2$	634454.2164
	636363.8430	O_3	634461.7341		635051.0139
	636366.2480		634519.7678		635144.2269
	636393.5680	$O_3(\nu_{1,3})$	635316.5654		636052.9909
	636420.2310		636672.3675		636659.6978
H_2O	556936.0020	$O_3(2\nu_2)$	636155.1303		637307.2949
	620700.8070	$O_3(\nu_{1,3}+\nu_2)$	634988.3326	R4:640.B10UF:CLO.C1-25	
	645766.0100		636266.8508	^{81}BrO	650175.8041
	645905.6200	$O_2^{17}O$	635763.2268		650177.2087
	752033.2270		635763.4934		650177.7979
HNO_3	635089.2789		635763.6269		650178.6151

Continues next page

Table 12.17: Table 12.3 continued

	650179.0310		620700.8070		650595.2013
	650179.4142		645766.0100		650599.5548
	650180.4285		645905.6200		650795.8109
	650181.3811		752033.2270		650796.1034
CH_3COCH_3	648392.1602	$H_2^{32}S$	650374.1860	O_3	650732.9663
	648415.1283	HNO_3	648337.4208	$O_3(\nu_{1,3})$	648890.8087
	648422.7222		648916.5334		650510.8450
	648460.4078		649032.1913		650978.7020
	648611.4259		650287.6161		650983.0165
	648615.8408		650483.0066		651225.6634
	648777.1645		650582.7236	$O_3(\nu_2)$	648489.8807
	648797.2636		650713.1148		651192.8448
	648828.6017	$HNO_3(\nu_6)$	648400.5846		651250.7562
	648881.4045		650614.5741	$O_3(\nu_{1,3}+\nu_2)$	649584.2351
	649006.4714	$HNO_3(\nu_7)$	649411.2209		650111.6106
	649058.5459		649774.3276	$O_2^{17}O$	648373.6161
	649126.1157		650184.0758		648373.9670
	649235.1963		650927.7925		648373.9787
	649400.6346		651027.2113		648374.0518
	649837.4307		651079.3631		648374.0615
	650552.8406		651171.0657		649275.2349
	650675.5449	$HNO_3(\nu_8)$	649634.7465		649275.6618
	651301.5484		650859.1985		649275.8339
^{35}ClO	649445.0400	$HNO_3(\nu_9)$	648486.9195		649970.1201
	649445.0400		648694.6807		649970.4631
	649445.0400		648694.6974		649970.6726
	649445.0400		649728.3300		649970.7157
	649451.1700		650018.9228		649970.7749
	649451.1700		650021.6410		649981.3999
	649451.1700		650199.9431		649981.6061
	649451.1700		650303.8379		650010.5882
	650628.9967	$HO^{35}Cl$	648618.0026		650010.8169
	650629.1177	HO_2	648613.8526		650042.5398
	650629.3322		648617.4877		650042.7459
	650629.8570		649701.4773		650159.5639
	651298.1297		649701.5134		650159.7719
	651298.7393		650426.8147		650159.9428
	651298.9924		650426.8484		650167.9240
	651299.1048		650575.0063		650334.5414
H_2O	556936.0020		650575.0245		650334.7582

Continues next page

Table 12.18: Table 12.3 continued

650334.9084		651089.4900		649236.3027
650335.0010		651089.6032		650796.7454
650335.0448		651089.6136		650861.9971
650335.0478		651089.6387		651299.9130
650461.4706		651174.7048		651306.2637
650461.6905		651175.1442	$^{32}SO_2(\nu_2)$	648946.2944
650496.9314		651175.4069		650669.2850
650497.4014		651175.4728		650916.7971
650497.6139		651175.5281	$^{34}SO_2$	648737.5970
650523.9865		651175.5403		650055.9800
650524.2255		651246.0665	R4:640.B11LF:BRO.C1-25	
650524.3879		651246.4343	CH_3COCH_3	634437.0853
650524.4849		651246.6651		634492.7001
650524.5238		651246.7791		634547.1516
650524.5270		651246.7843		634563.6259
650720.4274		651246.8152		634628.0619
650720.6912	$O^{17}OO$	648791.8277		634683.3872
650720.8672		648791.8712		634873.3676
650720.9691		648792.1789		635224.7746
650721.0000		648792.2674		635249.0050
650721.0095		648792.3892		635352.9646
650857.0769		648792.4291		635387.6431
650857.0860		649794.7104		635407.4553
650857.1135		649794.9197		635728.3277
650889.0320		650605.6360		635750.0632
650889.4268		650605.8348		636302.1082
650889.6667		650605.8560		636322.9889
650889.7352		651273.7164		637011.5617
650889.7877		651273.7186		637085.4436
650911.7313		651273.7536		637160.5773
650912.0235	$O_2^{18}O$	649137.1089		637216.4495
650912.2151		649138.5046		637289.5615
650912.3224		649152.1201		637402.7158
650912.3442		649152.9292	$CH_3^{35}Cl$	636288.1819
650912.3608		650552.6825		636288.8365
650951.1646	$O_2^{18}O(\nu_2)$	649088.2012		636288.8439
650951.2825		651149.6155		636449.0467
650951.4690	$^{32}SO_2$	648381.4661		636449.5669
651088.9544		648694.4365		636591.1990
651089.2805		649052.1202		636591.5976

Continues next page

Table 12.19: Table 12.3 continued

	636714.5472	H_2O	556936.0020	$O_3(2\nu_2)$	636155.1303
	636714.5705		620700.8070	$O_3(\nu_{1,3}+\nu_2)$	634988.3326
	636714.8377		645766.0100		636266.8508
	636714.8650		645905.6200	$O_2^{17}O$	635763.2268
	636819.0577		752033.2270		635763.4934
	636819.2426	HNO_3	635089.2789		635763.6269
	636819.2783		635432.1434		635763.7172
	636904.6166		635439.0872		636396.0542
	636904.6553		635546.7294		636396.6046
	636904.7673		636414.7874		636396.7385
	636971.2472		636423.7620		636396.8567
	636971.3213		636850.0072		636997.5285
	637018.8285		637192.8717		636997.9465
	637018.8590		637234.7106		636998.0732
	637018.8763		637259.9950		636999.1116
	637018.9108		637267.8610		636999.8142
	637047.4014		637269.3732		637000.8255
	637047.4075	$HNO_3(\nu_6)$	635000.3006	$O^{17}OO$	634713.6891
	637047.4516		637042.0547		634713.7493
	637047.4617	$HNO_3(\nu_7)$	634677.0351		634713.8846
	637056.9255		635859.0265	$O_2^{18}O$	636124.0614
	637056.9275		636220.2437	$O_2^{18}O(\nu_2)$	635776.4506
	637056.9784		636481.7563		635928.1758
	637056.9804	$HNO_3(\nu_8)$	636311.7392		637047.7805
CH_3OH	636238.2680	$HNO_3(\nu_9)$	636191.9062	$O^{18}OO$	634438.7221
	636259.8546		636194.7659		635241.1461
	636263.3859		636209.1040		635573.4715
	636264.0656		636211.9636	$^{32}SO_2$	634782.4646
	636274.0770		636219.6352		634898.4145
	636279.9980		636219.6427		635127.0040
	636287.1936		636572.6435		635324.7873
	636290.7110		636572.7197		636086.5257
	636304.3550	$HO^{35}Cl$	635870.0222		636090.0579
	636311.6900	$HO^{37}Cl$	634788.5280	$^{32}SO_2(\nu_2)$	634692.0861
	636333.4700	HO_2	636598.8986		637056.6346
	636337.4190		636602.4359	$^{34}SO_2$	634454.2164
	636363.8430	O_3	634461.7341		635051.0139
	636366.2480		634519.7678		635144.2269
	636393.5680	$O_3(\nu_{1,3})$	635316.5654		636052.9909
	636420.2310		636672.3675		636659.6978

Continues next page

Table 12.20: Table 12.3 continued

	637307.2949		650629.8570		649701.4773
R4:640.B11UF:BRO.C1-25			651298.1297		649701.5134
^{81}BrO	650175.8041		651298.7393		650426.8147
	650177.2087		651298.9924		650426.8484
	650177.7979		651299.1048		650575.0063
	650178.6151	H_2O	556936.0020		650575.0245
	650179.0310		620700.8070		650595.2013
	650179.4142		645766.0100		650599.5548
	650180.4285		645905.6200		650795.8109
	650181.3811		752033.2270		650796.1034
CH_3COCH_3	648392.1602	$H_2^{32}S$	650374.1860	O_3	650732.9663
	648415.1283	HNO_3	648337.4208	$O_3(\nu_{1,3})$	648890.8087
	648422.7222		648916.5334		650510.8450
	648460.4078		649032.1913		650978.7020
	648611.4259		650287.6161		650983.0165
	648615.8408		650483.0066		651225.6634
	648777.1645		650582.7236	$O_3(\nu_2)$	648489.8807
	648797.2636		650713.1148		651192.8448
	648828.6017	$HNO_3(\nu_6)$	648400.5846		651250.7562
	648881.4045		650614.5741	$O_3(\nu_{1,3}+\nu_2)$	649584.2351
	649006.4714	$HNO_3(\nu_7)$	649411.2209		650111.6106
	649058.5459		649774.3276	$O_2^{17}O$	648373.6161
	649126.1157		650184.0758		648373.9670
	649235.1963		650927.7925		648373.9787
	649400.6346		651027.2113		648374.0518
	649837.4307		651079.3631		648374.0615
	650552.8406		651171.0657		649275.2349
	650675.5449	$HNO_3(\nu_8)$	649634.7465		649275.6618
	651301.5484		650859.1985		649275.8339
^{35}ClO	649445.0400	$HNO_3(\nu_9)$	648486.9195		649970.1201
	649445.0400		648694.6807		649970.4631
	649445.0400		648694.6974		649970.6726
	649445.0400		649728.3300		649970.7157
	649451.1700		650018.9228		649970.7749
	649451.1700		650021.6410		649981.3999
	649451.1700		650199.9431		649981.6061
	649451.1700		650303.8379		650010.5882
	650628.9967	$HO^{35}Cl$	648618.0026		650010.8169
	650629.1177	HO_2	648613.8526		650042.5398
	650629.3322		648617.4877		650042.7459

Continues next page

Table 12.21: Table 12.3 continued

650159.5639		650912.3608		650552.6825
650159.7719		650951.1646	$O_2^{18}O(\nu_2)$	649088.2012
650159.9428		650951.2825		651149.6155
650167.9240		650951.4690	$^{32}SO_2$	648381.4661
650334.5414		651088.9544		648694.4365
650334.7582		651089.2805		649052.1202
650334.9084		651089.4900		649236.3027
650335.0010		651089.6032		650796.7454
650335.0448		651089.6136		650861.9971
650335.0478		651089.6387		651299.9130
650461.4706		651174.7048		651306.2637
650461.6905		651175.1442	$^{32}SO_2(\nu_2)$	648946.2944
650496.9314		651175.4069		650669.2850
650497.4014		651175.4728		650916.7971
650497.6139		651175.5281	$^{34}SO_2$	648737.5970
650523.9865		651175.5403		650055.9800
650524.2255		651246.0665	R4:640.B12LF:N2O.C1-25	
650524.3879		651246.4343	CH_3COCH_3	632212.0287
650524.4849		651246.6651		632212.0378
650524.5238		651246.7791		632216.8170
650524.5270		651246.7843		632243.7575
650720.4274		651246.8152		632637.0342
650720.6912	$O^{17}OO$	648791.8277		632664.6671
650720.8672		648791.8712		632678.7391
650720.9691		648792.1789		632700.6596
650721.0000		648792.2674		632826.7957
650721.0095		648792.3892		632847.4916
650857.0769		648792.4291		632866.7451
650857.0860		649794.7104		632927.1414
650857.1135		649794.9197		633168.1041
650889.0320		650605.6360		633197.7241
650889.4268		650605.8348		633374.8170
650889.6667		650605.8560		633385.4845
650889.7352		651273.7164	H_2O	556936.0020
650889.7877		651273.7186		620700.8070
650911.7313		651273.7536		645766.0100
650912.0235	$O_2^{18}O$	649137.1089		645905.6200
650912.2151		649138.5046		752033.2270
650912.3224		649152.1201	HNO_3	631750.8291
650912.3442		649152.9292		631759.4840

Continues next page

Table 12.22: Table 12.3 continued

	631766.8126		632558.8404	$O_3(\nu_{1,3}+\nu_2)$	631929.2002
	631770.0138		632649.6401	$O_2^{17}O$	631902.3885
	631774.1257		632666.5927		631902.6927
	631782.6466		632773.4467		631902.8045
	631794.4115		632877.8473		631902.9204
	631811.6338		632978.4548	$O^{17}OO$	633130.4022
	631837.6664		633074.1444		633130.7602
	631858.1117		633163.9080	$O_2^{18}O$	631775.2923
	631877.4590		633246.8274		633178.4482
	631896.3016		633322.0509		633597.3311
	631938.8027		633388.7783		633760.9558
	632034.8446		633525.1451		633762.0906
	632148.8480		633565.4857	$O_2^{18}O(\nu_2)$	632137.4749
	632189.1235		633909.2417	$O^{18}OO$	631959.6261
	632219.7624	$HNO_3(\nu_7)$	632721.5576		633860.4277
	632360.1195		632799.0808	$O^{18}OO(\nu_2)$	633034.3066
	632448.0967		632826.1549	$^{32}SO_2$	632193.3697
	632535.8512		633190.7436		633349.4620
	632597.8138	$HNO_3(\nu_9)$	632080.5403		633791.4652
	632844.6590		632137.3061		633849.2943
	632876.3616		632137.3200	$^{32}SO_2(\nu_2)$	632195.9831
	632880.9913		633436.2757	$^{34}SO_2$	632474.6378
	632912.7602		633441.3435		633147.7364
	633027.6914		633600.8042	R4:640.B12UF:N2O.C1-25	
	633146.2743		633600.8219	^{79}BrO	652880.5319
	633578.8659		633826.2903		652881.8917
	633770.9327	$HO^{35}Cl$	632057.8077		652882.5651
	633825.8146	HO_2	633329.0046		652883.2781
	633829.8071		633333.7137		652883.7212
	633848.8746	O_3	632177.0500		652883.9628
	633854.1264		633352.9979		652885.0993
	633858.1189		634028.0793		652885.9708
$HNO_3(\nu_6)$	632085.0641	$O_3(\nu_{1,3})$	632833.8294	CH_3COCH_3	651716.9611
	632110.1209		632949.7372		652362.6384
	632122.1764		633243.8371		652363.3640
	632171.1923		633377.2058		652584.0251
	632253.7847		633855.9280		652891.7722
	632272.8340		634020.9595		653056.9170
	632349.2741	$O_3(\nu_2)$	631906.3437		653058.5797
	632452.1889	$O_3(2\nu_2)$	633538.2627		653082.3445

Continues next page

Table 12.23: Table 12.3 continued

	653159.1605		652935.1501	$N_2O(\nu_2)$	653089.2474
	653210.7728	$HNO_3(\nu_7)$	651874.4817	$N^{15}NO$	652787.0903
	653235.2940		652103.5264	O_3	651723.7773
	653311.8791		652331.5856		653762.5698
	653612.7817		652559.7686	$O_3(\nu_{1,3})$	652066.8398
$CH_3^{37}Cl$	652962.8523		652789.2855		652842.8928
	652963.0568		653021.5114		653417.9746
	653068.7870		653154.5640	$O_3(\nu_2)$	651819.8765
	653068.9292		653184.1016		652188.1959
	653155.5452		653258.0855		652270.6460
	653155.6365		653419.0929		653460.2649
	653223.0762		653501.0720	$O_3(\nu_{1,3}+\nu_2)$	652737.5290
	653223.1280		653753.2260		653091.9105
	653271.3230	$HNO_3(\nu_9)$	651715.2943		653606.3783
	653271.3440		651715.3606	$O_2^{17}O$	651706.3065
	653271.3581		651859.4050		651706.6745
	653271.3824		651869.7697		651706.8353
	653300.2922		651869.8196		651706.8930
	653300.2962		651870.3762		651719.2363
	653300.3289		651870.4260		651720.0848
	653300.3362		652349.5192		651721.0174
	653309.9488		652352.2394		651721.8654
	653309.9505		653867.7700		652649.3584
	653309.9877	$HO^{35}Cl$	653312.9426		652649.6139
	653309.9893	HO_2	652077.6973		653939.0769
H_2CO	653970.1550		652077.8316		653939.3493
H_2O	556936.0020		652782.0864	$O_2^{18}O$	652162.9684
	620700.8070		652782.2730		652321.8443
	645766.0100		653223.8481		653052.3818
	645905.6200		653224.0584		653769.0994
	752033.2270		653228.7041	$O_2^{18}O(\nu_2)$	652824.9209
HNO_3	651934.0981		653228.9149		653326.2707
	651940.4017	NO	651771.4200	$O^{18}OO$	652818.5971
	652156.4541		651772.9276		653357.8186
	652162.7577		651773.1484	$^{32}SO_2$	652529.7204
	652428.6213	NO_2	653126.2317		653109.7211
	652790.5934		653251.6802		653882.8936
	652899.0599		653288.4701		653928.0468
	653893.2885		653327.8563	$^{32}SO_2(\nu_2)$	653385.2828
$HNO_3(\nu_6)$	651971.6874	N_2O	652833.7897		653711.4804

Continues next page

Table 12.24: Table 12.3 continued

$^{34}SO_2$	652652.8650		626569.6534		625344.9466
	652745.7910		626588.7876		626621.9820
	653367.5968		626912.4796		626825.2410
R4:640.B13LF:HCL.C1-25			626956.9594	$HNO_3(\nu_6)$	626353.6227
^{81}BrO	624764.8570	CH_3CN	624344.0986	$HNO_3(\nu_7)$	626166.3604
	624766.3907		624344.1105		626412.1046
	624766.7040		624498.4440		626414.9281
	624767.9257		624629.1049		626653.1461
	624768.0666		624629.1122		626890.4827
	624768.8034		624736.0997		627060.8108
	624769.5930		624736.1036	$HNO_3(\nu_9)$	624314.3397
	624770.6246		624819.3430		624352.8456
CH_3COCH_3	624458.8035		624819.3430		624352.8940
	624484.1342		624819.3430		625085.6322
	624666.9312		624878.8642		625085.7032
	624670.4364		624914.5729		626452.5348
	624787.3645		624926.4775		626452.5486
	624804.9332	$CH_3^{37}Cl$	626926.9793	$HO^{35}Cl$	625074.8710
	624838.5155		626926.9977	$HO^{37}Cl$	624378.8940
	624839.9336		626927.2082	HO_2	625660.3542
	624850.8608		626927.2299		625663.7997
	624862.7086		627028.7082		626579.9359
	624867.9658		627028.8690		626587.0677
	624981.5533	CH_3OH	626626.1888		626607.4541
	625051.4489	$H^{35}Cl$	625901.6030	O_3	624480.5315
	625118.5039		625918.7560		625371.4686
	625121.9134		625932.0070		625894.7151
	625149.4917	$H^{37}Cl$	624964.3740		626397.2442
	625214.9148		624977.8210	$O_3(\nu_{1,3})$	625011.4391
	625312.5684		624988.3340		625051.2336
	625498.4002	H_2O	556936.0020		625797.9205
	625520.8596		620700.8070		626784.5400
	625778.3140		645766.0100	$O_3(\nu_2)$	625280.8257
	625799.7547		645905.6200		625324.2654
	625821.4055		752033.2270		625611.7040
	625965.5985	H_2O_2	625044.1800		625793.5621
	625988.1987		626608.9004		626654.6988
	626042.8376	$H_2^{32}S$	626474.6250		626723.5181
	626065.0045	HNO_3	624484.4450	$O_3(2\nu_2)$	624182.6861
	626307.7811		624775.5300	$O_3(\nu_{1,3}+\nu_2)$	625303.2213

Continues next page

Table 12.25: Table 12.3 continued

$O_2^{17}O$	625009.5694		625091.8080		661157.5676
	625009.7126		625563.6585		661295.7173
	625009.7872		625939.4177		661408.8233
	625010.1853	$O_2^{18}O(\nu_2)$	625288.0490		661408.8266
	625010.3980	$^{32}SO_2$	624344.4890		661496.8230
	625010.9574		624887.4758		661559.7415
	627011.8296		626087.3249		661559.7435
$O^{17}OO$	624294.2586		626168.2253		661559.7472
	625771.8878		626491.4639	^{13}CO	661067.2801
	625772.0998		626809.5350	H_2O	556936.0020
	625772.1813	$^{32}SO_2(\nu_2)$	625311.3135		620700.8070
	625782.9166		625933.5079		645766.0100
	625783.1392	$^{34}SO_2$	624243.5693		645905.6200
	625783.2331		624254.4853		752033.2270
	625783.2556		626043.4993	H_2O_2	661379.1913
	625869.5705	R4:640.B13UF:HCL.C1-25		HNO_3	658918.9445
	625869.8353	CH_3COCH_3	658736.4294		659083.5267
	625869.9452		659141.9589		659149.3708
	626087.3102		659394.5600		659157.9297
	626087.4871		659429.8682		659197.9058
	626087.5337		659458.8662		659206.8279
	626316.5749		659466.9782		659215.3868
	626316.6915		659489.6115		659610.9966
	626490.4223		659545.9211		660198.7192
	626490.6886		659573.0392		660833.4591
	626490.8207		659687.5133		661197.9981
	626490.8434		660297.3018		661204.0841
	626490.8992		660354.3088		661516.2296
	626739.7505		660416.3709	$HNO_3(\nu_6)$	658840.5959
	626740.1668		660421.6529		658921.3152
	626740.3135		660427.2895		659693.2415
	626740.3841		660584.0327		660301.0002
	626740.4437		660658.4791	$HNO_3(\nu_7)$	658726.7466
	626867.1427		660663.2810		658771.9978
	626867.4905		660899.6418		659723.0210
	626867.5992		661295.8745		659728.5791
	626867.6809		661398.7990		660087.1556
	626867.7085		661464.4956	$HNO_3(\nu_9)$	658805.1738
	626867.7442		661538.4666		659380.2908
$O_2^{18}O$	625090.4623	CH_3CN	660994.4320		660084.0947

Continues next page

Table 12.26: Table 12.3 continued

	660084.1128		660877.3393		624981.5533
$HO^{37}Cl$	661305.9426		661047.7728		625051.4489
HO_2	660115.6907	$O^{18}OO(\nu_2)$	659555.3155		625118.5039
	660115.8615		659643.0706		625121.9134
	660485.6655	$^{32}SO_2$	659079.8201		625149.4917
	660485.7114		659338.2952		625214.9148
O_3	658815.2932		659421.0105		625312.5684
	659594.8149		659885.9532		625498.4002
	660360.2258		659898.5409		625520.8596
	661458.3584		660472.6960		625778.3140
$O_3(\nu_{1,3})$	658757.9619		660918.3140		625799.7547
	659212.6286		661332.4780		625821.4055
	659465.1985		661510.7760		625965.5985
	660962.4607	$^{32}SO_2(\nu_2)$	658749.3593		625988.1987
$O_3(\nu_2)$	659091.0854		659897.0724		626042.8376
	659753.5588		660076.5090		626065.0045
$O_3(2\nu_2)$	659760.7611		660266.8785		626307.7811
	660004.8028		660849.8281		626569.6534
$O_3(\nu_{1,3}+\nu_2)$	658828.3385		661138.2660		626588.7876
	659847.7538	$^{34}SO_2$	658797.5170		626912.4796
$O_2^{17}O$	659880.6775	R4:640.B14LF:O3.C1-25			626956.9594
	659974.6147	^{81}BrO	624764.8570	CH_3CN	624344.0986
	659975.7197		624766.3907		624344.1105
	660080.3628		624766.7040		624498.4440
	660080.5427		624767.9257		624629.1049
	660238.0752		624768.0666		624629.1122
	660238.6076		624768.8034		624736.0997
	660238.7111		624769.5930		624736.1036
	660238.8557		624770.6246		624819.3430
$O^{17}OO$	661271.3080	CH_3COCH_3	624458.8035		624819.3430
	661271.5427		624484.1342		624819.3430
$O_2^{18}O$	660150.1537		624666.9312		624878.8642
	661263.8286		624670.4364		624914.5729
$O_2^{18}O(\nu_2)$	658787.5784		624787.3645		624926.4775
	659055.3845		624804.9332	$CH_3^{37}Cl$	626926.9793
	659918.0986		624838.5155		626926.9977
	661075.4086		624839.9336		626927.2082
	661369.6259		624850.8608		626927.2299
$O^{18}OO$	659110.3746		624862.7086		627028.7082
	660762.6847		624867.9658		627028.8690

Continues next page

Table 12.27: Table 12.3 continued

CH_3OH	626626.1888		626607.4541		626490.4223
$H^{35}Cl$	625901.6030	O_3	624480.5315		626490.6886
	625918.7560		625371.4686		626490.8207
	625932.0070		625894.7151		626490.8434
$H^{37}Cl$	624964.3740		626397.2442		626490.8992
	624977.8210	$O_3(\nu_{1,3})$	625011.4391		626739.7505
	624988.3340		625051.2336		626740.1668
H_2O	556936.0020		625797.9205		626740.3135
	620700.8070		626784.5400		626740.3841
	645766.0100	$O_3(\nu_2)$	625280.8257		626740.4437
	645905.6200		625324.2654		626867.1427
	752033.2270		625611.7040		626867.4905
H_2O_2	625044.1800		625793.5621		626867.5992
	626608.9004		626654.6988		626867.6809
$H_2^{32}S$	626474.6250		626723.5181		626867.7085
HNO_3	624484.4450	$O_3(2\nu_2)$	624182.6861		626867.7442
	624775.5300	$O_3(\nu_{1,3}+\nu_2)$	625303.2213	$O_2^{18}O$	625090.4623
	625344.9466	$O_2^{17}O$	625009.5694		625091.8080
	626621.9820		625009.7126		625563.6585
	626825.2410		625009.7872		625939.4177
$HNO_3(\nu_6)$	626353.6227		625010.1853	$O_2^{18}O(\nu_2)$	625288.0490
$HNO_3(\nu_7)$	626166.3604		625010.3980	$^{32}SO_2$	624344.4890
	626412.1046		625010.9574		624887.4758
	626414.9281		627011.8296		626087.3249
	626653.1461	$O^{17}OO$	624294.2586		626168.2253
	626890.4827		625771.8878		626491.4639
	627060.8108		625772.0998		626809.5350
$HNO_3(\nu_9)$	624314.3397		625772.1813	$^{32}SO_2(\nu_2)$	625311.3135
	624352.8456		625782.9166		625933.5079
	624352.8940		625783.1392	$^{34}SO_2$	624243.5693
	625085.6322		625783.2331		624254.4853
	625085.7032		625783.2556		626043.4993
	626452.5348		625869.5705	R4:640.B14UF:O3.C1-25	
	626452.5486		625869.8353	CH_3COCH_3	658736.4294
$HO^{35}Cl$	625074.8710		625869.9452		659141.9589
$HO^{37}Cl$	624378.8940		626087.3102		659394.5600
HO_2	625660.3542		626087.4871		659429.8682
	625663.7997		626087.5337		659458.8662
	626579.9359		626316.5749		659466.9782
	626587.0677		626316.6915		659489.6115

Continues next page

Table 12.28: Table 12.3 continued

	659545.9211		660198.7192		660080.3628
	659573.0392		660833.4591		660080.5427
	659687.5133		661197.9981		660238.0752
	660297.3018		661204.0841		660238.6076
	660354.3088		661516.2296		660238.7111
	660416.3709	$HNO_3(\nu_6)$	658840.5959		660238.8557
	660421.6529		658921.3152	$O^{17}OO$	661271.3080
	660427.2895		659693.2415		661271.5427
	660584.0327		660301.0002	$O_2^{18}O$	660150.1537
	660658.4791	$HNO_3(\nu_7)$	658726.7466		661263.8286
	660663.2810		658771.9978	$O_2^{18}O(\nu_2)$	658787.5784
	660899.6418		659723.0210		659055.3845
	661295.8745		659728.5791		659918.0986
	661398.7990		660087.1556		661075.4086
	661464.4956	$HNO_3(\nu_9)$	658805.1738		661369.6259
	661538.4666		659380.2908	$O^{18}OO$	659110.3746
CH_3CN	660994.4320		660084.0947		660762.6847
	661157.5676		660084.1128		660877.3393
	661295.7173	$HO^{37}Cl$	661305.9426		661047.7728
	661408.8233	HO_2	660115.6907	$O^{18}OO(\nu_2)$	659555.3155
	661408.8266		660115.8615		659643.0706
	661496.8230		660485.6655	$^{32}SO_2$	659079.8201
	661559.7415		660485.7114		659338.2952
	661559.7435	O_3	658815.2932		659421.0105
	661559.7472		659594.8149		659885.9532
^{13}CO	661067.2801		660360.2258		659898.5409
H_2O	556936.0020		661458.3584		660472.6960
	620700.8070	$O_3(\nu_{1,3})$	658757.9619		660918.3140
	645766.0100		659212.6286		661332.4780
	645905.6200		659465.1985		661510.7760
	752033.2270		660962.4607	$^{32}SO_2(\nu_2)$	658749.3593
H_2O_2	661379.1913	$O_3(\nu_2)$	659091.0854		659897.0724
HNO_3	658918.9445		659753.5588		660076.5090
	659083.5267	$O_3(2\nu_2)$	659760.7611		660266.8785
	659149.3708		660004.8028		660849.8281
	659157.9297	$O_3(\nu_{1,3}+\nu_2)$	658828.3385		661138.2660
	659197.9058		659847.7538	$^{34}SO_2$	658797.5170
	659206.8279	$O_2^{17}O$	659880.6775	R5H:2T5.B15LF:OH.C1-25	
	659215.3868		659974.6147	H_2O	2462933.0320
	659610.9966		659975.7197		2531917.8110

Continues next page

Table 12.29: Table 12.3 continued

	2547436.4782
	2567177.1320
	2630959.5200
	2640473.8360
OH	2514298.7300
	2514316.7050
	2514353.4900
$O_3(\nu_{1,3})$	2513510.4489
	2514240.3740
$O_3(\nu_2)$	2514385.5333
	2514593.0117
	2514784.7726
	2514961.5137
	2515123.9199
	2515272.6626
	2515408.4005
$O_2^{18}O$	2513742.9096
$O^{18}OO$	2513320.8019
$^{32}SO_2$	2513384.4424
R5H:2T5.B15UF:OH.C1-25	
H_2O	2462933.0320
	2531917.8110
	2547436.4782
	2567177.1320
	2630959.5200
	2640473.8360
R5H:2T5.B16LF:OH.C1-25	
H_2O	2462933.0320
	2531917.8110
	2547436.4782
	2567177.1320
	2630959.5200
	2640473.8360
HO_2	2509318.5449
	2509318.5449
	2511090.2884
	2511090.2884
OH	2509935.4400
	2509949.0100
	2509988.1500
O_3	2509560.4399
	2509611.2736
	2510614.2022
	2510875.7362
	2510933.7261
$O_3(\nu_{1,3})$	2509599.8979
$O_3(\nu_2)$	2509207.0106
	2509247.0031
$O^{18}OO$	2510299.3261
$^{32}SO_2$	2509357.0265
	2510469.9025
R5H:2T5.B16UF:OH.C1-25	
H_2O	2462933.0320
	2531917.8110
	2547436.4782
	2567177.1320
	2630959.5200
	2640473.8360
O_3	2536301.7542
$O_3(\nu_{1,3})$	2534560.2526
	2535126.4983
$O^{18}OO$	2535208.0603
R5H:2T5.B17LF:PT.C1-25	
H_2O	2462933.0320
	2531917.8110
	2547436.4782
	2567177.1320
	2630959.5200
	2640473.8360
$HO^{35}Cl$	2502016.9641
O_2	2502323.9230
O_3	2501411.4461
	2501727.5474
	2502751.7710
$O_3(\nu_2)$	2502324.3793
	2502973.9957
R5H:2T5.B17UF:PT.C1-25	
H_2O	2462933.0320
	2531917.8110
	2547436.4782
	2567177.1320
	2630959.5200
	2640473.8360
O_3	2542119.3911
	2543208.4034
$O_3(\nu_{1,3})$	2542175.6118
	2542657.8486
$O_3(\nu_2)$	2543331.2660
	2544322.6785
$O_3(2\nu_2)$	2543146.7986
$O^{18}OO$	2542168.8045
	2543721.7419
$^{32}SO_2$	2544199.8515
R5V:2T5.B18LF:OH.C1-25	
H_2O	2462933.0320
	2531917.8110
	2547436.4782
	2567177.1320
	2630959.5200
	2640473.8360
OH	2514298.7300
	2514316.7050
	2514353.4900
$O_3(\nu_{1,3})$	2513510.4489
	2514240.3740
$O_3(\nu_2)$	2514385.5333
	2514593.0117
	2514784.7726
	2514961.5137
	2515123.9199
	2515272.6626
	2515408.4005
$O_2^{18}O$	2513742.9096
$O^{18}OO$	2513320.8019
$^{32}SO_2$	2513384.4424
R5V:2T5.B18UF:OH.C1-25	
H_2O	2462933.0320
	2531917.8110
	2547436.4782
	2567177.1320

Continues next page

Table 12.30: Table 12.3 continued

	2630959.5200
	2640473.8360
R5V:2T5.B19LF:OH.C1-25	
H_2O	2462933.0320
	2531917.8110
	2547436.4782
	2567177.1320
	2630959.5200
	2640473.8360
HO_2	2509318.5449
	2509318.5449
	2511090.2884
	2511090.2884
OH	2509935.4400
	2509949.0100
	2509988.1500
O_3	2509560.4399
	2509611.2736
	2510614.2022
	2510875.7362
	2510933.7261
$O_3(\nu_{1,3})$	2509599.8979
$O_3(\nu_2)$	2509207.0106
	2509247.0031
$O^{18}OO$	2510299.3261
$^{32}SO_2$	2509357.0265
	2510469.9025
R5V:2T5.B19UF:OH.C1-25	
H_2O	2462933.0320
	2531917.8110
	2547436.4782
	2567177.1320
	2630959.5200
	2640473.8360
O_3	2536301.7542
$O_3(\nu_{1,3})$	2534560.2526
	2535126.4983
$O^{18}OO$	2535208.0603
R5V:2T5.B20LF:PT.C1-25	
H_2O	2462933.0320
	2531917.8110
	2547436.4782
	2567177.1320
	2630959.5200
	2640473.8360
$HO^{35}Cl$	2502016.9641
O_2	2502323.9230
O_3	2501411.4461
	2501727.5474
	2502751.7710
$O_3(\nu_2)$	2502324.3793
	2502973.9957
R5V:2T5.B20UF:PT.C1-25	
H_2O	2462933.0320
	2531917.8110
	2547436.4782
	2567177.1320
	2630959.5200
	2640473.8360
O_3	2542119.3911
	2543208.4034
$O_3(\nu_{1,3})$	2542175.6118
	2542657.8486
$O_3(\nu_2)$	2543331.2660
	2544322.6785
$O_3(2\nu_2)$	2543146.7986
$O^{18}OO$	2542168.8045
	2543721.7419
$^{32}SO_2$	2544199.8515
R1B:118.B21LF:PT.C1-25	
O_2	118750.3430
$O_2(\nu_1)$	119039.3139
$O^{17}O$	118687.6979
	118737.7202
	118804.0320
$O^{18}O$	118759.8102
O_3	114979.2000
	118364.5000
	119277.6200
R1A:118.B22LD:PT.C0-128	
O_2	118750.3430
$O_2(\nu_1)$	119039.3139
$O^{17}O$	118687.6979
	118737.7202
	118804.0320
$O^{18}O$	118759.8102
O_3	114979.2000
	118364.5000
	119277.6200
R2:190.B23LD:H2O.C0-128	
CH_3COCH_3	176754.0405
	176756.3792
	177786.1645
	177837.1126
	178874.8160
	178912.0856
	179982.9373
	179987.0518
	180005.8142
	180149.9393
	181098.1317
	181105.1070
CH_3CN	183930.8684
CH_3OH	181296.0300
	181771.0500
	183124.9773
	183853.0000
	183879.9600
HCN	177259.8176
	177261.1836
	177263.4450
H_2O	183310.1170
HNO_3	176828.3550
	177398.2186
	177834.1207
	177918.0674
	178391.8006
	178646.4767
	178822.9762
	179214.8564

Continues next page

Table 12.31: Table 12.3 continued

	179570.4437		181315.8547		200724.1429
	179892.5122		181362.3790		200730.8313
	180035.1820	$OC^{32}S$	182427.1956		200737.5084
	180101.5200	O_3	176829.2761		204271.4822
	180183.6335		178577.0671		204464.1283
	180446.1425		180001.2900		205136.7427
	180625.2698		183967.0403		205138.5639
	180682.4323		184377.8200		205212.5450
	180725.3575	$O_3(\nu_{1,3})$	177420.9586		206138.9278
	180894.4179		177915.5696		206199.7596
	181084.1006		180424.1450		207212.9118
	181179.1123		180631.7528		207261.5274
	181253.3038		182377.0023	CH_3CN	202320.4492
	181403.7376		183854.7692		202340.1000
	181537.0375		183892.9893		202351.4500
	181559.8656	$O_3(\nu_2)$	177028.2271		202351.4500
	181594.4162		178714.3385		202355.6100
	181630.5718		182180.0402	CH_3OH	201072.0504
	181654.6355	$O_3(2\nu_2)$	179922.8155		201089.2756
	181677.9981	$O_2^{18}O$	181023.4500		201445.4885
	181758.0067		181090.1200		205791.2813
	181770.4400		181430.4698	^{35}ClO	204346.0000
	181772.0400		183815.9900		204351.6300
	181789.2000		184087.0920		204352.2200
	181790.8200	$O^{18}OO$	177776.8700		204356.8600
	181848.4498	$^{32}SO_2$	179006.1051		204357.4800
	181927.2235		179560.9541		204362.5570
	181995.4626		180045.2785		204491.5050
	183371.1814		182705.8900		204491.9374
	183413.8725		183582.7100		204493.3344
	183867.6273	$^{32}SO_2(\nu_2)$	179076.3654		204497.9715
$HNO_3(\nu_7)$	179981.9689		179941.2004		205168.7432
	180264.9863	$^{34}SO_2$	184287.7358		205175.4649
$HNO_3(\nu_9)$	181240.9944	R2:190.B23UD:H2O.C0-128			205176.8563
	181262.6503	CH_3COCH_3	199590.9109		205177.4267
	181262.6520		199613.4146	^{37}ClO	200897.3378
	181271.8094		199635.8342		200897.8638
	181288.1016		200328.3162		200902.3004
	181288.1033		200458.8932		200902.9097
	181315.8486		200627.6726		200906.6905

Continues next page

Table 12.32: Table 12.3 continued

	200907.2946		206765.0232		206496.0360
	200911.1624		206847.1622		206504.4510
	200911.6721		206895.9348	$O_3(2\nu_2)$	203207.6007
H_2O	183310.1170		206901.4468		205320.8744
$H_2^{18}O$	203407.5200		206939.9384	$O_2^{18}O$	201466.8808
H_2O_2	204574.7000		206951.2528		202229.5092
HNO_3	199548.2214		206956.7648		203997.9605
	200243.8295		207022.4627		205730.4003
	200831.2765		207095.6166	$O^{18}OO$	199549.0969
	200886.9849	$HNO_3(\nu_6)$	207130.3913		205850.8977
	201481.4027		207228.9863		206272.3015
	202030.4782	$HNO_3(\nu_7)$	204784.7830	$^{32}SO_2$	199415.8756
	202485.9261		205066.3461		200287.5300
	202537.3283		205349.3440		200809.1800
	203004.8250		205638.8099		203391.5500
	203320.6304		205951.4550		203570.1500
	203435.6245	$HNO_3(\nu_9)$	200439.4517		204246.7598
	203832.1916		200439.4684		204384.3000
	204196.8195		204748.2657		205300.5700
	204337.4451		204748.2734	$^{32}SO_2(\nu_2)$	199756.9742
	204531.6485		206229.3526		201972.1800
	204718.8340		206229.4915		202562.4700
	204838.6805		206243.0382		203652.7000
	205062.5770		206282.3452		204331.6700
	205119.7921		206297.0141	$^{34}SO_2$	201376.4835
	205376.7458		206328.3762		203504.2123
	205611.2000		206370.8296		204136.2298
	205736.9662		206375.4431		204525.1791
	205824.7169	HO_2	200617.4700	R3:240.B24LD:O3.C0-128	
	206018.7703	N_2O	200975.2600	CO	230538.0000
	206194.7518	$N_2O(\nu_2)$	201055.2631	HNO_3	230012.5652
	206230.4862		201435.1295		231627.3370
	206353.9761	$OC^{32}S$	206745.1610		231661.0304
	206497.6860	O_3	199384.3602		231694.3543
	206594.6855		203352.3120		231730.5651
	206627.0566		203453.1720		231777.6757
	206628.6816		206132.0490		231862.6453
	206663.1951	$O_3(\nu_{1,3})$	203881.8298		232050.6553
	206703.2186	$O_3(\nu_2)$	204958.6184		232178.5970
	206743.1987		205214.0363		235167.5730

Continues next page

Table 12.33: Table 12.3 continued

	236148.0695
$O^{18}O$	233946.1790
O_3	229575.0227
	231281.4919
	232986.7731
	235709.8400
	237146.1921
$O_3(\nu_{1,3})$	231990.9848
	234355.3078
	234557.5814
	236067.7980
	237314.4297
$O_3(\nu_2)$	235867.6556
$O_2^{18}O$	232525.0900
	232723.6689
	233351.1600
	234056.0600
	234183.6000
	235082.0900
	236620.9400
$O^{18}OO$	234339.9800
	236876.3866
$^{32}SO_2$	234187.0526
	235151.7201
	236216.6848
	237068.8700
R3:240.B24UD:O3.C0-128	
HNO_3	244142.8772
	244176.3496
	244209.1879
	244244.0750
	244287.0548
	244356.1585
	244369.9016
	244513.3716
	244528.0770
	244731.9485
	246093.7146
	247810.6065
O_3	242318.7357
	243453.7000
	244145.6952
	244158.0400
	247761.7700
	248183.3800
	249788.6000
$O_3(\nu_{1,3})$	243063.5194
	244217.2315
	244404.1242
	248720.8421
$O_3(\nu_2)$	243382.3207
	246512.6283
	246551.3991
$O_2^{18}O$	244355.1638
	245795.8877
	248321.2300
$O^{18}OO$	242998.1087
$^{32}SO_2$	244254.2177
	245339.2295
	245563.4226
	248057.4013
R3:240.B25LD:CO.C0-128	
CO	230538.0000
HNO_3	230012.5652
	231627.3370
	231661.0304
	231694.3543
	231730.5651
	231777.6757
	231862.6453
	232050.6553
	232178.5970
	235167.5730
	236148.0695
$O^{18}O$	233946.1790
O_3	229575.0227
	231281.4919
	232986.7731
	235709.8400
	237146.1921
$O_3(\nu_{1,3})$	231990.9848
	234355.3078
	234557.5814
	236067.7980
	237314.4297
$O_3(\nu_2)$	235867.6556
$O_2^{18}O$	232525.0900
	232723.6689
	233351.1600
	234056.0600
	234183.6000
	235082.0900
	236620.9400
$O^{18}OO$	234339.9800
	236876.3866
$^{32}SO_2$	234187.0526
	235151.7201
	236216.6848
	237068.8700
R3:240.B25UD:CO.C0-128	
HNO_3	244142.8772
	244176.3496
	244209.1879
	244244.0750
	244287.0548
	244356.1585
	244369.9016
	244513.3716
	244528.0770
	244731.9485
	246093.7146
	247810.6065
O_3	242318.7357
	243453.7000
	244145.6952
	244158.0400
	247761.7700
	248183.3800
	249788.6000
$O_3(\nu_{1,3})$	243063.5194

Continues next page

Table 12.34: Table 12.3 continued

	244217.2315		183124.9773		181848.4498
	244404.1242		183853.0000		181927.2235
	248720.8421		183879.9600		181995.4626
$O_3(\nu_2)$	243382.3207	HCN	177259.8176		183371.1814
	246512.6283		177261.1836		183413.8725
	246551.3991		177263.4450		183867.6273
$O_2^{18}O$	244355.1638	H_2O	183310.1170	$HNO_3(\nu_7)$	179981.9689
	245795.8877	HNO_3	176828.3550		180264.9863
	248321.2300		177398.2186	$HNO_3(\nu_9)$	181240.9944
$O^{18}OO$	242998.1087		177834.1207		181262.6503
$^{32}SO_2$	244254.2177		177918.0674		181262.6520
	245339.2295		178391.8006		181271.8094
	245563.4226		178646.4767		181288.1016
	248057.4013		178822.9762		181288.1033
R1B:118.B26LD:PT.C0-128			179214.8564		181315.8486
O_2	118750.3430		179570.4437		181315.8547
$O_2(\nu_1)$	119039.3139		179892.5122		181362.3790
$O^{17}O$	118687.6979		180035.1820	$OC^{32}S$	182427.1956
	118737.7202		180101.5200	O_3	176829.2761
	118804.0320		180183.6335		178577.0671
$O^{18}O$	118759.8102		180446.1425		180001.2900
O_3	114979.2000		180625.2698		183967.0403
	118364.5000		180682.4323		184377.8200
	119277.6200		180725.3575	$O_3(\nu_{1,3})$	177420.9586
R2:190.B27LM:HCN.C1-11			180894.4179		177915.5696
CH_3COCH_3	176754.0405		181084.1006		180424.1450
	176756.3792		181179.1123		180631.7528
	177786.1645		181253.3038		182377.0023
	177837.1126		181403.7376		183854.7692
	178874.8160		181537.0375		183892.9893
	178912.0856		181559.8656	$O_3(\nu_2)$	177028.2271
	179982.9373		181594.4162		178714.3385
	179987.0518		181630.5718		182180.0402
	180005.8142		181654.6355	$O_3(2\nu_2)$	179922.8155
	180149.9393		181677.9981	$O_2^{18}O$	181023.4500
	181098.1317		181758.0067		181090.1200
	181105.1070		181770.4400		181430.4698
CH_3CN	183930.8684		181772.0400		183815.9900
CH_3OH	181296.0300		181789.2000		184087.0920
	181771.0500		181790.8200	$O^{18}OO$	177776.8700

Continues next page

Table 12.35: Table 12.3 continued

$^{32}SO_2$	179006.1051		204357.4800		205376.7458
	179560.9541		204362.5570		205611.2000
	180045.2785		204491.5050		205736.9662
	182705.8900		204491.9374		205824.7169
	183582.7100		204493.3344		206018.7703
$^{32}SO_2(\nu_2)$	179076.3654		204497.9715		206194.7518
	179941.2004		205168.7432		206230.4862
$^{34}SO_2$	184287.7358		205175.4649		206353.9761
R2:190.B27UM:HCN.C1-11			205176.8563		206497.6860
CH_3COCH_3	199590.9109		205177.4267		206594.6855
	199613.4146	^{37}ClO	200897.3378		206627.0566
	199635.8342		200897.8638		206628.6816
	200328.3162		200902.3004		206663.1951
	200458.8932		200902.9097		206703.2186
	200627.6726		200906.6905		206743.1987
	200724.1429		200907.2946		206765.0232
	200730.8313		200911.1624		206847.1622
	200737.5084		200911.6721		206895.9348
	204271.4822	H_2O	183310.1170		206901.4468
	204464.1283	$H_2^{18}O$	203407.5200		206939.9384
	205136.7427	H_2O_2	204574.7000		206951.2528
	205138.5639	HNO_3	199548.2214		206956.7648
	205212.5450		200243.8295		207022.4627
	206138.9278		200831.2765		207095.6166
	206199.7596		200886.9849	$HNO_3(\nu_6)$	207130.3913
	207212.9118		201481.4027		207228.9863
	207261.5274		202030.4782	$HNO_3(\nu_7)$	204784.7830
CH_3CN	202320.4492		202485.9261		205066.3461
	202340.1000		202537.3283		205349.3440
	202351.4500		203004.8250		205638.8099
	202351.4500		203320.6304		205951.4550
	202355.6100		203435.6245	$HNO_3(\nu_9)$	200439.4517
CH_3OH	201072.0504		203832.1916		200439.4684
	201089.2756		204196.8195		204748.2657
	201445.4885		204337.4451		204748.2734
	205791.2813		204531.6485		206229.3526
^{35}ClO	204346.0000		204718.8340		206229.4915
	204351.6300		204838.6805		206243.0382
	204352.2200		205062.5770		206282.3452
	204356.8600		205119.7921		206297.0141

Continues next page

Table 12.36: Table 12.3 continued

	206328.3762		203504.2123		636904.6166
	206370.8296		204136.2298		636904.6553
	206375.4431		204525.1791		636904.7673
HO_2	200617.4700	R4:640.B28LM:HO2.C1-11			636971.2472
N_2O	200975.2600	CH_3COCH_3	634437.0853		636971.3213
$N_2O(\nu_2)$	201055.2631		634492.7001		637018.8285
	201435.1295		634547.1516		637018.8590
$OC^{32}S$	206745.1610		634563.6259		637018.8763
O_3	199384.3602		634628.0619		637018.9108
	203352.3120		634683.3872		637047.4014
	203453.1720		634873.3676		637047.4075
	206132.0490		635224.7746		637047.4516
$O_3(\nu_{1,3})$	203881.8298		635249.0050		637047.4617
$O_3(\nu_2)$	204958.6184		635352.9646		637056.9255
	205214.0363		635387.6431		637056.9275
	206496.0360		635407.4553		637056.9784
	206504.4510		635728.3277		637056.9804
$O_3(2\nu_2)$	203207.6007		635750.0632	CH_3OH	636238.2680
	205320.8744		636302.1082		636259.8546
$O_2^{18}O$	201466.8808		636322.9889		636263.3859
	202229.5092		637011.5617		636264.0656
	203997.9605		637085.4436		636274.0770
	205730.4003		637160.5773		636279.9980
$O^{18}OO$	199549.0969		637216.4495		636287.1936
	205850.8977		637289.5615		636290.7110
	206272.3015		637402.7158		636304.3550
$^{32}SO_2$	199415.8756	$CH_3^{35}Cl$	636288.1819		636311.6900
	200287.5300		636288.8365		636333.4700
	200809.1800		636288.8439		636337.4190
	203391.5500		636449.0467		636363.8430
	203570.1500		636449.5669		636366.2480
	204246.7598		636591.1990		636393.5680
	204384.3000		636591.5976		636420.2310
	205300.5700		636714.5472	H_2O	556936.0020
$^{32}SO_2(\nu_2)$	199756.9742		636714.5705		620700.8070
	201972.1800		636714.8377		645766.0100
	202562.4700		636714.8650		645905.6200
	203652.7000		636819.0577		752033.2270
	204331.6700		636819.2426	HNO_3	635089.2789
$^{34}SO_2$	201376.4835		636819.2783		635432.1434

Continues next page

Table 12.37: Table 12.3 continued

	635439.0872		636396.0542		650179.4142
	635546.7294		636396.6046		650180.4285
	636414.7874		636396.7385		650181.3811
	636423.7620		636396.8567	CH_3COCH_3	648392.1602
	636850.0072		636997.5285		648415.1283
	637192.8717		636997.9465		648422.7222
	637234.7106		636998.0732		648460.4078
	637259.9950		636999.1116		648611.4259
	637267.8610		636999.8142		648615.8408
	637269.3732		637000.8255		648777.1645
$HNO_3(\nu_6)$	635000.3006	$O^{17}OO$	634713.6891		648797.2636
	637042.0547		634713.7493		648828.6017
$HNO_3(\nu_7)$	634677.0351		634713.8846		648881.4045
	635859.0265	$O_2^{18}O$	636124.0614		649006.4714
	636220.2437	$O_2^{18}O(\nu_2)$	635776.4506		649058.5459
	636481.7563		635928.1758		649126.1157
$HNO_3(\nu_8)$	636311.7392		637047.7805		649235.1963
$HNO_3(\nu_9)$	636191.9062	$O^{18}OO$	634438.7221		649400.6346
	636194.7659		635241.1461		649837.4307
	636209.1040		635573.4715		650552.8406
	636211.9636	$^{32}SO_2$	634782.4646		650675.5449
	636219.6352		634898.4145		651301.5484
	636219.6427		635127.0040	^{35}ClO	649445.0400
	636572.6435		635324.7873		649445.0400
	636572.7197		636086.5257		649445.0400
$HO^{35}Cl$	635870.0222		636090.0579		649445.0400
$HO^{37}Cl$	634788.5280	$^{32}SO_2(\nu_2)$	634692.0861		649451.1700
HO_2	636598.8986		637056.6346		649451.1700
	636602.4359	$^{34}SO_2$	634454.2164		649451.1700
O_3	634461.7341		635051.0139		649451.1700
	634519.7678		635144.2269		650628.9967
$O_3(\nu_{1,3})$	635316.5654		636052.9909		650629.1177
	636672.3675		636659.6978		650629.3322
$O_3(2\nu_2)$	636155.1303		637307.2949		650629.8570
$O_3(\nu_{1,3}+\nu_2)$	634988.3326	R4:640.B28UM:HO2.C1-11			651298.1297
	636266.8508	^{81}BrO	650175.8041		651298.7393
$O_2^{17}O$	635763.2268		650177.2087		651298.9924
	635763.4934		650177.7979		651299.1048
	635763.6269		650178.6151	H_2O	556936.0020
	635763.7172		650179.0310		620700.8070

Continues next page

Table 12.38: Table 12.3 continued

	645766.0100		650599.5548	650335.0010
	645905.6200		650795.8109	650335.0448
	752033.2270		650796.1034	650335.0478
$H_2^{32}S$	650374.1860	O_3	650732.9663	650461.4706
HNO_3	648337.4208	$O_3(\nu_{1,3})$	648890.8087	650461.6905
	648916.5334		650510.8450	650496.9314
	649032.1913		650978.7020	650497.4014
	650287.6161		650983.0165	650497.6139
	650483.0066		651225.6634	650523.9865
	650582.7236	$O_3(\nu_2)$	648489.8807	650524.2255
	650713.1148		651192.8448	650524.3879
$HNO_3(\nu_6)$	648400.5846		651250.7562	650524.4849
	650614.5741	$O_3(\nu_{1,3}+\nu_2)$	649584.2351	650524.5238
$HNO_3(\nu_7)$	649411.2209		650111.6106	650524.5270
	649774.3276	$O_2^{17}O$	648373.6161	650720.4274
	650184.0758		648373.9670	650720.6912
	650927.7925		648373.9787	650720.8672
	651027.2113		648374.0518	650720.9691
	651079.3631		648374.0615	650721.0000
	651171.0657		649275.2349	650721.0095
$HNO_3(\nu_8)$	649634.7465		649275.6618	650857.0769
	650859.1985		649275.8339	650857.0860
$HNO_3(\nu_9)$	648486.9195		649970.1201	650857.1135
	648694.6807		649970.4631	650889.0320
	648694.6974		649970.6726	650889.4268
	649728.3300		649970.7157	650889.6667
	650018.9228		649970.7749	650889.7352
	650021.6410		649981.3999	650889.7877
	650199.9431		649981.6061	650911.7313
	650303.8379		650010.5882	650912.0235
$HO^{35}Cl$	648618.0026		650010.8169	650912.2151
HO_2	648613.8526		650042.5398	650912.3224
	648617.4877		650042.7459	650912.3442
	649701.4773		650159.5639	650912.3608
	649701.5134		650159.7719	650951.1646
	650426.8147		650159.9428	650951.2825
	650426.8484		650167.9240	650951.4690
	650575.0063		650334.5414	651088.9544
	650575.0245		650334.7582	651089.2805
	650595.2013		650334.9084	651089.4900

Continues next page

Table 12.39: Table 12.3 continued

	651089.6032		650796.7454		636714.5705
	651089.6136		650861.9971		636714.8377
	651089.6387		651299.9130		636714.8650
	651174.7048		651306.2637		636819.0577
	651175.1442	$^{32}SO_2(\nu_2)$	648946.2944		636819.2426
	651175.4069		650669.2850		636819.2783
	651175.4728		650916.7971		636904.6166
	651175.5281	$^{34}SO_2$	648737.5970		636904.6553
	651175.5403		650055.9800		636904.7673
	651246.0665	R4:640.B29LM:HOCL.C1-11			636971.2472
	651246.4343	CH_3COCH_3	634437.0853		636971.3213
	651246.6651		634492.7001		637018.8285
	651246.7791		634547.1516		637018.8590
	651246.7843		634563.6259		637018.8763
	651246.8152		634628.0619		637018.9108
$O^{17}OO$	648791.8277		634683.3872		637047.4014
	648791.8712		634873.3676		637047.4075
	648792.1789		635224.7746		637047.4516
	648792.2674		635249.0050		637047.4617
	648792.3892		635352.9646		637056.9255
	648792.4291		635387.6431		637056.9275
	649794.7104		635407.4553		637056.9784
	649794.9197		635728.3277		637056.9804
	650605.6360		635750.0632	CH_3OH	636238.2680
	650605.8348		636302.1082		636259.8546
	650605.8560		636322.9889		636263.3859
	651273.7164		637011.5617		636264.0656
	651273.7186		637085.4436		636274.0770
	651273.7536		637160.5773		636279.9980
$O_2^{18}O$	649137.1089		637216.4495		636287.1936
	649138.5046		637289.5615		636290.7110
	649152.1201		637402.7158		636304.3550
	649152.9292	$CH_3^{35}Cl$	636288.1819		636311.6900
	650552.6825		636288.8365		636333.4700
$O_2^{18}O(\nu_2)$	649088.2012		636288.8439		636337.4190
	651149.6155		636449.0467		636363.8430
$^{32}SO_2$	648381.4661		636449.5669		636366.2480
	648694.4365		636591.1990		636393.5680
	649052.1202		636591.5976		636420.2310
	649236.3027		636714.5472	H_2O	556936.0020

Continues next page

Table 12.40: Table 12.3 continued

	620700.8070	$O_3(\nu_{1,3}+\nu_2)$	634988.3326	R4:640.B29UM:HOCL.C1-11	
	645766.0100		636266.8508	^{81}BrO	650175.8041
	645905.6200	$O_2^{17}O$	635763.2268		650177.2087
	752033.2270		635763.4934		650177.7979
HNO_3	635089.2789		635763.6269		650178.6151
	635432.1434		635763.7172		650179.0310
	635439.0872		636396.0542		650179.4142
	635546.7294		636396.6046		650180.4285
	636414.7874		636396.7385		650181.3811
	636423.7620		636396.8567	CH_3COCH_3	648392.1602
	636850.0072		636997.5285		648415.1283
	637192.8717		636997.9465		648422.7222
	637234.7106		636998.0732		648460.4078
	637259.9950		636999.1116		648611.4259
	637267.8610		636999.8142		648615.8408
	637269.3732		637000.8255		648777.1645
$HNO_3(\nu_6)$	635000.3006	$O^{17}OO$	634713.6891		648797.2636
	637042.0547		634713.7493		648828.6017
$HNO_3(\nu_7)$	634677.0351		634713.8846		648881.4045
	635859.0265	$O_2^{18}O$	636124.0614		649006.4714
	636220.2437	$O_2^{18}O(\nu_2)$	635776.4506		649058.5459
	636481.7563		635928.1758		649126.1157
$HNO_3(\nu_8)$	636311.7392		637047.7805		649235.1963
$HNO_3(\nu_9)$	636191.9062	$O^{18}OO$	634438.7221		649400.6346
	636194.7659		635241.1461		649837.4307
	636209.1040		635573.4715		650552.8406
	636211.9636	$^{32}SO_2$	634782.4646		650675.5449
	636219.6352		634898.4145		651301.5484
	636219.6427		635127.0040	^{35}ClO	649445.0400
	636572.6435		635324.7873		649445.0400
	636572.7197		636086.5257		649445.0400
$HO^{35}Cl$	635870.0222		636090.0579		649445.0400
$HO^{37}Cl$	634788.5280	$^{32}SO_2(\nu_2)$	634692.0861		649451.1700
HO_2	636598.8986		637056.6346		649451.1700
	636602.4359	$^{34}SO_2$	634454.2164		649451.1700
O_3	634461.7341		635051.0139		649451.1700
	634519.7678		635144.2269		650628.9967
$O_3(\nu_{1,3})$	635316.5654		636052.9909		650629.1177
	636672.3675		636659.6978		650629.3322
$O_3(2\nu_2)$	636155.1303		637307.2949		650629.8570

Continues next page

Table 12.41: Table 12.3 continued

	651298.1297		649701.5134	650159.7719
	651298.7393		650426.8147	650159.9428
	651298.9924		650426.8484	650167.9240
	651299.1048		650575.0063	650334.5414
H_2O	556936.0020		650575.0245	650334.7582
	620700.8070		650595.2013	650334.9084
	645766.0100		650599.5548	650335.0010
	645905.6200		650795.8109	650335.0448
	752033.2270		650796.1034	650335.0478
$H_2^{32}S$	650374.1860	O_3	650732.9663	650461.4706
HNO_3	648337.4208	$O_3(\nu_{1,3})$	648890.8087	650461.6905
	648916.5334		650510.8450	650496.9314
	649032.1913		650978.7020	650497.4014
	650287.6161		650983.0165	650497.6139
	650483.0066		651225.6634	650523.9865
	650582.7236	$O_3(\nu_2)$	648489.8807	650524.2255
	650713.1148		651192.8448	650524.3879
$HNO_3(\nu_6)$	648400.5846		651250.7562	650524.4849
	650614.5741	$O_3(\nu_{1,3}+\nu_2)$	649584.2351	650524.5238
$HNO_3(\nu_7)$	649411.2209		650111.6106	650524.5270
	649774.3276	$O_2^{17}O$	648373.6161	650720.4274
	650184.0758		648373.9670	650720.6912
	650927.7925		648373.9787	650720.8672
	651027.2113		648374.0518	650720.9691
	651079.3631		648374.0615	650721.0000
	651171.0657		649275.2349	650721.0095
$HNO_3(\nu_8)$	649634.7465		649275.6618	650857.0769
	650859.1985		649275.8339	650857.0860
$HNO_3(\nu_9)$	648486.9195		649970.1201	650857.1135
	648694.6807		649970.4631	650889.0320
	648694.6974		649970.6726	650889.4268
	649728.3300		649970.7157	650889.6667
	650018.9228		649970.7749	650889.7352
	650021.6410		649981.3999	650889.7877
	650199.9431		649981.6061	650911.7313
	650303.8379		650010.5882	650912.0235
$HO^{35}Cl$	648618.0026		650010.8169	650912.2151
HO_2	648613.8526		650042.5398	650912.3224
	648617.4877		650042.7459	650912.3442
	649701.4773		650159.5639	650912.3608

Continues next page

Table 12.42: Table 12.3 continued

	650951.1646	$O_2^{18}O(\nu_2)$	649088.2012		625214.9148
	650951.2825		651149.6155		625312.5684
	650951.4690	$^{32}SO_2$	648381.4661		625498.4002
	651088.9544		648694.4365		625520.8596
	651089.2805		649052.1202		625778.3140
	651089.4900		649236.3027		625799.7547
	651089.6032		650796.7454		625821.4055
	651089.6136		650861.9971		625965.5985
	651089.6387		651299.9130		625988.1987
	651174.7048		651306.2637		626042.8376
	651175.1442	$^{32}SO_2(\nu_2)$	648946.2944		626065.0045
	651175.4069		650669.2850		626307.7811
	651175.4728		650916.7971		626569.6534
	651175.5281	$^{34}SO_2$	648737.5970		626588.7876
	651175.5403		650055.9800		626912.4796
	651246.0665	R4:640.B30LM:HO2.C1-11			626956.9594
	651246.4343	^{81}BrO	624764.8570	CH_3CN	624344.0986
	651246.6651		624766.3907		624344.1105
	651246.7791		624766.7040		624498.4440
	651246.7843		624767.9257		624629.1049
	651246.8152		624768.0666		624629.1122
$O^{17}OO$	648791.8277		624768.8034		624736.0997
	648791.8712		624769.5930		624736.1036
	648792.1789		624770.6246		624819.3430
	648792.2674	CH_3COCH_3	624458.8035		624819.3430
	648792.3892		624484.1342		624819.3430
	648792.4291		624666.9312		624878.8642
	649794.7104		624670.4364		624914.5729
	649794.9197		624787.3645		624926.4775
	650605.6360		624804.9332	$CH_3^{37}Cl$	626926.9793
	650605.8348		624838.5155		626926.9977
	650605.8560		624839.9336		626927.2082
	651273.7164		624850.8608		626927.2299
	651273.7186		624862.7086		627028.7082
	651273.7536		624867.9658		627028.8690
$O_2^{18}O$	649137.1089		624981.5533	CH_3OH	626626.1888
	649138.5046		625051.4489	$H^{35}Cl$	625901.6030
	649152.1201		625118.5039		625918.7560
	649152.9292		625121.9134		625932.0070
	650552.6825		625149.4917	$H^{37}Cl$	624964.3740

Continues next page

Table 12.43: Table 12.3 continued

	624977.8210	$O_3(\nu_{1,3})$	625011.4391		626739.7505
	624988.3340		625051.2336		626740.1668
H_2O	556936.0020		625797.9205		626740.3135
	620700.8070		626784.5400		626740.3841
	645766.0100	$O_3(\nu_2)$	625280.8257		626740.4437
	645905.6200		625324.2654		626867.1427
	752033.2270		625611.7040		626867.4905
H_2O_2	625044.1800		625793.5621		626867.5992
	626608.9004		626654.6988		626867.6809
$H_2^{32}S$	626474.6250		626723.5181		626867.7085
HNO_3	624484.4450	$O_3(2\nu_2)$	624182.6861		626867.7442
	624775.5300	$O_3(\nu_{1,3}+\nu_2)$	625303.2213	$O_2^{18}O$	625090.4623
	625344.9466	$O_2^{17}O$	625009.5694		625091.8080
	626621.9820		625009.7126		625563.6585
	626825.2410		625009.7872		625939.4177
$HNO_3(\nu_6)$	626353.6227		625010.1853	$O_2^{18}O(\nu_2)$	625288.0490
$HNO_3(\nu_7)$	626166.3604		625010.3980	$^{32}SO_2$	624344.4890
	626412.1046		625010.9574		624887.4758
	626414.9281		627011.8296		626087.3249
	626653.1461	$O^{17}OO$	624294.2586		626168.2253
	626890.4827		625771.8878		626491.4639
	627060.8108		625772.0998		626809.5350
$HNO_3(\nu_9)$	624314.3397		625772.1813	$^{32}SO_2(\nu_2)$	625311.3135
	624352.8456		625782.9166		625933.5079
	624352.8940		625783.1392	$^{34}SO_2$	624243.5693
	625085.6322		625783.2331		624254.4853
	625085.7032		625783.2556		626043.4993
	626452.5348		625869.5705	R4:640.B30UM:HO2.C1-11	
	626452.5486		625869.8353	CH_3COCH_3	658736.4294
$HO^{35}Cl$	625074.8710		625869.9452		659141.9589
$HO^{37}Cl$	624378.8940		626087.3102		659394.5600
HO_2	625660.3542		626087.4871		659429.8682
	625663.7997		626087.5337		659458.8662
	626579.9359		626316.5749		659466.9782
	626587.0677		626316.6915		659489.6115
	626607.4541		626490.4223		659545.9211
O_3	624480.5315		626490.6886		659573.0392
	625371.4686		626490.8207		659687.5133
	625894.7151		626490.8434		660297.3018
	626397.2442		626490.8992		660354.3088

Continues next page

Table 12.44: Table 12.3 continued

	660416.3709	$HNO_3(\nu_6)$	658840.5959		660238.8557
	660421.6529		658921.3152	$O^{17}OO$	661271.3080
	660427.2895		659693.2415		661271.5427
	660584.0327		660301.0002	$O_2^{18}O$	660150.1537
	660658.4791	$HNO_3(\nu_7)$	658726.7466		661263.8286
	660663.2810		658771.9978	$O_2^{18}O(\nu_2)$	658787.5784
	660899.6418		659723.0210		659055.3845
	661295.8745		659728.5791		659918.0986
	661398.7990		660087.1556		661075.4086
	661464.4956	$HNO_3(\nu_9)$	658805.1738		661369.6259
	661538.4666		659380.2908	$O^{18}OO$	659110.3746
CH_3CN	660994.4320		660084.0947		660762.6847
	661157.5676		660084.1128		660877.3393
	661295.7173	$HO^{37}Cl$	661305.9426		661047.7728
	661408.8233	HO_2	660115.6907	$O^{18}OO(\nu_2)$	659555.3155
	661408.8266		660115.8615		659643.0706
	661496.8230		660485.6655	$^{32}SO_2$	659079.8201
	661559.7415		660485.7114		659338.2952
	661559.7435	O_3	658815.2932		659421.0105
	661559.7472		659594.8149		659885.9532
^{13}CO	661067.2801		660360.2258		659898.5409
H_2O	556936.0020		661458.3584		660472.6960
	620700.8070	$O_3(\nu_{1,3})$	658757.9619		660918.3140
	645766.0100		659212.6286		661332.4780
	645905.6200		659465.1985		661510.7760
	752033.2270		660962.4607	$^{32}SO_2(\nu_2)$	658749.3593
H_2O_2	661379.1913	$O_3(\nu_2)$	659091.0854		659897.0724
HNO_3	658918.9445		659753.5588		660076.5090
	659083.5267	$O_3(2\nu_2)$	659760.7611		660266.8785
	659149.3708		660004.8028		660849.8281
	659157.9297	$O_3(\nu_{1,3}+\nu_2)$	658828.3385		661138.2660
	659197.9058		659847.7538	$^{34}SO_2$	658797.5170
	659206.8279	$O_2^{17}O$	659880.6775	R4:640.B31LM:BRO.C1-11	
	659215.3868		659974.6147	^{81}BrO	624764.8570
	659610.9966		659975.7197		624766.3907
	660198.7192		660080.3628		624766.7040
	660833.4591		660080.5427		624767.9257
	661197.9981		660238.0752		624768.0666
	661204.0841		660238.6076		624768.8034
	661516.2296		660238.7111		624769.5930

Continues next page

Table 12.45: Table 12.3 continued

	624770.6246		624819.3430		624352.8456
CH_3COCH_3	624458.8035		624819.3430		624352.8940
	624484.1342		624819.3430		625085.6322
	624666.9312		624878.8642		625085.7032
	624670.4364		624914.5729		626452.5348
	624787.3645		624926.4775		626452.5486
	624804.9332	$CH_3^{37}Cl$	626926.9793	$HO^{35}Cl$	625074.8710
	624838.5155		626926.9977	$HO^{37}Cl$	624378.8940
	624839.9336		626927.2082	HO_2	625660.3542
	624850.8608		626927.2299		625663.7997
	624862.7086		627028.7082		626579.9359
	624867.9658		627028.8690		626587.0677
	624981.5533	CH_3OH	626626.1888		626607.4541
	625051.4489	$H^{35}Cl$	625901.6030	O_3	624480.5315
	625118.5039		625918.7560		625371.4686
	625121.9134		625932.0070		625894.7151
	625149.4917	$H^{37}Cl$	624964.3740		626397.2442
	625214.9148		624977.8210	$O_3(\nu_{1,3})$	625011.4391
	625312.5684		624988.3340		625051.2336
	625498.4002	H_2O	556936.0020		625797.9205
	625520.8596		620700.8070		626784.5400
	625778.3140		645766.0100	$O_3(\nu_2)$	625280.8257
	625799.7547		645905.6200		625324.2654
	625821.4055		752033.2270		625611.7040
	625965.5985	H_2O_2	625044.1800		625793.5621
	625988.1987		626608.9004		626654.6988
	626042.8376	$H_2^{32}S$	626474.6250		626723.5181
	626065.0045	HNO_3	624484.4450	$O_3(2\nu_2)$	624182.6861
	626307.7811		624775.5300	$O_3(\nu_{1,3}+\nu_2)$	625303.2213
	626569.6534		625344.9466	$O_2^{17}O$	625009.5694
	626588.7876		626621.9820		625009.7126
	626912.4796		626825.2410		625009.7872
	626956.9594	$HNO_3(\nu_6)$	626353.6227		625010.1853
CH_3CN	624344.0986	$HNO_3(\nu_7)$	626166.3604		625010.3980
	624344.1105		626412.1046		625010.9574
	624498.4440		626414.9281		627011.8296
	624629.1049		626653.1461	$O^{17}OO$	624294.2586
	624629.1122		626890.4827		625771.8878
	624736.0997		627060.8108		625772.0998
	624736.1036	$HNO_3(\nu_9)$	624314.3397		625772.1813

Continues next page

Table 12.46: Table 12.3 continued

	625782.9166		625933.5079		645766.0100
	625783.1392	$^{34}SO_2$	624243.5693		645905.6200
	625783.2331		624254.4853		752033.2270
	625783.2556		626043.4993	H_2O_2	661379.1913
	625869.5705	R4:640.B31UM:BRO.C1-11		HNO_3	658918.9445
	625869.8353	CH_3COCH_3	658736.4294		659083.5267
	625869.9452		659141.9589		659149.3708
	626087.3102		659394.5600		659157.9297
	626087.4871		659429.8682		659197.9058
	626087.5337		659458.8662		659206.8279
	626316.5749		659466.9782		659215.3868
	626316.6915		659489.6115		659610.9966
	626490.4223		659545.9211		660198.7192
	626490.6886		659573.0392		660833.4591
	626490.8207		659687.5133		661197.9981
	626490.8434		660297.3018		661204.0841
	626490.8992		660354.3088		661516.2296
	626739.7505		660416.3709	$HNO_3(\nu_6)$	658840.5959
	626740.1668		660421.6529		658921.3152
	626740.3135		660427.2895		659693.2415
	626740.3841		660584.0327		660301.0002
	626740.4437		660658.4791	$HNO_3(\nu_7)$	658726.7466
	626867.1427		660663.2810		658771.9978
	626867.4905		660899.6418		659723.0210
	626867.5992		661295.8745		659728.5791
	626867.6809		661398.7990		660087.1556
	626867.7085		661464.4956	$HNO_3(\nu_9)$	658805.1738
	626867.7442		661538.4666		659380.2908
$O_2^{18}O$	625090.4623	CH_3CN	660994.4320		660084.0947
	625091.8080		661157.5676		660084.1128
	625563.6585		661295.7173	$HO^{37}Cl$	661305.9426
	625939.4177		661408.8233	HO_2	660115.6907
$O_2^{18}O(\nu_2)$	625288.0490		661408.8266		660115.8615
$^{32}SO_2$	624344.4890		661496.8230		660485.6655
	624887.4758		661559.7415		660485.7114
	626087.3249		661559.7435	O_3	658815.2932
	626168.2253		661559.7472		659594.8149
	626491.4639	^{13}CO	661067.2801		660360.2258
	626809.5350	H_2O	556936.0020		661458.3584
$^{32}SO_2(\nu_2)$	625311.3135		620700.8070	$O_3(\nu_{1,3})$	658757.9619

Continues next page

Table 12.47: Table 12.3 continued

	659212.6286		661332.4780		234557.5814
	659465.1985		661510.7760		236067.7980
	660962.4607	$^{32}SO_2(\nu_2)$	658749.3593		237314.4297
$O_3(\nu_2)$	659091.0854		659897.0724	$O_3(\nu_2)$	235867.6556
	659753.5588		660076.5090	$O_2^{18}O$	232525.0900
$O_3(2\nu_2)$	659760.7611		660266.8785		232723.6689
	660004.8028		660849.8281		233351.1600
$O_3(\nu_{1,3}+\nu_2)$	658828.3385		661138.2660		234056.0600
	659847.7538	$^{34}SO_2$	658797.5170		234183.6000
$O_2^{17}O$	659880.6775	R1A:118.B32LW:PT.C1-4			235082.0900
	659974.6147	O_2	118750.3430		236620.9400
	659975.7197	$O_2(\nu_1)$	119039.3139	$O^{18}OO$	234339.9800
	660080.3628	$O^{17}O$	118687.6979		236876.3866
	660080.5427		118737.7202	$^{32}SO_2$	234187.0526
	660238.0752		118804.0320		235151.7201
	660238.6076	$O^{18}O$	118759.8102		236216.6848
	660238.7111	O_3	114979.2000		237068.8700
	660238.8557		118364.5000	R3:240.B33UW:O3.C1-4	
$O^{17}OO$	661271.3080		119277.6200	HNO_3	244142.8772
	661271.5427	R3:240.B33LW:O3.C1-4			244176.3496
$O_2^{18}O$	660150.1537	CO	230538.0000		244209.1879
	661263.8286	HNO_3	230012.5652		244244.0750
$O_2^{18}O(\nu_2)$	658787.5784		231627.3370		244287.0548
	659055.3845		231661.0304		244356.1585
	659918.0986		231694.3543		244369.9016
	661075.4086		231730.5651		244513.3716
	661369.6259		231777.6757		244528.0770
$O^{18}OO$	659110.3746		231862.6453		244731.9485
	660762.6847		232050.6553		246093.7146
	660877.3393		232178.5970		247810.6065
	661047.7728		235167.5730	O_3	242318.7357
$O^{18}OO(\nu_2)$	659555.3155		236148.0695		243453.7000
	659643.0706	$O^{18}O$	233946.1790		244145.6952
$^{32}SO_2$	659079.8201	O_3	229575.0227		244158.0400
	659338.2952		231281.4919		247761.7700
	659421.0105		232986.7731		248183.3800
	659885.9532		235709.8400		249788.6000
	659898.5409		237146.1921	$O_3(\nu_{1,3})$	243063.5194
	660472.6960	$O_3(\nu_{1,3})$	231990.9848		244217.2315
	660918.3140		234355.3078		244404.1242

Continues next page

Table 12.48: Table 12.3 continued

	248720.8421	$^{32}SO_2$	244254.2177		118737.7202
$O_3(\nu_2)$	243382.3207		245339.2295		118804.0320
	246512.6283		245563.4226	$O^{18}O$	118759.8102
	246551.3991		248057.4013	O_3	114979.2000
$O_2^{18}O$	244355.1638	R1B:118.B34LW:PT.C1-4			118364.5000
	245795.8877	O_2	118750.3430		119277.6200
	248321.2300	$O_2(\nu_1)$	119039.3139		
$O^{18}OO$	242998.1087	$O^{17}O$	118687.6979		

Id: line_data_table.tex,v 1.19 2004/02/12 00:09:46 bill Exp

Appendix A. Refraction

The derivation of refracted $\phi_t^{\rm refr}$ (orbit plane projected geodetic angle) eq. 6.4 and refracted path length eq. 10.12 are given here. The derivation is shown in the equivalent Earth center, H, coordinate system. The same derivation also applies to the Earth ellipsoid R coordinate system if we use geocentric angles. Figure A.1 shows the refracted quantities in relation to their unrefracted counterparts. In this context we want the pointing angle $\chi_{\rm eq}^{\rm refr}$ that points to the same altitude H_t as the the unrefracted $\chi_{\rm eq}$. Likewise we want the new horizontal location $\phi_t^{\rm refr}$ caused by the additional path lengthening. Finally we want an algorithm for computing the path lengthening between any two levels.

A spherical Earth is assumed. Layering the atmosphere in concentric shells and successively applying Snell's law it can be shown that

$$\sin\chi_{\rm eq}^{\rm refr} = \frac{\mathcal{N}_t H_t}{\mathcal{N} H} \tag{A.1}$$

Eq. A.1 is the spherical polar coordinate form of Snell's law as given by [4]. Referring to figure A.2 we can write the following relationships

$$\cos\chi_{\rm eq}^{\rm refr} = {\rm d}H/{\rm d}s \tag{A.2}$$

$$\tan\chi_{\rm eq}^{\rm refr} = H{\rm d}\gamma/{\rm d}H \tag{A.3}$$

γ is the geocentric orbit plane projected angle which is, in the equivalent Earth center system, the geodetic orbit plane projected angle ϕ.

Combining eq. A.1 with eq. A.2 gives

$${\rm d}s = \frac{\mathcal{N} H {\rm d}H}{\sqrt{\mathcal{N}^2 H^2 - \mathcal{N}_t^2 H_t^2}}, \tag{A.4}$$

which is the path length differential.

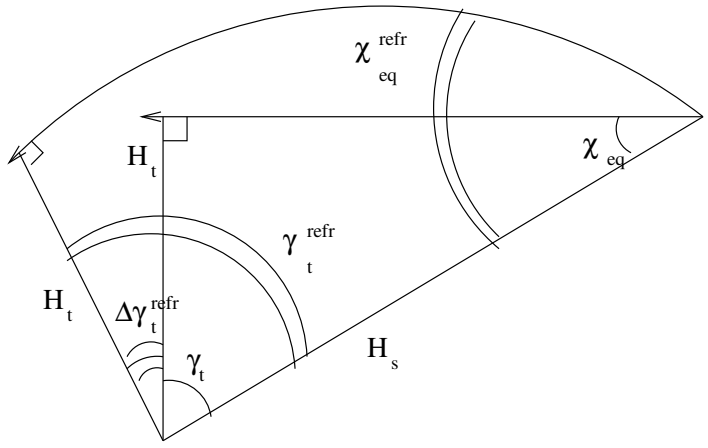

Figure A.1: The difference between refracted and unrefracted quantities.

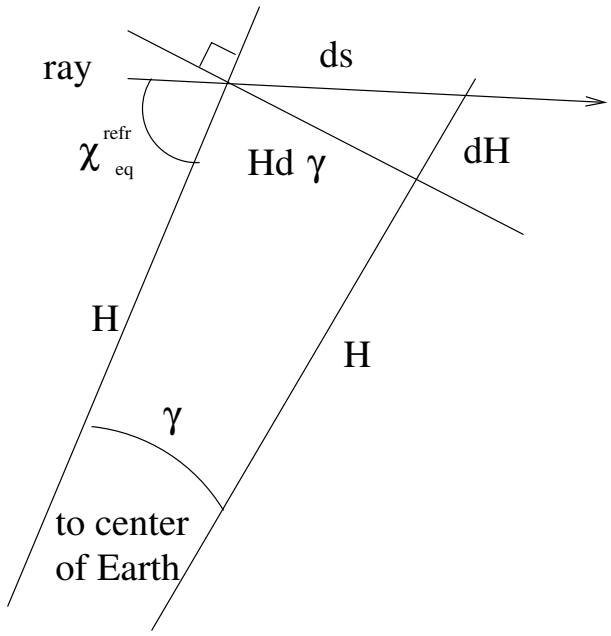

Figure A.2: The geometry of a refracted ray.

Combining eq. A.1 with eq. A.3 and substituting $\gamma = \phi$ gives

$$\mathrm{d}\phi = \frac{\mathcal{N}_t H_t \mathrm{d}H}{H\sqrt{\mathcal{N}^2 H^2 - \mathcal{N}_t^2 H_t^2}} \tag{A.5}$$

Adding and subtracting $(\mathcal{N}_t H_t \mathrm{d}H) \,/\, \left(H\sqrt{\mathcal{N}_t^2 H^2 - \mathcal{N}_t^2 H_t^2}\right)$ to eq. A.5 and integrating gives

$$\begin{aligned} \phi_t^{\mathrm{refr}} &= \phi_{\mathrm{geom}} + \int_{\mathrm{MAX}(H_t, H^{\oplus})}^{H_s} \frac{\mathcal{N}_t H_t \mathrm{d}H}{H} \\ &\times \left(\frac{1}{\sqrt{\mathcal{N}^2 H^2 - \mathcal{N}_t^2 H_t^2}} \right. \\ &- \left. \frac{1}{\sqrt{\mathcal{N}_t^2 H^2 - \mathcal{N}_t^2 H_t^2}} \right). \end{aligned} \tag{A.6}$$

Eq. A.6 conveniently gives ϕ_t^{refr} as an additive correction to ϕ_{geom}, which is available from Level 1 orbit attitude data.

Appendix B. Temperature Derivatives of Pointing Angles

This appendix gives the derivation of the temperature derivatives with respect to pointing angles, eq. 8.10. Differentiating eq. D.2 with respect to temperature (ignoring offset terms in the hydrostatic function like $R_o - \overset{\star}{R}_o$) gives

$$\frac{\mathrm{d}\chi_{\mathrm{eq}}^{\mathrm{refr}}}{\mathrm{d}f_{lm}^T} = \left(\frac{\mathcal{N}_t}{H_s} \frac{\mathrm{d}H_t}{\mathrm{d}f_{lm}^T} + \frac{H_t}{H_s} \frac{\mathrm{d}\mathcal{N}_t}{\mathrm{d}f_{lm}^T} \right) / \cos \chi_{\mathrm{eq}}^{\mathrm{refr}} \tag{B.1}$$

χ replaces $\chi_{\mathrm{eq}}^{\mathrm{refr}}$ when it is an integration angle as in eq. 8.10. Multiply eq. B.1 by $H_s \sin \chi_{\mathrm{eq}}^{\mathrm{refr}} / \mathcal{N}_t H_t = 1$ gives

$$\frac{\mathrm{d}\chi_{\mathrm{eq}}^{\mathrm{refr}}}{\mathrm{d}f_{lm}^T} = \tan \chi_{\mathrm{eq}}^{\mathrm{refr}} \left(\frac{1}{H_t} \frac{\mathrm{d}H_t}{\mathrm{d}f_{lm}^T} + \frac{1}{\mathcal{N}_t} \frac{\mathrm{d}\mathcal{N}_t}{\mathrm{d}f_{lm}^T} \right) \tag{B.2}$$

If we neglect the $\frac{\mathrm{d}\mathcal{N}_t}{\mathrm{d}f_{lm}^T} = (1 - \mathcal{N}_t)\, \eta_l^T \eta_m^T / T_t$ term, we get eq. 8.10. $\frac{\mathrm{d}H_t}{\mathrm{d}f_{lm}^T}$ is evaluated from eq. 5.31.

Now we move on to the much more complex $\frac{\partial}{\partial \chi_{\mathrm{eq}}^{\mathrm{refr}}} \left(\frac{\partial \chi_{\mathrm{eq}}^{\mathrm{refr}}}{\partial f_{lm}^T} \right)$ term. We first use the chain rule $\frac{\mathrm{d}}{\mathrm{d}\chi_{\mathrm{eq}}^{\mathrm{refr}}} = \frac{\mathrm{d}H_t}{\mathrm{d}\chi_{\mathrm{eq}}^{\mathrm{refr}}} \frac{\mathrm{d}}{\mathrm{d}H_t}$. Evaluating $\frac{\mathrm{d}H_t}{\mathrm{d}\chi_{\mathrm{eq}}^{\mathrm{refr}}}$ gives for heights above the Earth surface gives

$$\frac{\mathrm{d}H_t}{\mathrm{d}\chi_{\mathrm{eq}}^{\mathrm{refr}}} = \frac{1}{\left(\frac{1}{H_t} + \frac{1}{\mathcal{N}_t} \frac{\mathrm{d}\mathcal{N}_t}{\mathrm{d}H_t} \right) \tan \chi_{\mathrm{eq}}^{\mathrm{refr}}}, \tag{B.3}$$

or for heights below the Earth surface,

$$\frac{\mathrm{d}H_t}{\mathrm{d}\chi_{\mathrm{eq}}^{\mathrm{refr}}} = \frac{H_t}{\tan \chi_{\mathrm{eq}}^{\mathrm{refr}}}. \tag{B.4}$$

It is easy to show that $\frac{\mathrm{d}\mathcal{N}_t}{\mathrm{d}H_t} = (1 - \mathcal{N}_t) \ln 10 \frac{\mathrm{d}\zeta_t}{\mathrm{d}H_t}$ where $\frac{\mathrm{d}\zeta_t}{\mathrm{d}H_t}$ is embedded in eq. 10.11. Differentiating eq. B.2 with respect to $\chi_{\mathrm{eq}}^{\mathrm{refr}}$ gives

$$\begin{aligned}
\frac{\partial}{\partial \chi_{\mathrm{eq}}^{\mathrm{refr}}} \left(\frac{\partial \chi_{\mathrm{eq}}^{\mathrm{refr}}}{\partial f_{lm}^T} \right) &= \left(\frac{1}{H_t} \frac{\mathrm{d}H_t}{\mathrm{d}f_{lm}^T} + \frac{1}{\mathcal{N}_t} \frac{\mathrm{d}\mathcal{N}_t}{\mathrm{d}f_{lm}^T} \right) / \cos^2 \chi_{\mathrm{eq}}^{\mathrm{refr}} \\
&- \frac{\tan \chi_{\mathrm{eq}}^{\mathrm{refr}}}{H_t} \frac{\mathrm{d}H_t}{\mathrm{d}\chi_{\mathrm{eq}}^{\mathrm{refr}}} \left(\frac{1}{H_t} \frac{\mathrm{d}H_t}{\mathrm{d}f_{lm}^T} - \frac{\mathrm{d}}{\mathrm{d}H_t} \frac{\mathrm{d}H_t}{\mathrm{d}f_{lm}^T} \right) \\
&- \frac{\tan \chi_{\mathrm{eq}}^{\mathrm{refr}}}{\mathcal{N}_t} \frac{\mathrm{d}H_t}{\mathrm{d}\chi_{\mathrm{eq}}^{\mathrm{refr}}} \left(\frac{1}{\mathcal{N}_t} \frac{\mathrm{d}\mathcal{N}_t}{\mathrm{d}H_t} \frac{\mathrm{d}\mathcal{N}_t}{\mathrm{d}f_{lm}^T} - \frac{\mathrm{d}}{\mathrm{d}H_t} \frac{\mathrm{d}\mathcal{N}_t}{\mathrm{d}f_{lm}^T} \right)
\end{aligned} \tag{B.5}$$

where $\frac{\mathrm{d}}{\mathrm{d}H_t} \frac{\mathrm{d}\mathcal{N}_t}{\mathrm{d}f_{lm}^T} = \frac{(\mathcal{N}_t - 1) \ln 10 \eta_l^T \eta_m^T}{T_t} \frac{\mathrm{d}\zeta_t}{\mathrm{d}H_t}$ and $\frac{\mathrm{d}}{\mathrm{d}H_t} \frac{\mathrm{d}H_t}{\mathrm{d}f_{lm}^T} = \frac{2}{H_t} \frac{\mathrm{d}H_t}{\mathrm{d}f_{lm}^T} + \frac{\eta_l^T \eta_m^T}{T_t}$. If we set all $\frac{\mathrm{d}\mathcal{N}_t}{\mathrm{d}f_{lm}^T} = 0$ and $\frac{\mathrm{d}\mathcal{N}_t}{\mathrm{d}H_t} = 0$ then eq. 8.10 results.

An experimental program was developed that included both $\frac{\mathrm{d}H_t}{\mathrm{d}f_{lm}^T}$ and $\frac{\mathrm{d}\mathcal{N}_t}{\mathrm{d}f_{lm}^T}$; however, the contribution from $\frac{\mathrm{d}\mathcal{N}_t}{\mathrm{d}f_{lm}^T}$ was negligible, even in the troposphere, so it is not included in production software. *This is a topic that should be revisited because I think the $\mathcal{N}_t$ should be more apparent than I was computing near the Earth surface.*

Appendix C. ECR to LOSF transformation

A prescription for converting satellite pointing into ϕ_t is given here. This is needed in order to find ϕ_t operationally and to form a theoretical basis for radiance sensitivities to various misalignment angles to be discussed later. *All angles in this section are geocentric*. The solution to this problem is worked in the *Earth Centered Rotating* or ECR frame. This differs from Earth Centered Inertial (ECI) mostly but not entirely by a longitude rotation. The z-axis of the ECR coordinate does precess about the z-axis of ECI. ECR is more convenient because it uses spacecraft location (longitude and latitude). There is another frame called instrument pointing where the z-axis is the FOV direction and the x-z plane is the elevation scan plane and the y axis perpendicular to it. The limb tangent is defined as a point along the FOV direction where the normal to the underlying figure ellipsiod (eq. 5.1) intersects it at a right angle. The pointing boresight vector is $\vec{n}_{\rm d} = (0, 0, 1)$ in the instrument pointing frame is transformed into ECR coordinates according to

$$\vec{n}_{\rm d} = (0, 0, 1)\,(\mathbf{ACF})^t \tag{C.1}$$

where $\mathbf{A}$ is a ECR to local orbital frame transformation matrix, $\mathbf{C}$ is the local orbital frame to satellite platform frame transformation matrix, and $\mathbf{F}$ is the satellite platform frame to instrument pointing frame transformation matrix. The local orbital frame has the z-axis pointing to the center of orbit (or Earth), x-axis is in the flight orbital plane (would be the velocity direction if orbit were perfectly circular), and y-axis is out of this plane. The satellite platform has an internal frame of reference which is used for mounting the instruments. This frame is maintained as close as possible to the orbital frame so as to keep the instruments properly aligned relative to the Earth. To do so the satellite is constantly pitching (rotating about the y-axis in the orbital frame) to keep its internal frame coaligned with the orbital frame. The alignment is not perfect and changes with time; the coordinate transformation is given by the $\mathbf{C}$ matrix which has yaw (z-axis rotation), pitch (y-axis rotation) and roll (x-axis rotation) angles. The instrument is mounted with respect to the satellite's internal frame and has its own boresight coordinate, as previously described with the transformation matrix $\mathbf{F}$. This is somewhat simplistic but complete in that other misalignment angles can be folded into these described here.

The $\mathbf{A}$ matrix is the most complicated and has been developed previously [13]. *This older work uses some different conventions from the usual but due to the complexity of the problem I am not going to alter this material for now.* The $\mathbf{A}$ matrix is

$$\mathbf{A} = \begin{bmatrix} \frac{\cos\mu_a \sin\lambda}{\cos\beta'} - \sin\mu_a \sin\beta' \cos\mu_r \cos\lambda & \sin\mu_a \cos\beta' & -\cos\lambda\cos\mu \\ \frac{\sin\mu_a \sin\lambda}{\cos\beta'} + \cos\mu_a \sin\beta' \cos\mu_r \cos\lambda & -\cos\mu_a \cos\beta' & -\cos\lambda\sin\mu \\ -\cos\beta' \cos\mu_r \cos\lambda & -\sin\beta' & -\sin\lambda \end{bmatrix} \tag{C.2}$$

where β' is the orbit incline angle *relative to the north pole or z-axis in ECR*; it is positive if on the descending node the spacecraft travels from west to east or negative if the satellite travels westerly on the descending node. β' *in the ECR frame* can be computed from the spacecraft velocity (in ECR coordinates) according to

$$\sin\beta' = \frac{\cos\lambda\,(v_y \cos\mu - v_x \sin\mu)}{\sqrt{v_x^2 + v_y^2 + v_z^2}} \tag{C.3}$$

where v_x, v_y, v_z are components of the satellite velocity in the ECR frame with an Earth motion correction ($\vec{v} = \vec{v}_{\rm ecr} + \omega\,(0,0,1) \times \vec{R}_s$, ω is Earth's radial velocity, $7.292115 \times 10^{-5}\ {\rm s}^{-1}$). Nominally the orbit incline angle for EOS, which is given as 98.14°, is $\beta' = -8.14°$ in this convention (i.e. $\sin\beta' = \cos\beta$. *I need to verify the exact relationship between β' and the Aura incline angle β at a later time.* However, β', is invariant only in the ECI but not the ECR frame and therefore the inclination and subsequently orbit plane projected minor axis will have to be recomputed for each satellite location. μ, λ are geocentric longitude (east is positive, west is negative) and latitude (north is positive, south is negative) μ_a is the longitude where the orbit plane crosses the equator and is given by $\mu_a = \mu - \mu_r$ where μ_r is a longitude angle of the spacecraft relative to μ_a which is given by $\sin\mu_r = -\tan\lambda\tan\beta'$. Angle μ_r is not uniquely defined by this relation. The choice is based on whether the satellite is in the ascending or descending node. Use $90 \leq \mid \mu_r \mid \leq 180$ for the ascending node, or $0 \leq \mid \mu_r \mid \leq 90$ for the descending node.

The satellite platform transformation matrix is a three axis rotation given by

$$\mathbf{C} = \begin{bmatrix} \cos\vartheta\cos\psi & -\cos\vartheta\sin\psi\cos\varphi + \sin\vartheta\sin\varphi & \cos\vartheta\sin\psi\cos\varphi + \sin\vartheta\cos\varphi \\ \sin\psi & \cos\psi\cos\varphi & -\cos\psi\sin\varphi \\ -\sin\vartheta\cos\psi & \sin\vartheta\sin\psi\cos\varphi + \cos\vartheta\sin\varphi & -\sin\vartheta\sin\psi\cos\varphi + \cos\vartheta\cos\varphi \end{bmatrix} \tag{C.4}$$

where φ, ϑ, and ψ are roll, pitch, and yaw angles. The order of rotations is roll, yaw, and pitch—like UARS. The matrix will be slightly modified if the order of rotations are altered but this is straightforward to derive. The $\mathbf{C}$ matrix is nearly an identity matrix if the satellite is operating properly.

The instrument field-of-view pointing (IFOVP) frame transform matrix $\mathbf{F}$ is

$$\mathbf{F} = \begin{bmatrix} \cos\alpha_t\sin\epsilon_t & -\sin\alpha_t & \cos\alpha_t\cos\epsilon_t \\ \sin\alpha_t\sin\epsilon_t & \cos\alpha_t & \sin\alpha_t\cos\epsilon_t \\ -\cos\epsilon_t & 0 & \sin\epsilon_t \end{bmatrix} \tag{C.5}$$

where ϵ_t is the elevation or vertical scanning angle (nominally 25° with increasing positive values pointing lower) and α_t is a azimuth or horizon scanning angle (nominally 0°). The MLS scan program predominantly determines this matrix.

The unit vector normal to the ellipse and perpendicular to the boresight is given by

$$\vec{n}_\perp = \frac{(\vec{n}_d \times \vec{n}_s) \times \vec{n}_d}{\parallel (\vec{n}_d \times \vec{n}_s) \times \vec{n}_d \parallel} = \frac{(\vec{n}_d \cdot \vec{n}_d)\,\vec{n}_s - (\vec{n}_s \cdot \vec{n}_d)\,\vec{n}_d}{\parallel (\vec{n}_d \cdot \vec{n}_d)\,\vec{n}_s - (\vec{n}_s \cdot \vec{n}_d)\,\vec{n}_d \parallel} \tag{C.6}$$

where $\vec{n}_s = (\cos\lambda\cos\mu, \cos\lambda\sin\mu, \sin\lambda)$ is a unit vector pointing to the satellite. $\vec{n}_\perp$ has to also be the normal vector to the eq. 5.1 ellipsiod which is

$$\vec{n}_\perp = \frac{(b\cos\lambda_t\cos\mu_t, b\cos\lambda_t\sin\mu_t, a\sin\lambda_t)}{\sqrt{b^2\cos^2\lambda_t + a^2\sin^2\lambda_t}} \tag{C.7}$$

where λ_t and μ_t are the field-of-view limb tangent latitude and longitude in ECR. These angles are extracted by equating eq. C.6 and eq. C.7.

The geocentric limb tangent horizontal angle γ_t (see eq. 5.5) is computed as follows. The spacecraft orbital component is given by

$$\gamma = 180 \pm \cos^{-1}(\cos\mu_r\cos\lambda) \tag{C.8}$$

Use $-$ if $\lambda \geq 0.0$ or $+$ when $\lambda < 0.0$. Next is to compute the limb tangent orbit projected angle $\Delta\gamma_t$. This is done by finding the angle between planes formed by the orbit plane and the pointing plane and projecting the satellite to tangent angle onto the orbit plane. A vector perpendicular to the orbit plane is

$$\vec{n}_v = \frac{[(1,0,0)\,\mathbf{A}^t] \times \vec{n}_s}{\parallel [(1,0,0)\,\mathbf{A}^t] \times \vec{n}_s \parallel} \tag{C.9}$$

A vector perpendicular to the pointing plane is

$$\vec{n}_x = \frac{\vec{n}_s \times \vec{n}_d}{\parallel \vec{n}_d \times \vec{n}_s \parallel} \tag{C.10}$$

The dot product of $\vec{n}_v$ and $\vec{n}_x$ is the cosine of the angle separating these planes, which is the projection angle for getting the tangent horizontal angle. This is computed with

$$\Delta\gamma_t = \tan^{-1}\left\{\vec{n}_v \cdot \vec{n}_x \tan\left[\cos^{-1}\left(\vec{n}_s \cdot \vec{n}_e\right)\right]\right\}. \tag{C.11}$$

where $\vec{n}_e$ is a vector pointing from the center of the Earth to the tangent point on the Earth ellipsoid given by

$$\vec{n}_e = \left(a\cos\lambda_t\cos\mu_t, a\cos\lambda_t\sin\mu_t, b\sin\lambda_t\right)/\sqrt{a^2\cos^2\lambda_t + b^2\sin^2\lambda_t}. \tag{C.12}$$

And finally $\gamma_t = \gamma + \Delta\gamma_t$. γ_t is easily converted into the independent horizontal coordinate ϕ_t with eq. 5.4.

The tangent height and distance from the spacecraft is easily computed from these relations

$$\begin{aligned} h_t &= \vec{n}_\perp \cdot \left(\vec{R}_s - \vec{R}_t^{\oplus}\right) \\ s_t &= -\vec{n}_d \cdot \left(\vec{R}_s - \vec{R}_t^{\oplus}\right) \end{aligned} \tag{C.13}$$

The intent is to have the orbit and pointing planes coaligned; however, there will be slight misalignments. For the sake of simplicity, once the tangent geodetic angle is established then one can use eq. 5.2 and its equivalent circular Earth for the radiative transfer and statevector gridding calculations. The actual ellipse traced by the tangent will be a bit smaller because the center will be displaced from the orbital center and will behave like a chord of a circle. One does not want to use the tangent traced ellipse for the radiative transfer equation because the viewing plane by definition goes through the center of the earth and in this sense eq. 5.2 is more accurate for radiative transfer. The ϕ_t angle is invariant in either ellipse. The most accurate equation is to use eq. 5.2 with eq. 5.3 having β and c include perturbations due to attitude changes. The true viewing β is computed from

$$\cos\beta'' = \left(\frac{\vec{n}_s \times \vec{n}_d}{\parallel \vec{n}_d \times \vec{n}_s \parallel}\right) \cdot (0,0,1) \tag{C.14}$$

and β in eqs. 5.3 and 5.5 is $90 - \beta''$. Currently we are setting $\beta' = \beta''$ for Aura-MLS and feel the the added level of sophistication implied in eq. C.14 is not necessary. If we consider the UARS MLS viewing geometry where $\alpha_t = 90$, β'' would be the compliment of β'.

The procedure described above will have a tangent location error of a few arcseconds and 30 meters in altitude. This is caused by a light speed aberration effect that takes account of the time it takes for light to travel from the tangent to the observer. One can think of the limb tangent ellipsoid

normal being scanned vertically at a rate of the projection of the satellite and Earth component velocities upon it and computing the vertical offset caused by the amount of time it takes light to travel s_t kilometers. This is given by

$$(\Delta\alpha_{t,\mathrm{ls}}, \Delta\epsilon_{t,\mathrm{ls}}, \Delta\gamma_{\mathrm{t,ls}}) = \tan^{-1}\left\{\left[\vec{v}_s + \vec{\omega}\times\left(R^{\oplus}\vec{n}_e + h_t\vec{n}_\perp\right)\right]\mathbf{ACF}/\mathsf{c}\right\} \tag{C.15}$$

where $\Delta\alpha_{t,\mathrm{ls}}$ is the change in azimuth angle, $\Delta\epsilon_{t,\mathrm{ls}}$ is the change in elevation angle, and $\Delta\gamma_{\mathrm{t,ls}}$ is the change in γ_t, $\vec{v}_s$ is the satellite velocity, $\vec{\omega}$ is the Earth angular velocity, all in ECR and c is the speed of light. $\Delta\epsilon_{t,\mathrm{ls}}$ for EOS MLS is about two arcseconds and should be used to correct the instrument elevation angle used in the transformations. The impact of the azimuth and geocentric corrections can probably be neglected.

The transformation between ECR and the two dimensional LOSF vectors in subsection 4.2 is given by

$$\vec{n}_{\mathrm{d}}\,(\mathrm{LOSF}) = \vec{n}_{\mathrm{d}}\,(\mathrm{ECR})\,(\mathbf{H})^t\,, \tag{C.16}$$

where the ECR to LOSF transformation matrix is

$$\mathbf{H} = \begin{bmatrix} \cos\mu'_a & \sin\mu'_a & 0 \\ \sin\beta''\sin\mu'_a & -\sin\beta''\cos\mu'_a & \cos\beta'' \\ \cos\beta''\sin\mu'_a & -\cos\beta''\cos\mu'_a & -\sin\beta'' \end{bmatrix} \tag{C.17}$$

where $\mu'_a = \mu - \mu'_r$. μ'_r is a longitude angle of the spacecraft relative to μ'_a which is given by $\sin\mu'_r = -\tan\lambda\tan\beta''$. Angle μ'_r is not uniquely defined by this relation. The choice is based on whether the satellite is in the ascending or descending node. Use $90 \leq| \mu'_r |\leq 180$ for the ascending node, or $0 \leq| \mu'_r |\leq 90$ for the descending node. It can be shown that the z component of a vector in the LOSF frame vanishes for any ECR vector of the form $\propto (\cos\mu\cos\lambda, \sin\mu\cos\lambda, \sin\lambda)$. Matrix $\mathbf{H}$ cannot be folded into eq. C.1 because β'' is not known until eq. C.14 is evaluated; however, the Aura-MLS viewing geometry with perfect instrument alignment and attitude control ($\varphi = \psi = \alpha = 0$) is a special case where $\beta' = \beta''$.

Appendix D. Geometric and Attitude Models

This appendix contains material of a historical nature from UARS MLS. It contains a detailed model for the encoder angle. It also contains algorithms for computing the radiance sensitivities to the radiometer offset angles, spacecraft attitude angles, the Earth and satellite radii. Some of these algorithms were incorporated in the UARS MLS L2PC file creation but were not considered necessary for data production. They are currently not a part of the EOS MLS algorithm package.

Limb tangent pressure is the independent vertical coordinate for the radiance profile. The vertical coordinate is the ellipsoid normal in a plane defined by the spacecraft location, center of Earth and the limb tangent. The radiometers on the EOS MLS view the limb using different optics. Despite using a common receiving antenna, there are small differences in the FOV directions. The co-polarized plane of the FOVs may not be contained within the defined viewing plane. Additionally, spacecraft misalignments may cause the scan to have an azimuth component. Therefore each radiometer's scan has a pointing reference that is independent of the others. However we believe that the differences are confined to a constant and unvarying (within one scan) offset. This allows one to create a model linking all the scan pointings to a single pointing profile with offsets. This eliminates many elements in the statevector and improves pointing knowledge provided that the offset model is accurate. A model that deals with this issue is given at length in [14]. It is reproduced here. Note that the angles here are in the geocentric (not equivalent circular) Earth system.

The geometric quantities include, pointing sensitivity, derivatives due to variations in the satellite orbital radius, earth radius, spacecraft yaw, pitch, and roll attitude angles, and the instrument FOV pointing offset angles. The following definitions for angles and heights are:

$\zeta_t^{\rm ref}$**:** The tangent pressure of one (240 GHz for EOS MLS) of the radiometers. This radiometer is the pointing reference for the instrument.

α_t**:** The azimuth pointing angle (in eq. C.5) in the IFOVP frame . This is actually a sum of a reference angle, a thermal contribution, an encoder contribution (the vertical antenna scanner), a radiometer offset, and a light-speed correction. The reference angle is 0° which means the FOV direction is parallel to spacecraft orbital motion. The radiometer offset is the azimuthal difference between pointing reference radiometer and the radiometer of question.

ϵ_t**:** The elevation pointing angle (in eq. C.5) in the IFOVP frame. This is actually a sum of a reference angle, a thermal contribution, an encoder contribution, a radiometer offset, and a light speed correction. The EOS orbit places the reference angle nominally at 25.2°(?) which directs the FOV into the atmosphere, and the encoder varies about $\pm 1^\circ$ about the reference in order to measure the radiance profile.

φ**:** The "combined" spacecraft/instrument roll angle. This includes the spacecraft roll, and roll-like contributions from the instrument reference axes and spacecraft axes. Angles α_t and ϵ_t locate the FOV direction relative to the instrument reference axes.

ψ**:** The "combined" spacecraft/instrument yaw angle. This is the spacecraft yaw, and yaw-like contributions from the instrument reference axes and spacecraft axes.

ϑ**:** The "combined" spacecraft/instrument pitch angle. This is the spacecraft pitch, and pitch-like contributions from the instrument reference axes and spacecraft axes.

R_t^{ref}**:** The geocentric tangent of ζ_t^{ref}. See figure 5.1.

H_t^{ref}**:** The geocentric tangent of ζ_t^{ref} in the equivalent Earth coordinates. See figure 5.2.

R_t**:** A non-reference radiometer FOV direction geocentric tangent.

H_t**:** A non-reference radiometer FOV direction geocentric tangent relative to equivalent Earth center.

R_s**:** The geocentric spacecraft orbital height.

H_s**:** The geocentric spacecraft orbital height relative to equivalent circular Earth center.

$R_t^{\oplus}$**:** The geocentric Earth radius, Magnitude of eq. 5.10 evaluated at ϕ_t.

$H_t^{\oplus}$**:** The "equivalent circle" Earth radius. Magnitude of eq. 5.21 evaluated at ϕ_t.

$\chi^{\text{refr, ref}}$**:** The refracted pointing angle in the plane defined by $\vec{R}_s$ and $\vec{R}_t$ for the reference radiometer

$\chi_{\text{eq}}^{\text{refr, ref}}$**:** The refracted pointing angle in the plane defined by $\vec{H}_s$ and $\vec{H_t}^{\text{ref}}$ for the reference radiometer.

χ^{refr}**:** The refracted pointing angle in the plane defined by $\vec{R}_s$ and $\vec{R}_t$.

$\chi_{\text{eq}}^{\text{refr}}$**:** The refracted pointing angle in the plane defined by $\vec{H}_s$ and $\vec{H}_t$

$\Delta\chi$**:** $\chi_{\text{eq}}^{\text{refr}} - \chi^{\text{refr}}$, the difference between pointing angles in the equivalent Earth and ellipsoid Earth coordinates.

Note that angle χ is always in the x-y plane of the LOSF. The radiance calculations are convolved with an antenna pattern that is an angular function, hence it is convenient to express the radiance derivative as an angular quantity and use the chain rule

$$\frac{\partial I}{\partial x} = \frac{\partial I}{\partial \chi^{\text{refr}}} \frac{\mathrm{d}\chi^{\text{refr}}}{\mathrm{d}x}, \tag{D.1}$$

where x = α_t, ϵ_t, ϑ, ψ, φ, ζ^{ref}, R^s, and $R^{\oplus}$. The $\frac{\partial I}{\partial \chi^{\text{refr}}}$ derivative is easily computed from the radiance versus pointing angle functions from the antenna convolution calculation described later. The functional forms of $\chi\left(\mathbf{x}\right)$ are presented. The tangent heights are related to the refracted angle according to

$$\sin \chi^{\text{refr}} = \mathcal{N}_t \frac{R_t}{R_s} \tag{D.2}$$

where $\chi_{\text{eq}}^{\text{refr}}$ includes a correction to the pointing due to atmospheric refraction, $\mathcal{N}_t$, given in eq. 6.3. R_t, and R_s are the tangent point and satellite heights. Eq. D.2 works for Earth reflecting rays also.

Another way of writing eqn. D.2 which is more useful for the attitude derivative calculation is

$$\mathcal{N}_t^2 R_t^2 = R_s^2 - \left(\vec{R}_s \cdot \vec{n}_d\right)^2, \tag{D.3}$$

where $\vec{n}_d$ is an unit vector in the FOV direction and $\vec{R}_s$ is the vector from the instrument to the equivalent Earth center. Eq. D.3 simplifies to

$$\mathcal{N}_t^2 R_t^2 = R_s^2 \left(1 - e_z^2\right), \tag{D.4}$$

where $e_z = \cos\chi^{\text{refr}}$ is given by

$$\begin{aligned} e_z &= -\cos\alpha_t \cos\epsilon_t + \sin\vartheta\cos\psi \\ &+ \sin\alpha_t \cos\epsilon_t \sin\vartheta \sin\psi \cos\varphi \\ &+ \sin\alpha_t \cos\epsilon_t \cos\vartheta \sin\varphi \\ &- \sin\epsilon_t \sin\vartheta \sin\psi \cos\varphi \\ &+ \sin\epsilon_t \cos\vartheta \cos\varphi. \end{aligned} \tag{D.5}$$

This is derived from applying the $\mathbf{C}$ and $\mathbf{F}$ transform matricies to $\vec{n}_d = [0, 0, 1]$ in the instrument pointing frame and substituting $\vec{R}_s = [0, 0, -R_s]$.

Eqn. D.3 requires $e_z = \cos\chi^{\text{refr}}$ and to *first order* (for the EOS MLS observation configuration), $\alpha \approx 0.0$, $\varphi \approx 0.0$, and $\psi \approx 0.0$ would simplify to $e_z = \frac{\mathcal{N}_t R_t}{R_s} = \cos(\epsilon_t + \vartheta)$ or in other words, χ^{refr} is the sum of all the elevation (pitch) angles between the EOS and the FOV direction. However, sensitivity to pointing is great and *second* order effects could be important and therefore contributions from the yaw, ψ, and roll, φ, angles are included. Although formally retained in the UARS MLS foward model description—the source of this material—the impacts of off-elevation angles was totally ignored and this did not seem to cause problems, hence it may be ignored for the EOS MLS case also.

The pointing angle for each of the MLS radiometers can be expressed as a function of the reference radiometer pointing angle according to

$$\chi^{\text{refr}} = \chi^{\text{ref,refr}} + \arccos e_z - \arccos e_z^{\text{ref}} \tag{D.6}$$

The difference between e_z and e_z^{ref} being the inclusion of an offset contribution to the effects of α_t and ϵ_t in e_z. The geometric derivatives are:

$$\frac{\mathrm{d}I}{\mathrm{d}\zeta^{\text{ref}}} = \frac{\mathrm{d}I}{\mathrm{d}\chi^{\text{refr}}} \frac{\mathrm{d}\chi_{\text{eq}}^{\text{refr}}}{\mathrm{d}\zeta^{\text{ref}}}, \tag{D.7}$$

$$\frac{\mathrm{d}I}{\mathrm{d}H_s} = \frac{\mathrm{d}I}{\mathrm{d}\chi^{\text{refr}}} \frac{\mathrm{d}\chi^{\text{refr}}}{\mathrm{d}H_s}, \tag{D.8}$$

$$\frac{\mathrm{d}I}{\mathrm{d}H^{\oplus}} = \frac{\mathrm{d}I}{\mathrm{d}\chi^{\text{refr}}} \frac{\mathrm{d}\chi^{\text{refr}}}{\mathrm{d}H^{\oplus}}, \tag{D.9}$$

and

$$\frac{\mathrm{d}I}{\mathrm{d}\wp} = \frac{\mathrm{d}I}{\mathrm{d}\chi^{\text{refr}}} \frac{\mathrm{d}\chi^{\text{refr}}}{\mathrm{d}\wp}, \tag{D.10}$$

where $\wp = \epsilon_t + \Delta\chi, \alpha_t, \varphi, \psi$, or ϑ. The derivative forms are given here because they will be later combined with the general forward model derivative to get the radiance sensitivities. When the radiances are weighted by the antenna gain pattern and integrated (see eq. 3.1), which is done in the $\chi^{\rm refr}$ coordinate, cubic spline coefficients are calculated which give the radiance first derivatives in the first product appearing in the chain-rule above. $\frac{{\rm d}\chi^{\rm refr}}{{\rm d}\zeta^{\rm ref}}$ is obtained from eq. D.2 and differentiating eq. D.4. To evaluate eqs. D.8 and D.9 substitute $e_z = \sqrt{1.0 - \mathcal{N}_t^2 \frac{R_t^2}{R_s^2}}$ followed by eq. D.2 and differentiate. Likewise eq. D.10 where $\wp$ is any one of the five angles appearing in eq. D.5 is evaluated by combining eqs. D.2, D.5, and D.6 and differentiating.

The instrument elevation encoder angle, nominally ϵ_t, can be determined from absolute pointing $\chi^{\rm refr}$ by solving eq. D.5.

$$\cos\epsilon_t = \frac{e_z}{A} \pm B\left(A^2 + B^2\right)\sqrt{A^2 + B^2 - e_z^2}, \tag{D.11}$$

or

$$\sin\epsilon_t = \frac{e_z}{B} \mp A\left(A^2 + B^2\right)\sqrt{A^2 + B^2 - e_z^2}, \tag{D.12}$$

where

$$\begin{aligned} A &= -\cos\alpha_t \sin\vartheta \cos\psi + \sin\alpha_t \sin\vartheta \sin\psi \cos\varphi \\ &+ \sin\alpha_t \cos\vartheta \sin\varphi, \qquad \text{(D.13)} \\ B &= -\sin\vartheta \sin\psi \sin\varphi + \cos\vartheta \cos\varphi. \qquad \text{(D.14)} \end{aligned}$$

This is useful because the MLS makes angular measurements of its FOV-direction called the encoder angle (used to compute ϵ_t and α_t) and this information can be incorporated into the pressure-temperature-constituent mixing ratio retrievals using eq. D.11 as the foward model.

Appendix E. The MLS State Vector

For the purposes of the forward model, the state vector is any *independent* variable for which a radiance derivative is computed. The establishment of a particular state vector is given elsewhere [14]. Basically it consists of the experimental objectives, which are the atmospheric variables listed in table 2.1 and any other independent supporting variables. In practice, only a subset of the latter whose uncertainty is sufficiently large to impact the estimated values and uncertainties of the experimental objective is formally considered part of the state vector. Here we give the basic elements that create the forward model, which is an expansion of eq. 3.1 and a geometric scanning model.

Combining these models with the calculation in eq. 3.1, which is detailed later, gives the state vector in table E.1.

Table E.1: A proposed EOS MLS state vector by component.

Component	description	model
f^{k}	atmospheric profiles	radiative transfer
$\mathsf{f}^{\mathrm{H2O}}$	water profile	radiative transfer Scan model
f^{T}	Temperature Profile	Radiative transfer Hydrostatic function Scan Model
$\vec{\zeta}_t$	Tangent pressure, 118 GHz Radiometer	Radiative transfer Scan Model
$\vec{\phi}_t$	Orbit tangent geodetic angle	Radiative transfer Scan Model Earth Ellipsoid model Geopotential model
ϵ_{off} α_{off}	Radiometer offsets elevation/azimuth	Radiative transfer
$R_s\left(\phi_t\right)$	Spacecraft geocentric height	Radiative transfer
$\mathsf{f}^{\mathrm{refgeopot}}$	Reference Geopotential	Scan Model
φ,ϑ,ψ	roll, pitch, yaw alignments	Radiative transfer Scan model(?)
f^{ν}	line frequency shift profile	Radiative transfer
$\mathsf{f}^{\omega^{\mathrm{k}}}$ $\mathsf{f}^{\mathrm{n^k}}$	P and T broadening	Radiative transfer
r_u r_l	Side band ratios	Radiative transfer
I_{bsl}	Additive Radiance Offset	Radiative transfer

Appendix F. Catalogue Generation and Maintanance Programs

F.1 Introduction

In the directory `/users/bill/eos_fwd_mdl/spectroscopy/line_lister` are programs for generating and maintaining a JPL catalogue swept list of lines to consider for the EOS and UARS MLS experiments.

F.2 Programs

These programs make the catalogue data base.

`make_template.pro`: A program to create a file called `line_data_table.tex.uc` which contains the first two header lines but has no line data in it. `uc` means "under construction".

`make_line_table.pro`: This program takes a molecule name and an EOS or UARS band designation and creates a catalogue subset of lines that should be considered. It produces a file, `data_for_`**spectag**`.tex`.

`merge_continuum_lines.pro`: This program assigns bands to lines in the `line_data_table.tex.uc` file that must accompany the continuum function.

`sweep_over_catalogue.pro`: This program reads the file, `molecule_data_base.txt` containing the molecules to consider and repeatedly calls `make_line_table.pro` generating catalogue subset files for each **molecule**.

`merge_files.pro`: This file merges all the available `data_for_`**spectag**`.tex` files into the `line_data_table.tex.uc` acording to some rules. The original `line_data_table.tex.uc` is overwritten.

`update_lineshape.pro`: updates all lineshape data in `line_data_table.tex.uc` to be in agreement with that in the `s`**spectag**`.cat` files.

`read_molecule_file.pro`: Reads the file `molecule_data_base.txt`.

`read_mol_dbase.pro`: Reads a molecular data base file (e.g. `mol_data_table.tex`).

`read_spect_dbase.pro`: Reads a molecular data base file (e.g. `mol_data_table.tex`) and a line data base file. This program will read for example either a `line_data_table.tex.uc` or a `data_for_`**spectag**`.tex` file.

`read_cont_designator_file.pro`: Reads a `b`**spectag**`.cat` file.

`proc_tex_string.pro`: A LaTeXstring processing subroutine used by `read_mol_dbase.pro` and `read_spect_dbase.pro`

proc_tex_stra.pro: A LaTeXstring processing subroutine used by `read_spect_dbase.pro`.

check_partition_function.pro: Compares the partition function in `mol_data_table.tex` to `catdir.cat`.

plot_spectrum.pro: Plots a stick spectrum showing approximate strengths, molecule id, and frequencies of lines in an EOS band.

F.3 Procedure

Use the following procedure to automatically generate lines for EOS and UARS MLS missions.

1. Delete all files of name `data_for_??????.tex`. This is not always necessary after one gets started making and updating `line_data_table.tex.uc` but should be done the very first time the `line_data_table.tex.uc` is made.

2. Run `make_template.pro`. This will make a file called `line_data_table.tex.uc`.

3. Run `make_line_table.pro` 3 times for molecules, H$_{2}$O, H$_{2}\wedge${18}$O, and O$_{2}$ with eos band = 0. The program will prompt for a frequency range. Choose 0.0 to 3000000.0. This will populate the catalogue with all significant lines of H_2O, $H_2^{18}O$, and O_2. The user can add other molecules at a later time.

4. Run `merge_continuum_lines.pro`.

5. Run `merge_files.pro`.

6. Run `sweep_over_catalogue.pro` for each or a collection of eos band(s) to consider. A negative sign on the band number means consider the lower sideband frequencies.

7. Run `merge_files.pro`.

8. Repeat 5 and 6 until all bands are done. Repeat for UARS bands.

9. cp `line_data_table.tex.uc` to `line_data_table.tex` and place it int the `MLSPGS` directory.

A shell script exists for doing the above procedure automatically called `run_build_catalogue.cmd`.

F.4 Maintanance

Over time, new line shape data and even line position data become available. The new line shape data will need to be added to the `/users/bill/catalogue/jpl_catalogue/s`**spectls**`.cat` file. New line by line calculations will require importing the affected `/users/bill/catalogue/jpl_catalogue/c`**spectag**`.cat` file from the JPL

catalogue web site (URL: http://spec.jpl.nasa.gov). You will also need to import the `/users/bill/catalogue/jpl_catalogue/catdir.cat` file from the JPL catalogue web site. You may need to update the `mol_data_table.tex` file by hand if the partition function has changed and the JPL catalogue partition function value is used instead of the HITRAN value. More on this later. After these file updates, one can run `make_line_table.pro` on the affected molecule for the affected band followed by a `merge_files.pro` run. If necessary repeat for other affected bands for UARS and EOS. If the only changes are line shape parameters (e.g. modified `/users/bill/catalogue/jpl_catalogue/s` **spectls**`.cat` files), then the whole file can be brought up to date by running `update_lineshape.pro`. It is much quicker than running `make_line_table.pro` followed by `merge_files.pro`.

F.5 Program Descriptions

F.5.1 `make_template.pro`

Inputs: None

This program creates a file called `line_data_table.tex.uc` which contains the first two header lines but has no line data in it.

F.5.2 `make_line_table.pro`

Inputs: molecule, eos_band

Keywords: mol_file, molecule_file, thresh, del_nu, del_lse, uars, lo_frq, hi_frq

This program finds the approriate subset of JPL catalogue lines for **molecule** to be applied to radiative transfer calculations for **eos_band**. **eos_band** is a vector (or scalar) of signed integers representing the frequency space covered by the bands to be considered. A negative sign is for the lower sideband and a positive sign is for the upper sideband. The program determines the minimum and maximum frequency including the channel band width covered by the vector of bands inputted. The frequency bounds are extended an additional 500 MHz above and below the extrema so as to ensure that the lineshape is behaving like ν^2 for lines beyond these extrema at 100 hPa or above. Lines that are far enough away from the targeted bands are treated as continuum contributions and are not included in line $\times$ line calculations. Excluding lines having a ν^2 absorption behavior is done because lineshape theory is very poor in the wings of lines. Another option is to set **eos_band** = 0 where the program will prompt the user to input a frequency range (or get it from **lo_frq, hi_frq** if supplied). And another option is to set **uars** = 1 which interprets **eos_band** as an UARS MLS band(s). If non zero **eos_band** is supplied, the program sets a field which is written out called **eos_bands** or **uars_bands** to contain the band characters (e.g. **eos_band** = [-2,3,22] $\rightarrow$ **eos_bands**, or **uars_bands** when **uars** flag is set = B2L, B3U, B22U). If **eos_band** = 0, then **eos_bands** and **uars_bands** are blank. The program first reads the appropriate JPL catalogue line file, `/users/bill/catalogue/jpl_catalogue/c`**spectag**`.cat`. The strengths are multiplied by the ratio of the JPL partition function to the `mol_data_table.tex` (default, but changeable with **mol_file** keyword) partition function which corrects the strength

for the vibrational partition function where ever it is applicable. The appropriate subset of lines are extracted from the line file and tested for strength. Strength is tested by doing a very simple optically-thin radiative transfer calculation assuming 500 km path length at the line shape maximum. The **molecule** mixing ratio is read from the `molecule_data_base.txt` (default, but changeable with **molecule_file** keyword) file. Brightness exceeding 0.01 K (default, but changeable with **thresh** keyword) are kept. The line frequencies, strengths, lower state energies, and quantum numbers are read from the JPL catalogue. The line shape data (pressure broadening coefficient, temperature dependence, pressure shift coefficient, temperature dependence, and four interference coefficients) come from one of three sources based on a heirarchial procedure. Initially based on the quantum number designations, the program will look for this data in a `/users/bill/catalogue/jpl_catalogue/s`**spectls**`.cat` file. Next it will look for this data in a HITRAN file. If this fails then it uses default values in the `molecule_data_base.txt` file. Whenever possible whose details are not perfectly worked out yet, the JPL quantum numbers are matched with the HITRAN quantum numbers when combining JPL line data with HITRAN shape data. Unfortunately these catalogues don't use the same quantum number formats and when these can't be identified then a match based on lower state energy and transition frequency is attempted. This is dicey because the two catalogues do not place the lines at exactly the same frequency. They often differ by one or two parts per million or more. A field called **ref** is set to **M**, **H**, or **G** to let the user know if the lineshape data for the particular line came from the `/users/bill/catalogue/jpl_catalogue/s`**spectls**`.cat` file, HITRAN data base or `molecule_data_base.txt` file respectively. Finally degenerate and near degenerate lines are collapsed into one line. Lines having the same lower state energy (default, but changeable with the **del_lse** keyword) and within 0.5 MHz (default, but changeable with the **del_nu** keyword) are collapsed into a single line where the frequency, lower state energy, line shape data is a strength weighted average and the strength is the sum of the individual lines. When lines are combined, the quantum number format field indicates the number of combined lines and the quantum numbers are for one of the component lines. The line collapsing feature can be turned off by setting **del_nu** to any negative number. *It is very important when tabulating measured line shape data in the* `/users/bill/catalogue/jpl_catalogue/s`**spectls**`.cat` *file that all degenerate level quantum numbers are included.* A file containing the line data including band designations and line shape data source called `data_for_`**spectag**`.tex` is written.

F.5.3 `sweep_over_catalogue.pro`

Inputs: eos_band

Keywords: mol_file, molecule_file, thresh, del_nu, del_lse, uars

This program successively calls `make_line_table.pro` for each **molecule** in `molecule_data_base.txt` (default, but changeable with **molecule_file** keyword) and writes a collection of `data_for_`**spectag**`.tex` files. The input parameters are described under `make_line_table.pro`.

F.5.4 `merge_continuum_lines.pro`

Inputs: None

This program reads in turn each `/users/bill/catalogue/jpl_catalogue/b`**spectag**`.cat` and matches the molecule, and quantum numbers in the `line_data_table.tex.uc` file and adds the supplied **eos_bands** and **uars_bands** to the latter file. The purpose of this operation is to ensure that the line set for the designated molecules are included so as to make the auxiliary continuum function given in `mol_data_table.tex` work properly. The `/users/bill/catalogue/jpl_catalogue/b`**spectag**`.cat` file is maintained by hand and contains quantum numbers and **eos_bands** and **uars_bands** fields. A separate `/users/bill/catalogue/jpl_catalogue/b`**spectag**`.cat` file is created for each species that has a continuum.

F.5.5 `merge_files.pro`

Inputs: None

This program merges all the available `data_for_`**spectag**`.tex` files into `line_data_table.tex.uc` acording to the following rules

1. New lines (based on quantum number designations) in `data_for_`**spectag**`.tex` are added to `line_data_table.tex.uc` and sorted by frequency.

2. If an existing line in `line_data_table.tex.uc` has the same quantum numbers and quantum number format as a line in `data_for_`**spectag**`.tex` then the former is overwritten by the latter except for the band designation fields. The band desigantion field is combined (ie a mathematical union).

A caveat. If one runs the `make_line_table.pro` program with the line combiner turned on and merges, followed by a run with the line combiner turned off and merges, the `line_data_table.tex.uc` file will duplicate the combined line and its components. This may be what you want if you wish to distinguish the DACS bands from the standard filter banks. Another trap is if `make_line_table.pro` program is run for the same band(s) but with different **del_nu** or **del_lse** values. The merged file may have extraneous lines. Also if the `make_line_table.pro` program is run on an updated `/users/bill/catalogue/jpl_catalogue/c`**spectag**`.cat` file and merged into `line_data_table.tex.uc` may also cause problems if the lines are combined differently. Therefore one should delete the line data in `line_data_table.tex.uc` for the affected **molecule** before merging. The same is also true if one *increases* **thresh**. However, if the only change is in the lineshape file (`/users/bill/catalogue/jpl_catalogue/s`**spectls**`.cat`), the file merger program does the right thing.

F.5.6 `update_lineshape.pro`

Inputs: None

This program overwrites the line shape data in a `line_data_table.tex.uc` with data present in `/users/bill/catalogue/jpl_catalogue/s`**spectls**`.cat` files where there

is a molecule id and quantum number match. It leaves all other lines unaffected and does not change the number lines in the file. This program is a quick way to import line shape data into the `line_data_table.tex.uc` file.

F.5.7 `read_molecule_file.pro`

Inputs: filename

Outputs: molecule, spectag, spectls, hitran, hitran_iso, hitran_frac, nom_mr, dflt_wc, dflt_nc

Reads the `molecule_data_base.txt` file. See file description of `molecule_data_base.txt` for a description of the output fields.

F.5.8 `read_mol_dbase.pro`

Inputs: mol_file, species

Outputs: mol_data

keywords: molID, readID

Reads a `mol_data_table.tex` file. **mol_data** is a structure. **species** is either a null string or a vector of molecule names in LaTeXformat. A null string returns a vector sturcture **mol_data** containing all species in the file whereas inputted species names returns only the requested species if present in `mol_data_table.tex`. See file description of `mol_data_table.tex` for a description of the structure components and the output fields. **molID, readID** are character strings containing tracking information for CVS.

F.5.9 `read_spect_dbase.pro`

Inputs: mol_file, line_file, species

Outputs: sps_data

keywords: molID, lineID, readID

Reads `mol_data_table.tex` and `line_data_table.tex` files. **sps_data** is a structure. **species** is either a null string or a vector of molecule names in LaTeXformat. A null string returns a vector sturcture **sps_data** containing all species in the file whereas inputted species names returns only the requested species if present in `mol_data_table.tex`. See file description of `mol_data_table.tex` and `line_data_table.tex` for a description of the structure components and the output fields. **lineID, molID, readID** are character strings containing tracking information for CVS.

F.5.10 `read_continuum_designator_file.pro`

Inputs: filename

Outputs: qnu, qnl, uars_bands, eos_bands

Reads a `b`**spectag**`.cat` file whose name is the input **filename**. The outputs are: **qnu, qnl**, upper and lower quantum numbers for the lines in the file (both are 12 character strings), **uars_bands** are the UARS bands that use lines having these quantum numbers, and **eos_bands** are the EOS bands that use lines having these quantum numbers.

F.5.11 `proc_tex_string.pro`

Inputs: lu

Outputs: sps_name, buff

Processes an ASCII LaTeXformat line in `mol_data_table.tex` already opened with logical unit **lu**. It returns the molecule name **sps_name** and a string of data contents in **buff**.

F.5.12 `proc_tex_stra.pro`

Inputs: lu

Outputs: sps_name, buff, stra, strb,qnu, qnl, ref

Processes an ASCII LaTeXformat line in `line_data_table.tex` already opened with logical unit **lu**. It returns the molecule name **sps_name**, a string of data contents **buff**, **stra**, **strb**, **qnu**, **qnl**, and **ref**. The latter 5 fields need to preserve the string nature of its contents.

F.5.13 `check_partition_function.pro`

Inputs: None

This program compares the partition functions in `/users/bill/catalogue/jpl_catalogue/catd`
to those in `mol_data_table.tex` and writes the result by molecule as percent difference at 300, 225, and 150 K. This program is used to check for obvious errors in the partition functions cause by hand transcription. It should be noted however that the partition functions in `mol_data_table.tex` are where applicable, spin-rotation-vibration and are sometimes larger than those in `/users/bill/catalogue/jpl_catalogue/catdir.cat`.

F.5.14 `plot_spectrum.pro`

Inputs: eos_band

keywords: uars

This file reads the `/users/bill/mlspgs/tables/mol_data_table.tex` and `/users/bill/mlspgs/tables/line_data_table.tex` and plots a simple stick spectrum showing, position, strength, and molecule of selected lines for the inputted **eos_band**, a signed integer, negative is lower sideband, positive is upper sideband. The calculation is a simple optically thin 500 km radiative transfer computation at line center using the mixing ratio supplied in `molecule_data_base.txt`. Lines exceeding 100 K are truncated to 100 K. This program runs on the spectral data base files currently in the `mlspgs` directory. If keyword flag **uars** is set, then the spectrum applies to the UARS instrument; however, I don't think this feature is working at present.

F.6 File Descriptions

F.6.1 `molecule_data_base.txt`

This file contains the pertainent list of molecules to consider. It is maintained by hand. This file contains the fields **molecule, spectag, spectls, hitran, hitran_iso, hitran_frac, nom_mr, dflt_wc, dflt_nc**. The fields are:

molecule: The molecule name in LaTeXnotation.

spectag: JPL catalogue spectag ID.

spectls: A corresponding spectag ID for getting the line shape data. This is different from **spectag** because in many cases I will refer to the parent isotope lineshape data for minor isotopes and for excited vibrational states.

hitran: HITRAN catalogue file name.

hitran_iso: HITRAN cataloge isotope ID number.

hitran_frac: Isotopic fraction, usually from HITRAN data base.

nom_mr: A representative concentration to use when selecting lines for **molecule**.

dflt_wc: Pressure broadening coefficient for **molecule**.

dflt_nc: Temperature dependence of the pressure broadening for **molecule**.

This contains a fairly comprehensive list of molecules which may be observable with microwave–far infrared instruments. Some of these molecules are not in the JPL catalogue. These are designated with **spectag** = `000000` or `???99?`. In the latter case a psuedo jpl catalogue file was created from the HITRAN catalogue. Unfortunately the HITRAN catalogue appears to use a greater strength cut-off limit which means the reconstructed line catalogues are only partial listings of lines.

F.6.2 `mol_data_table.tex`

This file contains data for the same list of molecules in `molecule_data_base.txt` that is common for all its line spectrum. This file contains the fields: **name, abun, mass, q(3), cont(6)**

name: The molecule name in LaTeXnotation.

abun: Naturally occuring isotopic abundance.

mass: atomic mass in AMU.

q(3): Partition function value (*not logarithm of*) at 300, 225, and 150 K.

cont(6): 6 parameters describing this molecule's continuum.

This file is currently maintained by hand. The partition function values come from either the HITRAN catalogue, adjusted JPL catalogue or JPL catalogue. I preferably use the HITRAN because it contains the vibrational partition function whereas for most molecules, the JPL does not. Some cases I used an adjusted JPL catalogue value which is derived by multiplying the JPL spin rotation q by the vibration q derived from the excited vibrational states given in the JPL catalogue. The JPL q calculation contains more rotational states than does HITRAN. There are some instances where the HITRAN q will be larger than the JPL q for the higher temperatures (due to vibrational q) whereas the JPL has a larger q at lower temperatures (due to more rotational states). I have used the larger of the two values therefore some partition function values for a given molecule are a mix of JPL and HITRAN values. Also note that some of the molecules in `catdir.cat` are not in the standard JPL catalogue. These molecules having **spectag** = `???99?` are molecules reconstructed from the HITRAN catalogue to fill in missing species. Therefore if you import a new `catdir.cat`, don't forget to add the extra molecules. For this reason I have a backup copy called `catdir.cat.sav`. The `catdir.cat` files are kept in `/users/bill/catalogue/jpl_catalogue` directory.

The fields above are combined in structures **mol_data** and **sps_data** with variables names like **mol_data(*)."field"** or **sps_data(*)."field"** where**"field"** is any one of the field names given above.

F.6.3 `line_data_table.tex`

This file contains line data for all or a subset of molecules listed in `mol_data_table.tex`. Files `line_data_table.tex.uc` and `data_for_`**spectag**`.tex` have identical formats. This file contains the fields **name, no_lines, frq, gse, ist, wc, nc, ps, ns, int1, n1, int2, n2, qnfmt, qnu, qnl, uars_bands, eos_bands, ref**

name: The molecule name in LaTeXnotation.

no_lines: number of lines for **name**

frq(*): Line frequency in MHz.

ist(*): log integrated strength in nm^2 MHz.

gse(*): Lower state energy in cm^{-1}.

wc(*): Pressure broadening coefficient at 300 K in MHz hPa^{-1}.

nc(*): Temperature exponent of the pressure broadening coefficient.

ps(*): Pressure shift coefficient at 300 K in MHz hPa^{-1}.

ns(*): Temperature exponent of the pressure shift coefficient.

int1(*): Line interference coefficient at 300 K in hPa^{-1}.

n1(*): Temperature exponent of the line interference coefficient.

int2(*): Line interference coefficient at 300 K in hPa^{-1}.

n2(*): Temperature exponent of the line interference coefficient.

qnfmt(*): Quantum number format which is an integer of the form **qnfmt** = $D * 10000 + Q * 100 + H * 10 + NQN$ where D is the number of degenerate lines combined, Q indicates the type of molecule, H is a 3-bit code for existence of half integer quantum numbers, and NQN is the number of quantum numbers. See web site (URL: http://spec.jpl.nasa.gov) for full description of fields Q, H, and NQN.

qnu(*): Upper state quantum numbers. Applies to one of the combined lines if **qnfmt** > 9999.

qnl(*): Lower state quantum numbers. Applies to one of the combined lines if **qnfmt** > 9999.

uars_bands(*): A string indicating which eos bands should use this line.

eos_bands(*): A string indicating which uars bands should use this line.

ref(*): The source for the line shape data.

This file is automatically maintained using the programs above.

The fields above are combined in the structure **sps_data** with variables name **sps_data(*).“field”** where **“field”** is any one of the field names given above.

F.7 Initial Program Runs

Table F.1 gives the collection of bands and thresholds that are used for running `sweep_over_catalogue.pro`

Table F.1: Inputs to `sweep_over_catalogue.pro` runs.

Bands	Mission	Thresholds	
		Initial	Goal
-1, -21, -22, -26, -32, -34	EOS	1.0	0.1
-2, -3, -4, -5, -6, -23, -27	EOS	0.05	0.01
2, 3, 4, 5, 6, 23, 27	EOS	0.05	0.01
-7, -8, -9, -24, -25, -33	EOS	1.0	0.1
7, 8, 9, 24, 25, 33	EOS	1.0	0.1
-10, -11, -28, -29	EOS	0.05	0.01
10, 11, 28, 29	EOS	0.05	0.01
-12	EOS	0.05	0.01
12	EOS	0.05	0.01
-13, -14, -30, -31	EOS	0.05	0.01
13, 14, 30, 31	EOS	0.05	0.01
-15, -18	EOS	0.5	0.1?
15, 18	EOS	0.5	0.1?
-16, -19	EOS	0.5	0.1?
16, 19	EOS	0.5	0.1?
-17, -20	EOS	0.5	0.1?
17, 20	EOS	0.5	0.1?
-1, 1	UARS	0.1	NA
-2, -3, -4	UARS	0.01	NA
2, 3, 4	UARS	0.01	NA
-5, -6, 5, 6	UARS	0.01	NA

Appendix G. Unpublished UARS MLS forward model paper

The unpublished UARS MLS forward model paper whose last version was written in 20 May 1998 is presented here. This paper is only a draft copy and there exist some typographical errors.

The UARS MLS Radiance Model

WG READ and Z. Shippony

Jet Propulsion Laboratory, California Institute of Technology, Pasadena, Ca.

Abstract. The mathematical description of the MLS forward model is described. The basic features include a local thermodynamic equilibrium (LTE) radiative transfer calculation which is averaged over the instrument's spectral and spatial responses.

Introduction

The 12 September 1991 launch of the Upper Atmosphere Research Satellite (UARS) is the initial phase of NASA's Mission to Planet Earth program of long-term space-based research into global atmospheric change [Reber, 1993 []]. The UARS platform carries ten instruments which make measurements of processes involving energy inputs, dynamics, chemistry, and photochemistry to be studied on a global scale. The overall mission objective is to improve our understanding of upper atmospheric processes which will provide accurate forecasting of the impacts of policy decisions regarding anthropogenic industrial activities [WMO 1991 []]. The satellite experiments strive to produce measurements of "atmospheric state," those are constituent concentrations, temperatures, winds, etc.; however, one should appreciate that such quantities are inferred from remotely measured spectra. This paper describes the model which relates the radiances measured by the Microwave Limb Sounder (MLS), one of ten experiments on UARS, to atmospheric state. This model in addition to providing the means to determine the atmospheric state is also necessary for error characterizations [Rodgers, 1990 []].

The MLS scientific objective is to monitor fluctuations in the Earth's ozone layer and its anthropogenically produced destructive agent, chlorine monoxide over time and space [e.g. Waters et al., 1993a [] and Waters et al., 1993b []]. Other relevent measurements include temperature [Fishbein et al., 1993 []], and water vapor [Harwood et al., 1993 []]. These data have already been used to advance our understanding of ozone loss during the northern hemisphere winter [Manney, 1994 []]. Since launch, detailed data analysis have provided additional retrievals of nitric acid [Santee et al., 1994 []], sulfur dioxide from Mt. Pinatubo [Read et al., 1993 []], and upper tropospheric water vapor [Read et al., 1995 []]. As mentioned before, the MLS constituent concentrations are derived from microwave and millimeter spectral measurements. This paper describes the MLS measurement model used to relate atmospheric state to measured spectra and referred to as the *forward model* hereafter. The forward model is used by a retrieval algorithm described by Froidevaux et al. [Froidevaux et al., 1996 []] to infer atmospheric state.

MLS Overview

The MLS is a vertically scanned limb thermal radiance hetrodyne receiving instrument mounted at 90 degrees to UARS orbital motion. The UARS platform is in a nearly circular 585 km orbit inclined 57 degrees to the equator. This viewing geometry allows latitude coverage from 80 degrees in one hemisphere to 34 degrees in the other hemisphere. The orbit plane precesses at the rate of 5 degrees a day relative to the sun. The platform is designed to keep one side away from the sun at all times to keep it out of the field-of-view of the limb viewing instruments and the other side in the sun where the solar panel is mounted. After 36 days of orbital precession, the solar illuminated side of UARS switches sides. When this happens, the UARS executes a 180 degree yaw maneuver which restores the proper spacecraft solar illumination and causes the hemispheric coverage to invert. This orbital configuration allows a complete sampling of local time for the study of diurnal effects.

The MLS "measures" ClO, O_3, H_2O, and O_2 by measuring the spectral intensity or radiance of their molecular emissions in the microwave and millimeter regions using vertically scanned limb sounding. The MLS instrument has three hetrodyne receivers with local oscillator frequencies at 63.2 GHz, 203.3 GHz, and 184.8 GHz. Each of these "double sideband" receivers are tuned to receive radiation in one or more 500 MHz wide bands offsetted by 0.3–2.8 GHz above and below the local oscillator frequency. An emission line from each of the target molecules is spectrally located on one side of the local oscillator frequency in the center of a

received band (except O_2 which has a line on both sides of the local oscillator in the center of the band). Each band is spectrally resolved into 15 channels having nominal frequency offsets of ±191, ±95, ±47, ±23, ±11, ±5, ±2, and 0 MHz relative to band center with respective variable spectral widths approximately 128, 64, 32, 16, 8, 4, 2, and 2 MHz. The radiation (at all frequencies) is received through an antenna system which has a measured half power beam width of 9.8 km, 3.0 km, and 3.7 km for the receivers. The differences in beam width are proportional to the receiver wavelengths. The field-of-view of the antenna system is vertically scanned from the top of the atmosphere (∼ 87 km) to the Earth's surface in 65.536 seconds. The scan proceeds in 32 discete steps taking 2.048 seconds which includes time for moving the antenna and measuring the radiation (∼ 1.8 s). The scan step spacing for normal operations varies from 5 km in the mesosphere, to 1 km in the lower stratosphere, to 3 km in the troposphere, followed by a 3 step retrace which returns the FOV to the top. During the 3 step retrace and 3 other 2.048 s intervals, the instrument is internally calibrated by looking at either cold space (having known radiation) or an internally maintained and measured "hot" target. Although radiation at all received frequencies is collected through the same primary optics system, it is eventually separated into individual paths before being detected. Therefore the field-of-view directions (however one defines this) of the three receivers will not exactly coincide and needs to be characterized before launch. The details of the design operation and calibration of MLS can be found in [Jarnot, et al., 1996 []]. This technique offers the following features: 1) the limb sounding geometry provides an extremely long pathlength (∼ 400 km) which allows detection of minute concentrations of trace atmospheric constituents, 2) the vertical scanning provides vertically resolved data, 3) the microwave and millimeter wavelengths can incorporate solid state signal processing technologies which allow fabrication of receivers having high signal sensitivities with high spectral resolution and good calibration stability, and 4) the long wavelengths are not affected by scattering or emission of aerosols even following large volcanic eruptions. The spectral strength of the species targeted for measurement depends on the species abundance, the spectral location of the species' emissions relative to the MLS receiver frequency and bandpass, spectroscopic line strengths, and spectral line shape. The first and last items are highly sensitive to altitude. In fact, the O_2 measurement, a species with an invarient and well known abundance allows easy separation of those items and exists to provide the altitude measurement. This altitude measurement simplifies determination of abundances for the other targeted molecules. The O_2 signal also provides the temperature measurement.

In addition to the targeted molecules, any molecule can have emissions which affect the radiance measurement and may need to be considered. Table 1 lists the species considered for modelling MLS radiances. The following subsections give the results from a simple radiance calculation around the MLS receiver frequencies. The program interfaces with the *JPL Submillimeter, Millimeter, and Microwave Spectral Catalog*[Pickett et al., 1992 []] for the spectral lines and strengths. Vertical profiles for the species in Table 1 used "typical" abundances and the line shape data was the same for all species and assumed a value representative of the target molecule line.

63 GHz Spectrum

Figure 1 is a survey calculation of a radiometric spectrum between 62.0 and 64.5 GHz for three limb paths having tangent pressures at 1, 10, and 22 hPa. The two detected MLS spectral regions are bounded by the dashed and dotted lines with channel 1 being furthest from the LO and channel 15 is nearest. The measured spectrum is obtained by folding the spectrum in figure 1 at the LO frequency (the two bounded regions should coincide) and adding the two overlayed spectra with weights r_u and r_l (which sum to one). The channel bandwidths specified above are deployed symetrically with the widest channels furthest from band center (ie 1 and 15) and becoming successively narrower towards the middle. This is the Band 1 measurement. As can be seen each band is centered on one O_2 line. The O_2 lines are choosen from a manifold of magnetic dipole transitions involving a change in total angular momentum arising from the electron spin and molecular rotational angular momenta. The choice is based on a pair of lines which produces a radiance growth curve relative to tangent pressure in the middle to lower mesosphere and exhibits a high degree of temperature insensitivity in the weak signal limit. The instrument averages the signals received in each band according to a pre-lauched determined weight called a sideband ratio and produces a single spectrum. Therefore, the MLS produces a spectrum dominated by one spectral line feature which is of course emissions from two O_2 lines. The three ray paths having a different limb tangent pressure clearly shows the effect of pressure broadening on the line which is exploited for the pressure measurement [Fishbein et al., 1996 []]. The flattening of the tops of the O_2 lines oc-

Table 1. JPL Catalog species included in radiance calculations. Atoms not preceded with isotope numbers assume the most naturally occuring isotope and the quantity in parenthesis indicates an excited vibrational state.

I think this list is not complete - bill

O(atom)	OH	NH_3	CH_3D	OD	$^{15}NH_3$	H_2O	NH_2D	H_2O(v2)	^{18}OH
HDO	$H_2^{18}O$	CN	HCN	CO	$H^{13}CN$	$HC^{15}N$	DCN	^{13}CO	HCO+
CH_2NH	N_2H+	$C^{18}O$	$H^{13}CO$+	DCO+	H_2CO	$^{13}CH_2NH$	$CH_2^{15}NH$	CH_2ND	NO
$HC^{18}O$+	$H_2^{13}CO$	O_2	O_2(v1)	CH_3OH	$H_2C^{18}O$	HO_2	$O^{17}O$	$O^{18}O$	H_2S
PH_3	H_2O_2	HDS	HCl	$H^{37}Cl$	CH_3CCH	CH_3CN	CH_2CO	CHDCO	CS
SiO	N_2O	^{13}CS	^{29}SiO	$C^{34}S$	^{30}SiO	H_2CS	HCOOH	NO_2	$H_2^{13}CS$
$H^{13}COOH$	DCOOH	HCOOD	SO	SO(v1)	$H_2C^{34}S$	O_3	O_3(v2)	O_3(v1,3)	O_3(2v2)
$O^{17}OO$	$^{17}OO_2$	^{34}SO	$S^{18}O$	$O^{18}OO$	$^{18}OO_2$	$O^{18}OO$(v2)	$^{18}OO_2$(v2)	ClO	HOCl
C_2H_3CN	^{37}ClO	$HO^{37}Cl$	C_2H_5CN	OCS	SiS	$O^{13}CS$	^{29}SiS	$OC^{34}S$	^{18}OCS
^{30}SiS	$Si^{34}S$	HNO_3	SO_2	$H^{79}Br$	$H^{81}Br$	^{79}BrO	^{81}BrO	$ClNO_3$	$^{37}ClNO_3$

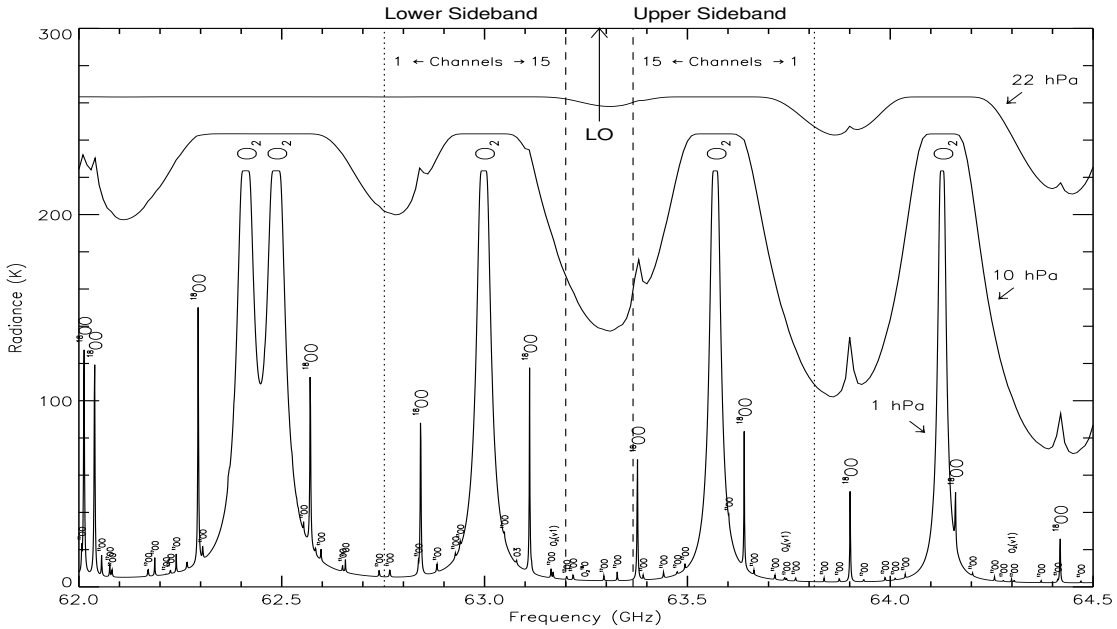

Figure 1. Radiance spectrum of three limb viewing paths in vicinity of 63 GHz radiometer. The three curves indicate limb paths having different tangent pressures. The calculations used an isothermal atmosphere and a hydrostatic model. The isothermal temperature values were varied among the three curves so as to separate them.

Table 2. Species which affect Band 1.

Species	Altitude Range km
O_2	5-80
$O^{18}O$	20-80
$O^{17}O^{\dagger}$	20-80

† Not included in V0003 retrievals but will be included in subsequent versions.

curs when the optical depth becomes so large that the atmosphere is effectively a blackbody emitter which is one of the effects used to infer atmospheric temperature. Clearly, $O^{18}O$ has significant features and this needs to be included. Although the spectrum shows this feature as being distinct, it does not present itself this way in individual MLS spectra because these features are located in the rather wide edge channels of the band and causes distortion in the measured O_2 line shape. Minor contributions in order of importance are $O^{17}O$, vibrationally exicted O_2 and ozone. Table 2 lists molecules considered in Band 1 measurement computations.

Table 3. Species which affect Bands 2 and 3.

Species	Altitude Range km
ClO	15–50
HNO_3	15–40
H_2O_2	20–40
SO_2	15–35
O_3	15–40
$H_2^{18}O$	0–30
$^{18}OO_2$	15–50
N_2O	0–35
H_2O	0–30
N_2 & $O_2^{\dagger}$	0–40
$HDO^{\ddagger}$	0–30
$H_2O_{liq}^{\ddagger}$	0–20
$O_3(v2)^{\wr}$	15–40
$CH_3CN^{\diamond}$	15–40

† This is the collision induced absorption and magnetic dipole absorption.
‡ Included in current V0003 processing but will be excluded in V0004.
≀ Included in V0004.
◇ Replaces SO_2 in V0005 processing.

205 GHz Spectrum

Figure 2 is a survey calculation of a radiometric spectrum between 198.0 and 208.0 GHz for two limb paths having tangent pressures of 46 and 4.6 hPa. This receiver measures spectra in three regions as indicated in the figure by B2, B3, and B4 referred to as Band 2, Band 3, and Band 4. Identical to the 63 GHz radiometer, each band spectrum is the combination of radiances from two spectral regions offset by an equal amount above and below the local oscillator frequency. Each band is further subdivided into 15 channels in the usual way. Band 2 is centered on a group of ClO lines (spread across 25 MHz) at 204.35 GHz. Band 3 is centered on an H_2O_2 line at 204.57 GHz. During the MLS science definition phase H_2O_2 was believed to be much more abundant and an important species in the hydrogen cycle. After the instrument design was finalized and being built, it was realized that H_2O_2 was much less abundant and below the 65 second detection limit of the radiometer. This Band is currently used to extend the bandwidth of the ClO measurement. Band 4 is centered on the 206.13 GHz ozone line. Note that the complimentary frequencies below the local oscillator for these bands are in regions of little spectral activity so as to provide minimal interference with the target measurement.

Table 3 lists the molecules included in the calculation of bands 2 and 3 radiances. Spectra in the lower stratosphere and upper troposphere show sloping wing features from $H_2^{18}O$, O_3, and N_2O. Note that some of the emission is received by the lower frequency sideband. HNO_3 and $^{18}OO_2$ are very weak but clearly recognizable if lots of radiometric data are averaged. SO_2 which is not shown has a line at 204.25 GHz and is easily detected if abundances exceed 10 ppbv as happened following the Mt. Pinatubo eruption on 15 June 1991 [Read et al., 1993 []]. Another molecule, CH_3CN (not shown), also has a group of lines at 202.3 GHz which is in the lower sideband and would be observable if its concentration exceeds 20 pptv. In band 2, the SO_2 and CH_3CN interfere with each other strongly but are distinguishable because SO_2 has a line in band 4 whereas CH_3CN does not; however, the band 4 SO_2 line interferes heavily with HNO_3 which creates a situation where only 2 of these three molecules can be independently retrieved. In V0005 the decision has been made to retrieve CH_3CN and HNO_3 and ignore SO_2. This decision is based on the fact that nominal SO_2 concentrations are below the detection limit which is a result of its conversion to aerosols through well understood processes. Hence SO_2 is observable only during perturbed situations—like that after a large volcanic eruption. CH_3CN is expected to be a tropospheric source

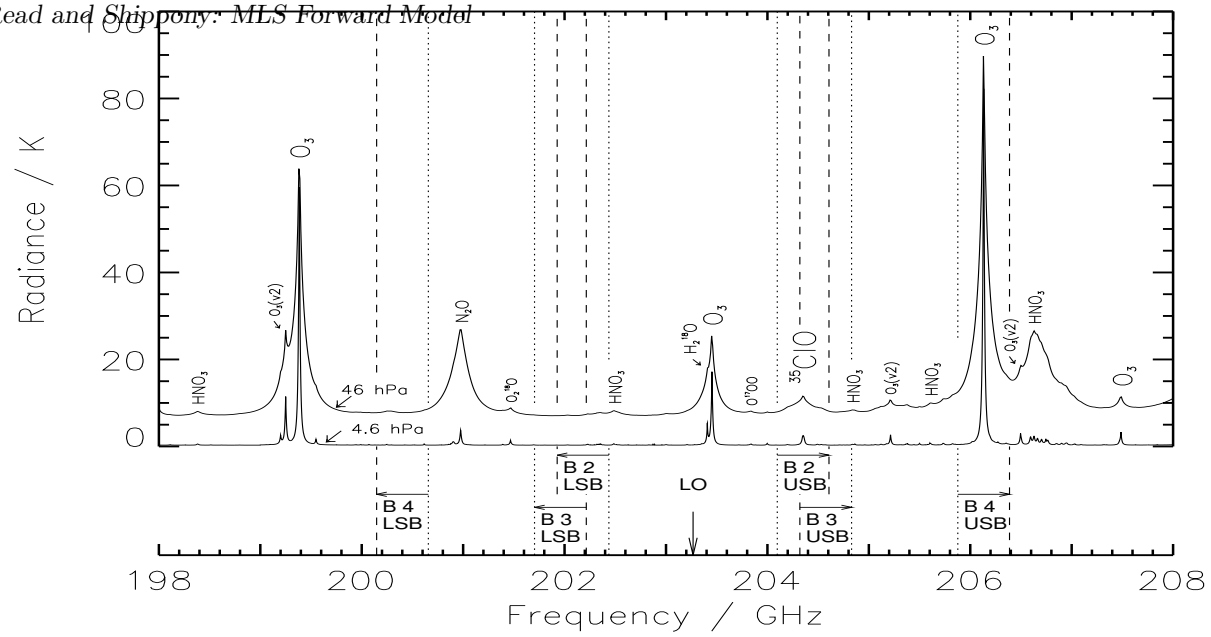

Figure 2. Radiance spectrum of two limb viewing paths in vincinity of 203.2 GHz radiometer. The two curves indicate limb paths having different tangent pressures. The calculations used an isothermal atmosphere, a hydrostatic model and $\sim$ 2 ppbv ClO in the lower stratosphere.

gas and will be present all the time. V0004 retrievals which retrieved SO_2 always showed persistently high values at least 10 times greater than expected was suspicious. Therefore based on the current understanding of atmospheric chemistry, it is more reasonable to believe that this is really CH_3CN. Also the spectrum is generally better fit with CH_3CN. Special processing will be done after volcaninic events to get SO_2 in V0005. The radiances exhibit a slowly decaying background absorption with height which can be partially explained by including a dry air collision induced absorption (CIA) model. CIA for nitrogen has been measured [Dagg et al., 1985 [], and references therein] and this absorption has been seen in the observations. The V0003 processing uses a simple empirical function measured from MLS radiances to account for emission from all possible effects from N_2 & O_2 in the atmosphere. Version 0004 uses a N_2 CIA function derived from experimental measurements and a line by line calculation for O_2 to estimate its contribution. V0005 uses the dry calibration function (includes both O_2 and N_2) derived from upper tropospheric humidity studies which is described in a later section. HDO contributes about 0.01 K to the continuum in the lower stratosphere and increases slightly at lower altitudes. This species is deemed superflous and will be neglected in V0004 and beyond. Liquid water can contribute significantly to the continuum at very low concentration; however, experience has shown no effect attributable to this and aerosols are undetectable. Condensed water is more likely to be ice which is expected to be detectable when concentrations exceed 0.005 g/m^3. These conditions can occur in strong convective systems and the effects have been observed in the MLS radiances in the upper troposphere. Nevertheless, condensed water is also neglected in future processing at least for the stratospheric retrievals. As the FOV is scanned down, the radiometric signal becomes dominated by emissions from the N_2 & O_2 continua and H_2O and the small spectral features in bands 2 and 3 wash-out. Since the air continua is expected to be only effected by pointing and temperature in a known way, this signal can be used to infer upper tropospheric water vapor providing new data in the poorly sampled altitudes about 3-4 km below the hygropause [Read et al., 1995 []].

Band 4 is used to measure ozone. This and other species affecting band 4 are listed in Table 4. Sloping tails from HNO_3 and N_2O can be seen in the spectra. Note that N_2O is actually coming from the lower frequency sideband. The impact of HNO_3 on the spec-

Table 4. Species which affect Bands 4.

Species	Altitude Range km
O_3	15–70
HNO_3	15–40
SO_2	15–35
$O^{18}OO$	15–50
N_2O	0–35
H_2O	0–30
HO_2	20–60
N_2 & $O_2^{\dagger}$	0–40
$H_2O_{liq}^{\ddagger}$	0–20
$O_3(v2)^{\wr}$	15–40

† This is the collision induced absorption and magnetic dipole absorption.
‡ Included in current V0003 processing but will be excluded in future processing.
≀ Included in future processing.

trum is severe enough that its abundances can be independently retrieved and used for scientific analysis [Santee et al., 1994 []]. The excited vibrational ozone $O_3(v2)$ is not included in V0003 but from figure 2 it will clearly interfere with the quality of the HNO_3 retrieval and is included in V0004 and beyond. The lower sideband also contains a SO_2 line at 200.29 GHz which is about 2 K at 20 ppbv. Although totally masked by the much stronger O_3 line in the upper frequency sideband, this feature shows clearly in the difference spectrum generated between the measured and calculated during the early post launch period when Pinatubo SO_2 was present. The SO_2 line however interferes strongly with the HNO_3 feature as described previously. The heavy ozone isotope $O^{18}OO$ has two very weak lines at the edges of the upper frequency sideband and causes a slight distortion in the measured O_3 line spectrum. It is included to model this effect. HO_2 emits at 200.62 GHz in the lower frequency sideband and when averaged over the broadly banded channel 1 at the sideband edge is expected to have a signal strength of 0.01 K using expected abundances and is probably superflous. Finally the dry air continua (from N_2 & O_2 emissions) and all phases of H_2O contribute similarly as described for Bands 2 & 3.

183 GHz Spectrum

Figure 3 is a survey calculation of a radiometric spectrum between 182.0 and 187.0 GHz for two limb paths having tangent pressures of 46 and 4.6 hPa. This receiver measures spectra in two regions as indicated in the figure by B5 and B6 referred to as Band 5 and Band 6. This radiometer like the others is also a double side band receiver having 15 channels per band. The lower frequency sideband of Band 5 is tuned on the 183.31 GHz water vapor line. This line is strong and provides good signal strength up to the upper mesosphere. The line strength is strong enough that the spectral emission at the edge of the receiver bandwidth has saturated near the hygropause. Line saturation provides an atmospheric temperature measurement. Small shifts in the line position inside the band are also easily detected in the upper statosphere and this is caused by changes in molecular velocity mostly due the relative motion of the Earth to the satellite. Because of its great strength, interfering species are relatively less important and have been ignored. Only two appear important, O_3 and CH_3Cl. Ozone contributes only to the background continuum giving it some slope. Although CH_3Cl is within the broadly banded channel 15 of the upper frequency sideband it is about 1 K in the lower stratosphere (less above) and has no distinctly resolvable spectral feature apart from a spectral slope. Currently both of these are ignored in current V0003 production processing; however, O_3 is added in V0004. Band 6 is centered on the 184.38 GHz line of ozone and is 4 times stronger than the 206.16 GHz ozone line. Interestingly, most of the interferring lines in the Band 6 spectrum come from additional ozone lines which are included in the calculation. Current and future processing includes H_2O because of its spectral proximity and great strength. The 184.38 GHz ozone line is sufficiently strong to allow easy detection well into the mesosphere and to observe molecular velocity changes. The background continuum arises from dry air emission and condensed phases of water. It is treated similarly to Bands 2–4. Table 5 gives the species included in current V0003 processing and those planned for V0004 and V0005.

MLS measurement Definition

The MLS instrument has been described elsewhere [Barath et al., 1993 []]. The instrument is a hetrodyne receiver operating at centimeter and millimeter wavelengths. It receives thermal radiation (Watts m^{-2} Hz^{-1} $Ster^{-1}$) from the atmospheric limb. The radiation passes through an antenna system, into a hetrodyne mixer, through a spectrometer and finally into a square law detector which converts power linearly into volts which is digitized and recorded. Periodically, the receiver-detector electronics measure thermal radiation from blackbody sources of known temperatures—one being an internal absorber maintained at $\sim$ 300 K, the

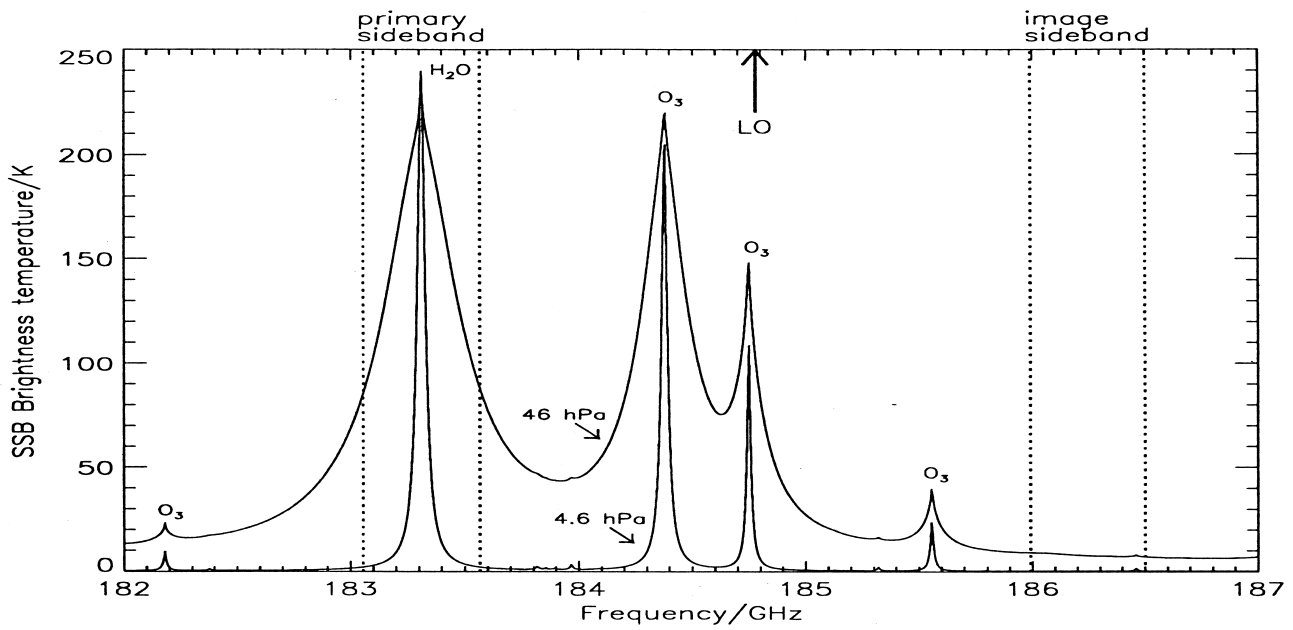

Figure 3. Radiance spectrum of two limb viewing paths in vincinity of 184.8 GHz radiometer. The two curves indicate limb paths having different tangent pressures. The calculations used an isothermal atmosphere, a hydrostatic model.

Table 5. Species which affect Bands 5 & 6.

Species	Altitude Range km
H_2O	0–90
$O_3^{\dagger}$	15–80
N_2 & $O_2^{\ddagger}$	0–40
$H_2O_{liq}^{\wr}$	0–20

† Not included in V0003 Band 5 processing, but will be included in future versions.
‡ This is the collision induced absorption and O_2 magnetic dipole emission.
≀ Included in current V0003 processing but will be excluded in future processing.

other being the 2.7 K cosmic background. This is the basic in-orbit calibration operation which allows easy conversion from engineering quantities (e.g. volts), into an atmospheric observable, thermal radiance. The calibration procedure takes into account temporal drifts in the electronics while determining the limb radiance. Imperfections in the antenna, limitations in the pattern measurement equipment and differences in optical paths while viewing the atmospheric limb, cold space and the MLS internal target are included in radiometric calibration and yields the following definition for calibrated radiance [Jarnot, et al., 1996 []].

$$\begin{aligned} \dot{I} &= r_{\mathrm{u}} \frac{\int_{\nu_{1\mathrm{o}}}^{\infty} \int_{\Omega_A} I\left(\nu, \Omega, \underline{x}\right) \Phi\left(\nu\right) G\left(\Omega\right) \mathrm{d}\Omega \mathrm{d}\nu}{\int_{\nu_{1\mathrm{o}}}^{\infty} \int_{\Omega_A} \Phi\left(\nu\right) G\left(\Omega\right) \mathrm{d}\Omega \mathrm{d}\nu} \\ &+ r_{\mathrm{l}} \frac{\int_{-\infty}^{\nu_{1\mathrm{o}}} \int_{\Omega_A} I\left(\nu, \Omega, \underline{x}\right) \Phi\left(\nu\right) G\left(\Omega\right) \mathrm{d}\Omega \mathrm{d}\nu}{\int_{-\infty}^{\nu_{1\mathrm{o}}} \int_{\Omega_A} \Phi\left(\nu\right) G\left(\Omega\right) \mathrm{d}\Omega \mathrm{d}\nu}, \quad (1) \end{aligned}$$

where $\dot{I}$ is the measured radiance, r_{u} is the higher frequency (relative to the LO) side band ratio for the channel, r_{l} is the lower sideband ratio (both numbers must sum to one), $I\left(\nu, \Omega, x\right)$ is the limb radiance, $\Phi\left(\nu\right)$ is the instrument spectral response, and $G\left(\Omega\right)$ is the antenna response or field-of-view. Eqn. 1 is channel specific and the filter function Φ, sideband ratios, r

changes with channel and the antenna pattern G depends on radiometer. For simplicity, these quantities have not been subscripted but remember that eqn. 1 is evaluated 90 times for MLS at each scan step. The antenna gain is a function of solid angle Ω and a weak function of frequency which is ignored within each radiometer. The spectral response function Φ is a function of frequency ν. Limb spectral power I is a function of solid angle, frequency, and state vector x. The antenna is not integrated over 4π ster radians but instead over a small solid angular section given by Ω_A which contains all the available measurable response. However, the pattern is normalized over this small solid angle. *Rick, Bob, Joe, we probably should make sure we are comfortable with this statement. Later in the paper when the antenna averaging calculation is discussed, I will present a conversion of eqn. 1 into a standard convolution format which by necessity forces an "infinite range" integration or an entire hemisphere or 2π ster radians of solid angle (which actually gets collapsed into one dimension) and the pattern is normalized with respect to this integral. This allows the fast fourier transform technique to be used. Based on the equation above it seems probable that there may be a distortion error introduced by the forward calculation.* The units of radiance, $\overset{\bullet}{I}$ and $I(\nu, \Omega, \underline{x})$ are *watts / Hz* or spectral power. If the atmosphere is an isotropic blackbody, then $I(\nu, \Omega, \underline{x}) = h\nu / \left(\exp\left\{\frac{h\nu}{kT}\right\} - 1\right)$, the spectral power Planck blackbody equation where h is Planck's constant, k is Boltzmann's constant, T is temperature. Since calibration uses reference thermal emitters based on temperature measurements and to maintain traditions from radio astronomy it is conceptually easier to understand I when expressed in temperature units. This is done with no loss of accuracy by dividing both sides of eqn. 1 by Boltzmann's constant. The temperature-like quantity is approximately equivalent to the temperature of a blackbody emitter but differs because the Rayliegh-Jeans approximation (commonly used in radio astronomy) is slightly inadequate and not employed here.

Eqn. 1 require the following assumptions (*Bob or Rick, can you check these*):

1. Calibration targets are spatially isotropic blackbody emitters that completely fill the non-baffle portion of the receiver aperture with radiation. This assumption allows absolute knowledge of spectral power emission from a temperature measurement. In addition, the instrument optics gain and blackbody transmitter functions need not be known.
2. Antenna gain functions are frequency independent over Φ. This allows separation of the frequency and solid angle dependence in the power integrals for calibration.
3. The spectral response acts as an impulse function relative to the received radiation for all radiometer views except the limb view. Additionally the radiation from the sideband above the local oscillator is equal to that of the sideband below the local oscillator for all views except the limb view. This allows removal of the Planck spectral power function in the frequency integration of the power integrals for calibration and the separation of equation 1 into individual sideband contributions as given.
4. The spectral response function F_i is indentical for all switching mirror positions and independent of scan. This permits the use of a relative spectral response measurement in the forward model.
5. Conversion of received power into counts is linear.

The Inversion Problem

The inversion problem simply stated is rewriting eqn. 1 as $\underline{x} = F\left(\overset{\bullet}{\underline{I}}, ?\right)$; however, the state vector $\underline{x}$ is unlikely to be uniquely defined by this relationship without the inclusion of additional models and measurements which are designated by ?. The objective is to establish a complete and independent set of variables which are overconstrained by the measurement system. After the statevector has been established, the MLS inversion problem is solved [Froidevaux et al., 1996 []].

The State Vector The MLS state vector selection process is shown pictorially in fig 4. We begin by clearly defining the measurement objective, in this case being vertical profiles of atmospheric constituents $\underline{f}$ and temperature $\underline{T}$, and the source of information which are an ensemble of MLS radiances $\overset{\bullet}{\underline{I}}$. The model which connects these, the subject of this paper, will require additional variables in addition to $\underline{f}$ and $\underline{T}$. These variables are $\underline{w}$ and are also part of the state vector. Unfortunately, limitations in the measurement/retrieval system do not sufficiently constrain the state vector, therefore we must add additional constraints or information. These measurements fall under the general catagory of virtual measurements or *a priori* estimates. These latter quantities are connected to the state vector by the virtual measurement model (or *a priori* model). This model is discussed in Froidevaux et al., 1996 []. The

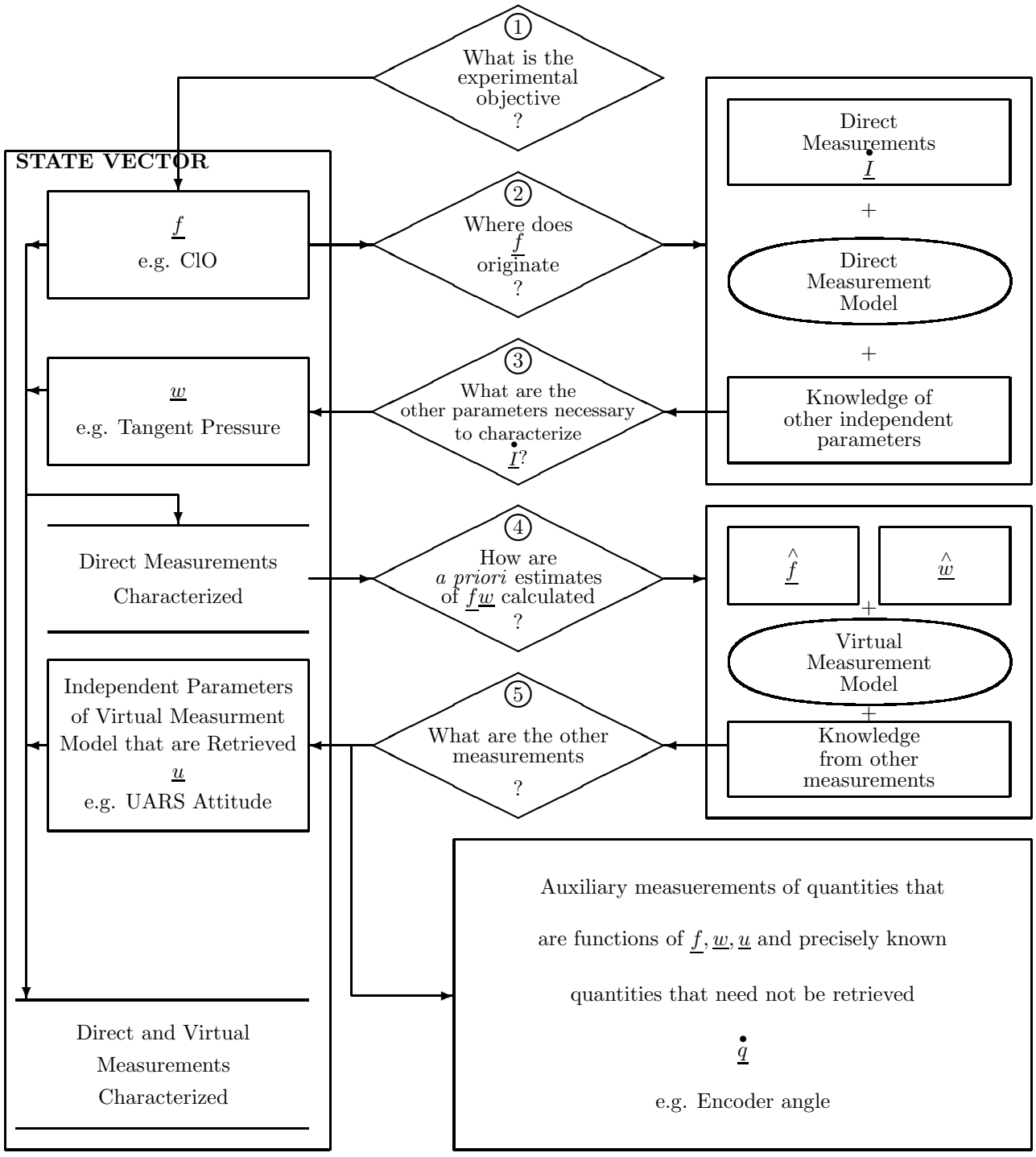

Figure 4. Schematic of Selection Process for MLS State Vector

purpose of the virtual measurement model is to provide a method for obtaining parts or all of $\underline{f}$ and $\underline{w}$ where the direct measurement model is inadequate. In the course of incorporating these measurements and accompanying models, new unknown independent quantities $\underline{u}$ may need to be retrieved. The virtual measurement model, like the direct measurment model will need additional measured data in addition to that already supplied by previous estimates of $\hat{\underline{w}}$ and $\hat{\underline{f}}$ and these measurements are indentified in $\dot{\underline{q}}$. When all the "unknown" independent variables are covered by additional measurements and models then the state vector is complete and defined. The state vector is now defined as $\underline{x} = (\underline{f}, \underline{T}, \underline{w}, \underline{u})$.

For MLS, $\underline{f}$ are all the atmospheric constituent profiles targeted for measurement e.g. ClO, O_3, H_2O, and temperature. $\underline{w}$ includes limb pointing altitude (in pressure units), contaminant species, e.g. SO_2, HNO_3, N_2O among a few, the field of view direction offset angles among the three principal receivers in the instrument, total molecular line of sight velocity profile, magnetic field parameters, the limb path tangential Earth radius and satellite radius, and instrumental radiometric offset and in V0005 an extinction coefficient. A future version may include horizontal and cross-track line-of-sight gradient (linear model) effects in $\underline{w}$. Since $\underline{w}$ includes all the independent variables of the direct measurement model that are not in $\underline{f}$, it would include all the instrument calibration data such as sideband ratios, and spectroscopic data such as line broadening parameters and even fundemental constants like the Boltzmann. In practice however, only those items whose uncertainties are considered important are included. The retrieval methodology used by MLS has focused on random error sources and desires to ignore systematic errors in its error characterization during the retrieval process. Therefore potential state vector elements which will contribute only toward the systematic error budget or have negligible error have been excluded from the statevector and are treated as errorless constants in the direct measurement model. Although these decisions can appear arbitrary, this is why items such as linebroadening, sideband ratios are not part of $\underline{w}$. The virtual measurement model includes a stochastic model for estimating "future" profiles based combining previous ones (the $\hat{\underline{f}}$ and $\hat{\underline{w}}$) and an antenna scanning model incorporating a hydrostatic model for estimating limb tangent pressure. This model depends on UARS attitude data (specifically roll) which became part of the state vector ($\underline{u}$) because its uncertainty is believed to be reduced with MLS limb tangent pressure measurements. A stochastic model for the UARS measured attitude data is also part of the virtual measurement models. Finally a simple data transfer of UARS spacecraft data into $\underline{w}$ (e.g. radiometer offset). Virtual measurement data include climatologies for estimating $\underline{f}$ and National Centers for Enviromental Prediction (NCEP) daily temperature fields for $\underline{T}$. For estimating limb pointing (in pressure) we use the antenna scan angle measurements which is part of the instrument calibration [see Jarnot, et al., 1996 []] and UARS supplied attitude data. Other measurements which are incorporated are receiver FOV direction offsets, UARS instaneous ephemeris (this provides geometric quantities and an estimate of line of sight velocity), and a geomagnetic field model. These additional measurements do not add any new unknowns and form a complete self-contained measurement system. These quantities are in $\dot{\underline{q}}$. It is worth noting that some of the contaminant species in $\underline{w}$ are being retrieved on par with target species with great advantage (relative to climatology, e.g. HNO_3, [Santee et al., 1994 []]).

The choice of vertical coordinate, whether it be geometric height, pressure, density or even potential temperature is completely arbitrary because the hydrostatic model is included and temperature is part of the state vector. We have chosen pressure because it can be shown that optically thin radiances calculated at constant tangent pressure are fairly insensitive to atmospheric temperature and is the standard output coordinate used by the UARS distributed data archive center (DAAC). Detailed studies to examine which if any particular vertical coordinate has any advantage apart from that stated above has not been done. Table 6 summarizes the MLS statevector components.

The radiometer offset polynomial $\underline{\Delta I}$ is an additive polynomial to eqn. 1 and becomes an element in $\underline{w}$. It accounts for all spectrally flat calibration errors and forward modelling errors. This term places the emphasis on computing the spectral signature or differences between MLS channels accurately rather than absolute radiances. This has the desireable impact of isolating radiometric effects caused by the targeted constituent from other atmospheric species or unmodelled and excluded phenomenon. In practice, retrieved constituent profiles quite often produce radiometric fits that are no worse than ± 0.2 K in the signature yet differ by as much as 5 K in absolute magnitude and it is clear from validation work that the retrieved profile is accurate. This underscores the the neccessity of including $\underline{\Delta I}$ in the statevector. Moreover, even if all the measurement physics were known perfectly, the model would require

Table 6. MLS Statevector Composition.

$\underline{x}^{\diamond}$	description
$\underline{f}$	Atmospheric Concentrations
$\underline{T}$	Atmospheric Temperature
$\zeta^{63}_{\tan}$	63 GHz radiometer LOS† Tangent Pressure
δ^{63}_{183}	FOV‡ directional offset between 63 GHz and 183 GHz radiometers
δ^{63}_{205}	FOV directional offset between 63 GHz and 205 GHz radiometers
$\underline{v}$	LOS molecular velocity
$R^{\oplus}$	Geocentric Earth Radius
R^{s}	Geocentric UARS Orbital Radius
$\underline{B}$	Magnetic Field Magnitude
$\underline{\theta}$	Angle between B and LOS
$\underline{\phi}$	63 GHz radiometer polarization angle
$\underline{\Delta I}$	Radiometer band offset polynomial
$\frac{\mathrm{d}_{f,T}}{\mathrm{d}_s}$	profile LOS gradiant°

◇ *Underline* indicates vector of values. In terms of the individual components it indicates a vertical profile of numbers.

† LOS is limb path Line of Sight.

‡ FOV is Field of View.

○ This component is to be added in the future.

the addition of more new statevector components than could be retrieved with essentially a DC measurement. An important drawback at least for measurements of a non-saturated line is that the instrument band width is narrowed because the band edge channels are used to supply the offset information which affects the lowest retrievable altitude. This term is handled by the retrieval software. On bands 1,4–6 it is just a constant added to the radiances and retrieved at each limb view. On Bands 2 and 3 which overlap in frequency, a linear function is retrieved across all the channels in those bands. This paper discusses the calculation of absolute radiances and will not consider this term to be part of the foward model state vector.

In version V0005, the direct measurement model implimentation is different from that used in earlier versions. In particular, the measurement objective $\underline{f}$ includes geopotential height and an antenna scan model which is used to get the geopotential height is added to the direct measurement model. Instead of using encoder angles and UARS attitude data as measurements, the modified antenna scan model uses UARS determined heights which combine these measurements and others into a single parameter. The the direct measurements now include radiances and heights, and UARS attitude is eliminated from the statevector and there will be no $\underline{u}$. In addition a continuum absorption baseline has been added which adds a constant absorption to the total absorption coefficient in the opacity calculation described later. The continuum absorption will have a different behavior than that caused by instrumental calibration errors or an additive radiance offset. An atmospheric continuum will contribute most when the total atmospheric absorption is weakest and least when its strongest, therefore even though the continuum is spectrally flat, this will impart a spectral shape to the radiances. This is handled by having a species called "EXTINCTION" which is an additive offset added to the *absorption coefficient* and has units of km^{-1}. The details of the V0005 statevector is discussed in a future publication.

Approximate Function Beginning with a statevector $\overset{\star}{\underline{x}}$, and the instrument response functions $G(\Omega)$, $F(\nu)$, and sideband responses, r_{u} and r_{l}, the measured radiance, $\overset{\star}{I}$ can be calculated using eqn. 1. Although eqn. 1 is a non-linear equation, for inversion purposes, a linear approximation is needed. The optically thin radiances are nearly linear in concentrations. This has been successfully exploited in current MLS V0003 retrievals which assume eqn. 1 is completely linear [Froidevaux et al., 1996 []]. Encouraged by this success and further numerical experiments also support that eqn. 1 may be adequately represented with a second order Taylor series.

$$
\begin{aligned}
I &= \overset{\star}{I} + \sum_l \overset{\star}{K}_j \left(x_l - \overset{\star}{x_l}\right) \\
&\quad + \frac{1}{2} \sum_l \sum_k \overset{\star}{L}_{jk} \left(x_l - \overset{\star}{x_l}\right) \left(x_k - \overset{\star}{x_k}\right), \\
\overset{\star}{K}_l &= \frac{\partial \overset{\star}{I}_i}{\partial x_l}, \\
\text{and,} & \\
\overset{\star}{L}_{lk} &= \frac{\partial^2 \overset{\star}{I}}{\partial x_l \partial x_k} \qquad (2)
\end{aligned}
$$

The calculation of $\overset{\star}{I}$, first derivatives, $\overset{\star}{K}_k$ and second derivatives, $\overset{\star}{L}_{lk}$ is the subject of this paper. The overscore $\star$ indicates the Taylor series expansion or linearization point of eqn. 1. Currently, only the zeroth and first derivative terms are computed for processing. In the future, for most of the channels, non-linearity will be included by extending the power series to second order. This will have the advantage of high computational speed (fewer terms in nested sums), and high initial ac-

curacy at the linearization point (less need to find ways to compromise eqn. 1 for sake of speed).

The MLS inversion program, or level 2 (L2) processing, accesses the forward model through a file table. There is a file for each UARS yaw period. Within each file there are 8 linearization choices or $\underline{\overset{\star}{x}}$s to choose from. These nominally represent eight 20° wide zonal averages between 80°S to 80°N and the two flight orientations (northward or southward velocity) occuring each orbit. Each linearization choice within this file (called an L2PC file) has the statevector, $\underline{\overset{\star}{x}}$, radiances for the 90 MLS channels, $\underline{\overset{\star}{I}}$, and derivatives of radiance with respect to each state vector element, $\underline{\underline{\overset{\star}{K}}}$. The radiances and derivatives are tabulated as functions of limb tangent pressure between 1000.0 and 0.0001 hPa in 43 steps of $\frac{1}{6}$ in $\log_{10}$ pressure. This allows the L2 processing to account for non-linearities in the vertical dimension.

Forward model derivatives The MLS statevector has approximately 200 elements and the radiances and derivatives are needed for each element. These calculations are very time consuming and efficient methods are desired for computing the derivatives. This motivated the use of analytic rather than numerical methods (such as finite differences) for computing the derivative tables for the inversion program. Eqn. 1 defines the MLS radiance calculation and here we define $\overset{\star}{K}_k$, and $\overset{\star}{L}_{lk}$ used in eqn. 2. The following section defines the radiative transfer calculations and derivatives and subsequent section on instrumental effects includes the procedure to compute the full instrument radiances and derivatives.

Radiative Transfer Calculation

Discrete Radiative Transfer Equation

Radiative transfer equations for the special case of local thermodynamic equalibrium without scattering for polarized and isotropic radiation are given. The radiative transfer and its derivative forms are developed for the limb viewing geometry used by MLS as shown in figure 5. Each path is characterized by a frequency and the height (or pressure) of its nearest Earth center of mass contact also called tangent height (or pressure). A polarized calculation is necessary for the 63 GHz O_2 emission which is partially polarized by Earth's magnetic field. Lenoir [1967], has developed the radiative transfer equation for this situation and is given by

$$\frac{\mathrm{d}}{\mathrm{d}s}\underline{\underline{I}}(s) + \underline{\underline{\mathcal{G}}}(\underline{x},s)\,\underline{\underline{I}}(s) + \underline{\underline{I}}(s)\,\underline{\underline{\mathcal{G}}}^{t*}(\underline{x},s) = B(s)\left(\underline{\underline{\mathcal{G}}}(\underline{x},s) + \underline{\underline{\mathcal{G}}}^{t*}(\underline{x},s)\right), \tag{3}$$

where B is the Planck radiation function in K given by

$$B = \frac{h\nu}{k\left(\exp\left\{\frac{h\nu}{kT}\right\} - 1\right)}, \tag{4}$$

$\underline{\underline{I}}$ is the radiance (in K) tensor along path s, and $\underline{\underline{\mathcal{G}}}$ is the complex radiation propagation tensor given by

$$\underline{\underline{\mathcal{G}}}(\underline{x},s) = \frac{2\imath\pi\nu}{c}\sum_j \underline{\underline{\rho}}_j \mathcal{N}_j, \tag{5}$$

where $\imath = \sqrt{-1}$, c, is the speed of light, $\underline{\underline{\rho}}_j$ is a tensor which characterizes the polarization emitted (or absorbed) by the j'th transition, and $\mathcal{N}_j$ is the contribution of the j'th transition to the total complex index of refraction. The details regarding the evaluation of eqn. 5 is forthcoming. The radiation tensor contains the polarization properties and has the following form

$$\underline{\underline{I}} = \begin{bmatrix} I_{\parallel} & I_{|} + \imath I_{\circ} \\ I_{|} - \imath I_{\circ} & I_{\perp} \end{bmatrix}, \tag{6}$$

where $I_{\parallel}$ is the radiation component co-polarized with the receiver, $I_{\perp}$ is the cross-polarized component, and $I_{|}$ and $I_{\circ}$ are the linear and circular coherences respectively. Isotropic radiation has no coherence and $I_{\parallel} = I_{\perp} = I$. Consequently, the radiation tensor can be collapsed into a scalar equation giving [Chandrasekhar, 1960 []]

$$\frac{\mathrm{d}I(s)}{\mathrm{d}s} + \kappa(\underline{x},s)\,I(s) = \kappa(\underline{x},s)\,B(s), \tag{7}$$

where $\underline{\underline{\mathcal{G}}} \longrightarrow \kappa$, the absorption coefficient.

Eqn. 3 is solved by transformation into an integral equation,

$$\underline{\underline{I}}(s) = \underline{\underline{I}}(s_o)\,\underline{\underline{\mathcal{T}}}(\underline{x},s_o) + \int_{\underline{\underline{\mathcal{T}}}(\underline{x},s_o)}^{\underline{\underline{1}}} B\left(\underline{\underline{\mathcal{T}}}\right)\mathrm{d}\underline{\underline{\mathcal{T}}}, \tag{8}$$

where s_o is a point on the path, s where $\underline{\underline{I}}(s_o)$ is known and $\underline{\underline{\mathcal{T}}}$ is the transmission defined as

$$\begin{aligned} \underline{\underline{\mathcal{T}}} &= \underline{\underline{\tau}}\,\underline{\underline{\tau}}^{t*}, \\ \text{where} \\ \underline{\underline{\tau}} &= \exp\left\{-\int_{s''}^{s} \underline{\underline{\mathcal{G}}}(s')\,\mathrm{d}s'\right\}. \end{aligned} \tag{9}$$

This equation is discretized and evaluated with numerical methods (see Rosenkranz and Staelin, [1988], for numerical evaluation of the tensor form or Marks

and Rodgers, [1993], for an isotropic application). The exponentiation of a complex matrix is acomplished with Sylvester's identity (assuming distinct eigenvalues) [Gantmacher, 1959 []].

$$\underline{\underline{\tau}} = \sum_{i=1}^{2} \exp\{\lambda_i\} \prod_{j\neq i}^{2} \frac{-\int_{s''}^{s} \underline{\underline{\mathcal{G}}}(s')\,\mathrm{d}s' - \lambda_j \underline{\underline{1}}}{\lambda_i - \lambda_j} \tag{10}$$

where λ_i is an eigenvalue of the matrix argument in the exponential. Eqn. 8 is a differential transmittance equation and is not convenient for differentiation with the state vector (particularly the tensor equation). A better form is derived by integrating eqn. 8 by parts and obtaining the unusual looking differential temperature (or more precisely spectral power divided by k) integral equation,

$$\begin{aligned}\underline{\underline{I}}(s) = \underline{\underline{I}}(s_o)\,\underline{\underline{\mathcal{T}}}(\underline{x}, s_o) + B(s_o)\left(\underline{\underline{1}} - \underline{\underline{\mathcal{T}}}(\underline{x}, s_o)\right) \\ + \int_{B(s)}^{B(s_o)} \underline{\underline{\mathcal{T}}}(B)\,\mathrm{d}B,\end{aligned} \tag{11}$$

where $B(s_o)$ is the blackbody spectral power (in Kelvin) at s_o and $\underline{\underline{1}}$ is the identity matrix.

Eqn. 11 is solved in the usual way of partitioning the integrals into discrete steps. This process is shown in figure 5 for a limb path. This results in the following equation

$$\underline{\underline{I}}(s) = \sum_{i=N}^{t} \Delta B_i \underline{\underline{\mathcal{T}}}_{N-i+1} - \sum_{i=t}^{N} \Delta B_i \underline{\underline{\mathcal{T}}}_{N+i} \tag{12}$$

where i indicates layer boundary (and is decremented in the first sum), N is the layer index for the top of the atmosphere, t is the tangent layer or Earth surface ($t = 1$), $\underline{\underline{\mathcal{T}}}$ is given by eqn. 10 or in terms of layer transmittances according to

$$\begin{aligned}\underline{\underline{\tau}}_{N-i+1} &= \underline{\underline{\tau}}_{N-i} \underline{\underline{\Delta\tau}}_i = \prod_{j=N-1}^{i} \underline{\underline{\Delta\tau}}_i \\ \underline{\underline{\tau}}_{N+i} &= \underline{\underline{\tau}}_{N+i-1} \underline{\underline{\Delta\tau}}_{i-1} = \Upsilon \underline{\underline{\tau}}_{N-t+1} \prod_{j=t}^{i} \underline{\underline{\Delta\tau}}_i \\ \underline{\underline{\tau}}_1 &= \underline{\underline{\Delta\tau}}_N = \underline{\underline{1}}\end{aligned} \tag{13}$$

and ΔB_i is

$$\Delta B_i = \frac{B_{i-1} - B_{i+1}}{2},$$

with these exceptions:

$$\begin{aligned}\Delta B_1 &= \frac{B^{\oplus} - B_2}{2}, \\ \Delta B_N &= \frac{B_{N-1} + B_N}{2},\end{aligned}$$

in the first term, and

$$\Delta B_N = \frac{B_{N-1} + B_N}{2} - I(s_0), \tag{14}$$

in the second term. Filling in the details, $B^{\oplus} = B_1$, is the Earth surface value, $I(s_0)$, is the cosmic background, Υ, is the squareroot of the Earth reflectivity, B_i is the temperature at surface i (not an average value in the layer), and $\underline{\underline{\Delta\tau}}_i$ means field transmittance between surfaces i and $i+1$ with a slant path having an Earth tangent at surface t. Note that it is allowable to have t point to a surface below the surface of the Earth. The quantities $\underline{\underline{I}}$, $\underline{\underline{\mathcal{T}}}_i$, and $\underline{\underline{\Delta\tau}}_i$ depend on the limb tangent height t but a subscript indicating this has been omitted for notational simplicity. The analogous isotropic or scalar form of eqn. 12 is

$$I = \sum_{i=N}^{t} \Delta B_i \mathcal{T}_{N-i+1} - \sum_{i=t}^{N} \Delta B_i \mathcal{T}_{N+i} \tag{15}$$

where $\mathcal{T}$ is the scalar transmission function equivalent to $\underline{\underline{\mathcal{T}}}$ for isotropic radiation.

Evaluating Transmittance

The evaluation of the transmission function in eqn. 12 and eqn. 15 is described. The polarized and isotropic equations are analogous and presented together however be aware that the polarized form uses *field* absorption and dispersion coefficients whereas the scalar uses *power* absorption coefficient. This distinction is convenient because eqn. 10 shows that the transmission function used for the tensor calculation is the square root of that used in the scalar formula for isotropic radiation and a factor of two appearing in the exponential argument can be avoided. The propagation matrix (or absorption coefficient) is proportional to volume mixing ratio and the following form is used for incremental transmission,

$$\begin{aligned}\underline{\underline{\Delta\tau}}_i = \exp\Bigg\{ -\sum_l \sum_j \int_{s_{i+1}}^{s_i} \\ \underline{\underline{\rho}}_j(\theta,\phi)\,\beta_j^l(s, \mathcal{B}, \underline{T})\,F^l(s)\,\mathrm{d}s \Bigg\},\end{aligned} \tag{16}$$

where β is proportional (see eqn. 5) to the derivative of the complex refractive index with respect to volume mixing ratio and F is the mixing ratio function.

The $\underline{\underline{\rho}}_j(\theta,\phi)$ matrix establishes the emission tensor in the polarization basis established in eqn. 6. The two angles in this equation are defined in figure 6. The coordinate system IFOVPP is Instrument Field Of View

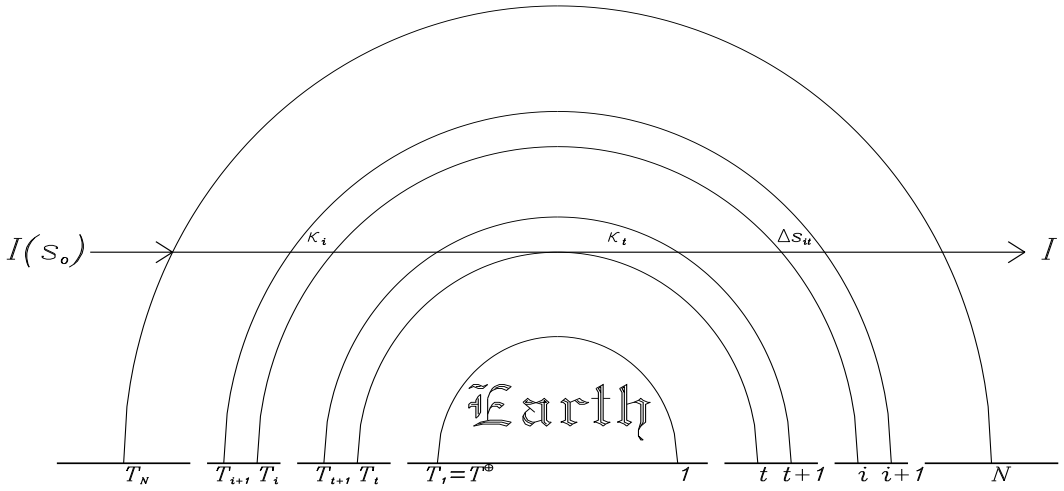

Figure 5. Layering notation for discrete radiative transfer calculations.

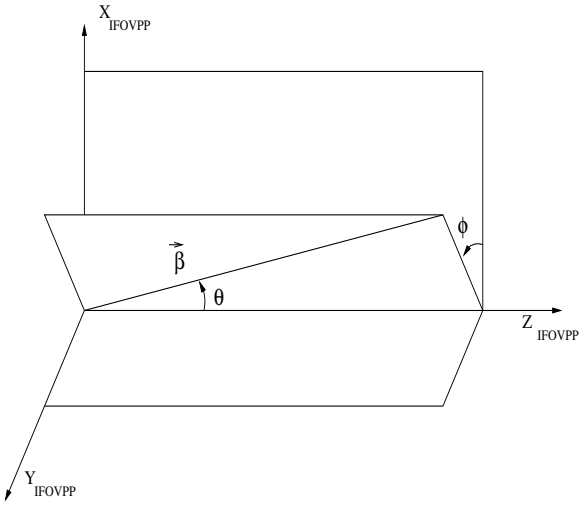

Figure 6. Angle definition for polarized radiative transfer

Plane Polarized. In this frame, the instrument FOV direction is the z-axis and receives polarized radiation whose electric field is parallel to the x axis. The y axis is parallel to the magnetic field component of the received radiation and makes a right-handed coordinate system with respect to the other axes. The Earth magnetic field vector has magnitude $\mathcal{B}$, and direction θ relative to the z-axis. The magnetic field vector and z-axis form a plane which is rotated through ϕ relative to the x-z plane in the IFOVPP coordinates as shown.

The details of $\underline{\underline{\rho}}_j\,(\theta, \phi)$, depend on the change in projection of total angular momentum in the molecule (designated as ΔM) along the geomagnetic vector. Only three such changes are important for most situations, ΔM = -1, 0, and 1. These are called σ_-, π, and σ_+ transitions. Beginning with the knowledge that the $\sigma_\pm$ transitions are circularly polarized and propagate along the magnetic field vector and the π transitions propagate with linear polarization perpendicular to $\underline{\mathcal{B}}$ it is possible to determine $\underline{\underline{\rho}}$. Lenoir [1968] has done this for a special case ($\phi = 0$) and it is extended here for the general case in figure 6 [see also Jackson, 1975 []]

$$\underline{\underline{\rho}}_{-1} = \begin{bmatrix} \cos^2\phi + \sin^2\phi\cos^2\theta & \cdots \\ -\sin\phi\cos\phi\sin^2\theta - \imath\cos\theta & \cdots \end{bmatrix},$$

$$\begin{array}{ll} \cdots & -\sin\phi\cos\phi\sin^2\theta + \imath\cos\theta \\ \cdots & \sin^2\phi + \cos^2\phi\cos^2\theta \end{array}\Bigg],$$

$$\underline{\underline{\rho}}_0 = \begin{bmatrix} \sin^2\phi\sin^2\theta & \sin\phi\cos\phi\sin^2\theta \\ \sin\phi\cos\phi\sin^2\theta & \cos^2\phi\sin^2\theta \end{bmatrix},$$

$$\underline{\underline{\rho}}_{+1} = \begin{bmatrix} \cos^2\phi + \sin^2\phi\cos^2\theta & \cdots \\ -\sin\phi\cos\phi\sin^2\theta + \imath\cos\theta & \cdots \\ \cdots & -\sin\phi\cos\phi\sin^2\theta - \imath\cos\theta \\ \cdots & \sin^2\phi + \cos^2\phi\cos^2\theta \end{bmatrix}, \quad (17)$$

where these matrices are normalized with respect to a unit vector and as such depend only on total angular quantum change, ΔM. Emission intensity depends on ΔM and overall quantum state and is incorporated in β of eqn. 16.

The independent variable of the integrand in eqn. 16 is transformed from horizontal path distance, s to vertical distance or height using a variable change because it is more convenient to express the components of the state vector in the vertical dimension. This is done by replacing s with H using

$$\begin{aligned} s &= \sqrt{H_N^2 - H_t^2} - \sqrt{H^2 - H_t^2}, \\ H &= h + R^{\oplus}, \end{aligned}$$

and

$$\mathrm{d}s = -\frac{H}{\sqrt{H^2 - H_t^2}}\mathrm{d}H, \quad (18)$$

where H is the center of Earth distance to s and includes the Earth radius and h refers to the vertical distance above the sea-level Earth.

The pressure dependence of β is approximately

$$\beta = AP^a, \quad (19)$$

where A and a are assumed constant between pressures $P(H_{i+1})$ and $P(H_i)$. The hydrostatic equation relates pressure to height according to

$$P = P_i \exp\left\{-\Delta H/\mathcal{H}\right\}, \quad (20)$$

where $\mathcal{H}$ is a scale height—a temperature dependent constant, $\Delta H = H - H_i$, and P_i is the pressure at h_i. Combining eqn. 19 and 20 gives the approximate functional behavior of β. Furthermore if β is known at two heights, then the following interpolation function results,

$$\beta(h) = \beta_i \exp\left\{\frac{\Delta\ln\beta_i}{\Delta h_i}(h - h_i)\right\}, \quad (21)$$

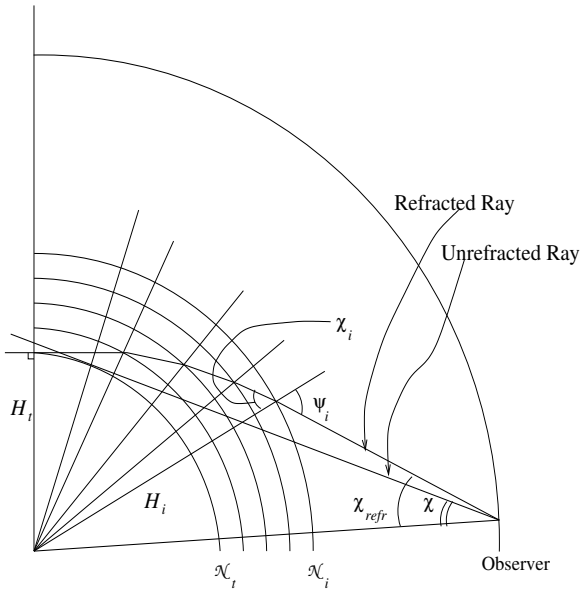

Figure 7. Geometry of refractive effects.

where $\Delta\ln\beta_i = \ln\frac{\beta_{i+1}}{\beta_i}$, $\Delta h_i = h_{i+1} - h_i$, and of course β_{i+1} and β_i are evaluated at h_{i+1} and h_i respectively.

The vertical profiles (e.g. constituent abundances, temperature, velocity, etc.) are generally composed of an infinite number of points with no particular function to constrain its shape. Since the number of measurements is finite and the instrument has finite resolution, it is necessary to greatly reduce the number of adjustable free parameters yet maintain sufficient flexibility so that any atmospheric profile shape can be recovered. The general approach is to express a vertical profile function as a linear combination of a set of basis functions,

$$F^l(h) = \sum_{m=1}^{M(l)} f_m^l \eta_m^l(h), \quad (22)$$

where $\eta_m^l(h)$ is the m'th basis function for l'th species, f_m^l is the m'th "adjustable parameter" for the l'th species, and $M(l)$ are the total number of coefficients and basis functions being used to describe the l'th species profile. Eqn. 22 will be described in more detail later.

The radiative transfer equations thus far assume an unrefracted straight-line ray path. Views in the lower stratosphere and troposphere will be refracted, causing a lengthening of the path length as shown in figure 7. The philosophy is to perform all calculations using unrefracted geometries, then correcting them for refraction. Referring to the figure, the refracted ray is treated as a

successive application of Snell's law which include the law of sines,

$$\begin{aligned}\sin\chi_i &= \frac{\overline{\mathcal{N}}_t}{\overline{\mathcal{N}}_{i-1}}\frac{H_t}{H_i},\\ \sin\psi_i &= \frac{\overline{\mathcal{N}}_t}{\overline{\mathcal{N}}_i}\frac{H_t}{H_i},\end{aligned} \tag{23}$$

where angles χ, and ψ are shown in the figure, and $\overline{\mathcal{N}}_i$ is the average refractive index in layer i. The refractive index is from Bean and Dutton, 1968 []

$$\mathcal{N} = 1 + 0.0000776\frac{P}{T}\left(1 + \frac{4810F^{\mathrm{H_2O}}}{T}\right), \tag{24}$$

where $F^{\mathrm{H_2O}}$ is the mixing ratio of water and the minor spectral dispersion contributions have been neglected. The refracted path length is determined from the geometry of figure 7 yielding,

$$\Delta s_i^{\mathrm{refr}} = H_{i+1}\cos\chi_{i+1} - H_i\cos\psi_i, \tag{25}$$

where angles χ_{i+1} and ψ_i are determined from eqn. 23. This equation is not very convenient but it can be combined with eqn. 23 and using first order approximations for divisions involving $\overline{\mathcal{N}}$ and $2H_t^2\ \left(\overline{\mathcal{N}}_t - \overline{\mathcal{N}}_{i+1}\right) \ll H_i^2 - H_t^2$ gives a more useful though less accurate form which relates the refracted path to the unrefracted path:

$$\Delta s_i^{\mathrm{refr}} = \Delta s_i\left[1 + \frac{H_t^2\left(\overline{\mathcal{N}}_t - \overline{\mathcal{N}}_{i+1}\right)}{\sqrt{\left(H_i^2 - H_t^2\right)\left(H_{i+1}^2 - H_t^2\right)}}\right]. \tag{26}$$

Unfortunately, eqn. 26 has a singularity at the tangent. This is circumvented by chosing a small enough step size where the difference between the refracted and unrefracted length can be neglected. Numerical experiments have shown that The approximations in eqn. 26 are good to 5% at the tangent and improves as one moves away from it.

Eqn. 26 is not adequate for the lower troposphere because the Taylor series representation is slowly converging and problems regarding the tangent point singularity are significant. An improved refractive treatment which is used in V0004 and V0005 is presented. Using figures from Goody , [1963], a differential form of the refracted pathlength can be derived and integrated giving the path length segments according to

$$\Delta s_i^{\mathrm{refr}} = \int_{H_i}^{H_{i+1}} \frac{\mathcal{N}H\mathrm{d}H}{\sqrt{\mathcal{N}^2H^2 - \mathcal{N}_t^2H_t^2}}. \tag{27}$$

The tangent point singularity can be removed by changing variables, viz. $x^2 = \mathcal{N}^2H^2 - \mathcal{N}_t^2H_t^2$, $2x\mathrm{d}x = 2\left(\mathcal{N}^2H + H^2\mathcal{N}\frac{\mathrm{d}\mathcal{N}}{\mathrm{d}H}\right)\mathrm{d}H$, etc. The integrand in eqn. 27 should replace eqn. 18, but instead as with eqn. 26, the transmittance integral will be scaled. This latter operation causes negligible error ($\ll$ 0.01K in radiative transfer calculations).

The incremental transmittance equation is derived by combining eqns. 16, 18, 21, 22, 26, or 27 to give

$$\begin{aligned}\underline{\underline{\Delta\tau}}_i &= \exp\left\{-\underline{\underline{\Delta\delta}}_i\right\}\\ \underline{\underline{\Delta\delta}}_i &= \sum_{l=1}^{NS}\sum_{m=1}^{M(l)}\sum_{\Delta M=-1}^{+1}\underline{\underline{\rho}}_{\Delta M}(\theta,\phi)\, f_m^l\Delta\delta_{ilm\Delta M}\end{aligned} \tag{28}$$

where $\underline{\underline{\Delta\delta}}_i$ is the total incremental opacity and the incremental opacity integral $\delta_{ilm\Delta M}$ is

$$\begin{aligned}\Delta\delta_{ilm\Delta M} &= \frac{\Delta s_i^{refr}}{\Delta s_i}\beta_{i\Delta M}^l\\ &\times \int_{h_i}^{h_{i+1}}\eta_m^l(H)\exp\left\{\frac{\Delta\ln\beta_{i\Delta M}^l}{\Delta H_i}\Delta H\right\}\\ &\times \frac{H}{\sqrt{H^2 - H_t^2}}\mathrm{d}H\end{aligned} \tag{29}$$

Changes in the magnetic field parameters along the integration path are neglected here but extension to the more general case is straightforward. The unpolarized form of equations 28 and 29 are identical except τ is a scalar, $\underline{\underline{\rho}}_{\Delta M}$ is eliminated along with the ΔM dependence, and β is real and is for power attenuation. The integral is evaluated with an eight point Gauss-Legendre quadrature.

Atmospheric Representation

Models and assumptions needed to evaluate the radiative transfer equation and its state-vector derivatives are described.

Line of Sight (LOS) Integration Hydrostatic balance is assumed over the full vertical extent in the atmosphere which is nominally 0–110 km. This important assumption allows rewriting cross section β which depends on pressure (or density) as a height function as described above. It also allows a single independent vertical variable which simplifies the state vector considerably as mentioned before. The hydrostatic relation is

$$h_i = \frac{g^{\oplus}{H_{\mathrm{eff}}^{\oplus}}^2}{g^{\oplus}H_{\mathrm{eff}}^{\oplus} - k\ln 10\sum_{q=1}^{NT}\left(T_qP_{qi}\right)} - H_{\mathrm{eff}}^{\oplus}, \tag{30}$$

where P_{qi} is the integral,

$$P_{qi} = \int_{\zeta^{\oplus}}^{\zeta_i} \frac{\eta_q(\zeta)}{\mathcal{M}(\zeta)} \mathrm{d}\zeta. \tag{31}$$

The superscript $\oplus$ indicates the value of that quantity at $H^{\oplus}$ which for convenience we choose to be the earth's surface. $g^{\oplus}$ is the gravitational acceleration (at the Earth's surface), $\mathcal{M}$ is the mean molecular mass, and T_q is a coefficient of a temperature profile having NT values and $\eta_q(\zeta)$ is the representation basis function. The independent variable is ζ which is $-\log\{P\}$. Eqn. 30 is oversimplistic because it assumes a non-rotating Earth and $1/H^2$ gravitational fall-off. These deficiencies can be virtually eliminated (see List, 1951 []) by defining $g^{\oplus} = -\mid \vec{\nabla}\mathcal{U} \mid$, the geopotential gradient and using an effective earth radius, $H^{\oplus}_{\text{eff}} = \frac{2g^{\oplus}}{-\left(\partial g^{\oplus}/\partial \mathrm{d}H\right)_{H=H^{\oplus}}}$ which satisfies two boundary conditions, namely, gravitational acceleration and its vertical gradient are correct for the spinning oblate Earth. The effective Earth radius used eqn. 30 is given in polynomial by List, 1951 []

$$\begin{aligned} H^{\oplus}_{\text{eff}} &= 2g^{\oplus} / \left(3.085462 \times 10^{-6}\right. \\ &+ \left. 2.27 \times 10^{-9} \cos 2\lambda - 2.0 \times 10^{-12} \cos 4\lambda\right). \end{aligned} \tag{32}$$

Eqn. 30 gives *geometric* (not geopotential) height because the quadratic dependence of gravitational acceleration in height is included.

The state vector discussion established the convention that ζ would be used as the independent variable for the constituent profiles and temperature. Beginning with a temperature profile which has been parameterized accordingly, eqn. 30 gives the heights needed to handle the geometric aspects of the opacity integration (see eqn. 29). A grid of ζ_i are chosen to give 1 km steps up to 70 km, and 2 km steps from 72 km to 110 km for a total of 91 layers.

Atmospheric Profiles Atmospheric constituents and temperature are represented by vertical functions composed of linear segments connecting points in $\zeta = -\log(P)$ in a connect-the-dots fashion. This is easily done using the form of eqn. 22 with ζ replacing h as the independent variable and the basis functions given by

$$\eta^l_m(\zeta) = \begin{array}{cc} 0 & \zeta \geq \zeta^l_{m+1} \\ \frac{\zeta^l_{m+1} - \zeta}{\Delta\zeta^l_m} & \zeta^l_{m+1} > \zeta \geq \zeta^l_m \\ \frac{\zeta - \zeta^l_{m-1}}{\Delta\zeta^l_{m-1}} & \zeta^l_m > \zeta > \zeta^l_{m-1} \\ 0 & \zeta^l_{m-1} \geq \zeta \end{array}, \tag{33}$$

which are triangular shaped functions having unit value at ζ^l_m and linearly going to zero on either side at ζ^l_{m-1} and ζ^l_{m+1}.

The species mixing ratios and temperature are input as an array of values versus ζ^l_m with the convention that basis function for a given coefficient goes from one at the peak to zero at the points adjacent. However this is not a complete specification of the function because there is no information delimiting the lower boundary or the upper boundary of the lowest and highest altitude coefficients. This is remedied by specifying two extra pressure levels in the ζ array where the first and last points are the lower and upper basis function 0 value. Temperature is an exception where the lowest pressure value indicates the unit peak for the first basis function and this function remains 1 for any $\zeta \leq \zeta_1$. Likewise the uppermost coefficient has unit value from ζ_{NT} to ∞. Hence, the temperature function is unambigously represented with a vector of pressure and temperature of equal dimension and never goes to zero at any altitude.

The representation basis needs to be converted to height for the benefit of eqn. 29. Combining height with the hydrostatic relation gives the following variable transform equation (for the upper triangular half)

$$\frac{H^l_{m+1} - H}{\Delta H^l_m} = \frac{\overline{T\mathcal{M}}^l_m H}{\overline{T}^l_m \overline{\mathcal{M}} H^l_m} \left(\frac{\zeta^l_m - \zeta}{\Delta\zeta^l_m}\right). \tag{34}$$

The unsubscripted mean variables $\overline{T}$ and $\overline{\mathcal{M}}$ are averages evaluated between H^l_m and H whereas the subscripted mean variables are between H^l_{m+1} and H^l_m. Currently, MLS processing neglects the ratio preceding the ζ triangular function and rewrites $\zeta \rightarrow H$, etc. The validity of this approximation is discussed. The mean molecular mass is constant from the surface to 0.003 hPa and varies slowly above hence the ratio $\overline{\mathcal{M}}^l_m / \overline{\mathcal{M}} = 1.0$ and can be neglected. The quadratic gravitational fall-off effect is worst at the Earth surface giving $H^l_{m+1}/H^l_m = 6377/6372 = 1.00078$ for a 5 km basis function (typical of MLS profiles) and can be neglected. The temperature effect is estimated by substituting

$$\begin{aligned} \overline{T}^l_m &= \left(T^l_{m+1} + T^l_m\right)/2.0, \\ \overline{T} &= \left(T^l_{m+1} + T^l_m + W^l_m\left(\zeta - \zeta^l_m\right)\right)/2.0, \\ \frac{\overline{T}}{\overline{T}^l_m} &= 1 + \frac{W^l_m\left(\zeta - \zeta^l_m\right)}{2\overline{T}^l_m}, \end{aligned} \tag{35}$$

where $W^l_m = \left(T^l_{m+1} - T^l_m\right) / \left(\zeta^l_{m+1} - \zeta^l_m\right)$, into eqn. 34 and neglecting effects due to mean molecular mass and

gravitatonal acceleration gives

$$\frac{H^l_{m+1}-H}{\Delta H^l_m} = \left[1+\frac{W^l_m}{2\overline{T}^l_m}\left(\zeta-\zeta^l_m\right)\right]\frac{\zeta^l_{m+1}-\zeta}{\Delta\zeta^l_m}. \quad (36)$$

The second term in the brackets will give the non linear behavior in the pressure basis function as a result of the direct substitution. When this is done in the forward model which is later used for retrievals, the "connecting" lines between the retrieved coefficients will be somewhat non linear in ζ. This approximation will cause errors in the column calculation. Integrating eqn. 36 over the triangular base and ratio this result with itself assuming $W^l_m = 0$ gives the percent error in the column.

$$\epsilon = \frac{W^l_m \Delta\zeta^l_m}{0.06\overline{T}^l_m} \quad (37)$$

A one percent error occurs with $\overline{T}^l_m = 250$ K and $W^l_m\Delta\zeta^l_m = 15$ K or in other words a 15 K temperature change across the representation basis. The atmosphere can exceed this for the choice of basis functions used by MLS and if a better variable transform is needed one can substitute

$$\begin{aligned}\frac{\zeta^l_{m+1}-\zeta}{\Delta\zeta^l_m} &\approx \frac{H^l_{m+1}-H}{\Delta H^l_m}\left[1-\frac{W^{l\prime}_m}{2\overline{T}^l_m}\left(H-H^l_m\right)\right]\\ \frac{\zeta-\zeta^l_{m-1}}{\Delta\zeta^l_{m-1}} &\approx \frac{H-H^l_{m-1}}{\Delta H^l_{m-1}}\left[1-\frac{W^{l\prime}_{m-1}}{2\overline{T}^l_{m-1}}\left(H-H^l_m\right)\right]\end{aligned} \quad (38)$$

into eqn. 33 and 29, which is approximate because $1/(1+x) \approx 1-x$ and $W^{l\prime}_m = \Delta T^l_m/\Delta H^l_m$. This form is used in V0004 and V0005.

Species Cross Section The cross section β are evaluated at the 91 heights which define the layers used in the LOS integration. The details regarding evaluation of β is deferred to the next section. Here we present the effective functional form of β that is necessary for the radiance derivative calculations. This is

$$\begin{aligned}\beta^l_i &= \beta^l_i\left(\overset{\star}{T},\overset{\star}{\nu},\overset{\star}{\mathcal{B}}\right)\left(\frac{T}{\overset{\star}{T}}\right)^{n^l_i}\\ &+ \frac{\partial\beta^l_i}{\partial\nu}\left(\nu-\overset{\star}{\nu}\right)+\frac{\partial\beta^l_{\Delta Mi}}{\partial\mathcal{B}}\left(\mathcal{B}-\overset{\star}{\mathcal{B}}\right)\end{aligned} \quad (39)$$

where $\overset{\star}{T}$, $\overset{\star}{\nu}$, and $\overset{\star}{\mathcal{B}}$, are the "linearization" values for the temperature, velocity shifted linecenter frequencies, and magnetic field strength. The power n^l_i, and partials with respect to line center frequency and magnetic field are computed with β and stored for later use for radiance derivative calculations.

Derivatives

The need to reduce computational time motivated an analytical approach to derivative computations which are the K_j's in eqn. 2. The differential temperature radiative transfer equation has a simple derivative form given by

$$\begin{aligned}\underline{\underline{\frac{\partial I}{\partial x_j}}} &= \sum_{i=N}^{t}\underline{\underline{\mathcal{Q}}}_{N-i+1}\underline{\underline{\mathcal{T}}}_{N-i+1}+\underline{\underline{\tilde{\mathcal{T}}}}_{N-i+1}\underline{\underline{\tilde{\mathcal{Q}}}}_{N-i+1}\\ &- \sum_{t}^{N}\underline{\underline{\mathcal{Q}}}_{N+i}\underline{\underline{\mathcal{T}}}_{N+i}+\underline{\underline{\tilde{\mathcal{T}}}}_{N+i}\underline{\underline{\tilde{\mathcal{Q}}}}_{N+i},\\ \underline{\underline{\mathcal{Q}}}_{N-i+1} &= \frac{1}{2}\frac{\partial\Delta B_i}{\partial x_j}\underline{\underline{1}}+\Delta B_i\underline{\underline{\mathcal{W}}}_{N-i+1},\\ \underline{\underline{\mathcal{Q}}}_{N+i} &= \frac{1}{2}\frac{\partial\Delta B_i}{\partial x_j}\underline{\underline{1}}+\Delta B_i\underline{\underline{\mathcal{W}}}_{N+i},\\ \underline{\underline{\mathcal{W}}}_1 &= 0.0,\\ \underline{\underline{\mathcal{W}}}_{N-i+1} &= \underline{\underline{\mathcal{W}}}_{N-i}+\underline{\underline{\tau}}_{N-i}\underline{\underline{\frac{\partial\Delta\tau_i}{\partial x_j}}}\left(\underline{\underline{\tau}}_{N-i+1}\right)^{-1},\\ \underline{\underline{\mathcal{W}}}_{N+t} &= \underline{\underline{\mathcal{W}}}_{N-t+1},\end{aligned}$$

and

$$\underline{\underline{\mathcal{W}}}_{N+i} = \underline{\underline{\mathcal{W}}}_{N+i-1}+\underline{\underline{\tau}}_{N+i-1}\underline{\underline{\frac{\partial\Delta\tau_{i-1}}{\partial x_j}}}\left(\underline{\underline{\tau}}_{N+i}\right)^{-1}. \quad (40)$$

The above equation requires $\frac{\partial\Delta B_i}{\partial x_j}$, which is zero, except for temperature, and $\underline{\underline{\frac{\partial\Delta\tau_i}{\partial x_j}}}$, which is a function of the total incremental opacity derivative, $\underline{\underline{\frac{\partial\Delta\delta_i}{\partial x_j}}}$ and evaluated with Sylvester's identity, eqn. 10. The incremental opacity derivative is the partial derivative of eqn. 28 with respect to state-vector element x_j.

Derivatives for unpolarized radiation simplify eqn. 40 giving,

$$\begin{aligned}\frac{\partial I}{\partial x_j} &= \sum_{i=N}^{t}\mathcal{Q}_{N-i+1}\mathcal{T}_{N-i+1}-\sum_{t}^{N}\mathcal{Q}_{N+i}\mathcal{T}_{N+i},\\ \mathcal{Q}_{N-i+1} &= \frac{\partial\Delta B_i}{\partial x_j}-\Delta B_i\mathcal{W}_{N-i+1},\\ \mathcal{Q}_{N+i} &= \frac{\partial\Delta B_i}{\partial x_j}-\Delta B_i\mathcal{W}_{N+i},\\ \mathcal{W}_1 &= 0.0,\\ \mathcal{W}_{N-i+1} &= \mathcal{W}_{N-i}+\frac{\partial\Delta\delta_i}{\partial x_j}\\ \mathcal{W}_{N+t} &= \mathcal{W}_{N-t+1},\end{aligned}$$

and

$$\mathcal{W}_{N+i} \quad = \quad \mathcal{W}_{N+i-1} + \frac{\partial \Delta\delta_{i-1}}{\partial x_j}, \tag{41}$$

where $\Delta\delta_i$ is the total incremental opacity which is the scalar form of eqn. 28.

Mixing Ratios The incremental opacity derivative follows immediately from eqn. 28

$$\underline{\underline{\frac{\partial \Delta\delta_i}{\partial f_m^l}}} = \sum_{\Delta M=-1}^{+1} \underline{\underline{\rho}}_{\Delta M}(\theta,\phi)\, \Delta\delta_{ilm\Delta M}. \tag{42}$$

and

$$\frac{\partial \Delta B_i}{\partial f_m^l} = 0.0 \tag{43}$$

Eqns. 42 and 43 are subsituted into eqn. 40 or eqn. 41. The incremental opacity integral, $\Delta\delta_{ilm\Delta M}$, having been computed for the radiance computation essentially gives the mixing ratio derivative without farther effort. Most of these terms are zero which significantly delimits the summation range in eqn. 40 or 41 and greatly speeds the calculation.

Temperature The temperature derivative consists of two parts, the temperature sensitivity of the radiative transfer equation, and the hydrostatic perturbation on the antenna pattern. The former contribution dominates for saturated radiances and when the FOV is narrower than the radiative transfer vertical smearing and is described here. The latter effect dominates for unsaturated radiances when the FOV is broader than the radiative transfer vertical smearing and is described later. The latter effect arises because *pressure* is the indepedent vertical coordinate for this problem and the antenna FOV shape being constant in height, varies in pressure depending on temperature. For band 1 (9.8 km Half Power Beam Width), hydrostatic FOV effect dominates the temperature effect on *subsaturated* radiances.

The temperature derivative of the differential Planck term $\frac{\partial \Delta B_i}{\partial T_q}$ is related to the Planck function according to eqn. 14 where the derivative is

$$\frac{\partial B_i}{\partial T_q} = \frac{B_i^2 \exp\left\{\frac{h\nu}{kT(H_i)}\right\}}{T^2(H_i)} \eta_q(H_i), \tag{44}$$

Terms $T(H_i)$ means evaluate eqn. 44 at H_i.

The temperature derivative of the incremental optical depth is

$$\underline{\underline{\frac{\partial \Delta\delta_i}{\partial T_q}}} = \sum_{l=1}^{NS} \sum_{m=1}^{M(l)} \sum_{\Delta M=-1}^{+1} \underline{\underline{\rho}}_{\Delta M}(\theta,\phi)\, f_m^l \frac{\partial \Delta\delta_{ilm\Delta M}}{\partial T_q}. \tag{45}$$

The temperature functional part of eqn. 39 is substituted into eqn. 29 and expanded

$$\begin{aligned}\frac{\partial \Delta\delta_{ilm\Delta M}}{\partial T_q} \quad = \quad & \frac{\Delta s_i^{refr}}{\Delta s_i} \int_{h_i}^{h_{i+1}} \eta_m^l(H) \left[\frac{\mathrm{d}}{\mathrm{d}T_q}\left\{\beta_{i\Delta M}^l \right.\right. \\ & \times \quad \left.\left. \left(\frac{T}{T_i}\right)^{n_i^l} \exp\left\{\frac{\Delta \ln \beta_{i\Delta M}^l}{\Delta H_i}\Delta H\right\}\right\} \right. \\ & \times \quad \left. \frac{H}{\sqrt{H^2 - H_t^2}} \right. \\ & + \quad \beta_{i\Delta M}^l \exp\left\{\frac{\Delta \ln \beta_{i\Delta M}^l}{\Delta H_i}\Delta H\right\} \\ & \times \quad \left.\left(\frac{T}{T_i}\right)^{n_i^l} \frac{\mathrm{d}}{\mathrm{d}T_q} \frac{H}{\sqrt{H^2 - H_t^2}}\right] \mathrm{d}H \end{aligned} \tag{46}$$

and contributions due to change in refractive path lengthening and distortions in the mixing ratio and temperature representation bases are ignored. The definition of $\Delta \ln \beta_{i\Delta M}^l$ is now $\ln\left(\frac{\beta_{i+1\Delta M}^l}{\beta_{i\Delta M}^l}\left(\frac{T}{T_{i+1}}\right)^{n_{i+1}^l}\left(\frac{T_i}{T}\right)^{n_i^l}\right)$. The first term is the thermal sensitivity of the absorption coefficient and is evaluated by substituting

$$\begin{aligned}&\frac{\mathrm{d}}{\mathrm{d}T_q}\left\{\beta_{i\Delta M}^l \left(\frac{T}{T_i}\right)^{n_i^l} \exp\left\{\frac{\Delta \ln \beta_{i\Delta M}^l}{\Delta H_i}\Delta H\right\}\right\} \quad = \\ &\beta_{i\Delta M}^l \left(\frac{T}{T_i}\right)^{n_i^l} \exp\left\{\frac{\Delta \ln \beta_{i\Delta M}^l}{\Delta H_i}\Delta H\right\} \eta_q(H) \\ &\times \left[n_i^l (H_{i+1} - H) + n_{i+1}^l (H - H_i)\right] / (T \Delta H_i) \end{aligned} \tag{47}$$

into eqn. 46. To simplify this calculation, $\eta_q(H)$, the temperature basis function for coefficient q is separated from the rest of eqn. 47 and kept inside the integral while remainder is pulled outside and replaced with a mean-value for the layer. The thermal sensitivity integral is approximated with

$$\begin{aligned}&\beta_{i\Delta M}^l \int_{h_i}^{h_{i+1}} \frac{\mathrm{d}}{\mathrm{d}T_q}\left(\frac{T}{T_i}\right)^{n_i^l} \\ &\times \exp\left\{\frac{\Delta \ln \beta_{i\Delta M}^l}{\Delta H_i}\Delta H\right\} \\ &\times \sum_{m=1}^{M(l)} f_m^l \eta_m^l(H)\, \mathrm{d}H \quad = \\ &\overline{\frac{\beta_i^l F_i^l n_i^l}{T_i}} \int_{h_i}^{h_{i+1}} \frac{\eta_q(H)\, H}{\sqrt{H^2 - H_t^2}} \mathrm{d}H, \end{aligned} \tag{48}$$

where the overscore indicates an average value of the product between H_i and H_{i+1}. The sum over species

coefficient bases in eqn. 45 has been pulled into the integral along with f_m^l which replaces the "fast" varying η_m^l terms with a more slowly varing F^l function which improves the validity of the approximation. The resulting integral in eqn. 48 can be solved analytically. It is likely in a future upgrade, eqn. 48 will be integrated more fully with Gauss quadrature.

The second term gives the incremental optical depth variation due to a path length change which arises when temperature varies but the pressures of the preselected integration grid are held constant. The path length change is based on the hydrostatic relation given in eqn. 30. The second term in eqn. 46 is

$$\sum_{l=1}^{NS} \beta_{i\Delta M}^l \int_{h_i}^{h_{i+1}} \exp\left\{\frac{\Delta \ln \beta_{i\Delta M}^l}{\Delta H_i}\Delta H\right\} \times \left(\frac{T}{T_i}\right)^{n_i^l} \sum_{m=1}^{M(l)} \eta_m^l(H) f_m^l \frac{\mathrm{d}}{\mathrm{d}T_q}\frac{H}{\sqrt{H^2-H_t^2}}\mathrm{d}H = \overline{\kappa_{i\Delta M}}\frac{\partial}{\partial T_q}\Delta s_i, \quad (49)$$

where

$$\frac{\partial}{\partial T_q}\Delta s_i = \frac{H_{i+1}\frac{\mathrm{d}H_{i+1}}{\mathrm{d}T_q} - H_t\frac{\mathrm{d}H_t}{\mathrm{d}T_q}}{\sqrt{H_{i+1}^2-H_t^2}} - \frac{H_i\frac{\mathrm{d}H_i}{\mathrm{d}T_q} - H_t\frac{\mathrm{d}H_t}{\mathrm{d}T_q}}{\sqrt{H_i^2-H_t^2}}. \quad (50)$$

The second term is zero if $i = t$ and the hydrostatic derivative as evaluated by differentiating eqn. 30 giving

$$\frac{\mathrm{d}H_i}{\mathrm{d}T_q} = \frac{g^{\oplus}k\ln 10 {H_{\mathrm{eff}}^{\oplus}}^2 P_{qi}}{\left[g^{\oplus}H_{\mathrm{eff}}^{\oplus} - k\ln 10\sum_{n=1}^{NT}(T_n P_{ni})\right]^2}. \quad (51)$$

These derivatives are evaluated on the preselected integration grid. As with eqn. 48, eqn. 49 would incorporate the sums, appearing in eqn. 45, over species mixing ratios and coefficients in the mean-layer-averaged *absorption coefficient*, $\kappa_{i\Delta M} = \sum\sum f\beta\eta$, premultiplying the path length derivative. This can be done because these sums can be separated from the integral in this application. Combining eqns. 44–51 with eqn. 40, or 41 gives the radiative transfer temperature derivative.

Molecular Velocity Molecular motion relative to the microwave receiver causes small spectral shifts in the emission spectrum. This causes observable changes in the calculated channel radiance. The MLS is sensitive to molecular motion along its FOV. The total

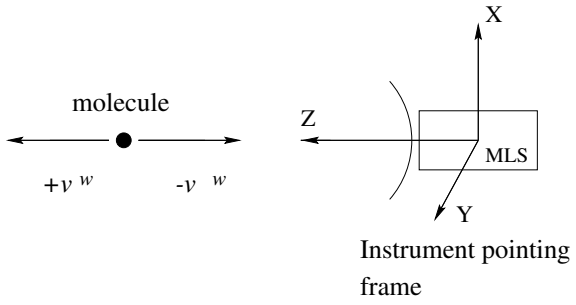

Figure 8. Molecular motion relative to MLS FOV axes.

effect is the sum of molecular motion due to Earth's rotation, satellite orbital motion, and motion in a "rotating" Earth reference frame commonly referred as wind. Referring to Figure 8 which shows the *instrument pointing* (IP) *frame* relative to molecular motion, the velocity is

$$v = v^{\oplus} - v^s + v^w \quad (52)$$

where superscripts $\oplus$, s, and w indicate Earth, satellite, and wind. All velocities are defined in the IP frame z axes as shown. Molecular motion causes its emission line frequency to shift according to

$$v_{\mathrm{obs}} = v_{\mathrm{rest}}\left(1.0 + \frac{v}{c}\right) \quad (53)$$

which describes the velocity effect upon the instrument's spectral response. In other words, a positive velocity or net molecular motion away from MLS is like observing a stationary molecule with the instrument spectral responses blue shifted.

The total velocity will use the temperature function eqn. 33 but with a different number of coefficients and resolution.

$$V(H) = \sum_{q=1}^{NV} v_q \eta_q(H). \quad (54)$$

H and ζ are considered completely interchangeable (see discussion under subsection *Atmospheric Profiles*) The derivative of the total incremental opacity with respect to total velocity is eqn. 45 with $T_q \to v_q$. The optical depth integral is

$$\frac{\partial\Delta\delta_{ilm\Delta M}}{\partial v_q} = \frac{\Delta s_i^{refr}}{\Delta s_i}\frac{\partial\beta_{i\Delta M}^l}{\partial v_q} \times \int_{h_i}^{h_{i+1}} \eta_m^l(H)\exp\left\{\frac{\Delta\ln\beta_{i\Delta M}^l}{\Delta H_i}\Delta H\right\} \times \frac{H}{\sqrt{H^2-H_t^2}}\mathrm{d}H. \quad (55)$$

The derivative of the cross section is expanded using the chain rule,

$$\frac{\partial\beta^l}{\partial v_q} = \frac{\eta_q\left(H_i\right)\nu_{\rm rest}\beta_i^l}{c\Delta H_i}\exp\left\{\frac{\ln\beta_i}{\Delta H_i}\Delta H\right\} \times \left[\frac{H_{i+1}-H}{\beta_i^l}\frac{\partial\beta_i^l}{\partial\nu}+\frac{H-H_i}{\beta_{i+1}^l}\frac{\partial\beta_{i+1}^l}{\partial\nu}\right], \quad (56)$$

where H is between H_i and H_{i+1}. Substituting eqn. 56 into eqn. 55 and using the mean-value-approximation (setting $\beta_i^l = \beta_{i+1}^l = 0.5\left(\beta_{i+1}^l+\beta_i^l\right)$, etc.) for everything except the representation basis and the path-length functions gives

$$\frac{\partial\Delta\delta_{ilm\Delta M}}{\partial v_q} = \frac{v_{\rm rest}}{c}\sum_{l=1}^{NS}\overline{f_i^l}\overline{\frac{{\rm d}\beta_i^l}{{\rm d}\nu}}\frac{\Delta s_i^{\rm refr}}{\Delta s_i} \times \int_{H_i}^{H_{i+1}}\eta_q\left(H\right)\frac{H{\rm d}H}{\sqrt{H^2-H_t^2}} \quad (57)$$

These integrals can be evaluated similarly to eqn. 48.

Geometric and Attitude The geometric derivatives include, pointing sensitivity, derivatives due to variations in the satellite orbital radius, earth radius, space craft yaw, pitch, and roll attitude angles, and the instrument field-of-view pointing angles. The following definitions for angles and heights are:

$\zeta^{\rm ref}$**:** The tangent pressure of one (63 GHz for MLS) of the radiometers. This radiometer is the pointing reference for the instrument.

α**:** The azimuth pointing angle which defines the instrument FOV direction. This is actually a sum of a reference angle, a thermal contribution, an encoder contribution (the vertical antenna scanner), and a radiometer offset. The reference angle is 90° which means the FOV direction is perpendicular to spacecraft orbital motion. The radiometer offset is the azimuthal difference between pointing reference radiometer and the radiometer of question.

ϵ**:** The elevation pointing angle which defines the instrument FOV direction. This is actually a sum of a reference angle, a thermal contribution, an encoder contribution, and a radiometer offset, The UARS orbit places the reference angle nominally at 23.3° which directs the FOV into the atmosphere, and the encoder varies about ±1° about the reference in order to measure the radiance profile.

φ**:** The "combined" spacecraft/instrument roll angle. This includes the spacecraft roll, and roll-like contributions from the instrument reference axes and spacecraft axes. Angles α and ϵ locate the FOV direction relative to the instrument reference axes.

ψ**:** The "combined" spacecraft/instrument yaw angle. This is the spacecraft yaw, and yaw-like contributions from the instrument reference axes and spacecraft axes.

ϑ**:** The "combined" spacecraft/instrument pitch angle. This is the spacecraft pitch, and pitch-like contributions from the instrument reference axes and spacecraft axes.

$H_t^{\rm ref}$**:** The geocentric tangent of $\zeta^{\rm ref}$.

H_t**:** The non-reference radiometer FOV direction geocentric tangent.

H_s**:** The geocentric spacecraft orbital height.

$H_\oplus$**:** The geocentric Earth radius.

$\chi^{\rm refr,ref}$**:** The refracted pointing angle in the plane defined by H_s and $H_t^{\rm ref}$.

$\chi^{\rm refr}$**:** The refracted pointing angle in the plane defined by H_s and H_t.

The radiance calculations are convolved with an antenna pattern which is an angular function (see *Sec.* Spatial and Spectral Effects), hence it is convenient to express the radiance derviative as an angular quantity and use the chain rule

$$\frac{\partial I}{\partial x} = \frac{\partial I}{\partial\chi^{\rm refr}}\frac{{\rm d}\chi^{\rm refr}}{{\rm d}x}, \quad (58)$$

where $x = \alpha$, ϵ, ϑ, ψ, φ, $\zeta^{\rm ref}$, H^s, and $H^\oplus$. The $\frac{\partial I}{\partial\chi^{\rm refr}}$ derivative is easily computed from the radiance versus pointing angle functions from the antenna convolution calculation described later. The functional forms of $\chi\left(\underline{x}\right)$ are presented. The tangent heights are related to the refracted angle according to

$$\chi^{\rm refr} = \arcsin\frac{\mathcal{N}_t H_t}{H_s}. \quad (59)$$

Another way of writing eqn. 59 which is more useful for the attitude derivative calculation is

$$\mathcal{N}_t^2 H_t^2 = H_s^2 - \left(\vec{H}_s\cdot\vec{e}\right)^2, \quad (60)$$

where $\vec{e}$ is an unit vector in the FOV direction and $\vec{H}_s$ is vector from the instrument to the Earth center. If these vectors are in the *vertical orbital frame*, then $\vec{H}_s = (0, 0, -H_s)$. Inserting this into eqn. 60 gives

$$\mathcal{N}_t^2 H_t^2 = H_s^2 \left(1 - e_z^2\right), \tag{61}$$

where e_z is the z component of $\vec{e}$ given by

$$\begin{aligned} e_z &= -\cos\alpha\cos\epsilon\sin\vartheta\cos\psi \\ &+ \sin\alpha\cos\epsilon\sin\vartheta\sin\psi\cos\varphi \\ &+ \sin\alpha\cos\epsilon\cos\vartheta\sin\varphi \\ &- \sin\epsilon\sin\vartheta\sin\psi\sin\varphi \\ &+ \sin\epsilon\cos\vartheta\cos\varphi. \end{aligned} \tag{62}$$

Eqn. 60 requires $e_z = \cos\chi^{\text{refr}}$ and to *first order* (for the UARS/MLS observation configuration), $\alpha \approx 90.0$, $\vartheta \approx 0.0$, and $\psi \approx 0.0$ (or 180.0) would simplify to $e_z = \frac{\mathcal{N}_t H_t}{H_s} = \cos(\epsilon + \varphi)$ or in other words, χ^{refr} is the sum of all the elevation (roll) angles between the UARS and the FOV direction. However, sensitivity to pointing is great and *second* order effects are important and therefore contributions from the yaw and pitch(ψ, ϑ) angles need to be retained.

The pointing angle for each of the MLS radiometers can be expressed as a function of the reference radiometer according to

$$\chi^{\text{refr}} = \chi^{\text{ref,refr}} + \arccos e_z - \arccos e_z^{\text{ref}} \tag{63}$$

The difference between e_z and e_z^{ref} being the inclusion of an offset contribution to α and ϵ in the former. The geometric derivatives are:

$$\frac{\partial I}{\partial \zeta^{\text{ref}}} = \frac{\partial I}{\partial \chi^{\text{refr}}} \frac{\mathrm{d}\chi^{\text{refr}}}{\mathrm{d}\zeta^{\text{ref}}}, \tag{64}$$

$$\frac{\partial I}{\partial H_s} = \frac{\partial I}{\partial \chi^{\text{refr}}} \frac{\mathrm{d}\chi^{\text{refr}}}{\mathrm{d}H_s}, \tag{65}$$

$$\frac{\partial I}{\partial H_t} = \frac{\partial I}{\partial \chi^{\text{refr}}} \frac{\mathrm{d}\chi^{\text{refr}}}{\mathrm{d}H_\oplus}, \tag{66}$$

and

$$\frac{\partial I}{\partial \wp} = \frac{\partial I}{\partial \chi^{\text{refr}}} \frac{\mathrm{d}\chi^{\text{refr}}}{\mathrm{d}\wp}. \tag{67}$$

When the radiances are weighted by the antenna gain pattern and integrated (see eqn. 1) which is done in the χ^{refr} coordinate, cubic spline coefficients are calculated which give the radiance first derivatives in the first product appearing in the chain-rule above. $\frac{\mathrm{d}\chi^{\text{refr}}}{\mathrm{d}\zeta^{\text{ref}}}$ is obtained from eqn. 59 and differentiating eqn. 30. Eqns. 65 and 66 substitute $e_z = \sqrt{1.0 - \mathcal{N}_t \frac{H_t^2}{H_s^2}}$ into eqn. 61 followed by eqn. 59 and differentiating. Likewise eqn. 67 where $\wp$ is any one of the five angles appearing in eqn. 62 is evaluated by combining eqns. 59, 61, 62, and 63 and differentiating.

The instrument elevation encoder angle, nominally ϵ, can be determined from absolute pointing χ^{refr} according to

$$\cos\epsilon = \frac{e_z}{A} \pm B\left(A^2 + B^2\right)\sqrt{A^2 + B^2 - e_z^2}, \tag{68}$$

or

$$\sin\epsilon = \frac{e_z}{B} \mp A\left(A^2 + B^2\right)\sqrt{A^2 + B^2 - e_z^2}, \tag{69}$$

where

$$\begin{aligned} A &= -\cos\alpha\sin\vartheta\cos\psi + \sin\alpha\sin\vartheta\sin\psi\cos\varphi \\ &+ \sin\alpha\cos\vartheta\sin\varphi, \end{aligned} \tag{70}$$

$$B = -\sin\vartheta\sin\psi\sin\varphi + \cos\vartheta\cos\varphi. \tag{71}$$

This is useful because the MLS makes angular measurements of its FOV-direction called the encoder angle and this information can be incorporated into the pressure-temperature-constituent mixing ratio retrievals using eqn. 68 as the foward model.

Magnetic field and Orientation The magnetic field strength derivative is obtained from combining eqn. 39 with eqn. 28 and 29 in a way quite analogous to velocity giving

$$\underline{\underline{\frac{\partial \Delta\delta_i}{\partial \mathcal{B}}}} = \sum_{l=1}^{NS} \sum_{m=1}^{M(l)} \sum_{\Delta M=-1}^{+1} \underline{\underline{\rho}}_{\Delta M}(\theta, \phi)\, f_m^l \frac{\partial \Delta\delta_{ilm\Delta M}}{\partial \mathcal{B}} \tag{72}$$

and

$$\begin{aligned} \frac{\partial \Delta\delta_{ilm\Delta M}}{\partial \mathcal{B}} &= \frac{\Delta s_i^{refr}}{\Delta s_i} \frac{\beta_{i\Delta M}^l}{\Delta H_i} \\ &\times \int_{h_i}^{h_{i+1}} \eta_m^l(H) \exp\left\{\frac{\Delta \ln \beta_{i\Delta M}^l}{\Delta H_i} \Delta H\right\} \\ &\times \left[\frac{H_{i+1} - H}{\beta_{i\Delta M}^l} \frac{\partial \beta_{i\Delta M}^l}{\partial \mathcal{B}}\right. \\ &+ \left.\frac{H - H_i}{\beta_{i+1\Delta M}^l} \frac{\partial \beta_{i+1\Delta M}^l}{\partial \mathcal{B}}\right] \\ &\times \frac{H}{\sqrt{H^2 - H_t^2}} \mathrm{d}H. \end{aligned} \tag{73}$$

This is similar to the velocity derivative, eqn. 57 except the magnetic field is assumed to have no vertical structure. The extension of eqn. 73 to include a magnetic field profile is easily deduced from inspection of eqn. 56. This integral is evaluated using a mean-layer approximation.

The orientation parameters θ and ϕ only affect the $\underline{\underline{\rho}}$ matrix giving.

$$\underline{\underline{\frac{\partial \Delta\delta_i}{\partial \wp}}} = \sum_{l=1}^{NS} \sum_{m=1}^{M(l)} \sum_{\Delta M=-1}^{+1} \underline{\underline{\frac{\partial \rho_{\Delta M}}{\partial \wp}}} (\theta, \phi)\, f_m^l \Delta\delta_{ilm\Delta M} \tag{74}$$

where $\wp \equiv \theta$, or ϕ. Differentiating $\underline{\underline{\rho}}_{\Delta M}$ with respect to θ gives,

$$\begin{aligned}
\underline{\underline{\frac{\partial \rho_{-1}}{\partial \theta}}} &= \begin{bmatrix} -2\sin^2\phi\sin\theta\cos\theta & \cdots \\ -2\sin\phi\cos\phi\sin\theta\cos\theta + \imath\sin\theta & \cdots \\ \cdots & -2\sin\phi\cos\phi\sin\theta\cos\theta - \imath\sin\theta \\ \cdots & -2\cos^2\phi\sin\theta\cos\theta \end{bmatrix} \\
\underline{\underline{\frac{\partial \rho_{0}}{\partial \theta}}} &= \begin{bmatrix} 2\sin^2\phi\sin\theta\cos\theta & \cdots \\ 2\sin\phi\cos\phi\sin\theta\cos\theta & \cdots \\ \cdots & 2\sin\phi\cos\phi\sin\theta\cos\theta \\ \cdots & 2\cos^2\phi\sin\theta\cos\theta \end{bmatrix} \\
\underline{\underline{\frac{\partial \rho_{+1}}{\partial \theta}}} &= \begin{bmatrix} -2\sin^2\phi\sin\theta\cos\theta & \cdots \\ -2\sin\phi\cos\phi\sin\theta\cos\theta - \imath\sin\theta & \cdots \\ \cdots & -2\sin\phi\cos\phi\sin\theta\cos\theta + \imath\sin\theta \\ \cdots & -2\cos^2\phi\sin\theta\cos\theta \end{bmatrix}
\end{aligned} \tag{75}$$

The corresponding derivative $\underline{\underline{\rho}}_{\Delta M}$ with respect to ϕ gives,

$$\begin{aligned}
\underline{\underline{\frac{\partial \rho_{-1}}{\partial \phi}}} &= \begin{bmatrix} -2\sin\phi\cos\phi\sin^2\theta & \cdots \\ -\left(\cos^2\phi - \sin^2\phi\right)\sin^2\theta & \cdots \\ \cdots & -\left(\cos^2\phi - \sin^2\phi\right)\sin^2\theta \\ \cdots & 2\sin\phi\cos\phi\sin^2\theta \end{bmatrix} \\
\underline{\underline{\frac{\partial \rho_{0}}{\partial \phi}}} &= \begin{bmatrix} 2\sin\phi\cos\phi\sin^2\theta & \cdots \\ \left(\cos^2\phi - \sin^2\phi\right)\sin^2\theta & \cdots \\ \cdots & \left(\cos^2\phi - \sin^2\phi\right)\sin^2\theta \\ \cdots & -2\sin\phi\cos\phi\sin^2\theta \end{bmatrix} \\
\underline{\underline{\frac{\partial \rho_{+1}}{\partial \phi}}} &= \begin{bmatrix} -2\sin\phi\cos\phi\sin^2\theta & \cdots \\ -\left(\cos^2\phi - \sin^2\phi\right)\sin^2\theta & \cdots \\ \cdots & -\left(\cos^2\phi - \sin^2\phi\right)\sin^2\theta \\ \cdots & 2\sin\phi\cos\phi\sin^2\theta \end{bmatrix}
\end{aligned} \tag{76}$$

These derivatives are substituted into eqn. 74 which eventually make their way into eqn. 40.

There exists a much simpler way to compute the ϕ radiance derivative. Using some suitable lineariazation value for ϕ, the radiative transfer is computed using eqns. 12, 13, 14, 16, 17, 28, and 29. The effect of ϕ is to rotate the polarization matrix about the FOV direction which can be written as

$$\begin{aligned}
\underline{\underline{I}} &= \begin{Bmatrix} I_{11} & I_{12} + \imath I_| \\ I_{12} - \imath I_| & I_{22} \end{Bmatrix} \\
I_{11} &= I_\parallel \cos^2\Delta\phi + I_\perp \sin^2\Delta\phi + 2I_| \sin\Delta\phi\cos\Delta\phi \\
I_{12} &= \left(I_\parallel - I_\perp\right)\sin\Delta\phi\cos\Delta\phi \\
&+ I_| \left(\cos^2\Delta\phi - \sin^2\Delta\phi\right) \\
I_{22} &= I_\parallel \cos^2\Delta\phi + I_\perp \sin^2\Delta\phi - 2I_| \sin\Delta\phi\cos\Delta\phi
\end{aligned} \tag{77}$$

The angle used here is $\Delta\phi$ because the above rotation is an additional rotation added to the linearization ϕ. Before rotating through $\Delta\phi$, the components $I_\parallel$ and $I_\perp$ represent radiances whose polarization are parallel and perpendicular to the instrument field of view pointing polarized (IFOVPP) x axis (see figure 6), and $I_|$ and $I_\circ$ are the linear and circular coherence respectively. Differentiating eqn. 77 at $\Delta\phi = 0$ gives

$$\underline{\underline{\frac{\partial I}{\partial \phi}}} = \begin{bmatrix} 2I_| & I_\parallel - I_\perp \\ I_\parallel - I_\perp & -2I_| \end{bmatrix}. \tag{78}$$

Or more simply, the radiance derivative with respect to ϕ for the co-polarized component (ie the instrument measured radiance) is twice the linear coherence. This result is always available when the radiative transfer is computed and provides a simple algorithm test for the more complicated eqn. 76.

Higher Order Derivatives

A significant problem with radiative transfer calculations is the large amount of computational time required—especially if high accuracy is desired to compliment the high inherent precision available from the measurements. The MLS deals with this problem by designing a nearly linear measurement system thereby reducing the forward model calculation (potentially an N^3 process) into a first order Taylor series evaluation (an N process) Froidevaux et al., 1996 []. The computation of the zero and first order terms of the Taylor series being described herein. Since the linearized forward model can handle a wide range of situations, the time taken to compute its coefficients is not as limiting an issue as it would be if the forward model had to be computed dynamically during the retrieval procedure. Nevertheless, the forward model is intrinsically

non-linear and the next enhancement of the MLS retrieval scheme will include it. The goal of course is not to sacrifice accuracy nor add computational time. A way to best achieve these objectives is to extend the Taylor series to second order. Although computational speed during the retrieval process will be increased, zero order accuracy (forward model calculation at the initial conditions) will be maintained and accuracy for state-vector values apart from the "linearization" point will be improved. It is worth noting however that the second order expansion causes the forward calculation to behave as an N^2 process but it has the following features:

1. The size of N in the Taylor series is determined by the retrieval resolution, whereas N in the forward calculation is determined by the PSIG. For high accuracy, the PSIG must have more steps than the number of basis functions, usually by at least a factor of two; hence, the Taylor series N will be at least twice as small as the forward calculation N.

2. It is expected that correlations between statevector elements will diminish in proportion to the height separation between them. Therefore, the "N^2" part of the problem can be made effectively much smaller than the total number of coefficients needed to span the vertical range. Although the same can be done with the forward calculation, the potential savings is not as great.

Evaluating a second order Taylor series representation of the forward calculation will be much faster than the forward model itself and is proposed as a future enhancement to the MLS inversion scheme. The second derivative with respect to state elements x_j and x_k has the same form as the first order equation 40 except $\underline{\underline{\mathcal{Q}}}_z$ is

$$\begin{aligned}
\underline{\underline{\mathcal{Q}}}_z &= \frac{1}{2}\frac{\partial^2 \Delta B_i}{\partial x_j \partial x_k}\underline{\underline{1}} + \frac{\partial \Delta B_i}{\partial x_j}\underline{\underline{\mathcal{W}}}^t_{k,z} \\
&+ \frac{\partial \Delta B_i}{\partial x_k}\underline{\underline{\mathcal{W}}}_{j,z} + \Delta B_i\left(\underline{\underline{\mathcal{X}}}_z + \underline{\underline{\mathcal{Y}}}_z + \underline{\underline{\mathcal{Z}}}_z\right) \\
&+ \Delta B_i \underline{\underline{\mathcal{W}}}_{j,z}\underline{\underline{\mathcal{T}}}^t_z \underline{\underline{\tilde{\mathcal{W}}}}_{k,z}\left(\underline{\underline{\mathcal{T}}}_z\right)^{-1}, \\
\underline{\underline{\mathcal{X}}}_1 &= \underline{\underline{\mathcal{Y}}}_1 = \underline{\underline{\mathcal{Z}}}_1 = 0.0, \\
\underline{\underline{\mathcal{X}}}_{N-i+1} &= \underline{\underline{\mathcal{X}}}_{N-i} \\
&+ \underline{\underline{\mathcal{W}}}_{k,N-i+1}\underline{\underline{\tau}}_{N-i+1}\underline{\underline{\frac{\partial \Delta\tau_i}{\partial x_j}}}\left(\underline{\underline{\tau}}_{N-i+1}\right)^{-1},
\end{aligned}$$

$$\begin{aligned}
\underline{\underline{\mathcal{Y}}}_{N-i+1} &= \underline{\underline{\mathcal{Y}}}_{N-i} + \underline{\underline{\tau}}_{N-i}\underline{\underline{\frac{\partial^2 \Delta\tau_i}{\partial x_j \partial x_k}}}\left(\underline{\underline{\tau}}_{N-i+1}\right)^{-1}, \\
\underline{\underline{\mathcal{Z}}}_{N-i+1} &= \underline{\underline{\mathcal{Z}}}_{N-i} \\
&+ \underline{\underline{\tau}}_{N-i}\underline{\underline{\frac{\partial \Delta\tau_i}{\partial x_j}}}\left(\underline{\underline{\tau}}_{N-i}\right)^{-1}\underline{\underline{\mathcal{W}}}_{k,N-i+1},
\end{aligned} \tag{79}$$

where subscript z is $N-i+1$ or $N+i$ following the example of eqn 40, and the $N+i$ expansions of $\mathcal{X}$, $\mathcal{Y}$, and $\mathcal{Z}$ are analogous to $\mathcal{W}$ in eqn 40 which is not shown here for brevity. A subscript k, or j has been added to $\mathcal{W}$ to indicate the state vector element being differentiated. Despite the complexity, everything in eqn. 79 has been evaluated previously except $\underline{\underline{\frac{\partial^2 \Delta\tau_i}{\partial x_j \partial x_k}}}$. Fortunately the scalar form is considerably simpler. The second derivative equation is identical to eqn. 41 but having a new definition for $\mathcal{Q}$ which is

$$\begin{aligned}
\mathcal{Q}_z &= \frac{\partial^2 \Delta B_i}{\partial x_j \partial x_k} - \frac{\partial \Delta B_i}{\partial x_j}\mathcal{W}_{k,z} \\
&- \frac{\partial \Delta B_i}{\partial x_k}\mathcal{W}_{j,z} + \Delta B_i \mathcal{W}_{j,z}\mathcal{W}_{k,z} \\
&- \Delta B_i \mathcal{X}^t_z \\
\mathcal{X}_1 &= 0.0 \\
\mathcal{X}_{N-i+1} &= \mathcal{X}_{N-i} + \frac{\partial^2 \Delta\delta_i}{\partial x_j \partial x_k}
\end{aligned} \tag{80}$$

As before subscript z is $N-i+1$ or $N+i$ and subscripts j and k indicate the state vector element derivative. The $N+i$ form for $\mathcal{X}$ is not shown but is entirely analogous to that for $\mathcal{W}$ in eqn. 41.

For the special case of second derivatives involving only mixing ratios, all the derivative terms except $\mathcal{W}$ vanish leaving a simple one term function (scalar case). In fact, for this case the extension to higher order derivatives is obvious. Inclusion of higher order terms will require further nesting of sums in the forward model calculation using a Taylor series and at some point will be uncompetetive with a direct forward model calculation. We feel that the second to third order transition probably represents a reasonble cut-off point—that is if convergence is not satisfactory at second order, then compute the forward model directly. Simplified numerical simulations have shown that this will work well for temperature (band 1), and ozone (band 4) retrievals. For band 1 having a 30K temperature deviation, the first order function is accurate to 1.5 K whereas the second order correction is accurate to 0.2 K. For band 4 ozone, the linearization error between a polar ozone hole situation and the equator amounts to a 0.0–0.4 K.

Including the second order term eliminates this error entirely (<0.01 K). The signals in bands 5 and 6 are more non-linear in mixing ratio and are not as amenable to this approach and will require an interactive computation with the forward model; however, if the linearization value is close, this method may suffice. Nevertheless, it will reduce the calculation from 90 to 30 channels worst case which is a considerable time savings.

Spectroscopy Considerations

The spectroscopy database used in the MLS forward model is described. Spectroscopy is the center-piece of these calculations and clearly one of the limiting obstacles confronting absolute accuracy (the other being instrument calibration and charaterization); therefore, we hope this application helps to re-enforce and promote the importance of basic spectroscopic work which does not always get the recognition it deserves in the scientific community. This section describes the absorption coefficient calculation and the values of the main parameters used; followed by a subsection discussing implementation with the radiative transfer calculation in the previous section.

Line Absorption Calculation

The absorption coefficient derivative with respect to mixing ratio β or "cross-section" is given by

$$\begin{aligned}\beta &= \sqrt{\frac{\ln 2}{\pi}}\frac{10^{-6}}{k}P\left(\sum_j 10^{\mathcal{S}_j}\,\mathrm{Voigt}\left(x_j,y_j,z_j\right)\right)\\ &/ \quad (Tw_d)\end{aligned} \tag{81}$$

where

$$\begin{aligned}\mathcal{S}_j &= \mathcal{I}_j\left(300\right)-\mathrm{Q\_LOG}\left(Q,T\right)\\ &+ \frac{E\ell_j}{1.600386}\left(\frac{1}{300}-\frac{1}{T}\right)\\ &+ \log\left[\frac{1-\exp\left\{-\nu_j/\left(20836.74T\right)\right\}}{1-\exp\left\{-\nu_j/6251022.0\right\}}\right],\end{aligned}$$

T is temperature in Kelvins, P is pressure in mbar, $\mathcal{I}_j\left(300\right)$ is the logarithm of the integrated intensity in nm^{2}MHz at 300 K, ν_j is the pressure shifted line center frequency in MHz, $E\ell_j$ is the ground state energy in cm^{-1}, Q_LOG is a log-linear partition function interpolation routine which gives the logarithm of the ratio of the partition function at T and 300K and uses calculated partition functions, Q at $T=300$, 225, and 150 Kelvins respectively as inputs, $w_d = 3.58117369\times10^{-7}\nu\sqrt{\frac{T}{\mathcal{M}}}$ MHz is the Doppler width, $\mathcal{M}$ is the absorber molecular mass (AMU), $\sqrt{\frac{\ln 2}{\pi}}\frac{10^{-6}}{k} = 3.402136078\times10^{9}$ K mb^{-1} nm^{-2} km^{-1}, is proportional to the receprical to Boltzmann constant, Voigt is the lineshape function and subscript j identifies the individual lines or quantum states in the molecule. The Voigt function is

$$\begin{aligned}\mathrm{Voigt}\left(x_j,y_j,z_j\right) &= \left(\frac{\nu}{\nu_j}\right)\left(\frac{1}{\pi}\int_{-\infty}^{\infty}\right.\\ &\times \frac{\left(y_j-Y_j\left(x_j-t\right)\right)\exp\left\{-t^2\right\}}{y_j^2+\left(x_j-t\right)^2}\mathrm{d}t\\ &+ \left.\frac{1}{\sqrt{\pi}}\frac{y_j-Y_jz_j}{z_j^2+y_j^2}\right)\end{aligned} \tag{82}$$

where $x_j = \frac{\sqrt{\ln 2}(\nu_j-\nu)}{w_d}$, $y_j = \frac{\sqrt{\ln 2}w_{cj}P}{w_d}\left(\frac{300}{T}\right)^{n_j}$, $z_j = \frac{\sqrt{\ln 2}(\nu_j+\nu)}{w_d}$, w_{cj} is the collision width at 300 Kelvins and 1 mbar, n_j is its temperature dependence, Y_j is an intramolecular line interference coefficient, ν_j is the line position frequency, ν is the radiative frequency, both in MHz. The $\left(\frac{\nu}{\nu_j}\right)^2$ term which is virtually constant over a Doppler width has been pulled outside the integral giving the well studied Voigt integral [Shippony and Read, 1993 []]. The line center frequency is pressure shifted according to

$$\nu_j = \nu_{j0}+\Delta\nu_{j0}P\left(\frac{300}{T}\right)^{\frac{1+6n_j}{4}}, \tag{83}$$

where ν_{j0} is the "zero pressure" line center frequency, $\Delta\nu_{j0}$ is pressure shift parameter, and the temperature dependence is dependent on n_j [Pickett, 1980 []]. The pressure shift correction is a feature that was added to V0005 process specifically for H_2O. This effect was discovered and characterized in [Pumphrey, 1998 []]. The interference coefficient is parameterized according to

$$Y_j = P\left(\delta_j\left(\frac{300}{T}\right)^{0.8}+\gamma_j\left(\frac{300}{T}\right)^{1.8}\right) \tag{84}$$

and applies only to oxygen [Liebe, 1992 []].

Partially polarized radiative transfer calculations add additional complications. The Voigt in eqn. 82 is replaced with

$$\begin{aligned}\mathrm{Voigt}\left(x_j,y_j,z_j\right) &= \left(\frac{\nu}{\nu_j}\right)^2\frac{1}{\pi}\int_{-\infty}^{\infty}\exp\left\{-t^2\right\}\\ &\times \sum_{M=M1}^{M2}\xi j,M,\Delta M\end{aligned}$$

$$\times \quad \frac{y_j - Y_j\left(x_{j,M,\Delta M} - t\right)}{\left(x_{j,M,\Delta M} - t\right)^2 + y_j^2}$$
$$+ \quad \frac{\imath\left(y_j Y_j + x_{j,M,\Delta M} - t\right)}{\left(x_{j,M,\Delta M} - t\right)^2 + y_j^2}\mathrm{d}t \tag{85}$$

where emission is from the jth transition with a ΔM selection rule. The three allowed selection rules for oxygen are $\Delta M = +1$, $\Delta M = 0$, and $\Delta M = -1$, referred to as σ_+, π, and σ_- respectively. The selection rule indicates a quantum number change relative to the initial state (higher energy) in an *emitting* molecule. The broadening parameter y_j, and interference coefficient Y_j are assumed unchanged from the zero field situation [Rosenkranz and Staelin, 1988 []], but the frequency offset parameter, $x_{j,M,\Delta M}$ is $-\sqrt{\ln 2}\left(\nu - \nu_j - \Delta\nu_{j,M,\Delta M}\right)/\omega_d$, where $\Delta\nu_{j,M,\Delta M}$ is the magnetically perturbed M transition frequency offset relative to the field-free transition whose selection rule is ΔM. The formulas for the line shifts are derived from first order perturbation theory and given in table 7 [Lenoir, 1968 []]. The Magnetic line strength as a fraction of the zero field strength is $\xi_{j,M,\Delta m}$ and given in Table 8 [Liebe, 1981 []].

The range of M values in the sum depend on the ΔJ and ΔM selection rules. A $\Delta J = +1$ or N^+ transition, $M1 = -N$, and $M2 = N$ for all ΔM transitions. For $\Delta J = -1$ or N^- transitions, $M1 = -N + 1$ and $M2 = N - 1$ for π transitions, $M1 = -N$, and $M2 = N - 2$ for σ_+, and $M1 = -N + 2$, and $M2 = N$ for σ_- lines. Magnetic perturbation is considered only for the primary O_2 isotope and is neglected for all other molecules.

MLS Spectral Constants

The MLS spectral constants for the species within the spectral bands is given here. Table 9 gives the partition function ground state energy and the integrated intensity. This data comes from the JPL Spectral Catalogue [Pickett et al., 1992 []]. The V0003 retrieval used data from an earlier version of the Catalogue [Poynter and Pickett, 1984 []]. These quantities are in normal typeset. V0004 used catalogue data from a more recent version (current at the time of V0004 processing) of the catalogue [Pickett et al., 1992 []] and where these values are different are indicated in italics. This table includes only a subset of lines used in the cross section calculations—the most important. For a given molecule, all lines (resolvable or not) within the MLS spectral band-pass are included in a line by line computation. Lines outside the band-pass are included only if needed which is based on a line selection criteria to be described later. Errors on the values in table 9 are not well characterized. Contributing factors are the molecular dipole moment, line frequency measurement, and the quantum mechanical calculation. Dipole moments can be measured using the microwave spectroscopy in a Stark cell to 0.01 Debye or better and is probably the limiting error source [Townes and Schawlow, 1955 []]; however, using molecular beam electric resonance techniques can reduce this error by 2 orders of magnitude. Line position frequencies can be routinely measured to within 100 kHz and is negligible, and if many molecular lines are measured and well fit with a quantum mechanical model, then this error source can in principle be reduced indefinitely. A typical aggragate value for all these sources assuming a 1 debye molecule is about 2% for the line strength (the non Voigt part in eqn. 81). This is broken down in more detail in the MLS validation papers [Waters et al., 1996 [], Fishbein et al., 1996 [], Lahoz, et al., 1996 [], Froidevaux et al., 1996 []]. Two molecules, ClO and HNO_3 inadvertendly used an obsolete catalogue calculation in V0003 which is rectified in V0004. The ClO linestrengths are increased by 7.5% which will reduce subsequent retrievals by the same amount (there will also be a minor temperature dependence which is not expected to exceed 1% of the total ClO). *Therefore before performing any scientific analyses with V0003 MLS ClO data, reduce the values by 7.5% and add 1% additional error.* The HNO_3 catalogue change is negligible and since no V0003 product is available, is inconsequential.

Table 10 contains the lineshape parameters. These quantities have changed during the course of the mission and values used for V0003, V0004, and V0005 are given. A single error estimate when available is given in percent which applies to the broadening function, and values are for air broadening unless otherwise stated. As before more lines are included than listed and the calculations do allow for line dependent linewidths to be used. Since producing V0003 data products, some linewidths have been remeasured and these are highlighted with different typeset, italics for V0004 and sans serif for V0005 where these values are different from V0003 and added molecules. Errors are listed only for those molecules where the broadening function (which includes the temperature dependence) is measured for both N_2 and O_2 for the target spectral line in the catalogue. An exception to this is made when a sufficient number of lines are measured allowing a highly confident estimate based on its quantum state. Lines with-

Table 7. Magnetically perturbed O_2 line displacements relative to its zero field position as a function of field strength H.

	$\Delta\nu_{j,M,\Delta M}$ Functions	
	N^+ Line	N^- Line
σ_+	$-2.8026H\frac{M(N-1)+N}{N(N+1)}$	$2.8026H\frac{M(N+2)+N+1}{N(N+1)}$
π	$-2.8026H\frac{M(N-1)}{N(N+1)}$	$2.8026H\frac{M(N+2)}{N(N+1)}$
σ_-	$-2.8026H\frac{M(N-1)-N}{N(N+1)}$	$2.8026H\frac{M(N+2)-N-1}{N(N+1)}$

Table 8. Magnetically perturbed O_2 line intensities relative to its zero field line strength.

	$\xi_{j,M,\Delta M}$ Functions	
	N^+ Line	N^- Line
σ_+	$\frac{3(N+M+1)(N+M+2)}{4(N+1)(2N+1)(2N+3)}$	$\frac{3(N-M)(N-M-1)}{4N(2N+1)(2N-1)}$
π	$\frac{3\left((N+1)^2-M^2\right)}{(N+1)(2N+1)(2N+3)}$	$\frac{3\left(N^2-M^2\right)}{N(2N+1)(2N-1)}$
σ_-	$\frac{3(N-M+1)(N-M+2)}{4(N+1)(2N+1)(2N+3)}$	$\frac{3(N+M)(N+M-1)}{4N(2N+1)(2N-1)}$

out errors are estimates based a number of assumptions such as isotopic and quantum state invariance, nitrogen broadening, and educated guesses. The N_2O line broadening error is somewhat large because there was an unresolved but rather large difference between the two references cited in the table and has been incorporated in the table. Lines outside the instrument bandwidth also include quantum state specific linewidths where available and this will be expanded further in the future. Details are not discussed here and a nearly identical listing appears in Rosenkranz [1993]. Intramolecular line broadening interference parameters are zero for all molecules except the principal O_2 isotope. This species uses $\delta = 0.0003427$ hPa^{-1}, and -0.0000820 hPa^{-1}, and $\gamma = -0.0008874$ hPa^{-1} and -0.0004864 hPa^{-1} for the lower and upper frequency tabular line for V0003 retrievals. These are revised to $\delta = 0.000208$ hPa^{-1} and -0.0000668 hPa^{-1}, and $\gamma = 0.000094$ hPa^{-1} and -0.000614 hPa^{-1} for V0004 and V0005. A complete listing for all the lines used in the line by line calculations are given in Liebe , [1991] (V0003 products) and Liebe , [1992] (V0004 and V0005). New broadening and pressure shift parameters for 183 GHz H_2O and 184 GHz O_3 were determined from MLS data based on optimizing the spectral fit [Pumphrey, 1998 []]. These values are larger than the corresponding laboratory values beyond the error estimates. Despite this, these revised values are being used in V0005 because we believe they may be compensating for errors associated with radiometer offsets or O_2 linewidth. Both target molecules optimally fit to broader linewidths by roughly the same amount which lends support that a systematic effect may be acting here.

This line data is incorporated into eqn. 81 which is then used by eqn. 29 for radiative transfer calculations in one of two ways. The first method which uses a pre-frequency averaged value per channel computes the β spectrum line by line and the result is averaged across the channel using channel's spectral response. These calculations are performed for each height in the preselected integration grid (PSIG) and the result is tabulated. The temperature, velocity, and magnetic field sensitivities are computed according to the requirements of eqn. 39 and tabulated with the β's. The second computational use is for frequency (not channel) specific radiative transfer computations. This application requires many more evaluations of eqn. 12 or eqn. 15 and a line by line and a quasi continuum approach is used. In this calculation, the β spectrum is computed as before and differenced from another β spectrum which

Table 9. MLS spectral data from JPL Spectral Catalogue.

molecule	ν_j MHz	Q(300K)	Q(225K)	Q(150K)	$E\ell_j$ cm^{-1}	$\mathcal{I}_j$(300K) $\log(nm^2MHz)$
O_2	62,997.971	2.3398	2.2152	2.0398	343.7484	-6.6076
	63,568.520	2.3398	2.2152	2.0398	438.4418	-6.7441
^{18}OO	62,842.424	2.6649	2.5402	2.3649	325.3585	-6.8966
	63,111.000	2.6649	2.5402	2.3649	368.7314	-6.9560
	63,376.687	2.6649	2.5402	2.3649	414.8060	-7.0227
	63,639.955	2.6649	2.5402	2.3649	463.5807	-7.0964
^{17}OO[a b]	*62,882.5809*	*3.4302*	*3.3051*	*3.1290*	*292.5225*	*-7.5570*
	62,766.4891	*3.4302*	*3.3051*	*3.1290*	*292.5262*	*-7.5878*
	63,163.8268	*3.4302*	*3.3051*	*3.1290*	*334.3115*	*-7.6147*
	63,048.6585	*3.4302*	*3.3051*	*3.1290*	*334.3152*	*-7.6436*
ClO[a]	204,346.000[d]	3.5149	3.3578	3.1485	14.2541	-2.8166
	V0004↪	*3.5250*	*3.3632*	*3.1537*	*13.0222*	*-2.7855*
	204,351.925[d]	3.5149	3.3578	3.1485	14.2522	-2.8990
	V0004↪	*3.5250*	*3.3632*	*3.1537*	*13.0203*	*-2.8678*
	204,357.170[d]	3.5149	3.3578	3.1485	14.2512	-2.9837
	V0004↪	*3.5250*	*3.3632*	*3.1537*	*13.0193*	*-2.9525*
	204,362.557[d]	3.5149	3.3578	3.1485	14.2508	-3.0685
	V0004↪	*3.5250*	*3.3632*	*3.1537*	*13.0189*	*-3.0373*
O_3	184,377.820	3.5506	3.3484	3.0787	39.7506	-4.0808
	206,132.050	3.5506	3.3484	3.0787	323.6207	-4.7207
$O^{18}OO$	206,272.302	3.5472	3.3599	3.0959	49.1007	-4.6914
	205,850.898	3.5472	3.3599	3.0959	436.3999	-4.8985
^{18}OOO	202,229.509	3.8582	3.6708	3.4065	328.7227	-5.0311
	202,385.562	3.8582	3.6708	3.4065	7.9927	-5.7597
	204,592.000	3.8582	3.6708	3.4065	1007.9151	-6.1461
O_3(v2)[b]	*206,496.036*	*3.5506*	*3.3484*	*3.0787*	*873.1248*	*-6.0181*
H_2O	183,310.091	2.2507	2.0645	1.8040	136.1639	-3.6472
$H_2^{18}O$	203,407.520	2.2544	2.0682	1.8076	134.7832	-3.5657
HDO[e]	207,345.710	2.1669	1.9803	1.7185	513.2071	-4.2844
H_2O_2	204,574.715	3.9914	3.7616	3.4494	475.3349	-3.2027
HNO_3[a]	206,594.744[d]	4.4462	4.2589	3.9947	53.2579	-2.9444
	206,594.686[c d]	4.4462	4.2589	3.9947	53.2579	*-2.9445*
	206,353.966[d]	4.4462	4.2589	3.9947	190.3144	-3.6231
	206,353.976[c d]	4.4462	4.2589	3.9947	*190.3143*	*-3.6232*
	206,194.740[d]	4.4462	4.2589	3.9947	211.1913	-3.6241
	206,194.752[c d]	4.4462	4.2589	3.9947	*211.1912*	-3.6241
	205,824.699[d]	4.4462	4.2589	3.9947	255.4339	-3.6455
	205,824.717[c d]	4.4462	4.2589	3.9947	255.4339	-3.6455

Table 9. (continued)

molecule	ν_j MHz	Q(300K)	Q(225K)	Q(150K)	$E\ell_j$ cm^{-1}	$\mathcal{I}_j$(300K) log(nm^{2}MHz)
SO_2	204,246.772	3.7721	3.5845	3.3202	118.6848	-3.0440
	204,384.300	3.7721	3.5845	3.3202	38.3677	-4.1892
	200,287.530	3.7721	3.5845	3.3202	203.4634	-3.0624
N_2O	200,975.260	2.6972	2.5724	2.3965	23.4641	-4.0066
HO_2	200,616.725[d]	3.6380	3.4530	3.1895	25.5087	-3.2061

[a]The calculation includes many more lines—only the four strongest are listed.
[b]Molecule added to V0004 and subsequent processing.
[c]Improved catalogue data [Pickett et al., 1992 []] used in V0004.
[d]This frequency is composed of multiple lines—actual calculation includes each individual line separately.
[e]Included in V0003 processing but will be excluded in future versions.

is a line by line computation using only the molecular lines (nominally those in Table 8) in the receiver bandwidth. This residual which is computed for each PSIG height is stored as a discrete frequency function which can be accurately interpolated with cubic spline owing to its smooth structure. This is the "quasi continuum" part of the function and reduces the line by line component of the subsequent radiative transfer calculation considerably which of course speeds it up. The individual line data which must be evaluated with eqn. 81 is also stored in the line by line and quasi continuum file. The temperature and velocity sensitivity of the continuum part is also part of this file which allows the user to correct for changes in these parameters. The distinction and use of these two approaches are described in the next section.

There are also two important background continuum functions to consider, dry air and H_2O. The dry air continuum is mostly from N_2 collision induced absorption (CIA) [Borysow and Frommhold, 1986 [], Dagg et al., 1985 [] and references cited therein] but will include similar effects from O_2, CO_2 and others. It will also include a contribution from the magnetic dipole O_2 in the far wings of those lines. In V0003, this effect was characterized empirically from fitting a pressure function to the band 2 radiances in the lower to middle stratosphere which are assumed to be dry.

$$\kappa = 1.36 \times 10^{-18} P^{1.54} \nu^2 \left(\frac{300}{T}\right)^3. \qquad (86)$$

The ν^2 is assumed for extension to other frequencies. This function is not used for 63 GHz (O_2) analysis. Although this function fit the radiances well, the pressure power dependence is unphysical because it should be P^2. Therefore in V0004 the approach was to use a function that fits Dagg et al. [1985], N_2 CIA measurements over a range of frequencies between 0.0–450 GHz and 200K–350K. This produces the function

$$\begin{aligned} \kappa &= 1.07 \times 10^{-19} P^2 \nu^2 \left(\frac{300}{T}\right)^{3.68} \\ &\times \exp\left\{-1.85 \times 10^{-12} \nu^2\right\}, \end{aligned} \qquad (87)$$

which fits the experimental data to within 5% or better. This function is then added to the O_2 β calculation eqn. 82 with the weights 0.79/0.21 for the dry continuum contribution. Subsequent to this a new UTH retrieval was developed which required a more characteristic function than that provided by eqn. 87. A scheme was used to screen the data for the driest radiances and fit this to dry air (assuming no water) in the *troposphere*. The new function was much closer to the expected P^2 giving some confidence that the nature of the radiometric signal is properly understood. This new function is

$$\begin{aligned} \kappa &= 1.68 \times 10^{-19} P^2 \nu^2 \left(\frac{300}{T}\right)^{3.05} \\ &\times \exp\left\{-1.85 \times 10^{-12} \nu^2\right\}, \end{aligned} \qquad (88)$$

This function used V0004 pointing and temperature (which is NCEP analysis degraded to 3 per decade resolution) and is only used for the interim "V490"

Table 10. MLS Line Shape data.

molecule	ν_{j0} MHz	$\mathcal{M}$ AMU	w_{cj} MHz/hPa	n_j	error[a] %	$\Delta\nu_{j0}$[b] MHz/hPa
O_2	62,997.971	32.0	1.211[cd]	0.8[cd]	···	···
	V0004↪		*1.139*[e]		1	···
	63,568.520	32.0	1.182[cd]	0.8[cd]	···	···
	V0004↪		*1.11*[e]		2	···
^{18}OO	62,842.424	34.0	1.2[f]	0.8[f]	···	···
	V0004↪		*1.139*[g]	*0.8*[g]	···	···
	63,111.000	34.0	1.2[f]	0.8[f]	···	···
	V0004↪		*1.125*[f]	*0.8*[g]	···	···
	63,376.687	34.0	1.2[f]	0.8[f]	···	···
	V0004↪		*1.110*[f]	*0.8*[g]	···	···
	63,639.955	34.0	1.2[f]	0.8[f]	···	···
	V0004↪		*1.095*[f]	*0.8*[f]	···	···
^{17}OO[hi]	*62,882.581*	*33.0*	*1.155*[g]	*0.8*[g]	···	···
	62,766.489	*33.0*	*1.155*[g]	*0.8*[g]	···	···
	63,163.827	*33.0*	*1.139*[g]	*0.8*[g]	···	···
	63,048.659	*33.0*	*1.139*[g]	*0.8*[g]	···	···
ClO[h]	204,346.000[j]	51.0	2.529[k]	0.62[k]	3	···
	204,351.925[j]	51.0	2.529[k]	0.62[k]	3	···
	204,357.170[j]	51.0	2.529[k]	0.62[k]	3	···
	204,362.557[j]	51.0	2.529[k]	0.62[k]	3	···
O_3	184,377.820	48.0	2.373[l]	0.697[l]	3	···
	V0005↪		2.49[m]		1	0.0[n]
	206,132.050	48.0	2.168[l]	0.745[l]	3	···
$O^{18}OO$	206,272.302	50.0	2.2[f]	0.76[f]	···	···
	205,850.898	50.0	2.2[f]	0.76[f]	···	···
	V0004↪		*2.1*[g]		···	···
^{18}OOO	202,229.509	50.0	2.34[f]	0.76[f]	···	···
	V0004↪		*2.13*[g]	*0.76*[g]	···	···
	202,385.562	50.0	2.34[f]	0.76[f]	···	···
	204,592.000	50.0	2.34[f]	0.76[f]	···	···
	V0004↪		*2.00*[g]	*0.76*[g]	···	···
O_3(v2)[i]	*206,496.036*	*48.0*	*2.140*[g]	*0.76*[g]	···	···
H_2O	183,310.091	18.0	2.830[o]	0.75[o]	3	···
	V0005↪	18.0	3.12[m]	0.75[m]	2	-0.157[m]
$H_2^{18}O$	203,407.520	20.0	2.830[g]	0.75[g]	5	···
HDO[p]	207,345.710	19.0	2.919[q]	0.75[g]	···	···
H_2O_2	204,574.715	34.0	2.910[q]	0.75[t]	···	···

Table 10. (continued)

molecule	ν_{j0} MHz	$\mathcal{M}$ AMU	w_{cj} MHz/hPa	n_j	error[a] %	$\Delta\nu_{j0}$[b] MHz/hPa
HNO_3[h]	206,594.686[j]	63.0	3.27[q]	0.75[t]	···	···
	V0004↪		*3.330*[r]	*0.65*[r]	5	···
	206,353.976[j]	63.0	3.27[q]	0.75[t]	···	···
	V0004↪		*3.160*[r]	*0.83*[r]	5	···
	206,194.752[j]	63.0	3.27[q]	0.75[t]	···	···
	V0004↪		*3.260*[r]	*0.72*[r]	5	···
	205,824.717[j]	63.0	3.27[q]	0.75[t]	···	···
	V0004↪		*3.170*[r]	*0.80*[r]	5	···
SO_2	204,246.772	64.0	2.85[s]	0.75[t]	···	···
	V0004↪		*2.92*[u]	*0.78*[u]	5	···
	204,384.300	64.0	2.85[s]	0.75[t]	···	···
	V0004↪		*2.92*[u]	*0.78*[u]	···	···
	200,287.530	64.0	2.85[s]	0.75[t]	···	···
	V0004↪		*2.92*[u]	*0.78*[u]	···	···
N_2O	200,975.260	44.0	2.43[v]	0.87[v]	7	···
HO_2	200,616.725[j]	33.0	3.1[t]	0.75[t]	···	···
	V0004↪	33.0	*2.5*[t]	0.75[t]	···	···

[a]This error refers to the broadening function between at least 200–300 K for the future values.

[b]Calculations assume no pressure shift if data is missing.

[c]Liebe, 1977 [].

[d]Liebe, 1991 [].

[e]Liebe, 1992 [].

[f]Uses an average value based on most abundant isotope.

[g]Uses the same value as most abundant isotope.

[h]The calculation includes many more lines—only the four strongest are listed.

[i]To be included in future processing.

[j]This frequency is composed of multiple lines—actual calculation includes each individual line separately.

[k]Oh and Cohen, 1994 [].

[l]Oh and Cohen, 1992 [].

[m]Pumphrey, 1998 [].

[n]Value measured by Pumphrey, 1998 [] is not significantly different from zero.

[o]Bauer et al., 1989 [] and Goyette and DeLucia, 1990 []

[p]Included in current V0003 processing but will be excluded in future versions.

[q]Goyette et al., 1988 [] but for a different line and no temperature dependence.

[r]E. A. Cohen, unpublished work. Some lines were not measured but were estimated from other measured lines using a J correction.

[s]Meier, 1978 [], Nitrogen broadening only and no temperature dependence.

[t]An experiential guess.

[u]C. Ball and F. C. DeLucia unpublished work. only 204246.772 line was measured, same function applied to the other lines.

[v]Margottin-Maclou, 1985 [] and Colmont, 1987 [].

UTH product. Due to pointing biases between V0004 and V0005 and using the NCEP temperatures on a 6 per decade $\log(P)$ vertical resolution, the dry function needed to be recharacterized and the new function is

$$\begin{aligned}\kappa &= 1.90\times10^{-19}P^2\nu^2\left(\frac{300}{T}\right)^{2.79}\\ &\times \exp\left\{-1.85\times10^{-12}\nu^2\right\},\end{aligned} \tag{89}$$

Eqns. 88 and 89 include O_2 hence one does not add emissions for this molecule as was done for V0004 with eqn. 87 V0005 uses eqn. 89 for all its retrievals. Contributions due to stratospheric gases, e.g. N_2O, ClO, O_3, HNO_3, etc. are excluded and must be added in all cases.

The water vapor continuum has also undergone evolution through the versions. In V0003 and V0004 the Liebe function [Liebe, 1981 []]

$$\begin{aligned}\beta &= 4.76\times10^{-16}P^2\nu^2\left(\frac{300}{T}\right)^{3}\\ &\times \left(1.0+31.6f_{\mathrm{h2o}}\left(\frac{300}{T}\right)^{7.5}\right)\end{aligned} \tag{90}$$

is added to the summed contribution from 7 lines Rosenkranz [1993] for all bands. This function was unsatisfactory for the UTH retrieval because the calculated absorption in the 203 GHz region is too small. This is also supported by laboratory work [Godon et al., 1992 []]. Therefore this function was recharacterized assuming the same functional form as dry air. Maximum radiance values as a function of height and assuming 100% ice relative humidity was assumed in this characterization. The temperature dependence was borrowed from the laboratory work Godon et al., 1992 [] and the magnitude fit. This function includes absorption from lines and continuum and assumes a P^2 for all this. It also neglects water vapor self-broadening and is used only for the V490 UTH retrieval. The function is

$$\beta = 5.66\times10^{-5}P^2\left(\frac{300}{T}\right)^{4.20} \tag{91}$$

The resulting β (Km^{-1}) is multiplied by the water vapor mixing ratio to give the absorption coefficient, κ. This function has no frequency dependence and is only used for band 2 radiances which represents a frequency range between 202–205 GHz. As with the dry air continuum, the water vapor continuum was recharacterized for the V0005 retrieval. In this case Vaisala sonde measurements were used to establish the atmospheric wetness rather than selecting the maximum radiance values at a given height and assuming 100% ice relative humidity. The resulting function is

$$\beta = 5.29\times10^{-5}P^2\left(\frac{300}{T}\right)^{3.67} \tag{92}$$

This function will be used in all retrievals involving bands 2–4 including UTH. The Liebe continuum plus line by line is used in the other bands.

Line Selection

Which lines to include in the line by line calculations is considered here. The line selection procedure will include any line within a specified band width which is 660 MHz for the MLS bands except Bands 2 and 3 which is treated as a single unit having 880 MHz bandwidth with a center frequency halfway between them. Each band has two sets of lines because both side bands are received. Outside these specified bandwidths a simple radiance difference formula is used

$$\Delta I_j = \frac{1.714\times10^{13}P^2w\Delta f10^{\mathcal{I}_j}}{\Delta\nu_j^2}\tau, \tag{93}$$

where P is pressure in hPa, w is the broadening parameter, Δf is the mixing ratio, $\mathcal{I}$ is the *JPL Catalog* line strength in nm^2MHz for the jth line, $\Delta\nu$ is the frequency offset from the target frequency including the bandwidth and the test line, and τ is an attenuation factor. The temperature dependent quantities are tabulated at 300 K and are not adjusted because factors of two errors are tolerable for this purpose. The mixing ratios use a "typical" mid-latitude profile. The premultiplicative constant assumes a 500 km path length, 300 K temperature and a factor of ten increase to account for profile variations. The attenuation factor $\tau = 1.0$ for line selection used for V0003 processing and will use the following function for subsequent processing (V0004 and beyond)

$$\begin{aligned}\tau &= \exp\left\{-5.35\times10^{-17}P^2\nu^2\right.\\ &\times \left.\exp\left[-1.85\times10^{-12}\nu^2\right]\right\},\end{aligned} \tag{94}$$

which accounts for N_2 CIA which is always present. This additional factor helps to eliminate many unnecessary lines near the surface which would not penetrate a dense atmosphere. The algorithm accounts for unresolved lines based on the pressure broadening width by adding the contributions and treating it as a single line. All lines exceding the selection threshold of $\Delta I_j > 0.01$ K are included in the line by line calculation described in the previous subsection.

Spatial and Spectral Effects

This section discusses the mathematical interface including approximations, between the instrument and the radiative transfer calculations. Reviewing eqn. 1, there are two effects, spectral and spatial (or antenna) averaging.

Frequency Averaging

The instrument processes radiation through a series of filter banks which are composed of 15 narrow band pass filters. The instrument's spectral response is measured prior to launch and is characterized by $F_i(\nu)$. These functions describe the relative sensitivity of the instrument at any frequency and its effect is accounted through evaluation of an averaging integral. This integral is evaluated using one of two methods, fast and approximate, and exact.

Approximate Depending on the spectral characteristics and the signal strength, a considerable computational savings can be realized by integrating the β over frequency and using this in the radiative transfer calculation. This reduces the frequency averaged radiative transfer computation to a single evaluation of eqn. 12 or eqn. 15. This approximation causes a second order error according to

$$\begin{aligned}\Delta I &= \frac{B}{2}\left\{\int_{\nu_0}^{\nu_1} F(\nu)\left[\int_0^s \kappa(\nu,s)\,\mathrm{d}s\right]^2 \mathrm{d}\nu\right. \\ &- \left.\left[\int_0^s\int_{\nu_0}^{\nu_1} F(\nu)\,\kappa(\nu,s)\,\mathrm{d}\nu\mathrm{d}s\right]^2\right\}. \qquad (95)\end{aligned}$$

This equation is derived by assuming an isothermal atmosphere, expanding the transmission exponential and truncating at the second order term, and assuming no frequency variation in the Planck function across the MLS channel. This expansion is differenced from one using frequency averaged β's which when combined with mixing ratios become absorption coefficients κ above. Neglecting the frequency response of B across the MLS channel bandwidth is an excellent approximation, and neglecting temperature gradiants although not necessary leads to a simplier equation and does not add any error in itself. The spectral function is normalized to unit area with inverse frequency units. In general an error occurs only when the second order term in an exponential is important. Radiances of 10 K, 20 K, and 40 K single sideband will have second order contributions of 2%, 8%, and 17% respectively. The pre-frequency average approximation also has a second order contribution which helps to cancel some of the error caused by neglecting the more time consuming approach. The amount of error realized depends on the ratio of the channel bandwidth to the frequency structure of κ. This is hard to determine without case by case studies but a simple estimate can be made by assuming a path averaged absorption coefficient having a linear frequency response. This gives the radiance error,

$$\Delta I \approx -\frac{B}{24}\Delta s^2\Delta\kappa^2\exp\left\{-\overline{\kappa}\Delta s\right\}, \qquad (96)$$

where Δs is the path length, and $\Delta\kappa$ is the path averaged absorption coefficient difference across the channel bandwidth, and $\overline{\kappa}$ is the frequency averaged absorption coefficient. Eqn. 96 predicts that prefrequency averaged calculations cause an overestimation of radiances and since the error tends to be greater in the center channels than the wing channels the usual result will lead to an underestimation of profile concentrations when retrievals are performed. In practice, for microwave work, channel bandwidths can be made quite narrow and the pre-frequency averaging approximation (PFA) can work quite well—even for strong signals.

A description of errors caused by the PFA approximation as it applies to MLS is given. If the band width is larger than the line width, then this approximation can only be used when single sideband radiances are less than 10–20 K (2–10% error). For MLS, 10 K "narrow" high altitude line signals occur only for O_2 (band 1), H_2O (band 5) and O_3 (band 6) and this approximation is not used here. The MLS ozone line in band 4 is significantly pressure broadened when the signal strength is 10 K which effectively "smooths" the spectral structure relative to the receiver bandwidths and the PFA approximation works quite well for this molecule at all heights despite having 50 K signal strengths. Other MLS species, ClO, SO_2, HNO_3 and all the other contaminant species have signal strengths less than 10 K and the PFA approximation is essentially exact. The upper tropospheric water continuum has no spectral structure and the frequency averaging approximation is valid regardless of signal strength. Breaking the errors by band gives the following results. Band 1, (O_2), the PFA approximation causes large errors–any where from 2 K to 70 K. This approximation is not applied to band 1 (except for derivative calculations). Bands 2–4, (ClO, O_3, SO_2, HNO_3, and upper tropospheric H_2O), radiance error is less than 0.13 K in any channel at any height and the approximation is acceptable for these bands. Band 5 (H_2O) uses the PFA calculation on the 5 outermost channels where the maximum error is not expected to exceed 2.3 K (or 3%) in any channel at any height. The center five channels do not use the PFA

approximation because it can have errors as large as 15 K. Band 6 (O_3) uses the PFA approximation on the 12 outermost channels and the "exact" calculation on the center three channels. The PFA errors on band 6 are less than 1.4 K for the affected channels. In V0004 and V0005 processing, the PFA approximation is not used at all on bands 5 and 6.

Exact The MLS forward model calculation uses a weighted spectral response radiance averaging calculation (eqn. 1) where the PFA approximation is likely to cause large errors. This applies to all of band 1, the center 5 channels in band 5, and the center 3 channels in band 6. V0004 and V0005 will perform the full frequency averaging calculation to all channels in band 5 and 6. The current version (V0003) does this integration using an Aitkins Δ^2 method. This approach evaluates the integral using a series of numerical quadratures using a small number of integration points and projecting the "exact answer" based on the convergence property of the series. The integrals use 25, 13, and 7 radiative transfer calculations on equally spaced frequency grids. The radiometric calculations at 13 and 7 points are a subset of the 25 point calculation and therefore only 25 radiometric evaluations are needed for each affected MLS channel. The spectral responses are quite complicated and these are represented with 161 points. The radiative transfer calculations are interpolated to the same 161 frequency points using a cubic spline. The integral is evaluated with a 161 point Simpson Rule. The 25, 13, and 7 point based integrations are processed with the Aitkins procedure which gives the final result. This technique has been compared to a 161 point integration with 161 radiative transfer calculations with negligible difference. This method works very well when the frequency dependence of the radiative transfer varies monotonically. Although this situation exist for most channels considered a notable exception are the wing channels of band 1 where a 80 K signal from ^{18}OO appears in the very broad channels. The current Aitkins application can be in error by 2–3 K in this situation. This problem was discovered subsequent to V0003 processing and therefore will exist in that product. The Aitkins could not be adequately adapted or modified to work well for this case because it required equal frequency spacings in the radiative transfer calculations and a smooth well behaved monotonic radiative transfer function. This is fixed using an adaptive integration procedure which bifurcates the integration step until convergence is reached. This approach requires more time and effort but appears to be accurate to 0.2 K in most cases for the wing channels in band 1. This method is used in V0004 and 5.

The exact computation is at least 25 times slower (if Aitkins is used) than the PFA computation. The derivatives should also be computed this way but this would be prohibitively long especially for the magnetic channels which are an additional 8 times longer on account of the complex matrix algebra involved. Additional time is invested computing absorption cross sections β's, which are conveniently tabulated for the PFA case. The previously described line by line plus continuum file greatly helps to speed this aspect of the calculation. Therefore a scaling approximation is used for the derivatives. This approximation computes the radiances and derivatives with the PFA approximation and then only the radiances with full frequency averaging. The radiances from these two calculations are ratioed and the derivatives are scaled by this ratio. This approximation of course assumes that the scaling ratio is a constant of the change variable which of course is not strictly valid but it seems to work well (less than 10% error in the derivative) for the impacted MLS channels. This will be re-evaluated for the non-linear V0005 retrieval where high first order derivative accuracy is required.

Field of View Effects

The far-field beam width of the MLS receiver is larger than the vertically projected limb path smearing due to radiative transfer and must be considered. Variations in the antenna response arising from frequency changes within an MLS radiometer is neglected allowing separation between the spatial and frequency averaging calculations. The calculation is a weighted average of the radiances with the antenna gain function as given in eqn. 1 and for polarized radiation is given by

$$\begin{aligned} \overset{\bullet}{I}(\epsilon_p, \psi_p) &= \frac{1}{4\pi}\mathrm{Tr}\int_0^{2\pi}\int_{-\frac{\pi}{2}}^{\frac{\pi}{2}} \underline{\underline{I}}(\epsilon,\psi) \\ &\times \underline{\underline{G}}(\epsilon_p,\psi_p;\epsilon,\psi)\cos\epsilon d\epsilon d\alpha, \end{aligned} \quad (97)$$

where $\underline{\underline{G}}$ is the polarized far field antenna gain function and the trace (Tr) of the integrated area is 4π. Angles ψ and ϵ are azimuth and elevation angles in the instrument pointing reference frame and the subscript p indicates the field of view direction or more simply, the tangent height. The antenna gain matrix contains the co-polarized, cross-polarized, linear and circular coherent antenna patterns for the radiometer and must be presented in the same polarization basis as the radiance, see eqn 6. The unpolarized radiance has a diagonal polarization matrix with both elements equal. The evaluation of this integral can be sped up considerably by

using the fast Fourier transform theory of convolutions. This relies on the assumption that the antenna pattern is invarient throughout the scan which is believed to be true. Using the following coordinate transform in Barrett [1970]:

$$\xi \cong \psi \cos \epsilon_p; \chi \cong \epsilon - \epsilon_p, \tag{98}$$

and,

$$\mathrm{d}\psi \cong \frac{\mathrm{d}\xi}{\cos \epsilon_p} \simeq \frac{\mathrm{d}\xi}{\cos \epsilon}; \mathrm{d}\epsilon \cong \mathrm{d}\chi, \tag{99}$$

where small angular displacements from the origin, $\epsilon = \epsilon_p$ and $\psi = 0.0$ are required. The χ here refers to χ_{refr} in figure 8 which is the refracted elevation angle. The unrefracted elevation angle (χ in figure 8) is easily computed from the tangent height, e.g. $H_t = H_s \sin \chi$. The corresponding refracted χ, from successive application of eqn. 23 through the layers, is

$$\sin \chi_{refr} = \mathcal{N}_t \frac{H_t}{H_s}$$

where $\mathcal{N}_t$ is the tangent height refractive index and the refractive index at the UARS-MLS is unity. This is the χ to be used (both χ and χ_p) in the following field of view equations. These are substituted into eq. 97 to give,

$$\overset{\bullet}{I}(\xi_p, \chi_p) = \mathrm{Tr} \int_{-\infty}^{\infty} \int_{-\infty}^{\infty} \underline{\underline{I}}(\xi, \chi)\, \underline{\underline{G}}(\xi_p, \chi_p; \xi, \chi)\, \mathrm{d}\xi \mathrm{d}\chi, \tag{100}$$

where $\mathrm{Tr}\underline{\underline{G}}$ is now normalized to yield unity when integrated over all area. Eqn. 100 is written as a convolution integral:

$$\begin{aligned} \overset{\bullet}{I}(\xi_p, \chi_p) &= \mathrm{Tr} \int_{-\infty}^{\infty} \int_{-\infty}^{\infty} \underline{\underline{I}}(\xi, \chi) \\ &\times \underline{\underline{G}}(\xi_p - \xi, \chi_p - \chi)\, \mathrm{d}\xi \mathrm{d}\chi, \end{aligned} \tag{101}$$

where $\mathrm{Tr}\underline{\underline{G}}$ is the mirror image of the antenna pattern Barrett [1970]. This equation also requires a small angle approximation ($\ll 5^\circ$ in both dimensions) which is appropriate for 93.1%, 97.5%, and 92.1% of the power received by the MLS antenna for band1, bands 2-4, and bands 5 and 6 respectively [Jarnot, et al., 1996 []]. The purpose for developing eqn. 101 is that it is amenable to solution using fast Fourier transforms which is an $N \log N$ process which is much faster than directly integrating eq. 97 which is an N^2 process. Another simplification is to integrate in the vertical dimension (χ) only, taking advantage of neglecting the effect of the slight curvature of the earth and possible cross-track atmospheric gradients in the radiance function. Assuming $\overset{\bullet}{I}$ depends only on the vertical scan coordinate χ gives:

$$\overset{\star}{I}(\chi_p) = \mathrm{Tr} \int_{-\infty}^{\infty} \underline{\underline{I}}(\chi)\, \underline{\underline{G}}(\chi_p - \chi)\, \mathrm{d}\chi. \tag{102}$$

The matrix multiplication in eqn. 102 can be expanded to yield a four term sum.

$$\begin{aligned} \overset{\star}{I}(\chi_p) &= \int_{-\infty}^{\infty} I_\perp(\chi)\, G_\perp(\chi_p - \chi)\, \mathrm{d}\chi \\ &+ 2 \int_{-\infty}^{\infty} I_|(\chi)\, G_|(\chi_p - \chi)\, \mathrm{d}\chi \\ &+ 2 \int_{-\infty}^{\infty} I_\circ(\chi)\, G_\circ(\chi_p - \chi)\, \mathrm{d}\chi \\ &+ \int_{-\infty}^{\infty} I_\parallel(\chi)\, G_\parallel(\chi_p - \chi)\, \mathrm{d}\chi. \end{aligned} \tag{103}$$

The four antenna pattern components $G_\perp$, $G_|$, $G_\circ$, and $G_\parallel$ represent the normalized cross-polarized, linear coherence, circular coherence, and co-polarized antenna gain functions respectively. The patterns $G_|$ and $G_\circ$ were not measured and are not needed for unpolarized signals where $I_| = I_\circ = 0$ but will have to be ignored for the polarized case. The unpolarized radiation requires $I_\perp = I_\parallel$ and the four terms collapse to a single term:

$$\overset{\star}{I}(\chi_p) = \int_{-\infty}^{\infty} I_\parallel(\chi)\, \overline{G}(\chi_p - \chi)\, \mathrm{d}\chi, \tag{104}$$

where $\overline{G}$ is $G_\parallel + G_\perp$. Eqn. 104 is used for polarized radiation but in this case it is an approximation. It is expected to be a reasonable approximation because the peak gain in $G_\parallel$ is 30 db greater than $G_\perp$ for the 63 GHz radiometer.

One dimensional Fourier transforms are applied to solve this integral. The Fourier transform theorem of convolutions is

$$\mathcal{F}t\left(\overset{\star}{I}(\chi_p)\right) = \mathcal{F}t\left(\overset{\star}{I}(\chi)\right) \times \mathcal{F}t\left(\overline{G}(\chi)\right). \tag{105}$$

The Fourier transform of the antenna gain pattern can be taken and stored as such. An advantage to doing this in addition to avoiding repetitive Fourier transforms is that the autocorrelation of the field pattern should be zero beyond twice the aperture distance and the first point in the pattern is the normalization factor. Truncating the aperture autocorrelation pattern accordingly provides noise filtering; however, this is not done in our calculations because of uncertainty of the precise aperture size.

The parameter derivatives in eq. 2 can be complicated by field of view effects. The instrument derivative

function is given by (based on eqn. 104 the extension to the more general eqn. 97 is straightforward):

$$\begin{aligned}\frac{\partial \overset{\star}{I}}{\partial x} &= \int_{-\infty}^{\infty}\left[\frac{\partial \overset{\star}{I}}{\partial x}+\overset{\star}{I}\frac{\partial}{\partial x}\left(\frac{\partial \eta}{\partial x}\right)\right]G(\chi_p-\chi)\,\mathrm{d}\chi \\ &+ \frac{\partial \chi_p}{\partial x}\int_{-\infty}^{\infty}\overset{\star}{I}\frac{\partial G(\chi_p-\chi)}{\partial(\chi_p-\chi)}\mathrm{d}\chi \\ &- \int_{-\infty}^{\infty}\frac{\partial \chi}{\partial x}\overset{\star}{I}\frac{\partial G(\chi_p-\chi)}{\partial(\chi_p-\chi)}\mathrm{d}\chi \end{aligned} \quad (106)$$

where x is the state vector parameter to be differentiated. In most cases x is non geometrical (e.g. mixing ratios) and all the terms involving $\frac{\partial \chi}{\partial x} = 0$ and eqn. 106 is merely convolving the pattern with the radiance derivative which was developed in the previous section. Important exceptions are temperature, Earth radius, and the orbital radius. Remember that the antenna beam width is an angular property. Changes in these parameters will alter the far field antenna beam width as projected in ζ (or height) which is the independent variable. It is easy to appreciate the fact that the antenna beam width at the limb tangent will increase with increasing orbital height. Since pressure is the vertical gridding coordinate, then temperature changes the antenna shape through the hydrostatic function.

The pointing derivatives in eqn. 106 are:

$$\begin{aligned}\frac{\partial \chi}{\partial T_q} &= \frac{\tan\chi}{h}\frac{\partial h}{\partial T_q} \\ \frac{\partial}{\partial \chi}\left(\frac{\partial \chi}{\partial T_q}\right) &= \frac{2+\tan^2\chi}{h}\frac{\partial h}{\partial T_q}+\frac{\eta_q(\zeta(h))}{T(h)} \\ \frac{\partial \chi}{\partial h^s} &= -\frac{\tan\chi}{h^s} \\ \frac{\partial}{\partial \chi}\left(\frac{\partial \chi}{\partial h^s}\right) &= -\frac{1}{h^s\cos^2\chi} \\ \frac{\partial \chi}{\partial R^{\oplus}} &= -\frac{\tan\chi}{h_t} \\ \frac{\partial}{\partial \chi}\left(\frac{\partial \chi}{\partial R^{\oplus}}\right) &= -\frac{1}{h_t\cos^2\chi}\end{aligned} \quad (107)$$

The $\frac{\partial G(\chi_p-\chi)}{\partial(\chi_p-\chi)}$ term is evaluated using the FFT derivative property

$$\mathcal{F}t\left(\frac{\partial G(\chi)}{\partial \chi}\right) = \imath q\mathcal{F}t(G(\chi)), \quad (108)$$

where q is the aperture independent coordinate (number of wavelengths), and $\imath$ is $\sqrt{-1}$. This definition is convenient because the pattern is stored as $\mathcal{F}tG(\chi)$ and insures internal consistency between the pattern and its derivative.

There is a second derivative form of eqn. 106 which is given by:

$$\begin{aligned}\frac{\partial^2 \overset{\star}{I}}{\partial x\partial y} &= \int_{-\infty}^{\infty}\left(\frac{\partial^2 I}{\partial x\partial y}+\frac{\partial I}{\partial x}\frac{\partial^2\chi}{\partial\chi\partial y}\right. \\ &+ \left.\frac{\partial I}{\partial y}\frac{\partial^2\chi}{\partial\chi\partial x}+I\frac{\partial^3\chi}{\partial\chi\partial x\partial y}\right)G(\chi_p-\chi)\,\mathrm{d}\chi \\ &+ \int_{-\infty}^{\infty}\left(\frac{\partial I}{\partial x}+I\frac{\partial^2\chi}{\partial\chi\partial x}\right)\left(\frac{\partial\chi_p}{\partial y}-\frac{\partial\chi}{\partial y}\right) \\ &\times \frac{\partial G(\chi_p-\chi)}{\partial(\chi_p-\chi)}\mathrm{d}\chi \\ &+ \int_{-\infty}^{\infty}\left(\frac{\partial I}{\partial y}+I\frac{\partial^2\chi}{\partial\chi\partial y}\right)\left(\frac{\partial\chi_p}{\partial x}-\frac{\partial\chi}{\partial x}\right) \\ &\times \frac{\partial G(\chi_p-\chi)}{\partial(\chi_p-\chi)}\mathrm{d}\chi \\ &+ \int_{-\infty}^{\infty}I\left(\frac{\partial^2\chi_p}{\partial x\partial y}-\frac{\partial^2\chi}{\partial x\partial y}\right)\frac{\partial G(\chi_p-\chi)}{\partial(\chi_p-\chi)}\mathrm{d}\chi \\ &+ \int_{-\infty}^{\infty}I\left(\frac{\partial\chi_p}{\partial x}-\frac{\partial\chi}{\partial x}\right)\left(\frac{\partial\chi_p}{\partial y}-\frac{\partial\chi}{\partial y}\right) \\ &\times \frac{\partial^2 G(\chi_p-\chi)}{\partial(\chi_p-\chi)^2}\mathrm{d}\chi\end{aligned} \quad (109)$$

Eqn 109 will be applied to temperature, mixing ratios and its cross derivatives. Any geometric derivative involving mixing ratio is zero and those for temperature are given in eqn. 107 plus the following forms:

$$\begin{aligned}\frac{\partial^2\chi}{\partial T_{q'}\partial T_q} &= \frac{\tan^3\chi}{H^2}\frac{\partial H}{\partial T_{q'}}\frac{\partial H}{\partial T_q} \\ &+ \frac{\tan\chi}{H}\frac{\partial^2 H}{\partial^2\chi}\partial T_{q'}\partial T_q \\ \frac{\partial^3\chi}{\partial\chi\partial T_{q'}\partial T_q} &= \frac{3+\tan^2\chi}{H}\frac{\partial^2 H}{\partial T_{q'}\partial T_q} \\ &+ \frac{3\tan^4\chi+5\tan^2\chi}{H^2}\frac{\partial H}{\partial T_{q'}}\frac{\partial H}{\partial T_q} \\ &+ \frac{2+\tan^2\chi}{HT}\left(\eta_q\frac{\partial H}{\partial T_{q'}}+\eta_{q'}\frac{\partial H}{\partial T_q}\right)\end{aligned} \quad (110)$$

The hydrostatic temperature derivatives are given by:

$$\begin{aligned}\frac{\partial H}{\partial T_q} &= \frac{k\ln 10}{H_{\mathrm{eff}}^{\oplus 2}g^{\oplus}}\left(H+H_{\mathrm{eff}}^{\oplus}-H^{\oplus}\right)^2 P_q \\ \frac{\partial^2 H}{\partial T_{q'}\partial T_q} &= 2\left\{\frac{k\ln 10}{H_{\mathrm{eff}}^{\oplus 2}g^{\oplus}}\right\}^2\left(H+H_{\mathrm{eff}}^{\oplus}-H^{\oplus}\right)^3 P_q P_{q'}\end{aligned} \quad (111)$$

Higher order derivatives for the satellite and Earth radius are deemed uneccessary at this time.

Sidebands

The MLS is a hetrodyne receiver and the spectral response has two distinct frequency bandpasses having significant gain. The spectral shape of each bandpass is measured and is the $F_i(\nu)$ in eqn. 1. Nominally the spectral response for the bandpass (or side band) containing the target molecule species is measured and normalized against itself in the spectral response function. However its gain relative to the other sideband must be known in order calculate the radiances. This is expressed as a sideband ratio which are the r_u and r_l in eqn. 1. These two numbers must sum to one and vary by channel. The unmeasured spectral response for the side band not containing the target line is assumed to be the mirror image of the target. This is true only if there is no spectral gradient in the sideband ratio function (this information is folded into the spectral response measurement). It is clear that spectral gradients do exist in the sideband response function (see Jarnot, et al., 1996 []) and therefore the approximation is somewhat invalid. In band 1 where the O_2 signal is in both sidebands, this approximation was used for V0003 retrievals; however, the upper and lower side band shapes were measured separately for the broadband wing channels and these are now incorporated into V0004 retrievals. In that case, the radiance calculations were affected by as much as 1 K at some altitudes. It is possible given the measured sideband ratios and the spectral response function for the one sideband to "deconvolve" the sideband spectral gradient from the filter shape to get pure filter response. This can now be mirror imaged and the estimated sideband spectral gradient superimposed upon it to get the a better estimate of the filter function for the unmeasured sideband. This was not done in practice because it is expected to be unimportant for the following reasons: 1) for all bands other than band 1 the received radiation does not have strong spectral features or gradients in the non-target sideband hence the calculation is insensitive to the filter function, and 2) the approximation in band 1 is now applied to the narrower center channels where the side band gradient is relatively small compared to the nominal channel width and the approximation will be more valid.

Sideband ratios are measured prior to launch as part of instrument calibration. Post launch investigations have shown some problems with achieving a good fit with measured spectra. Some of the problem has been attributed to errors in the side band ratios. Consequently, V0004 the sideband ratios were adjusted for band 1 [D. Wu,*personal communication*] and band 5. Then in V0005 they were adjusted again for band 5 and band 6. These values are in [Pumphrey, 1998 []].

Future Improvements

The MLS forward model and inversion procedure is an evolving process. This paper is an attempt to cover much of the evolution beginning with the first "public domain" version V0003 and our recently released V0004 version. The MLS group is now proceding toward a better V0005 version which will further expand the capabilities of the MLS data and the infrastructure of that development is also been presented in this paper. Two significant forward model issues we hope to include in the future are an accurate high speed computational model so that the retrieval can be iterated, and a correction for line of sight gradients.

High Speed Forward Model

A high speed forward model will eliminate nonlinearity errors through iterative inversion. Fortunately, the radiances in bands 1–4 are quite linear in mixing ratio or temperature as evidenced by our successful validation efforts to date (see Fishbein et al., 1996 [], Froidevaux et al., 1996 [], Lahoz, et al., 1996 [], and Waters et al., 1996 []). Given this and the need for high accuracy (due to good instrument precision) which limits one's ability to use approximations, a fast forward model is needed. Preliminary tests have demonstrated that expanding the radiative transfer calculation to 2nd order is a solution to this problem. High accuracy is maintained by virtue of using a detailed forward model and the high degree of existing linearity allows this approach to successfully acount for the residual non-linearity, and it is fast to evaluate. The highly non-linear bands 5 (for H_2O) and band 6 (O_3) is not amenable to this approach and will require a forward model calculation at each iteration. Fortunately, this impacts only 30 out of 90 channels. The center channels on band 1 (O_2 for pointing and temperature) have been rendered unusable because the radiometric calculations are quite non-linear in the magnetic parameters and the tabulation of "linearization points" was poorly conceived. This will be remedied in the future by adding additional linearization values for the theta angle and storing the calculated result as a tensor. This will allow exact calculation of the third magnetic angle, ϕ, through tensor rotation. The "improved" model will neglect magnetic

line-of-sight gradients and this approximation will require further study. The mathematical development for these calculations have been presented herein.

Line-of-Sight Gradients

The retrievals for V0003 and V0004 neglect the effect of line-of-sight gradients on the retrievals. Although a minor effect, experimental iterative retrievals show a degraded radiometric fit where these gradients are large for temperature when the line sight path crosses the southern hemisphere vortex hence it is indirectly detectable in the data. A simple (but untested) algorithm for handling line of sight gradients is presented here. The cross track gradient also needs to be included and will for sake of simplicity assume that the cross track and line of sight are orthogonal during the MMAF. For a given profile coefficient projected onto a plane surface (like a 2D mapped field) can be fit to this equation:

$$f_m^l = f_{m,o}^l + G_m^l\,(\text{los})\,H_m^l\sqrt{1-\frac{H_t}{H}} + G_m^l\,(\text{ct})\,\Delta L \quad (112)$$

where $f_{m,o}^l$ is the coefficient value at a reference location based on the limb tangent location at a given MMIF, $G_m^l\,(\text{los})$ is the line-of-sight gradient in the coefficient, $G_m^l\,(\text{ct})$ is the cross track gradient, and ΔL is the distance between the current MMIF and the reference one. Eqn. 112 assumes that the gradient is a plane and the cross-track and line of sight paths are orthogonal which allows $G_m^l\,(\text{los})$ to be MMIF independent and $G_m^l\,(\text{ct})$ to be line of sight independent. The state vector which contains f_m^l is replaced with $f_{m,o}^l$, $G_m^l\,(\text{los})$, and $G_m^l\,(\text{ct})$. Eqn. 112 is substituted into eqn. 28 and the forward model is computed in the usual way. Note that eqn. 112 is H dependent and that part will have to be included in the integral in eqn. 29. Radiance derivatives with respect to $G_m^l\,(\text{los})$, and $G_m^l\,(\text{ct})$ are needed and computed with eqn. 40–43. The same form is usable for temperature however the situation gets much more complicated (see discussion on temperature derivatives and substitute eqn. 112 for T_q).

The gradients problem would be handled this way. The coefficients file (L2PC) would compute the forward model including derivatives for $G_m^l\,(\text{los})$ and $G_m^l\,(\text{ct})$ using no gradient as a linearization value. The retrieval program would perform a full-up no gradient retrieval. It would then have to "map" the fields and determine estimates for $G_m^l\,(\text{los})$ and $G_m^l\,(\text{ct})$. After doing so it would use those values in the state vector and keeping the gradients constrained, repeat the inversion which produces the gradient corrected fields and hopefully a better radiometric fit. In theory, the gradient profiles could be fit simultaneously with the profiles but this would probably not be prudent given the tripling of the number of profile-related adjustable parameters. Needless to say, this is going to add considerable complications to the inversion program too and is not an immediate goal for version 5.

Acknowledgments. The research described here, done at the Jet Propulsion Laboratory, California Institute of Technology, was under contract with the National Aeronautics and Space Administration and funded through its UARS Project.

References

Barath, F. T., M. C. Chavez, R. E. Cofield, D. A. Flower, M. A. Frerking, M. B. Gram, W. M. Harris, J. R. Holden, R. F. Jarnot, W. G. Kloezeman, G. J. Klose, G. K. Lau, M. S. Loo, B. J. Maddison, R. J. Mattauch, R. P. McKinney, G. E. Peckham, H. M. Pickett, G. Siebes, F. S. Soltis, R. A. Suttie, J. A. Tarsala, J. W. Waters, and W. J. Wilson, The Upper Atmosphere Research Satellite Microwave Limb Sounder Instrument, *J. Geophys. Res.,* , vol. *98*, 10751–10762, 1993.

Barrett, A. H. Fundementals of Radio Astronomy, *MIT notes*, 1970.

Bauer, A., M. Godon, M. Khedder, and J. M. Hartmann, Temperature and Perturber Dependences of Water Vapor Line-Broadening Experiments at 183 GHz; Calculations below 1000 GHz, *J. Quant. Spectrosc. Radiat. Transfer*, vol. *41*, 49–54, 1989.

Bean, B. R. and J. D. Dutton, *Radio Meteorology*, ??? pp., Dover Publications, New York, 1968.

Borysow, A. and L. Frommhold, Collision-Induced Rototranslational Absorption Spectra of N_2–N_2 Pairs for Temperatures from 50 to 300 K., *Astrophys. J.,* , vol. *311*, 1043–1057, 1986.

Chance, K., K. W. Jucks, D. G. Johnson, and W. A. Traub, The Smithsonian Astrophysical Observatory Database SAO92., *J. Quant. Spectrosc. Radiat. Transfer*, vol. *52*, 447–457, 1994.

Chandrasekhar, S., *Radiative Transfer*, 303 pp., Dover Publications, New York, 1960.

Colmont, J. M., N. Semmoud-Monnanteuil, Pressure Broadening of the N_2O J=9←8 Rotational Transition by N_2O, N_2, and O_2., *J. Mol. Spectrosc.*, vol. *126*, 240–242, 1987.

Dagg, I. R., A. Anderson, S. Yan, W. Smith, and L. A. A. Read, 1985, Collision-induced Absorption in Nitrogen at Low Temperatures, *Can. J. Phys.*, vol. *63*, 625–631, 1985.

Fishbein, E. F., L. S. Elson, L. Froidevaux, G. L. Manney, W. G. Read, J. W. Waters, and R. W. Zurek, MLS Observations of Stratospheric Waves in Temperature and O_3 During the 1992 Southern Winter, *Geophys. Res. Lett.,* , vol. *20*, 1255–1258, 1993.

Fishbein, E. F., R. E. Cofield, L. Froidevaux, R. F. Jarnot, T. Lungu, W. G. Read, Z. Shippony, J. W. Waters, I. S. McDermid, T. J. McGee, U. Singh, M. Gross, A. Hauchecorne, and M. E. Gelman, Validation of UARS MLS Temperatures and Pressure Measurements, *J. Geophys. Res.,* , *101*, 9983–10016, 1996.

Froidevaux, L., W. G. Read, T. A. Lungu, R. E. Cofield, E. F. Fishbein, D. A. Flower, R. F. Jarnot, B. P. Ridenoure, Z. Shippony, J. W. Waters, J. J. Margitan, I. S. McDermid, R. A. Stachnik, G. E. Peckham, G. Braathen, T. Deshler, J. Fishman, D. J. Hofmann, and S. J. Oltmans, Validation of UARS MLS Ozone Measurements, *J. Geophys. Res.,* , special issue on UARS data validation, *J. Geophys. Res.,* , *101*, 10017–10060, 1996.

Froidevaux, L., J. W. Waters, W. A. Lahoz, and W. A. Drew, Microwave Limb Sounder (MLS) Level 2/3A Data Processing: Software Requirements, *UARS MLS Group Document*, version 1.0, 15 July 1988.

Gantmacher, F. R., *The Theory of Matrices, Vol. 1*, Chelsea, New York, 1959.

Godon, M., J. Carlier, and A. Bauer, Laboratory Studies of Water Vapor Absorption in the Atmospheric Window at 213 GHz, *J. Quant. Spectrosc. Radiat. Transfer*, vol. *47*, 275–285, 1992.

Goody, R., A Note on the Refraction of a Twilight Ray, *J. Atmos. Sci.*, vol. *20*, 502–505, 1963.

Goyette, T. M. and F. C. DeLucia, The Pressure Broadening of the $3_{12} \rightarrow 2_{20}$ Transition of Water Between 80 K and 600 K, *J. Mol. Spectrosc.*, vol. *143*, 346–358, 1990.

Goyette, T. M., W. L. Eberstein, S. L. Shostak, F. C. DeLucia, and P. Helminger, Pressure Broadening of NO_2, CF_2Cl_2, HDO, and HOOH by O_2, N_2 in the Millimeter Wave Region, *J. Quant. Spectrosc. Radiat. Transfer*, vol. *40*, 129–134, 1988.

Harwood, R. S., E. S. Carr, L. Froidevaux, R. F. Jarnot, W. A. Lahoz, C. L. Lau, G. E. Peckham, W. G. Read, P. D. Ricaud, R. A. Suttie, and J. W. Waters, Springtime Stratospheric Water Vapour in the Southern Hemisphere as Measured by MLS, *Geophys. Res. Lett.,* , vol. *20*, 1235–1238, 1993.

Jackson, J. D., *Classical Electrodynamics*, 848 pp., John Wiley & Sons, New York, 1975.

Jarnot, R. F., R. E. Cofield, J. W. Waters, D. A. Flower, and G. E. Peckham, Calibration of the Microwave Limb Sounder on the Upper Atmosphere Research Satellite, *J. Geophys. Res.,* , vol. *101*, 9957–9982, 1996.

Lahoz, W. A., L. Froidevaux, R. S. Harwood, C. L. Lau, G. E. Peckham, H. C. Pumphrey, W. G. Read, Z. Shippony, M. R. Suttie, R. A. Suttie, and J. W. Waters, Data Validation of 183 GHz UARS MLS H_2O Measurements, *J. Geophys. Res.,* , *101*, 9957–9982, 1996.

Lenoir, W. B., Propagation of Partially Polarized Waves in a Slightly Anisotropic Medium, *J. App. Phys.,* vol. *38*, 5283–5290, 1967.

Lenoir, W. B., Microwave Spectrum of Molecular Oxygen in the Mesosphere, *J. Geophys. Res.,* , vol. *73*, 361–376, 1968.

Liebe, H. J., P. W. Rosenkranz, and G. A. Hufford, Atmospheric 60-GHz Oxygen Spectrum: New Laboratory Measurements and Line Parameters, *J. Quant. Spectrosc. Radiat. Transfer*, vol. *48*, 629–643, 1992.

Liebe, H. J., G. A. Hufford, and R. O. DeBolt, Measurements of the 60-GHz O_2 Spectrum of Air, *1991 North American Radio Science Meeting URS1 F*, Session 66, London, Ontario, Canada, June 24–28, 1991.

Liebe, H. J., Modelling Attenuation and Phase of Radio Waves in Air at Frequencies Below 1000 GHz., *Radio Science*, vol. *16*, 1183–1199, 1981.

Liebe, H. J., G. G. Gimmestad, and J. D. Hopponen, Atmospheric Oxygen Microwave Spectrum Experiment versus Theory, *I. E. E. E. Trans. Ant. Prop.*, vol. *AP-25*, 327–335, 1977.

List, R. J., *Smithsonian Meteorological Tables*, Smithsonian Miscellaneous Collections, vol. *114*, Smithsonian Institution, Washington D. C., 1951.

Manney, G. L., L. Froidevaux, J. W. Waters, R. W. Zurek, W. G. Read, L. S. Elson, J. B. Kumer, J. L. Mergenthaler, A. E. Roche, A. O'Neill, R. S. Harwood, I. MacKenzie, and R. Swinbank, Chemical Depletion of Ozone in the Arctic Lower Stratosphere During Winter 1992-93, *Nature*, vol. *370*, 429–434, 1994.

Margottin-Maclou, M., P. Dahoo, A. Henry, and L. Henry, Self-Broadening Parameters in the ν_3 Band of $^{14}N_2^{16}O$., *J. Mol. Spectrosc.*, vol. *111*, 275–290, 1985.

Marks, C. J., C. D. Rodgers, A Retrieval Method for Atmospheric Composition from Limb Emission Measurements, *J. Geophys. Res.,* , vol. *98*, 14939–14953, 1993.

D. Meier, Linewidth and Intensity Measurements of SO_2 Lines at 94 GHz with Self-Broadening and Broadening by H_2O and N_2., *J. Quant. Spectrosc. Radiat. Transfer*, vol. *19*, 323–329, 1978.

Oh, J. J. and E. A. Cohen, Pressure Broadening of ClO by N_2 and O_2 near 204 and 649 GHz and new Frequency Measurements between 632 and 725 GHz, *J. Quant. Spectrosc. Radiat. Transfer*, vol. *54*, 151–156, 1994.

Oh, J. J. and E. A. Cohen, Pressure Broadening of Ozone Lines near 184 and 206 GHz by Nitrogen and Oxygen. *J. Quant. Spectrosc. Radiat. Transfer*, vol. *48*, 405–408, 1992.

Pickett, H. M., Effects of Velocity Averaging on the Shapes of Absorption Lines., *J. Chem. Physics*, *73*, 6090–6094, 1980.

Pickett, H. M., R. L. Poynter, E. A. Cohen, Submillimeter, Millimeter, and Microwave Spectral Line Catalog, *JPL Publication 80-23, Rev 3*, 217pp., Jet Propulsion Laboratory, Pasadena, Ca. 1992.

Poynter, R. L. and H. M. Pickett, Submillimeter, Millimeter, and Microwave Spectral Line Catalog, *JPL Publication 80-23, Rev 2*, 165pp., Jet Propulsion Laboratory, Pasadena, Ca. 1984.

Pumphrey, H. C., S. Buehler, and R. S. Harwood, Instrumental and Spectral Parameters: Their Effect on and Measurement by Microwave Limb Sounding of the Atmosphere., submitted to ? 1998.

Read, W. G., L. Froidevaux, and J. W. Waters, Microwave Limb Sounder Measurement of Stratospheric SO_2 From the Mt. Pinatubo Volcano, *Geophys. Res. Lett.,* , vol. *20*, 1299-1302, 1993.

Read, W. G., J. W. Waters, D. A. Flower, L. Froidevaux, R. F. Jarnot, D. L. Hartmann, R. S. Harwood, and R. B. Rood, Upper-Tropospheric Water Vapor from UARS MLS, *Bull. Am. Meteorol. Soc.,* , vol. *76*, 2381–2389, 1995.

Reber, C. A., The Upper Atmosphere Research Satellite, *Geophys. Res. Lett.,* , vol. *20*, 1215–1218, 1993.

Rodgers, C. D., Characterization and Error Analysis of Profiles Retrieved From Remote Sounding Measurements, *J. Geophys. Res.,* , vol. *95*, 5587–5595, 1990.

Rosenkranz, P. W., D. H. Staelin, Polarized Thermal Microwave Emission from Oxygen in the Mesosphere, *Radio Science*, vol. *23*, 721–729, 1988.

Rosenkranz, P. W., Absorption of Microwaves by Atmospheric Gases, *Atmospheric Remote Sensing bby Microwave Radiometry*, M. A. Janssen, Ed., Chapter 2, pp. 37–90, John Wiley & Sons, New York, 1993.

Santee, M. L., W. G. Read, J. W. Waters, L. Froidevaux, G. L. Manney, D. A. Flower, R. F. Jarnot, R. S. Harwood, and G. E. Peckham, Interhemispheric Differences in HNO_3 Related to Polar Ozone Depletion, *Science*, vol. *267*, 849–852, 1994.

Shippony, Z., and W. G. Read, A Highly Accurate Voigt Function Algorithm, *J. Quant. Spectrosc. Radiat. Transfer*, vol. *50*, 635–646, 1993.

Townes, C. H., and A. L. Schawlow, *Microwave Spectroscopy*, 698 pp., Dover Publications, New York, 1975.

Waters, J. W., L. Froidevaux, W. G. Read, G. L. Manney, L. S. Elson, D. A. Flower, R. F. Jarnot, and R. S. Harwood, Stratospheric ClO and Ozone from the Microwave Limb Sounder on the Upper Atmosphere Research Satellite, *Nature*, vol. *362*, 597–602, 1993a.

Waters, J. W., L. Froidevaux, G. L. Manney, W. G. Read, and L. S. Elson, MLS Observations of Lower Stratospheric ClO and O_3 in the 1992 Southern Hemisphere Winter, *Geophys. Res. Lett.,* , vol. *20*, 1219–1222, 1993.

Waters, J. W., W. G. Read, L. Froidevaux, T. A. Lungu, V. S. Perun, R. A. Stachnik, R. F. Jarnot, R. E. Cofield, E. F. Fishbein, D. A. Flower, J. R. Burke, J. C. Hardy, L. L. Nakamura, B. P. Ridenoure, Z. Shippony, R. P. Thurstans, L. M. Avallone, D. W. Toohey, R. L. deZafra, and D. T. Shindell, Validation of UARS MLS ClO Measurements, *J. Geophys. Res.,* , *101*, 10091–10127, 1996.

WMO, Scientific Assessment of Ozone Depletion: 1991, World Meteorological Organization Global Ozone Research and Monitoring Project Report # 25, WMO, Washington D. C., 1991.

Jet Propulsion Laboratory
M.S. 183–701, Pasadena, Ca. 91109

This preprint was prepared with AGU's LaTeX macros v4, with the extension package 'AGU^{++}' by P. W. Daly, version 1.5g from 1998/09/14.

Bibliography

1. M. Abramowitz and I. A. Stegun. *Handbook of Mathematical Functions*. Dover, New York, 1965. National Bureau of Standards Applied Mathematics Series 55 (U.S. Government Printing Office, Washington, D.C., 1964).

2. B. J. Drouin. Temperature dependent pressure induced lineshape of the HCl J = 1 $\leftarrow$ 0 rotational transition in nitrogen and oxygen. *J. Quant. Spectrosc. Radiat. Transfer*, 83(1):63–81, 2004.

3. B. J. Drouin, J. Fisher, and R.R. Gamache. Temperature dependent pressure induced lineshape of O_3 rotational transitions in air. *J. Quant. Spectrosc. Radiat. Transfer*, 83(3–4):321–331, 2004.

4. R. Goody. A note on the refraction of a twilight ray. *J. Atmos. Sci.*, 20:502–505, 1963.

5. R. F. Jarnot, H. M. Pickett, and M. J. Schwartz. EOS MLS Level 1 Data Processing, Algorithm Theoretical Basis. Level 1 ATBD JPL D-15210, Jet Propulsion Laboratory, Mail Stop 183–701, 4800 Oak Grove Drive, Pasadena, Ca., 91109-8099, 22 June 2004. Version 2.0.

6. H. J. Liebe, G. A. Hufford, and M. G. Cotton. Propagation modeling of moist air and suspended water/ice particles at frequencies below 1000 Ghz. In *52nd Specialists' Meeting of the Electromagnetic Wave Propagation Panel*, Palma De Mallorca, Spain, May 17–21 1993. Adv. Group for Aerosp. Res. and Dev.

7. H. J. Liebe, P. W. Rosenkranz, and G. A. Hufford. Atmospheric 60-GHz oxygen spectrum: New laboratory measurements and line parameters. *J. Quant. Spectrosc. Radiat. Transfer*, 48:629–643, 1992.

8. N. J. Livesey. EOS MLS Retrieval Processes Algorithm Theoretical Basis. Level 2 ATBD JPL D-16159, Jet Propulsion Laboratory, Mail Stop 183–701, 4800 Oak Grove Drive, Pasadena, Ca., 91109-8099, 21 June 2004. Version 1.3.

9. J. J. Oh and E. A. Cohen. Pressure broadening of ClO by N_2 and O_2 near 204 and 649 GHz and new frequency measurements between 632 and 725 GHz. *J. Quant. Spectrosc. Radiat. Transfer*, 54:151–156, 1994.

10. J. R. Pardo, E. Serabyn, and J. Cernicharo. Submillimeter atmospheric transmission measurements on Mauna Kea during extremely dry El Niño conditions: Implications for broadband opacity contributions. *J. Quant. Spectrosc. Radiat. Transfer*, 68:419–433, 2001.

11. H. M. Pickett. Effects of velocity averaging on the shapes of absorption lines. *J. Chem. Physics*, 73:6090–6094, 1980.

12. H. C. Pumphrey. Validation of a new prototype water vapor retrieval for the UARS Microwave Limb Sounder. *J. Geophys. Res.*, 104(D8):9399–9412, 1999.

13. W. G. Read. UARS-MLS direct measurement model for radiative spectral intensity. Technical report, Jet Propulsion Laboratory, Mail Stop 183–701, 4800 Oak Grove Drive, Pasadena, Ca., 91109-8099, January 18 1988. Version 2.1.

14. W. G. Read and Z. Shippony. The UARS MLS radiance model. Unpublished paper, 1998.

15. Michael J. Schwartz, W. V. Snyder, and W. G. Read. EOS MLS mesosphere-specific forward model algorithm theoretical basis document. Mesosphere Specific ATBD JPL D-28534, Jet Propulsion Laboratory, Mail Stop 183–701, 4800 Oak Grove Drive, Pasadena, Ca., 91109-8099, 4 June 2004. Version 1.0.

16. Z. Shippony and W. G. Read. A highly accurate Voigt function algorithm. *J. Quant. Spectrosc. Radiat. Transfer*, 50:635–646, 1993.

17. C. C. Tscherning, editor. *The Geodesist's Handbook*, volume 58. Bureau Central De L'Association Internatiale De Géodésie, 1984.

18. J. W. Waters and L. Froidevaux. An Overview of the EOS MLS Experiment. Overview ATBD JPL D-15745, Jet Propulsion Laboratory, Mail Stop 183–701, 4800 Oak Grove Drive, Pasadena, Ca., 91109-8099, 2 April 2004. Version 2.0.

19. D. L. Wu and J. H. Jiang. EOS MLS algorithm theoretical basis for cloud measurements. Technical Report JPL D-19299, Jet Propul. Lab., Pasadena, Calif., 4 June 2004. Version 1.0.